DTIC File Copy

AD-A223 301

Scientific and Engineering Studies

Compiled 1987

Signal Processing Studies

A. H. Nuttall

PUBLISHED BY

NAVAL UNDERWATER SYSTEMS CENTER

NEWPORT LABORATORY, NEWPORT, RHODE ISLAND

NEW LONDON LABORATORY, NEW LONDON, CONNECTICUT

Scientific and Engineering Studies

Compiled 1987

Signal Processing Studies

A. H. Nuttall

PUBLISHED BY

NAVAL UNDERWATER SYSTEMS CENTER

NEWPORT LABORATORY, NEWPORT, RHODE ISLAND

NEW LONDON LABORATORY, NEW LONDON, CONNECTICUT

90 06 25 040

Foreword

This collection of technical reports addresses the following topics: the response of a linear-FM correlator for multiple signals, where the reference and signal amplitude modulations may be mismatched; the performance of two different types of normalizers subject to widely different interferences, such as Weibull, log-normal, Gaussian, and for received signals that have undergone a very general model of fading; the performance of an OR-ing device that must also indicate the correct signal channel of an incoherent combiner of separated signal components; a new procedure for accurate, efficient evaluation of Bessel transforms, which is an extension of Filon's method for Fourier transforms; a highly efficient procedure for evaluation of polynomials and exponentials of polynomials for equi-spaced arguments along an arbitrary line in the complex plane; and the estimation of signal and noise powers of a signal that is amplitude-modulated in a known way.

Some of the material presented here is based heavily on the author's earlier work, which can be found in the following volumes in addition to the referenced technical reports:

Performance of Detection and Communication Systems, NUSC Scientific and Engineering Studies, 1974;

Spectral Estimation, NUSC Scientific and Engineering Studies, 1977;

Coherence Estimation, NUSC Scientific and Engineering Studies, 1979;

Receiver Performance Evaluation and Spectral Analysis, NUSC Scientific and Engineering Studies, 1981;

Signal Processing Studies, NUSC Scientific and Engineering Studies, 1983;

Signal Processing Studies, NUSC Scientific and Engineering Studies, 1985;

Signal Processing Studies, NUSC Scientific and Engineering Studies, 1986.

Dr. William A. Von Winkle
Associate Technical Director
for Technology
NAVAL UNDERWATER SYSTEMS CENTER

Compiled 1987

Table of Contents

Technical Report 7543
4 October 1985

Linear FM Correlator Response for Multiple Targets; Mismatched Reference and Signal Amplitude Modulations

A. H. Nuttall

ABSTRACT

The response of a linear-FM correlator to a target with multiple point-highlights is derived in closed form. The transmitted signal and reference waveform amplitude modulations need not be equal in shape or length, nor do the highlight strengths, time delays, and frequency shifts have to be matched by the reference parameters. The fundamental calculation required is the cross-ambiguity function between two waveforms of different shapes and lengths, each belonging to the general class composed of a sum of cosines. In particular, this class includes the rectangular, Hanning, and Hamming functions, as well as a variety of optimum cases.

The effect of mainlobe broadening for frequency mismatch, as well as the possibility of supressing the sidelobes of the receiving filter response by deliberate mismatching, is displayed for a variety of cases. The accompanying loss in detectability is also investigated, being of the order of .5 dB in signal-to-noise ratio, if the reference waveform length is selected appropriately. Programs are furnished that allow a user to consider his own multiple target structure and reference waveforms with arbitrary time-bandwidth product.

TABLE OF CONTENTS

TABLE OF CONTENTS

LIST OF ILLUSTRATIONS

LIST OF ILLUSTRATIONS (Cont'd)

LIST OF SYMBOLS

FM	Frequency modulation
t	Time
$s(t)$	Signal complex envelope
f	Frequency
f_c	Frequency of carrier
$w(t)$	Received waveform
A_d	Amplitude of d-th target highlight (complex)
t_d	Time delay of d-th target highlight
f_d	Frequency shift of d-th target highlight
$r(t)$	Reference waveform
$q(t)$	Reference complex envelope
t_r	Time delay of reference
f_r	Frequency shift of reference
θ_r	Phase of reference
$c(t_r, f_r)$	Correlator signal output
$\underline{c}(t_r, f_r)$	Correlator output complex envelope
B_d	Complex phasor of d-th path
χ_{sq}	Cross-ambiguity function of s and q
τ	Time delay parameter
ν	Frequency shift parameter

LIST OF SYMBOLS (Cont'd)

$\underline{s}(t)$	Signal low-pass amplitude modulation
$\underline{g}(t)$	Reference low-pass amplitude modulation
β	Rate of instantaneous frequency
T	Signal duration
W	Signal bandwidth
$\bar{\chi}_{ab}$	Symmetric cross-ambiguity function of a and b
x	Normalized time variable, t/T
y	Normalized frequency variable, f/W
x_d	Normalized time delay of d-th path, t_d/T
y_d	Normalized frequency shift of d-th path, f_d/W
x_r	Normalized time delay of reference, t_r/T
y_r	Normalized frequency shift of reference, f_r/W
Δ_x	Difference in delays, x_r-x_d
Δ_y	Difference in shifts, y_r-y_d
a_k	k-th coefficient of signal $\underline{s}(t)$
b_ℓ	ℓ-th coefficient of reference $\underline{g}(t)$
χ_0	Normalized cross-ambiguity function
$A(f)$	Fourier transform of $a(t)$
$B(f)$	Fourier transform of $b(t)$
H	Height of ideal ambiguity function
L	Duration of local reference

LINEAR-FM CORRELATOR RESPONSE FOR MULTIPLE TARGETS; MISMATCHED REFERENCE AND SIGNAL AMPLITUDE MODULATIONS

INTRODUCTION

For target ranging and Doppler estimation on potential targets, a narrowband linear-FM (frequency modulation) waveform with rectangular amplitude modulation is often transmitted. Receiver processing for this signal is relatively simple, consisting of cross-correlation of the received waveform with a suitably time delayed (and possibly frequency shifted) replica of a linear-FM reference, generally utilizing the same rectangular amplitude modulation.

However, the receiver response can be cluttered by significant sidelobes for mismatched reference time delay guesses, due to a poor cross ambiguity function between the transmitted signal and the reference signal. Furthermore, significant broadening of the peak response can occur for mismatched frequency shifts.

Since the received waveform, consisting of multiple highlight echoes and noise, does not have to be necessarily processed with the matched filter, the possibility exists of suppressing sidelobes by using deliberately mismatched references. For recorded data that are to be

subjected to close scrutiny, a variety of situations can be investigated, and the maximum amount of information gleaned from a limited amount of data.

In order to determine how worthwhile this prospect can be, it is necessary to evaluate the noise-free responses of several candidate transmitted signals and local references. The class of waveforms should allow for different lengths as well as different shapes, including rectangular, Hanning, and Hamming functions as particular examples. Here we will derive equations and present programs for determining linear-FM correlator responses for signals with arbitrary

time-bandwidth product,
reference time delay and frequency shift,
number of targets,
target strengths,
target phases,
target time delays,
target frequency shifts, and
mismatched reference (envelope and duration).

As a necessary by-product of the investigation, the cross ambiguity between two different waveforms is derived for arbitrary

time delay

frequency shift,

time durations, and

amplitude shapes,

in the class of waveforms consisting of a sum of finite-duration cosines.

CROSS-CORRELATOR OUTPUT

GENERAL RESULT

The transmitted signal is presumed to be narrowband, with a dependence on time t of the form

$$s(t)\ \exp(i2\pi f_c t)\ , \tag{1}$$

where s(t) is the complex envelope and f_c is the carrier frequency. More precisely, (1) is the analytic signal corresponding to the transmitted waveform. The received (analytic) waveform after target reflection, but exclusive of noise, is given by

$$w(t) = \sum_d A_d\ s(t - t_d)\ \exp[i2\pi(f_c + f_d)(t - t_d)]\ , \tag{2}$$

where

$$\left.\begin{array}{l} A_d = \text{amplitude (complex)} \\ t_d = \text{time delay} \\ f_d = \text{frequency shift} \end{array}\right\} \begin{array}{l}\text{of d-th} \\ \text{target} \\ \text{highlight.}\end{array} \tag{3}$$

That is, each highlight is modeled as a point target with some strength, phase shift, range, and Doppler set of values.

The reference waveform to be used at the receiver has the form

$$r(t) = q(t - t_r) \exp[i2\pi(f_c + f_r)(t - t_r) + i\theta_r] , \qquad (4)$$

where

$$\left.\begin{aligned} q(t) &= \text{complex envelope} \\ t_r &= \text{time delay} \\ f_r &= \text{frequency shift} \\ \theta_r &= \text{phase} \end{aligned}\right\} \text{ of reference.} \qquad (5)$$

The reference complex envelope q(t) need not match transmitted signal s(t), nor need any of the reference parameters t_r, f_r, θ_r be identical to those in the received waveform w(t) in (2) and (3).

The signal output of the cross-correlator in the receiver is given by*

$$c(t_r,f_r) = \int dt\ w(t)\ r^*(t) . \qquad (6)$$

For matched filter processing at the receiver, the analytic signal of the filter output is given by (6), where t_r represents the time variable; the physical envelope is the magnitude of (6).

*Integrals without limits are over the range of nonzero integrand.

Correlator output c is obtained by substituting (2) and (4) in (6); the derivation is carried in appendix A, with the result for the complex envelope of (6) being given by (A-5) as

$$\underline{c}(t_r, f_r) = \sum_d B_d\, \chi_{sq}(t_r - t_d,\, f_r - f_d)\ , \tag{7}$$

where B_d is a complex phasor with the same strength as the d-th path amplitude A_d and a uniform distribution in angle, while

$$\chi_{sq}(\tau, \nu) = \int dt\ s(t)\ q^*(t - \tau)\ \exp(-i2\pi\nu t) \tag{8}$$

is the cross-ambiguity function of waveforms s(t) and q(t), at time delay τ and frequency shift ν. An alternative symmetric version of the cross-ambiguity function is defined in appendix B and some properties are discussed. The correlator output physical envelope is given by the magnitude of (7).

LINEAR-FM

When the transmitted signal s and local reference q employ linear-FM, we can express them according to

$$s(t) = \underline{s}(t)\ \exp(i\pi\beta t^2)\ ,$$
$$q(t) = \underline{q}(t)\ \exp(i\pi\beta t^2)\ , \tag{9}$$

where $\underline{s}(t)$ and $\underline{q}(t)$ are low-pass amplitude modulations centered at time $t = 0$. The instantaneous frequency of both functions in (9) is βt; if the

signal duration is T seconds and the frequency sweeps across a bandwidth of W Hz in that time, then we have

$$\beta = \pm \frac{W}{T} = \pm \frac{\text{frequency sweep}}{\text{signal duration}} , \tag{10}$$

where the + corresponds to an up sweep and the - to a down sweep.

The noise-free complex envelope of the correlator output (7) is then given in (A-12) by

$$\underline{c}(t_r, f_r) = \sum_d B_d \exp[-i\pi(f_r - f_d)(t_r - t_d)] *$$

$$* \bar{\chi}_{\underline{sq}}(t_r - t_d, f_r - f_d - \beta(t_r - t_d)) , \tag{11}$$

where $\bar{\chi}_{\underline{sq}}$ is the symmetric cross-ambiguity function of the low-pass amplitude modulations.

At this point, it is convenient to define a normalized time variable and a normalized frequency variable according to

$$x = \frac{t}{T} , \qquad y = \frac{f}{W} ; \tag{12}$$

the most important range of these new dimensionless variables x,y is -1,+1. Combining (10)-(12), we obtain

$$\underline{c}(t_r, f_r) = \sum_d B_d \exp[-i\pi TW(x_r - x_d)(y_r - y_d)]*$$

$$* \bar{\chi}_{\underline{sq}}[T(x_r - x_d), W(y_r - y_d \mp (x_r - x_d))] \tag{13}$$

for the linear-FM correlator complex envelope response. The physical envelope is $|\underline{c}(t_r, f_r)|$ versus reference time variable t_r. A multiple-highlight target is characterized by specification of

$$\left.\begin{array}{ll} \text{strength parameter} & B_d \\ \text{normalized time delay} & x_d \\ \text{normalized frequency shift} & y_d \end{array}\right\} \text{ for each path } d. \tag{14}$$

For a specified normalized local reference frequency shift y_r, we will plot the magnitude of response (13) versus normalized time parameter x_r in the -1,+1 range.

EXAMPLES OF LOW-PASS MODULATIONS

In this section, we present results for three common types of low-pass modulations $\underline{s}(t)$ and $\underline{q}(t)$ in (9). Numerical evaluation and graphical results are deferred to the next section.

RECTANGULAR ENVELOPES

Let both low-pass modulations be rectangular and of equal duration:

$$\underline{s}(t) = \underline{q}(t) = \frac{1}{\sqrt{T}} \qquad \text{for} \quad -\frac{T}{2} < t < \frac{T}{2} \, . \tag{15}$$

This corresponds to linear-FM that is abruptly turned on, held at constant amplitude, and abruptly turned off, at the transmitter as well as in the receiver processor.

The symmetric cross-ambiguity function is (see appendix B)

$$\overline{\chi}_{\underline{sq}}(\tau,\nu) = \int dt \; \underline{s}\left(t + \frac{\tau}{2}\right) \underline{q}^*\left(t - \frac{\tau}{2}\right) \exp(-i2\pi\nu t) =$$

$$= \frac{\sin\left[\pi\nu(T - |\tau|)\right]}{\pi\nu T} \qquad \text{for } -T < \tau < T \, , \tag{16}$$

and zero otherwise. In anticipation of its use in (13), we also have

$$\overline{\chi}_{\underline{sq}}(Tx,\, Wy) = \frac{\sin\left[\pi TWy(1 - |x|)\right]}{\pi TWy} \qquad \text{for } |x| < 1 \, , \tag{17}$$

and zero otherwise, which is seen to depend only on the time-bandwidth product TW, and not on these variables separately. This is one reason for introducing normalized variables in (12); it allows response (13) to depend only on TW and the normalized parameters listed in (14). This property is true only for narrowband waveforms, that is, $f_c \gg W$.

A program for the calculation of response (13) coupled with (17) is furnished in appendix C under the title Rectangular Envelopes. Inputs required of the user are collected at the top in lines 20-80. The target amplitudes and phases to be input in lines 50 and 60, respectively, are the magnitudes and arguments of the complex numbers $\{B_d\}$ in (13). The normalized reference frequency shift $y_r = f_r/W$ in line 20 is kept constant for a single plot, while the reference time delay $x_r = t_r/T$ is varied over -1,+1 in loop 180-340. The magnitude, $|\underline{c}(t_r,f_r)|$, is plotted on a linear ordinate.

Each term in (13) peaks when the second argument of the cross-ambiguity function is zero; see (17). Thus, each term peaks at reference time $x_r = x_d \pm(y_r - y_d)$, which depends on the particular highlight delay and shift values x_d, y_d and on the local reference frequency shift y_r. However, the peak amplitude in (17) is scaled down to the value $1-|x_r-x_d| = 1 - |y_r-y_d|$, which depends on the mismatch between the reference frequency shift and the particular highlight frequency shift.

Furthermore, the peak <u>broadens</u> for nonzero frequency mismatch. To see this, let

$$\Delta_x = x_r - x_d, \qquad \Delta_y = y_r - y_d \tag{18}$$

in (13) to obtain

$$\overline{\chi}_{\underline{sq}}\left(T\Delta_x,\ W(\Delta_y \mp \Delta_x)\right) = \frac{\sin\left[\pi TW(\Delta_y \mp \Delta_x)(1 - |\Delta_x|)\right]}{\pi TW(\Delta_y \mp \Delta_x)} , \tag{19}$$

by use of (17). Now in the neighborhood of the peak at $\Delta_x = \pm\, \Delta_y$, let $\Delta_x = \pm\, \Delta_y + \varepsilon$; then

$$\overline{\chi}_{\underline{sq}}\left(T\Delta_x,\ W(\Delta_y \mp \Delta_x)\right) = \frac{\sin\left[\pi TW(\mp\varepsilon)(1 - |\Delta_y \pm \varepsilon|)\right]}{\pi TW\,(\mp\,\varepsilon)} =$$

$$\cong \frac{\sin\left[\pi TW(1 - |\Delta_y|)\varepsilon\right]}{\pi TW\varepsilon} \quad \text{for small } |\varepsilon| . \tag{20}$$

The sharpness of this function of ε in the neighborhood of the peak at $\varepsilon = 0$ is proportional to $[TW(1 - |\Delta_y|)]^{-1}$. Thus if $|\Delta_y| = .5$, that is,

$$|y_r - y_d| = .5, \qquad \text{or} \qquad |f_r - f_d| = .5\ W, \tag{21}$$

the width of the peak is approximately doubled (in addition to the peak amplitude being halved, according to (20)).

GAUSSIAN ENVELOPES

In this example, both low-pass modulations have identical Gaussian envelopes:

$$\underline{s}(t) = \underline{g}(t) = \exp(-\pi t^2/T^2) \quad \text{for all } t. \tag{22}$$

The effective time duration T is defined such that

$$\underline{s}(\pm \tfrac{T}{2}) = \exp(-\pi/4) = .456, \quad \text{versus } \underline{s}(0) = 1. \tag{23}$$

The spectrum of this waveform is (see (B-2))

$$\underline{S}(f) = T \exp(-\pi T^2 f^2); \tag{24}$$

thus the effective spectral width is 1/T, since

$$\underline{S}(\pm \tfrac{1}{2T}) = T \exp(-\pi/4) = .456\, \underline{S}(0), \tag{25}$$

which is the analog to (23).

The symmetric cross-ambiguity function is easily determined from (B-6) as

$$\overline{\chi}_{\underline{sg}}(\tau,\nu) = \frac{T}{\sqrt{2}} \exp\left[-\frac{\pi}{2}\left(\frac{\tau^2}{T^2} + T^2\nu^2\right)\right] \quad \text{for all } \tau,\nu. \tag{26}$$

Then, as needed for (13),

$$\overline{\chi}_{\underline{sg}}(Tx,Wy) = \frac{T}{\sqrt{2}} \exp\left[-\frac{\pi}{2}(x^2 + T^2W^2y^2)\right] \quad \text{for all } x,y\,. \tag{27}$$

A program for the calculation of correlator response (13), by means of relation (27), is given in appendix C, under the title Gaussian Envelopes.

In particular, using definition (18) again, the significant term required in (13) is

$$\overline{\chi}_{\underline{sq}}(T\Delta_x, W(\Delta_y \mp \Delta_x)) =$$

$$= \frac{T}{\sqrt{2}} \exp\left[-\frac{\pi}{2}\left\{(1+T^2W^2)\left(\Delta_x \mp \Delta_y \frac{T^2W^2}{1+T^2W^2}\right)^2 + \Delta_y^2 \quad \frac{T^2W^2}{1+T^2W^2}\right\}\right]. \tag{28}$$

Now for fixed frequency mismatch Δ_y, i.e., fixed $f_r - f_d$, the <u>shape</u> of (28) is totally independent of the value of Δ_y. The peak value is reduced by the factor

$$\exp\left[-\frac{\pi}{2}\,\Delta_y^2\,\frac{T^2W^2}{1+T^2W^2}\right], \tag{29}$$

and the location of the peak is delayed to

$$\Delta_x = \pm\,\Delta_y\,\frac{T^2W^2}{1+T^2W^2}, \tag{30}$$

but there is <u>no broadening</u> of the response versus Δ_x, regardless of the value of Δ_y. This is in distinction to the case of rectangular envelopes in the previous subsection; it is due to the rounded shoulders of the Gaussian envelope (22), in contrast to the rectangular case in (15).

If we combine (9), (10), and (22) for this example, we have, for the complex envelope of transmitted signal and reference,

$$s(t) = q(t) = \exp\left[-\pi \frac{t^2}{T^2} \pm i\pi \frac{W}{T} t^2\right] . \tag{31}$$

The instantaneous frequency is $\pm \frac{W}{T}t$, which takes on values $\pm W/2$ at $t = \pm T/2$; this is consistent with the results in (23)-(25).

ARBITRARY ENVELOPES AND DURATIONS

The low-pass modulation of the transmitted signal is now

$$\underline{s}(t) = \sum_k a_k \exp(i2\pi kt/T) \quad \text{for } |t| < T/2 , \tag{32}$$

and zero otherwise; the summation on k is over all nonzero complex coefficients $\{a_k\}$. Observe that T here is the total nonzero extent of $\underline{s}(t)$, meaning that the effective extent of $\underline{s}(t)$ could be significantly less than T. If $a_{-k} = a_k$ = real, then (32) is a cosine expansion, and includes modulations such as rectangular, Hanning, Hamming, Blackman [1], Harris [2], and Nuttall [3], which are known to have very good sidelobe behavior in the frequency transform domain.

The low-pass modulation of the reference is taken to be

$$q(t) = \sum_{\ell} b_{\ell} \exp(i2\pi\ell t/L) \quad \text{for } |t| < L/2 , \tag{33}$$

and zero otherwise. The duration L of the local reference is unrelated to T; L can be larger or smaller than T. The number of nonzero complex coefficients $\{b_{\ell}\}$ is also unrelated to that above in (32).

The derivation of the cross-ambiguity function between $\underset{\sim}{s}$ and $\underset{\sim}{g}$ is carried out in appendix D, including all the generality introduced above; the end result is given by (D-7). The linear-FM correlator complex envelope response is given in (D-9), and a program for this result is given in appendix C, under the title Arbitrary Envelopes and Durations.

GRAPHICAL RESULTS

This section is divided into several parts, corresponding to the different envelope examples given above. In all but a few cases, the time bandwidth product is kept fixed at

$$TW = 50, \tag{34}$$

and the frequency sweep is upward versus time. Identification of the delay and shift parameters is according to the normalized variables introduced in (12), namely,

$$x_r = t_r/T, \; y_r = f_r/W, \; x_d = t_d/T, \; y_d = f_d/W; \tag{35}$$

the latter variables in (35) are explained in (2)-(5). The abscissa on every plot is x_r over the range -1,+1; thus each plot can be viewed as the envelope of the correlator or matched filter response versus time. Although the response may be nonzero outside this range, it is significant only within the plotted region for all the examples considered.

RECTANGULAR ENVELOPES

The first plot in figure 1 is for equal-duration rectangular envelopes for the transmitted signal as well as the local reference, and a single highlight (point target) at $x_d = 0$, $y_d = 0$; that is, there is no time delay or frequency shift of the target. (Actually, the only quantities that matter are differences of variables; see (13)). The response in figure 1 for zero Doppler mismatch, $y_r = 0$, peaks at $x_r = 0$ and has a narrow mainlobe with adjacent nulls approximately at $\pm(TW)^{-1} = \pm.02$ (for TW >> 1); see (17) and (19). However, there are significant sidelobes of peak

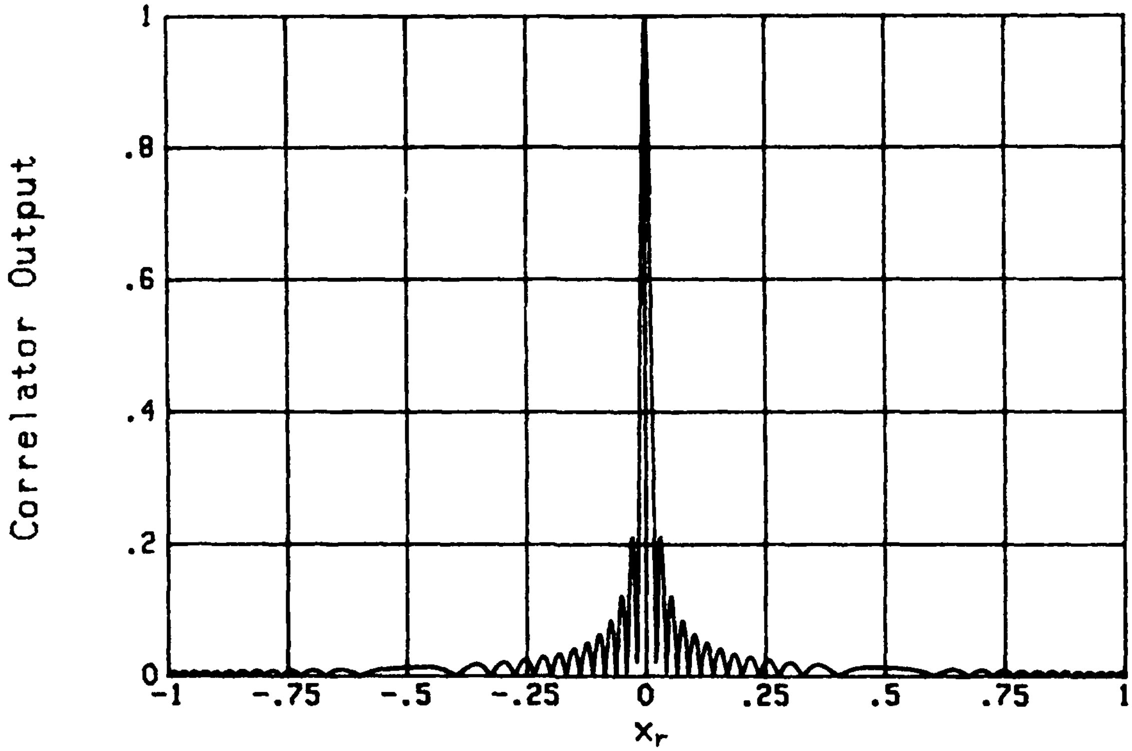

Figure 1. Rectangular Envelopes, $y_r = 0$

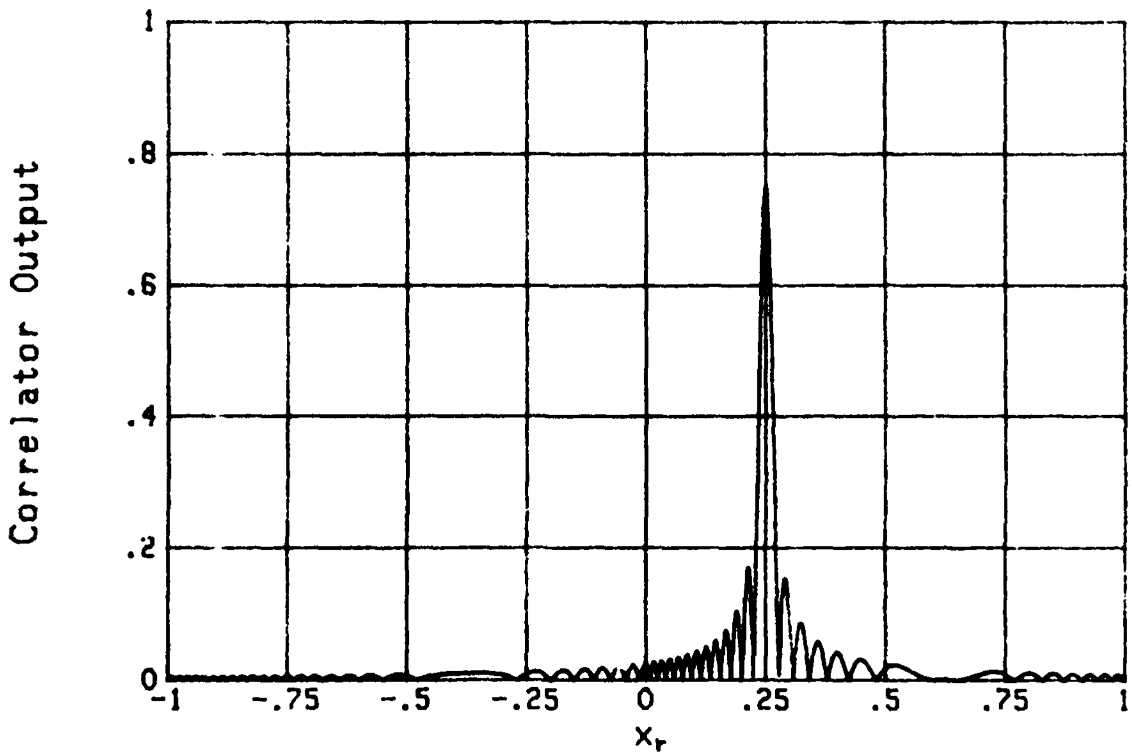

Figure 2. Rectangular Envelopes, $y_r = .25$

amplitude approximately $2/(3\pi) = .21 = -13.5$ dB, and a smear of sidelobes near $x_r = 0$. These sidelobes will tend to obscure a weak close-by highlight.

The series of results in figures 2 through 4 correspond to different amounts of frequency mismatch between the local reference and the received signal. For convenience, all this uncertainty is taken up by the reference variable, that is, $y_r = .25, .5, .75$, respectively, with $y_d = 0$; however, this mismatch can occur in practice due to unknown target Doppler. The peak response and sidelobes decrease proportionately as the frequency mismatch increases. However, significant broadening of the response also occurs, as predicted in (18)-(21); in fact, the mainlobe width for $y_r = .5$ in figure 3 is approximately double that for $y_r = 0$ in figure 1. The movement of the peak location along the x_r axis is due to the inherent large ambiguity of linear-FM along the 45° line in x_r,y_r space.

Figure 5 depicts the normalized correlator response for two equal-strength highlights separated only in time delay. This is depicted by the small diagram in the upper left with two dots at $x_d,y_d = 0,0$ and $.06,0$, respectively. That is, one highlight is at the origin in x_d,y_d space, and the other is displaced along the x_d axis, which corresponds to a slightly larger range. (A rotating target model which leads to these multiple highlight locations in x_d,y_d space is described in the next section.) Since the first null in figure 1 occurred at $x_r = \pm.02$, these two responses are sufficiently separated to see their individual peaks

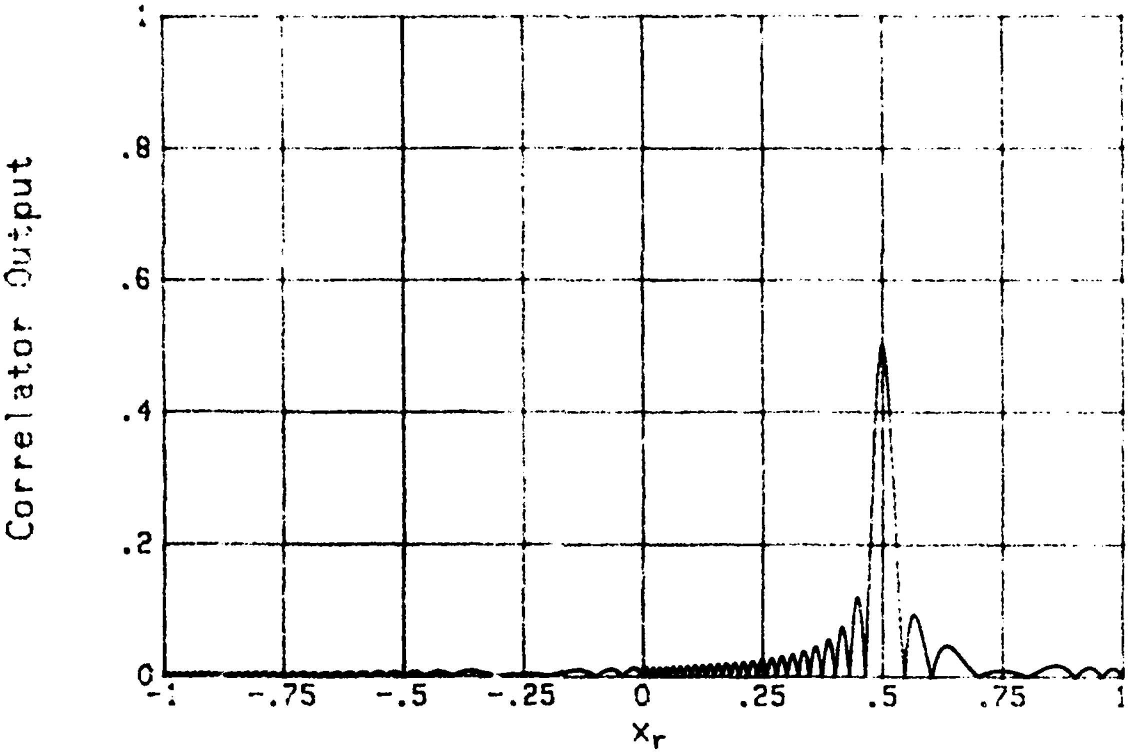

Figure 3. Rectangular Envelopes, y_r = .5

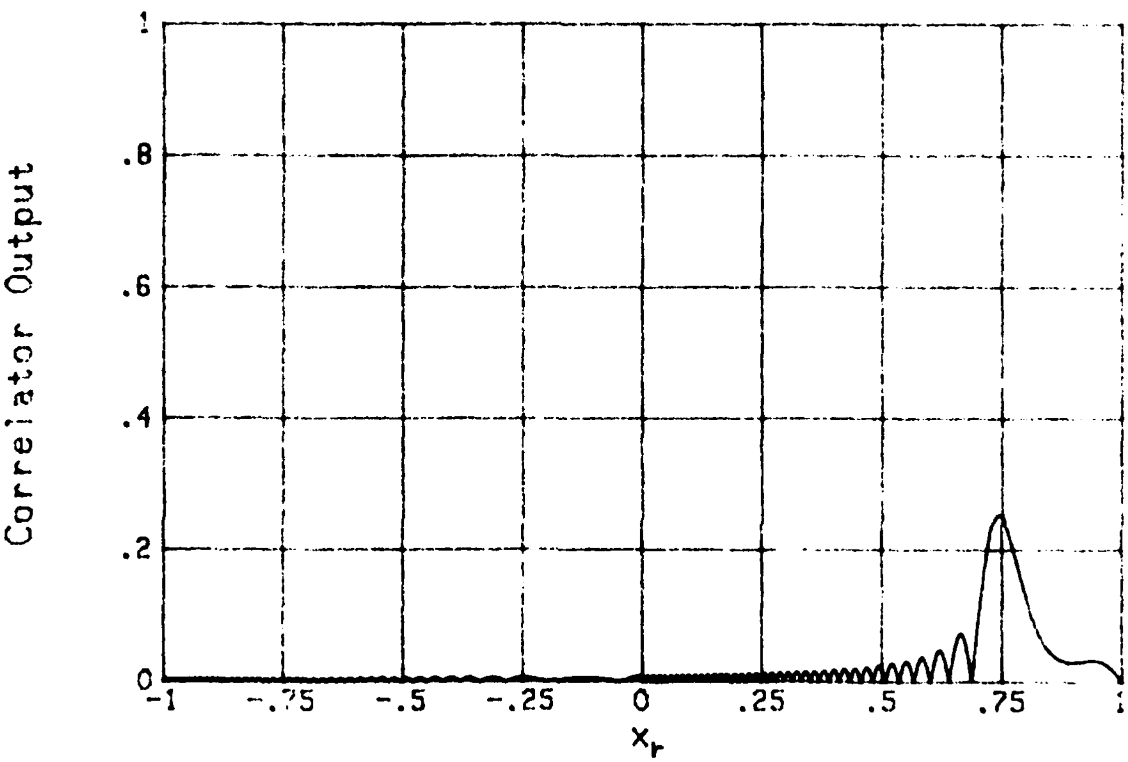

Figure 4. Rectangular Envelopes, y_r = .75

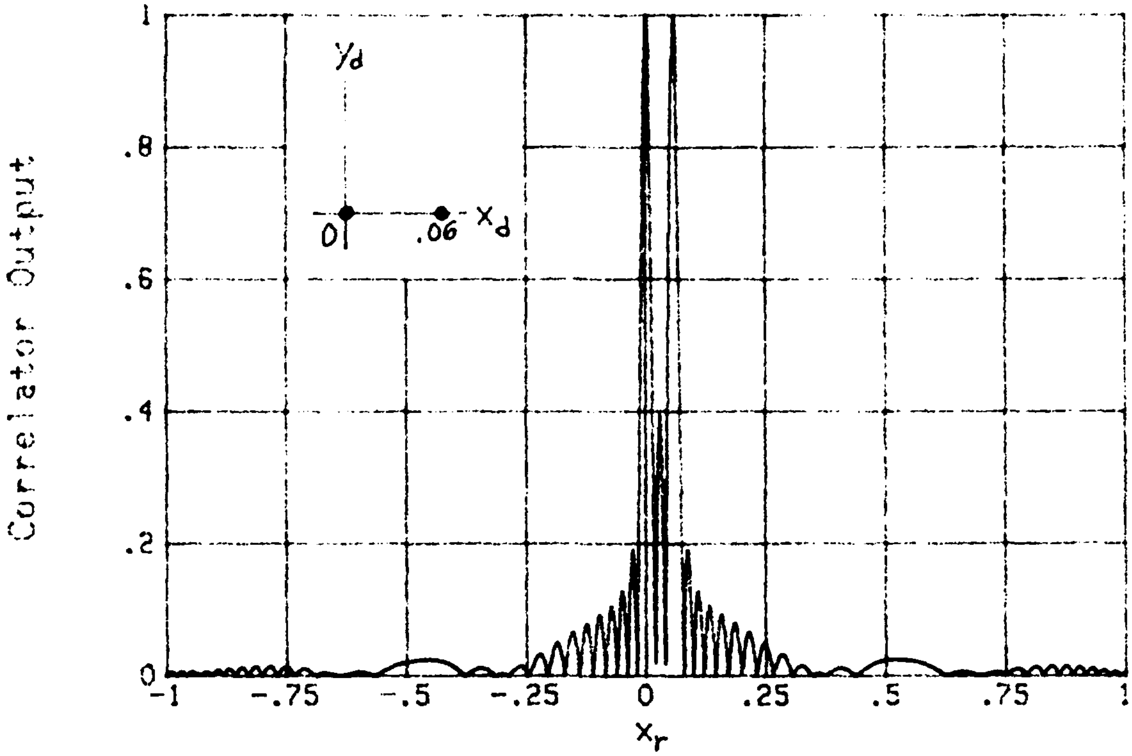

Figure 5. Rectangular Envelopes,
Two Separated Highlights, $y_r = 0$

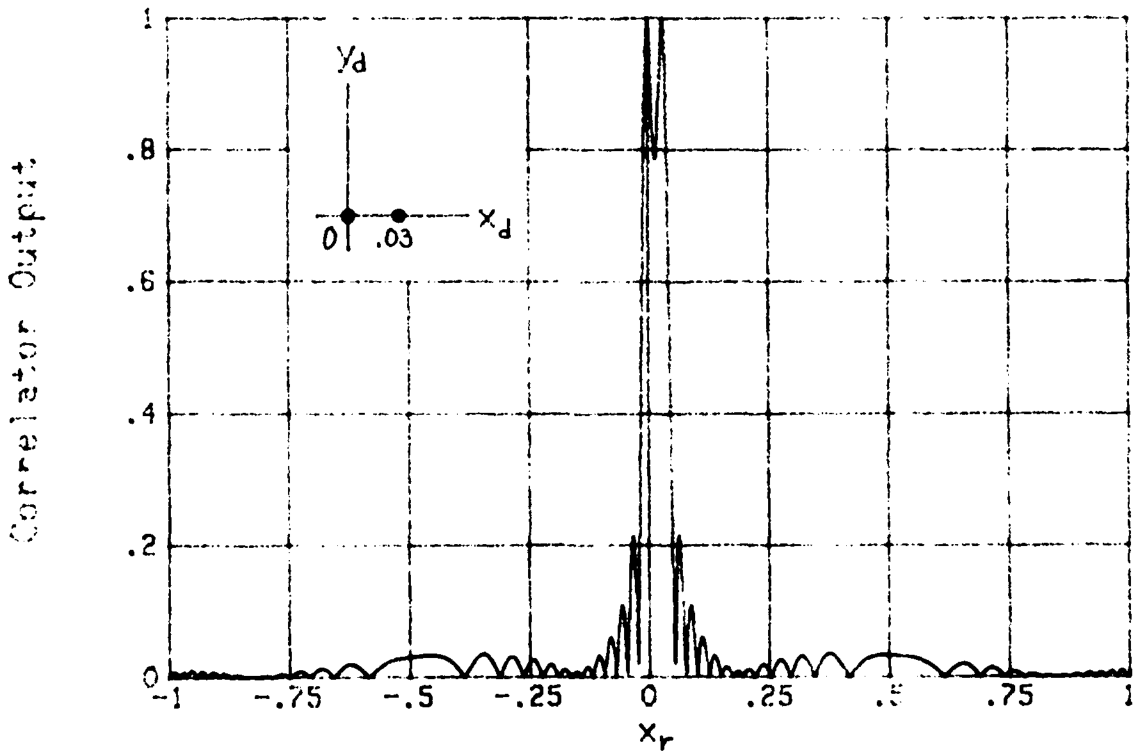

Figure 6. Rectangular Envelopes,
Two Close Highlights, $y_r = 0$

clearly. However, there is a very large spurious peak between the two, of amplitude approximately 40 percent = -8 dB of the desired peaks. This undesired peak is the result of an unfortunate and uncontrollable vector addition of sidelobes, according to (13).

The only change in figure 6 is to move the two highlights closer in range, namely to separation .03 in x_d. For this case of zero frequency mismatch, $y_r = 0$, the two responses can be resolved. However, when the frequency mismatch is increased to $y_r = .25$, the two highlights cannot be resolved, as shown by figure 7. This is due to the broadening of the response for $y_r \neq 0$, as previously described in figures 1 through 4. Again, movement of the peaks along the x_r axis is due to the tilted elliptical nature of the ambiguity function of linear-FM.

An example for three equal-strength separated highlights is depicted in figure 8. The small diagram in the upper left indicates that two of the highlights, namely those at 0,0 and .06,.06, are on the same 45° line in x_d,y_d space. This means that, for an up-sweep in frequency, these two correlator responses overlap and are indistinguishable. This may be seen as follows: each term in response (13) peaks when the second argument of the cross-ambiguity function is zero; see (17). Thus each term peaks when

$$x_r = x_d + y_r - y_d \quad \text{(for up-sweep).} \tag{36}$$

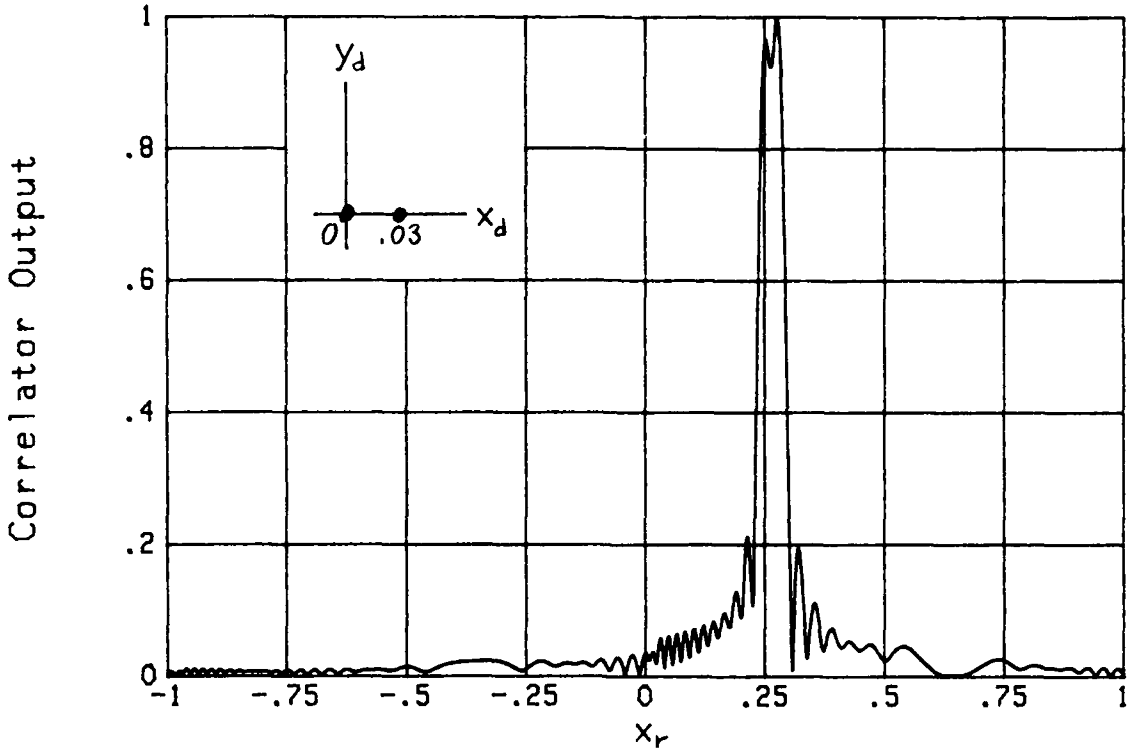

Figure 7. Rectangular Envelopes, Two Close Highlights, y_r = .25

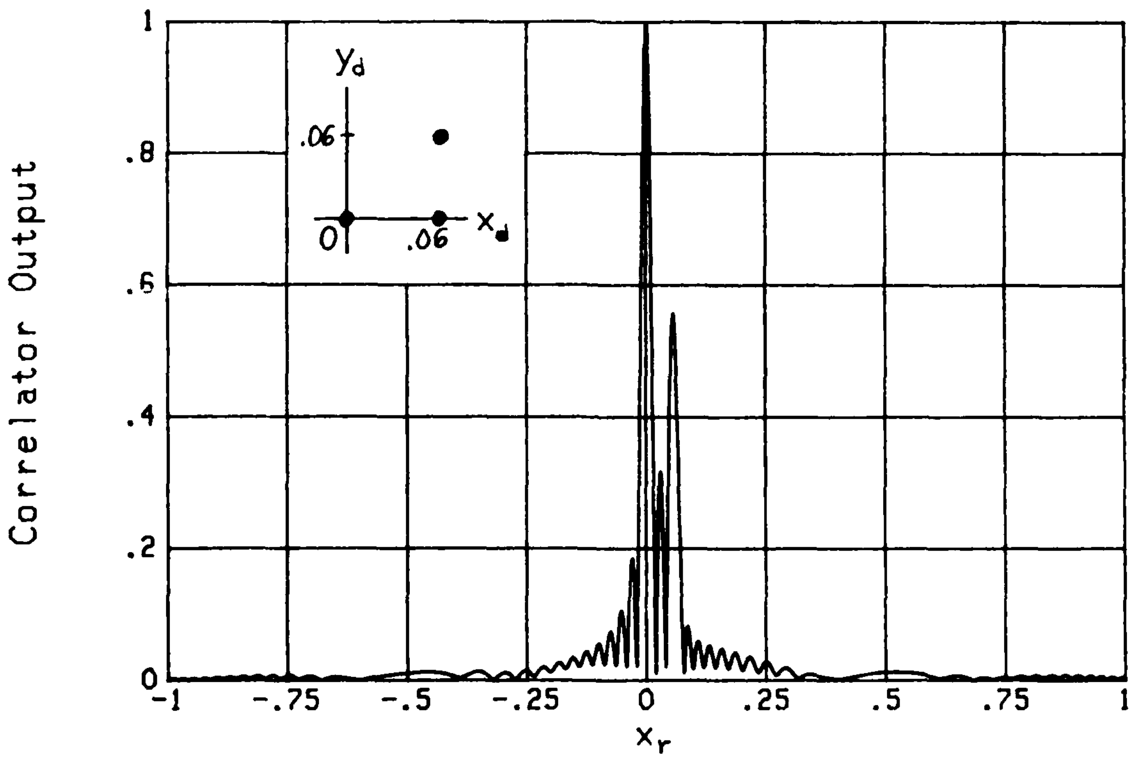

Figure 8. Rectangular Envelopes, Three Highlights, y_r = 0

But if $x_d - y_d$ takes on the same value for two different highlights, the same value of x_r results in (36). Thus all those highlights along any particular 45° line in x_d, y_d space will lead to overlapping responses at the correlator output. For a down-sweep of the linear-FM, all highlights along a common −45° line in x_d, y_d space will have overlapping correlator responses.

In addition to the overlapping responses in figure 8, a very large spurious peak, of relative amplitude equal to 60 percent = −4.4 dB of the smaller single-highlight response, is also indicated. The exact amplitude of this spurious response depends on the particular phases of the three highlights; these were 0,0,.283 radians for the example in figure 8. Similarly, the value of the response at $x_r = 0$ depends crucially on the phases of the two highlights on a common 45° line and has been normalized at unity.

The unnormalized response for a four-highlight target is given in figure 9; from left to right on the small diagram of the x_d, y_d plane, the relative highlight strengths are .9, 1, .8, .9. Since none of these highlights lie on common 45° lines, all four are resolved; in addition, there is a large spurious response between the third and fourth desired peaks. When the frequency mismatch is increased to $y_r = .43$ in figure 10, the inherent broadening associated with a rectangular envelope causes the two middle responses to coalesce, while the overall level of the response decreases.

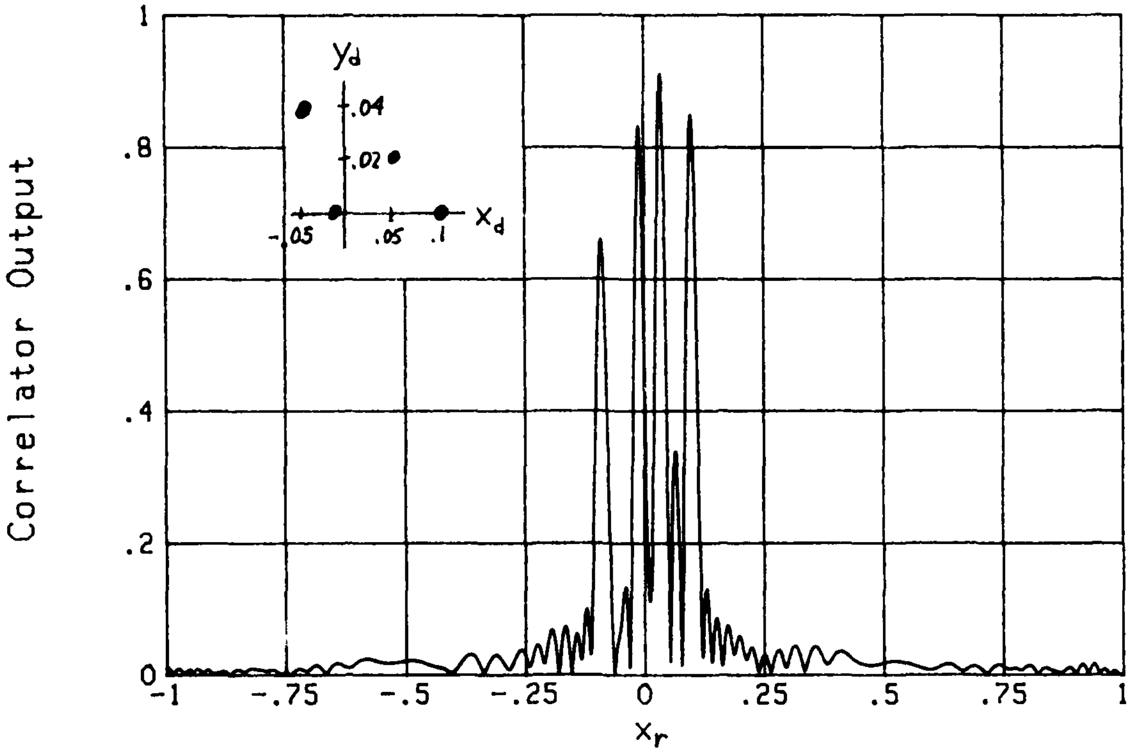

Figure 9. Rectangular Envelopes, Four Highlights, $y_r = 0$

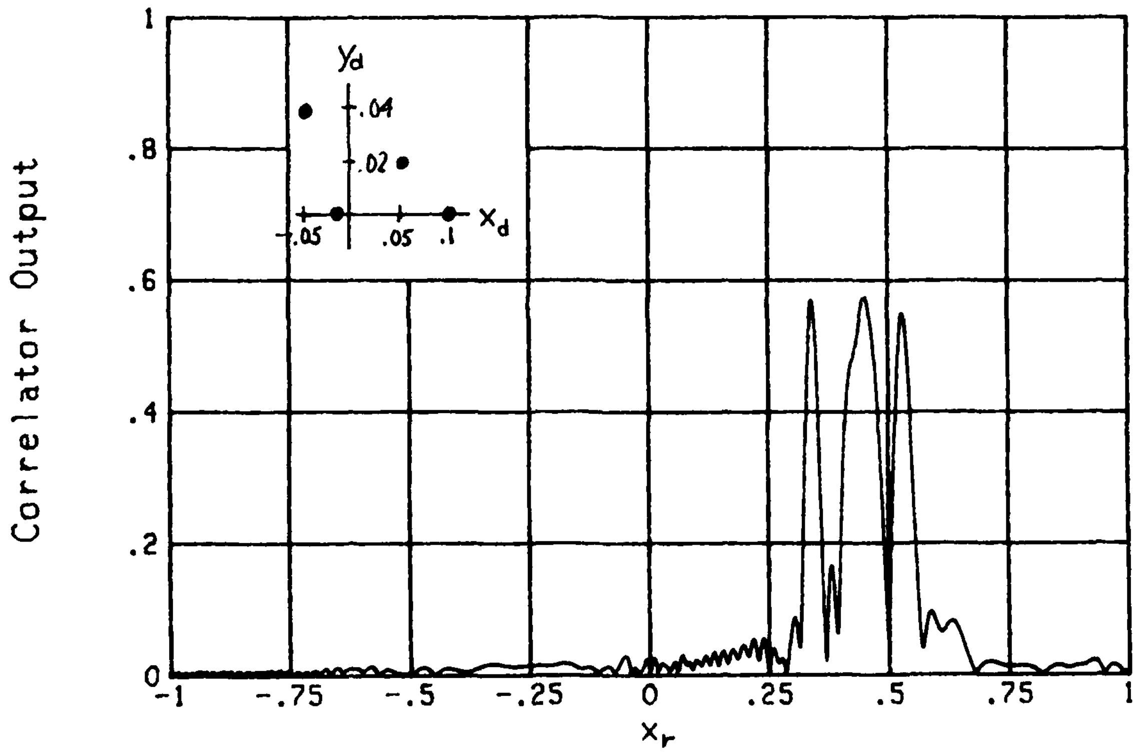

Figure 10. Rectangular Envelopes, Four Highlights, $y_r = .43$

The effect of using a down-sweep of the linear-FM, on a couple of the multiple highlights structures above, is depicted in figures 11 and 12. Specifically, in figure 11, none of the three highlights lie on a common -45° line, and so are resolved at the correlator output; contrast this result with figure 8 for an up-sweep. On the other hand, exactly the opposite happens for the four highlight case shown in figure 12. Namely, one pair of highlights lies on a common -45° line and the other pair nearly so; the correlator response in figure 12 displays only two peaks, in contrast with figure 9 which resolved all four contributions.

One conclusion from these observations is that it can be very difficult to decipher, from the correlator response, exactly what the detailed target highlight structure is. This is true even if both the up- and down-sweep responses are available. Fundamentally, each highlight is characterized by two location parameters, namely x_d, y_d; but both sweep responses contain insufficient information to resolve all the ambiguities of linear-FM in the general case. These ambiguities will not be eliminated by the use of different amplitude modulations, either; rather, it is the linear-FM which must be modified, in order to alleviate the problems. Of course, the requisite data processing will then be significantly more time-consuming.

GAUSSIAN ENVELOPES

In an effort to control the undesirable sidelobes associated with rectangular amplitude modulation, the possibility of employing a Gaussian modulation will now be investigated. The definitions of signal duration T

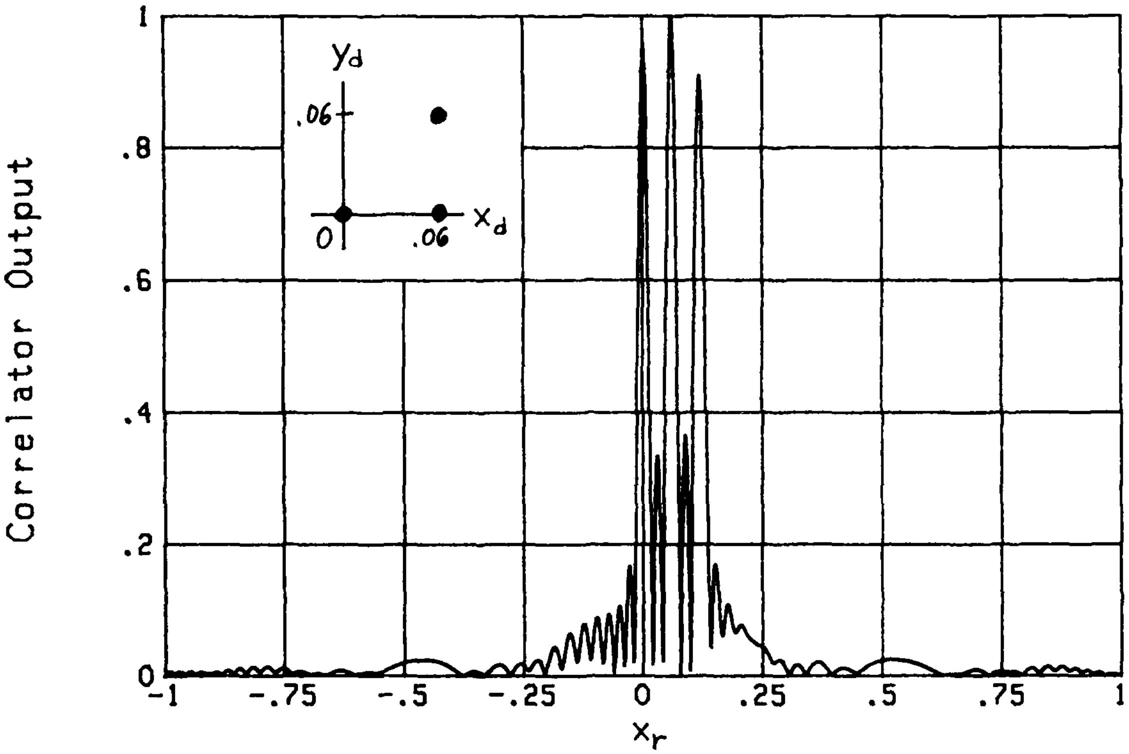

Figure 11. Rectangular Envelopes, Three Highlights, $y_r = 0$, Downsweep

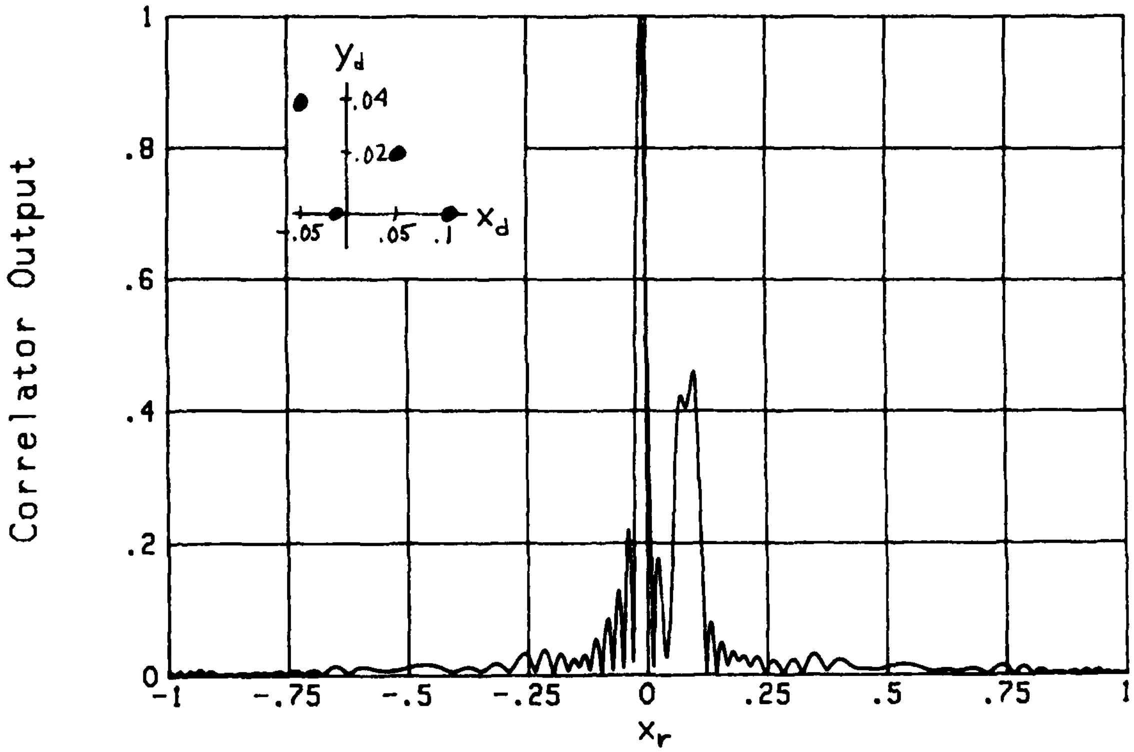

Figure 12. Rectangular Envelopes, Four Highlights, $y_r = 0$, Downsweep

and bandwidth W are according to (22)-(25) and (31); that is, T and W are effective measures of duration and bandwidth. The transmitted signal and reference waveform have the same duration.

The first result in figure 13 is a superposition of five different responses, each corresponding to a different frequency mismatch. Two points are to be observed: there is no pulse broadening and there are no sidelobes. These properties confirm the analysis in (28)-(30). This leads to the result in figure 14 for two highlights, which should be compared with the rectangular envelope case in figure 5.

For two closely-spaced highlights, a frequency-mismatch does not cause loss of resolution; see figures 15 and 16, which illustrate that the resolution is just as good at $y_r = .25$ as at $y_r = 0$. A direct comparison of these results with figures 6 and 7 reveals significantly different behavior.

The three highlight example of figure 8 is reconsidered in figure 17. The spurious sidelobe is now totally absent, although the two highlights at x_d, y_d equal to 0,0 and .06,.06 still overlap at $x_r = 0$. For a down-sweep of the linear-FM, figure 18 illustrates resolution of the three highlights and the absence of sidelobes.

The four highlight example previously investigated in figures 9 and 10 is reconsidered in figures 19 and 20. The same conclusion regarding fixed resolution and lack of sidelobes is again realized.

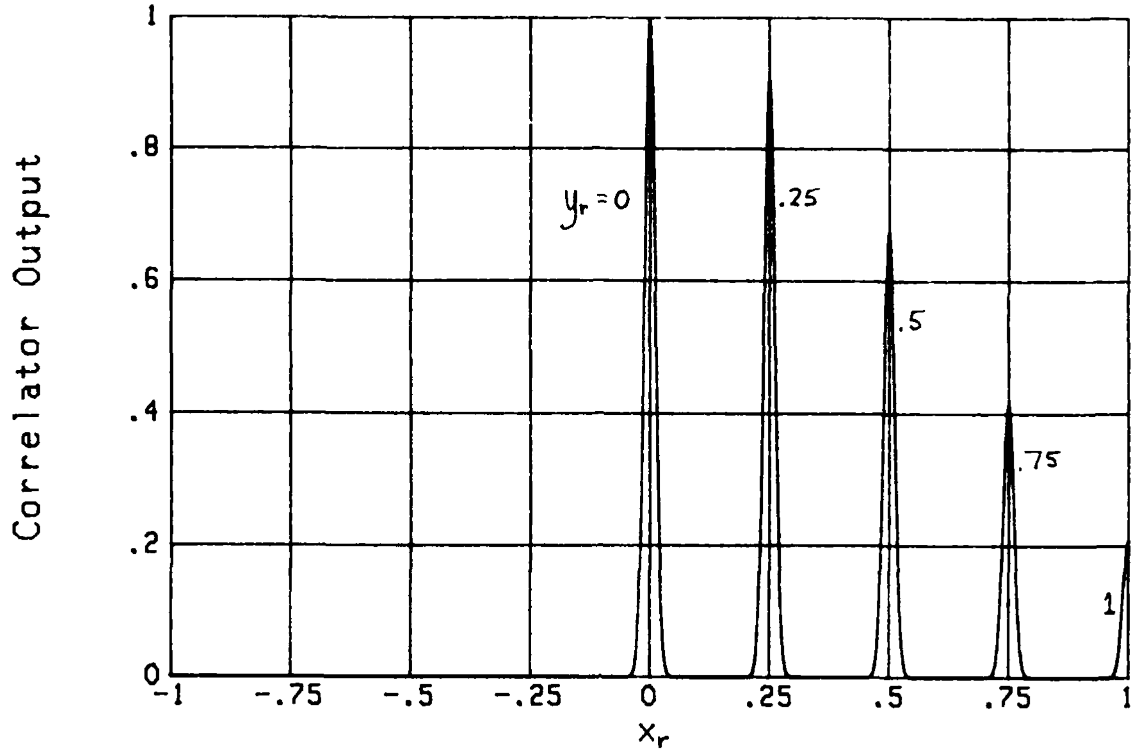

Figure 13. Gaussian Envelopes, Superposed Responses for Various y_r

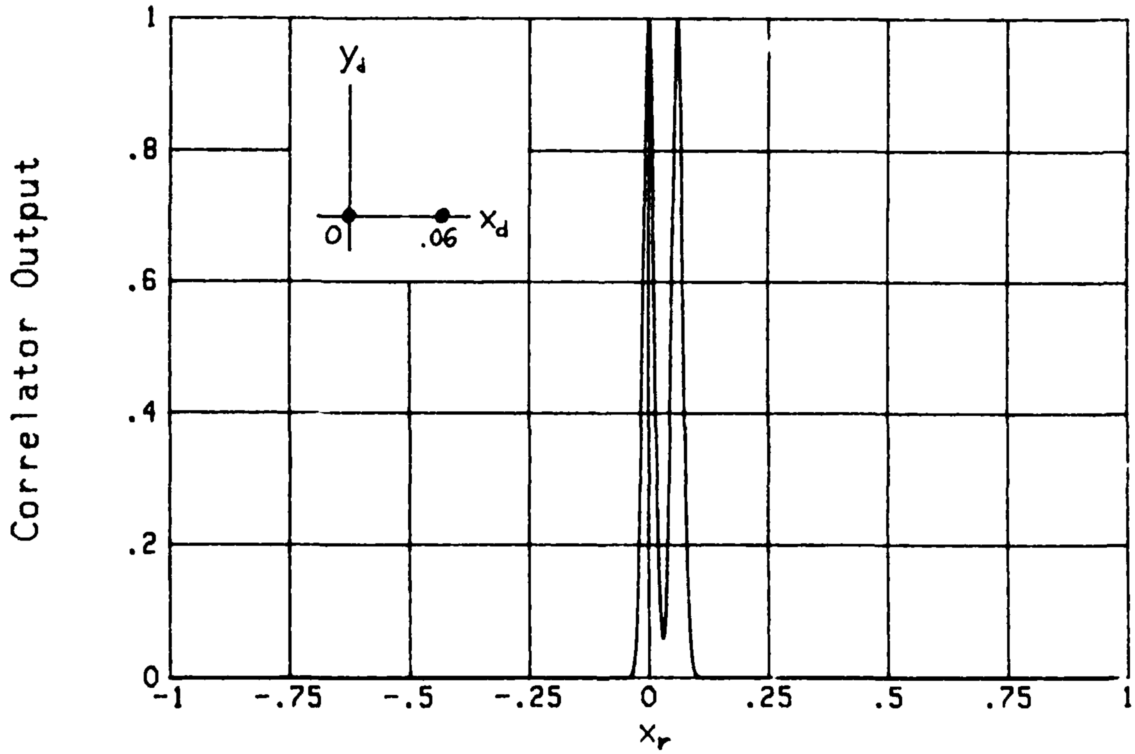

Figure 14. Gaussian Envelopes, Two Separated Highlights, $y_r = 0$

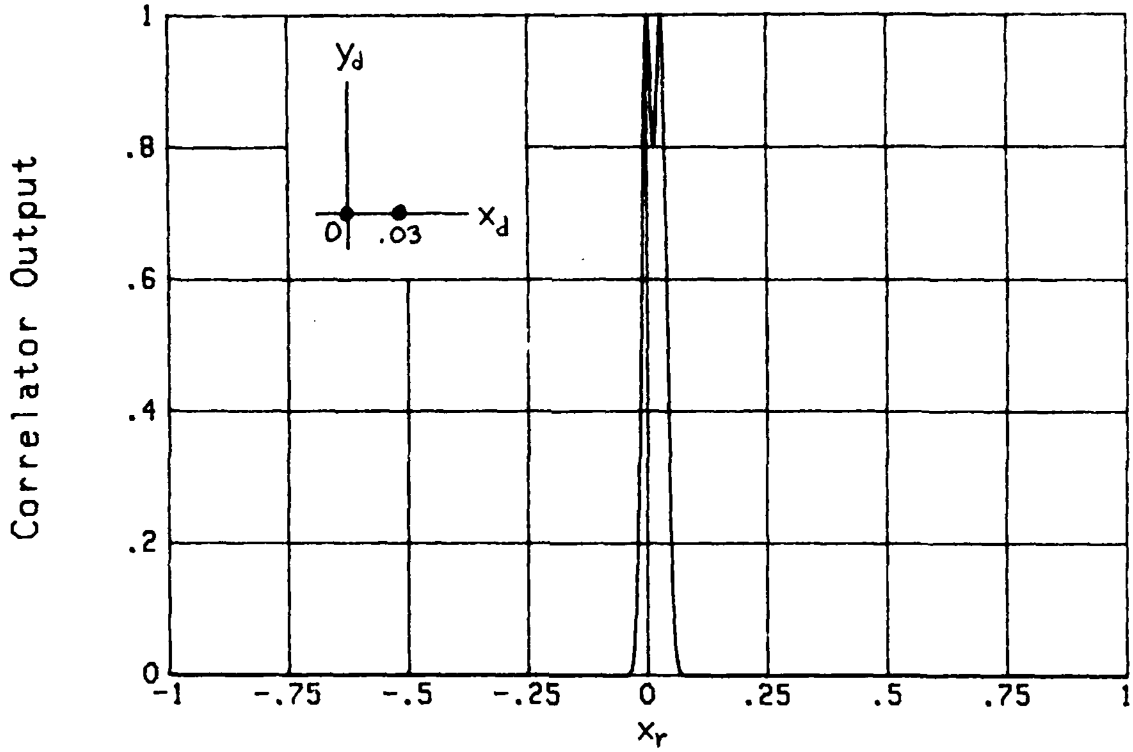

Figure 15. Gaussian Envelopes, Two Close Highlights, $y_r = 0$

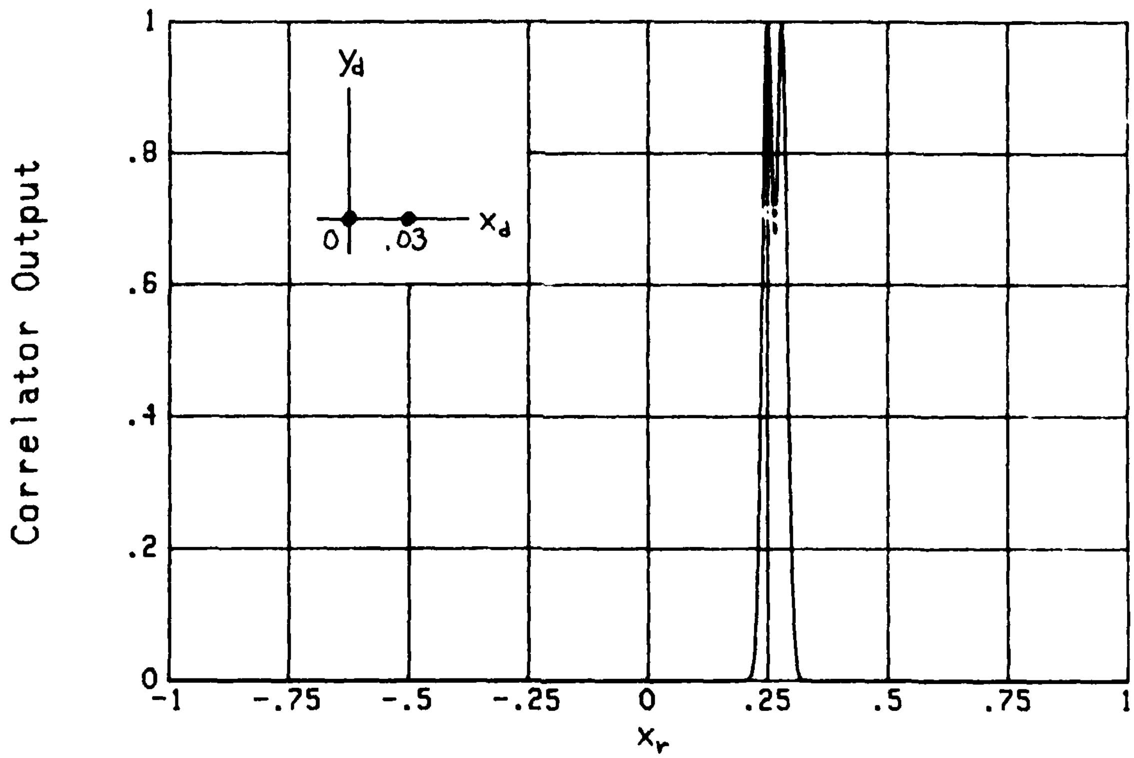

Figure 16. Gaussian Envelopes, Two Close Highlights, $y_r = .25$

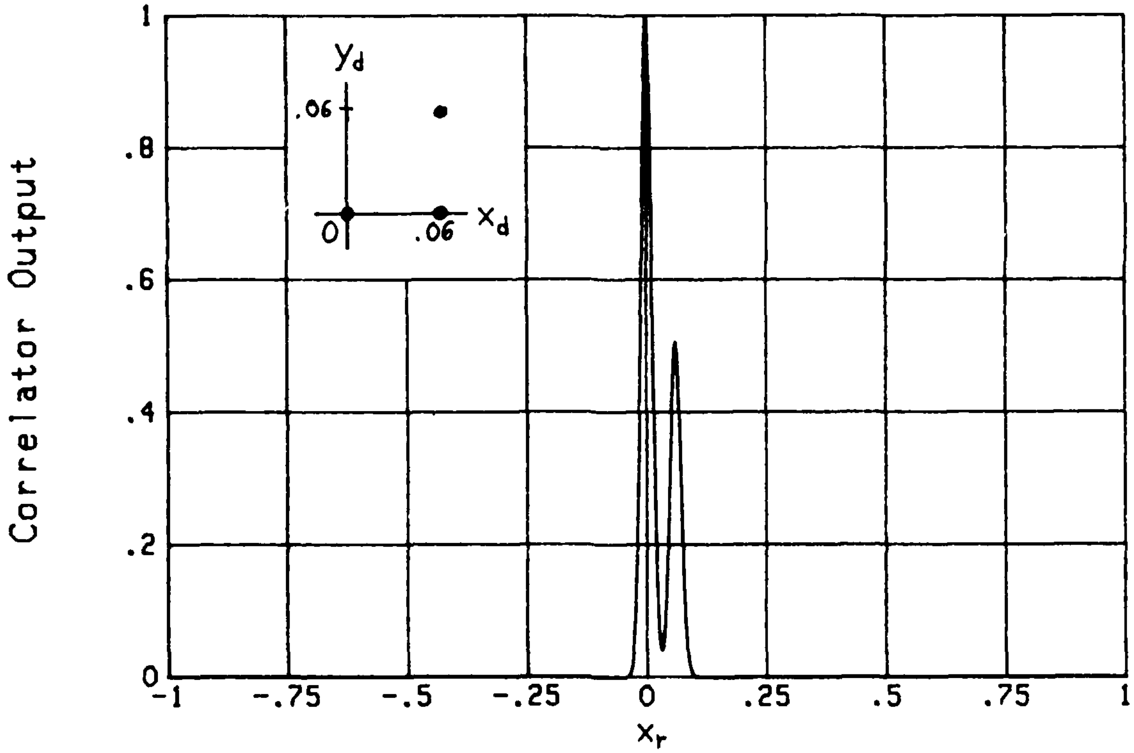

Figure 17. Gaussian Envelopes,
Three Highlights, $y_r = 0$

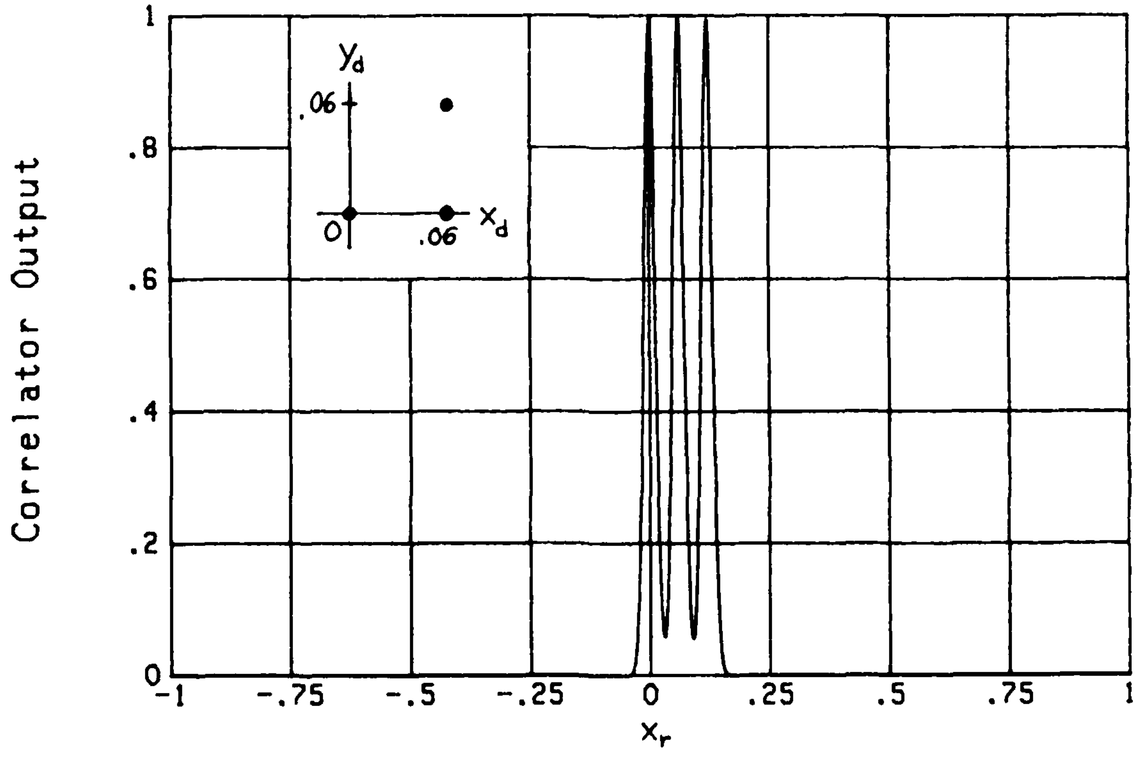

Figure 18. Gaussian Envelopes,
Three Highlights, $y_r = 0$, Downsweep

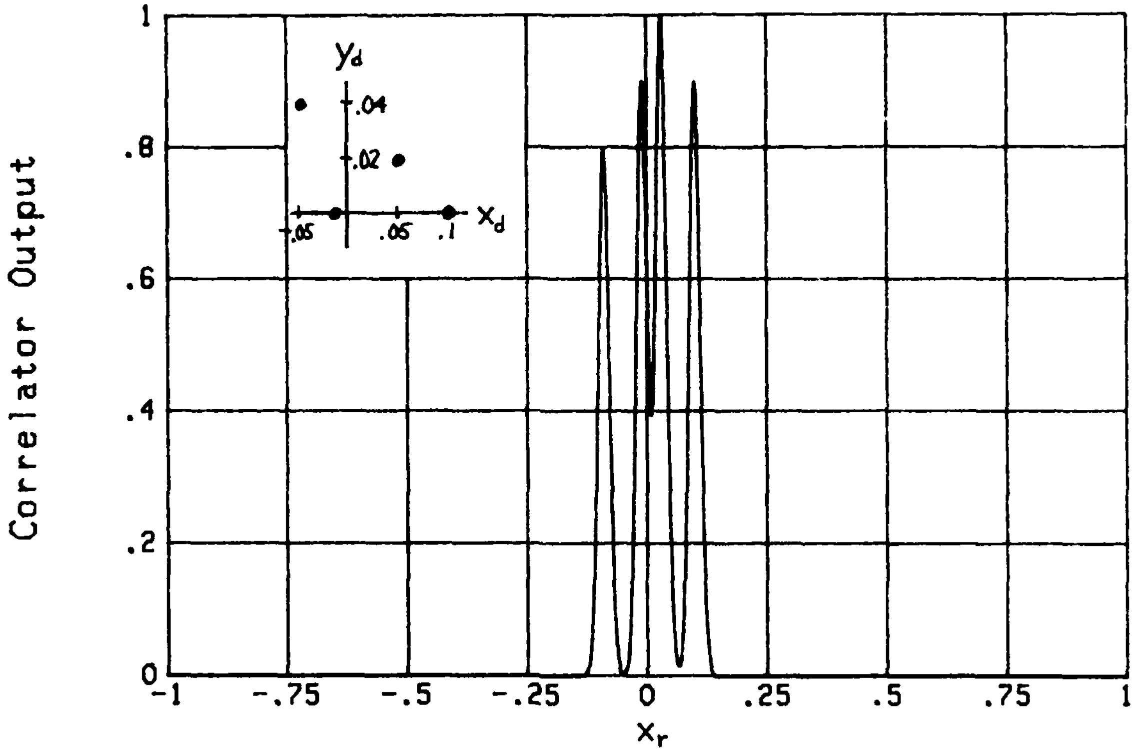

Figure 19. Gaussian Envelopes,
Four Highlights, $y_r = 0$

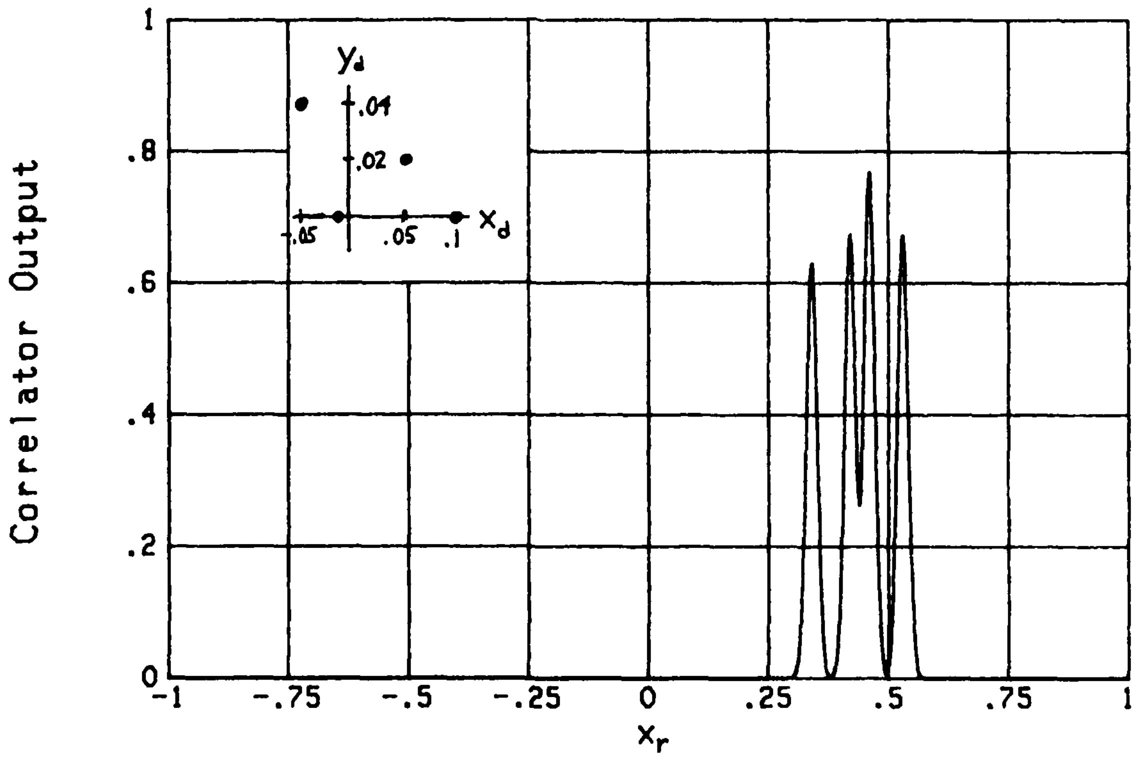

Figure 20. Gaussian Envelopes,
Four Highlights, $y_r = .43$

ARBITRARY ENVELOPES AND DURATIONS

The high quality of the correlator response for Gaussian amplitude modulation emphasizes the need for shaping the transmitted and reference signals. However, we must approximate the Gaussian function by some finite duration waveform, in practice. Also, for a given transmitted signal and corresponding received waveform, the possibility of utilizing a mismatched reference modulation needs to be considered. The mechanism for achieving this goal is afforded by the waveforms given by (32) and (33) and the correlator response derived in appendix D.

The first result in figure 21 for one highlight corresponds to rectangular transmitted signal and Hanning reference envelopes, of equal duration; that is, $L=T$. Very low sidelobes are achieved over the entire range of time delay, x_d; however, the mainlobe width is broadened, relative to figure 1. When the frequency mismatch is increased from $y_r = 0$ to .5, figure 22 illustrates the absence of sidelobes but a pronounced low-level pedastal; the plot has been normalized at peak value 1.

To narrow the mainlobe width and deduce the importance of different durations, the series of results in figures 23-26 for $L/T = .8, 1.2, 1.4, 1.6$, respectively, were computed. These all correspond to one highlight with no frequency mismatch. As L/T increases, figures 21 and 23-26 indicate that a trade-off between mainlobe width and sidelobe level takes place. The ratio of durations, $L/T = 1.4$, in figure 25 realizes sidelobes of relative

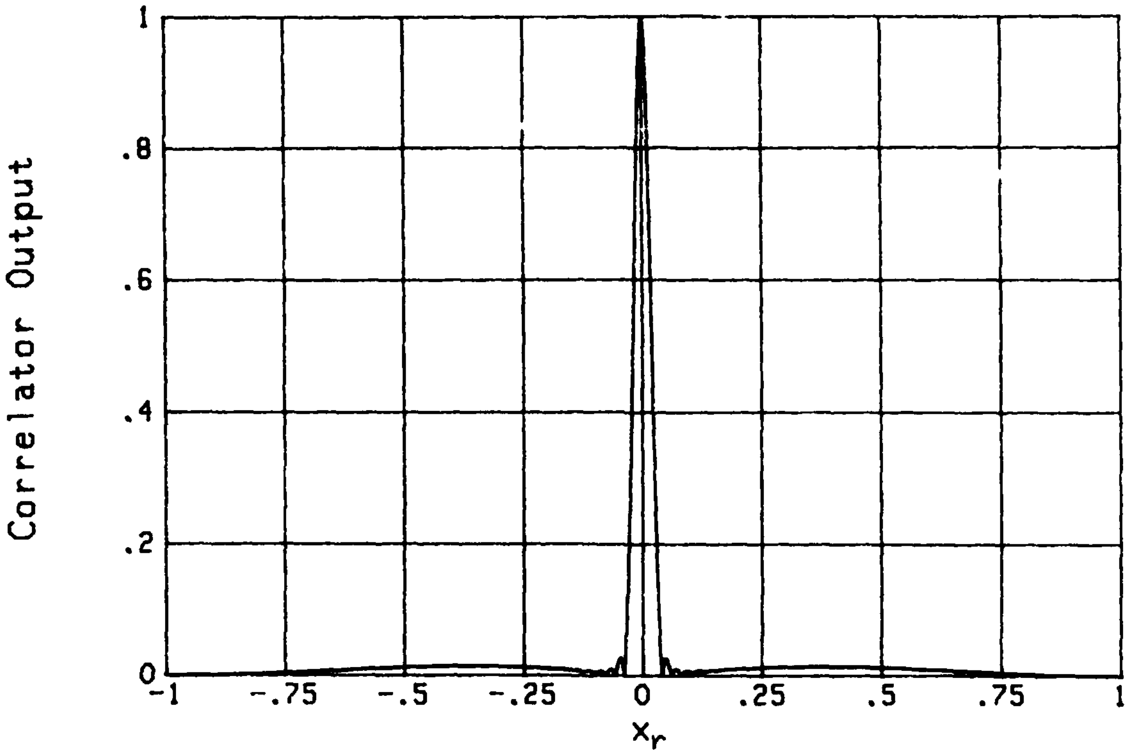

Figure 21. Rectangular-Hanning Envelopes,
y_r = 0, L/T = 1

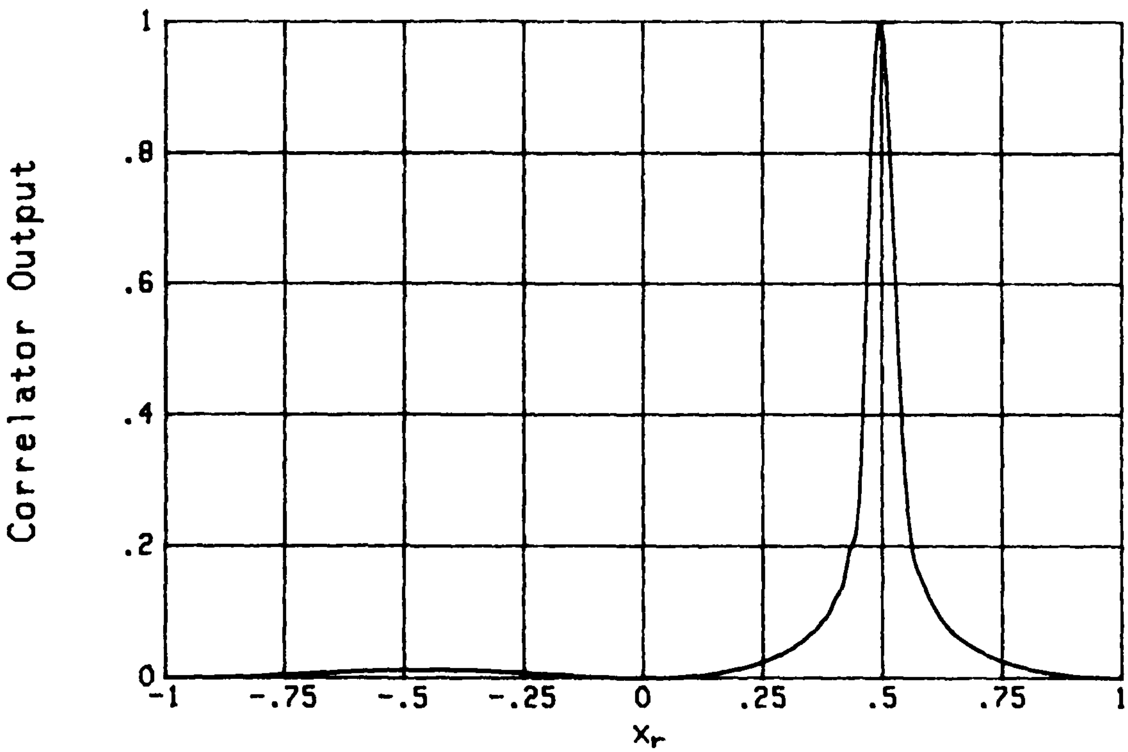

Figure 22. Rectangular-Hanning Envelopes,
y_r = .5, L/T = 1

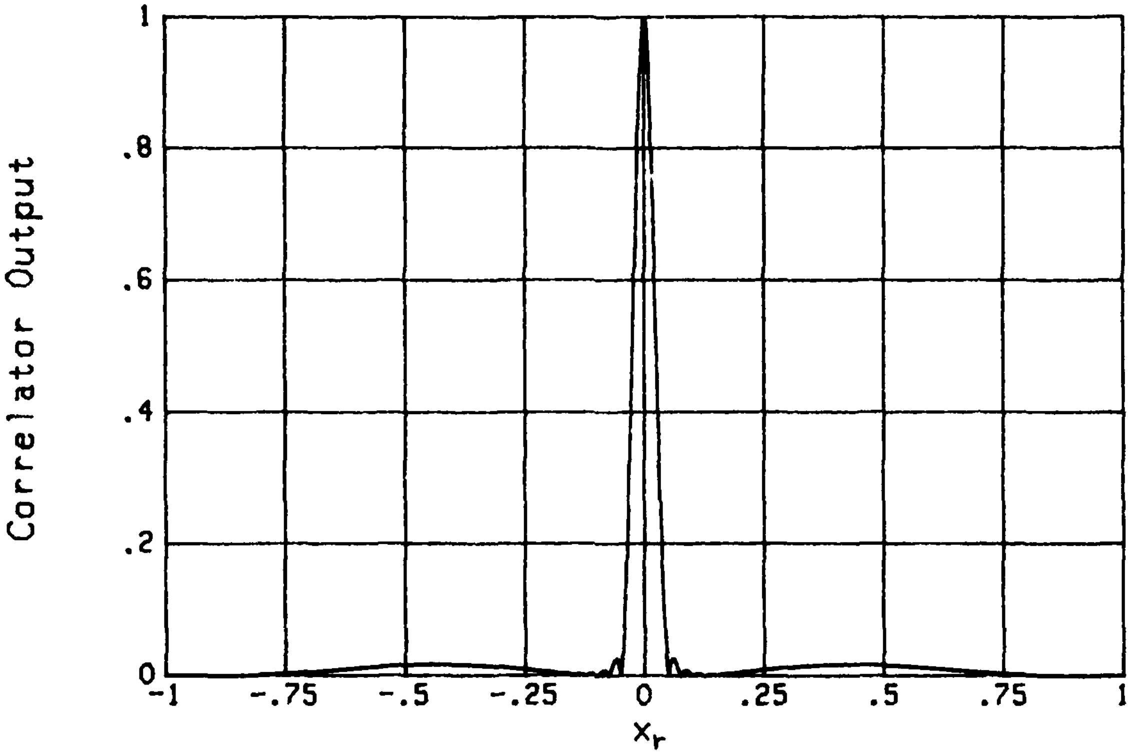

Figure 23. Rectangular-Hanning Envelopes, $y_r = 0$, $L/T = .8$

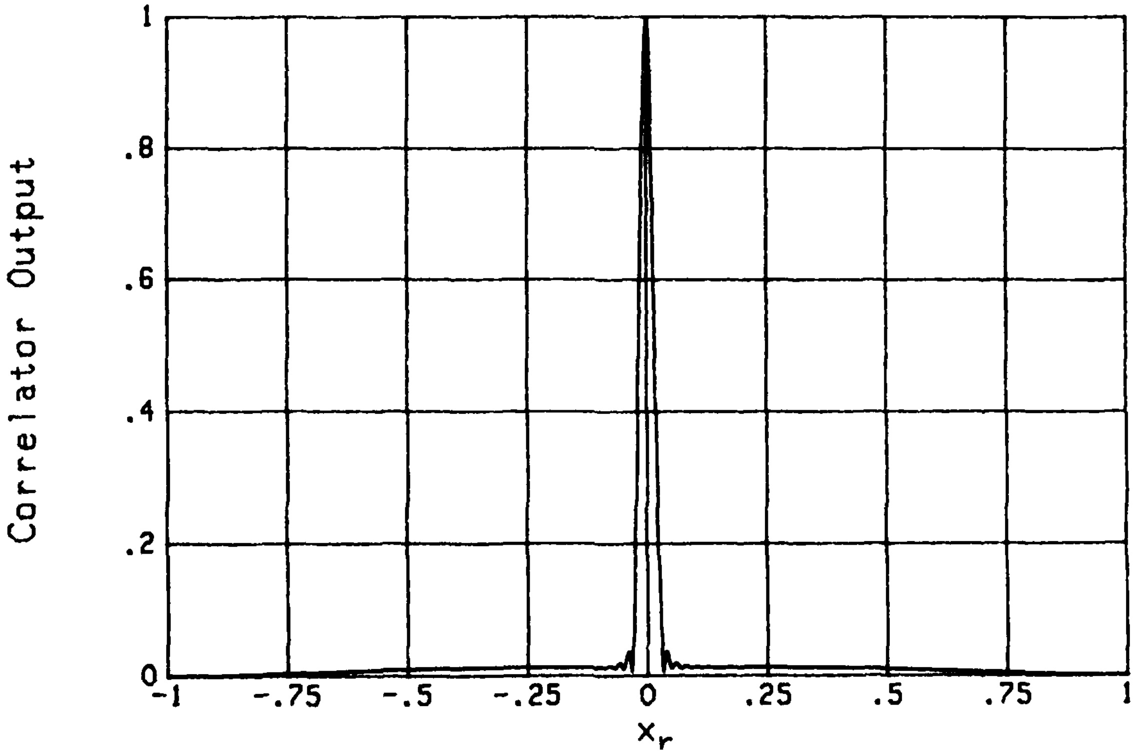

Figure 24. Rectangular-Hanning Envelopes, $y_r = 0$, $L/T = 1.2$

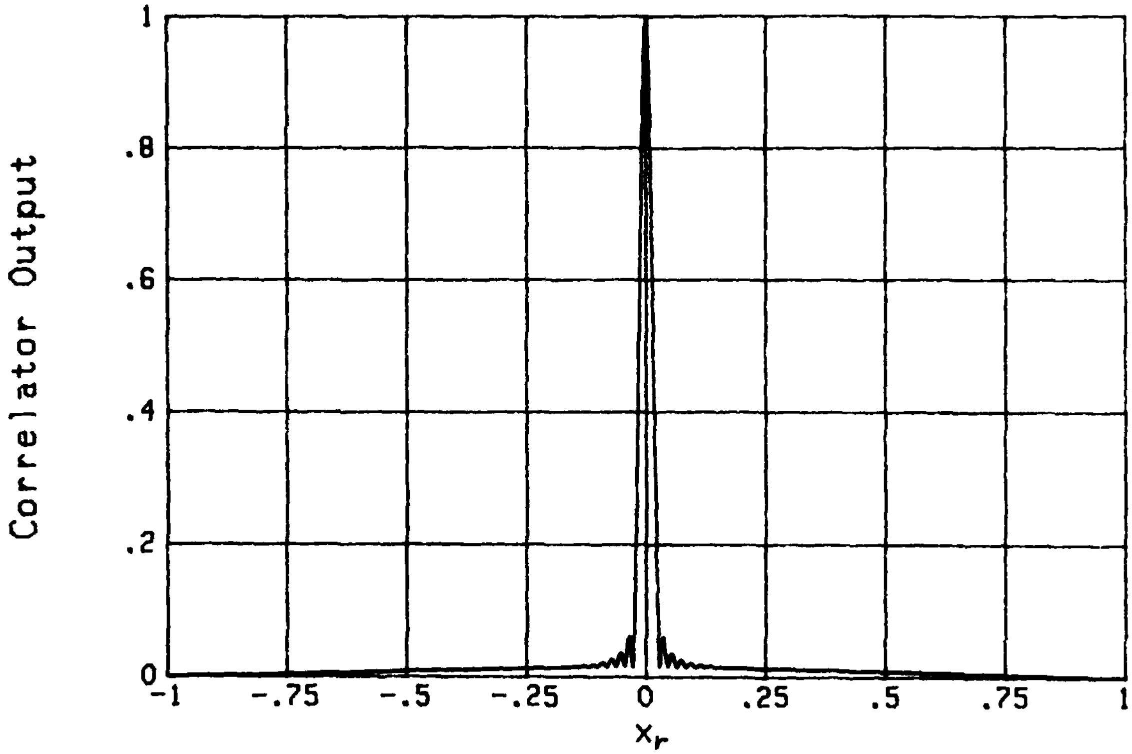

Figure 25. Rectangular-Hanning Envelopes,
$y_r = 0$, L/T = 1.4

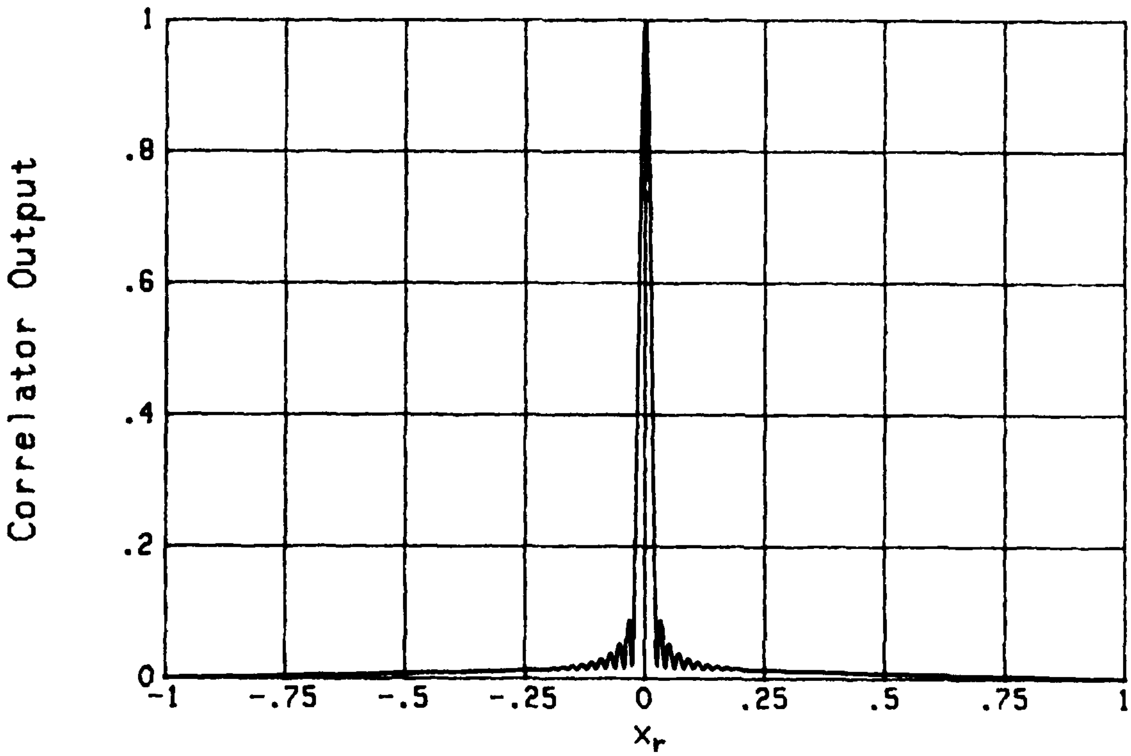

Figure 26. Rectangular-Hanning Envelopes,
$y_r = 0$, L/T = 1.6

amplitude 6 percent = -24 dB and a comparable mainlobe width to that of figure 1. Increasing L/T beyond this value begins to yield significant sidelobes, as indicated in figure 26. The loss in signal detectability due to the use of mismatched signal and reference waveforms is investigated quantitatively two sections hence.

The effect of frequency mismatch for this rectangular-Hanning pairing, with L/T = 1.4, is studied in figures 27 and 28. When coupled with figure 25 for $y_r = 0$, they indicate maintenance of a narrow mainlobe and suppression of sidelobes. Thus, these desirable features can be realized, for a rectangular transmission, by using a longer-duration Hanning reference for crosscorrelation, even with frequency mismatch.

The correlator response of this pairing, for two highlights separated by .06 in time delay, is depicted in figure 29. The sidelobe level is markedly better than the corresponding case in figure 5. When this time delay difference is decreased to .03 in figure 30, the two individual responses are not resolved. This result is somewhat poorer than figure 6, due to a slightly widened mainlobe for the rectangular-Hanning pair of envelopes.

When the earlier three- and four-highlight cases are reconsidered in figures 31 and 32, respectively, the results for the sidelobes are about as expected, by now. Comparison with figures 8 and 9, respectively, confirms the advantages to be accrued by utilizing a mismatched reference.

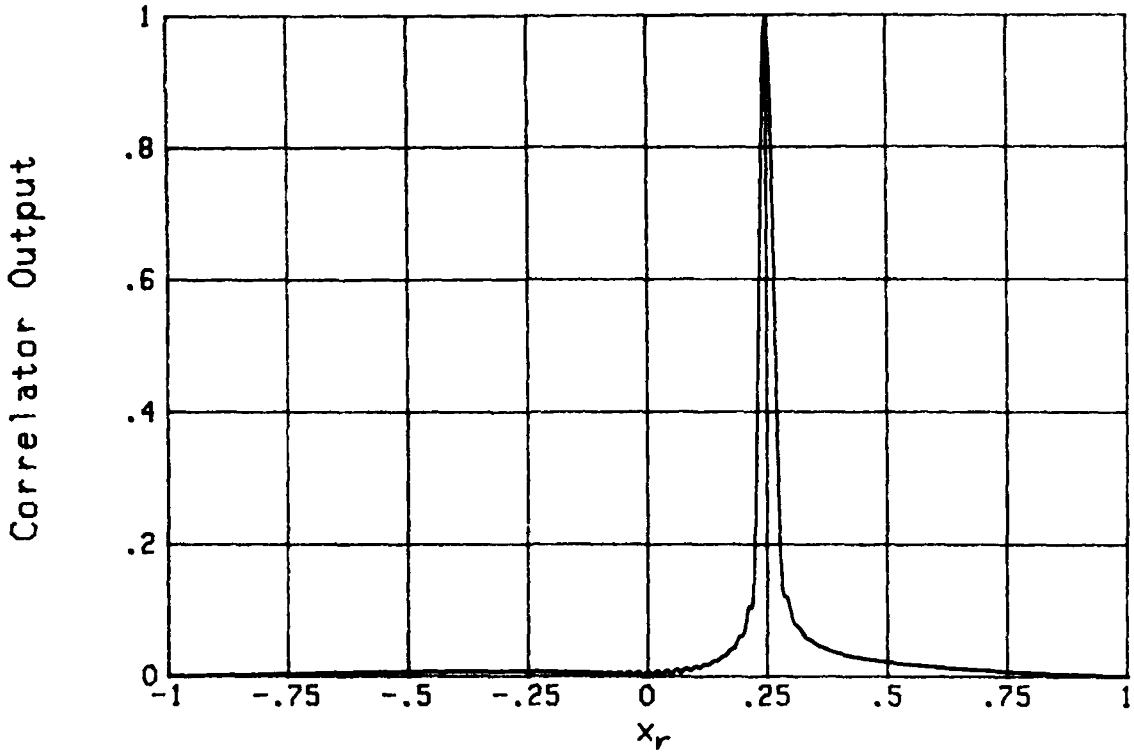

Figure 27. Rectangular-Hanning Envelopes, $y_r = .25$, $L/T = 1.4$

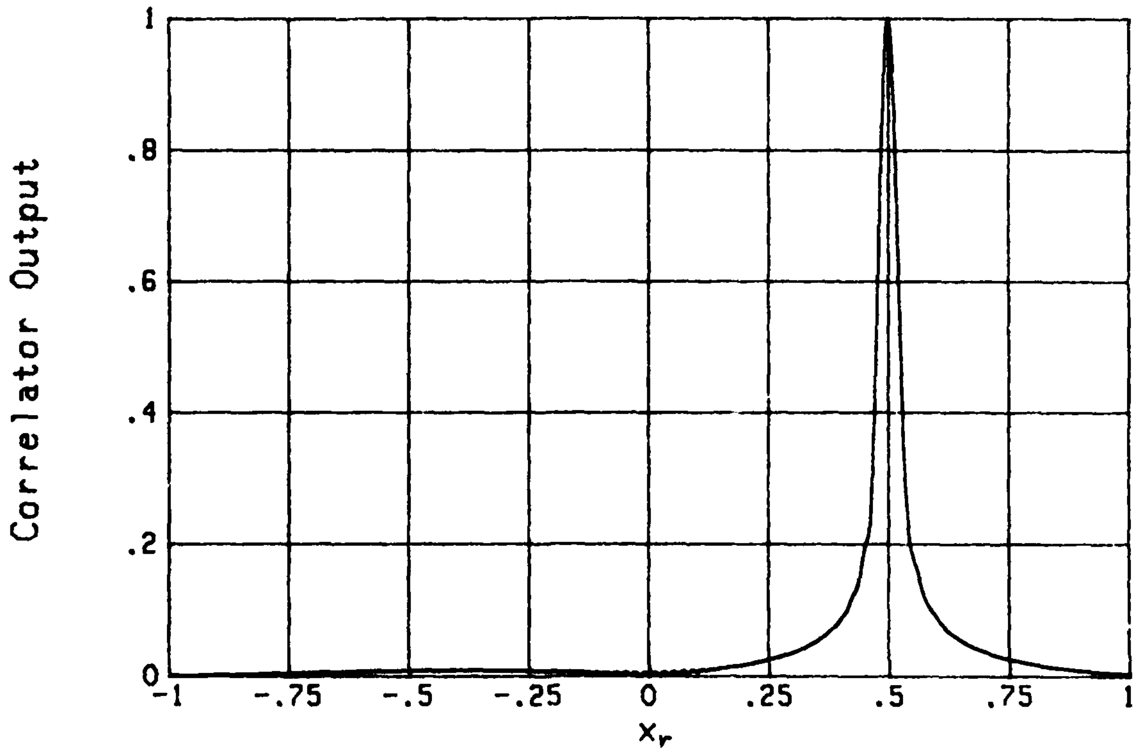

Figure 28. Rectangular-Hanning Envelopes, $y_r = .5$, $L/T = 1.4$

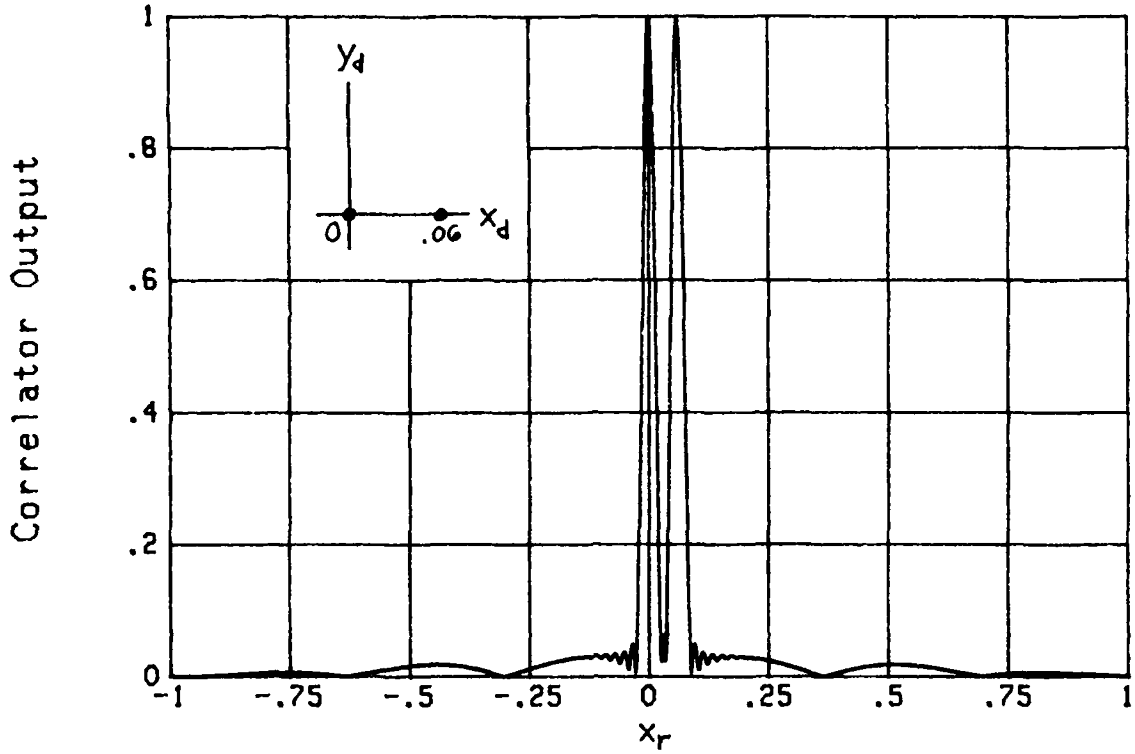

Figure 29. Rectangular-Hanning Envelopes, Two Separated Highlights, $y_r = 0$, $L/T = 1.4$

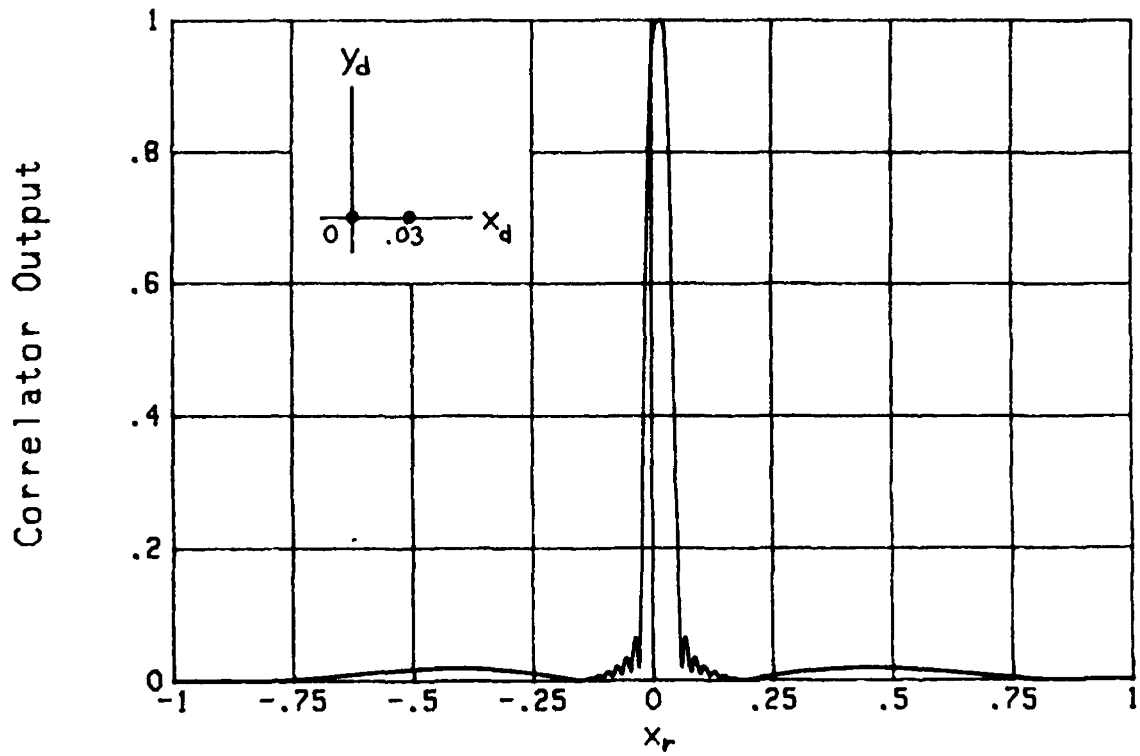

Figure 30. Rectangular-Hanning Envelopes, Two Close Highlights, $y_r = 0$, $L/T = 1.4$

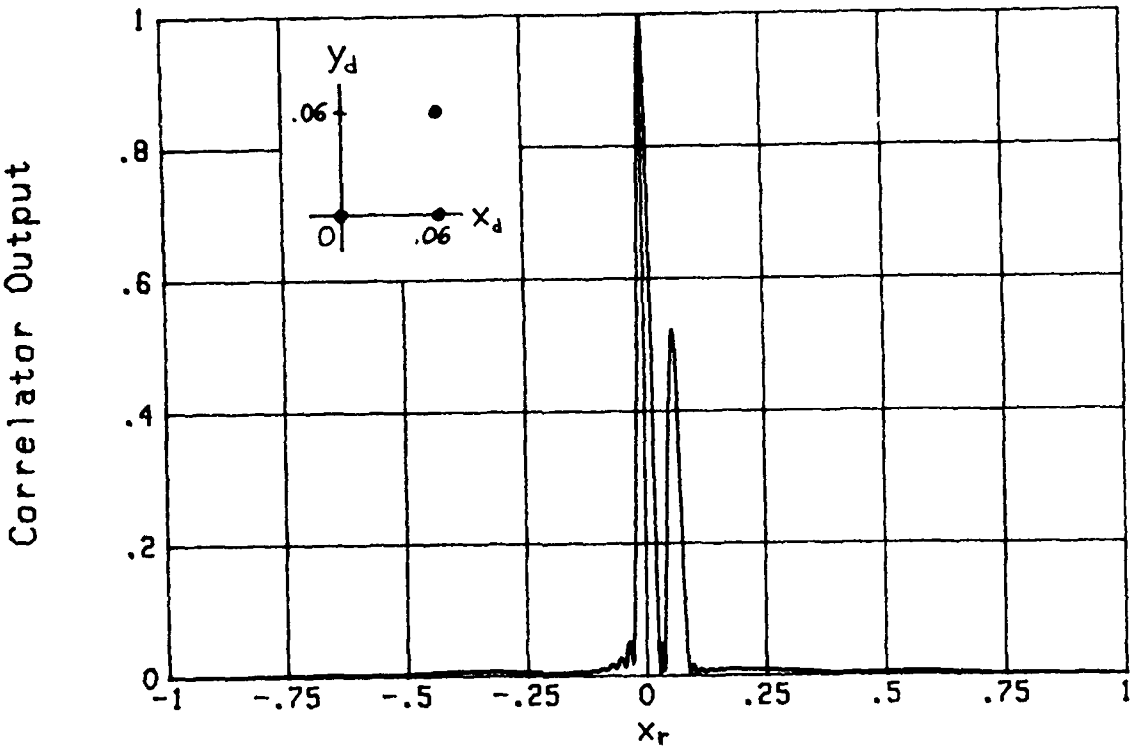

Figure 31. Rectangular-Hanning Envelopes, Three Highlights, $y_r = 0$, L/T = 1.4

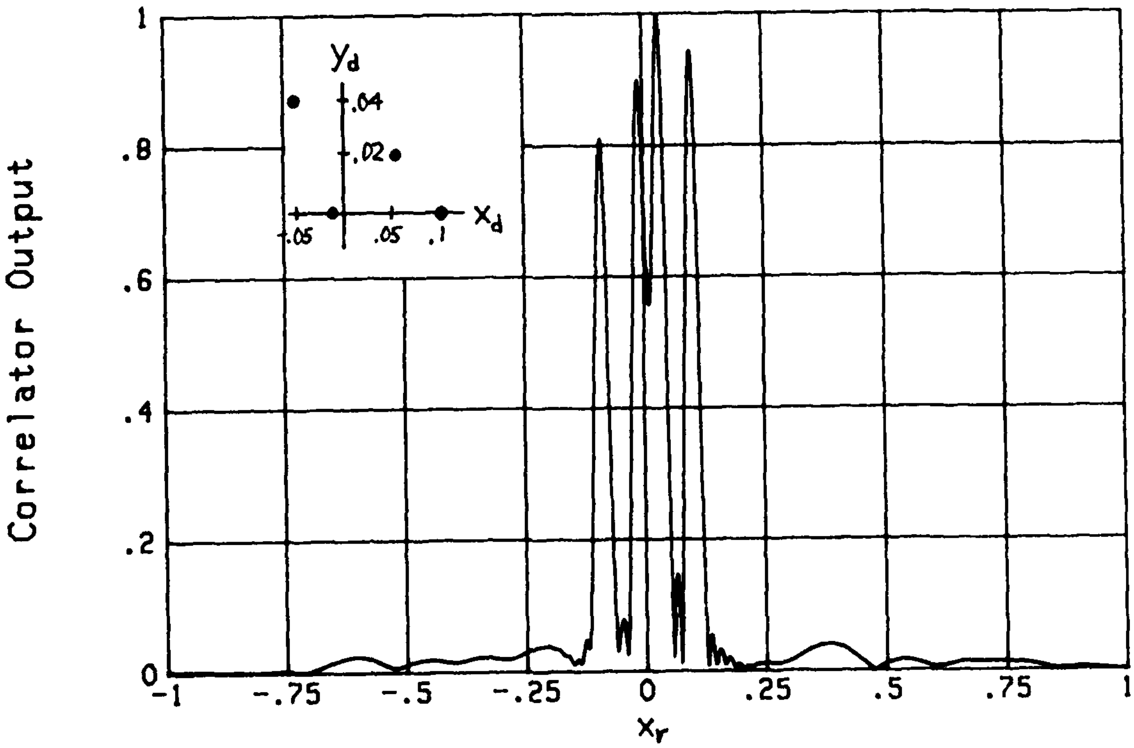

Figure 32. Rectangular-Hanning Envelopes, Four Highlights, $y_r = 0$, L/T = 1.4

The possibility of shaping both the transmitted and reference waveforms according to a Hanning weighting is considered in figures 33 and 34, for two close highlights. One important difference adopted in these two particular figures is that, since T is the overall signal duration in (32), the effective duration of a Hanning function is about T/2. To afford a reasonable comparison with the earlier results for rectangular and Gaussian envelopes, where T measured the effective duration, the value of TW was doubled here. Thus we have TW = 100, but T(eff) W $\cong$ 50, still, in figures 33 and 34. The case of nonzero frequency mismatch, y_r = .25 in the latter figure, reveals even better resolution capability than for y_r = 0, and the virtual absence of any sidelobes.

Instead of forcing the edge values of the waveforms to zero (as for Hanning), the possibility of allowing a nonzero pedastal is considered in figures 35 and 36. This is a compromise between rectangular and Hanning functions. In particular, we tried $a_{-1} = a_1 = .2$, $a_0 = 1$, in (32) and (33), along with L = 1, leading to a waveform center value of 1.4 and edge values of .6. The results for y_r = 0 and .5, respectively, with TW restored to a value of 50, reveal substantially reduced sidelobes relative to the rectangular envelopes case and a narrow mainlobe. A slight broadening of the peak for nonzero frequency mismatch is also evident in figure 36.

The devastating effect of overlapping correlator responses is depicted in figures 37 and 38 for rectangular equal-duration envelopes. The former figure has two equal-amplitude highlights with phases 0 and 3.71 radians,

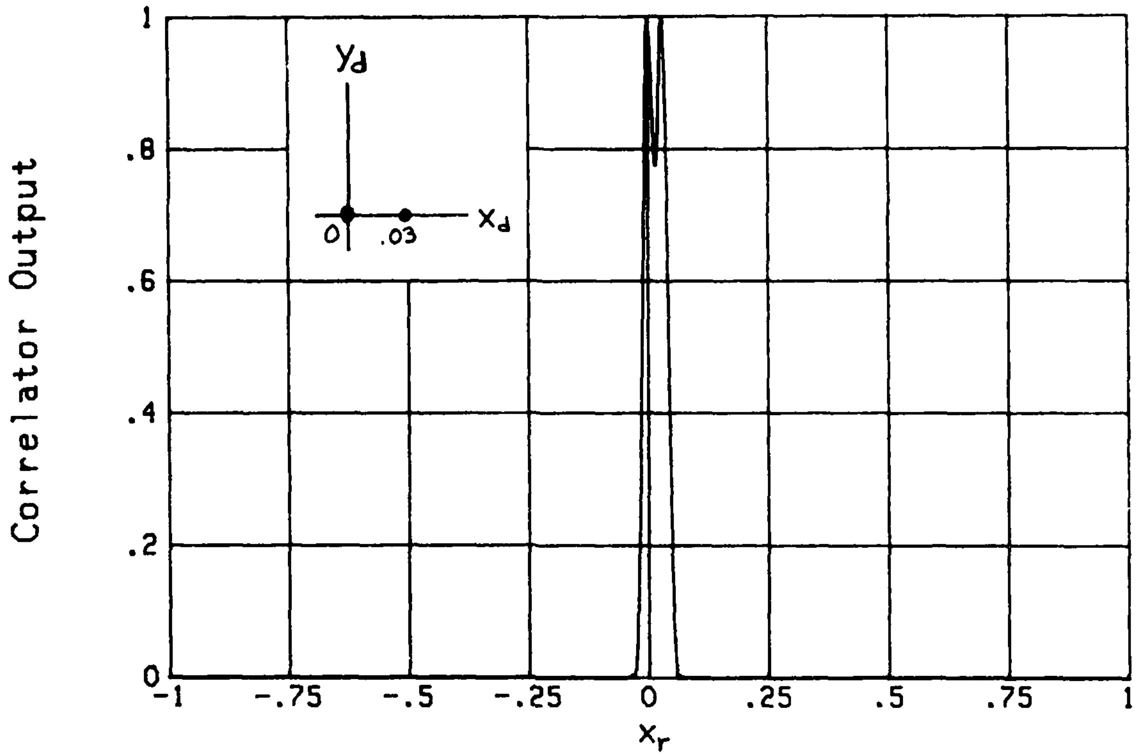

Figure 33. Hanning Envelopes, Two Close Highlights, $y_r = 0$

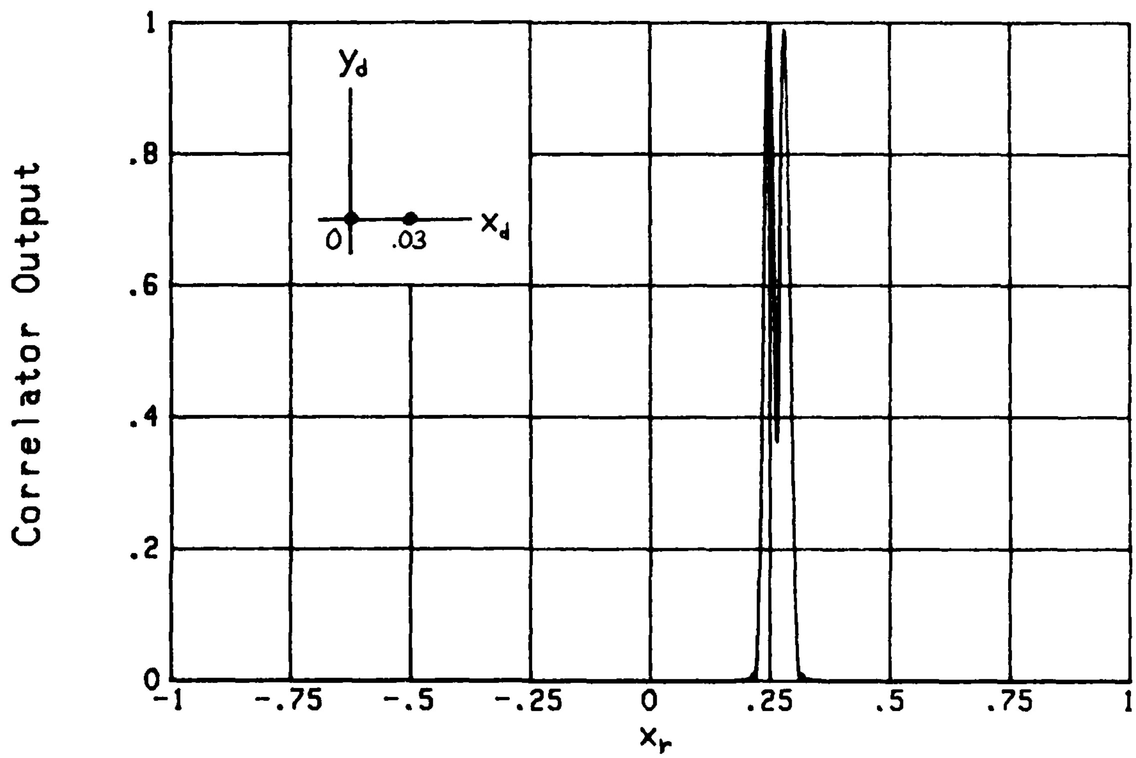

Figure 34. Hanning Envelopes, Two Close Highlights, $y_r = .25$

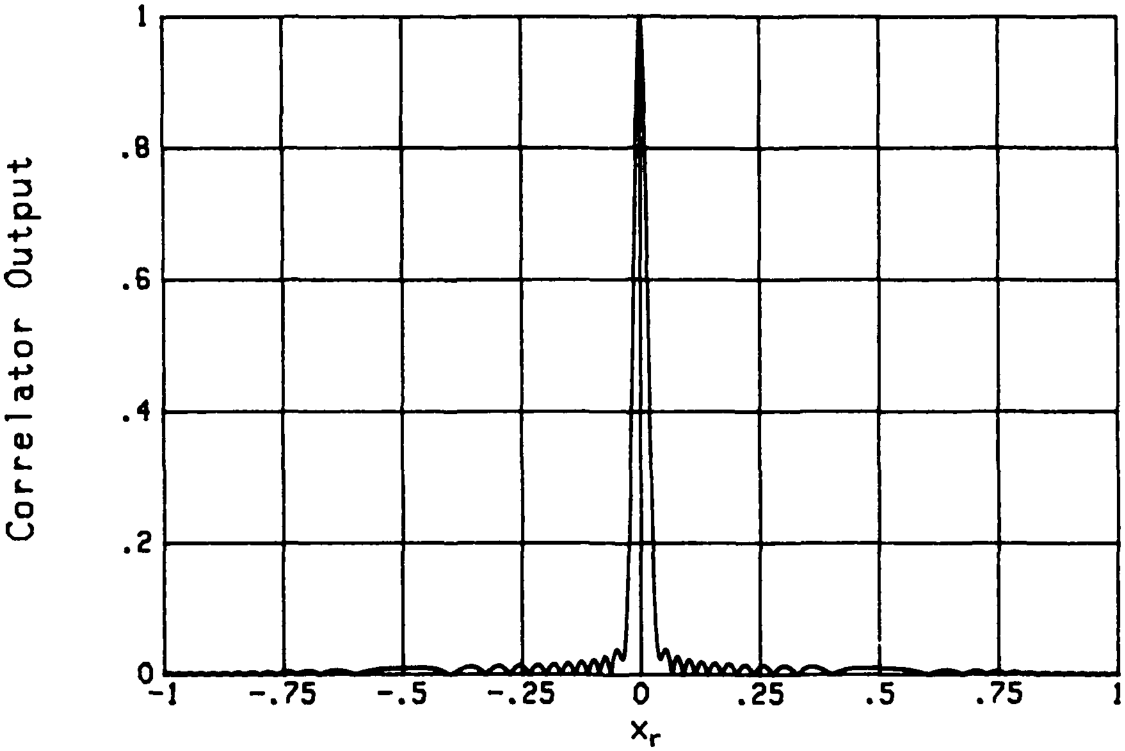

Figure 35. Pedestal Envelopes, $y_r = 0$

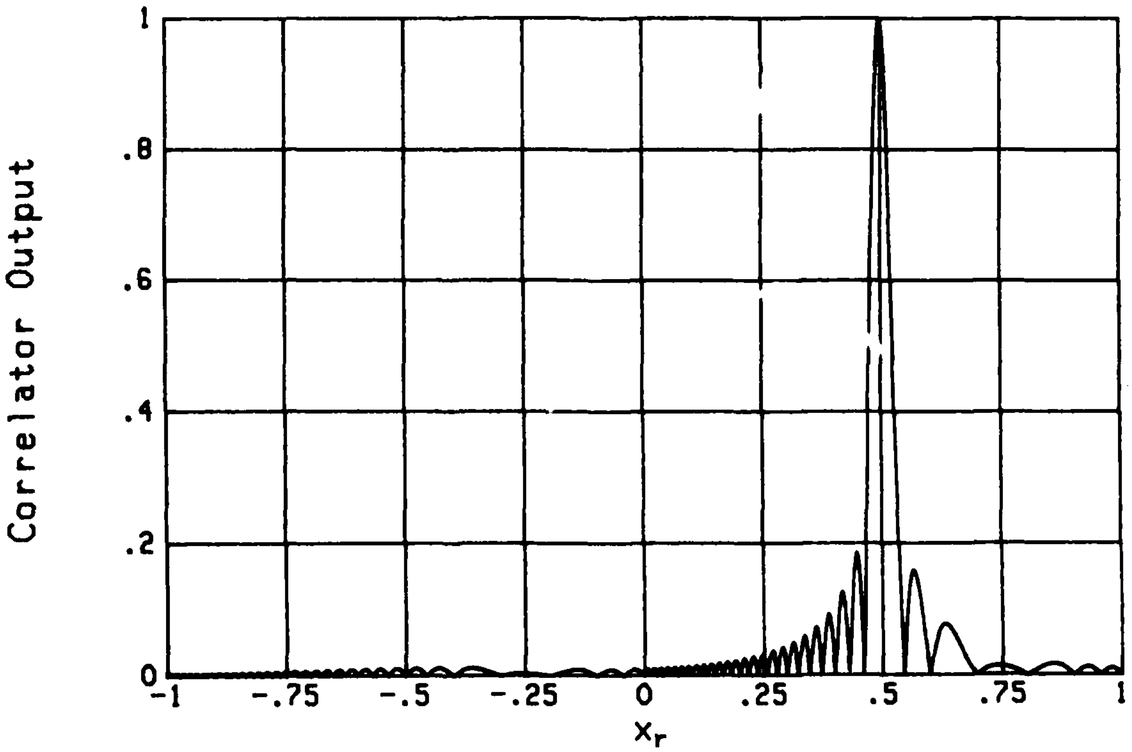

Figure 36. Pedestal Envelopes, $y_r = .5$

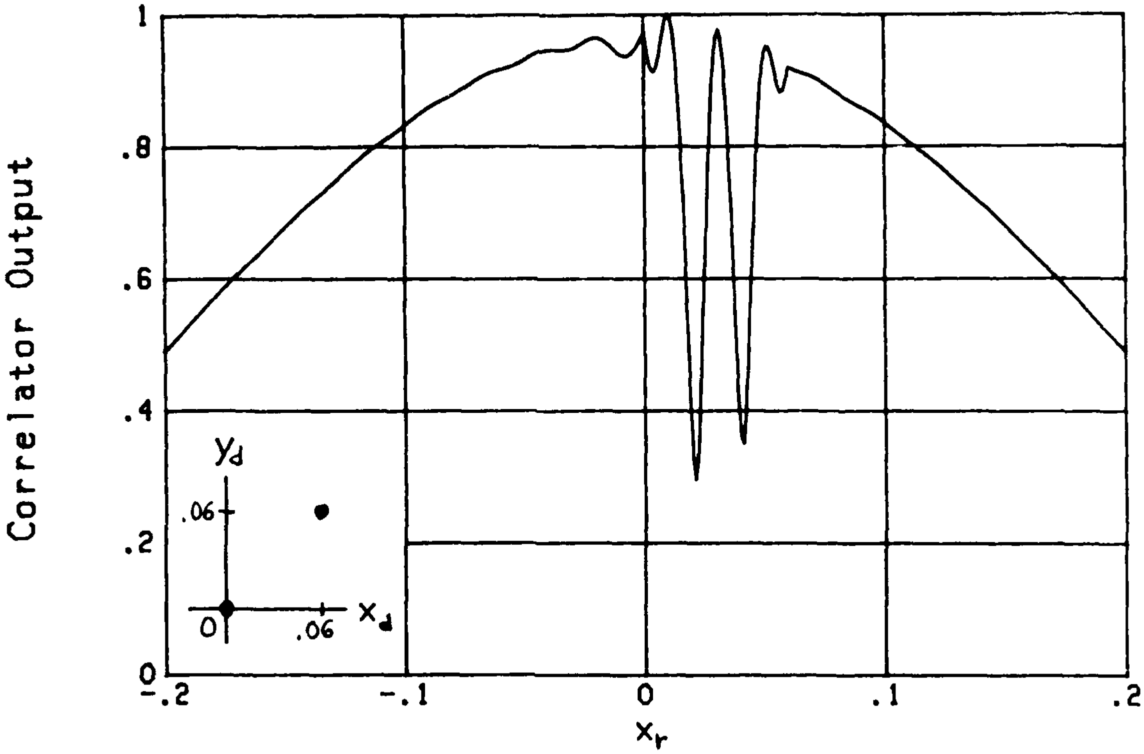

Figure 37. Overlapping Responses,
Two Highlights, $y_r = 0$

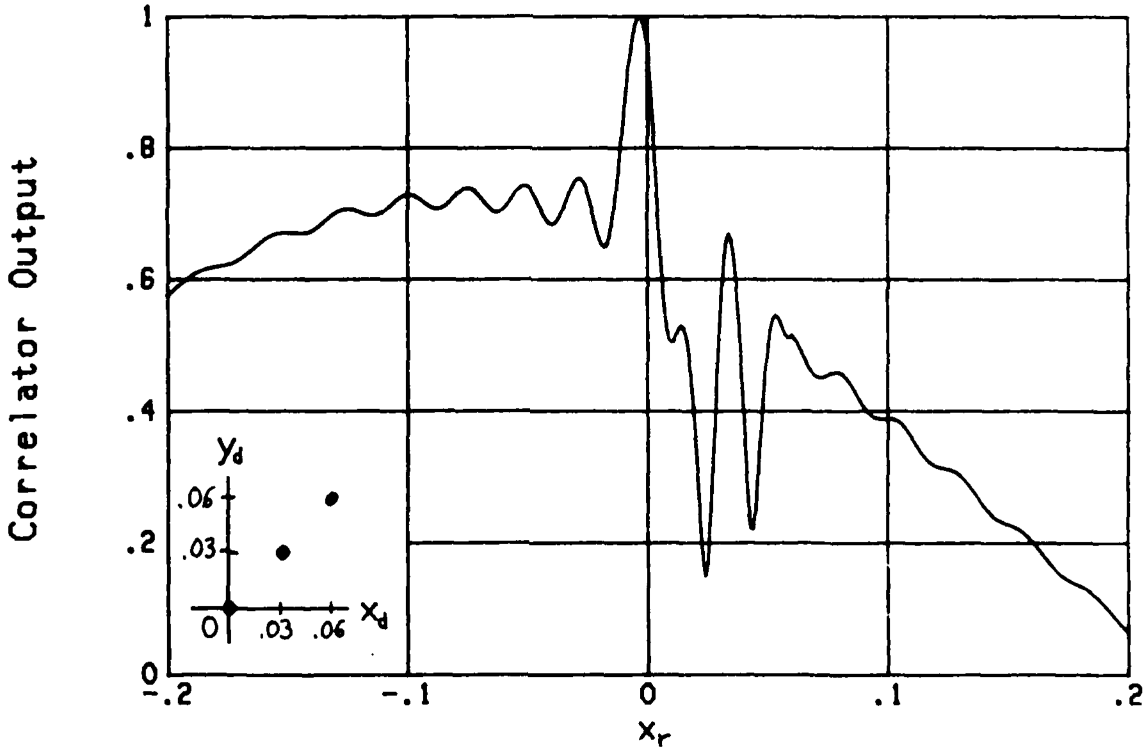

Figure 38. Overlapping Responses,
Three Highlights, $y_r = 0$

located as indicated in the small diagram at the bottom left. Use of up-sweep linear-FM causes these two highlight correlator responses to coalesce, leading to a broad response and numerous spurious peaks where the sidelobes of each highlight happen to interact constructively or destructively. (Notice that the abscissa covers the range -.2,.2 here, rather than -1,1.) Whereas the true target is located at $x_r = 0$ on this plot, the indicated multiple peaks are at .01, .03, .05.

A case of three equal-strength highlights is considered in figure 38, with phases 0, 2.2, 4.73 radians. Again there is a broad response with a pronounced spurious peak at $x_r = .035$. One way of becoming alerted to the fact that a particular peak may be spurious, is if there is a broad response surrounding it; compare figures 37 and 38 with the earlier ones.

A ROTATING MULTIPLE-HIGHLIGHT TARGET MODEL

In order to see how dispersions in x_d,y_d space, such as considered above, can arise in practice, consider a distant line target rotating with angular rate ω; see figure 39. The angle θ=0 corresponds to the plane wave arrival angle of incident energy at carrier frequency f_c. A highlight is presumed present at origin 0 with parameter values $t_d = 0$, $f_d = 0$; i.e., $x_d = 0$, $y_d = 0$. (The absolute range to 0 and the radial movement of 0 have been absorbed in differences between reference parameters t_r,f_r and t_d,f_d, with no loss in generality.) The angular rotational rate, ω, of the line target is equal to $d\theta/dt$.

The incremental round-trip time delay to the highlight at cylindrical coordinates r,θ is

$$t_d = \frac{2r \sin \theta}{c} \quad \text{seconds} \tag{37}$$

relative to the origin 0, where c is the speed of sound. And the frequency shift is

$$f_d = \frac{-2v(\text{radial})}{c} f_c = \frac{-2f_c}{c} \frac{d}{dt} (r\sin\theta) = \frac{-2f_c \; r \; \omega \cos\theta}{c} \quad . \tag{38}$$

For sample values $\omega = 1°/\text{sec} = \frac{\pi}{180}$ rad/sec,

$$r = 100 \text{ ft}, \; c = 5000 \text{ ft/sec}, \; f_c = 3000 \text{ Hz}, \; T = .5 \text{ sec}, \; W = 100 \text{ Hz}, \tag{39}$$

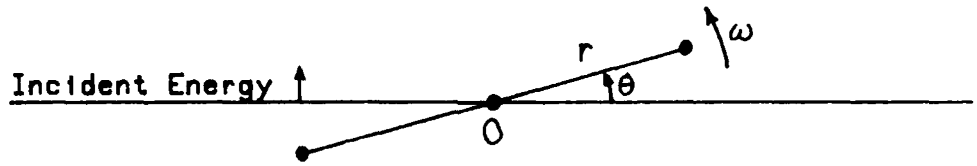

Figure 39. Rotating Line Target

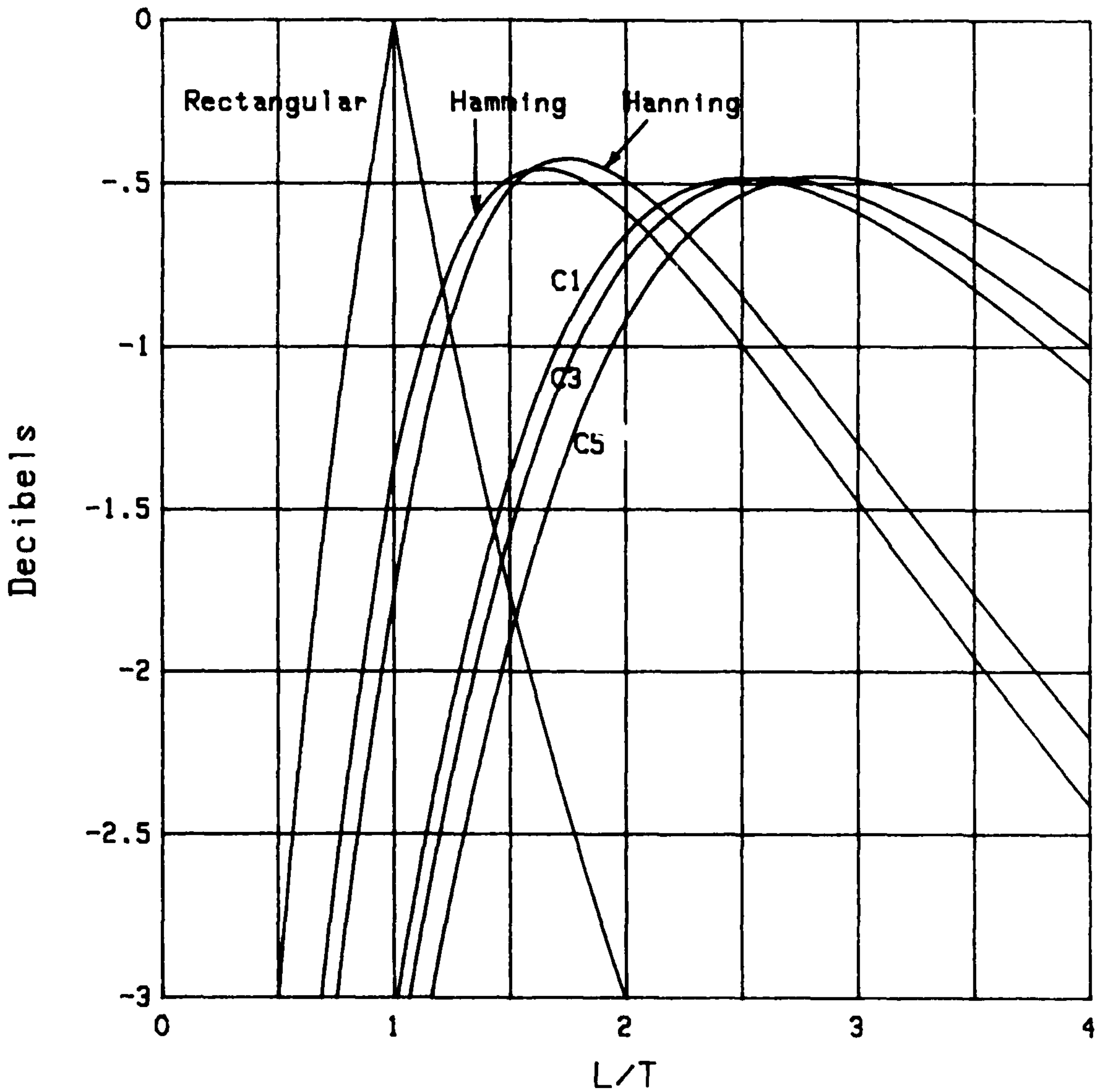

Figure 40. Loss in Detectability

substitution in (37) and (38) yields

$$x_d = \frac{t_d}{T} = .08 \sin \Theta, \quad y_d = \frac{f_d}{W} = -.0209 \cos \Theta . \tag{40}$$

Thus if $\Theta = 14.65°$, we obtain

$$x_d = .0202, \quad y_d = -.0202, \tag{41}$$

which lie on a common -45° line and will, therefore, lead to complete correlator response overlap for down-sweep of the linear-FM. On the other hand, for $\Theta = -14.65°$,

$$x_d = -.0202, \quad y_d = -.0202, \tag{42}$$

meaning overlap for an up-sweep.

Generally, for up-sweep linear-FM, rotating targets that are <u>approaching broadside</u> (relative to plane wave arrival angle) can lead to overlap in the correlator response, regardless of quadrant (Θ) and direction of rotation ($\mathrm{sgn}(\omega)$). Conversely, for down-sweep linear-FM, rotating targets that are <u>approaching endfire</u> can be subject to overlap, regardless of quadrant and direction of rotation. The exact amount and effect depends on all the parameters listed in (37) and (38), in addition to the signal duration T and bandwidth W.

Since t_d and f_d in (37) and (38) are both linearly proportional to target radius r, multiple highlights for a line target all occur on the same line through the origin in x_d, y_d space. Thus, when overlap occurs for one pair of highlights, it can occur for all highlights. Use of both up- and down-sweeps of the linear-FM will guarantee at least one nonambiguous response for a line target.

LOSS OF DETECTABILITY CAUSED BY MISMATCH

In the presence of white noise over the band of the received waveform, the local reference should match the transmitted signal, in order to maximize the deflection for each highlight individually. But earlier results have demonstrated that sidelobes can be significantly suppressed by deliberate mismatch of the local reference. Here we will quantitatively evaluate the loss in detectability caused by this mismatch, for a low-frequency application.

Suppose the real received waveform is

$$s(t) + n(t), \tag{43}$$

where $n(t)$ is white noise with a *double*-sided spectral density N_d watts/Hz. For deterministic reference waveform $r(t)$, the output of a correlator is proportional to

$$x = \int dt\, [s(t) + n(t)]\, r(t). \tag{44}$$

The mean and variance of output random variable x readily follow as

$$m_x = \int dt\, s(t)\, r(t),$$
$$\sigma_x^2 = N_d \int dt\, r^2(t), \tag{45}$$

respectively.

The output power deflection is defined as

$$d^2 = \frac{m_x^2}{\sigma_x^2} = \frac{\left[\int dt\, s(t)\, r(t)\right]^2}{N_d \int dt\, r^2(t)}. \tag{46}$$

This quantity is maximized when the local reference is chosen according to $r(t) = s(t)$, resulting in optimum deflection value

$$d_0^2 = \frac{\int dt\ s^2(t)}{N_d} = \frac{E_s}{N_d} . \qquad (47)$$

We shall be interested in the ratio of the actual deflection, d^2 in (46), to the optimum value, d_0^2 in (47), for a variety of choices of reference $r(t)$.

The relative power deflection of interest is therefore

$$R = \frac{d^2}{d_0^2} = \frac{\left[\int dt\ s(t)\ r(t)\right]^2}{\int dt\ s^2(t)\ \int dt\ r^2(t)} , \qquad (48)$$

which is seen to be independent of the absolute levels of both signal $s(t)$ and reference $r(t)$; however, it does depend on the relative <u>shapes</u> of $s(t)$ and $r(t)$.

The particular case we shall study here is a rectangular envelope for the transmitted signal,

$$s(t) = 1 \quad \text{for } |t| < T/2, \qquad (49)$$

and the arbitrary envelopes for the reference that were previously given in (33). In particular, we allow here

$$r(t) = \sum_{\ell \geq 0} B_\ell \cos(2\pi\ell t/L) \qquad \text{for } |t| < L/2, \qquad (50)$$

where the coefficients $\{\beta_\ell\}$ are restricted to be real. This class allows rectangular, Hanning, Hamming, etc., functions [3]. Reference duration L can be larger or smaller than transmitted duration T.

The quantities needed in (48) follow readily upon use of (49) and (50):

$$\int dt\; s^2(t) = T,$$

$$\int dt\; r^2(t) = L\left[\beta_0^2 + \frac{1}{2}\sum_{\ell\geq 1}\beta_\ell^2\right] \equiv LD,$$

$$\int dt\; s(t)\, r(t) = \left\{\begin{array}{ll} \beta_0\, L & \text{for } L \leq T \\ \\ T\sum_{\ell\geq 0}\beta_\ell\, \operatorname{sinc}(\ell T/L) & \text{for } L \geq T \end{array}\right\}. \tag{51}$$

Combining (51) and (48), the relative power deflection is given by

$$R = \left\{\begin{array}{ll} \dfrac{L}{T}\,\dfrac{1}{D}\,\beta_0^2 & \text{for } \dfrac{L}{T} \leq 1 \\ \\ \dfrac{T}{L}\,\dfrac{1}{D}\left[\sum_{\ell\geq 0}\beta_\ell\, \operatorname{sinc}(\ell T/L)\right]^2 & \text{for } \dfrac{L}{T} \geq 1 \end{array}\right\}. \tag{52}$$

The dB loss in detectability relative to the matched reference case is then given by $10 \log_{10} R$. This quantity is plotted in figure 40 for six different choices of reference, versus the duration ratio L/T. This figure

reveals that a Hanning reference loses only .4 dB if the ratio L/T = 1.75 is utilized. However, even at the smaller ratio L/T = 1.4 (as utilized in figures 27-32), the loss is only .5 dB. This appears to be very tolerable, considering the large improvement in sidelobes that can be realized then.

SUMMARY

The correlator response for a variety of transmitted signals and reference waveforms has been derived and plotted for several examples, including targets with multiple highlights. The generality of the programs listed in appendix C allows the user to numerically investigate his own cases of interest, in terms of the multiple-highlight response, for a wide range of parameter mismatches and transmitted-receiver pairs of waveforms selected.

Significantly reduced sidelobe levels are achieved at the expense of slightly broadened mainlobe response and about .5 dB loss in detectability. The length of a Hanning local reference waveform should be about 40 percent greater than that of a rectangular envelope transmitted signal, in order to achieve a reasonable compromise between sidelobe levels, mainlobe width, and detectability. Re-design or reshaping of the transmitted and reference signals can accomplish even more in terms of sidelobe reduction; however, a transmitter peak power limitation would then not be fully exploited. The interaction of such practical limitations precludes specification of any unique design.

APPENDIX A. DERIVATION OF CORRELATOR OUTPUT

GENERAL CASE

The noise-free correlator output is obtained by substituting (2) and (4) in (6):

$$c(t_r,f_r) = \int dt\; w(t)\; r^*(t) =$$

$$= \int dt \sum_d A_d\; s(t-t_d)\; q^*(t-t_r)\; \exp[i2\pi(f_d-f_r)t + i\,\phi - i\,\Theta_r], \qquad \text{(A-1)}$$

where temporary variable

$$\phi = 2\pi\; [(f_c+f_r)t_r - (f_c+f_d)t_d]. \qquad \text{(A-2)}$$

The cross-ambiguity function between (complex envelope) signal s(t) and reference q(t) is defined as

$$\chi_{sq}(\tau,\nu) = \int dt\; s(t)\; q^*(t-\tau)\; \exp(-i2\pi\nu t) \qquad \text{(A-3)}$$

for arbitrary time delay τ and frequency shift ν; some useful properties and alternative forms for the cross-ambiguity function are given in appendix B. Employment of (A-2) and (A-3) in (A-1) yields correlator output

$$c(t_r,f_r) = \exp[i2\pi(f_c+f_r)t_r - i\Theta_r]\; \underline{c}(t_r,f_r), \qquad \text{(A-4)}$$

where

$$\underline{c}(t_r,f_r) = \sum_d B_d\; \chi_{sq}(t_r-t_d,\; f_r-f_d) \qquad \text{(A-5)}$$

and

$$B_d = A_d \exp[-i2\pi(f_c+f_r)t_d] \ . \qquad (A-6)$$

Each of the exponentials in (A-6) is virtually a random phase shift, since each highlight delay t_d is unknown and f_c is a high-frequency carrier. For example, at a carrier frequency of $f_c = 3000$ Hz, an incremental target delay of 1 msec (5 foot range) causes a phase shift of $2\pi(3000)(.001)$ radians = 1080°. Thus the complex phasors $\{B_d\}$ in (A-5) can reasonably be taken as statistically independent vectors, each uniformly distributed in angle over 2π radians.

The magnitude of (A-4) or (A-5), $|\underline{c}(t_r,f_r)|$, is the physical envelope of the correlator output, versus reference time delay t_r and frequency shift f_r, that would be observed in the absence of noise. The general result in (A-4) and (A-5) applies for any transmitted signal and reference pair.

LINEAR-FM

We now specialize this general result to the particular case of linear-FM; specifically, let signal

$$s(t) = \underline{s}(t) \exp(i\pi\beta t^2), \qquad (A-7)$$

where $\underline{s}(t)$ is a low-pass amplitude modulation. The instantaneous frequency is βt Hz, which is zero at time $t=0$; thus $\underline{s}(t)$ should be centered around $t=0$

in order that s(t) correctly represent a complex envelope. Similarly, for the reference, let

$$q(t) = \underline{q}(t)\ \exp(i\pi\beta t^2). \tag{A-8}$$

Substitution of (A-7) and (A-8) in (A-3) immediately yields the relation

$$\chi_{sq}(\tau,\nu) = \chi_{\underline{sq}}(\tau,\nu-\beta\tau)\ \exp(-i\pi\beta\tau^2) \tag{A-9}$$

in terms of the cross-ambiguity function of low-pass amplitude modulations $\underline{s}(t)$ and $\underline{q}(t)$ (which can be complex). Alternatively, using the symmetric version, $\overline{\chi}$, of the cross-ambiguity function, χ, as defined in (B-6), we have

$$\chi_{sq}(\tau,\nu) = \overline{\chi}_{\underline{sq}}(\tau,\nu-\beta\tau)\ \exp(-i\pi\nu\tau) \tag{A-10}$$

and

$$\overline{\chi}_{sq}(\tau,\nu) = \overline{\chi}_{\underline{sq}}(\tau,\nu-\beta\tau). \tag{A-11}$$

This enables (A-5) to be expressed as

$$\underline{c}(t_r,f_r) = \sum_d B_d\ \exp[-i\pi(f_r-f_d)(t_r-t_d)]\,\overline{\chi}_{\underline{sq}}(t_r-t_d,f_r-f_d-\beta(t_r-t_d)). \tag{A-12}$$

This is the general result for the complex envelope of the linear-FM correlator output, in the absence of noise.

BEHAVIOR OF (A-11)

The fundamental quantity in (A-12) governing the correlator output is the cross-ambiguity function of low-pass modulations $\underline{s}(t)$ and $\underline{q}(t)$. If these modulations are unimodal, centered at $t=0$, and of approximate extent T, then cross ambiguity function $\overline{\chi}_{\underline{sq}}(\tau,\nu)$ in (B-6) or (B-7) has approximate extents T,1/T respectively in the τ,ν plane. Therefore

$$\overline{\chi}_{\underline{sq}}(Tx, y/T) \equiv \chi_o(x, y) \qquad \text{(A-13)}$$

has approximate extents 1,1 in the x,y plane.

It also follows from (A-11) that

$$\overline{\chi}_{sq}(\tau, \nu) = \overline{\chi}_{\underline{sq}}(\tau, \nu - \beta\tau) = \chi_o\left(\frac{\tau}{T}, T\nu - TW\frac{\tau}{T}\right). \qquad \text{(A-14)}$$

For fixed frequency shift ν, as we increment τ, the variation in the second argument of χ_o is magnified by the factor TW over that of the first argument. Thus, we are then taking virtually a <u>vertical</u> slice in the normalized ambiguity function χ_o; this magnification means that a time slice (in τ) of $\overline{\chi}_{sq}$ cuts through the <u>frequency</u> domain peaks and sidelobes of the ambiguity function $\overline{\chi}_{\underline{sq}}$.

APPENDIX B. CROSS-AMBIGUITY FUNCTIONS AND PROPERTIES

DEFINITIONS

The cross-ambiguity function between two arbitrary complex functions a(t) and b(t) is defined as

$$\chi_{ab}(\tau,\nu) = \int dt\ a(t)\ b^*(t-\tau)\ \exp(-i2\pi\nu t)\ , \tag{B-1}$$

where τ and ν are time delay and frequency shift parameters, respectively. If we define the Fourier transform of each function according to

$$\begin{aligned} A(f) &= \int dt\ a(t)\ \exp(-i2\pi ft)\ , \\ B(f) &= \int dt\ b(t)\ \exp(-i2\pi ft)\ , \end{aligned} \tag{B-2}$$

an alternative form to (B-1) is obtained:

$$\chi_{ab}(\tau,\nu) = \int df\ A(f+\nu)\ B^*(f)\ \exp(i2\pi\tau f)\ . \tag{B-3}$$

VOLUME CONSERVATION

Since the volume integral

$$\iint d\tau\ d\nu\ \left|\chi_{ab}(\tau,\nu)\right|^2 =$$

$$= \iint d\tau\ d\nu \iint dt_1\ dt_2\ a(t_1)\ b^*(t_1-\tau)\ a^*(t_2)\ b(t_2-\tau)\ \exp(-i2\pi\nu(t_1-t_2)) =$$

$$= \int d\tau \iint dt_1\ dt_2\ a(t_1)\ b^*(t_1-\tau)\ a^*(t_2)\ b(t_2-\tau)\ \delta(t_1-t_2) =$$

$$= \int d\tau \int dt_1\ |a(t_1)|^2\ |b(t_1-\tau)|^2 = \int dt_1\ |a(t_1)|^2 \int du\ |b(u)|^2 =$$

$$= \chi_{aa}(0,0)\ \chi_{bb}(0,0)\ , \tag{B-4}$$

it follows that

$$\iint d\tau\ d\nu\ \frac{\left|\chi_{ab}(\tau,\nu)\right|^2}{\chi_{aa}(0,0)\ \chi_{bb}(0,0)} = 1, \tag{B-5}$$

independent of the particular waveshapes of functions a(t) and b(t). Thus, no matter how the volume (B-4) under cross-ambiguity function $\chi_{ab}(\tau,\nu)$ is moved about in the τ,ν plane, it must be conserved according to relation (B-5).

SYMMETRIC VERSION

A symmetric version of the cross-ambiguity function is possible and preferred in some cases; namely, define

$$\bar{\chi}_{ab}(\tau,\nu) = \int dt\ a\left(t + \frac{\tau}{2}\right) b^*\left(t - \frac{\tau}{2}\right) \exp(-i2\pi\nu t) \ . \tag{B-6}$$

By use of (B-2), an equivalent form is

$$\bar{\chi}_{ab}(\tau,\nu) = \int df\ A\left(f + \frac{\nu}{2}\right) B^*\left(f - \frac{\nu}{2}\right) \exp(+i2\pi\tau f) \ , \tag{B-7}$$

which retains the same symmetry. A simple change of integration variable readily reveals that the two forms of the cross-ambiguity function are related according to

$$\chi_{ab}(\tau,\nu) = \bar{\chi}_{ab}(\tau,\nu) \exp(-i\pi\nu\tau) \ . \tag{B-8}$$

In particular,

$$\left|\chi_{ab}(\tau,\nu)\right| = \left|\bar{\chi}_{ab}(\tau,\nu)\right| \ ; \tag{B-9}$$

that is, both forms of the cross-ambiguity function have equal magnitudes for all τ,ν. There immediately follows the same conservation as in (B-5):

$$\iint d\tau\ d\nu\ \frac{\left|\bar{\chi}_{ab}(\tau,\nu)\right|^2}{\bar{\chi}_{aa}(0,0)\ \bar{\chi}_{bb}(0,0)} = 1. \tag{B-10}$$

AUTO AMBIGUITY PROPERTIES

Suppose that functions a(t) and b(t) are equal to some common signal:

$$a(t) = b(t) = s(t). \tag{B-11}$$

Then (B-5) (or (B-10)) yields the relation

$$\iint d\tau \, d\nu \left| \frac{\chi_{ss}(\tau,\nu)}{\chi_{ss}(0,0)} \right|^2 = 1 \, . \tag{B-12}$$

Now if signal s(t) is of duration T seconds and bandwidth W Hertz, then $\chi_{ss}(\tau,\nu)$ extends approximately over a region of width 2T in τ, and 2W in ν. If a negligible volume is contained under the peak of $\chi_{ss}(\tau,\nu)$ at the origin, which is reasonable and possible for TW >> 1, and <u>if</u> the relative ambiguity function magnitude could be maintained absolutely flat away from the origin, of height H, (B-12) yields

$$2T \; 2W \; H^2 = 1 \, , \qquad H = \frac{1}{2\sqrt{TW}} \, . \tag{B-13}$$

In fact, this situation is impossible to attain, and the ambiguity function $\chi_{ss}(\tau,\nu)$ develops wiggles versus τ,ν. Even for a good signal design, factors of 2 or larger are expected; thus a ballpark estimate is that

$$\text{peaks of } \left| \frac{\chi_{ss}(\tau,\nu)}{\chi_{ss}(0,0)} \right| \sim \frac{1}{\sqrt{TW}} \quad \text{for a good signal,} \tag{B-14}$$

but this can be expected to be exceeded occasionally.

As an example, for time bandwidth product TW = 50, (B-14) yields relative peaks of height .14; actual numerical calculation for a rectangular linear-FM yields some peaks of value .21, which are 50 percent greater than estimate (B-14). These peaks are in addition to the large elliptical mainlobe, along a diagonal in the τ,ν plane, that is inherent in a linear-FM waveform.

APPENDIX C. PROGRAMS FOR CORRELATOR RESPONSE

Three main programs are furnished here, corresponding to the examples of low-pass modulations presented in the main body of the report. They are, respectively,

Rectangular Envelopes,

Gaussian Envelopes, and

Arbitrary Envelopes and Durations.

The last program contains a subroutine, SUB Cross_ambiguity, which calculates the cross-ambiguity function between (32) and (33) for arbitrary τ, v, T, L, $\{a_k\}$, $\{b_\ell\}$. More details are found in appendix D.

```
 10  ! RECTANGULAR ENVELOPES
 20    Yr=0.                          !  REFERENCE FREQUENCY SHIFT fr/W
 30    Tw=50.                         !  TIME-BANDWIDTH PRODUCT TW
 40    Sweep=+1.                      !  UP/DOWN FREQUENCY SWEEP
 50    DATA .9,.9,0.,0.,0.            !  TARGET AMPLITUDES
 60    DATA 0.,0.,0.,0.,0.            !  TARGET PHASES
 70    DATA 0.,.06,0.,0.,0.           !  TARGET TIME DELAYS td/T
 80    DATA 0.,0.,0.,0.,0.            !  TARGET FREQUENCY SHIFTS fd/W
 90    DIM Ad(1:5),Pd(1:5),Xd(1:5),Yd(1:5)
100    READ Ad(*),Pd(*),Xd(*),Yd(*)
110    DOUBLE N                       !  INTEGER
120    GINIT
130    PLOTTER IS "GRAPHICS"
140    GRAPHICS ON
150    WINDOW -1.,1.,0.,1.
160    GRID .25,.2
170    T1=PI*Tw
180    FOR Xr=-1. TO 1. STEP .001     !  REFERENCE TIME DELAY tr/T
190    Cr=Ci=0.
200    FOR N=1 TO 5
210    IF Ad(N)=0. THEN 320
220    T2=Xr-Xd(N)
230    T3=Yr-Yd(N)
240    T4=T1*(T3-Sweep*T2)
250    T5=1.-ABS(T2)
260    T5=MAX(0.,T5)
270    IF T4<>0. THEN T5=SIN(T4*T5)/T4
280    T6=Ad(N)*T5
290    T7=Pd(N)-T1*T2*T3
300    Cr=Cr+T6*COS(T7)
310    Ci=Ci+T6*SIN(T7)
320    NEXT N
330    PLOT Xr,SQR(Cr*Cr+Ci*Ci)
340    NEXT Xr
350    PENUP
360    END
```

```
10  ! GAUSSIAN ENVELOPES
20    Yr=0.                              !  REFERENCE FREQUENCY SHIFT fr/W
30    Tw=50.                             !  TIME-BANDWIDTH PRODUCT TW
40    Sweep=+1.                          !  UP/DOWN FREQUENCY SWEEP
50    DATA .9,.9,0.,0.,0.                !  TARGET AMPLITUDES
60    DATA 0.,0.,0.,0.,0.                !  TARGET PHASES
70    DATA 0.,.06,0.,0.,0.               !  TARGET TIME DELAYS td/T
80    DATA 0.,0.,0.,0.,0.                !  TARGET FREQUENCY SHIFTS fd/W
90    DIM Ad(1:5),Pd(1:5),Xd(1:5),Yd(1:5)
100   READ Ad(*),Pd(*),Xd(*),Yd(*)
110   DOUBLE N                           !  INTEGER
120   GINIT
130   PLOTTER IS "GRAPHICS"
140   GRAPHICS ON
150   WINDOW -1.,1.,0.,1.
160   GRID .25,.2
170   T1=PI*Tw
180   P2=PI/2.
190   Tw2=Tw*Tw
200   FOR Xr=-1. TO 1. STEP .001         !  REFERENCE TIME DELAY tr/T
210   Cr=Ci=0.
220   FOR N=1 TO 5
230   IF Ad(N)=0. THEN 330
240   T2=Xr-Xd(N)
250   T3=Yr-Yd(N)
260   T4=P2*(T2*T2+Tw2*(T3-Sweep*T2)*(T3-Sweep*T2))
270   IF T4>25. THEN 330
280   T5=EXP(-T4)
290   T6=Ad(N)*T5
300   T7=Pd(N)-T1*T2*T3
310   Cr=Cr+T6*COS(T7)
320   Ci=Ci+T6*SIN(T7)
330   NEXT N
340   PLOT Xr,SQR(Cr*Cr+Ci*Ci)
350   NEXT Xr
360   PENUP
370   END
```

```
10   ! ARBITRARY ENVELOPES AND DURATIONS
20     Yr=0.                          !  REFERENCE FREQUENCY SHIFT fr/W
30     Tw=50.                         !  TIME-BANDWIDTH PRODUCT TW
40     Sweep=+1.                      !  UP/DOWN FREQUENCY SWEEP
50     DATA 1.,0.,0.,0.,0.            !  TARGET AMPLITUDES
60     DATA 0.,0.,0.,0.,0.            !  TARGET PHASES
70     DATA 0.,0.,0.,0.,0.            !  TARGET TIME DELAYS td/T
80     DATA 0.,0.,0.,0.,0.            !  TARGET FREQUENCY SHIFTS fd/W
90     DIM Ad(1:5),Pd(1:5),Xd(1:5),Yd(1:5),Xr(-1000:1000),Env(-1000:1000)
100    READ Ad(*),Pd(*),Xd(*),Yd(*)
110    DOUBLE I,N                     !  INTEGERS
120    T1=PI*Tw
130    FOR I=-1000 TO 1000
140    Xr(I)=Xr=.001*I                !  REFERENCE TIME DELAY tr/T
150    Cr=Ci=0.
160    FOR N=1 TO 5
170    A=Ad(N)
180    IF A=0. THEN 270
190    T2=Xr-Xd(N)
200    T3=Yr-Yd(N)
210    CALL Cross_ambiguity(T2,Tw*(T3-Sweep*T2),Zr,Zi)
220    T4=Pd(N)-T1*T2*T3
230    T5=COS(T4)
240    T6=SIN(T4)
250    Cr=Cr+A*(T5*Zr-T6*Zi)
260    Ci=Ci+A*(T5*Zi+T6*Zr)
270    NEXT N
280    Env(I)=SQR(Cr*Cr+Ci*Ci)
290    NEXT I
300    Big=MAX(Env(*))
310    MAT Env=Env/(Big)
320    GINIT
330    PLOTTER IS "GRAPHICS"
340    GRAPHICS ON
350    WINDOW -1.,1.,0.,1.
360    GRID .25,.2
370    PLOT Xr(*),Env(*)
380    PENUP
390    END
400    !
```

```
410   SUB Cross_ambiguity(X,Y,Zr,Zi)   !  Tau/T,Nu*T
420   R=1.2                            !  L/T
430   DATA 0.,0.,0.,1.,0.,0.,0.        !  a(-3:3)      real
440   DATA 0.,0.,.5,1.,.5,0.,0.        !  b(-3:3)  coefficients
450   Zr=Zi=0.
460   R1=MAX(-.5*(1.+X),-.5*(R-X))
470   R2=MIN(.5*(1.-X),.5*(R+X))
480   IF R1>=R2 THEN SUBEXIT
490   DOUBLE Ks,Ls                     !  INTEGERS
500   ALLOCATE A(-3:3),B(-3:3)
510   READ A(*),B(*)
520   Dif=PI*(R2-R1)
530   Sum=PI*(R2+R1)
540   Tx=PI*X
550   FOR Ls=-3 TO 3
560   B=B(Ls)
570   IF B=0. THEN 720
580   T1=Ls/R
590   FOR Ks=-3 TO 3
600   A=A(Ks)
610   IF A=0. THEN 710
620   V=Y-Ks+T1
630   Arg=Tx*(Ks+T1)-Sum*V
640   IF V<>0. THEN 670
650   Ts=Dif
660   GOTO 680
670   Ts=SIN(Dif*V)/V
680   Tab=A*B*Ts
690   Zr=Zr+Tab*COS(Arg)
700   Zi=Zi+Tab*SIN(Arg)
710   NEXT Ks
720   NEXT Ls
730   SUBEND
```

APPENDIX D. CROSS-AMBIGUITY FUNCTION FOR ARBITRARY ENVELOPES AND DURATIONS

The symmetric cross-ambiguity function is obtained by substituting (32) and (33) in (B-6):

$$\bar{\chi}_{\underline{s}\underline{q}}(\tau,\nu) = \int dt\ \underline{s}\left(t+\frac{\tau}{2}\right) q^*\left(t-\frac{\tau}{2}\right) \exp(-i2\pi\nu t) =$$

$$= \sum_{k,\ell} a_k\ b_\ell^* \int_{t_1}^{t_2} dt\ \exp\left[i2\pi\left\{\frac{k}{T}\left(t+\frac{\tau}{2}\right) - \frac{\ell}{L}\left(t-\frac{\tau}{2}\right) - \nu t\right\}\right] \quad \text{for } t_1 < t_2\ , \tag{D-1}$$

where

$$t_1 = \max\left\{-\frac{T}{2}-\frac{\tau}{2},\ -\frac{L}{2}+\frac{\tau}{2}\right\}\ ,$$
$$t_2 = \min\left\{\frac{T}{2}-\frac{\tau}{2},\ \frac{L}{2}+\frac{\tau}{2}\right\}\ ; \tag{D-2}$$

$\bar{\chi}_{\underline{s}q}$ is zero if $t_1 \geq t_2$. The relation in (D-1) and (D-2) holds for arbitrary τ, whether larger or smaller than T and/or L, and for arbitrary L/T values. Actual integration of (D-1) yields

$$\bar{\chi}_{\underline{s}\underline{q}}(\tau,\nu) = \frac{T}{\pi} \sum_{k,\ell} a_k\ b_\ell^*\ \frac{1}{v}\ \sin\left[\pi v \frac{t_2 - t_1}{T}\right] \exp\left[i\pi\left\{\frac{\tau}{T}\left(k+\ell\,\frac{T}{L}\right) - v\,\frac{t_2+t_1}{T}\right\}\right], \tag{D-3}$$

where

$$v = \nu T - k + \ell\frac{T}{L} \quad (= v_{k\ell})\ . \tag{D-4}$$

Now define a function

$$Z(X,Y,R) = \sum_{k,\ell} a_k\, b_\ell^* \,\frac{1}{V}\, \sin\left[\pi V(R_2-R_1)\right]\, \exp\left[i\pi\left\{X(k+\ell/R)-V(R_2+R_1)\right\}\right] \quad \text{for } R_1 < R_2 , \tag{D-5}$$

where

$$R_1 = \max\left\{-\frac{1}{2}(1+X),\ -\frac{1}{2}(R-X)\right\} ,$$

$$R_2 = \min\left\{\ \frac{1}{2}(1-X),\ \ \frac{1}{2}(R+X)\right\} ,$$

$$V = Y - k + \ell/R \quad (=V_{k\ell}) ; \tag{D-6}$$

Z is zero for $R_1 \geq R_2$. Then the cross-ambiguity function in (D-3) can be expressed as

$$\tilde{\chi}_{\underline{sq}}(\tau,\nu) = \frac{T}{\pi}\, Z\left(\frac{\tau}{T},\ \nu T,\ \frac{L}{T}\right) \qquad \text{for all } \tau,\nu. \tag{D-7}$$

A program for the evaluation of function Z is furnished in appendix C in subroutine SUB Cross_ambiguity. The ratio of durations, R = L/T, must be input in line 420, and the coefficients $\{a_k\}$ and $\{b_\ell\}$ must be entered in lines 430 and 440, respectively; here, these coefficients are presumed to be real. Also, the number of nonzero coefficients in (32) and (33) is assumed to cover the range -3 to +3, but could be easily extended. The range of coefficients currently programmed in this subroutine is sufficient to encompass all the optimum cases presented in [3]. The particular $\{b_\ell\}$ example listed in line 440 corresponds to the low-pass modulation (see (33))

$$0+0+\frac{1}{2}\exp(-i2\pi t/L)+1+\frac{1}{2}\exp(i2\pi t/L)+0+0 =$$

$$= 1+\cos(2\pi t/L) \qquad \text{for } |t| < L/2 , \tag{D-8}$$

which is recognized as Hanning.

The linear-FM correlator complex envelope response is then given, according to (13), by

$$\underline{c}(t_r,f_r) = \frac{T}{\pi} \sum_d B_d \exp[-i\pi TW(x_r - x_d)(y_r - y_d)] \,*$$

$$* \; Z\Big(x_r - x_d,\ TW(y_r - y_d \mp (x_r - x_d)),\ L/T\Big) \; . \qquad \text{(D-9)}$$

A program for the calculation of the magnitude of $\underline{c}$ is also presented in appendix C, under the title Arbitrary Envelopes and Durations. The number of nonzero highlight strengths, $\{B_d\}$, is currently programmed at 5 in line 90, but is easily extended. The amplitudes and phases of $\{B_d\}$ are entered in lines 50 and 60, while the corresponding time delays and frequency shifts are inputted in lines 70 and 80.

REFERENCES

1. R. B. Blackman and J. W. Tukey, The Measurement of Power Spectra from the Point of View of Communications Engineering, Dover Publications, Inc., New York, 1959.
2. F. J. Harris, "On the Use of Windows for Harmonic Analysis with the Discrete Fourier Transform," Proc. IEEE, Vol. 66, No. 1, pp. 51-83, January 1978.
3. A. H. Nuttall, "Some Windows with Very Good Sidelobe Behavior," IEEE Trans. on Acoustics, Speech, and Signal Processing, Vol. ASSP-29, No. 1, pp. 84-91, February 1981. Also NUSC Technical Report 6239, 9 April 1980.

Technical Report 8075
17 August 1987

Operating Characteristics of Log-Normalizer for Weibull and Log-Normal Inputs

A. H. Nuttall

ABSTRACT

The false alarm and detection probabilities of a log-normalizer, subject to either log-normal or Weibull input statistics, are derived for general input signal and noise strengths and number of normalizer samples, N. Plots of the exceedance distribution function versus the threshold, as well as the receiver operating characteristics (i.e., detection probability P_D vs. false alarm probability P_F) are plotted for N=∞, 64, 32, 16 and for various values of the normalizer input deflection statistic d. In addition, simulation results, based on 8.4 million trials, are superposed for purposes of confirming or rejecting the theoretical results.

Plots of the exceedance distribution function are carried out on the extremes of the distribution, to the point where the tail probabilities are 1E-6. The receiver operating characteristics vary over the range of (P_F, P_D) equal to (1E-6, 1E-6) through (.5, .99). It is found that the theoretical analysis for the log normal input is exact for all N, whereas the approximate theoretical analysis for the Weibull input is sufficiently accurate only for large N, and not on the tails of the distribution.

TABLE OF CONTENTS

LIST OF ILLUSTRATIONS

LIST OF SYMBOLS

N	Number of normalizer samples, (2)
d	Normalizer input deflection, (29),(30)
P_D	Detection probability, (6)
P_F	False alarm probability, (6)
EDF	Exceedance Distribution Function
ROC	Receiver Operating Characteristic
x_n	Input to Log-Normalizer, figure 1
y_n	Normalizer input, figure 1, (1)
z	Normalizer output, figure 1, (4),(28)
y_0	Candidate signal-bearing sample, (4)
$\hat{\mu}(y)$	Sample mean of normalizer input, (2)
$\hat{\sigma}(y)$	Sample standard deviation of normalizer input, (3)
T	Threshold at normalizer output, (5)
w_n	Fundamental random variables, (7)
a,b	Arbitrary scaling and power law, (7)
p_w	Probability density function of random variable w, (8)
Q_w	Exceedance distribution function of random variable w, (9)
Φ	Cumulative distribution function of normalized Gaussian random variable, (12)
ϕ	Probability density function of normalized Gaussian random variable, (12)
$\tilde{v}_n$	Log distorted version of w_n, (16)
$\mu(\tilde{v})$	Mean of $\tilde{v}$, (17)
$\sigma(\tilde{v})$	Standard deviation of $\tilde{v}$, (17)
v_n	Normalized random variable, (17)
α,β	Constants, (19),(20)

LIST OF SYMBOLS (Cont'd)

$\hat{\mu}(v)$	Sample mean of normalized random variable, (24)
$\hat{\sigma}(v)$	Sample standard deviation of normalized random variable, (24)
v_0	Normalized signal-bearing random variable, (25)
η, ν	Constants, (27)
r	Normalizer input scaling parameter, (29),(30)
H_0	Hypothesis that signal is absent in y_0, (31)
m	Auxiliary constant = $(N-1)/2$, (36)
σ_N^2	Auxiliary variance = $r^2 + 1/N$, (37)
d_r'	Modified deflection parameter, (38),(39)
T_r'	Modified threshold, (38),(39)
$\tilde{\Phi}$	Inverse Φ function, (44)
t	Sample random variable, (46)
γ	Euler's constant = .57721, (49)
$\mu(t)$	Mean of random variable t, (50),(53)
$\sigma(t)$	Standard deviation of random variable t, (50),(54)
h_1, h_2	Auxiliary constants, (52)
ρ	Normalized correlation coefficient, (54),(55)
$\{x_n\}_1^N$	Sequence $x_1, x_2, \ldots, x_N$

OPERATING CHARACTERISTICS OF LOG-NORMALIZER FOR WEIBULL AND LOG-NORMAL INPUTS

INTRODUCTION

The detection of the presence of a weak signal of unknown location and strength in background noise of unknown strength is often accomplished by comparing a candidate signal-bearing detection sample of the observed process with a local estimate of the background level based on N samples of the (hopefully) noise-only process. The local neighborhood can be time, space, or frequency, depending on the application. In order to obtain a stable estimate of the background level, the number of samples, N, should be large; however, if the background is nonstationary, nonhomogeneous, or nonwhite, or if decision and processing time is at a premium, N should be kept as small as reasonably possible. The tradeoff between these conflicting requirements and the dependence on the number of normalizer samples, N, is of interest in this study. Related work is available in [1,2,3].

Since the performance of the normalizer procedure outlined above is adversely affected by the presence of any outliers or noise bursts anywhere in the total of N+1 samples used to make a decision about signal presence or absence in the candidate sample, some form of limiting device

should precede the normalization. The particular combination that we consider in detail here is depicted in figure 1, where ℓn is the natural

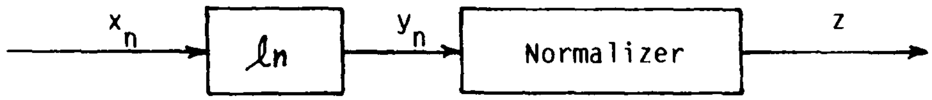

Figure 1. Log-Normalizer

logarithm. The logarithmic device tends to saturate at large input amplitudes and suppress their effect on the normalizer output z. The input sequence of random variables, $\{x_n\}$, (the detector output sequence), is presumed to be statistically independent and limited to positive values, giving logarithmic output

$$y_n = \ell n(x_n) \quad . \tag{1}$$

The particular normalizer we consider here is described as follows: call y_0 the candidate signal-bearing sample at the normalizer input, and let $y_1, y_2, \ldots, y_N$ be the N noise-only basis samples employed to extract an estimate of the background level at the normalizer input. Despite the notation, these N samples can (and probably will) surround the candidate sample y_0 in location, whether that be time, space, frequency, etc. The sample mean of the normalizer input noise-only samples is

$$\hat{\mu}(y) = \frac{1}{N} \sum_{n=1}^{N} y_n \quad , \tag{2}$$

while the corresponding sample standard deviation is defined as

$$\hat{\sigma}(y) = \left\{ \frac{1}{N-1} \sum_{n=1}^{N} [y_n - \hat{\mu}(y)]^2 \right\}^{1/2} . \tag{3}$$

The output of the normalizer in figure 1, that we consider here, is a deflection measure, namely

$$z = \frac{y_0 - \hat{\mu}(y)}{\hat{\sigma}(y)} . \tag{4}$$

The numerator of (4) is an estimate of the difference in means (at the normalizer input) of the candidate signal-plus-noise sample, relative to the noise-only samples; the denominator of (4) is a measure of the inherent fluctuation of the background noise. The dimensionless ratio in (4) eliminates the dependence on absolute levels in favor of relative levels.

The normalizer output z is compared with a threshold T, and a decision made about signal presence in sample y_0 according to the rule

$$\left. \begin{array}{ll} z > T: & \text{declare signal present in } y_0 \\ z < T: & \text{declare signal absent in } y_0 \end{array} \right\} . \tag{5}$$

It is desired to evaluate the false alarm probability and the detection probability, that is,

$$P_F = \text{Prob}\ (z > T \mid \text{signal absent in } y_0),$$

$$P_D = \text{Prob}\ (z > T \mid \text{signal present in } y_0). \tag{6}$$

Both of these probabilities in (6) are exceedance distribution functions, that is, probabilities that random variable z is greater than a threshold value T. We will be interested in plots of (6) versus T, for various signal-to-noise ratios, as well as in plots of P_D versus P_F, the latter known as the receiver operating characteristics.

The normalizer input random variables $\{y_n\}_1^N$ are statistically independent and identically distributed, since inputs $\{x_n\}_1^N$ have been presumed to have these properties. When signal is absent in candidate sample y_0, its probability density function will be taken identical to that of $\{y_n\}_1^N$; however, when signal is present in y_0, its probability density function can be arbitrary.

CLASSES OF INPUT VARIABLES

The noise-only input samples $\{x_n\}_1^N$ to the log-normalizer in figure 1 will be taken from the class of random variables that can be generated from fundamental independent identically-distributed random variables $\{w_n\}$ according to the rule

$$x_n = a\, w_n^b \text{ for } 1 \le n \le N; \qquad a > 0,\ b > 0,\ w_n > 0\ . \tag{7}$$

The probability density function p_w of $\{w_n\}$ is arbitrary; the total class of random variables defined by (7) is that yielded by allowing parameters a and b to be any positive constants (independent of n).

To fix this concept of a class of random variables, consider the case where w_n is a random variable with the fundamental exponential probability density function

$$p_w(u) = \exp(-u) \quad \text{for } u > 0\ . \tag{8}$$

Then the exceedance distribution function of w_n is

$$Q_w(u) = \text{Prob}(w > u) = \int_u^\infty dv\ p_w(v) = \exp(-u) \quad \text{for } u > 0\ . \tag{9}$$

It then follows from (7) that the exceedance distribution function of x_n is

$$Q_x(u) = \text{Prob}(x > u) = \text{Prob}(a\, w^b > u) =$$

$$= \text{Prob}\left(w > (u/a)^{1/b}\right) = Q_w\left(\left(\frac{u}{a}\right)^{1/b}\right) = \exp\left[-\left(\frac{u}{a}\right)^{1/b}\right] \quad \text{for } u > 0 \,. \tag{10}$$

But this is just the exceedance distribution function of a Weibull variate* with shape factor 1/b and scaling $(1/a)^{1/b}$. Thus, the class of random variables that can be generated via (7) with arbitrary a,b, from the fundamental exponential probability density function in (8), is the general class of Weibull variates, as given by (10). (If b = 1/2, x is a Rayleigh variate, for example.)

As a second case, let w_n be a random variable with the fundamental log-normal exceedance distribution function

$$Q_w(u) = \Phi(-\ln u) \quad \text{for } u > 0 \,, \tag{11}$$

where

$$\Phi(t) \equiv \int_{-\infty}^{t} ds\, (2\pi)^{-1/2} \exp(-s^2/2) \equiv \int_{-\infty}^{t} ds\, \phi(s) \tag{12}$$

is the cumulative distribution function of a normalized Gaussian random variable. Then by an analogous procedure to (10), the exceedance distribution function of the random variable x_n generated according to (7) is

---

*See appendix A.

$$Q_x(u) = Q_w\left(\left(\frac{u}{a}\right)^{1/b}\right) = \Phi\left(\frac{\ell n(a) - \ell n(u)}{b}\right) \quad \text{for } u > 0 , \tag{13}$$

which is the exceedance distribution function of a general log-normal variate with additive factor $\ell n(a)$ and scaling $1/b$. The probability density function corresponding to (13) is

$$p_x(u) = \frac{1}{bu}\,\phi\left(\frac{\ell n(a) - \ell n(u)}{b}\right) \quad \text{for } u > 0 , \tag{14}$$

where ϕ was defined in (12). Thus, the class of random variables that can be generated via (7) with arbitrary a,b, from the fundamental log-normal exceedance distribution function in (11), is the general class of log-normal variates, as given by (13) and (14).

Returning to the general case for fundamental random variable w_n now, the output of the logarithmic device, (1), is given, upon use of (7), as

$$y_n = \ell n(x_n) = \ell n\ a + b\ \ell n\ w_n = \ell n\ a + b\ \tilde{v}_n \quad \text{for } 1 \le n \le N , \tag{15}$$

where we define

$$\tilde{v}_n = \ell n\ w_n . \tag{16}$$

Let the mean and standard deviation of $\tilde{v}_n$ be denoted by $\mu(\tilde{v})$ and $\sigma(\tilde{v})$, respectively. Then form the normalized random variable

$$v_n = \frac{\tilde{v}_n - \mu(\tilde{v})}{\sigma(\tilde{v})} \quad \text{for } 1 \le n \le N \,, \tag{17}$$

which has mean 0 and standard deviation 1. Substitution of (17) in (15) then yields log output

$$y_n = \alpha + \beta \, v_n \quad \text{for } 1 \le n \le N \,, \tag{18}$$

where constants

$$\alpha = \ln a + b \, \mu(\tilde{v}) \,, \quad \beta = b \, \sigma(\tilde{v}) \,. \tag{19}$$

A direct useful interpretation of these two constants in (19) follows directly from (18); namely, since $\{v_n\}$ are normalized random variables,

$$\alpha = \mu(y), \quad \beta = \sigma(y) \,. \tag{20}$$

These are fundamental statistics of the input to the normalizer in figure 1.

Equations (18) and (19) demonstrate that the output of the logarithmic device in figure 1, for general parameters a,b and random variables $\{w_n\}_1^N$ in transformation (7), can be handled through the linear transformation (18) of a normalized random variable, v_n, with zero mean and unit standard deviation. The new general parameters α,β are given by (19) or (20), where the required statistics are mean

$$\bar{\tilde{v}} = \mu(\tilde{v}) = \mu(\ln w) = \int du \, \ln(u) \, p_w(u) \quad , \tag{21}$$

and mean square

$$\overline{\tilde{v}^2} = \overline{(\ln w)^2} = \int du \, (\ln u)^2 \, p_w(u) \quad , \tag{22}$$

in terms of the probability density function of input variable w_n in figure 1. Also, except for the specified zero mean and unit standard deviation of v_n in (18), the statistics of v_n are completely arbitrary. Thus, we can use form (18) for the <u>general</u> normalizer input in the following, where α and β are arbitrary constants.

When we now employ (18), the sample quantities in (2) and (3) become

$$\hat{\mu}(y) = \alpha + \beta \, \hat{\mu}(v) \quad ,$$

$$\hat{\sigma}(y) = \beta \, \hat{\sigma}(v) \quad , \tag{23}$$

where

$$\hat{\mu}(v) = \frac{1}{N} \sum_{n=1}^{N} v_n \quad ,$$

$$\hat{\sigma}(v) = \left\{ \frac{1}{N-1} \sum_{n=1}^{N} \left[v_n - \hat{\mu}(v) \right]^2 \right\}^{1/2} \quad . \tag{24}$$

in terms of the normalized random variables $\{v_n\}_1^N$.

As noted in the paragraph following (6), the probability density function of random variable y_o is arbitrary for the signal-present hypothesis. Without loss of generality, let

$$y_o = \eta + \upsilon\, v_o \; , \tag{25}$$

where normalized random variable v_o has

$$\mu(v_o) = 0, \quad \sigma(v_o) = 1 \; . \tag{26}$$

The constants η and υ absorb the absolute scale of y_o; in fact (in analogy with (20)),

$$\eta = \mu(y_o), \quad \upsilon = \sigma(y_o) \; . \tag{27}$$

When we now combine (23) and (25) in the normalizer output z, as given by (4), there follows

$$z = \frac{d + rv_o - \hat{\mu}(v)}{\hat{\sigma}(v)} \; , \tag{28}$$

where constants

$$d = \frac{\eta - \alpha}{\beta} \; , \qquad r = \frac{\upsilon}{\beta} \; . \tag{29}$$

Thus, the general output z of the log-normalizer in figure 1, for the general class of inputs (7), can be expressed in the form (28) involving two fundamental constants d, r in (29); an arbitrary normalized random variable v_0; and the sample mean and standard deviation of the normalized random variables $\{v_n\}_1^N$ according to (24).

A useful physical interpretation of the constants in (29) is afforded by utilizing (20) and (27), namely

$$d = \frac{\mu(y_0) - \mu(y)}{\sigma(y)} , \qquad r = \frac{\sigma(y_0)}{\sigma(y)} . \tag{30}$$

Thus, parameter d measures the deflection criterion at the normalizer input, relative to the standard deviation for signal absent. The parameter r is a scaling quantity reflecting the relative fluctuating strengths at the normalizer input. The fundamental analysis problem is now to evaluate the false alarm and detection probabilities specified by (6), for the output random variable given by (28), where d and r are arbitrary constants, and v_0 and $\{v_n\}_1^N$ are normalized random variables.

CONSTANT FALSE ALARM RATE PROPERTY

The general output of the log-normalizer is given by (28). However, for hypothesis H_0 where signal is absent in candidate signal-bearing sample y_0, the statistics of normalizer input y_0 are identical to those of $\{y_n\}_1^N$, as noted in the paragraph under (6). In this case, (30) obviously reduces to

$$d = 0, \quad r = 1 \qquad \text{under } H_0 , \tag{31}$$

and (28) yields

$$z = \frac{v_0 - \hat{\mu}(v)}{\hat{\sigma}(v)} \qquad \text{under } H_0 , \tag{32}$$

in terms of the independent identically-distributed normalized random variables v_0 and $\{v_n\}_1^N$.

Since v_n in (17) is the normalized random variable corresponding to logarithmic distortion (16) of fundamental random variable w_n, and does not involve a or b, all scale factors involving constants a and b in (7) have disappeared in output z in (32), under hypothesis H_0. This means that the false alarm probability P_F in (6) cannot depend on a,b; put another way, the false alarm probability for the log-normalizer of figure 1, subjected to

the class of inputs given by (7), is the <u>same</u> for all members of the class, regardless of the values of a and b. Since the sample mean and sample standard deviation in (32) still depend on N, as seen by reference to (24), the false alarm probability will necessarily be a function of N, as well as depend on the <u>particular</u> probability density function of independent identically-distributed normalized random variables v_o and $\{v_n\}$. However, in general, there will be no need to investigate the false alarm probability for the general Weibull class in (10), but instead we can confine attention to the fundamental exponential probability density function of w_n as given by (8). Of course, v_n must then be the normalized random variable, as given by (16), (17), (21), and (22). More details on the statistics of Weibull variates and their logarithmically-distorted counterparts are given in appendix A.

A similar statement can be made with regard to the fundamental log-normal exceedance distribution function given by (11). In fact, the logarithmically transformed input, (16), to the normalizer has exceedance distribution function

$$Q_{\tilde{v}}(u) = \mathrm{Prob}(\tilde{v} > u) = \mathrm{Prob}(\ln w > u) = \mathrm{Prob}(w > \exp(u)) =$$

$$= Q_w(\exp(u)) = \Phi(-u) \quad \text{for all } u \,. \tag{33}$$

But this is the exceedance distribution function of a zero-mean unit variance Gaussian random variable. Thus, $\tilde{v}$ of (16) is already a normalized random variable, and Gaussian at that. Therefore, decision

variable z in (32) involves a collection of N+1 independent identically-distributed zero-mean unit-variance random variables v_0 and $\{v_n\}_1^N$. Again, the false alarm probability can only depend on N, and not on scale factors a and b in (13) and (14). Of course, the detection probability (6), as applied to (28), will depend additionally on parameters d and r in (29) and (30).

In summary, the log-normalizer in figure 1 will possess constant false alarm rate properties, that is, the same false alarm probability for all the members of the class of random variables generated according to (7), regardless of the values of a and b.

PERFORMANCE FOR LOG-NORMAL INPUT X

The problem of interest in this section is the evaluation of detection probability (6) for the decision variable z given by (28), when normalized random variables $\{v_n\}_1^N$ are independent identically-distributed zero-mean unit-variance Gaussian random variables; this is the case discussed in (33) et seq. Although the probability density function of normalized random variable v_0 is arbitrary, we will also take it here to be zero-mean unit-variance Gaussian. Reference to (15), (17), and (25) reveals that this is tantamount to assuming that the normalizer input $\{y_n\}_1^N$ in figure 1 is Gaussian with arbitrary mean and variance, while y_0 is also Gaussian with different arbitrary mean and variance. All these arbitrary parameters are collected together in (28) in the parameters d and r, according to (30). This situation is also equivalent to assuming log-normal excitations at the input of the log-normalizer of figure 1.

From (6) and (28), since $\hat{\sigma} > 0$,

$$P_D = \text{Prob}(z > T) = \text{Prob}\left(d + rv_0 - \hat{\mu}(v) > T\,\hat{\sigma}(v)\right) , \tag{34}$$

where $\hat{\mu}(v)$ and $\hat{\sigma}(v)$ are given by (24). It is shown in appendix B that $\hat{\mu}(v)$ and $\hat{\sigma}(v)$ are statistically independent, with probability density functions given by (B-16) and (B-20), respectively, (setting $\mu = 0$, $\sigma = 1$) as

$$p_\mu(u) = (2\pi/N)^{-1/2} \exp(-\frac{N}{2} u^2) \text{ for all } u \tag{35}$$

and

$$p_\sigma(u) = \frac{2\, m^m\, u^{2m-1} \exp(-mu^2)}{\Gamma(m)} \quad \text{for } u > 0; \quad m = \frac{N-1}{2} . \tag{36}$$

Now the quantity $d + rv_0 - \hat{\mu}(v)$ in (34) is a Gaussian random variable with mean d and variance $r^2 + 1/N \equiv \sigma_N^2$; see (B-16) or (35). Considering $\hat{\sigma}$ fixed for the moment, the conditional detection probability in (34) is then

$$P_{DC} = \int_{T\hat{\sigma}}^{\infty} dt \left(2\pi\sigma_N^2\right)^{-1/2} \exp\left[-\frac{(t-d)^2}{2\sigma_N^2}\right] = \Phi\left(\frac{d - T\hat{\sigma}}{\sigma_N}\right) , \tag{37}$$

upon use of (12). Averaging this result over the probability density function (36) of $\hat{\sigma}$, we have the unconditional detection probability

$$P_D = \int_0^{\infty} du\; \Phi\left(\frac{d - Tu}{\sigma_N}\right) \frac{2\, m^m\, u^{2m-1} \exp(-mu^2)}{\Gamma(m)} =$$

$$= \int_0^{\infty} dw\; \frac{w^{N-2} \exp(-w^2/2)}{2^{\frac{N-3}{2}}\, \Gamma\left(\frac{N-1}{2}\right)}\; \Phi(d_r' - T_r' w) , \tag{38}$$

where $N \geq 2$ and

$$d_r' \equiv \frac{d}{\sigma_N} = \frac{d}{\sqrt{r^2 + 1/N}},$$

$$T_r' \equiv \frac{T}{\sqrt{N-1}\,\sigma_N} = \frac{T}{\sqrt{N-1}\sqrt{r^2 + 1/N}}. \tag{39}$$

The fundamental parameters upon which P_D depends are

N, number of normalizer samples;

T, threshold at normalizer output;

d, deflection criterion (30);

r, scaling (30) . (40)

However, they show up, in integral result (38), collapsed into the three variables N, d_r', T_r'.

For signal absent, we have $d=0$ and $r=1$, as noted in (31). Then (38) and (39) reduce to the false alarm probability

$$P_F = \int_0^\infty dw \; \frac{w^{N-2} \exp(-w^2/2)}{2^{\frac{N-3}{2}} \Gamma\left(\frac{N-1}{2}\right)} \; \Phi\left(-T\sqrt{\frac{N}{N^2-1}}\, w\right) , \tag{41}$$

which depends only on N and T. Thus, given a particular number N of normalizer samples, threshold T can be selected to realize a specified value of false alarm probability P_F. This applies for the complete class of log-normal inputs, (13) or (14), into the log-normalizer in figure 1, and can be achieved without knowledge of a or b.

As $N \to \infty$, we have

$$\hat{\sigma} \to 1, \quad \sigma_N \to r \qquad \text{as } N \to \infty , \tag{42}$$

giving from (37),

$$P_D = \Phi\left(\frac{d - T}{r}\right), \qquad P_F = \Phi(-T) \qquad \text{for } N = \infty. \tag{43}$$

This yields

$$\tilde{\tilde{\Phi}}(P_D) = \frac{1}{r}\left[d + \tilde{\tilde{\Phi}}(P_F)\right] \qquad \text{for } N = \infty, \tag{44}$$

where $\tilde{\tilde{\Phi}}$ is the inverse Φ-function; this last result is useful for plotting receiver operating characteristics on normal-probability paper. It illustrates that for $N = \infty$, those curves are straight lines with slope $1/r$ and offset d/r at $P_F = .5$.

The actual numerical evaluations of false alarm probability (41) and detection probability (38) are undertaken in appendix C. The inputs to the functions considered there are the 3 parameters N, T_r', d_r' as given by (39), rather than the 4 fundamental parameters N,T,d,r listed in (40). This is no limitation, since for any given values of N,T,d,r, the quantities N, T_r', d_r' can be easily calculated via (39) and used as inputs to the procedures in appendix C.

PERFORMANCE FOR WEIBULL INPUT

Here we want to evaluate detection probability (6) for the decision variable z given by (28), when normalized random variables $\{v_n\}_1^N$ are independent identically-distributed zero-mean unit-variance log-distorted Weibull variates. Before we do that, we observe that detection probability (6) can be expressed generally as

$$P_D = \text{Prob}(z > T) = Q_z(T) = \text{Prob}\left(\frac{d + rv_0 - \hat{\mu}(v)}{\hat{\sigma}(v)} > T\right) =$$

$$= \text{Prob}\left(v_0 > \frac{t - d}{r}\right) = \int du \; Q_{v_0}\left(\frac{u - d}{r}\right) p_t(u) \; , \qquad (45)$$

where we used (28) and defined random variable

$$t = \hat{\mu}(v) + T\,\hat{\sigma}(v) \qquad (46)$$

in terms of the sample quantities in (24). The separation of functions in the last form in (45) is due to the fact that random variables v_0 and t are statistically independent of each other. When signal is absent, then $d = 0$, $r = 1$ according to (31), and (45) reduces to false alarm probability

$$P_F = \int du \; Q_{v_0}(u) \; p_t(u) \; . \qquad (47)$$

In the special case where $N \to \infty$, that is, a very large number of samples used in the normalizer, the sample quantities in (24) approach the true mean 0 and standard deviation 1 of normalized random variables $\{v_n\}$, and t tends to the constant 1. Then (45) and (47) reduce to

$$P_D = Q_{v_o}\left(\frac{T - d}{r}\right), \qquad P_F = Q_{v_o}(1) \qquad \text{for } N = \infty. \tag{48}$$

This limiting case can be used as a comparison with practical cases where N is large, but not infinite.

We now specialize the above general results to the case of log-distorted Weibull variates $\{v_n\}_1^N$. Although the probability density function of normalized random variable v_o is arbitrary, we will also take it here to be a normalized log-distorted Weibull variate. In this case, the exceedance distribution function of random variable v_o is given by (A-17) as

$$Q_v(u) = \exp\left[-\exp\left(-\gamma + \frac{\pi}{\sqrt{6}}\,u\right)\right] \quad \text{for all } u \;, \tag{49}$$

where $\gamma = .57721$ is Euler's constant. Thus, the detection and false alarm probabilities for $N = \infty$, as given generally by (48), are immediately available upon use of (49).

The probability density function of random variable t defined in (46) is a much more difficult task for finite N. To make any analytic progress, we have had to assume that t is Gaussian; this can be expected to be a fair approximation if the number of normalizer samples N entering the sample

quantities in (24) is large, according to the central limit theorem. However, we can anticipate that the approach of random variable t to normality will be faster near its mean, but considerably slower on the tails. This can lead to a significant bias in the calculation of small false alarm probabilities.

Thus, our assumption is that the probability density function of t in (46) is given by

$$p_t(u) = [2\pi\ \sigma^2(t)]^{-1/2} \exp\left[-\frac{(u-\mu(t))^2}{2\ \sigma^2(t)}\right]. \tag{50}$$

Combining (49) and (50) in (45), the detection probability is given (approximately) by

$$P_D = \int du \exp\left[-\exp\left(-\gamma + \frac{\pi}{\sqrt{6}}\frac{u-d}{r}\right)\right] *$$

$$* \left[2\pi\ \sigma^2(t)\right]^{-1/2} \exp\left[-\frac{(u-\mu(t))^2}{2\ \sigma^2(t)}\right] =$$

$$= (2\pi)^{-1/2} \int dx \exp\left[-\frac{x^2}{2} - \exp\left(h_1 + h_2\ x\right)\right] , \tag{51}$$

where constants

$$h_1 = -\gamma + \frac{\pi}{\sqrt{6}}\frac{\mu(t)-d}{r} , \qquad h_2 = \frac{\pi}{\sqrt{6}}\frac{\sigma(t)}{r} . \tag{52}$$

The false alarm probability follows upon setting $d = 0$, $r = 1$ in (52).

The fundamental parameters in integral result (51) are d and r, along with mean $\mu(t)$ and standard deviation $\sigma(t)$ of random variable t. The

complexity of random variable t, defined by (46) and (24), precludes us from evaluating mean $\mu(t)$ and standard deviation $\sigma(t)$ exactly. However, numerous simulations, each consisting of 100,000 trials, enabled us to extract the following rather accurate rules of thumb for the statistics of t.

First of all, for general definition (46), we have mean

$$\mu(t) = \mu\left\{\hat{\mu}(v)\right\} + T\,\mu\left\{\hat{\sigma}(v)\right\} , \tag{53}$$

and variance

$$\sigma^2(t) = \sigma^2\left\{\hat{\mu}(v)\right\} + T^2\,\sigma^2\left\{\hat{\sigma}(v)\right\} + 2T\,\sigma\left\{\hat{\mu}(v)\right\}\sigma\left\{\hat{\sigma}(v)\right\}\rho , \tag{54}$$

where ρ is the normalized correlation coefficient between $\hat{\mu}(v)$ and $\hat{\sigma}(v)$.

The simulation results alluded to above, for normalized random variables $\{v_n\}$ in (24) being log-distorted Weibull variates, are given by

$$\mu\left\{\hat{\mu}(v)\right\} = 0 \qquad \mu\left\{\hat{\sigma}(v)\right\} \cong 1 - \frac{.39}{N}$$

$$\sigma^2\left\{\hat{\mu}(v)\right\} = \frac{1}{N} \qquad \sigma^2\left\{\hat{\sigma}(v)\right\} \cong \frac{1.05}{N + 1.5}$$

$$\rho \cong -.55 . \tag{55}$$

Observe the large value of ρ, in contrast with the earlier case of a Gaussian input to the normalizer, where the sample mean and sample standard deviation were not only uncorrelated but in fact independent; see appendix B.

The quantities in (55) depend solely on N; when used in (53) and (54), it is seen that $\mu(t)$ and $\sigma(t)$ in (54) depend on both N and threshold T. Thus, the totality of fundamental parameters of relevance in detection probability (51) is d,r,N,T, just as for the Gaussian case in (40). Analytic evaluation of integral (51) is impossible; accordingly, numerical integration was employed.

An alternative approximation to the statistics of random variable t of (46) is undertaken in appendix D. Namely, for large threshold values T, where random variable t is dominated by sample standard deviation $\hat{\sigma}(v)$, it might be thought that a χ-approximation would have wider applicability than a Guassian one. This is indeed true, as will be demonstrated by the numerical results to follow; however, for small false alarm probabilities, the χ-approximation also falls short.

GRAPHICAL RESULTS

In this section, we will present graphical results for the exceedance distribution functions and receiver operating characteristics for both the Gaussian and the log-distorted Weibull inputs to the normalizer in figure 1. This corresponds, respectively, to log-normal and Weibull inputs (that is, detector outputs) to the logarithmic device in figure 1. The theoretical results of the previous two sections are augmented by simulation results, each based upon $2^{23} = 8.4$ million trials of decision variable (normalizer output) z given by (28) and (24).

The scaling parameter r, that is, the ratio of standard deviations in (30), is taken at 1 for all these results, in order to keep the number of plots at a reasonable level. The deflection parameter d in (30) is varied from 0 to values large enough to sweep out the important range of detection and false alarm probabilities of interest. The number of normalizer samples, N, is taken at the values ∞, 64, 32, 16, which appears to cover the most important range of practical use. Threshold value I in exceedance probabilities (6) is allowed to vary widely, so that the full range of detection and false alarm probabilities can be observed.

GAUSSIAN INPUT TO NORMALIZER

The exceedance distribution function (EDF), defined in (6), for $N=\infty$ is plotted in figure 2 versus threshold T, for deflection parameter d taking on values

$$d = 0(1)9 = 0,1,2,3,4,5,6,7,8,9 \ . \tag{56}$$

The arrow on the figure indicates the direction of increasing d; thus d=0, which is the false alarm probability, corresponds to the curve at the lower left. The results in figure 2 are based on (43); since the ordinate is according to a normal probability rule, these curves are perfectly straight lines. Exceedance probabilities ranging from 1E-6 to .999999 are covered when threshold T is varied over the range -5,5.

When N takes on the values 64, 32, 16, the corresponding results are displayed in figures 3, 4, 5, respectively. These graphs were obtained from (38)-(41), implemented by the procedures in appendix C. The exceedance distribution function for N=64 in figure 3 is fairly close to that for $N=\infty$ in figure 2; however, by the time the number of normalizer samples N has decreased to 16 in figure 5, significant curvature has developed in the results.

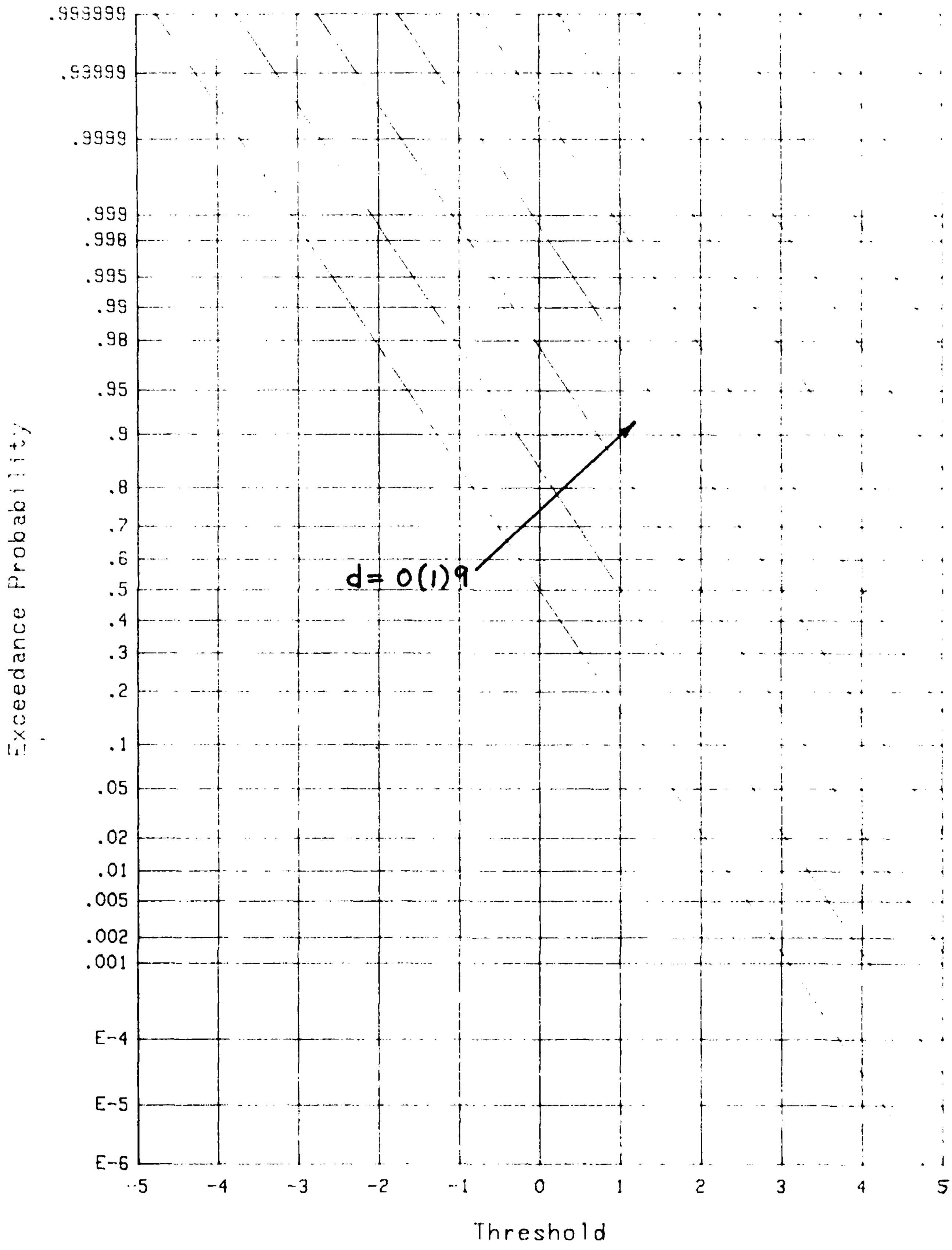

Figure 2. EDF for N = ∞; Gaussian

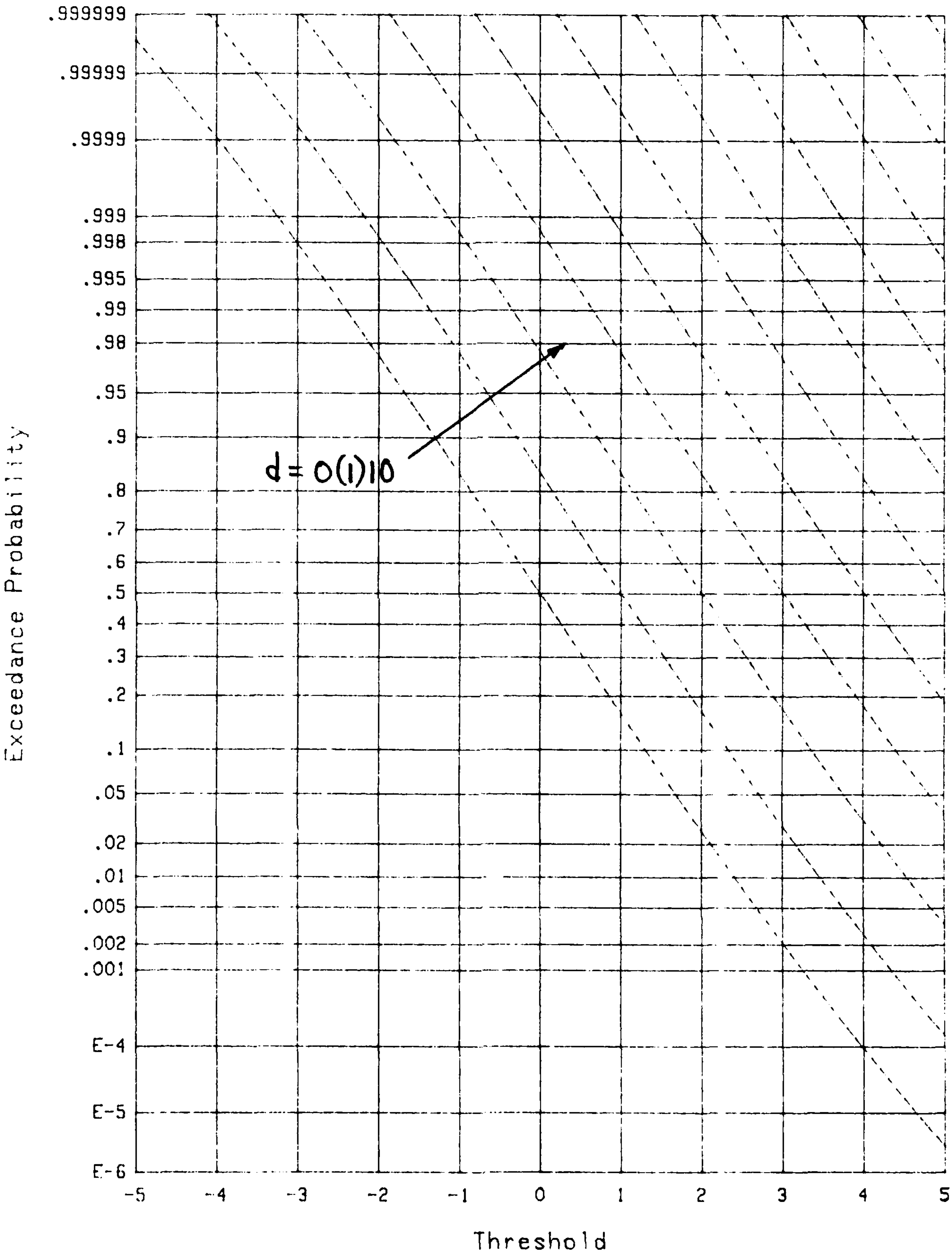

Figure 3. EDF for N = 64; Gaussian

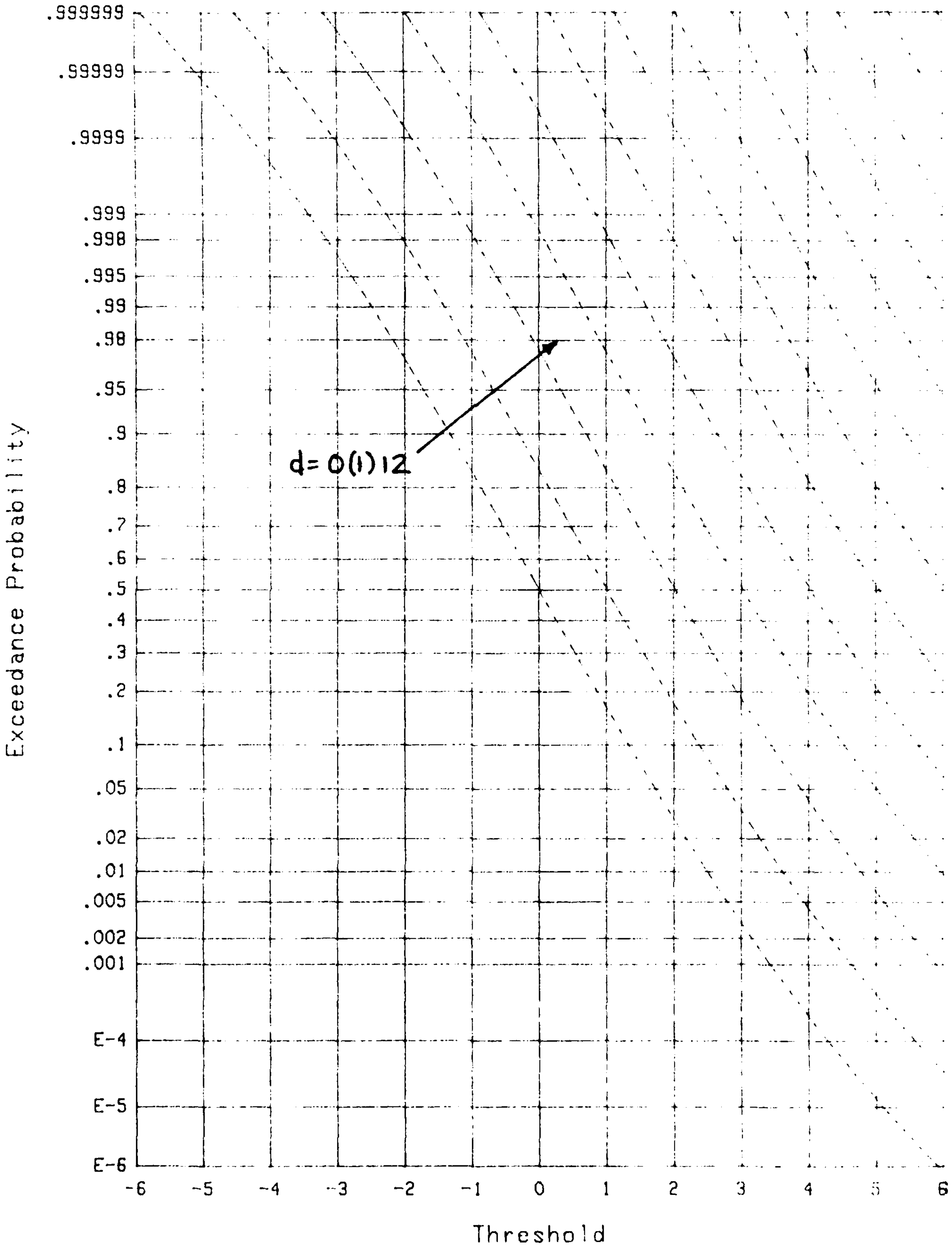

Figure 4. EDF for N = 32; Gaussian

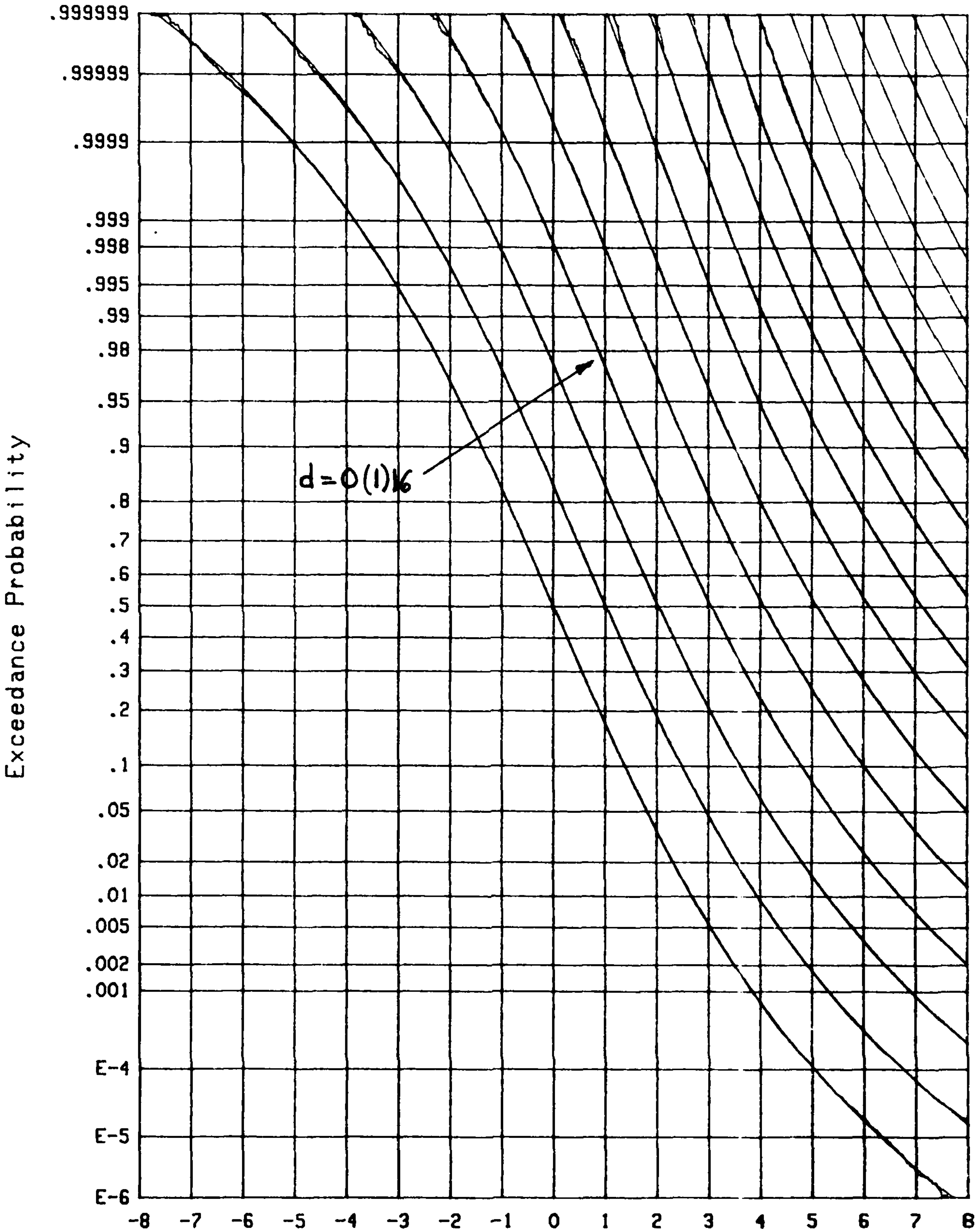

Figure 5. EDF for N = 16; Gaussian

Superposed in figure 5 are 11 simulation results for d=0(1)10, each based upon 8.4 million independent trials. Due to the large number of trials, the theoretical and simulation results are indistinguishable, except near the extremes of probability 1E-6 and .999999, where the jagged character of simulation results is manifested. This close agreement of results not only confirms the theoretical analysis but also lends credence to the use of simulation for the estimation of probabilities out on the tails of the distribution, provided that enough trials are conducted.

Figures 3, 4, 5 furnish information which enables the selection of the required threshold T to realize a specified false alarm probability for N = 64, 32, 16, respectively. For example, figure 5 with d = 0 indicates that to realize a false alarm probability of 1E-5 for N = 16, threshold T in (6) must be chosen as 6.3.

When threshold T is eliminated, and the detection probability plotted versus the false alarm probability, we obtain the receiver operating characteristics (ROC). The result for $N=\infty$ is given in figure 6, where both the abscissa and ordinate are plotted according to a normal probability scale. Deflection parameter d varies over the range

$$d = 0(.5)7.5 = 0,.5,1,1.5,\ \ldots,\ 7,7.5\ . \tag{57}$$

The arrow again points in the direction of increasing d; thus d=0 is the curve on the lower right. These curves are precisely the straight lines indicated by (44) with r=1.

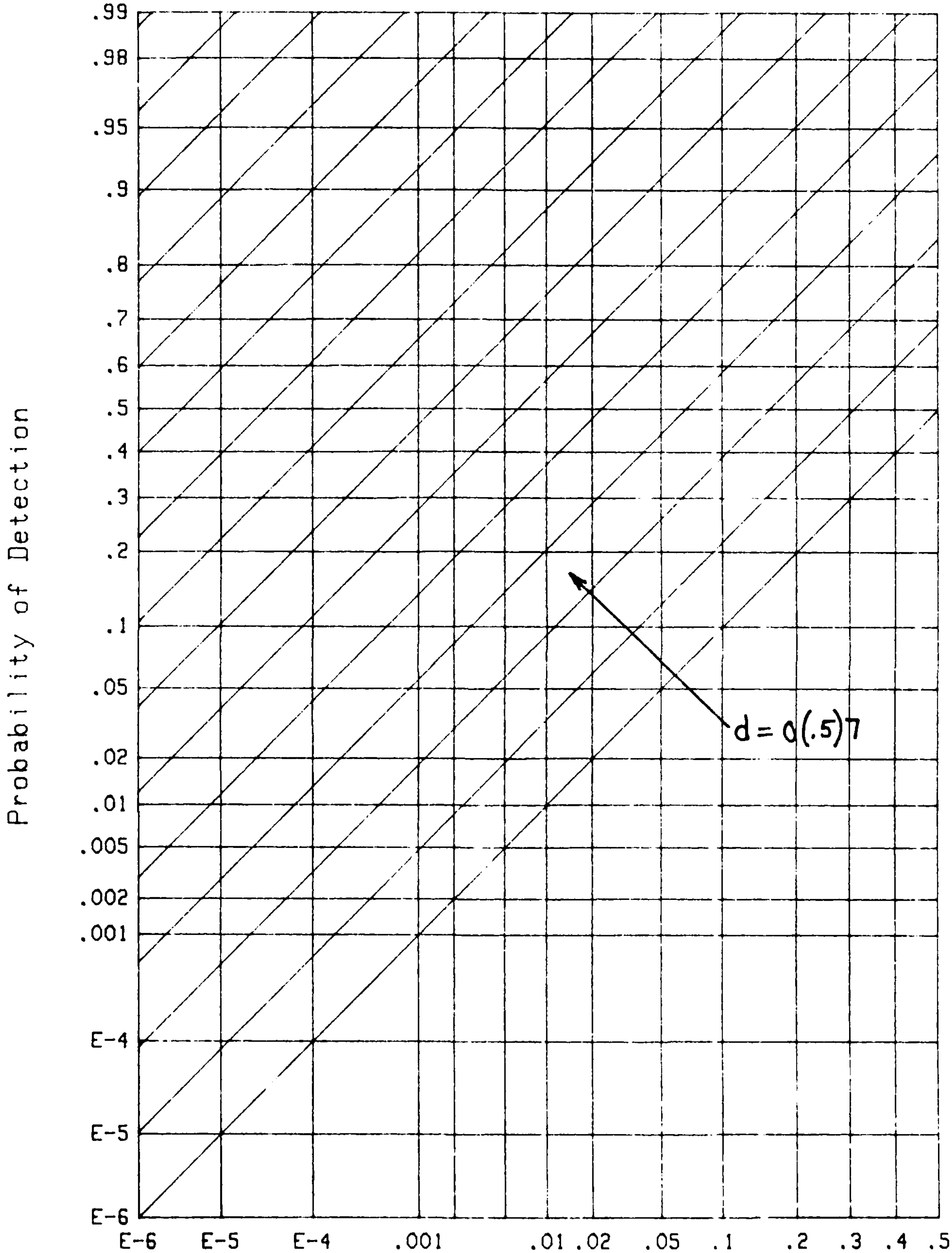

Figure 6. ROC for N = ∞; Gaussian

Corresponding receiver operating characteristics for N = 64, 32, 16 are presented in figures 7, 8, 9. The detection and false alarm probabilities both range down to 1E-6, while the upper limits have been truncated at .99 and .5, respectively. Values beyond these limits can be obtained from the earlier figures 2 through 5.

Superposed in figure 9 are ten simulation results for d = 1(1)10. Again, except for the small probability regions like $P_F < 1E-5$, the theoretical and simulation results are indistinguishable and overlay each other. It will be noticed that a characteristic wiggle in the receiver operating characteristics is duplicated for every simulation result, at a constant value of false alarm probability; for example, see the triangular bump in all 10 simulation results at $P_F \approx 1E-6$. The reason for this behavior is that when random variable z in (28) was simulated, the random numbers employed in (24) to generate $\hat{\mu}$ and $\hat{\sigma}$ were not changed when different d values were considered in (28). The reason for this deliberate choice was economy of computer execution time; that is, the time-consuming task of computation of (24) was done once for each trial, and used in (28) for all of the d values of interest. This repeated use of the same $\hat{\mu},\hat{\sigma}$ values for different d values gives a persistent systematic perturbation to the estimated receiver operating characteristics at a fixed false alarm probability. However, for 8.4 million trials, this bias is small, even for the rare events with probabilities greater than 1E-6, and was deemed acceptable in light of the greatly increased computer time required for the alternative approach of regeneration of $\hat{\mu}$ and $\hat{\sigma}$.

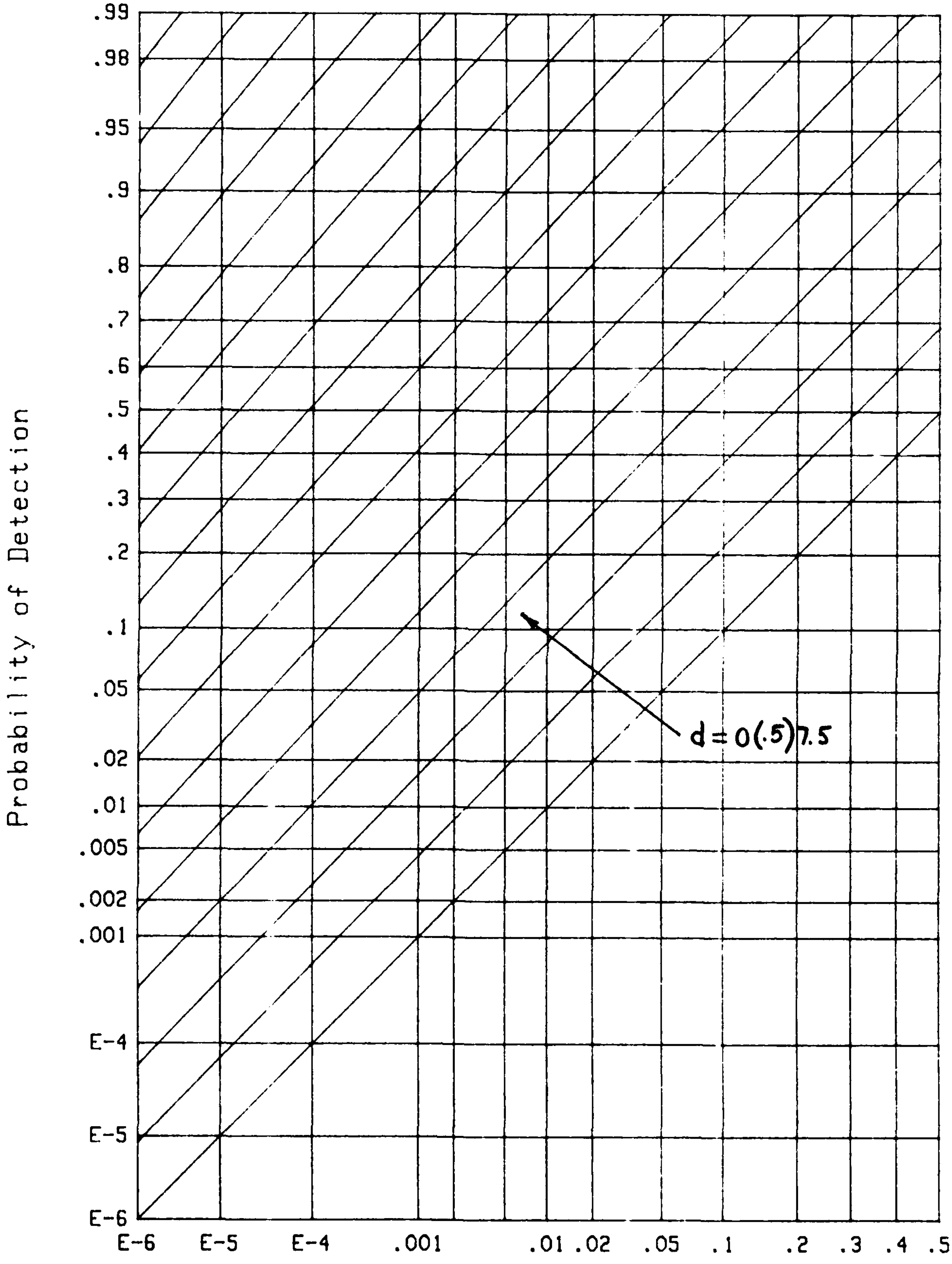

Figure 7. ROC for N = 64; Gaussian

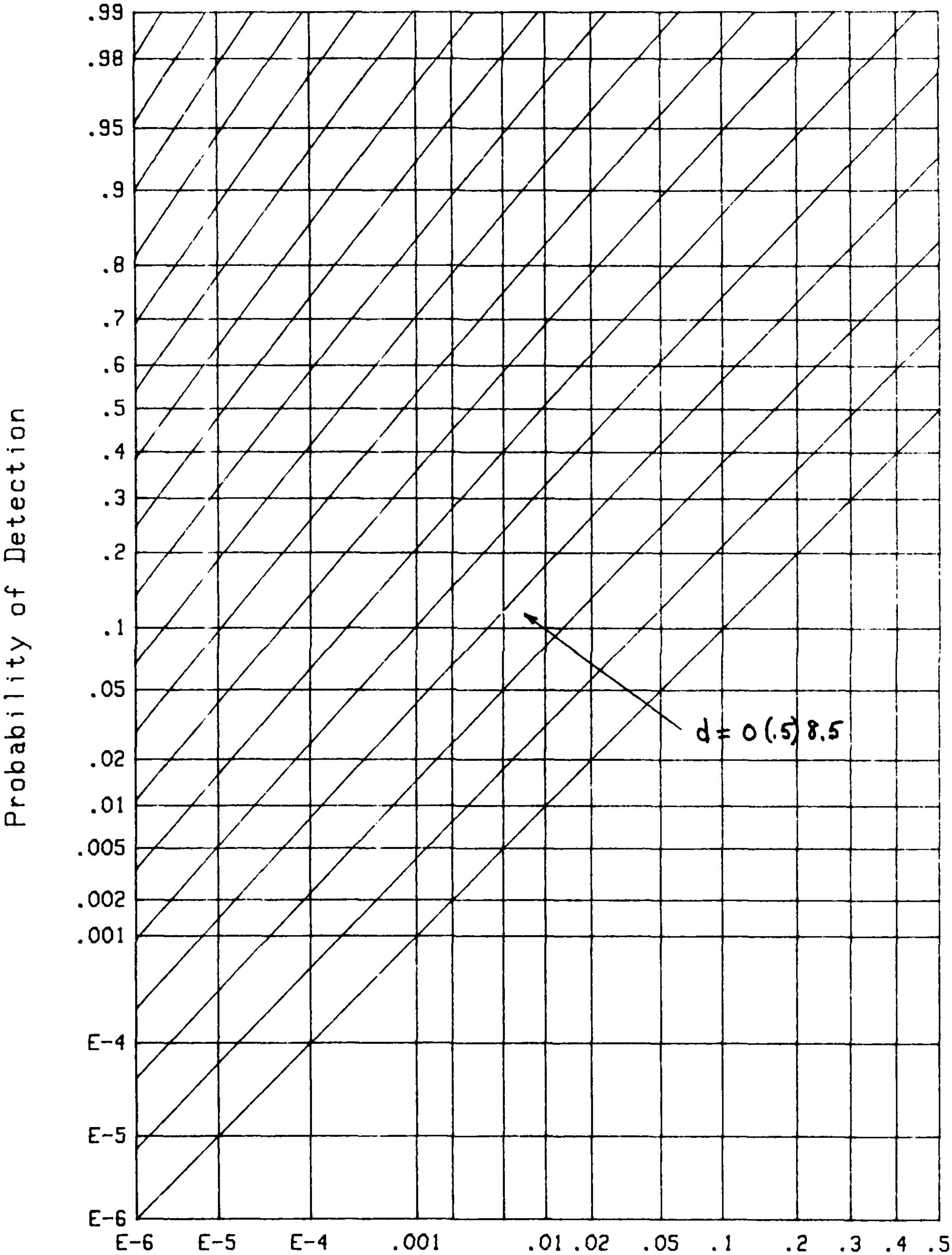

Figure 8. Probability of False Alarm

ROC for N = 32; Gaussian

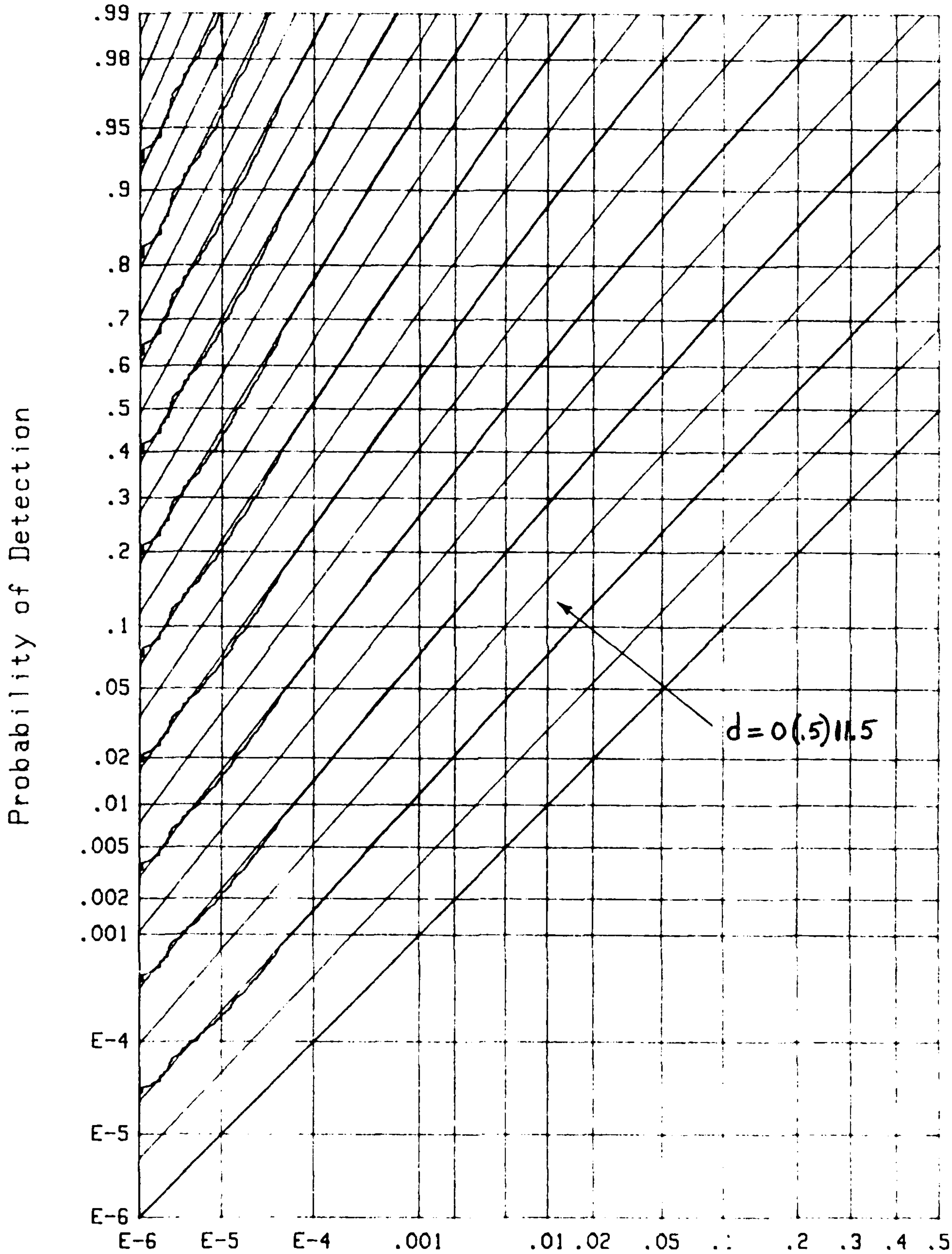

Figure 9. Probability of False Alarm
ROC for N = 16; Gaussian

As an example of the use of figures 6 through 9, the values of deflection d required to realize $P_F = 1E{-}5$ and $P_D = .5$ are

$$d = 4.3,\ 4.7,\ 5.1,\ 6.2 \quad \text{for } N = \infty,\ 64,\ 32,\ 16\ , \tag{58}$$

respectively. The cost of reducing N from ∞ to 16 is that d must be increased by the factor 6.2/4.3 = 1.44; whether this is tolerable depends on the application. The relation of deflection parameter d to any system input signal-to-noise ratio depends on the particular processor form preceding the logarithmic device in figure 1, and must be left to the user and his particular application.

LOG-WEIBULL INPUT TO NORMALIZER

When the input to the normalizer is a log-distorted Weibull variate, the performance is markedly different. The exceedance distribution function for $N = \infty$ is displayed in figure 10 and has a significant curvature when plotted on normal probability paper; these results are based upon the use of (48) and (49). The use of the notation 'Extreme' is explained in (A-7) et seq.

When N is decreased to 64, the corresponding exceedance distribution functions are given in figure 11. Due to the questionable assumptions required in the theoretical analysis of this case and used in (50) et seq., simulation results were also superposed for the values d = 0(.5)5. Agreement in the mid-range of probabilities is excellent. At the low end of the probability range, near 1E-6, the simulation results indicate a systematically lower exceedance probability than predicted by theory.

This erratic trend of the theoretical approximation is continued and accented in figure 12 for N=32 and in figure 13 for N=16. In fact, in the latter case, for threshold T=5, the simulation indicates exceedance probabilities for d=0 that are more than 2 orders of magnitude smaller than the theory predicts; see bottom right of figure 13. The discrepancies at the high end of probabilities are also considerable, as seen at the top left of the figure.

Also added to this particular figure is the result of using the χ-approximation for random variable t of (46), as detailed in appendix D. Although the improvement in probability values is over an order of magnitude, there is still another order of magnitude error left in this alternative approximate approach. The reason for the difficulty in the theoretical analysis is two-fold: (1) values of N like 16 or 32 are not large enough for the central limit theorem to have developed substantial accuracy on the tails; (2) the probability density function of a log-distorted Weibull variate, as given by (A-7), is distinctly non-Gaussian on the tails. The decay of (A-7) on the positive tail is much faster than Gaussian, while that on the negative tail is slower, being only exponential.

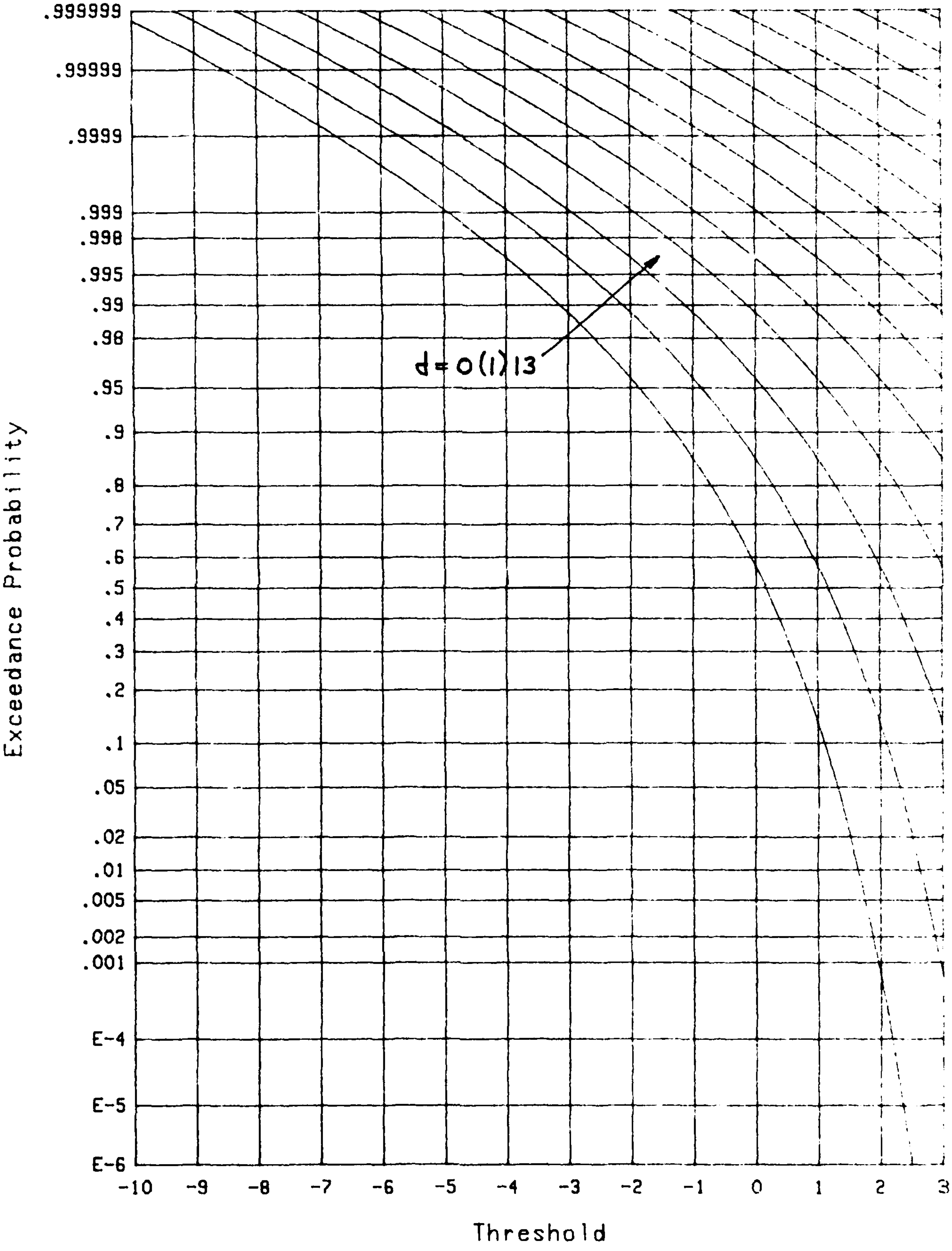

Figure 10. EDF for N = ∞; Extreme

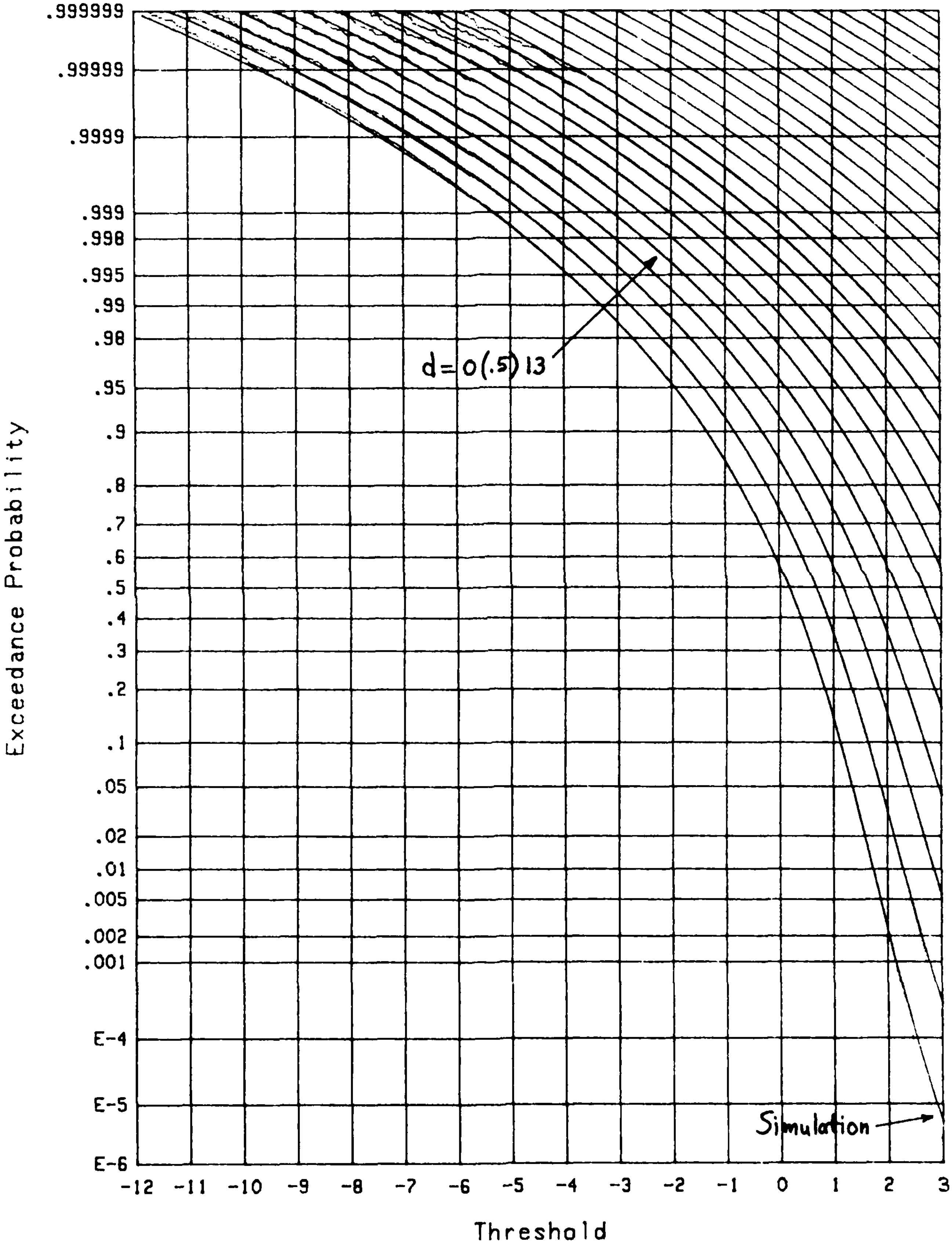

Figure 11. EDF for N = 64; Extreme

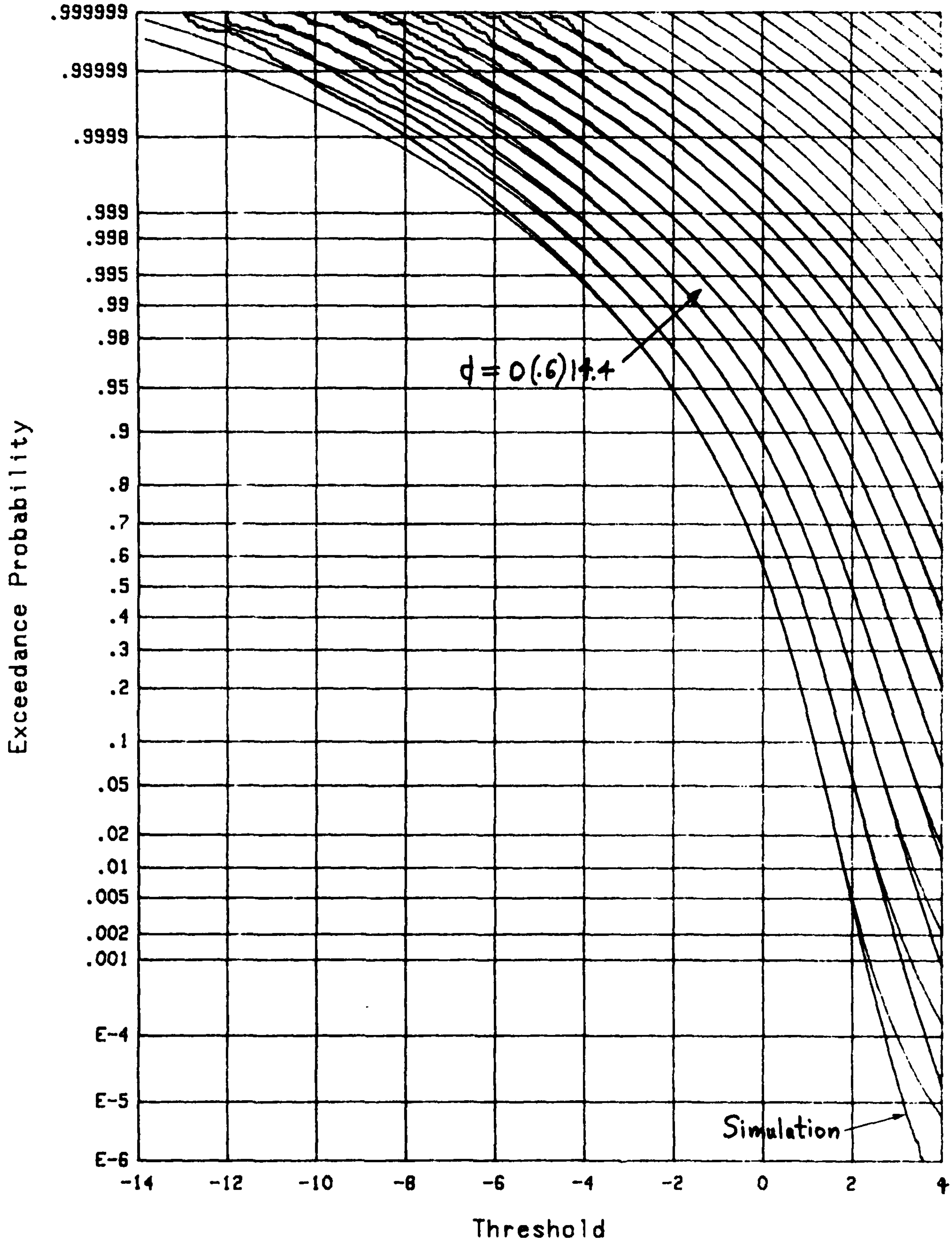

Figure 12. EDF for N = 32; Extreme

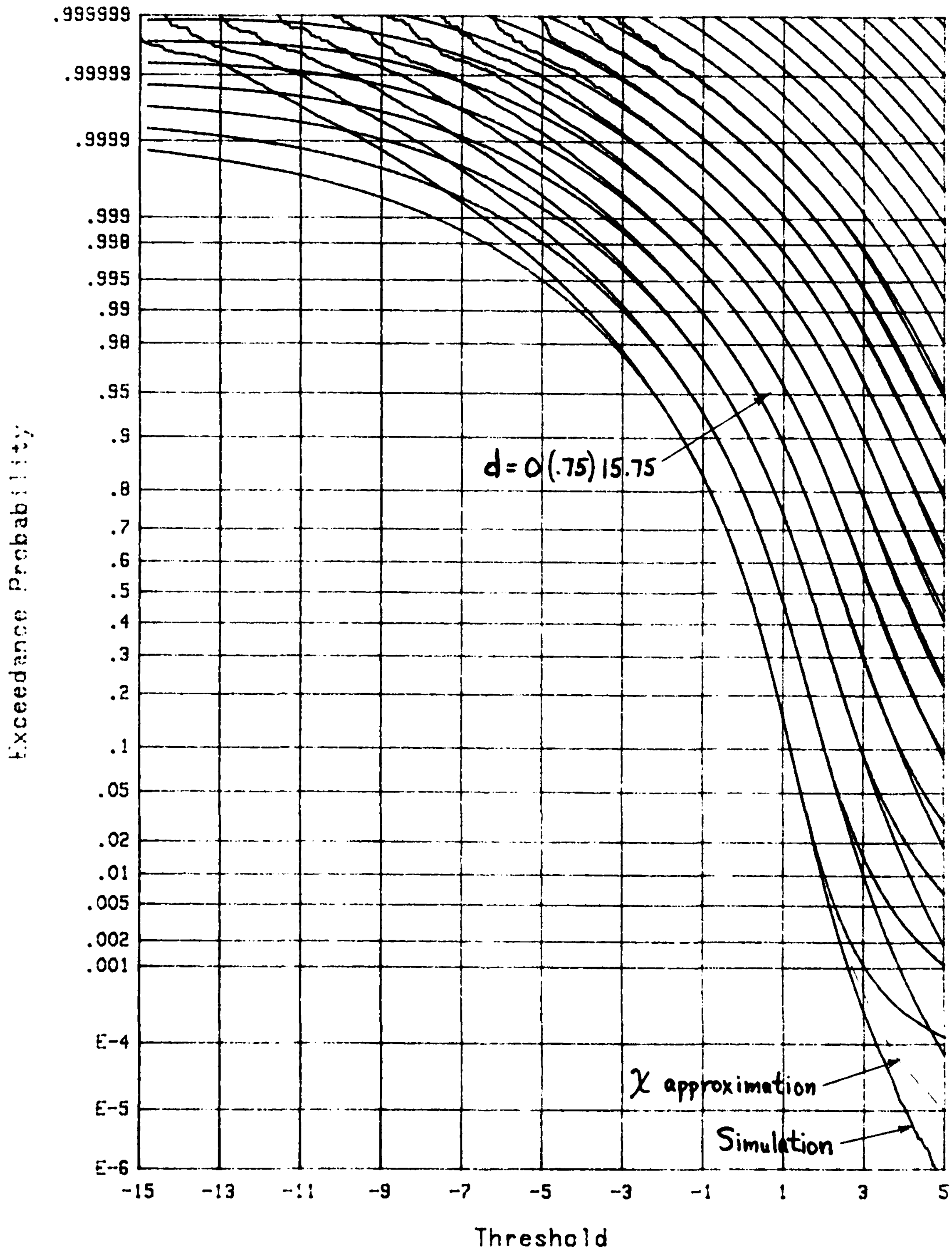

Figure 13. EDF for N = 16; Extreme

The receiver operating characteristics for $N=\infty$ are given in figure 14, while those for N = 64, 32, 16 are given in figures 15 through 17, respectively. The discrepancy between theory and simulation becomes progressively larger as N decreases, reaching the point in figure 17 where the theory is entirely invalid for false alarm probabilities less than approximately .001. The reason for the severe dip of the theoretical curves to the left of each figure is the inadequacy of the false alarm probability approximation, it being much too large for the larger threshold values; see bottom right of figure 13. On the other hand, the simulation results in these figures are all based on 8.4 million independent trials, making them trustworthy well down near the 1E-6 level of probability plotted here.

As an example of the use of figures 14 through 17, the values of d required to realize probabilities P_F = 1E-5 and P_D = .5 are

$$d = 2.2,\ 2.6,\ 2.9,\ 3.8 \quad \text{for } N = \infty,\ 64,\ 32,\ 16\ , \tag{59}$$

respectively. The latter three values are extracted from the simulation results in figures 15 through 17. Direct comparison of the absolute levels in (59) with the corresponding Gaussian results in (58) is not valid, because the shapes of the input probability density functions in the two cases are markedly different and are more important than the deflection criterion, defined by (30).

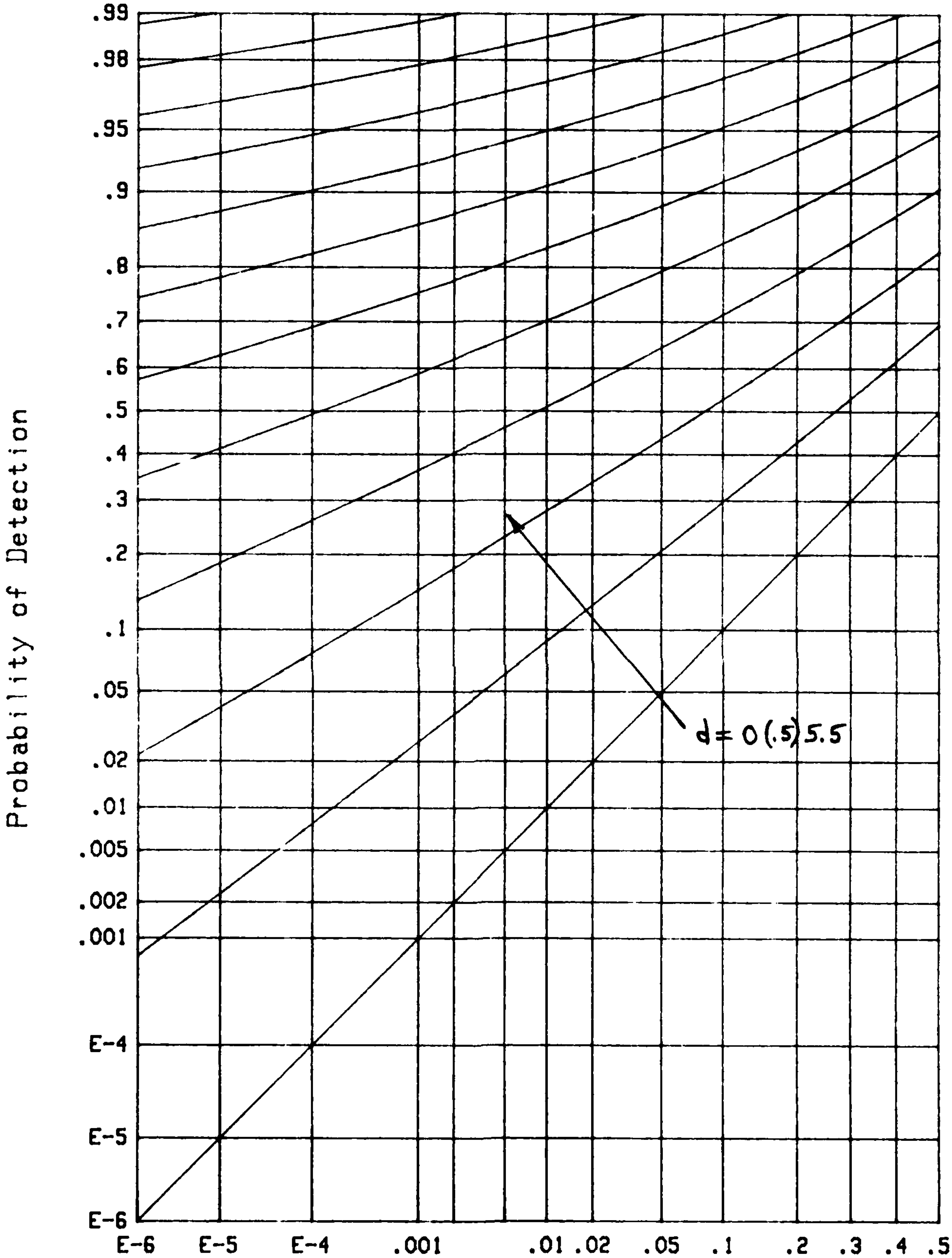

Figure 14. Probability of False Alarm

ROC for N = ∞; Extreme

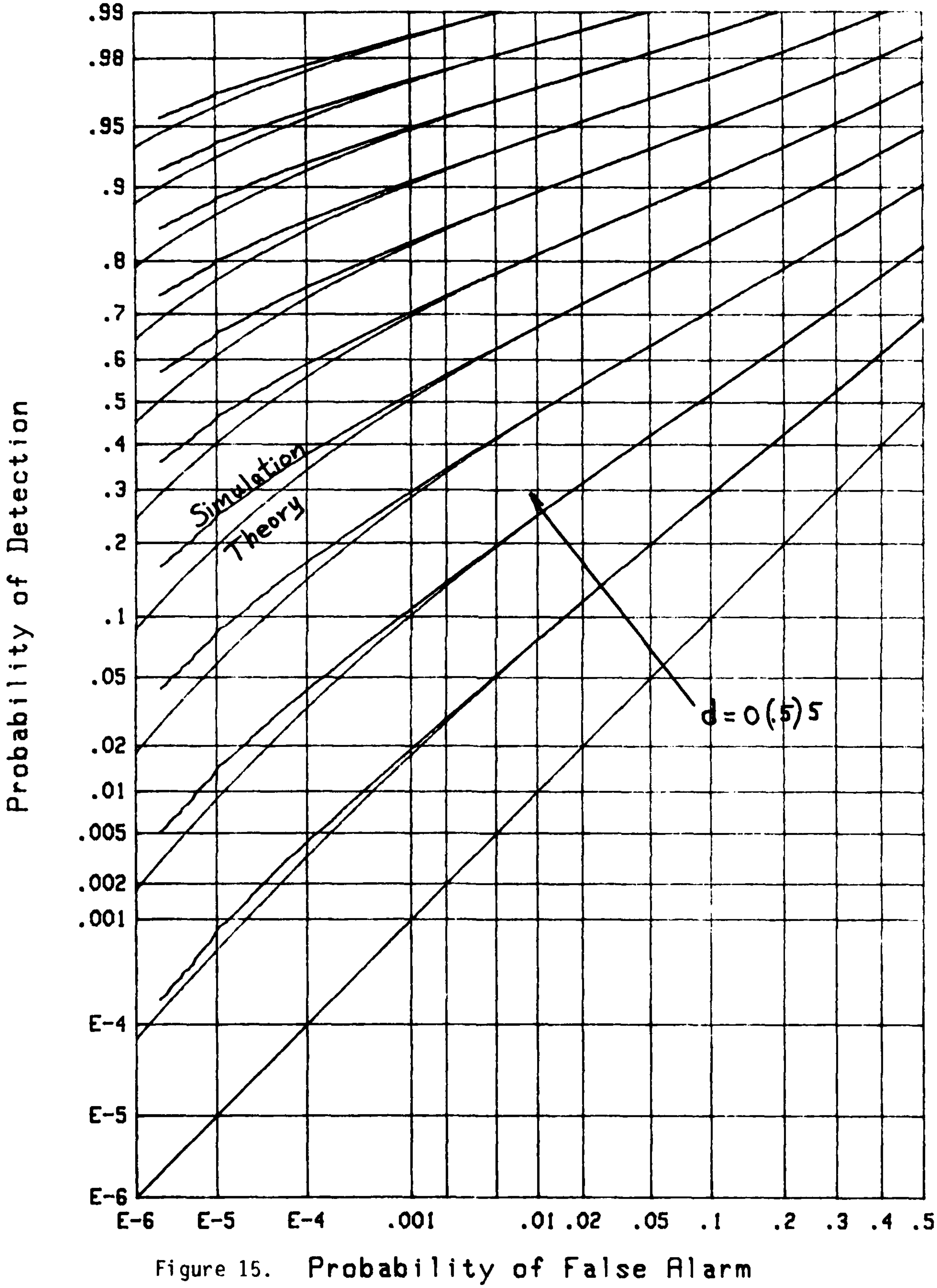

Figure 15. ROC for N = 64; Extreme

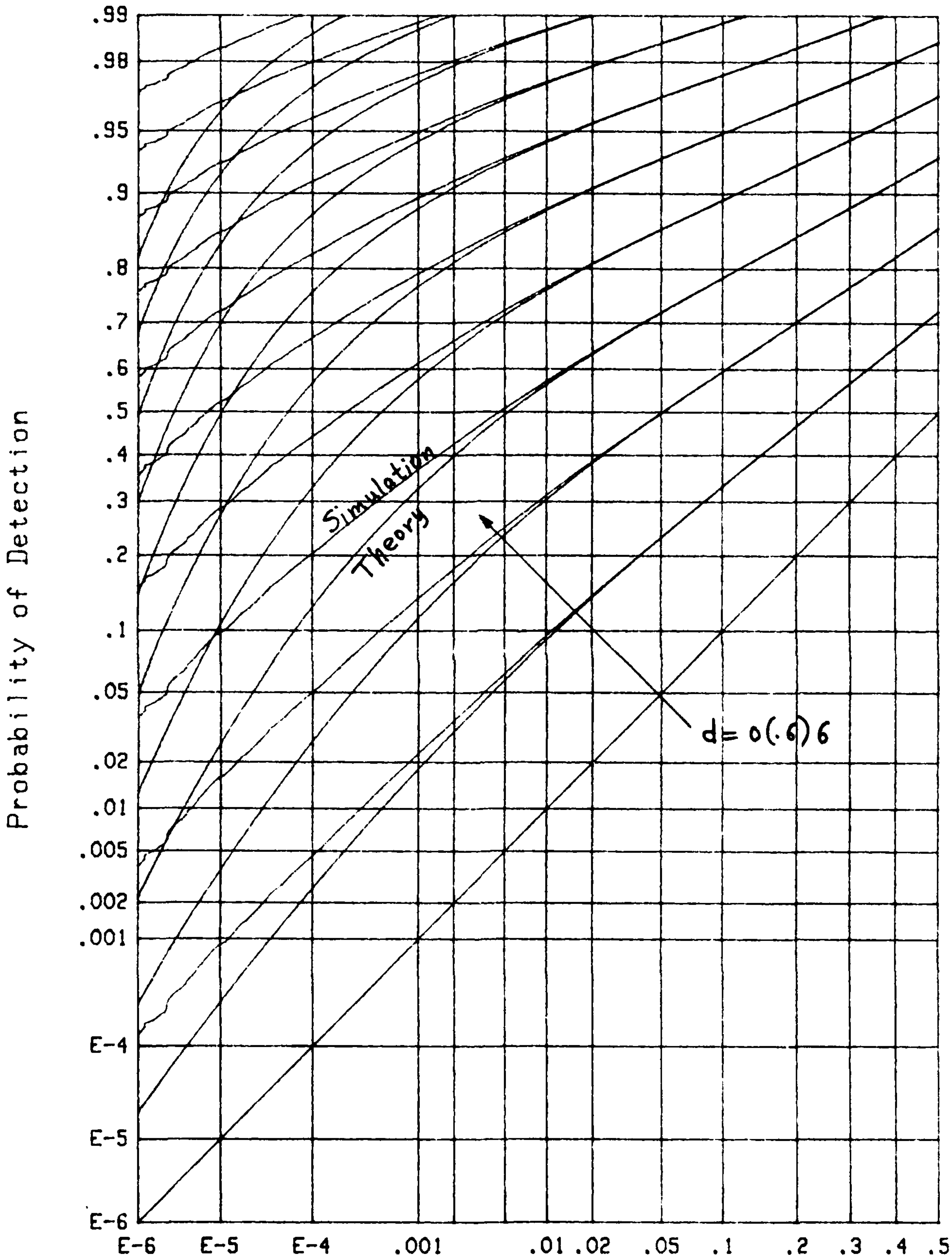

Figure 16. Probability of False Alarm

ROC for N = 32; Extreme

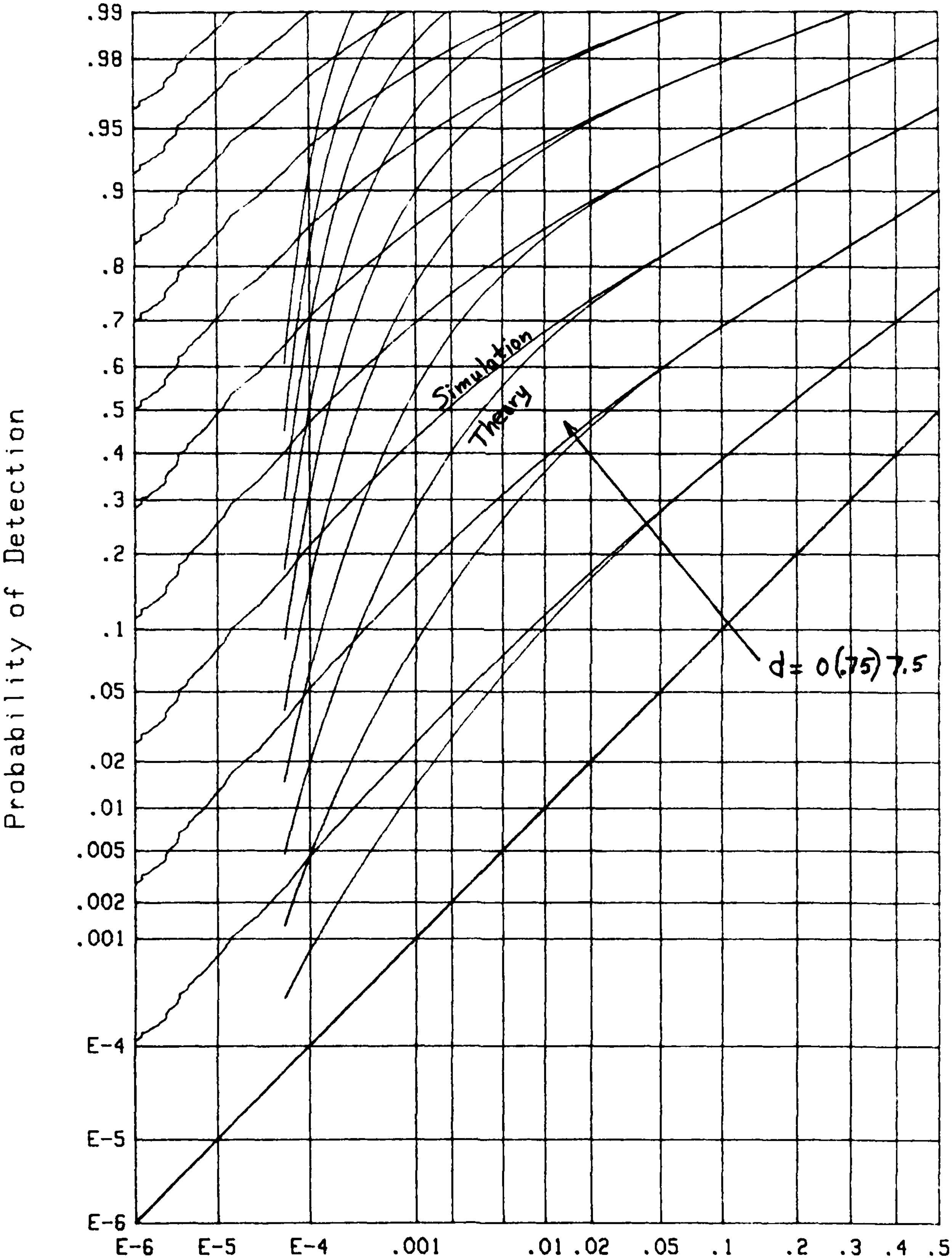

Figure 17. Probability of False Alarm

ROC for N = 16; Extreme

CONCLUSION

The performance of the normalizer with a Gaussian input is capable of exact analysis in terms of integrals which are readily evaluated via recursions. The main reason that this fortuitous situation obtains is the statistical independence of the sample mean and sample standard deviation for Gaussian random variables. However, for other inputs to the normalizer, these sample statistics are highly correlated with each other and create an untractable analysis problem.

An acceptable alternative in this latter case is simulation with a large number of trials. Here 8.4 million trials were employed, which allowed for estimation of tail probabilities in the 1E-6 range. If the false alarm probability could be evaluated theoretically, then simulation would only need to be conducted for the detection probability P_D. And if P_D were of interest only in the range (.5,.99) say, then as few as 10,000 trials would suffice for a decent estimate. However, it appears that, in general, even the analysis for the false alarm probability involves some unmanageable statistical relations.

APPENDIX A. WEIBULL VARIATES

The exceedance distribution function of a general Weibull random variable x is given by [8; p. 52]

$$Q_x(u) = \text{Prob}(x > u) = \exp\left[-\left(\frac{u}{a}\right)^{1/b}\right] \quad \text{for } u > 0;\ a > 0,\ b > 0\ . \qquad \text{(A-1)}$$

The corresponding probability density function of x is

$$p_x(u) = -Q_x'(u) = \frac{u^{\frac{1}{b}-1}}{a^{\frac{1}{b}}\, b} \exp\left[-\left(\frac{u}{a}\right)^{1/b}\right] \quad \text{for } u > 0\ . \qquad \text{(A-2)}$$

The ν-th moment of x is

$$\overline{x^\nu} = \int du\, u^\nu\, p_x(u) = a^\nu\, \Gamma(1 + b\nu) \quad \text{for } \nu > -1/b\ . \qquad \text{(A-3)}$$

The characteristic function of x is not available in closed form, for general b; however

$$\overline{\exp(i\xi x)} = (1 - i\xi a)^{-1} \quad \text{for } b = 1\ . \qquad \text{(A-4)}$$

The normalized cumulants of x, for general b, are independent of a; however, they do not approach zero as either $b \to 0$ or $b \to \infty$. Therefore x does not tend to Gaussian as the shape parameter b is changed.

LOG-DISTORTED WEIBULL VARIATE

As indicated in (1) and (15), we are interested in the log-distorted random variable

$$y = \ln x \,, \tag{A-5}$$

where x is a Weibull variate with probability density function (A-2). The exceedance distribution function of y is

$$Q_y(u) = \text{Prob}(y > u) = \text{Prob}(\ln x > u) = \text{Prob}(x > \exp(u)) =$$

$$= Q_x(\exp(u)) = \exp\left[-\frac{\exp(u/b)}{a^{1/b}}\right] \quad \text{for all } u \,, \tag{A-6}$$

where (A-1) was employed. The corresponding probability density function of random variable y is

$$p_y(u) = -Q_y'(u) = \frac{1}{b\, a^{1/b}} \exp\left[\frac{u}{b} - \frac{\exp(u/b)}{a^{1/b}}\right] \quad \text{for all } u \,, \tag{A-7}$$

which is a form of the probability density function for extreme values; see [4; (14.65)]. We will refer to (A-7) as an extreme value probability density function here.

The characteristic function of random variable y is

$$f_y(i\xi) = \overline{\exp(i\xi y)} = \overline{\exp(i\xi \ln x)} = \overline{x^{i\xi}} =$$

$$= a^{i\xi}\, \Gamma(1 + i\xi b) \; , \tag{A-8}$$

the last step by use of (A-3); this is a generalization of [4; page 344, exercise 14.4]. The actual numerical evaluation of the characteristic function in (A-8) for real ξ is best accomplished by employing (A-7):

$$f_y(i\xi) = \overline{\exp(i\xi y)} = \int du \, \exp(i\xi u) \, p_y(u) =$$

$$= \frac{1}{b\, a^{1/b}} \int_{-\infty}^{+\infty} du \, \exp(i\xi u) \, \exp\left[\frac{u}{b} - \frac{\exp(u/b)}{a^{1/b}}\right] \; . \tag{A-9}$$

This can be efficiently and accurately evaluated by use of a fast Fourier transform; the integrand decays very rapidly as $u \to \pm\infty$.

In anticipation of getting the cumulants of random variable y, we have from (A-8),

$$\ln f_y(i\xi) = i\xi \ln a + \ln \Gamma(1 + i\xi b) \; . \tag{A-10}$$

Now from [5: (6.1.33) and section 23.2] ,

$$\ln \Gamma(1+z) = -\gamma z + \sum_{n=2}^{\infty} (-1)^n \zeta(n)\ z^n/n\ , \tag{A-11}$$

where $\gamma = .57721$ is Euler's constant and

$$\zeta(n) = \sum_{k=1}^{\infty} \frac{1}{k^n}\quad . \tag{A-12}$$

In particular, $\zeta(2) = \pi^2/6$.

There then follows, from (A-10) and (A-11), the cumulants of random variable y as

$$\chi_y(n) = \left\{ \begin{array}{ll} \ln a - b\gamma & \text{for } n=1 \\ & \\ (-1)^n\, \zeta(n)(n-1)!\ b^n & \text{for } n \geq 2 \end{array} \right\} . \tag{A-13}$$

In particular, the variance of y is $\chi_y(2) = b^2\ \pi^2/6$. For $n \geq 2$, the normalized cumulant of y is

$$\frac{\chi_y(n)}{[\chi_y(2)]^{n/2}} = \left(-\frac{\sqrt{6}}{\pi}\right)^n\ \zeta(n)(n-1)!\ , \tag{A-14}$$

which is independent of both a and b; thus random variable y does not approach Gaussian as a and/or b approach any limits whatsoever. These results generalize [4; page 344, exercise 14.4].

NORMALIZED LOG-DISTORTED WEIBULL VARIATE

If a=b=1 in (7), then $x_n = w_n$, and it then follows from (16) and (1) that $\tilde{v}_n = \ln w_n = \ln x_n = y_n$. In this case, we can use (A-6) with a=b=1 to obtain the exceedance distribution function of $\tilde{v}_n$ as

$$Q_{\tilde{v}}(u) = \exp\left[-\exp(u)\right] \quad \text{for all } u . \tag{A-15}$$

Additionally, there follows from (A-13)

$$\mu(\tilde{v}) = \chi_y(1) = -\gamma = -.57721 ,$$

$$\sigma(\tilde{v}) = \left(\chi_y(2)\right)^{1/2} = \pi/\sqrt{6} . \tag{A-16}$$

We are now in position to determine the exceedance distribution function of the normalized log-distorted Weibull random variable v_n defined in (17), namely,

$$Q_v(u) = \text{Prob}(v > u) = \text{Prob}\left(\tilde{v} > \mu(\tilde{v}) + \sigma(\tilde{v})u\right) =$$

$$= Q_{\tilde{v}}\left(\mu(\tilde{v}) + \sigma(\tilde{v})u\right) = \exp\left[-\exp(-\gamma + \frac{\pi}{\sqrt{6}}\, u)\right] \quad \text{for all } u . \tag{A-17}$$

LOG-NORMAL VARIATES

For completeness, we list here the ν-th moment of log-normal variate x with probability density function as given by (14) and (12):

$$\overline{x^{\nu}} = \int du\ u^{\nu}\ p_x(u) = \frac{1}{b}\int_0^{\infty} \frac{du}{u}\ u^{\nu}\ \phi\left(\frac{\ln(a) - \ln(u)}{b}\right) =$$

$$= \frac{1}{\sqrt{2\pi}\,b}\int_{-\infty}^{+\infty} dt\ \exp\left[\nu t - \frac{1}{2}\left(\frac{t - \ln(a)}{b}\right)^2\right] = \exp\left[\nu \ln a + \frac{1}{2}\nu^2 b^2\right] \ . \tag{A-18}$$

APPENDIX B. INDEPENDENCE OF SAMPLE MEAN AND SAMPLE VARIANCE FOR GAUSSIAN RANDOM VARIABLES

Let $\{x_n\}_1^N$ be independent identically-distributed Gaussian random variables with mean and variance

$$\overline{x_n} = \mu , \quad \overline{(x_n - \mu)^2} = \sigma^2 \quad \text{for all } n . \tag{B-1}$$

Define sample mean

$$m = \frac{1}{N} \sum_{n=1}^{N} x_n , \tag{B-2}$$

and sample variance

$$v = g \sum_{n=1}^{N} (x_n - m)^2 , \tag{B-3}$$

where scale factor $g = 1/N$ or $1/(N-1)$ typically. ($N \geq 2$ required.)

We have, in vector notation

$$m = \frac{1}{N} 1^T X = \frac{1}{N}[1 \; 1 \; \ldots \; 1][x_1 \; x_2 \; \ldots \; x_N]^T , \tag{B-4}$$

and

$$v = g\left[\sum_{n=1}^{N} x_n^2 - m^2 N\right] = g\left[X^1 X - \frac{1}{N} X^T 1 \; 1^T X\right] = g \; X^T Q X , \tag{B-5}$$

where

$$Q = I - \frac{1}{N} 1 \, 1^T . \tag{B-6}$$

The joint characteristic function of m and v is

$$f(\xi,\phi) = \overline{\exp(i\xi m + i\phi v)} =$$

$$= \overline{\exp\left[i\xi \frac{1}{N} 1^T X + i\phi g \, X^T Q X \right]} . \tag{B-7}$$

Now the joint probability density function of vector X is

$$p(X) = \prod_{n=1}^{N} \left(\sqrt{2\pi}\,\sigma\right)^{-1} \exp\left[-\frac{(x_n - \mu)^2}{2\,\sigma^2} \right] =$$

$$= \left(2\pi\,\sigma^2\right)^{-N/2} \exp\left[-\frac{1}{2\sigma^2} \left(X^T X - 2\mu \, 1^T X + \mu^2 N \right) \right] . \tag{B-8}$$

Therefore

$$f(\xi,\phi) = (2\pi\,\sigma^2)^{-N/2} \int dX \, \exp\left[-\frac{1}{2\sigma^2} \left(X^T X - 2\mu \, 1^T X + \mu^2 N \right) + \right.$$

$$\left. + \, i \frac{\xi}{N} 1^T X + i\phi g \, X^T Q X \right] . \tag{B-9}$$

Now we use [6; (B-1)]

$$\int dX \, \exp\left[-\frac{1}{2} X^T M X + L^T X \right] = \left[\frac{(2\pi)^N}{\det M} \right]^{1/2} \exp\left[\frac{1}{2} L^T M^{-1} L \right] \tag{B-10}$$

with identifications

$$M = \frac{1}{\sigma^2} I - i2\phi g \, Q , \qquad L = \left(\frac{\mu}{\sigma^2} + i \frac{\xi}{N} \right) 1 . \tag{B-11}$$

Using the definition of Q in (B-6), there follows

$$M = \left(\frac{1}{\sigma^2} - i2\phi g\right) I + \frac{i2\phi g}{N} 1\, 1^T . \tag{B-12}$$

Now from [6; (21) and (22)],

$$\det M = \frac{1}{\sigma^{2N}} (1 - i2\sigma^2 \phi g)^{N-1} ,$$

$$M^{-1} = \frac{\sigma^2}{1 - i2\sigma^2\phi g} \left[I - \frac{i2\phi g \sigma^2}{N} 1\, 1^T\right] . \tag{B-13}$$

There follows

$$L^T M^{-1} L = N \sigma^2 \left(\frac{\mu}{\sigma^2} + i \frac{\xi}{N}\right)^2 \tag{B-14}$$

and

$$f(\xi,\phi) = \exp\left[i\xi\mu - \frac{1}{2} \xi^2 \frac{\sigma^2}{N}\right] \left(1 - i2\sigma^2 g\phi\right)^{\frac{1-N}{2}} . \tag{B-15}$$

Since this joint characteristic function factors, it follows that sample statistics m and v are statistically independent. Also the probability density functions are obviously

$$p_m(u) = \frac{1}{\sqrt{2\pi}\, \sigma/\sqrt{N}} \exp\left[- \frac{(u - \mu)^2}{2 \sigma^2/N}\right] \quad \text{for all } u \tag{B-16}$$

and

$$p_v(u) = \frac{u^{\frac{N-3}{2}} \exp\left(\frac{-u}{2\sigma^2 g}\right)}{\Gamma\left(\frac{N-1}{2}\right) \left(2\sigma^2 g\right)^{\frac{N-1}{2}}} \quad \text{for } u > 0 . \tag{B-17}$$

Thus sample mean m is Gaussian with mean μ and variance σ^2/N; while sample variance v is chi-squared of N-1 degrees of freedom with mean $\sigma^2(N-1)g$ and variance $2\sigma^4(N-1)g^2$. For the typical choice of gain $g = 1/(N-1)$, this implies that v has mean σ^2 and variance $2\sigma^4/(N-1)$, and therefore

$$\lim_{N\to\infty} p_v(u) = \delta(u - \sigma^2) \ . \tag{B-18}$$

The sample standard deviation

$$s = \sqrt{v} \tag{B-19}$$

has probability density function

$$p_s(u) = 2\, u\, p_v(u^2) = \frac{2\, u^{N-2} \exp(-u^2/\beta)}{\Gamma\left(\frac{N-1}{2}\right) \beta^{\frac{N-1}{2}}} \quad \text{for } u > 0 \tag{B-20}$$

where

$$\beta = \frac{2\sigma^2}{N-1} \quad \text{for } g = 1/(N-1) \ . \tag{B-21}$$

The k-th moment of s is

$$\overline{s^k} = \int du\, u^k\, p_s(u) = \int_0^\infty du \frac{2\, u^{N-2+k} \exp(-u^2/\beta)}{\Gamma\left(\frac{N-1}{2}\right) \beta^{\frac{N-1}{2}}} = \frac{\Gamma\left(\frac{N+k-1}{2}\right) \beta^{k/2}}{\Gamma\left(\frac{N-1}{2}\right)} \ . \tag{B-22}$$

In particular,

$$\overline{s^2} = \sigma^2 \ , \tag{B-23}$$

and [5; (6.1.47)]

$$\bar{s} = \sigma \left(\frac{2}{N-1}\right)^{1/2} \frac{\Gamma\left(\frac{N}{2}\right)}{\Gamma\left(\frac{N-1}{2}\right)} =$$

$$= \sigma \left(\frac{2}{N-1}\right)^{1/2} \left(\frac{N - \frac{3}{2}}{2}\right)^{1/2} \left[1 + \frac{1/16}{\left(N - \frac{3}{2}\right)^2} + 0\left(N - \frac{3}{2}\right)^{-3}\right] =$$

$$= \sigma \left[1 - \frac{1/4}{N - \frac{9}{8}} + 0\left(N - \frac{9}{8}\right)^{-3}\right] \left[1 + \frac{1/16}{\left(N - \frac{3}{2}\right)^2} + 0\left(N - \frac{3}{2}\right)^{-3}\right] =$$

$$= \sigma \left[1 - \frac{1/4}{N - \frac{9}{8}} + \frac{1/16}{\left(N - \frac{3}{2}\right)^2} + 0(N^{-3})\right] =$$

$$= \sigma \left[1 - \frac{1/4}{N - \frac{7}{8}} + 0(N^{-3})\right] \quad \text{as } N \to \infty \ . \qquad \text{(B-24)}$$

APPENDIX C. PROBABILITY RECURSIONS FOR GAUSSIAN CASE

The detection and false alarm probabilities are given in integral form in (38) and (41). These integrals have already been encountered in [1; appendix E], and evaluated in a recursive fashion. We will modify those results somewhat, in order to better suit the current forms.

First, we have, from (41) and (39),

$$P_F = \int_0^\infty dw \; \frac{w^{N-2}\exp(-w^2/2)}{2^{\frac{N-3}{2}}\,\Gamma\left(\frac{N-1}{2}\right)} \; \Phi(-T_1' w) \equiv P_F(N, T_1') \; . \tag{C-1}$$

Define

$$x_1 = \left(1 + T_1'^{\,2}\right)^{-1} , \quad \text{where } T_1' = T\sqrt{\frac{N}{N^2 - 1}} \; . \tag{C-2}$$

Then from [1; (E-17)], using identifications (that is, replacements from there to here)

$$r \rightarrow \frac{T_1'}{\left(1 + T_1'^{\,2}\right)^{1/2}} , \qquad K \rightarrow N-2 , \tag{C-3}$$

there follows the simple result

$$P_F(N,T_1') = \frac{1}{2} - \frac{1}{\pi}\mathrm{atn}(T_1') - \frac{1}{\pi}\, T_1'\, x_1 \sum_{k=0}^{\frac{N}{2}-2} b_k\, x_1^k \quad \text{for } N=2,4,6,\ldots, \tag{C-4}$$

where

$$b_o = 1\ , \qquad b_k = b_{k-1}\,\frac{k}{k+\frac{1}{2}} \qquad \text{for } k \geq 1\ . \tag{C-5}$$

A program for this false alarm probability is given in appendix E under the name FNPf246, where T_1' is represented by variable Tp.

Also,

$$P_F(N,T_1') = \frac{1}{2} - \frac{1}{2}\, T_1'\sqrt{x_1} \sum_{k=0}^{\frac{N-3}{2}} a_k\, x_1^k \qquad \text{for } N=3,5,7,\ldots, \tag{C-6}$$

where

$$a_o = 1\ , \qquad a_k = a_{k-1}\,\frac{k-\frac{1}{2}}{k} \qquad \text{for } k \geq 1\ . \tag{C-7}$$

These results are very tractable and efficient forms for recursive computer evaluation. A program for (C-6) is given in appendix E under the name FNPf357, where T_1' is represented by variable Tp.

The current form for detection probability $P_D = P_D(N,T_r',d_r')$ in (38) is identical to [1; (E-1)] if we make replacements

$$d_T \to d_r' , \qquad r \to \frac{T_r'}{\left(1 + T_r'^2\right)^{1/2}} , \qquad K \to N-2 . \tag{C-8}$$

(The curves in [1] are not directly applicable here because they employed the fundamental parameter $d_T \to d_r'$, which is $d/\left(r^2 + 1/N\right)^{1/2}$ here; however, the recursions derived there are immediately useable.) We can then use [1; (E-8)] to develop an expression for P_D, in terms of the auxiliary sequence $\{g(K)\}$ defined in [1; (E-7)]. In particular, [1; (E-9)] yields, with

$$x_r = \left(1 + T_r'^2\right)^{-1} , \tag{C-9}$$

the result

$$g(0) = T_r'\sqrt{x_r}\, \exp\left(-\frac{1}{2}\, d_r'^2 x_r\right) \Phi\left(d_r' T_r' \sqrt{x_r}\right) ; \tag{C-10}$$

[1; (E-13)] yields

$$g(1) = T_r' x_r \left[\frac{1}{\pi} \exp\left(-d_r'^2/2\right) + \left(\frac{2}{\pi}\right)^{1/2} d_r' \; g(0)\right] ; \tag{C-11}$$

and [1; (E-12)] yields

$$g(K) = x_r \left[h(K) g(K-1) + \frac{K-1}{K}\, g(K-2)\right] \quad \text{for } K \geq 2 , \tag{C-12}$$

with definition

$$h(K) = \frac{1}{\sqrt{2}}\, T_r' d_r' \, \frac{\Gamma\left(\frac{K+1}{2}\right)}{\Gamma\left(\frac{K}{2} + 1\right)} . \tag{C-13}$$

Then we can also use

$$h(0) = T_r' \, d_r' \left(\frac{\pi}{2}\right)^{1/2} , \quad h(1) = T_r' \, d_r' \left(\frac{2}{\pi}\right)^{1/2} ,$$

$$h(K) = h(K-2) \, \frac{K-1}{K} \quad \text{for } K \geq 2 . \tag{C-14}$$

Finally, $P_D = P_D(N,T_r',d_r')$ is given by [1; (E-8)] as

$$P_D = \begin{Bmatrix} \Phi(d_r') - \displaystyle\sum_{\substack{K=0 \\ K \text{ even}}}^{N-3} g(K) & \text{for } N=3,5,7, \ldots \\ \\ P_{D2} - \displaystyle\sum_{\substack{K=1 \\ K \text{ odd}}}^{N-3} g(K) & \text{for } N=4,6,8, \ldots \end{Bmatrix} , \tag{C-15}$$

where P_{D2} is the value of detection probability P_D for $N = 2$. Observe that the input parameters to P_D are N,T_r',d_r', rather than the fo·· fundamental parameters in (40); that is, N,1,d,r are collapsed into N,T_r',d_r' according to (39). Programs for (C-15) are furnished in appendix E under the names FNPd357 and FNPd246, respectively, where T_r' and d_r' are represented by variables Tp and Dp.

The quantity P_{D2} in (C-15) is evaluated according to the method in [1; appendix F]; an error tolerance and maximum number of terms must also be specified to terminate the infinite sum given by [1; (F-2)].

APPENDIX D. χ-APPROXIMATION FOR RANDOM VARIABLE t

Suppose we assume that the random variable t in (46) is a multiple of a χ-variate with K degrees of freedom; then its probability density function is [7; pages 5-7 for $\nu = 1/2$]

$$p_t(u) = \frac{u^{K-1} \exp\left(-u^2/\left(2A^2\right)\right)}{A^K \; 2^{\frac{K}{2}-1} \, \Gamma\left(\frac{K}{2}\right)} \quad \text{for } u > 0 \; . \tag{D-1}$$

Then the ν-th moment of random variable t is

$$\overline{t^\nu} = \int du \; u^\nu \; p_t(u) = \frac{2^{\nu/2} A^\nu \, \Gamma\left(\frac{K+\nu}{2}\right)}{\Gamma\left(\frac{K}{2}\right)} \; , \tag{D-2}$$

and in particular

$$\bar{t} = A \, \frac{\sqrt{2}\, \Gamma\left(\frac{K+1}{2}\right)}{\Gamma\left(\frac{K}{2}\right)} \; , \quad \overline{t^2} = A^2 K \; . \tag{D-3}$$

Then the ratio

$$R = \frac{\bar{t}}{\sqrt{\overline{t^2}}} = \frac{\Gamma\left(\frac{K+1}{2}\right)}{\sqrt{\frac{K}{2}}\, \Gamma\left(\frac{K}{2}\right)} = 1 - \frac{1}{4K+\frac{1}{2}} + O\left(K^{-3}\right) \; , \tag{D-4}$$

where the last result uses the development in (B-24) with N replaced by K+1.

Given a value for ratio R on the left side of (D-4), K can be solved for uniquely, since the ratio involving gamma functions increases monotonically from 0 to 1 as K goes from 0 to $+\infty$. In fact, to a good approximation for large K, the last part of (D-4) gives

$$K \cong \frac{1}{4(1-R)} - \frac{1}{8} . \tag{D-5}$$

Here we are allowing K in probability density function p_t in (D-1) to be arbitrary, that is, not limited to integer values. Then we can solve for the required value of A according to (D-3), as $A^2 = \overline{t^2}/K$. This procedure fits the assumed probability density function form in (D-1) to specified values of the first two moments of t given by (D-3), as given by simulation results (53)-(55).

If we now employ the χ-approximate probability density function for t given by (D-1) in detection probability result (45), along with (49), we obtain

$$P_D = \int_0^\infty du \, \exp\left[-\exp\left(-\gamma + \frac{\pi}{\sqrt{6}} \frac{u - d}{r}\right)\right] \frac{u^{K-1} \exp\left(-u^2/\left(2A^2\right)\right)}{A^K \, 2^{\frac{K}{2} - 1} \, \Gamma\left(\frac{K}{2}\right)} =$$

$$= \left[2^{\frac{K}{2} - 1} \Gamma\left(\frac{K}{2}\right)\right]^{-1} \int_0^\infty dx \, x^{K-1} \exp\left[-x^2/2 - \exp(h_1 + h_2 x)\right] , \tag{D-6}$$

where constants

$$h_1 = - \gamma - \frac{\pi}{\sqrt{6}} \frac{d}{r} , \qquad h_2 = \frac{\pi}{\sqrt{6}} \frac{A}{r} . \tag{D-7}$$

The numerical evaluation of (D-6) was undertaken for N = 16, and is discussed in the Graphical Results section of this report.

APPENDIX E. PROGRAMS

In this appendix, four programs are listed. They are written in BASIC for the Hewlett-Packard 9000 Model 520 Desk Top Computer. Their titles are

EDF - Gaussian,

EDF - Extreme,

Simulation-Extreme,

Plot-Simulation.

The first one computes the exceedance distribution function for a Gaussian input to the normalizer of figure 1, for N=16 (line 10) and for d = 0(1)12 (lines 960-970). This program is heavily based on the results of appendix C.

The second program computes the approximate exceedance distribution function for a log-distorted Weibull input to the normalizer of figure 1, for N=16 (line 10), r=1 (line 20), and d = 0(.75)7.5 (line 1070). It is based on numerical integration of (51) via Simpson's rule.

The third program simulates the normalizer output (28) and (24) for a log-distorted Weibull input, for N=16 (line 10), d = 0(.75)7.5 (line 20), r=1 (line 30), and 2^{23} = 8.4 million trials (line 40). The range of

values in z is (-15,5), which is divided into 1000 bins; see lines 60, 90, 100. The resultant histogram is then summed on the upper tail to yield the exceedance distribution function. The fourth program plots these simulation results for the exceedance distribution function vs threshold T.

Table E-1. EDF - Gaussian

```
10   Ns=16                                   !  NUMBER OF SAMPLES
20   X1=-7                                   !  THRESHOLD
30   X2=7                                    !   LIMITS
40   DIM A$[30],B$[30]
50   DIM Xlabel$(1:30),Ylabel$(1:30)
60   DIM Xcoord(1:30),Ycoord(1:30)
70   DIM Xgrid(1:30),Ygrid(1:30)
80   DOUBLE Lx,Ly,Nx,Ny,I,Ns,It
90   !
100  A$="Threshold"
110  B$="Exceedance Probability"
120  !
130  Lx=15
140  REDIM Xlabel$(1:Lx),Xcoord(1:Lx)
150  DATA -7,-6,-5,-4,-3,-2,-1,0,1,2,3,4,5,6,7
160  READ Xlabel$(*)
170  DATA -7,-6,-5,-4,-3,-2,-1,0,1,2,3,4,5,6,7
180  READ Xcoord(*)
190  !
200  Ly=27
210  REDIM Ylabel$(1:Ly),Ycoord(1:Ly)
220  DATA E-6,E-5,E-4,.001,.002,.005,.01,.02,.05
230  DATA .1,.2,.3,.4,.5,.6,.7,.8,.9,.95,.98,.99
240  DATA .995,.998,.999,.9999,.99999,.999999
250  READ Ylabel$(*)
260  DATA 1.E-6,1.E-5,1.E-4,.001,.002,.005,.01,.02,.05
270  DATA .1,.2,.3,.4,.5,.6,.7,.8,.9,.95,.98,.99
280  DATA .995,.998,.999,.9999,.99999,.999999
290  READ Ycoord(*)
300  !
310  Nx=15
320  REDIM Xgrid(1:Nx)
330  DATA -7,-6,-5,-4,-3,-2,-1,0,1,2,3,4,5,6,7
340  READ Xgrid(*)
350  !
360  Ny=27
370  REDIM Ygrid(1:Ny)
380  DATA 1.E-6,1.E-5,1.E-4,.001,.002,.005,.01,.02,.05
390  DATA .1,.2,.3,.4,.5,.6,.7,.8,.9,.95,.98,.99
400  DATA .995,.998,.999,.9999,.99999,.999999
410  READ Ygrid(*)
420  !
430  FOR I=1 TO Ly
440  Ycoord(I)=FNInvphi(Ycoord(I))
450  NEXT I
460  FOR I=1 TO Ny
470  Ygrid(I)=FNInvphi(Ygrid(I))
480  NEXT I
490  Y1=Ygrid(1)
500  Y2=Ygrid(Ny)
```

```
510    GINIT 180./240.                         !  VERTICAL PAPER
520    PLOTTER IS 505,"HPGL"
530    PRINTER IS 505
540    LIMIT PLOTTER 505,0.,180.,0.,240.       !  1 GDU = 2 mm
550    VIEWPORT 20.,120.,19.,132.
560  ! VIEWPORT 22.,85.,59.,122.               !  TOP OF PAPER
570  ! VIEWPORT 22.,85.,19.,62.                !  BOTTOM OF PAPER
580    WINDOW X1,X2,Y1,Y2
590  !   PRINT "VS2"
600    FOR I=1 TO Nx
610    MOVE Xgrid(I),Y1
620    DRAW Xgrid(I),Y2
630    NEXT I
640    FOR I=1 TO Ny
650    MOVE X1,Ygrid(I)
660    DRAW X2,Ygrid(I)
670    NEXT I
680    PENUP
690    LDIR 0
700    CSIZE 2.3,.5
710    LORG 5
720    Y=Y1-(Y2-Y1)*.02
730    FOR I=1 TO Lx
740    MOVE Xcoord(I),Y
750    LABEL Xlabel$(I)
760    NEXT I
770    CSIZE 3.,.5
780    MOVE .5*(X1+X2),Y1-.06*(Y2-Y1)
790    LABEL A$
800    CSIZE 2.3,.5
810    LORG 8
820    X=X1-(X2-X1)*.01
830    FOR I=1 TO Ly
840    MOVE X,Ycoord(I)
850    LABEL Ylabel$(I)
860    NEXT I
870    LDIR PI/2.
880    CSIZE 3.,.5
890    LORG 5
900    MOVE X1-.15*(X2-X1),.5*(Y1+Y2)
910    LABEL B$
920      PRINT "VS36"
```

```
930   Dx=(X2-X1)/100.
940   F1=SQR(Ns/(Ns+1))
950   F2=SQR(Ns/(Ns*Ns-1))
960   FOR I=0 TO 12
970   Ds=I                                  !  DEFLECTION d
980   Dp=Ds*F1                              !  d_r'
990   FOR It=0 TO 100
1000  T=X1+Dx*It                            !  THRESHOLD T
1010  Tp=T*F2                               !  T_r'
1020  IF Dp>0. THEN 1080
1030  IF Ns MODULO 2=0 THEN 1060
1040  Pd=FNPf357(Ns,Tp)
1050  GOTO 1120
1060  Pd=FNPf246(Ns,Tp)
1070  GOTO 1120
1080  IF Ns MODULO 2=0 THEN 1110
1090  Pd=FNPd357(Ns,Tp,Dp)
1100  GOTO 1120
1110  Pd=FNPd246(Ns,Tp,Dp)
1120  IF Pd<=0. THEN 1160
1130  IF Pd>=1. THEN 1160
1140  Y=FNInvphi(Pd)
1150  PLOT T,Y
1160  NEXT It
1170  PENUP
1180  NEXT I
1190  PAUSE
1200  PRINTER IS CRT
1210  PLOTTER 505 IS TERMINATED
1220  END
1230  !
1240  DEF FNInvphi(X)      !  AMS 55, 26.2.23
1250  IF X=.5 THEN RETURN 0.
1260  P=MIN(X,1.-X)
1270  T=-LOG(P)
1280  T=SQR(T+T)
1290  P=1.+T*(1.432788+T*(.189269+T*.001308))
1300  P=T-(2.515517+T*(.802853+T*.010328))/P
1310  IF X<.5 THEN P=-P
1320  RETURN P
1330  FNEND
1340  !
1350  DEF FNPf246(DOUBLE N,REAL Tp)      !  N=2,4,6,...
1360  DOUBLE Ks                          !  INTEGER
1370  Pf=.5-ATN(Tp)/PI
1380  IF N=2 THEN RETURN Pf
1390  X=1./(1.+Tp*Tp)
1400  S=Bx=1.
1410  FOR Ks=1 TO N/2-2
1420  Bx=Bx*X*Ks/(Ks+.5)
1430  S=S+Bx
1440  NEXT Ks
1450  Pf=Pf-Tp*X*S/PI
1460  RETURN Pf
1470  FNEND
1480  !
```

```
1490    DEF FNPf357(DOUBLE N,REAL Tp)       !  N=3,5,7,...
1500    DOUBLE Ks                           !  INTEGER
1510    X=1./(1.+Tp*Tp)
1520    S=Ax=1.
1530    FOR Ks=1 TO (N-3)/2
1540    Ax=Ax*X*(Ks-.5)/Ks
1550    S=S+Ax
1560    NEXT Ks
1570    Pf=.5*(1.-Tp*SQR(X)*S)
1580    RETURN Pf
1590    FNEND
1600    !
1610    DEF FNPd246(DOUBLE N,REAL Tp,Dp)    !  N=2,4,6,...
1620    Error=1.E-15                        !  Toleranc: in Pd for N=2
1630    Nterms=500                          !  Number of terms for N=2
1640    DOUBLE Ks                           !  INTEGER
1650    X=1./(1.+Tp*Tp)
1660    Rk=SQR(X)
1670    Tsq=Tp*Rk
1680    Dsq=Dp*Dp
1690    R=SQR(2./PI)
1700    A1=A0=EXP(-.5*Dsq)/PI
1710    A=A1*Dp/R
1720    B1=.5*PI-ATN(Tp)
1730    B=Rk
1740    Pd=A1*B1+A*B
1750    FOR Ks=2 TO Nterms
1760    F=FLT(Ks-1)
1770    T=Dsq*A1/F
1780    A1=A
1790    A=T
1800    Rk=Rk*Tsq
1810    T=(Rk+F*B1)/Ks
1820    B1=B
1830    B=T
1840    P=A*B
1850    Pd=Pd+P
1860    IF P<=Error*Pd THEN 1890
1870    NEXT Ks
1880    PRINT "500 TERMS IN FNPd246"
1890    IF N=2 THEN RETURN Pd
1900    G1=Tsq*EXP(-.5*Dsq*X)*FNPhi(Dp*Tsq)
1910    G=Tp*X*(A0+R*Dp*G1)
1920    F1=Tp*Dp/R
1930    F=Tp*Dp*R
1940    Pd=Pd-G
1950    IF N=4 THEN RETURN Pd
1960    FOR Ks=2 TO N-3
1970    R=(Ks-1)/Ks
1980    T=F1*R
1990    F1=F
2000    F=T
2010    T=X*(F*G+R*G1)
2020    G1=G
2030    G=T
2040    IF Ks MODULO 2=1 THEN Pd=Pd-G
2050    NEXT Ks
2060    RETURN Pd
2070    FNEND
2080    !
```

```
2090    DEF FNPd357(DOUBLE N,REAL Tp,Dp)   !  N=3,5,7,...
2100    DOUBLE Ks                          !  INTEGER
2110    X=1./(1.+Tp*Tp)
2120    Tsq=Tp*SQR(X)
2130    D2=.5*Dp*Dp
2140    G=Tsq*EXP(-D2*X)*FNPhi(Dp*Tsq)
2150    Pd=FNPhi(Dp)-G
2160    IF N=3 THEN RETURN Pd
2170    R=SQR(2./PI)
2180    G1=G
2190    G=Tp*X*(EXP(-D2)/PI+R*Dp*G1)
2200    F1=Tp*Dp/R
2210    F=Tp*Dp*R
2220    FOR Ks=2 TO N-3
2230    R=(Ks-1)/Ks
2240    T=F1*R
2250    F1=F
2260    F=T
2270    T=X*(F*G+R*G1)
2280    G1=G
2290    G=T
2300    IF Ks MODULO 2=0 THEN Pd=Pd-G
2310    NEXT Ks
2320    RETURN Pd
2330    FNEND
2340    !
2350    DEF FNPhi(X)          !  HART, page 140, #5708 & #5725
2360    Y=ABS(X)*.70710678118654746
2370    SELECT Y
2380    CASE <8.
2390    P=1631.76026875371470+Y*(456.261458706092631+Y*(86.0827622119485951+Y*
(10.0648589749095425+Y*.564189586761813614)))
2400    P=3723.50798155480672+Y*(7113.66324695404987+Y*(6758.21696411048589+Y*
(4032.26701083004974+Y*P)))
2410    Q=7542.47951019347576+Y*(2968.00490148230872+Y*(817.622386304544077+Y*
(153.077710750362216+Y*(17.8394984391395565+Y))))
2420    Q=3723.50798155480654+Y*(11315.1920818544055+Y*(15802.5359994020425+Y*
(13349.3465612844574+Y*Q)))
2430    Phi=.5*EXP(-Y*Y)*P/Q
2440    CASE <26.6
2450    P=2.97886562639399289+Y*(7.40974060596474179+Y*(6.16020985310963054+Y*
(5.01904972678426746+Y*(1.27536664472996595+Y*.564189583547755074))))
2460    Q=3.36907520698275277+Y*(9.60896532719278787+Y*(17.0814407474660043+Y*
(12.0489519278551290+Y*(9.39603401623505415+Y*(2.26052852076732697+Y)))))
2470    Phi=.5*EXP(-Y*Y)*P/Q
2480    CASE ELSE
2490    Phi=0.
2500    END SELECT
2510    IF X>0. THEN Phi=1.-Phi
2520    RETURN Phi
2530    FNEND
```

Table E-2. EDF - Extreme

```
10   Ns=16                    !  NUMBER OF SAMPLES
20   Rs=1.                    !  RATIO r
30   X1=-15
40   X2=5
50   Gamma=.577215664902
60   C1=-Gamma
70   C2=PI/SQR(6.)
80   F=SQR(.5/PI)
90   A=-8.                    !  LIMITS ON
100  B=8.                     !  INTEGRAL
110  Mean_mucv=0.
120  Var_mucv=1./Ns
130  Mean_sigcv=1.-.39/Ns
140  Var_sigcv=1.05/(Ns+1.5)
150  Rho=-.55
160  COM H1,H2
170  DIM A$[30],B$[30]
180  DIM Xlabel$(1:30),Ylabel$(1:30)
190  DIM Xcoord(1:30),Ycoord(1:30)
200  DIM Xgrid(1:30),Ygrid(1:30)
210  DOUBLE Lx,Ly,Nx,Ny,I,Ns,It
220  !
230  A$="Threshold"
240  B$="Exceedance Probability"
250  !
260  Lx=11
270  REDIM Xlabel$(1:Lx),Xcoord(1:Lx)
280  DATA -15,-13,-11,-9,-7,-5,-3,-1,1,3,5
290  READ Xlabel$(*)
300  DATA -15,-13,-11,-9,-7,-5,-3,-1,1,3,5
310  READ Xcoord(*)
320  !
330  Ly=27
340  REDIM Ylabel$(1:Ly),Ycoord(1:Ly)
350  DATA E-6,E-5,E-4,.001,.002,.005,.01,.02,.05,.1,.2,.3,.4,.5
360  DATA .6,.7,.8,.9,.95,.98,.99
370  DATA .995,.998,.999,.9999,.99999,.999999
380  READ Ylabel$(*)
390  DATA 1.E-6,1.E-5,1.E-4,.001,.002,.005,.01,.02,.05,.1,.2,.3,.4,.5
400  DATA .6,.7,.8,.9,.95,.98,.99
410  DATA .995,.998,.999,.9999,.99999,.999999
420  READ Ycoord(*)
430  !
440  Nx=11
450  REDIM Xgrid(1:Nx)
460  DATA -15,-13,-11,-9,-7,-5,-3,-1,1,3,5
470  READ Xgrid(*)
480  !
490  Ny=27
500  REDIM Ygrid(1:Ny)
510  DATA 1.E-6,1.E-5,1.E-4,.001,.002,.005,.01,.02..05,.1,.2,.3,.4,.5
520  DATA .6,.7,.8,.9,.95,.98,.99
530  DATA .995,.998,.999,.9999,.99999,.999999
540  READ Ygrid(*)
550  !
```

```
560    FOR I=1 TO Ly
570    Ycoord(I)=FNInvphi(Ycoord(I))
580    NEXT I
590    FOR I=1 TO Ny
600    Ygrid(I)=FNInvphi(Ygrid(I))
610    NEXT I
620    Y1=Ygrid(1)
630    Y2=Ygrid(Ny)
640    GINIT 180./240.                        !  VERTICAL PAPER
650    PLOTTER IS 505,"HPGL"
660    PRINTER IS 505
670    LIMIT PLOTTER 505,0.,180.,0.,240.      !  1 GDU = 2 mm
680    VIEWPORT 20.,120.,19.,132.
690  ! VIEWPORT 22.,85.,59.,122.              !  TOP OF PAPER
700  ! VIEWPORT 22.,85.,19.,62.               !  BOTTOM OF PAPER
710    WINDOW X1,X2,Y1,Y2
720  !   PRINT "VS2"
730    FOR I=1 TO Nx
740    MOVE Xgrid(I),Y1
750    DRAW Xgrid(I),Y2
760    NEXT I
770    FOR I=1 TO Ny
780    MOVE X1,Ygrid(I)
790    DRAW X2,Ygrid(I)
800    NEXT I
810    PENUP
820    CSIZE 2.3,.5
830    LORG 5
840    Y=Y1-(Y2-Y1)*.02
850    FOR I=1 TO Lx
860    MOVE Xcoord(I),Y
870    LABEL Xlabel$(I)
880    NEXT I
890    CSIZE 3.,.5
900    MOVE .5*(X1+X2),Y1-.06*(Y2-Y1)
910    LABEL A$
920    CSIZE 2.3,.5
930    LORG 8
940    X=X1-(X2-X1)*.01
950    FOR I=1 TO Ly
960    MOVE X,Ycoord(I)
970    LABEL Ylabel$(I)
980    NEXT I
990    LDIR PI/2.
1000   CSIZE 3.,.5
1010   LORG 5
1020   MOVE X1-.15*(X2-X1),.5*(Y1+Y2)
1030   LABEL B$
1040     PRINT "VS36"
1050   Dx=(X2-X1)/100.
1060   DIM P(0:100)
```

```
1070    FOR Ds=0. TO 7.5 STEP .75          !   DEFLECTION d
1080    FOR It=0 TO 100
1090    J=It
1100    Th=X2-Dx*It                         !   THRESHOLD
1110    Mut=Mean_mucv+Th*Mean_sigcv
1120    Temp=Var_mucv+Th*Th*Var_sigcv
1130    Temp=Temp+2.*Th*SQR(Var_mucv*Var_sigcv)*Rho
1140    Sigmat=SQR(Temp)
1150    H1=C1+C2*(Mut-Ds)/Rs
1160    H2=C2*Sigmat/Rs
1170    Sa=FNS(A)
1180    Sb=FNS(B)
1190    PRINT "FNS(A) = ";Sa;"    FNS(B) = ";Sb
1200    DOUBLE N,K,J
1210    N=2
1220    H=(B-A)*.5
1230    S=(Sa+Sb)*.5
1240    V=1.E10
1250    T=0.
1260    FOR K=1 TO N-1 STEP 2
1270    T=T+FNS(A+H*K)
1280    NEXT K
1290    S=S+T
1300    Vo=V
1310    V=(S+T)*H*2./3.
1320    IF ABS(V-Vo)<1.E-9 THEN 1360
1330    N=N+N
1340    H=H*.5
1350    GOTO 1250
1360    Pd=F*V
1370    IF Pd>.9999995 THEN 1400
1380    P(It)=FNInvphi(Pd)
1390    NEXT It
1400    FOR It=0 TO J-1
1410    PLOT X2-Dx*It,P(It)
1420    NEXT It
1430    PENUP
1440    NEXT Ds
1450    PAUSE
1460    PRINTER IS CRT
1470    PLOTTER 505 IS TERMINATED
1480    END
1490    !
1500    DEF FNInvphi(X)       !  AMS 55, 26.2.23
1510    IF X=.5 THEN RETURN 0.
1520    P=MIN(X,1.-X)
1530    T=-LOG(P)
1540    T=SQR(T+T)
1550    P=1.+T*(1.432788+T*(.189269+T*.001308))
1560    P=T-(2.515517+T*(.802853+T*.010328))/P
1570    IF X<.5 THEN P=-P
1580    RETURN P
1590    FNEND
1600    !
1610    DEF FNS(X)
1620    COM H1,H2
1630    T=.5*X*X+EXP(H1+H2*X)
1640    IF T>100. THEN RETURN 0.
1650    RETURN EXP(-T)
1660    FNEND
```

Table E-3. Simulation - Extreme

```
10    Ns=16                          !  NUMBER OF SAMPLES
20    DATA 0,.75,1.5,2.25,3.,3.75,4.5,5.25,6.,6.75,7.5   !  DEFLECTION d
30    Rs=1.                          !  SCALING r
40    Nt=2^20                        !  NUMBER OF TRIALS
50    A$="E-16-75to75-1-23"          !  FILE NAME
60    Nb=1000                        !  NUMBER OF BINS
70    Mean=-.577215664902            !  FOR Vt, LOG OF EXPONENTIAL
80    Sigma=PI/SQR(6.)               !    RANDOM VARIABLE
90      Zmin=-15.                    !  MINIMUM Z VALUE
100     Zmax=5.                      !  MAXIMUM Z VALUE
110   DOUBLE Ns,Nt,Nb,Kt,Ks,J        !  INTEGERS
120   DIM P0(1000),P1(1000),P2(1000),P3(1000),P4(1000),P5(1000)
130   DIM P6(1000),P7(1000),P8(1000),P9(1000),P10(1000),Edf(1:11000)
140   READ D0,D1,D2,D3,D4,D5,D6,D7,D8,D9,D10
150   A0=-Mean/Sigma
160   A1=1./Sigma
170   F=1./Ns
180   G=1./SQR(Ns-1)
190   Dz=(Zmax-Zmin)/Nb
200   FOR Kt=1 TO Nt                 !  SIMULATION
210   S1=S2=0.
220   FOR Ks=1 TO Ns
230   Vt=LOG(-LOG(RND))              !  UN-NORMALIZED RANDOM VARIABLE.
240   V=A1*Vt+A0                     !  ZERO MEAN, UNIT VARIANCE RV
250   S1=S1+V
260   S2=S2+V*V
270   NEXT Ks
280   Mc=S1*F                        !  SAMPLE MEAN
290   Sc=SQR(S2-Ns*Mc*Mc)*G          !  SAMPLE STANDARD DEVIATION
300   Vt=LOG(-LOG(RND))
310   V=A1*Vt+A0
320   C=Rs*V-Mc
330   Z=(D0+C)/Sc
340   J=INT((Z-Zmin)/Dz)
350   IF J<0 THEN J=0
360   IF J>Nb THEN J=Nb
370   P0(J)=P0(J)+1.
380   Z=(D1+C)/Sc
390   J=INT((Z-Zmin)/Dz)
400   IF J<0 THEN J=0
410   IF J>Nb THEN J=Nb
420   P1(J)=P1(J)+1.
430   Z=(D2+C)/Sc
440   J=INT((Z-Zmin)/Dz)
450   IF J<0 THEN J=0
460   IF J>Nb THEN J=Nb
470   P2(J)=P2(J)+1.
480   Z=(D3+C)/Sc
490   J=INT((Z-Zmin)/Dz)
500   IF J<0 THEN J=0
510   IF J>Nb THEN J=Nb
520   P3(J)=P3(J)+1.
```

```
530   Z=(D4+C)/Sc
540   J=INT((Z-Zmin)/Dz)
550   IF J<0 THEN J=0
560   IF J>Nb THEN J=Nb
570   P4(J)=P4(J)+1.
580   Z=(D5+C)/Sc
590   J=INT((Z-Zmin)/Dz)
600   IF J<0 THEN J=0
610   IF J>Nb THEN J=Nb
620   P5(J)=P5(J)+1.
630   Z=(D6+C)/Sc
640   J=INT((Z-Zmin)/Dz)
650   IF J<0 THEN J=0
660   IF J>Nb THEN J=Nb
670   P6(J)=P6(J)+1.
680   Z=(D7+C)/Sc
690   J=INT((Z-Zmin)/Dz)
700   IF J<0 THEN J=0
710   IF J>Nb THEN J=Nb
720   P7(J)=P7(J)+1.
730   Z=(D8+C)/Sc
740   J=INT((Z-Zmin)/Dz)
750   IF J<0 THEN J=0
760   IF J>Nb THEN J=Nb
770   P8(J)=P8(J)+1.
780   Z=(D9+C)/Sc
790   J=INT((Z-Zmin)/Dz)
800   IF J<0 THEN J=0
810   IF J>Nb THEN J=Nb
820   P9(J)=P9(J)+1.
830   Z=(D10+C)/Sc
840   J=INT((Z-Zmin)/Dz)
850   IF J<0 THEN J=0
860   IF J>Nb THEN J=Nb
870   P10(J)=P10(J)+1.
880   NEXT Kt
890   MAT P0=P0/(Nt)
900   MAT P1=P1/(Nt)
910   MAT P2=P2/(Nt)
920   MAT P3=P3/(Nt)
930   MAT P4=P4/(Nt)
940   MAT P5=P5/(Nt)
950   MAT P6=P6/(Nt)
960   MAT P7=P7/(Nt)
970   MAT P8=P8/(Nt)
980   MAT P9=P9/(Nt)
990   MAT P10=P10/(Nt)
1000  S0=S1=S2=S3=S4=S5=S6=S7=S8=S9=S10=0.
```

8 Jun 1987   14:18:02

```
1010    FOR J=Nb TO 0 STEP -1
1020    S0=S0+P0(J)
1030    IF S0=0. THEN 1060
1040    IF S0>=1. THEN 1070
1050    P0(J)=FNInvphi(S0)          !  P0(J)=Prob(Z0>=Zmin+J*Dz)
1060    NEXT J
1070    P0(J)=0.
1080    FOR J=Nb TO 0 STEP -1
1090    S1=S1+P1(J)
1100    IF S1=0. THEN 1130
1110    IF S1>=1. THEN 1140
1120    P1(J)=FNInvphi(S1)
1130    NEXT J
1140    P1(J)=0.
1150    FOR J=Nb TO 0 STEP -1
1160    S2=S2+P2(J)
1170    IF S2=0. THEN 1200
1180    IF S2>=1. THEN 1210
1190    P2(J)=FNInvphi(S2)
1200    NEXT J
1210    P2(J)=0.
1220    FOR J=Nb TO 0 STEP -1
1230    S3=S3+P3(J)
1240    IF S3=0. THEN 1270
1250    IF S3>=1. THEN 1280
1260    P3(J)=FNInvphi(S3)
1270    NEXT J
1280    P3(J)=0.
1290    FOR J=Nb TO 0 STEP -1
1300    S4=S4+P4(J)
1310    IF S4=0. THEN 1340
1320    IF S4>=1. THEN 1350
1330    P4(J)=FNInvphi(S4)
1340    NEXT J
1350    P4(J)=0.
1360    FOR J=Nb TO 0 STEP -1
1370    S5=S5+P5(J)
1380    IF S5=0. THEN 1410
1390    IF S5>=1. THEN 1420
1400    P5(J)=FNInvphi(S5)
1410    NEXT J
1420    P5(J)=0.
1430    FOR J=Nb TO 0 STEP -1
1440    S6=S6+P6(J)
1450    IF S6=0. THEN 1480
1460    IF S6>=1. THEN 1490
1470    P6(J)=FNInvphi(S6)
1480    NEXT J
1490    P6(J)=0.
1500    FOR J=Nb TO 0 STEP -1
1510    S7=S7+P7(J)
1520    IF S7=0. THEN 1550
1530    IF S7>=1. THEN 1560
1540    P7(J)=FNInvphi(S7)
1550    NEXT J
1560    P7(J)=0.
```

```
1570   FOR J=Nb TO 0 STEP -1
1580   S8=S8+P8(J)
1590   IF S8=0. THEN 1620
1600   IF S8>=1. THEN 1630
1610   P8(J)=FNInvphi(S8)
1620   NEXT J
1630   P8(J)=0.
1640   FOR J=Nb TO 0 STEP -1
1650   S9=S9+P9(J)
1660   IF S9=0. THEN 1690
1670   IF S9>=1. THEN 1700
1680   P9(J)=FNInvphi(S9)
1690   NEXT J
1700   P9(J)=0.
1710   FOR J=Nb TO 0 STEP -1
1720   S10=S10+P10(J)
1730   IF S10=0. THEN 1760
1740   IF S10>=1. THEN 1770
1750   P10(J)=FNInvphi(S10)
1760   NEXT J
1770   P10(J)=0.
1780   FOR J=1 TO Nb
1790   Edf(J)=P0(J)
1800   Edf(J+Nb)=P1(J)
1810   Edf(J+Nb*2)=P2(J)
1820   Edf(J+Nb*3)=P3(J)
1830   Edf(J+Nb*4)=P4(J)
1840   Edf(J+Nb*5)=P5(J)
1850   Edf(J+Nb*6)=P6(J)
1860   Edf(J+Nb*7)=P7(J)
1870   Edf(J+Nb*8)=P8(J)
1880   Edf(J+Nb*9)=P9(J)
1890   Edf(J+Nb*10)=P10(J)
1900   NEXT J
1910   CREATE DATA A$,396
1920   ASSIGN #1 TO A$
1930   PRINT #1;Edf(*)
1940   ASSIGN #1 TO *
1950   PAUSE
1960   END
1970   !
1980   DEF FNInvphi(X)                 !  AMS 55, 26.2.23
1990   IF X=.5 THEN RETURN 0.
2000   P=MIN(X,1.-X)
2010   T=-LOG(P)
2020   T=SQR(T+T)
2030   P=1.+T*(1.432788+T*(.189269+T*.001308))
2040   P=T-(2.515517+T*(.802853+T*.010328))/P
2050   IF X<.5 THEN P=-P
2060   RETURN P
2070   FNEND
```

Table E-4. Plot - Simulation

```
10   A$="E-16-75to75-1-23"
20   Zmin=-15.
30   Zmax=5.
40   X1=-15.
50   X2=5.
60   Nb=1000
70   ASSIGN #1 TO A$
80   READ #1;Edf(*)
90   ASSIGN #1 TO *
100  DIM Edf(1:11000)
110  DIM A$[30],B$[30]
120  DIM Xlabel$(1:30),Ylabel$(1:30)
130  DIM Xcoord(1:30),Ycoord(1:30)
140  DIM Xgrid(1:30),Ygrid(1:30)
150  DOUBLE Nb,Lx,Ly,Nx,Ny,I,K        !  INTEGERS
160  !
170  A$="Threshold"
180  B$="Exceedance Probability"
190  !
200  Lx=11
210  REDIM Xlabel$(1:Lx),Xcoord(1:Lx)
220  DATA -15,-13,-11,-9,-7,-5,-3,-1,1,3,5
230  READ Xlabel$(*)
240  DATA -15,-13,-11,-9,-7,-5,-3,-1,1,3,5
250  READ Xcoord(*)
260  !
270  Ly=27
280  REDIM Ylabel$(1:Ly),Ycoord(1:Ly)
290  DATA E-6,E-5,E-4,.001,.002,.005,.01,.02,.05
300  DATA .1,.2,.3,.4,.5,.6,.7,.8,.9,.95,.98,.99
310  DATA .995,.998,.999,.9999,.99999,.999999
320  READ Ylabel$(*)
330  DATA 1.E-6,1.E-5,1.E-4,.001,.002,.005,.01,.02,.05
340  DATA .1,.2,.3,.4,.5,.6,.7,.8,.9,.95,.98,.99
350  DATA .995,.998,.999,.9999,.99999,.999999
360  READ Ycoord(*)
370  !
380  Nx=11
390  REDIM Xgrid(1:Nx)
400  DATA -15,-13,-11,-9,-7,-5,-3,-1,1,3,5
410  READ Xgrid(*)
420  !
430  Ny=27
440  REDIM Ygrid(1:Ny)
450  DATA 1.E-6,1.E-5,1.E-4,.001,.002,.005,.01,.02,.05
460  DATA .1,.2,.3,.4,.5,.6,.7,.8,.9,.95,.98,.99
470  DATA .995,.998,.999,.9999,.99999,.999999
480  READ Ygrid(*)
490  !
```

```
500    FOR I=1 TO Ly
510    Ycoord(I)=FNInvphi(Ycoord(I))
520    NEXT I
530    FOR I=1 TO Ny
540    Ygrid(I)=FNInvphi(Ygrid(I))
550    NEXT I
560    Y1=Ygrid(1)
570    Y2=Ygrid(Ny)
580    GINIT 180./240.                          !  VERTICAL PAPER
590    PLOTTER IS 505,"HPGL"
600    PRINTER IS 505
610    LIMIT PLOTTER 505,0.,180.,0.,240.        !  1 GDU = 2 mm
620    VIEWPORT 20.,120.,19.,132.
630  ! VIEWPORT 22.,85.,59.,122.               !  TOP OF PAPER
640  ! VIEWPORT 22.,85.,19.,62.                !  BOTTOM OF PAPER
650    WINDOW X1,X2,Y1,Y2
660  !   PRINT "VS2"
670    FOR I=1 TO Nx
680    MOVE Xgrid(I),Y1
690    DRAW Xgrid(I),Y2
700    NEXT I
710    FOR I=1 TO Ny
720    MOVE X1,Ygrid(I)
730    DRAW X2,Ygrid(I)
740    NEXT I
750    PENUP
760    LDIR 0
770    CSIZE 2.3,.5
780    LORG 5
790    Y=Y1-(Y2-Y1)*.02
800    FOR I=1 TO Lx
810    MOVE Xcoord(I),Y
820    LABEL Xlabel$(I)
830    NEXT I
840    CSIZE 3.,.5
850    MOVE .5*(X1+X2),Y1-.06*(Y2-Y1)
860    LABEL A$
870    CSIZE 2.3,.5
880    LORG 8
890    X=X1-(X2-X1)*.01
900    FOR I=1 TO Ly
910    MOVE X,Ycoord(I)
920    LABEL Ylabel$(I)
930    NEXT I
940    LDIR PI/2.
950    CSIZE 3.,.5
960    LORG 5
970    MOVE X1-.15*(X2-X1),.5*(Y1+Y2)
980    LABEL B$
990      PRINT "VS36"
```

```
1000    Dz=(Zmax-Zmin)/Nb
1010    FOR I=1 TO Nb
1020    T=Edf(I)
1030    IF T=0. THEN 1050
1040    PLOT Zmin+Dz*I,T
1050    NEXT I
1060    PENUP
1070    FOR I=1 TO Nb
1080    T=Edf(I+Nb)
1090    IF T=0. THEN 1110
1100    PLOT Zmin+Dz*I,T
1110    NEXT I
1120    PENUP
1130    K=Nb*2
1140    FOR I=1 TO Nb
1150    T=Edf(I+K)
1160    IF T=0. THEN 1180
1170    PLOT Zmin+Dz*I,T
1180    NEXT I
1190    PENUP
1200    K=Nb*3
1210    FOR I=1 TO Nb
1220    T=Edf(I+K)
1230    IF T=0. THEN 1250
1240    PLOT Zmin+Dz*I,T
1250    NEXT I
1260    PENUP
1270    K=Nb*4
1280    FOR I=1 TO Nb
1290    T=Edf(I+K)
1300    IF T=0. THEN 1320
1310    PLOT Zmin+Dz*I,T
1320    NEXT I
1330    PENUP
1340    K=Nb*5
1350    FOR I=1 TO Nb
1360    T=Edf(I+K)
1370    IF T=0. THEN 1390
1380    PLOT Zmin+Dz*I,T
1390    NEXT I
1400    PENUP
1410    K=Nb*6
1420    FOR I=1 TO Nb
1430    T=Edf(I+K)
1440    IF T=0. THEN 1460
1450    PLOT Zmin+Dz*I,T
1460    NEXT I
1470    PENUP
```

```
1480    K=Nb*7
1490    FOR I=1 TO Nb
1500    T=Edf(I+K)
1510    IF T=0. THEN 1530
1520    PLOT Zmin+Dz*I,T
1530    NEXT I
1540    PENUP
1550    K=Nb*8
1560    FOR I=1 TO Nb
1570    T=Edf(I+K)
1580    IF T=0. THEN 1600
1590    PLOT Zmin+Dz*I,T
1600    NEXT I
1610    PENUP
1620    K=Nb*9
1630    FOR I=1 TO Nb
1640    T=Edf(I+K)
1650    IF T=0. THEN 1670
1660    PLOT Zmin+Dz*I,T
1670    NEXT I
1680    PENUP
1690    K=Nb*10
1700    FOR I=1 TO Nb
1710    T=Edf(I+K)
1720    IF T=0. THEN 1740
1730    PLOT Zmin+Dz*I,T
1740    NEXT I
1750    PENUP
1760    PAUSE
1770    PRINTER IS CRT
1780    PLOTTER 505 IS TERMINATED
1790    END
1800    !
1810    DEF FNInvphi(X)       !  AMS 55, 26.2.23
1820    IF X=.5 THEN RETURN 0.
1830    P=MIN(X,1.-X)
1840    T=-LOG(P)
1850    T=SQR(T+T)
1860    P=1.+T*(1.432788+T*(.189269+T*.001308))
1870    P=T-(2.515517+T*(.802853+T*.010328))/P
1880    IF X<.5 THEN P=-P
1890    RETURN P
1900    FNEND
```

REFERENCES

1. A. H. Nuttall and P. G. Cable, Operating Characteristics for Maximum Likelihood Detection of Signals in Gaussian Noise of Unknown Level; I. Coherent Signals of Unknown Level, NUSC Technical Report 4243, New London, CT, 27 March 1972.

2. P. G. Cable and A. H. Nuttall, Operating Characteristics for Maximum Likelihood Detection of Signals in Gaussian Noise of Unknown Level; II. Phase-Incoherent Signals of Unknown Level, NUSC Technical Report 4683, New London, CT, 22 April 1974.

3. A. H. Nuttall and P. G. Cable, Operating Characteristics for Maximum Likelihood Detection of Signals in Gaussian Noise of Unknown Level; III. Random Signals of Unknown Level, NUSC Technical Report 4783, New London, CT, 31 July 1974.

4. M. G. Kendall and A. Stuart, The Advanced Theory of Statistics, Volume 1, Distribution Theory, Third Edition, Hafner Publishing Co., New York, N.Y., 1969.

5. Handbook of Mathematical Functions, U. S. Department of Commerce, National Bureau of Standards, Applied Mathematics Series No. 55, U. S. Government Printing Office, Washington, DC, June 1964.

6. A. H. Nuttall, Operating Characteristics of Crosscorrelator With or Without Sample Mean Removal, NUSC Technical Report 7045, New London, CT, 14 August 1984.

7. A. H. Nuttall, "On the Distribution of a Chi-Squared Variate Raised to a Power," NUSC Technical Memorandum 831059, New London, CT, 19 April 1983.

8. W. Feller, An Introduction to Probability Theory and its Applications, Vol. II, J. Wiley and Sons, Inc., New York, N.Y., 1966.

Technical Report 8133
1 October 1987

Detection Performance of Normalizer for Multiple Signals Subject to Partially Correlated Fading With Chi-Squared Statistics

A. H. Nuttall

ABSTRACT

The false alarm and detection probabilities for a multi-pulse signal subject to partially correlated fading, in the presence of Gaussian noise of unknown level, are derived in closed form. The number K of signal pulses, as well as the number L of noise-only pulses used to estimate the noise background power level, are arbitrary. The power fading is characterized by a chi-squared distribution with 2m degrees of freedom and a normalized set of covariance coefficients $\{\rho_{k,j}\}$, all of which can be selected arbitrarily, in order to match an experimental realization or an actual measured situation. The performance capability of this processor depends additionally on the received signal-to-noise ratio.

This study is an extension of NUSC Technical Report 7707, to cover the case of a nonconstant threshold. Comparisons of this normalizer with the earlier results (for $L = \infty$) enable a quantitative evaluation of the losses incurred by lack of knowledge of the noise level. The important capability of constant false alarm rate is achieved by this normalizer.

Plots of the detection probability vs. false alarm probability are furnished for a variety of typical choices of the various parameters; however, the multitude of parameters and cases precludes a comprehensive all-encompassing compilation of numerical results. Accordingly, a general program in BASIC is listed, whereby additional results of interest to a particular user can be eaaily obtained, once numerical values are assigned to all the parameters.

TABLE OF CONTENTS

LIST OF ILLUSTRATIONS

LIST OF TABLES

LIST OF SYMBOLS

K	number of signal pulses added, figure 1
L	number of noise-only pulses, figure 1
m	fading parameter, table 1
ρ_{kj}	normalized covariance coefficient, table 1
ROC	Receiver Operating Characteristic
SNR	Signal-to-Noise Ratio
FFT	Fast Fourier Transform
$\overline{E_1}$	average received signal energy per pulse
N_0	single-sided noise spectral density level (watts/Hz)
K_e	equivalent number of samples, table 2
N	summary parameter, table 2
γ	sum of K signal squared-envelope samples
σ_n^2	noise power
a,b	auxiliary constants, (2)
R	scaled signal-to-noise ratio, (2)
Q_γ	exceedance distribution function of γ
Λ	scaled threshold, (3)
$E_n(x)$	exceedance function, (5)

LIST OF SYMBOLS (Cont'd)

$e_n(x)$	partial exponential, (6)
γ_o	sum of L noise-only squared-envelope samples
v	normalizer ratio output, (9)
$\tilde{v}$	alternative normalizer ratio, (10)
u	threshold, (11)
P_v	cumulative distribution function of v
$f(\xi)$	characteristic function, (12)
$p(u)$	probability density function, (13)
$H_\ell(x)$	hypergeometric function, (25)
P_D	detection probability, (30)
P_F	false alarm probability, (31)
ρ	exponential correlation coefficient, (32)

DETECTION PERFORMANCE OF NORMALIZER FOR MULTIPLE SIGNALS SUBJECT TO PARTIALLY CORRELATED FADING WITH CHI-SQUARED STATISTICS

INTRODUCTION

In a recent study [1], the detection performance capability of a multiple-pulse system subject to correlated fading was quantitatively delineated. It was assumed there that the noise level was known, so that a threshold could be set for an arbitrarily specified false alarm probability. Then the detection probability was evaluated as a function of the threshold level, the received signal-to-noise ratio, the number K of signal pulses, and the fading statistics.

Here we will extend these earlier results to cover the case where, additionally, the noise level is unknown and must be estimated on the basis of a finite number L of noise-only samples. The same approximation technique that was presented in [1] is used to determine the detection probability of this normalizer system. The reader is referred to [1] for additional background, motivation, interpretations, and related references. For the sake of brevity, we will employ the same notation and presume that the reader has complete familiarity with the earlier material and development.

PROBLEM DEFINITION

We will couch the problem in a particular setting, one with obvious appeal and application; however, it should be obvious how to extend this setting to a more general one, particularly in light of the arbitrary fading covariance coefficients that are allowed in the analysis.

Suppose a sequence of K tone bursts at a common center frequency are transmitted, as depicted in figure 1. Each rectangular slot symbolizes

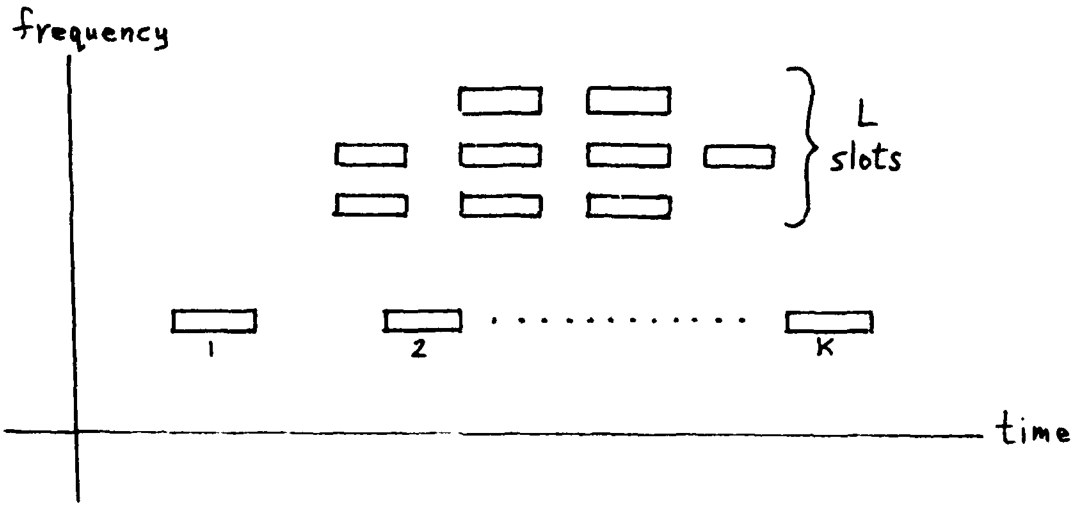

Figure 1. Time-Frequency Occupancy Diagram

a tone of duration T_1 seconds and approximate frequency bandwidth $1/T_1$ Hz. These bursts may be abutting in time or may be arbitrarily separated in time by several multiples of T_1. At the receiver, K narrowband filters of bandwidth $1/T_1$ Hz are sampled at the times of peak signal output (if present) and their squared envelopes are summed. Depending on the time separation between pulses, the signal strength may fade considerably; the

exact amount and frequency of the fading depends on the distribution of the fading and the covariance of the fading amplitude of adjacent (as well as separated) pulses.

It is presumed that, during a single tone of duration T_1 seconds, the fading is essentially constant, resulting in a constant amplitude scaling and phase shift applied to the pulse. The time separations between pulses in figure 1 are arbitrary, thereby allowing for an arbitrary degree of correlation between the fading factors applied to each pulse. Phase shifts can have arbitrary statistics and dependencies.

To establish a reference against which this sum of K matched filter outputs can be compared, for purposes of deciding on the presence or absence of signal, a group of L nonoverlapping noise-only slots, located arbitrarily in the time-frequency plane, are also energy-detected and summed. For very large L, this noise reference is very stable, and performance approaches that predicted by [1]. However, for moderate values of L and for small false alarm probabilities of interest, it is important to know how much degradation in performance is incurred by being forced to use this noisy reference.

An obvious implementation of the processing implied by figure 1 is to employ fast Fourier transforms. The L reference bins can then be an arbitrary collection of time and/or frequency bins. However, L cannot be so large that nonstationary and/or nonwhite noises cause their own kind of errors in noise power estimation. The tradeoff between these conflicting requirements will be assessed quantitatively in this investigation.

NORMALIZER PROBABILITIES

DEFINITIONS OF PARAMETERS

Very heavy reliance will be made here on the basis that was set up in [1]. Thus we have the following fundamental parameters of the detection procedure (the immediate references in tables 1 and 2 are to [1]):

K, number of potential-signal pulses added, (figure 1 and A-11);

m, signal fading parameter (power-scaling is chi-squared with 2m degrees of freedom), (13);

$\{\rho_{kj}\}$, normalized covariance coefficients of signal power-scalings $\{q_k\}$, (15);

$\frac{\overline{E_1}}{N_0}$, $\frac{\text{average received signal energy per pulse}}{\text{single-sided received noise spectral density level}}$, (9);

L, number of noise-only pulses added.

Table 1. Fundamental Parameters

In addition, there are two very useful auxiliary parameters that found frequent use in [1]:

K_e, $K^2 \Big/ \sum_{kj=1}^{K} \rho_{kj}$ = equivalent number of independent signal pulses, (10);

N, $m K_e$ = a summary parameter describing the distribution of the sum of power scalings, (A-24) and (A-29).

Table 2. Auxiliary Parameters

None of the parameters, m, K_e, N, need be integer. Also, N can be larger or smaller than K, the number of signal pulses.

PROBABILITIES FOR KNOWN NOISE LEVEL

The probability density function of the sum γ [1; (A-11)] of the K signal envelope-squared samples is given by [1; (B-4)]

$$p_\gamma(u) = \frac{\exp(-u/a)\ u^{K-1}}{a^{K-N}\ b^N\ \Gamma(K)}\ {}_1F_1\left(N;\ K;\ u\left(\frac{1}{a} - \frac{1}{b}\right)\right) \quad \text{for } u > 0\ , \tag{1}$$

where [1; (A-32),(B-3),(B-7)]

$$a = 2\sigma_n^2\ , \quad b = 2\sigma_n^2\ (1 + R)\ , \quad R = \frac{\overline{E}_1}{N_0}\ \frac{K}{N}\ . \tag{2}$$

The exceedance distribution function $Q_\gamma(u)$ of output sum γ is given by several alternative forms in [1; (B-9),(B-11),(B-13)]. For a fixed threshold (known noise level), the detection probability is

$$P_D = Q_\gamma(\Lambda, R, N, K) =$$

$$= 1 - \frac{1}{(1 + R)^N} \sum_{n=0}^{\infty} \frac{(N)_n}{n!} \left(\frac{R}{1 + R}\right)^n \left[1 - E_{K-1+n}(\Lambda)\right] , \ \Lambda = \frac{u}{2\sigma_n^2} , \qquad (3)$$

and the false alarm probability is [1; (B-10)]

$$P_F = E_{K-1}(\Lambda) , \qquad (4)$$

where we define the exceedance distribution function

$$E_n(x) = \exp(-x) \ e_n(x) , \qquad (5)$$

and

$$e_n(x) = \sum_{j=0}^{n} x^j/j! \qquad (6)$$

is the partial exponential [2; 6.5.11]. The results in (3) and (4) should be used for $L = \infty$, that is, for known noise level.

NORMALIZER RATIO

From this point on, L is presumed finite. Suppose a noise level estimate, γ_0, is obtained, based upon L independent measurements of noise-only bins. It is assumed that the average noise level in these L bins is the same as in the K potential-signal bins, but that this noise level is unknown. If we let

$$\gamma = \gamma(K, \bar{E}_1/N_0) \tag{7}$$

denote the sum of K signal bin outputs with average signal-to-noise ratio $\bar{E}_1/N_0$, then

$$\gamma_0 = \gamma(L, 0) \tag{8}$$

is the corresponding sum of L noise-only bins. Now define ratio

$$\upsilon = \frac{\gamma}{\gamma_0} = \frac{\gamma(K, \bar{E}_1/N_0)}{\gamma(L, 0)} \tag{9}$$

for sets of K and L pulses, respectively. The noise contributions to the total of K + L outputs are presumed independent of each other; however, the signal fading factors amongst the K signal outputs are correlated to an arbitrary degree. We are interested in the distribution of this normalizer ratio, υ.

When signal is absent, the ratio υ in (9) is independent of the absolute level of the received noise; therefore, we can expect the normalizer to achieve the important capability of constant false alarm rate. That means that a specified false alarm probability can be achieved without knowledge of the average noise power level.

The quantities γ and γ_0 are the sums of K and L squared-envelope samples, respectively, and are not the averages of these sampled quantities. In terms of the sample-average quantities, we could define a slightly different normalizer ratio

$$\tilde{\upsilon} \equiv \frac{\gamma/K}{\gamma_0/L} = \frac{L}{K}\,\upsilon \ . \tag{10}$$

It then readily follows that the cumulative distribution function of random variable $\tilde{\upsilon}$ is

$$P_{\tilde{\upsilon}}(u) = \text{Prob}(\tilde{\upsilon} < u) = \text{Prob}\left(\upsilon < \frac{K}{L}\,u\right) = P_{\upsilon}\left(\frac{K}{L}\,u\right) \ , \tag{11}$$

in terms of the cumulative distribution function of ratio υ in (9). Thus, a simple scale factor change allows for consideration of the alternative ratio $\tilde{\upsilon}$.

When we plot the detection probability versus the false alarm probability, that is, eliminate the threshold, the same performance characteristics result for random variable υ as for $\tilde{\upsilon}$. Accordingly, we will not use or refer to $\tilde{\upsilon}$ or $P_{\tilde{\upsilon}}(u)$ any further, but concentrate solely on normalizer ratio υ, given by (9).

NORMALIZER DISTRIBUTIONS

The characteristic function of noise-only random variable γ_0 can be found directly from [1; (A-13)] by setting A to zero and replacing K by L:

$$f_{\gamma_0}(\xi) = (1 - i\xi a)^{-L} \ , \quad a = 2\sigma_n^2 \ . \tag{12}$$

The corresponding probability density function of γ_0 is

$$p_{\gamma_0}(u) = \frac{u^{L-1}\exp(-u/a)}{\Gamma(L)\, a^L} \quad \text{for } u > 0\ . \tag{13}$$

The exceedance distribution function is

$$Q_{\gamma_0}(u) = \mathrm{Prob}(\gamma_0 > u) = E_{L-1}(u/a) \quad \text{for } u > 0\ , \tag{14}$$

in terms of the functions defined in (5) and (6).

The cumulative distribution function of ratio v in (9) is given by (since $\gamma_0 > 0$)

$$P_v(u) = \mathrm{Prob}(v < u) = \mathrm{Prob}\left(\frac{\gamma}{\gamma_0} < u\right) = \mathrm{Prob}\left(\gamma < u\gamma_0\right) =$$

$$= \int_0^\infty dy\ p_\gamma(y) \int_{y/u}^\infty dx\ p_{\gamma_0}(x) = \int_0^\infty dy\ p_\gamma(y)\ Q_{\gamma_0}(y/u) =$$

$$= \int_0^\infty dy\ \frac{\exp(-y/a)\ y^{K-1}}{a^{K-N}\ b^N\ \Gamma(K)}\ {}_1F_1\left(N;\ K;\ y\left(\frac{1}{a} - \frac{1}{b}\right)\right)\ E_{L-1}\left(\frac{y}{ua}\right) \tag{15}$$

for threshold $u > 0$, where we used (1) and (14). We now expand E_{L-1} according to (5) and (6) and integrate term-by-term,to obtain [3; 7.621 4]

$$P_v(u) = \left(\frac{a}{b}\right)^N \left(\frac{u}{1+u}\right)^K \sum_{\ell=0}^{L-1} \frac{(K)_\ell}{\ell!\ (1+u)^\ell}\ F\left(N,\ K+\ell\ ;\ K;\ \left(1 - \frac{a}{b}\right)\frac{u}{1+u}\right). \tag{16}$$

But from (2),

$$\frac{a}{b} = \frac{1}{1 + R}, \qquad R = \frac{\bar{E}_1}{N_o} \frac{K}{N}, \tag{17}$$

where the parameters involved are described in tables 1 and 2. Making these substitutions in (16), there follows for the cumulative distribution function of random variable υ,

$$P_\upsilon(u) = \frac{1}{(1 + R)^N} \left(\frac{u}{1 + u}\right)^K \sum_{\ell=0}^{L-1} \frac{(K)_\ell}{\ell!\,(1 + u)^\ell} F\left(N, K + \ell; K; \frac{R}{1 + R} \frac{u}{1 + u}\right). \tag{18}$$

An alternative more useful form is obtained when we use [2; 15.3.3]:

$$P_\upsilon(u) = \left(\frac{u}{1 + u}\right)^K \left(\frac{1 + u}{1 + u + R}\right)^N \sum_{\ell=0}^{L-1} \frac{(K)_\ell}{\ell!} \left(\frac{1 + R}{1 + u + R}\right)^\ell F\left(-\ell, K - N; K; \frac{R}{1 + R} \frac{u}{1 + u}\right) \tag{19}$$

for $u > 0$. This result is very attractive since the negative integer argument, $-\ell$, in the hypergeometric function causes termination of the series at ℓ terms. Thus, (19) is a closed form (albeit tedious) for the cumulative distribution function of υ, involving a finite number of elementary functions.

It should be noticed that the absolute noise level σ_n^2 does not appear in (18) or (19). (The cumulative distribution function for alternative normalizer ratio $\tilde{\upsilon}$ given by (10) can now easily be found by use of (11).)

COMPARISON WITH EARLIER RESULTS

The result (19) for the cumulative distribution function of normalizer ratio υ, operating in a partially correlated fading environment, is an approximation, having been based upon a characteristic function fitting procedure explained in [1; (A-24)-(A-28)]. Nevertheless, (19) is identical with the exact fading result for a related normalizer problem; namely, agreement with [4; (25)] is achieved under the following identifications:

TR 4783	Here	Interpretation
α	u	threshold
M	K	number of signal pulses
N	L	number of noise-only pulses
$\upsilon + 1$	N	m K_e, table 2
μ	R	$\frac{\overline{E}_1}{N_o}\frac{K}{N}$, (2)

Table 3. Identification of Variables

The identity of $\upsilon + 1$ with N is made by comparing [4; (24A)] with [1; (A-29)]. The final identity of μ with R utilizes [4; (24B)] and [1; (9)]:

$$\mu = \frac{\overline{R}_T}{\upsilon + 1} \rightarrow \frac{\overline{E}_T/N_o}{N} = \frac{\overline{E}_1 \; K/N_o}{N} = R \, , \tag{20}$$

where the arrow indicates transferrance from [4] to [1].

The approach in [4] proceeded as follows: the detection probability for nonfading signals in all the bins depended only on the total received signal-to-noise ratio R_T. When R_T was assigned the fading probability density function [4; (24A)], the average detection probability in [4; (25)] resulted. For the special case of fading parameter $\upsilon = M - 1$ there, numerous graphical results were given in [4; figures 1-36].

The current results here are more general, in that they allow for partially correlated fading (through parameter K_e) and a more general power-fading model (with 2m degrees of freedom). This means that $N = m\,K_e$ here is not restricted to be equal to the number of signal pulses, K, but is arbitrary. Thus the current numerical results will significantly augment and extend those in [4]. If N = K here, then $R = \overline{E_1}/N_o$ = signal-to-noise ratio per pulse, and (19) reduces to [4; (15B)], for which many numerical results were given in [4; figures 1-36].

SPECIAL CASES

For m = 1, which corresponds to Rayleigh amplitude fading, and for $\rho_{kj} = \delta_{kj}$, which corresponds to uncorrelated fading, then $K_e = K$, $N = K$, and we get from (19),

$$P_\upsilon(u) = \left(\frac{u}{1 + u + R}\right)^K \sum_{\ell=0}^{L-1} \frac{(K)_\ell}{\ell!} \left(\frac{1 + R}{1 + u + R}\right)^\ell , \qquad (21)$$

in agreement with [4; (15B)].

On the other hand, if R = 0, then (18) and (19) both reduce to

$$P_{\upsilon}^{(o)}(u) = \left(\frac{u}{1+u}\right)^{K} \sum_{\ell=0}^{L-1} \frac{(K)_{\ell}}{\ell!\ (1+u)^{\ell}} , \tag{22}$$

which is equal to $1 - P_F$, where P_F is the false alarm probability. Since noise level σ_n^2 is not involved in (22), threshold u can be selected to realize a given P_F, once K and L have been specified. This is a quantitative verification of the expected constant false alarm rate property of the normalizer.

Finally, in the special case of one signal pulse, $K = 1$, and Rayleigh amplitude fading, $m = 1$, then $K_e = 1$, $N = 1$, $R = \overline{E}_1/N_o$, and (19) yields

$$P_{\upsilon}(u) = \frac{u}{1+u+R} \sum_{\ell=0}^{L-1} \left(\frac{1+R}{1+u+R}\right)^{\ell} = 1 - \left(\frac{1+R}{1+u+R}\right)^{L} . \tag{23}$$

That is,

$$1 - P_{\upsilon}(u) = \left(1 + \frac{u}{1+R}\right)^{-L} , \tag{24}$$

which agrees with [5; (6)] when we make the identifications (from there to here) of $N \to L$, $T/N \to u$, $\gamma \to R$.

RECURSION FOR CUMULATIVE DISTRIBUTION FUNCTION

Let the hypergeometric function appearing in (19) be represented as follows:

$$H_{\ell}(x) \equiv \frac{(K)_{\ell}}{\ell!} F(-\ell, K-N; K; x) . \tag{25}$$

Then

$$H_0(x) = 1 \ , \qquad (26)$$

while (25) has the recursion [2; 15.2.10]

$$\ell H_\ell(x) = [K + 2\ell - 2 + (N - K + 1 - \ell)x]\, H_{\ell-1}(x) - (K + \ell - 2)(1 - x)H_{\ell-2}(x)$$

$$\text{for } \ell \geq 1 \ , \qquad (27)$$

where we define $H_{-1}(x) = 0$. In terms of (25), the cumulative distribution function of υ in (19) becomes

$$P_\upsilon(u) = \left(\frac{u}{1 + u}\right)^K \left(\frac{1 + u}{1 + u + R}\right)^N \sum_{\ell=0}^{L-1} \left(\frac{1 + R}{1 + u + R}\right)^\ell H_\ell\left(\frac{R}{1 + R}\,\frac{u}{1 + u}\right) . \qquad (28)$$

This form, in conjunction with recursion (27), was used for all the numerical results here, for L finite. The parameters appearing in (28) have all been explained in tables 1 and 2. The explicit dependence on the fundamental parameters is indicated below:

$$K_e = K_e(K, \{\rho_{kj}\}) \ ,$$

$$N = N(m, K, \{\rho_{kj}\}) \ ,$$

$$R = R(\overline{E_1}/N_0, m, K, \{\rho_{kj}\}) \ . \qquad (29)$$

In addition, the cumulative distribution function in (28) is a function of L and threshold u.

DETECTION AND FALSE ALARM PROBABILITIES

The detection probability is given by

$$P_D = \mathrm{Prob}(v > u \mid R > 0) = 1 - P_v(u) , \tag{30}$$

where $P_v(u)$ is available in (28). The false alarm probability is

$$P_F = \mathrm{Prob}(v > u \mid R = 0) = 1 - P_v^{(o)}(u) , \tag{31}$$

where $P_v^{(o)}(u)$ is available in (22). By allowing threshold u to vary over a wide range, P_D and P_F values can be obtained and plotted against each other, resulting in the standard receiver operating characteristics; the threshold is thereby eliminated from the plotted outputs. Programs for plotting P_D vs P_F, both for L finite as well as infinite, are listed in appendix A.

GRAPHICAL RESULTS

Due to the multitude of parameters appearing in this investigation (see tables 1 and 2), it is impossible to give a comprehensive compilation of encompassing numerical results. Considering just the covariance coefficients $\{\rho_{kj}\}_1^K$ for the moment, complete specification requires assignment of $K(K - 1)/2$ values to these quantities; to circumvent this difficulty, we consider numerically, here, only the very special case of exponential correlation, for which

$$\rho_{kj} = \rho^{|k-j|} \quad \text{for} \quad 1 \leq k,\ j \leq K\ , \tag{32}$$

and look at a couple of particular values for ρ. Our approach here, of necessity, is to give some representative sample receiver operating characteristics and a general computer program in BASIC, whereby additional results can easily by obtained once the user has specified all the particular values of interest in his application. This program allows for arbitrary covariance coefficients, $\{\rho_{kj}\}$, and is not limited to the specific example (32).

The particular cases we will investigate are as follows:

$$\begin{aligned} K &= 1,\ 2,\ 4, \\ L &= 16,\ 32,\ \infty, \\ m &= .5,\ 1, \\ \rho &= 0,\ .5\ . \end{aligned} \tag{33}$$

All possible combinations of these four fundamental variables lead to 30 plots, which appear below* in figures 2-31. (There are only 6 plots for $K = 1$, not 12, because the value of ρ is irrelevant for $K = 1$). The curves are indexed by the per-pulse signal-to-noise ratio, $\overline{E}_1/N_0$, in dB. The false alarm and detection probability pairs range from (poor quality) pair (.5,.01) up to (high quality) pairs near (1E-10,.999).

The number of signal pulses, K, is limited to the low values 1, 2, 4, because these seem to be the cases of most immediate practical use. The number of noise-only samples, L, is not evaluated for $L = 64$ because of the proximity of the results to those for $L = \infty$; conversely, results are not presented for $L = 8$, because a severe degradation in performance occurs, that probably cannot be tolerated. The fading parameter value $m = 1$ corresponds to Rayleigh amplitude fading (exponential power fading), while $m = .5$ corresponds to a deeper more-damaging form of fading. The correlation coefficient $\rho = 0$ corresponds to uncorrelated (independent) fading, while $\rho = .5$ allows for adjacent (equispaced) pulses in figure 1 to have some degree of dependent fading.

An explanation of the initial result in figure 2 follows: for $K = 1$, $m = 1$, $L = \infty$ (known noise level), the detection probability is plotted versus the false alarm probability for values of the latter between 1E-10 and .1. The value of the per-pulse signal-to-noise ratio, $\overline{E}_1/N_0$ in dB, varies over the range 6, 8, 10, ... , 42, giving detection probability values covering

* All the figures are collected together after the Summary section.

the range .01 to .999. The only difference in the accompanying pair, figures 3 and 4, is that L is reduced to 32 and 16, respectively.

The results in figures 5 through 7 correspond to the worst cases considered here. Namely, there is just one (fading) signal pulse, and m is .5, which means a very deep fading medium; see [1; figure 2]. The values of signal-to-noise ratio required for L = 16 in figure 7 are so large as to be physically unrealistic, except for the poorer quality region.

On the other hand, for K = 4 signal pulses, Rayleigh amplitude fading (m = 1), and uncorrelated fading (ρ = 0), the results in figures 20 through 22 are very encouraging, being physically reasonable over the whole range of plotted values. But when m is decreased to .5, and ρ is increased to .5, the results in figures 29 through 31, still for K = 4 pulses, indicate substantially increased signal-to-noise ratio requirements at the higher quality end of the performance region.

An alternative method of presenting the graphical results, which accounts for the losses incurred by not knowing the noise level, is to plot the required value of $\overline{E}_1/N_0$ vs L, for various values of the remaining parameters and for specified performance quality in terms of P_F and P_D. Two such cases are illustrated in figures 32 and 33. They show that the cost of not knowing the noise level is not severe for the high false alarm probabilities, but is quite significant for the lower more-desirable false alarm probabilities. For example, in figure 33 for K = 2 signal pulses, the signal-to-noise ratio must be about 1.5 dB larger at L = 10 noise pulses than

at $L = 100$, when $P_F = .01$. However, if we want to operate at $P_F = 1E-10$, the increased signal-to-noise ratio requirement is about 6 dB per pulse. The numbers are comparable for the $K = 1$ results in figure 32.

The asymptotes for large L in figures 32 and 33 can be found in some cases from earlier results in [1]. For example, reference to [1; figure 8] for $K = 2$, $\rho = .5$ gives $\overline{E}_1/N_o \cong 16.8$ dB, while $P_F = 1E-6$, $P_D = .9$, $m = 1$. Comparison with figure 33 here reveals that the performance requirement is virtually at this level by the time that $L = 100$.

SUMMARY

Although figures 32 and 33 are very informative, allowing for a ready assessment of the losses incurred by using a finite small value for L, the number of noise-only pulses, they also illustrate the voluminous compilation that would be needed for a thorough numerical investigation. For example, if: detection probabilities P_D were of interest for values .5, .9, .99, .999; number of signal pulses K for values 1, 2, ... , 10; fading parameter m for values .5, 1, 2; and fading correlation coefficient ρ for 0, .5, 1; this would require a total of 4*10*3*3 = 360 figures. The approach here is instead to present some representative receiver operating characteristics, in figures 2 through 31, from which information similar to that in figures 32 and 33 can be extracted, and to list a general program for the generation of additional receiver operating characteristics for whatever cases may be of interest to the user.

Some related work on the performance of a log-normalizer subject to Weibull or log-normal inputs has been published by the author in [6]; however, no fading was allowed, and the number of signal pulses was limited to K = 1. In a different vein, the performance of an or-ing device operating on the output of an incoherent combiner of multiple pulses was analyzed in [7]. These works augment and complement the analysis conducted here.

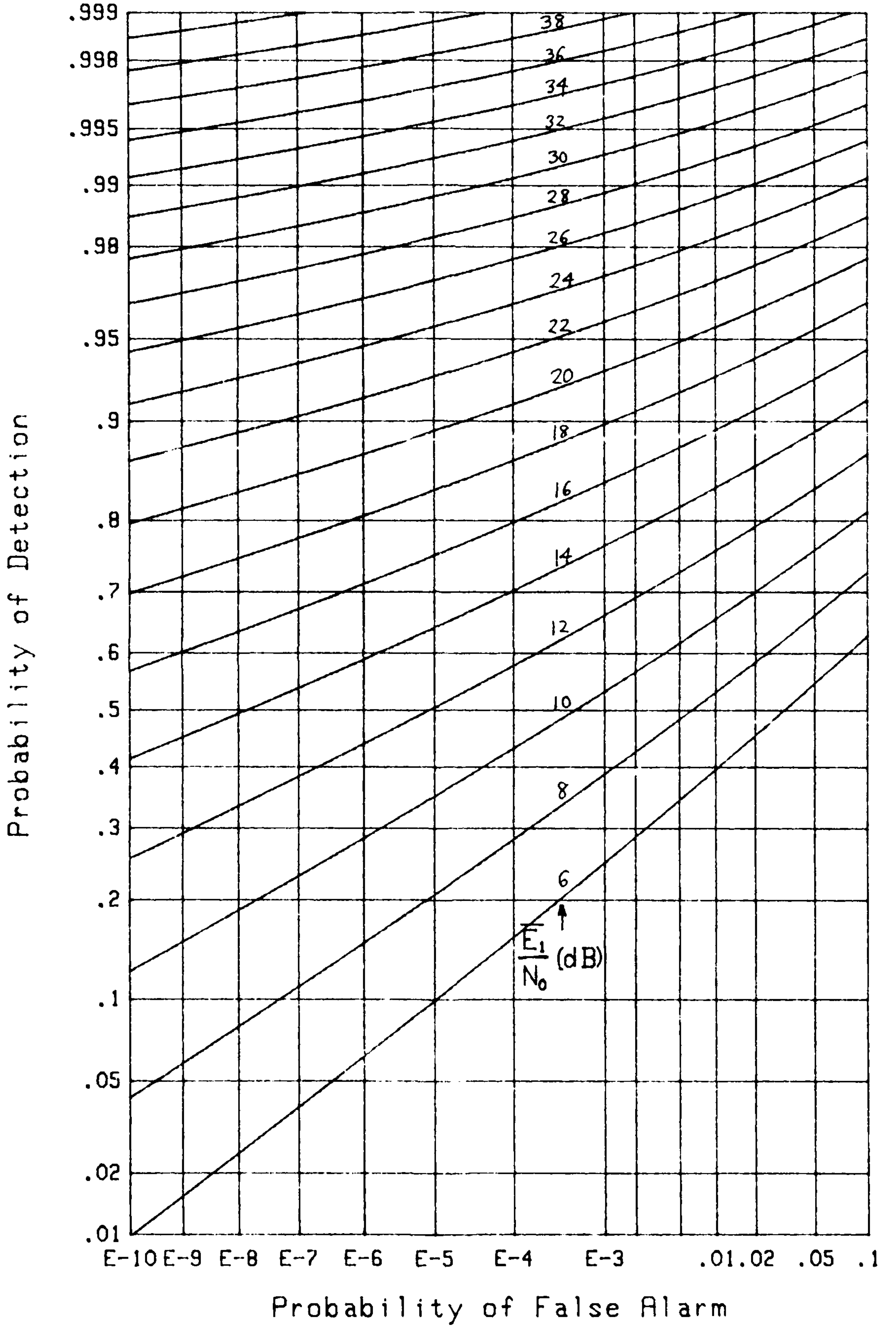

Figure 2. ROC for K=1, m=1, L=∞

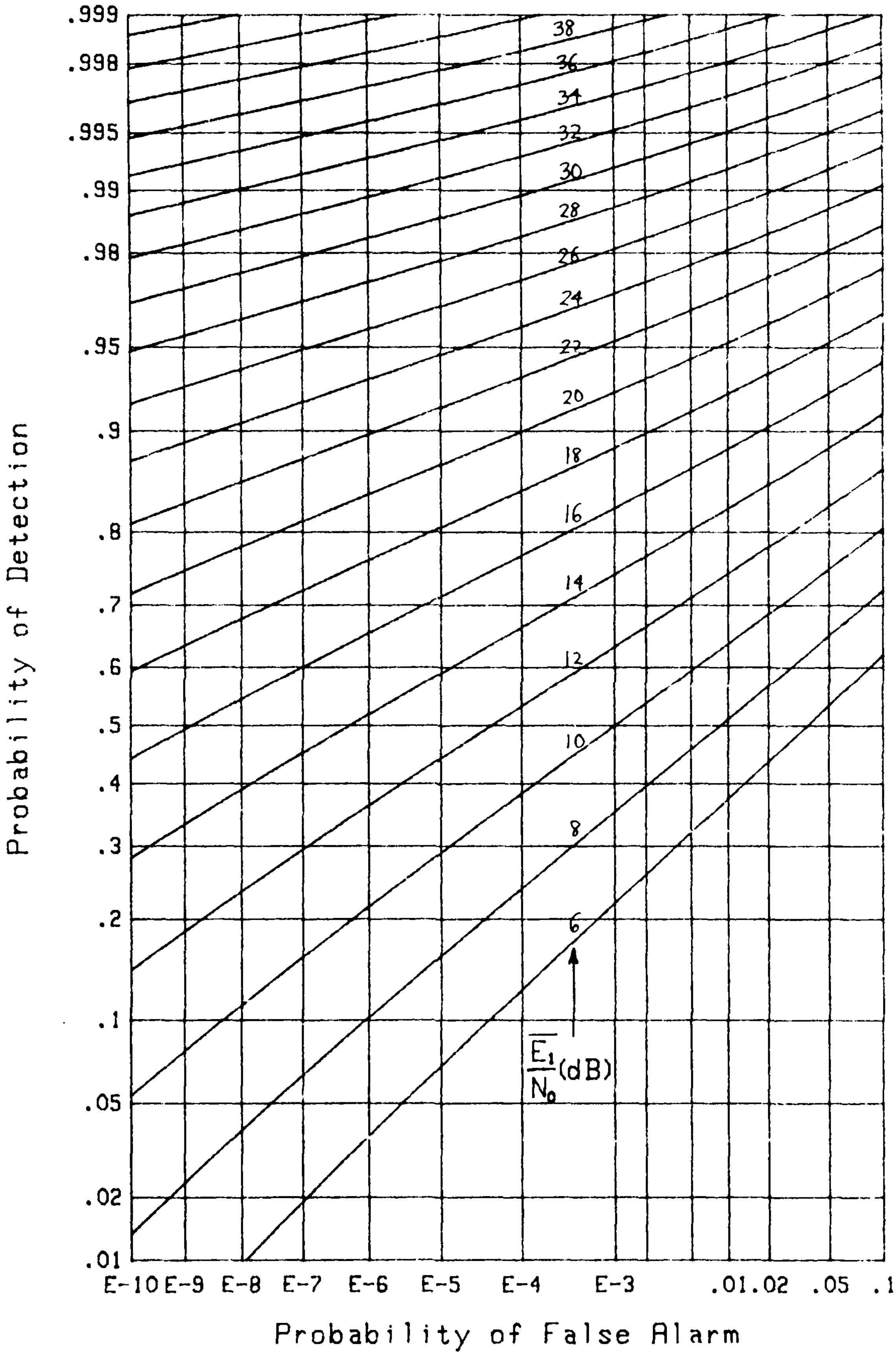

Figure 3. ROC for K=1, m=1, L=32

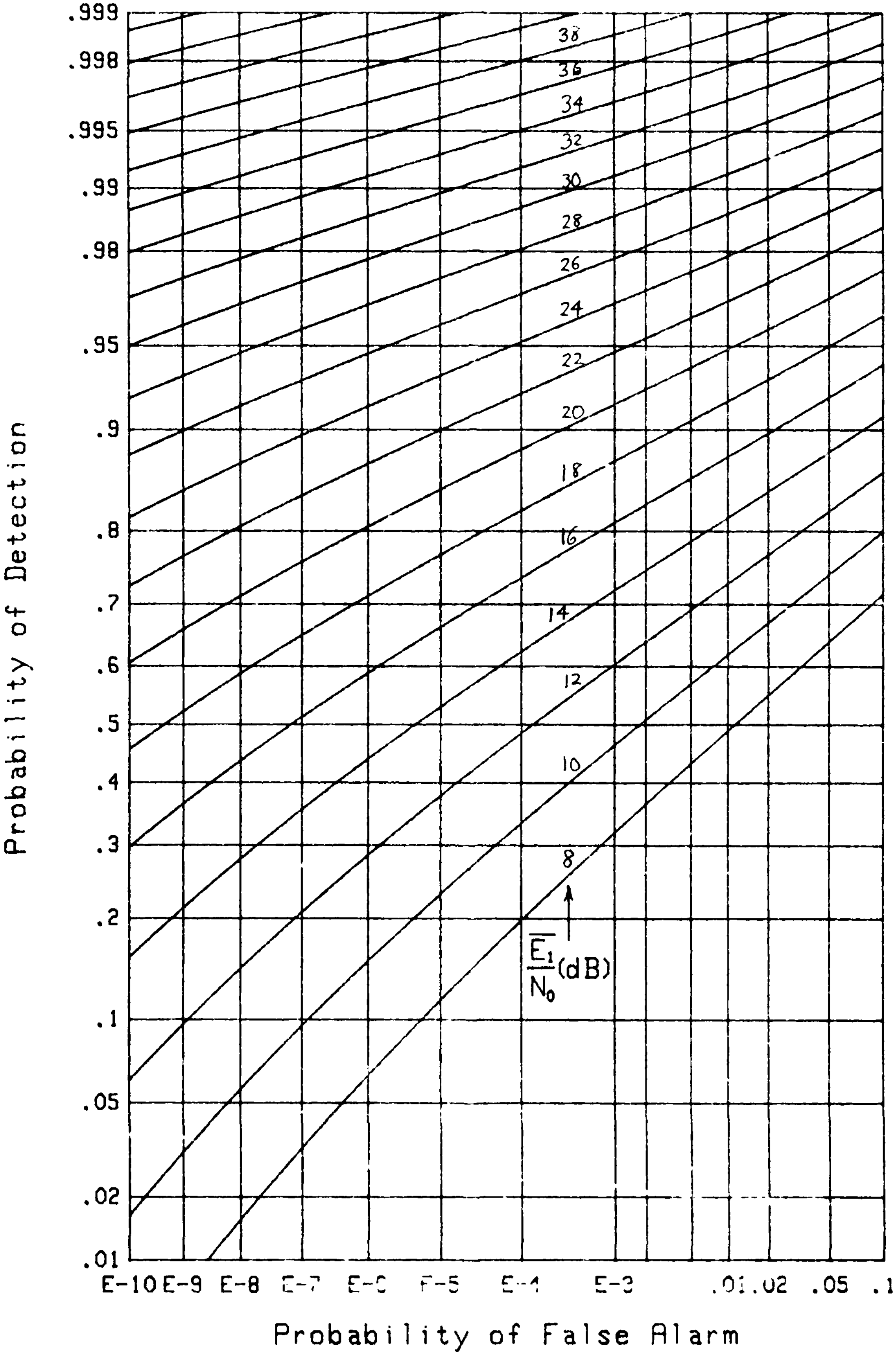

Figure 4. ROC for K=1, m=1, L=16

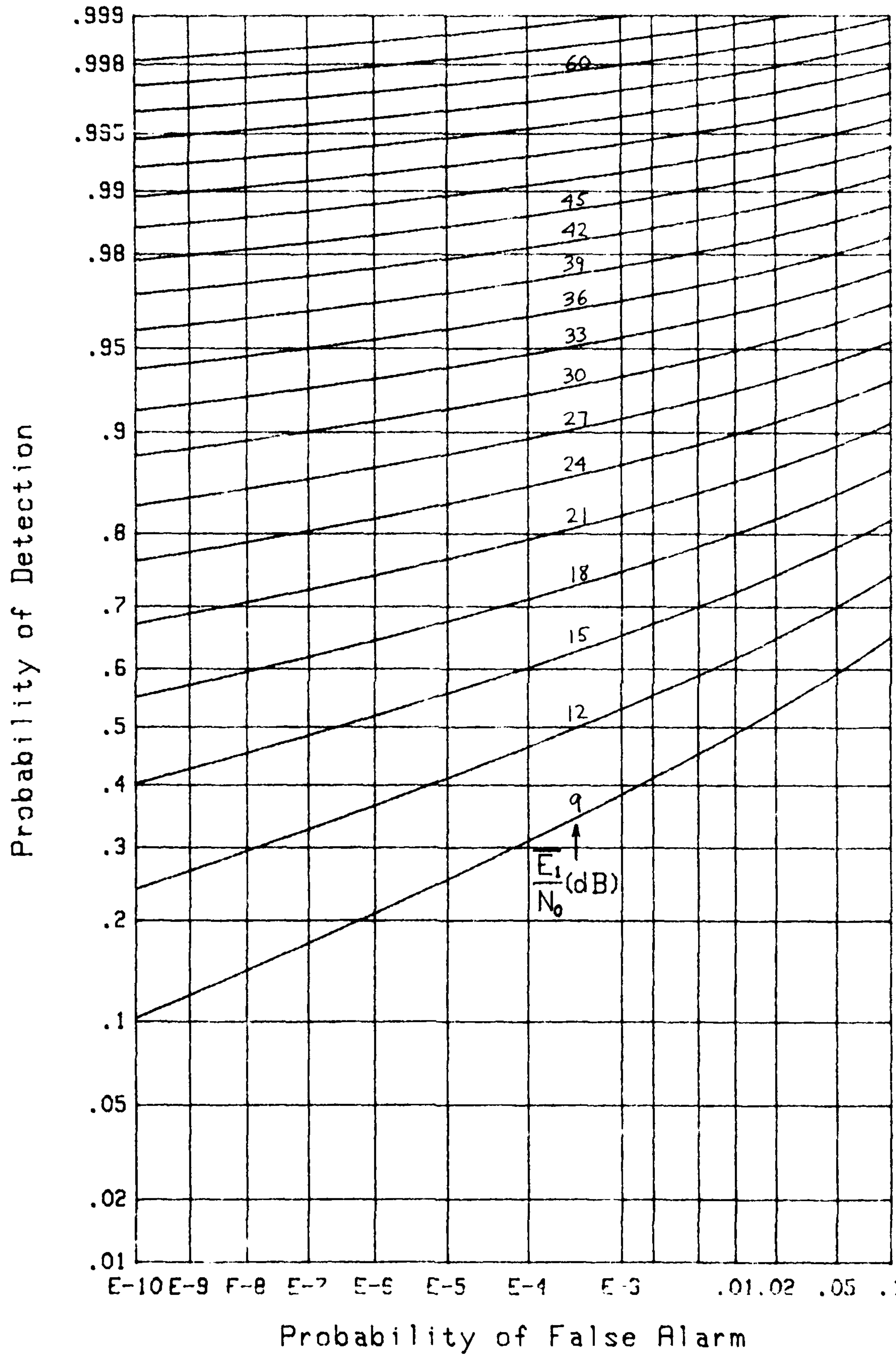

Figure 5. ROC for K=1, m=.5, L=∞

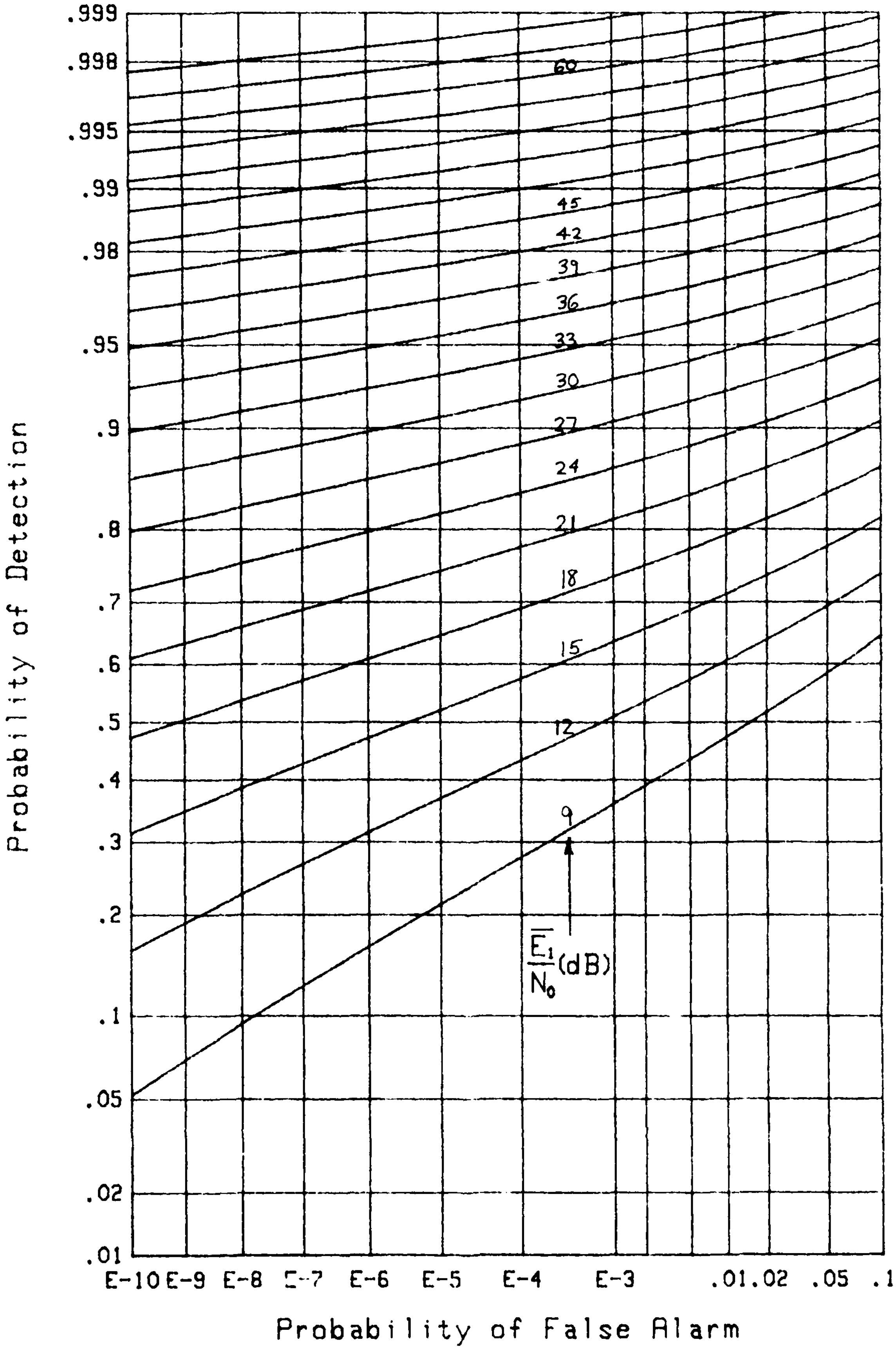

Figure 6. ROC for K=1, m=.5, L=32

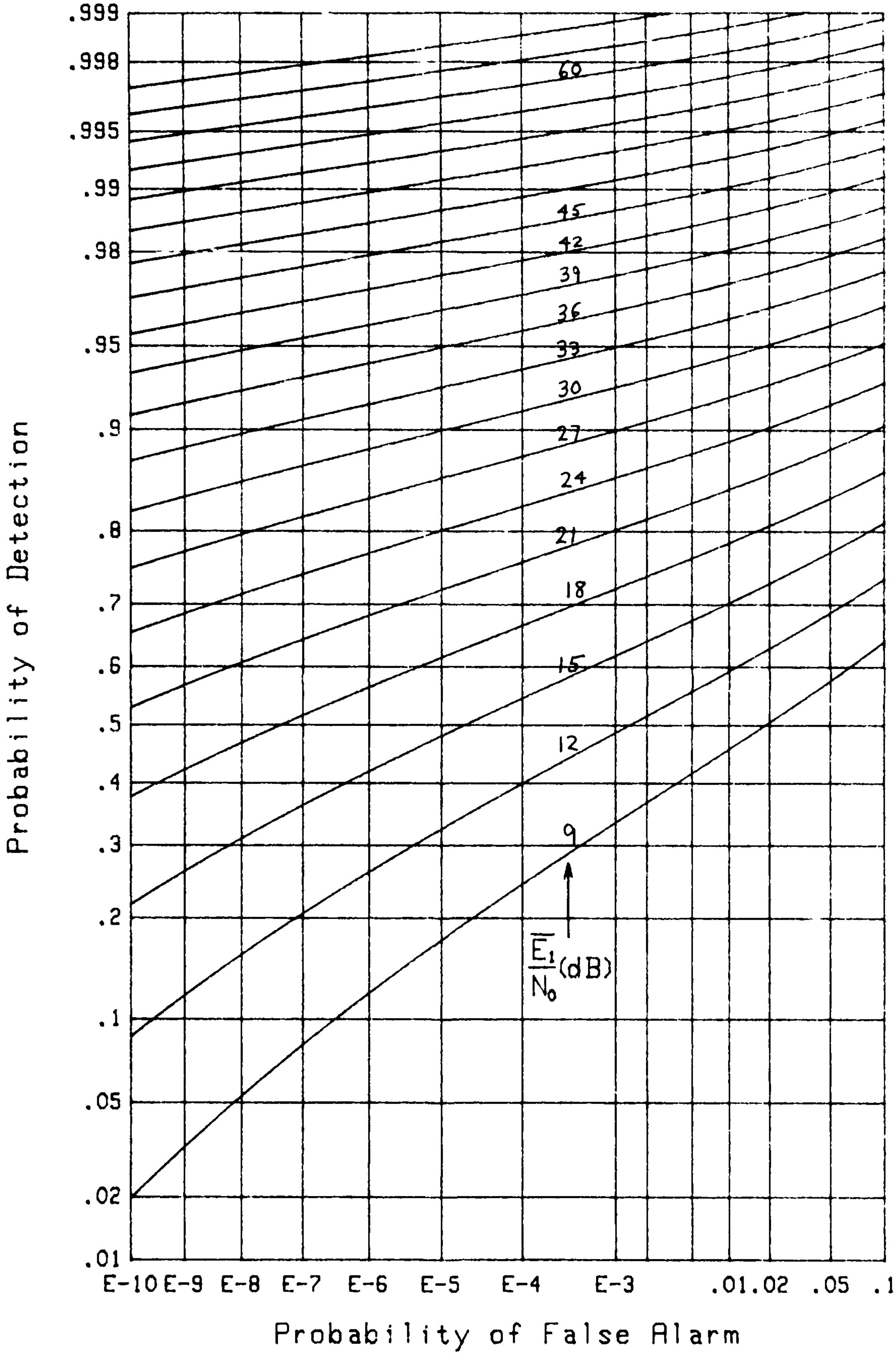

Figure 7. ROC for K=1, m=.5, L=16

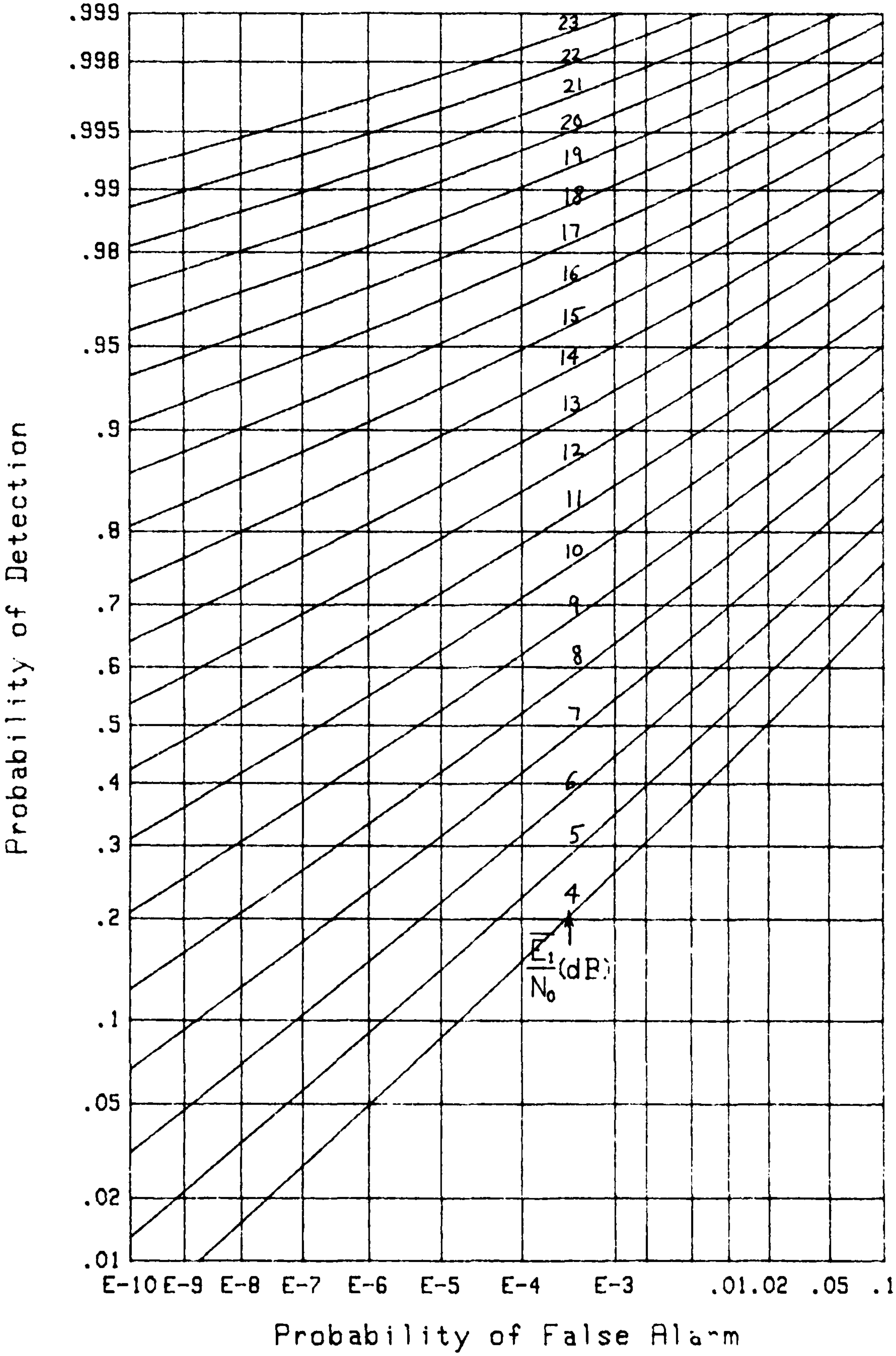

Figure 8. ROC for K=2, m=1, ρ=0, L=∞

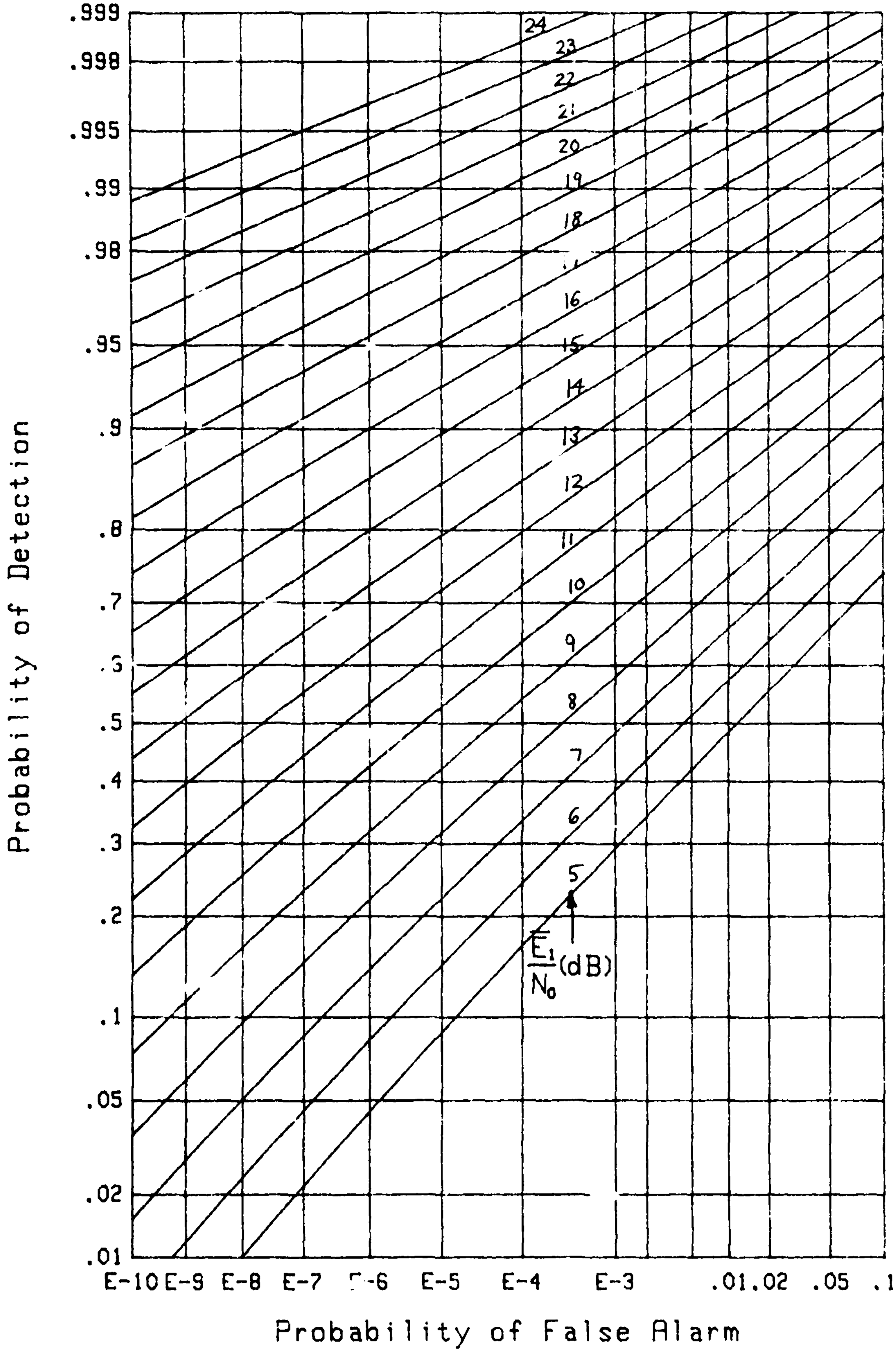

Figure 9. ROC for K=2, m=1, ρ=0, L=32

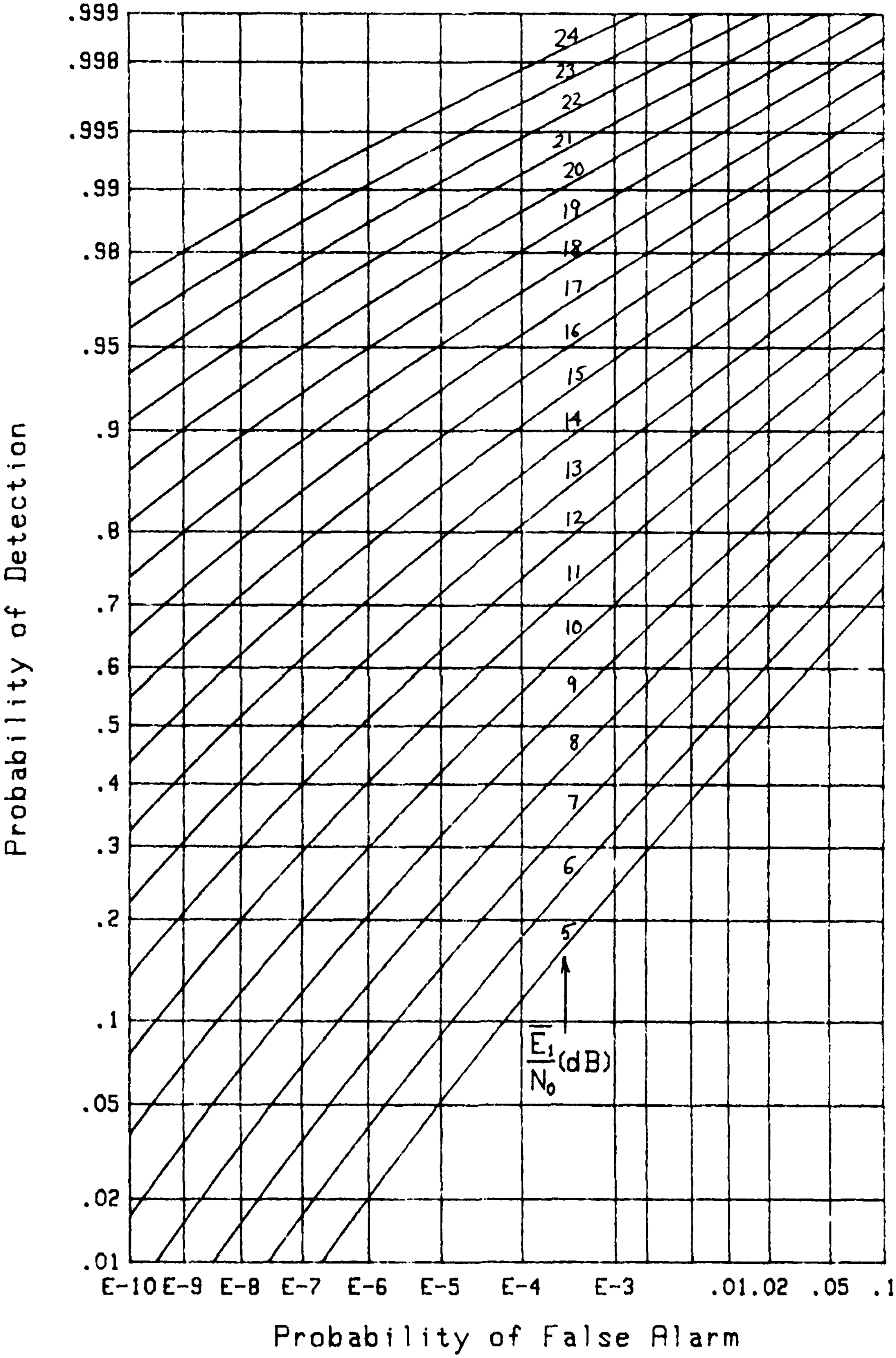

Figure 10. ROC for K=2, m=1, ρ=0, L=16

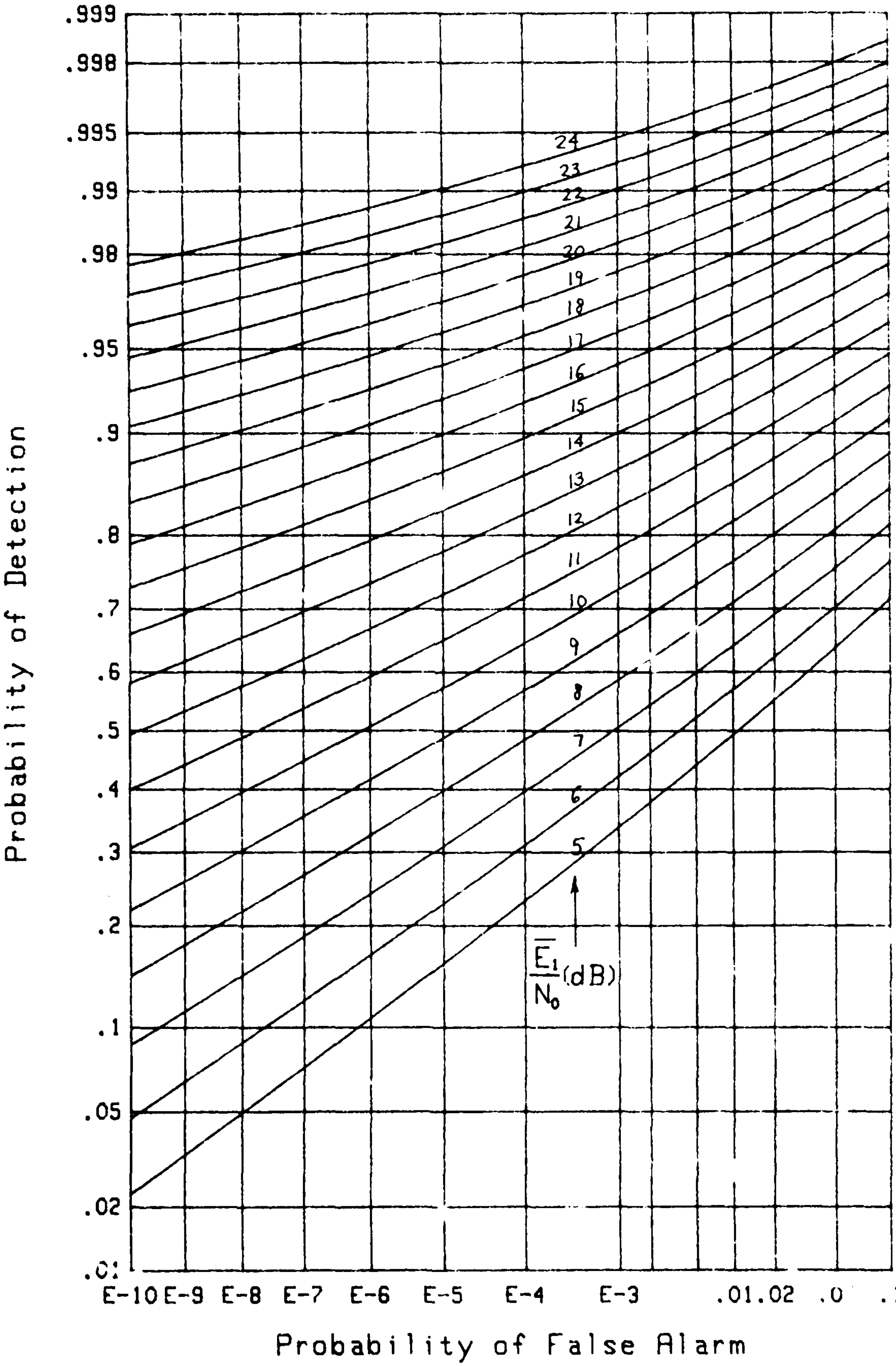

Figure 11. ROC for K=2, m=1, ρ=.5, L=∞

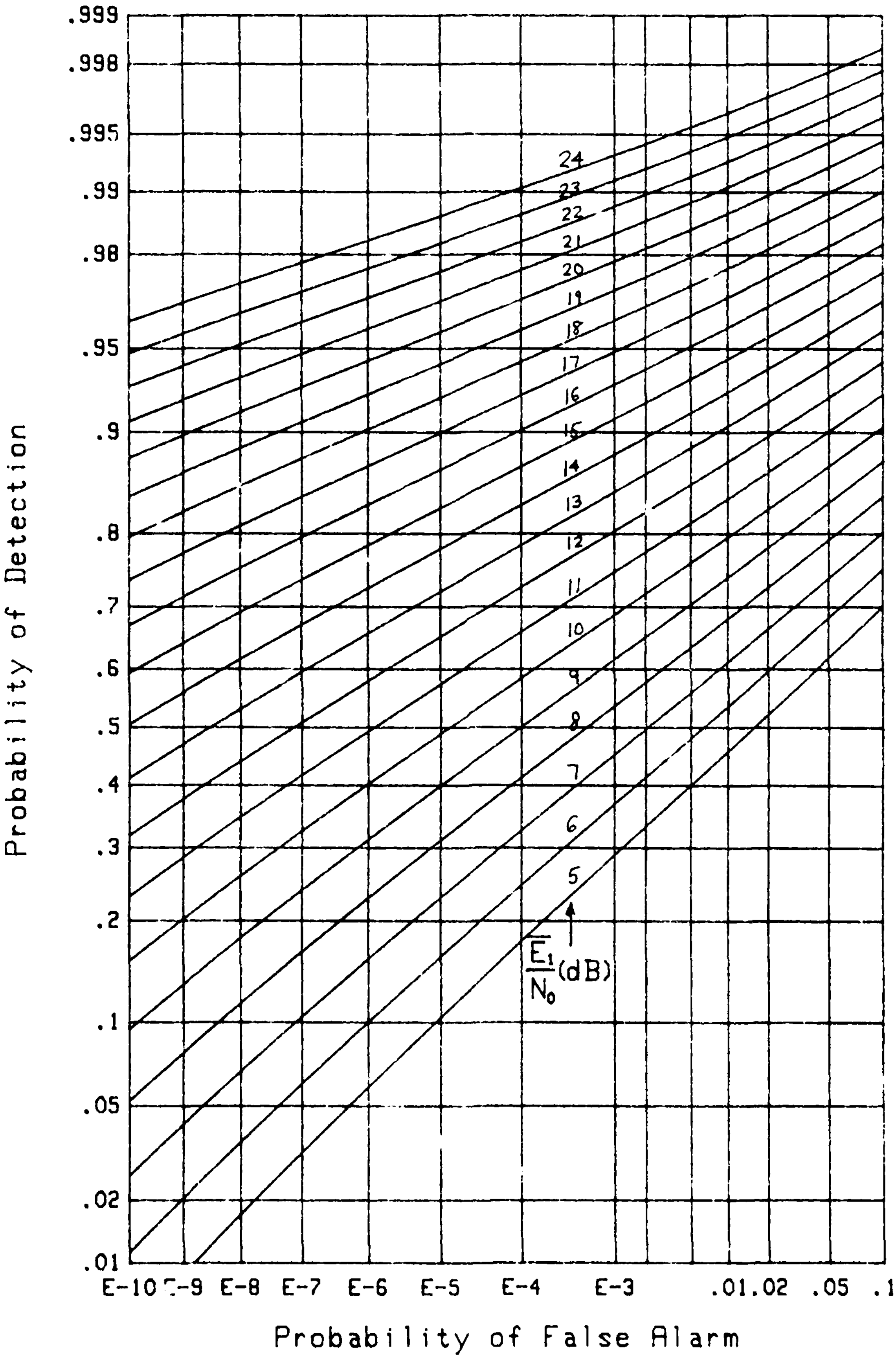

Figure 12. ROC for K=2, m=1, ρ=.5, L=32

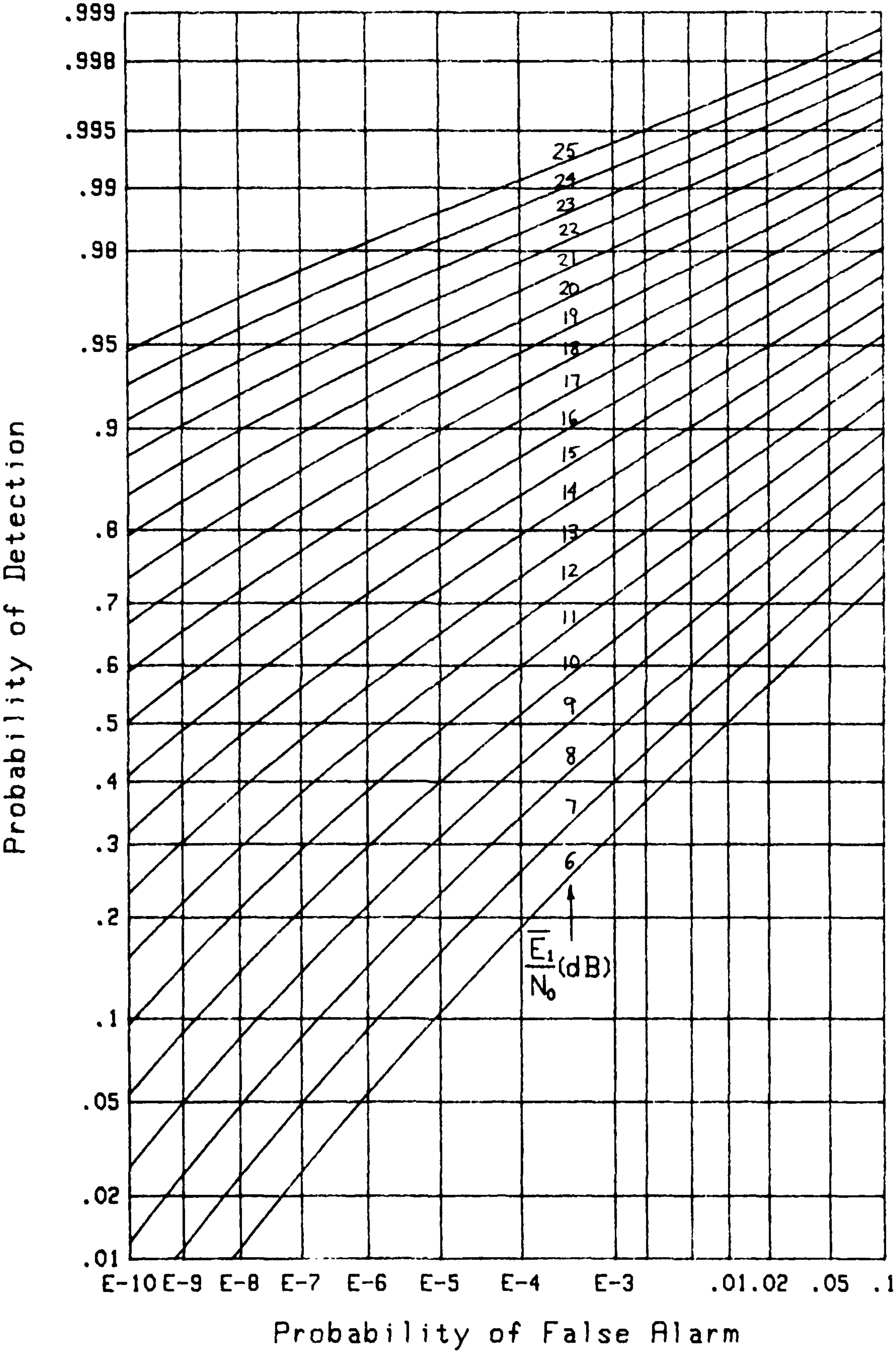

Figure 13. ROC for K=2, m=1, ρ=.5, L=16

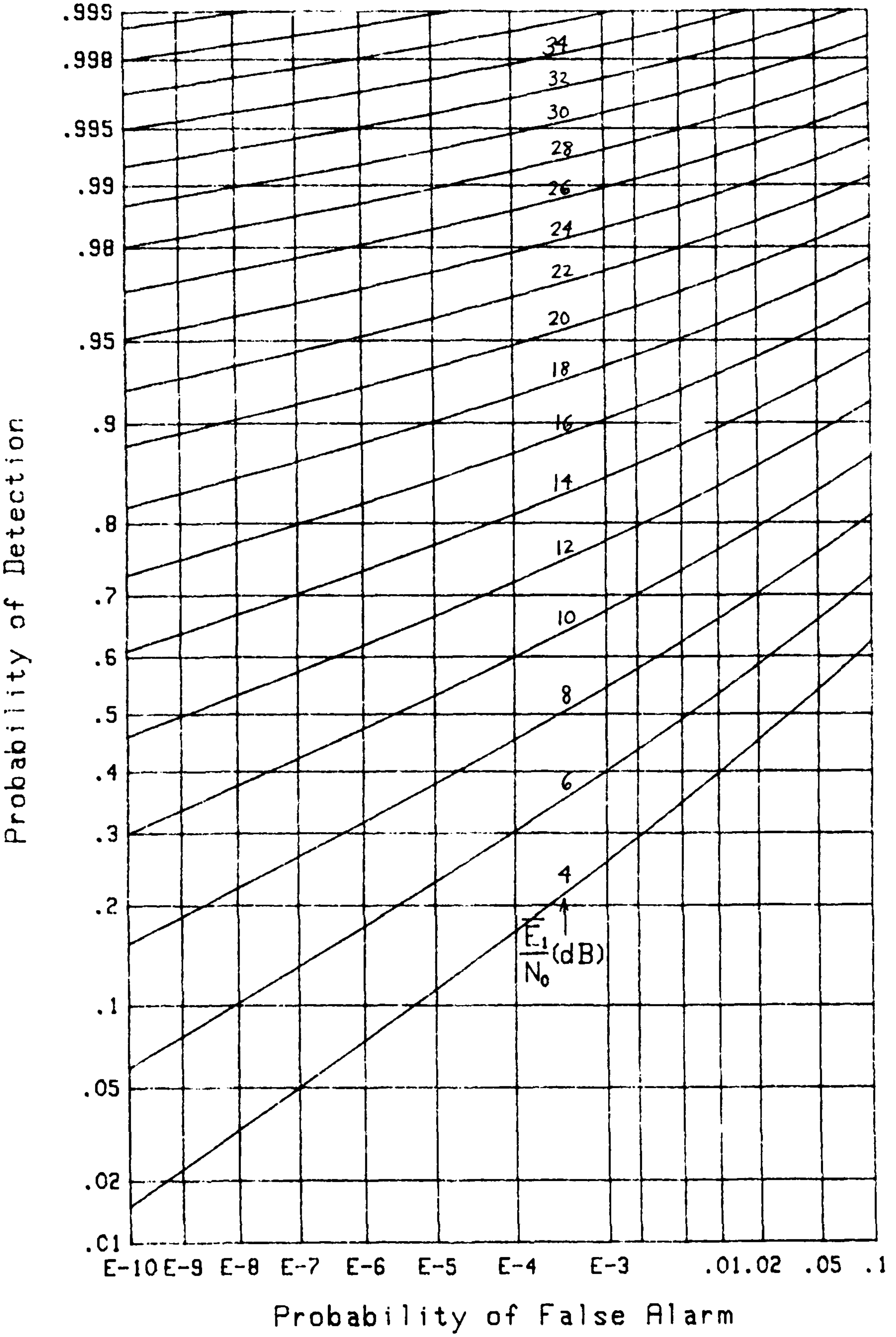

Figure 14. ROC for K=2, m=.5, ρ=0, L=∞

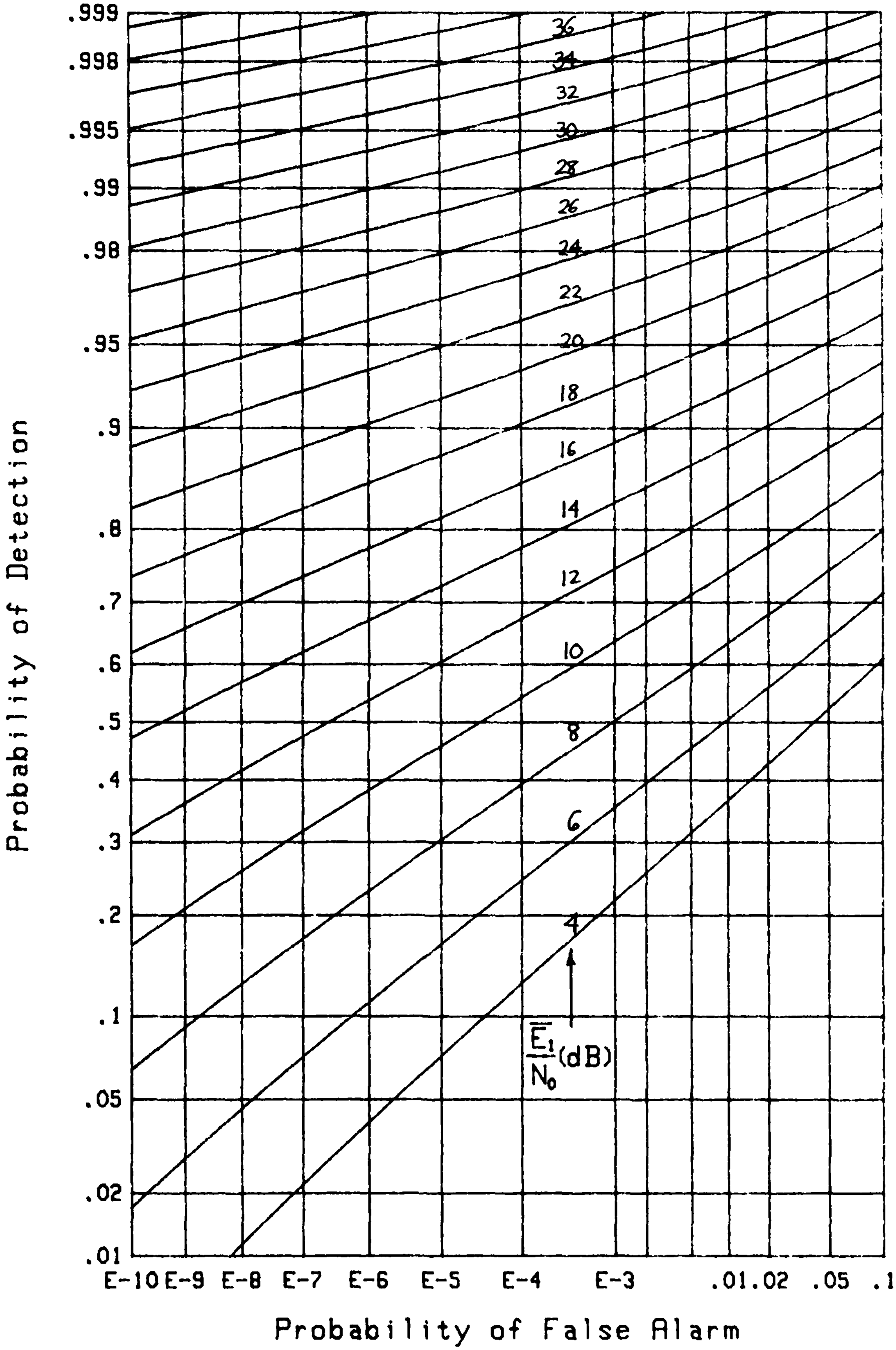

Figure 15. ROC for K=2, m=.5, ρ=0, L=32

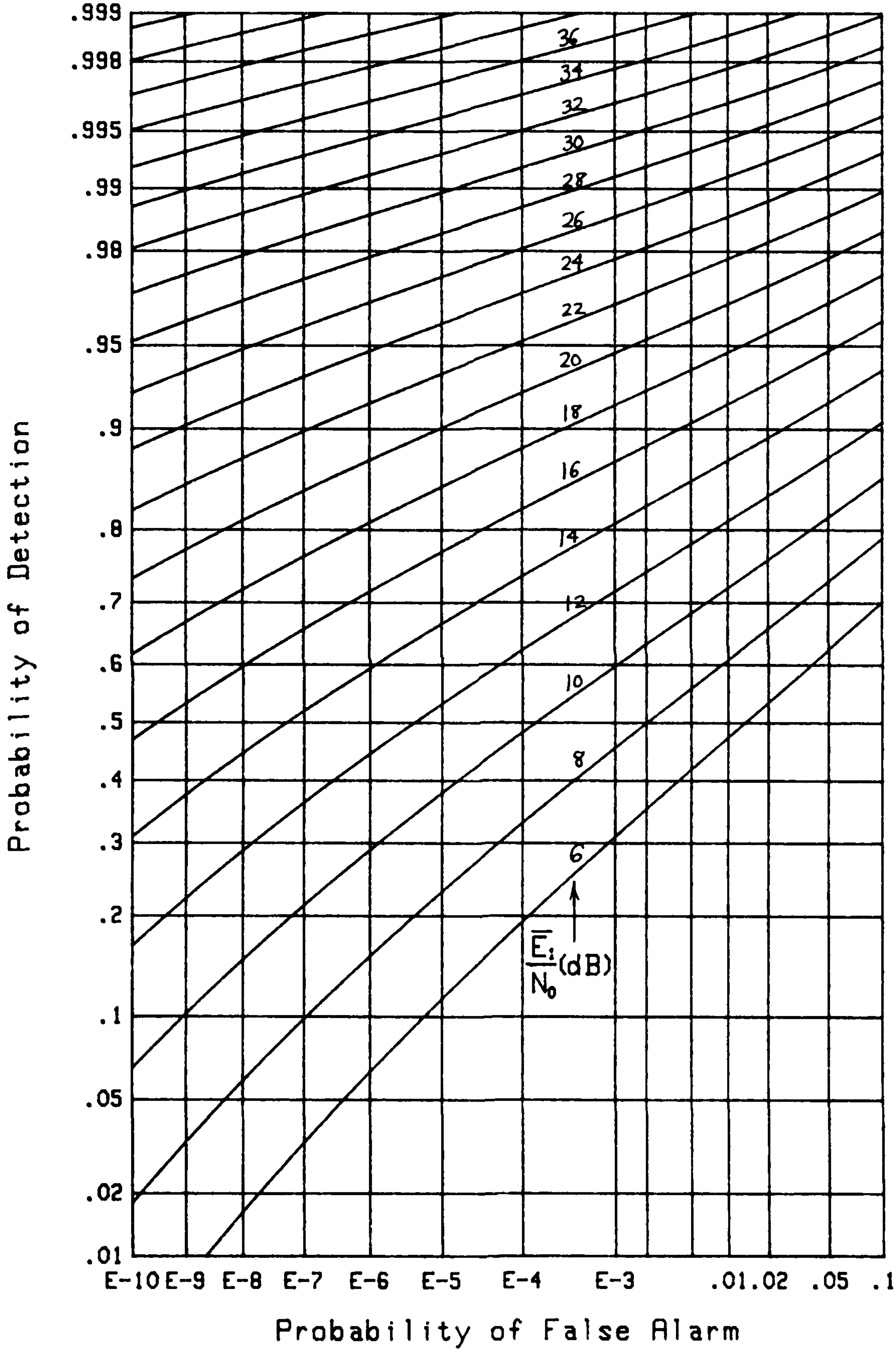

Figure 16. ROC for K=2, m=.5, ρ=0, L=16

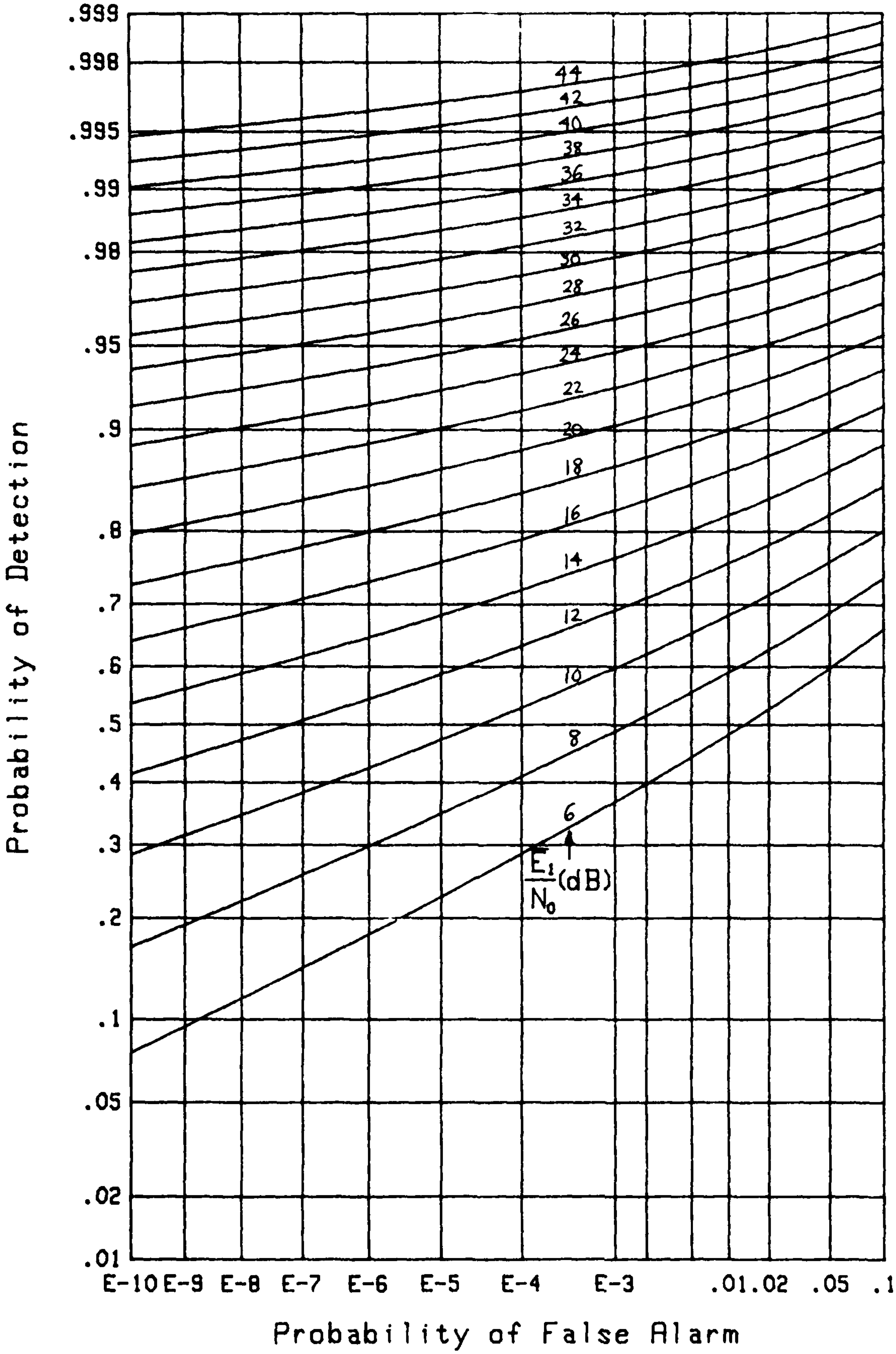

Figure 17. ROC for K=2, m=.5, ρ=.5, L=∞

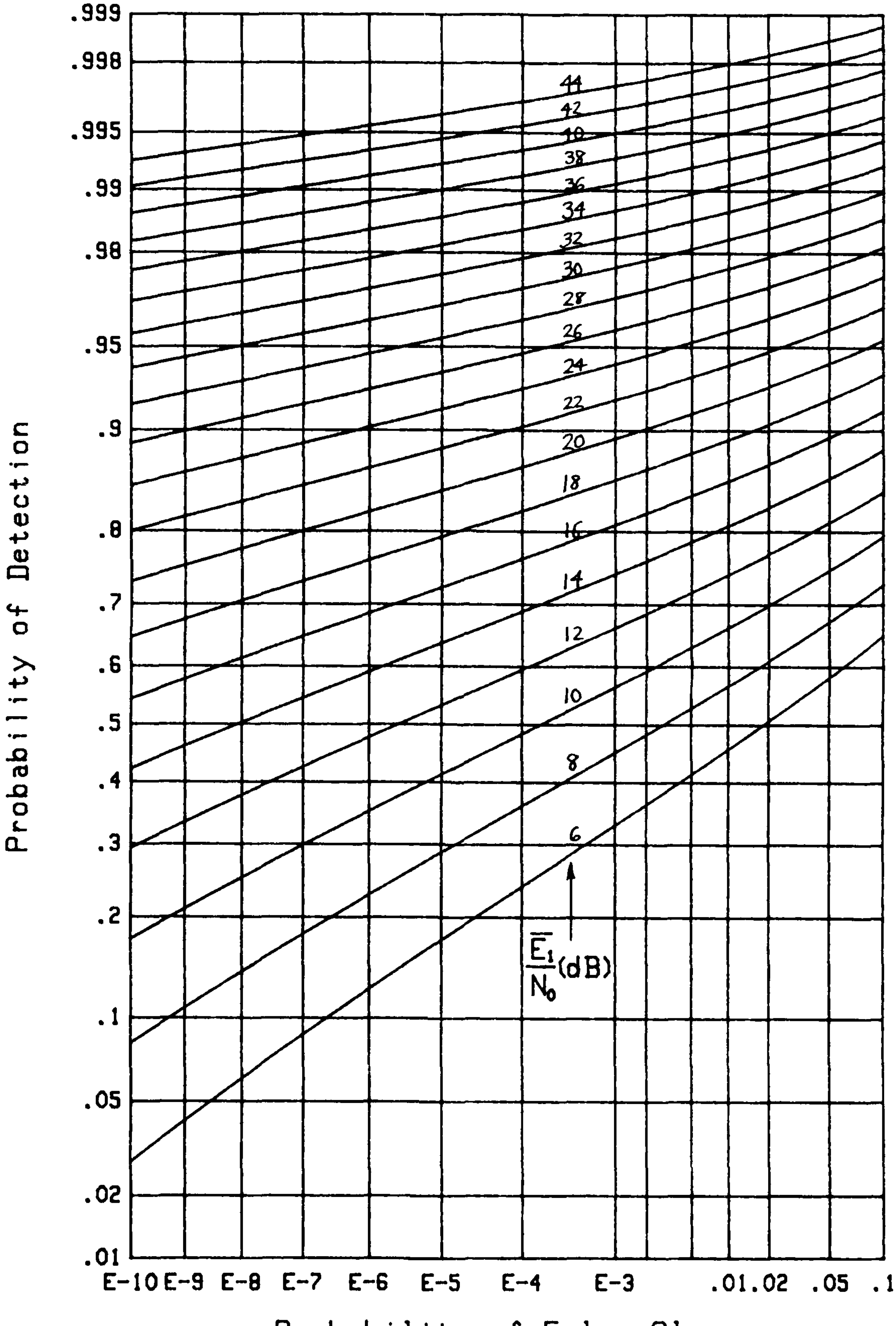

Figure 18. ROC for K=2, m=.5, ρ=.5, L=32

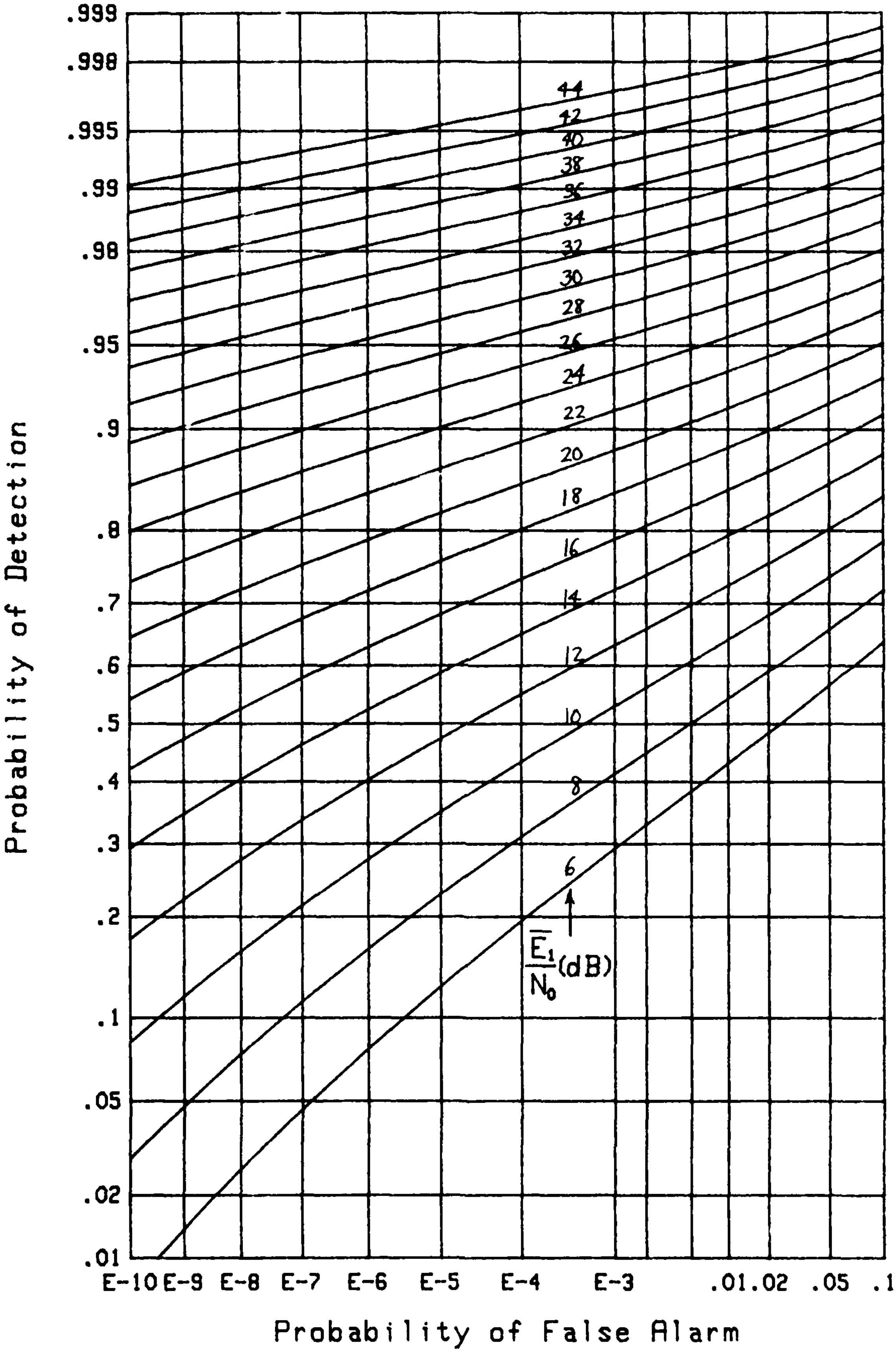

Figure 19. ROC for K=2, m=.5, ρ=.5, L=16

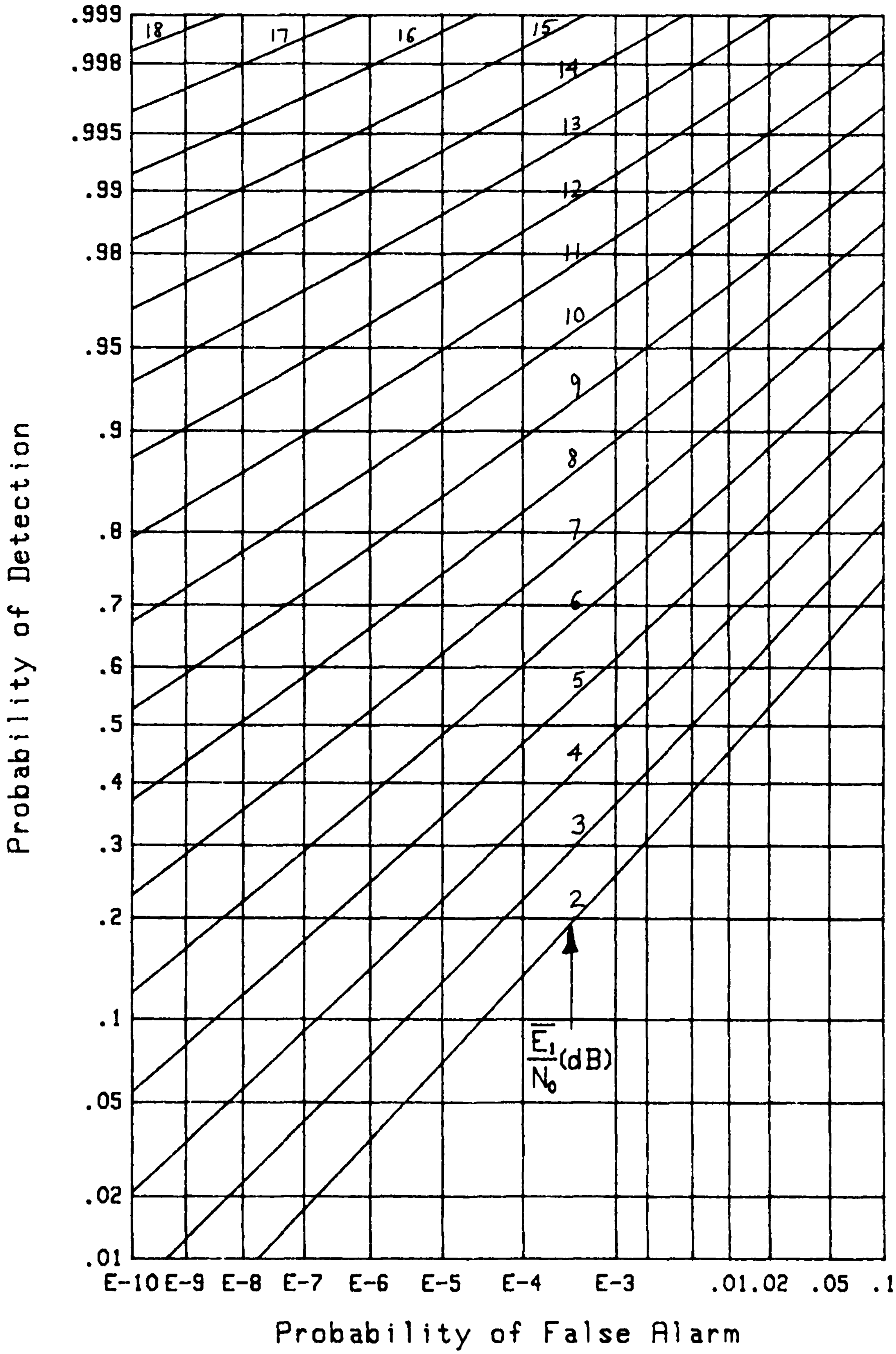

Figure 20. ROC for K=4, m=1, ρ=0, L=∞

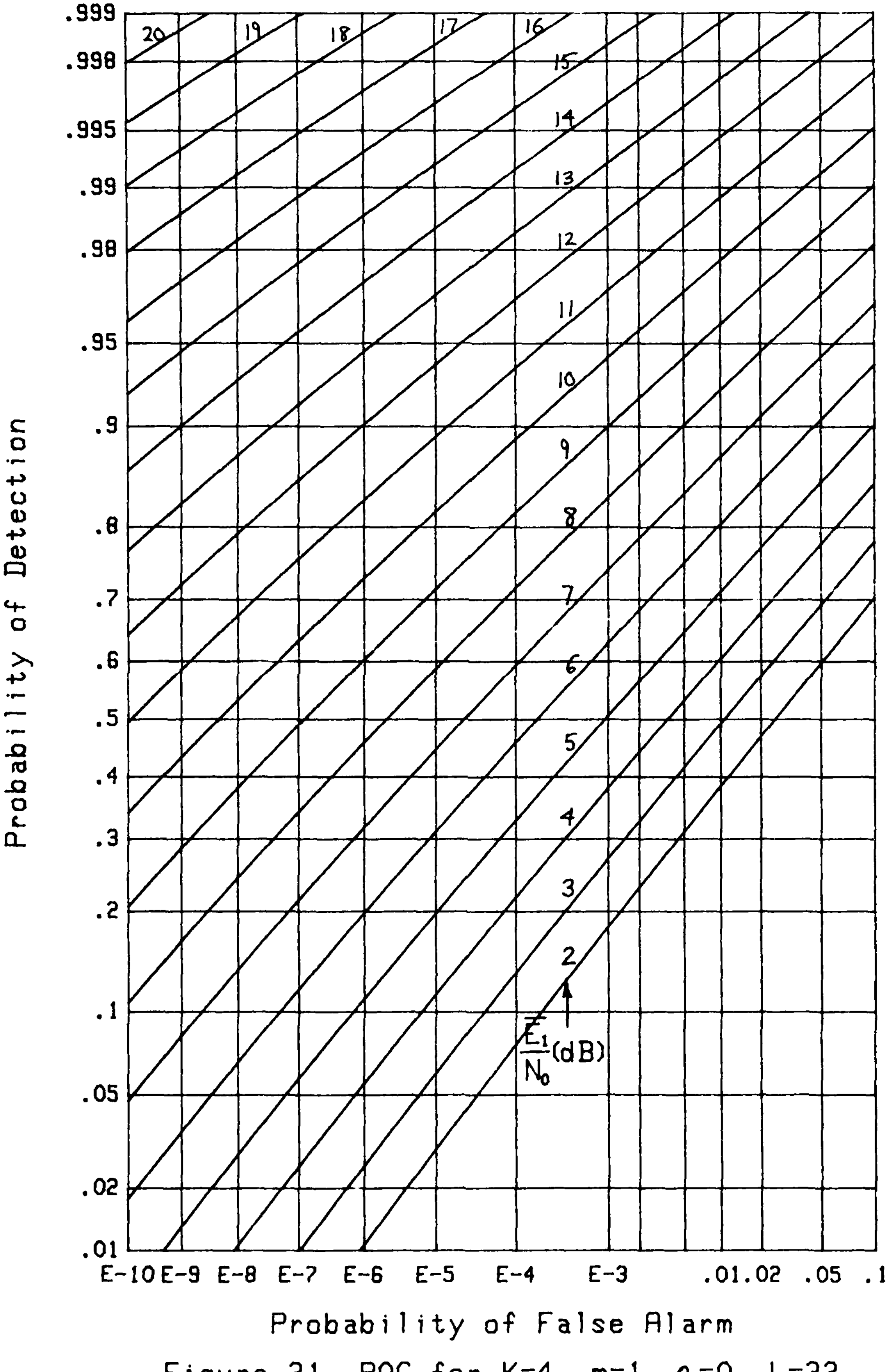

Figure 21. ROC for K=4, m=1, ρ=0, L=32

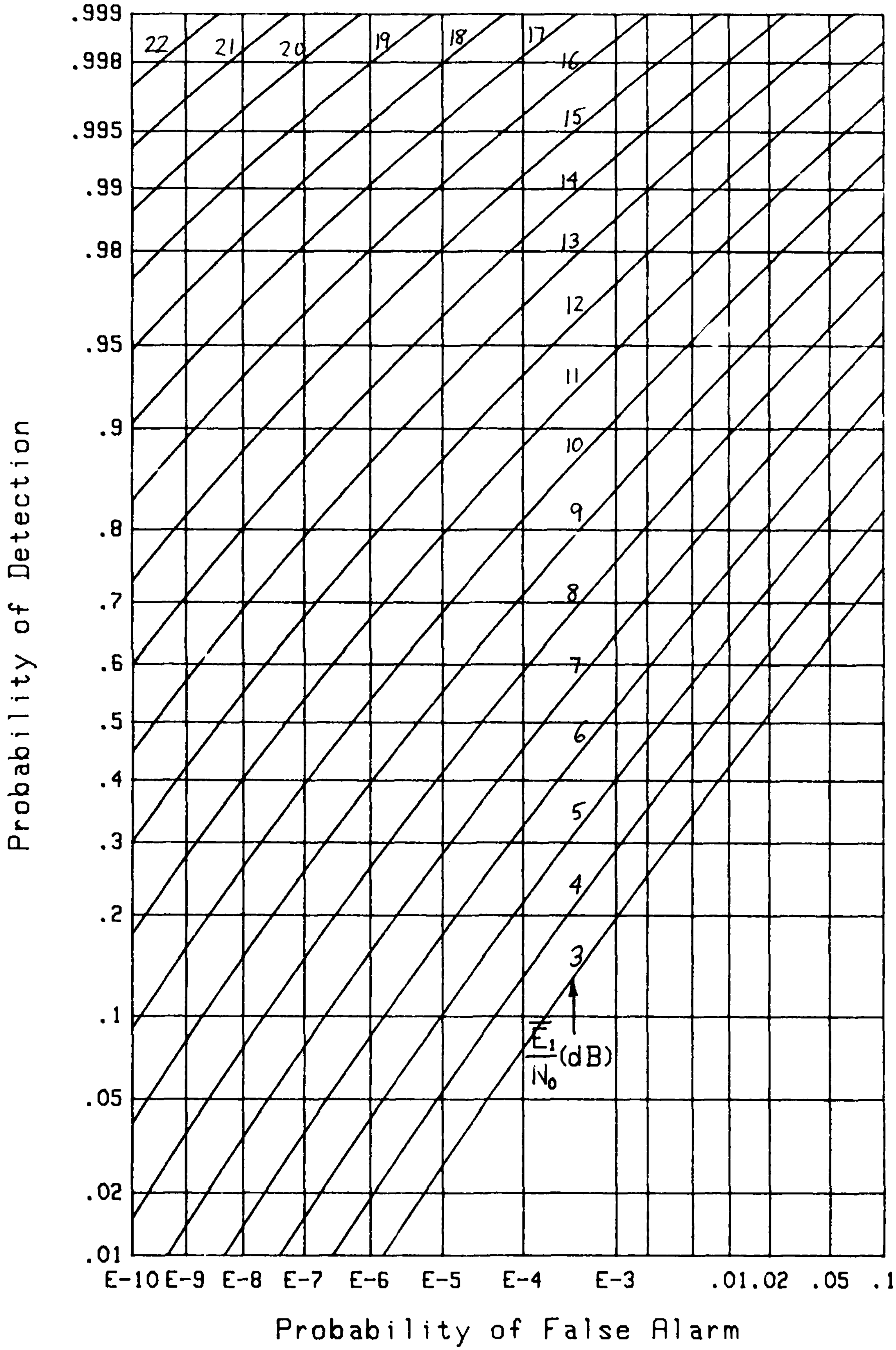

Figure 22. ROC for K=4, m=1, ρ=0, L=16

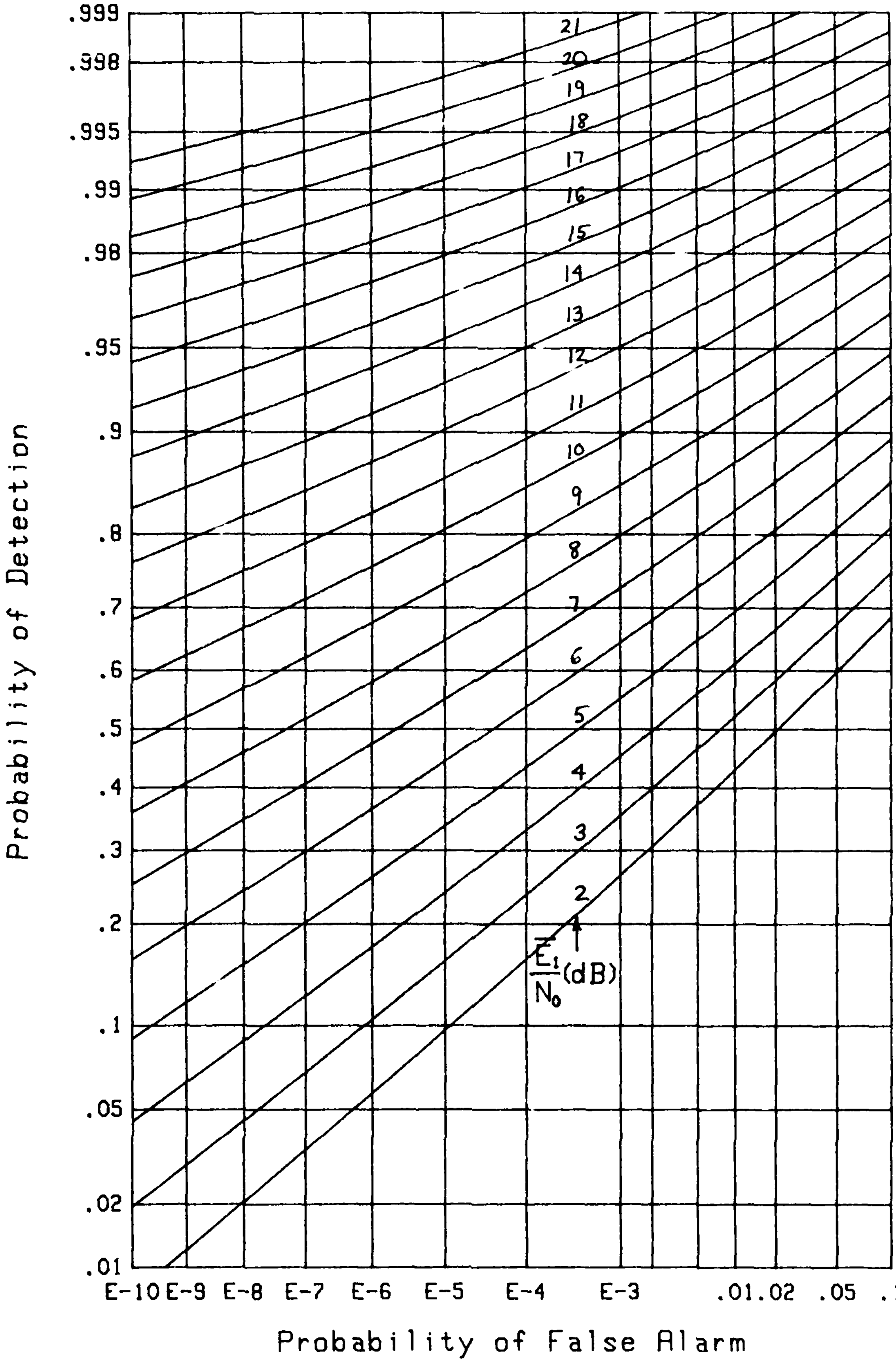

Figure 23. ROC for K=4, m=1, ρ=.5, L=∞

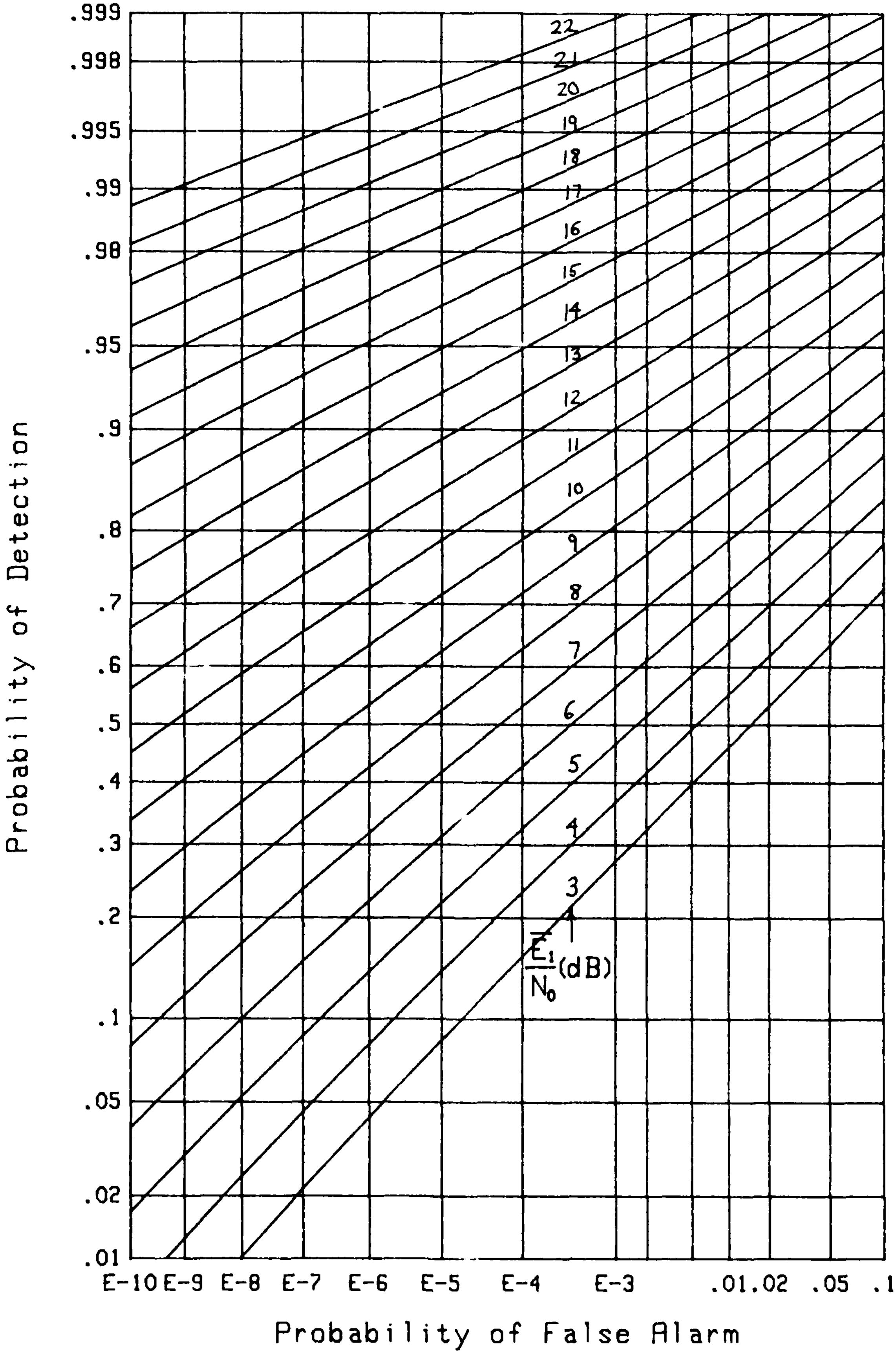

Figure 24. ROC for K=4, m=1, ρ=.5, L=32

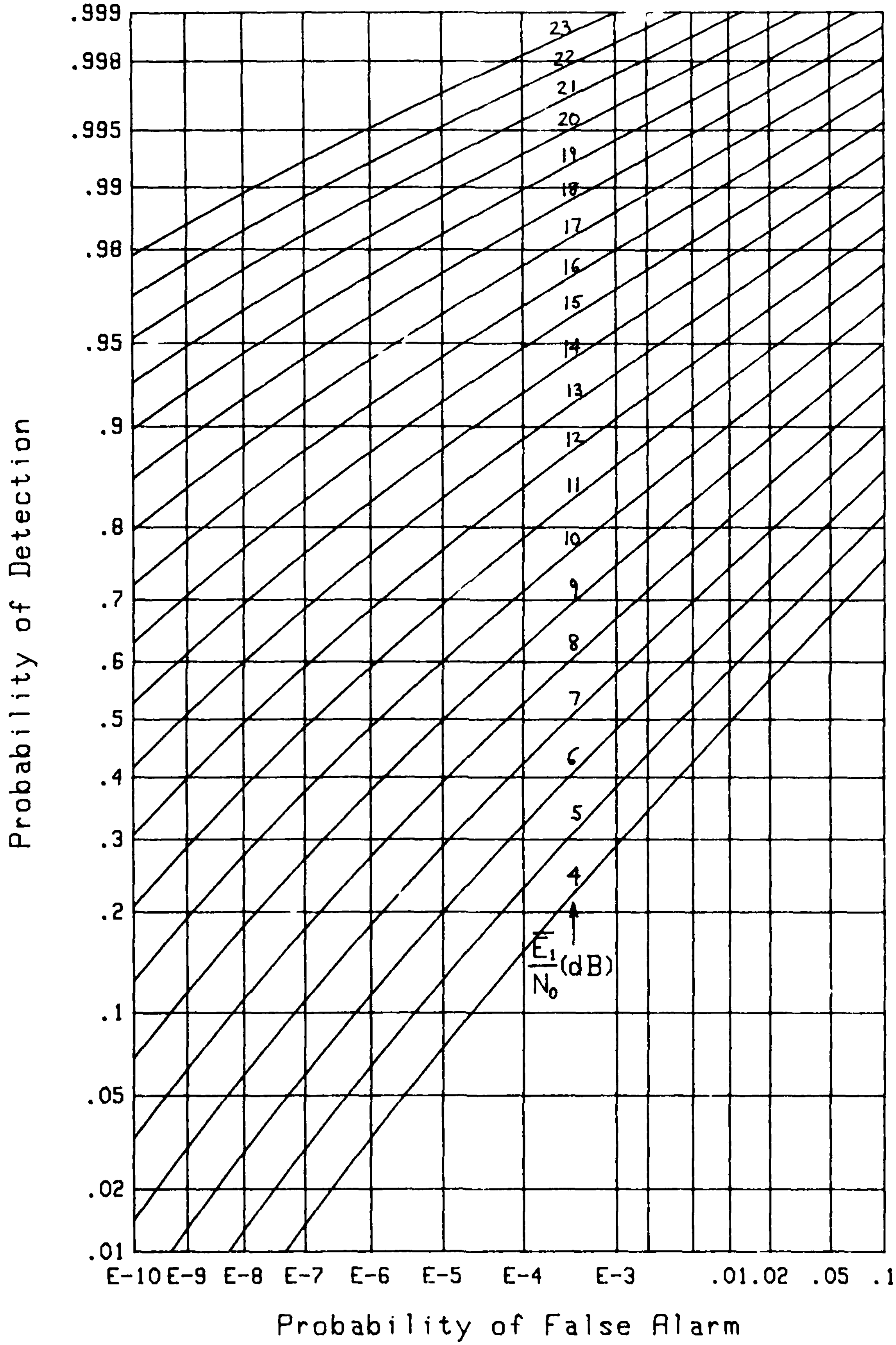

Figure 25. ROC for K=4, m=1, ρ=.5, L=16

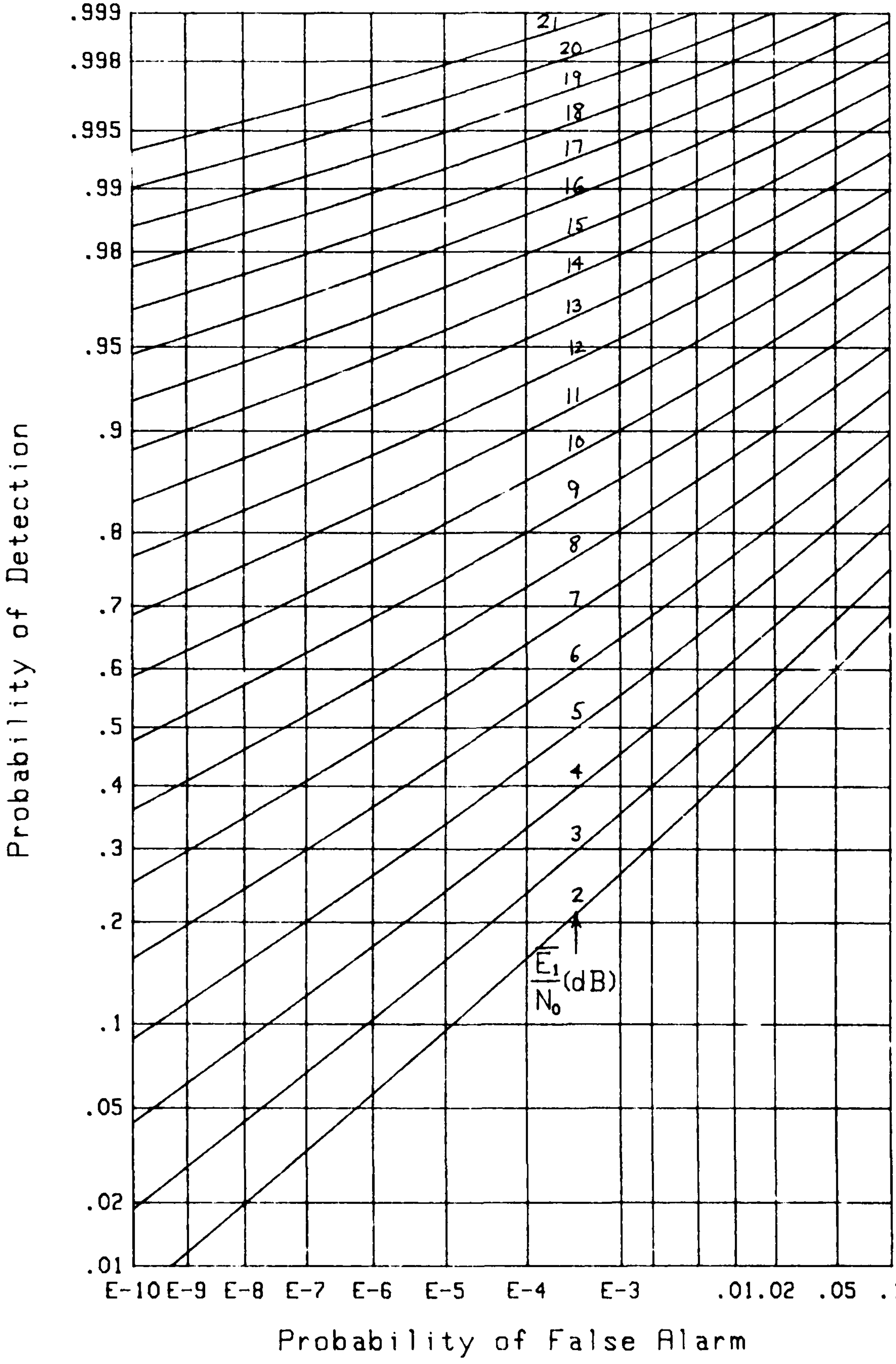

Figure 26. ROC for K=4, m=.5, ρ=0, L=∞

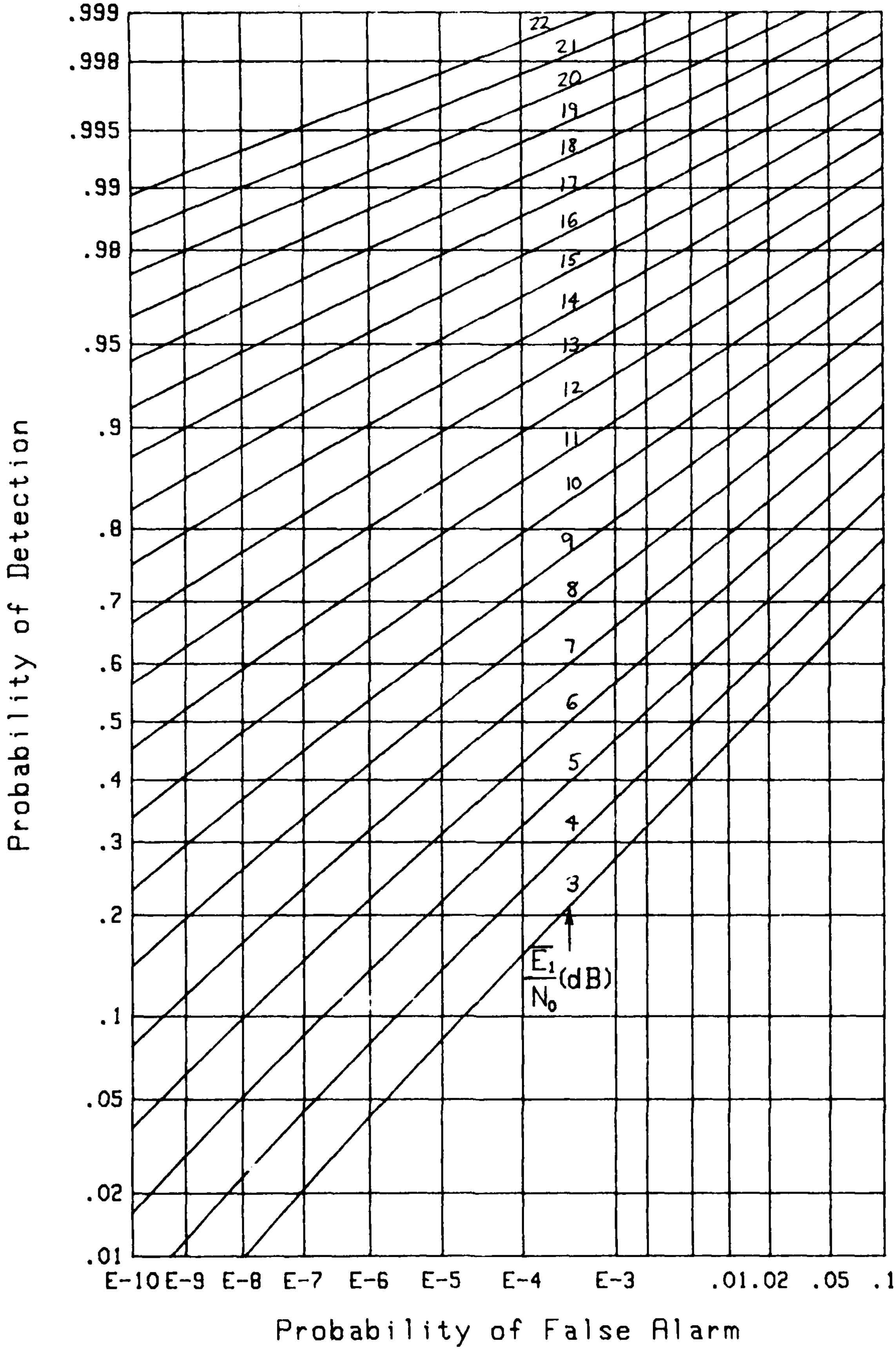

Figure 27. ROC for K=4, m=.5, ρ=0, L=32

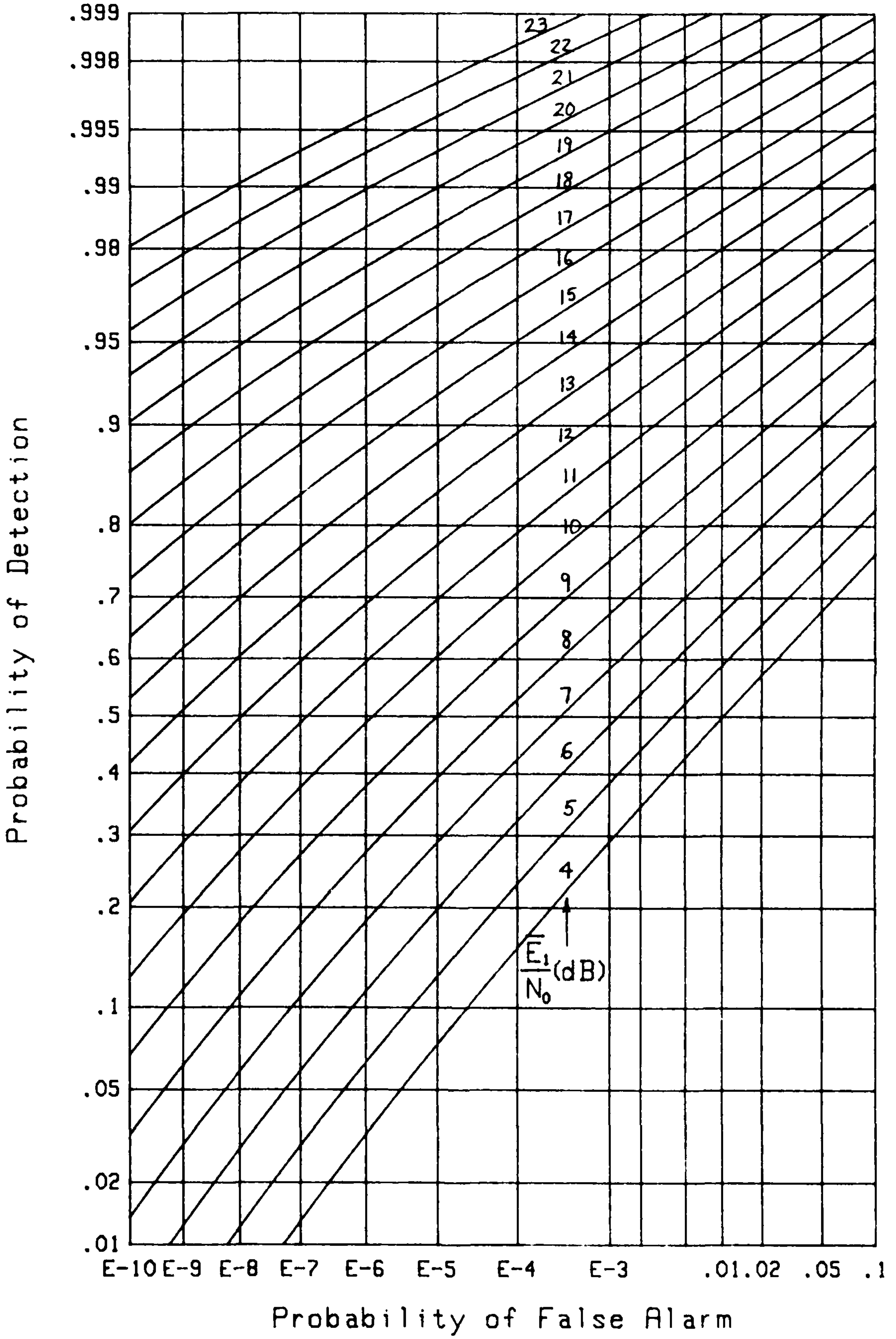

Figure 28. ROC for K=4, m=.5, ρ=0, L=16

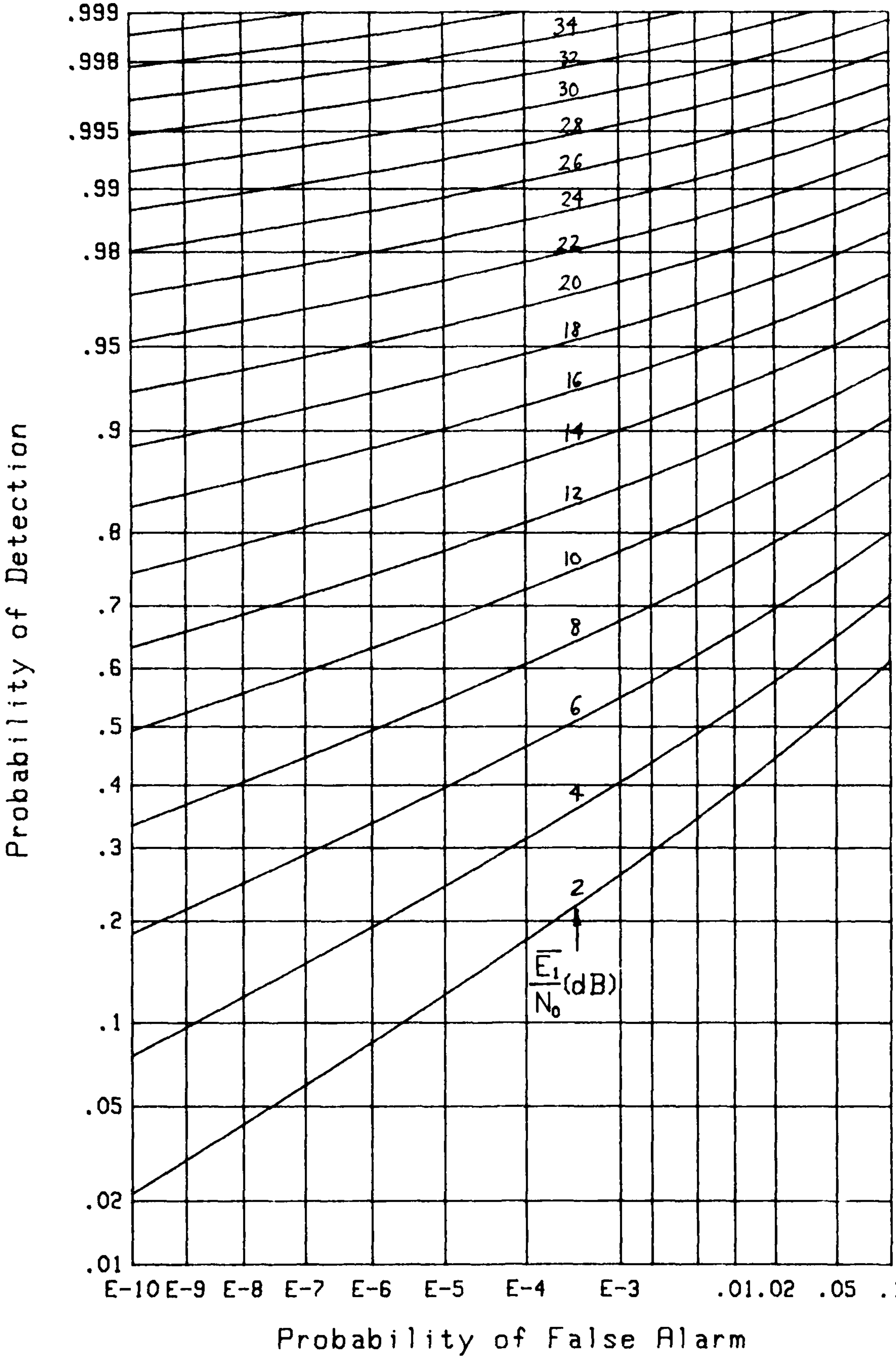

Figure 29. ROC for K=4, m=.5, ρ=.5, L=∞

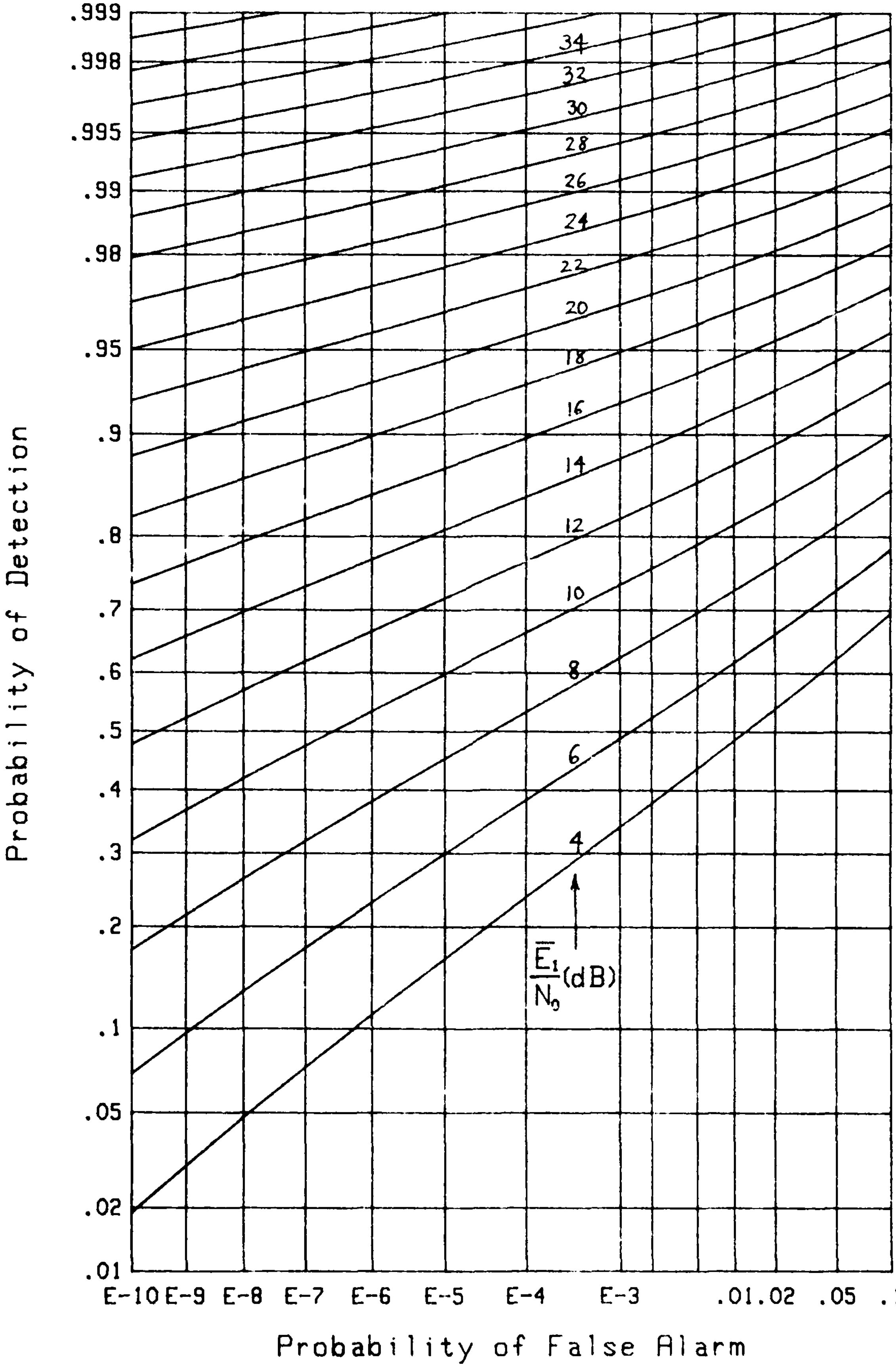

Figure 30. ROC for K=4, m=.5, ρ=.5, L=32

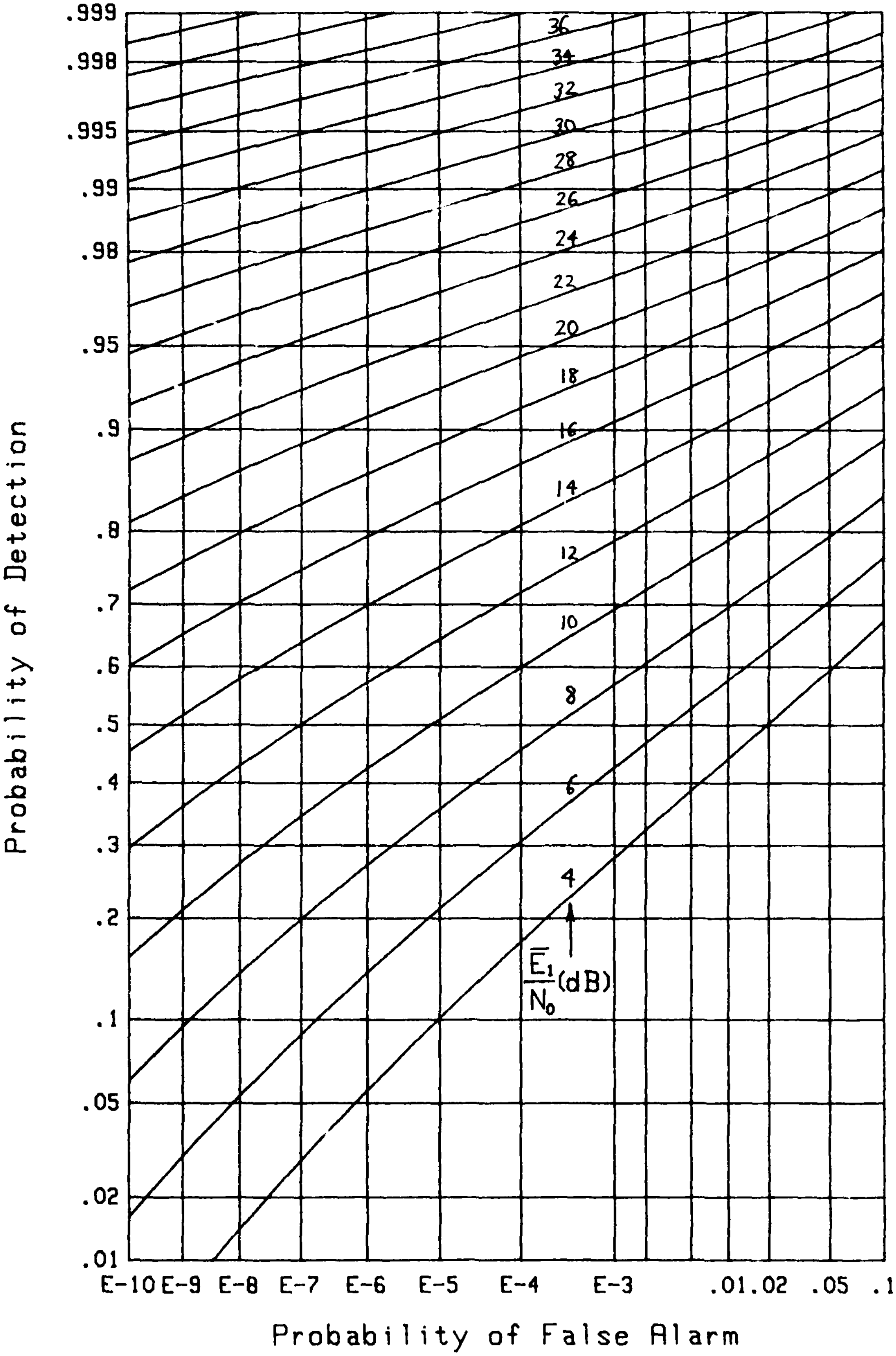

Figure 31. ROC for K=4, m=.5, ρ=.5, L=16

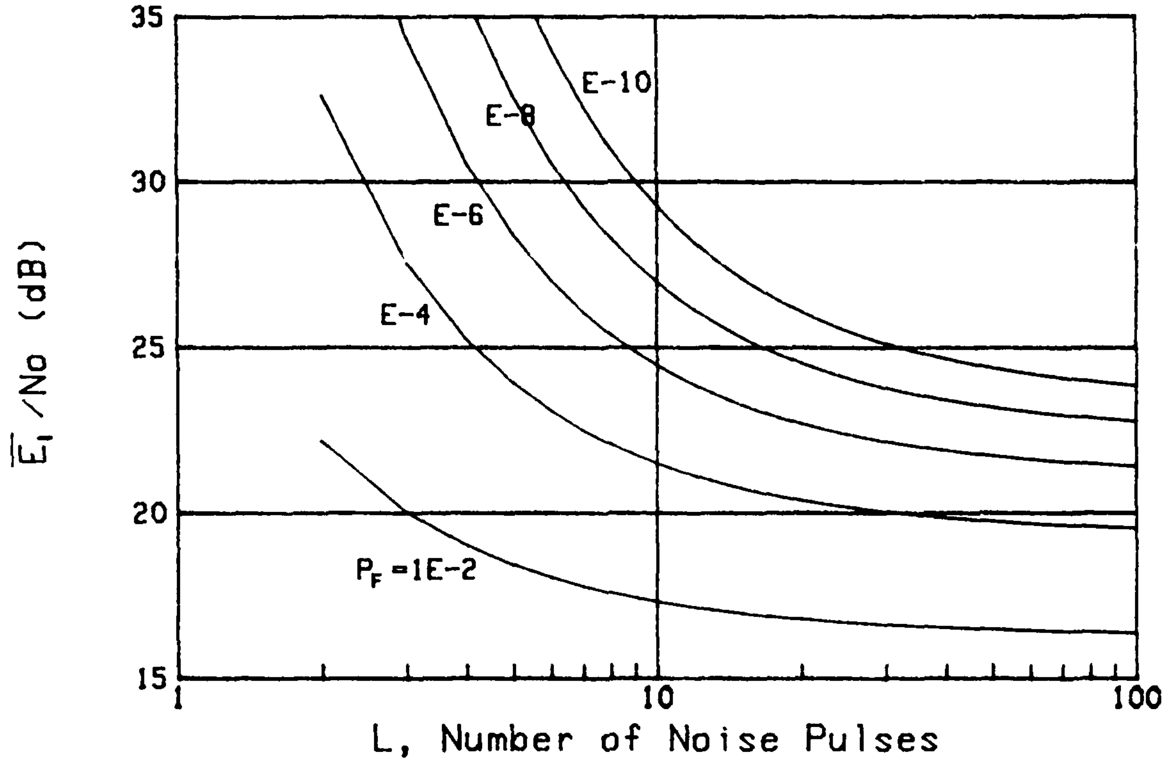

Figure 32. SNR for P_D =.9, K=1, m=1

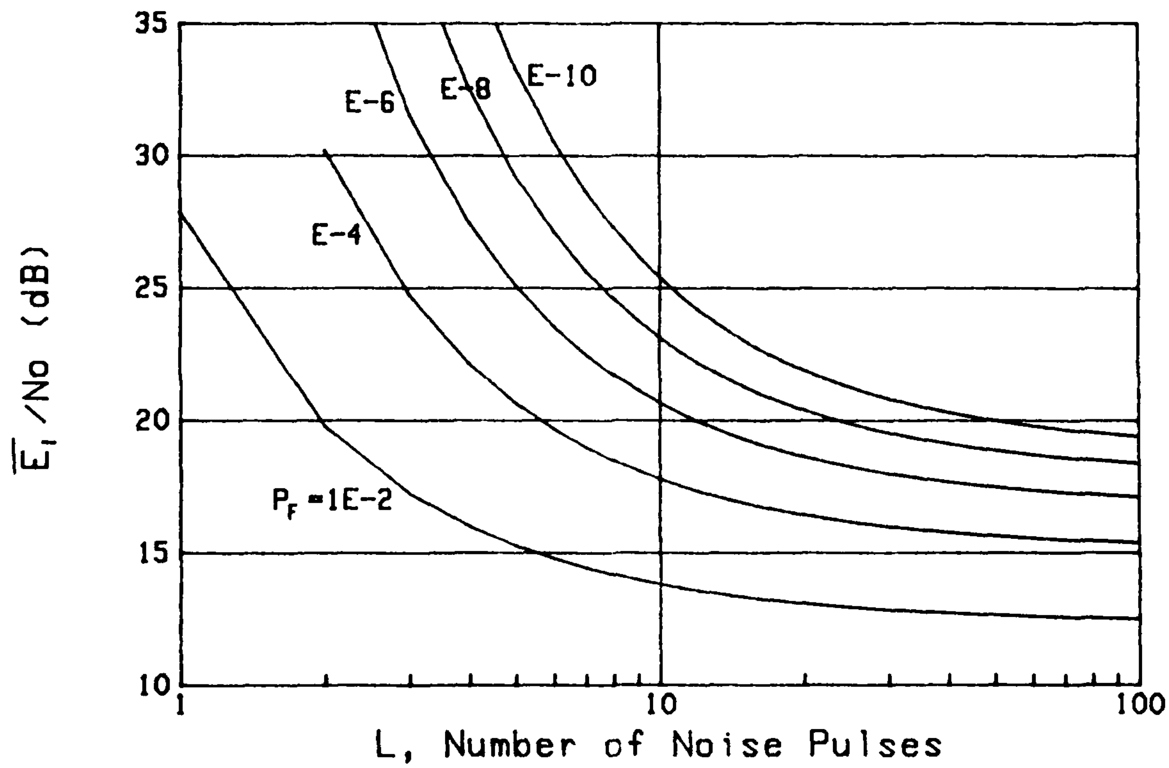

Figure 33. SNR for P_D =.9, K=2, m=1, ρ =.5

APPENDIX A

PROGRAM LISTINGS

There are two programs listed in this appendix, the first for L finite, the second for L infinite, where L is the number of noise-only pulses used to establish a reference. The fundamental parameters K,m,L are input in lines 20, 30, 40, while ρ is input in line 1400. The particular values of $\overline{E}_1/N_0$ (in dB) that are of interest are input in lines 340 and 350. Provision is made for 20 P_D vs P_F curves in lines 60-90; this can easily be changed to accommodate other cases.

The false alarm and detection probabilities are available in lines 1000 and 1130, respectively. The detection probability utilizes R and N as input variables; see table 2. The particular covariance programmed in lines 1390-1430 is exponential, but this, too, can easily be generalized.

To save space, the complete program for L infinite is not listed. Rather, just the essential false alarm and detection probability routines are listed at the end of the appendix; these are obviously not functions of L. The changes required to accommodate this case of infinite L should be obvious.

```
10   ! GENERATE PD-VS-PF NUMBERS FOR FINITE L
20     K=4                      !  NUMBER OF SIGNAL PULSES ADDED, K
30     Ms=.5                    !  FADING PARAMETER, m   (2m DOF)
40     L=16                     !  NUMBER OF NOISE PULSES ADDED, L
50     DIM U(100)
60     COM Pf(100),Pd1(100),Pd2(100),Pd3(100),Pd4(100),Pd5(100)
70     COM Pd6(100),Pd7(100),Pd8(100),Pd9(100),Pd10(100),Pd11(100)
80     COM Pd12(100),Pd13(100),Pd14(100),Pd15(100),Pd16(100),Pd17(100)
90     COM Pd18(100),Pd19(100),Pd20(100)
100    DOUBLE K,L,I,J           !  INTEGERS
110    S=0.
120    FOR I=1 TO K
130    FOR J=1 TO K
140    S=S+FNCov(I,J)           !  NORMALIZED COVARIANCE COEFFICIENTS
150    NEXT J
160    NEXT I
170    Ke=K*K/S                 !  EQUIVALENT NUMBER OF INDEPENDENT FADES
180    N=Ms*Ke                  !  N = m Ke
190    U=0.
200    U=U+.01
210    Pf=FNPf(U,K,L)
220    IF Pf>.1 THEN 200
230    U1=MAX(U-.01,.01)
240    U=U+.01
250    Pf=FNPf(U,K,L)
260    IF Pf>1E-10 THEN 240
270    U2=U
280    Delu=(U2-U1)/100.
290    FOR I=0 TO 100
300    U=U1+Delu*I
310    U(I)=U                   !  THRESHOLD VALUES
320    Pf(I)=FNPf(U,K,L)        !  PROBABILITY OF FALSE ALARM
330    NEXT I
340    FOR J=1 TO 20
350      E1nodb=2*J+2           !  SIGNAL-TO-NOISE RATIO PER PULSE, E1/No (dB)
360    E1no=10.^(.1*E1nodb)
370    R=E1no*K/N
380    FOR I=0 TO 100
390    U=U(I)
400    Pd=FNPd(U,R,N,K,L)       !  PROBABILITY OF DETECTION
410    IF J=1 THEN Pd1(I)=Pd
420    IF J=2 THEN Pd2(I)=Pd
430         !
440         !
590    IF J=19 THEN Pd19(I)=Pd
600    IF J=20 THEN Pd20(I)=Pd
610    NEXT I
620    NEXT J
630    FOR I=0 TO 100
640    Pf(I)=FNInvphi(Pf(I))
650    Pd1(I)=FNInvphi(Pd1(I))
660    Pd2(I)=FNInvphi(Pd2(I))
670      !
680      !
830    Pd19(I)=FNInvphi(Pd19(I))
840    Pd20(I)=FNInvphi(Pd20(I))
850    NEXT I
860    CALL A
870    END
880    !
```

```
890    DEF FNInvphi(X)        !  AMS 55, 26.2.23
900    IF X=.5 THEN RETURN 0.
910    P=MIN(X,1.-X)
920    T=-LOG(P)
930    T=SQR(T+T)
940    P=1.+T*(1.432788+T*(.189269+T*.001308))
950    P=T-(2.515517+T*(.802853+T*.010328))/P
960    IF X<.5 THEN P=-P
970    RETURN P
980    FNEND
990    !
1000   DEF FNPf(U,DOUBLE K,L) !  FALSE ALARM PROBABILITY
1010   IF U<=0. THEN RETURN 1.
1020   DOUBLE Ls                 !  INTEGER
1030   U1=U+1.
1040   K1=K-1
1050   S=T=EXP(K*LOG(U/U1))
1060   FOR Ls=1 TO L-1
1070   T=T*(K1+Ls)/(Ls*U1)
1080   S=S+T
1090   NEXT Ls
1100   RETURN 1.-S
1110   FNEND
1120   !
1130   DEF FNPd(U,R,N,DOUBLE K,L)  !  DETECTION PROBABILITY
1140   IF U<=0. THEN RETURN 1.
1150   DOUBLE Ls                     !  INTEGER
1160   U1=U+1.
1170   R1=R+1.
1180   U2=U/U1
1190   Ru=R1+U
1200   K2=K-2
1210   Nk=N-K+1
1220   Y=R1/Ru
1230   X=U2*R/R1
1240   X1=X-1.
1250   S=T=EXP(K*LOG(U2)+N*LOG(U1/Ru))
1260   Ho=0.
1270   H=1.
1280   FOR Ls=1 TO L-1
1290   T=T*Y
1300   J=K2+Ls
1310   A=((J+Ls+(Nk-Ls)*X)*H+J*X1*Ho)/Ls
1320   Ho=H
1330   H=A
1340   S=S+T*H
1350   NEXT Ls
1360   RETURN 1.-S
1370   FNEND
1380   !
1390   DEF FNCov(DOUBLE I,J)
1400     Rho=.5                   !  NORMALIZED COVARIANCE COEFFICIENT
1410   Cov=Rho^ABS(I-J)          !  EXPONENTIAL BEHAVIOR
1420   RETURN Cov
1430   FNEND
1440   !
```

```
1450    SUB A   !  PLOT PD VS PF ON NORMAL PROBABILITY PAPER
1460    COM Pf(*),Pd1(*),Pd2(*),Pd3(*),Pd4(*),Pd5(*)
1470    COM Pd6(*),Pd7(*),Pd8(*),Pd9(*),Pd10(*),Pd11(*)
1480    COM Pd12(*),Pd13(*),Pd14(*),Pd15(*),Pd16(*),Pd17(*)
1490    COM Pd18(*),Pd19(*),Pd20(*)
1500    DIM A$[30],B$[30]
1510    DIM Xlabel$(1:30),Ylabel$(1:30)
1520    DIM Xcoord(1:30),Ycoord(1:30)
1530    DIM Xgrid(1:30),Ygrid(1:30)
1540    DOUBLE N,Lx,Ly,Nx,Ny,I      ! INTEGERS
1550    !
1560    A$="Probability of False Alarm"
1570    B$="Probability of Detection"
1580    !
1590    Lx=12
1600    REDIM Xlabel$(1:Lx),Xcoord(1:Lx)
1610    DATA E-10,E-9,E-8,E-7,E-6,E-5,E-4,E-3,.01,.02,.05,.1
1620    READ Xlabel$(*)
1630    DATA 1E-10,1E-9,1E-8,1E-7,1E-6,1E-5,1E-4,.001,.01,.02,.05,.1
1640    READ Xcoord(*)
1650    !
1660    Ly=18
1670    REDIM Ylabel$(1:Ly),Ycoord(1:Ly)
1680    DATA .01,.02,.05,.1,.2,.3,.4,.5,.6,.7,.8,.9
1690    DATA .95,.98,.99,.995,.998,.999
1700    READ Ylabel$(*)
1710    DATA .01,.02,.05,.1,.2,.3,.4,.5,.6,.7,.8,.9
1720    DATA .95,.98,.99,.995,.998,.999
1730    READ Ycoord(*)
1740    !
1750    Nx=14
1760    REDIM Xgrid(1:Nx)
1770    DATA 1E-10,1E-9,1E-8,1E-7,1E-6,1E-5,1E-4
1780    DATA .001,.002,.005,.01,.02,.05,.1
1790    READ Xgrid(*)
1800    !
1810    Ny=18
1820    REDIM Ygrid(1:Ny)
1830    DATA .01,.02,.05,.1,.2,.3,.4,.5,.6,.7,.8,.9
1840    DATA .95,.98,.99,.995,.998,.999
1850    READ Ygrid(*)
1860    !
1870    FOR I=1 TO Lx
1880    Xcoord(I)=FNInvphi(Xcoord(I))
1890    NEXT I
1900    FOR I=1 TO Ly
1910    Ycoord(I)=FNInvphi(Ycoord(I))
1920    NEXT I
1930    FOR I=1 TO Nx
1940    Xgrid(I)=FNInvphi(Xgrid(I))
1950    NEXT I
1960    FOR I=1 TO Ny
1970    Ygrid(I)=FNInvphi(Ygrid(I))
1980    NEXT I
1990    X1=Xgrid(1)
2000    X2=Xgrid(Nx)
2010    Y1=Ygrid(1)
2020    Y2=Ygrid(Ny)
2030    Scale=(Y2-Y1)/(X2-X1)
```

```
2040    GINIT 200./260.                              !  VERTICAL PAPER
2050    PLOTTER IS 505,"HPGL"
2060    PRINTER IS 505
2070     PRINT "VS4"
2080    LIMIT PLOTTER 505,0.,200.,0.,260.            !  1 GDU = 2 mm
2090    VIEWPORT 22.,85.,19.,122.
2100  ! VIEWPORT 22.,85.,59.,122.                    !  TOP OF PAPER
2110  ! VIEWPORT 22.,85.,19.,62.                     !  BOTTOM OF PAPER
2120    WINDOW X1,X2,Y1,Y2
2130    FOR I=1 TO Nx
2140    MOVE Xgrid(I),Y1
2150    DRAW Xgrid(I),Y2
2160    NEXT I
2170    FOR I=1 TO Ny
2180    MOVE X1,Ygrid(I)
2190    DRAW X2,Ygrid(I)
2200    NEXT I
2210    CSIZE 2.3,.5
2220    LORG 5
2230    Y=Y1-(Y2-Y1)*.02
2240    FOR I=1 TO Lx
2250    MOVE Xcoord(I),Y
2260    LABEL Xlabel$(I)
2270    NEXT I
2280    CSIZE 3.,.5
2290    MOVE .5*(X1+X2),Y1-.06*(Y2-Y1)
2300    LABEL A$
2310    MOVE .5*(X1+X2),Y1-.1*(Y2-Y1)
2320      LABEL "Figure 31. ROC for K=4, m=.5,  =.5, L=16"
2330    CSIZE 2.3,.5
2340    LORG 8
2350    X=X1-(X2-X1)*.01
2360    FOR I=1 TO Ly
2370    MOVE X,Ycoord(I)
2380    LABEL Ylabel$(I)
2390    NEXT I
2400    LDIR PI/2.
2410    CSIZE 3.,.5
2420    LORG 5
2430    MOVE X1-.15*(X2-X1),.5*(Y1+Y2)
2440    LABEL B$
2450    PENUP
2460    PLOT Pf(*),Pd1(*)
2470    PENUP
2480    PLOT Pf(*),Pd2(*)
2490    PENUP
2500                  !
2510                  !
2820    PLOT Pf(*),Pd19(*)
2830    PENUP
2840    PLOT Pf(*),Pd20(*)
2850    PENUP
2860    PAUSE
2870    PRINTER IS CRT
2880    PLOTTER 505 IS TERMINATED
2890    SUBEND
```

```
 10     DEF FNPf(Thr,DOUBLE K)  !  FALSE ALARM PROBABILITY
 20     DOUBLE J                !  INTEGER
 30     S=T=EXP(-Thr)
 40     FOR J=1 TO K-1
 50     T=T*Thr/J
 60     S=S+T
 70     NEXT J
 80     RETURN S
 90     FNEND
100     !
110     DEF FNPd(Thr,R,N,DOUBLE K)   !  TR 7707, APP. C-1
120     Error=1.E-10
130     DOUBLE K1,Ks                 !  INTEGERS
140     Et=EXP(Thr)
150     K1=K-1
160     N1=N-1.
170     R1=1.+R
180     Q=R/R1
190     E=Te=1.
200     FOR Ks=1 TO K1
210     Te=Te*Thr/Ks
220     E=E+Te
230     NEXT Ks
240     S=B=MAX(Et-E,0.)
250     T=1.
260     FOR Ks=1 TO 1000
270     Te=Te*Thr/(K1+Ks)
280     B=MAX(B-Te,0.)
290     T=T*Q*(N1+Ks)/Ks
300     Pr=T*B
310     S=S+Pr
320     IF ABS(Pr)<=Error*ABS(S) THEN 350
330     NEXT Ks
340     PRINT "1000 TERMS AT:";K;N;Thr;R;Pr/S
350     Pd=1.-EXP(-Thr-N*LOG(R1))*S
360     RETURN Pd
370     FNEND
```

REFERENCES

1. A. H. Nuttall and F. S. Eby, Signal-to-Noise Ratio Requirements for Detection of Multiple Pulses Subject to Partially Correlated Fading With Chi-Squared Statistics of Various Degrees of Freedom, NUSC Technical Report 7707, Naval Underwater Systems Center, New London, CT, 2 June 1986.

2. Handbook of Mathematical Functions, U. S. Department of Commerce, National Bureau of Standards, Applied Mathematics Series No. 55, U. S. Government Printing Office, Washington, D.C., June 1964.

3. I. S. Gradshteyn and I. M. Ryzhik, Table of Integrals, Series, and Products, Academic Press, Inc., New York, NY, 1980.

4. A. H. Nuttall and P. G. Cable, Operating Characteristics for Maximum Likelihood Detection of Signals in Gaussian Noise of Unknown Level: III. Random Signals of Unknown Level, NUSC Technical Report 4783, Naval Underwater Systems Center, New London, CT, 31 July 1974.

5. D. R. Morgan, "Two-Dimensional Normalization Techniques," IEEE Journal of Oceanic Engineering, vol. OE-12, no. 1, pp. 130-142, January 1987.

6. A. H. Nuttall, Operating Characteristics of Log-Normalizer for Weibull and Log-Normal Inputs, NUSC Technical Report 8075, Naval Underwater Systems Center, New London, CT, 17 August 1987.

7. A. H. Nuttall, Operating Characteristics for Indicator Or-ing of Incoherently Combined Matched Filter Outputs, NUSC Technical Report 8121, Naval Underwater Systems Center, New London, CT, 21 September 1987.

Technical Report 8121
21 September 1987

Operating Characteristics for Indicator Or-ing of Incoherently Combined Matched-Filter Outputs

A. H. Nuttall

ABSTRACT

The false alarm and detection probabilities for a processor that incoherently combines M matched filter outputs and then subjects these summed quantities to or-ing amongst N channels are derived for general M, N, and signal-to-noise ratios. A probability of correct detection occurs only when the signal channel output exceeds a threshold and all other noise channel outputs. Receiver operating characteristics are plotted for the 40 possible combinations of M=1(1)10 with N=1, 10, 100, 1000, for signal-to-noise ratios ranging over values diverse enough to cover false-alarm, detection probability pairs from (.01,.5) to (1E-10,.999). Also, the required signal-to-noise ratio to realize specified false alarm and detection probabilities are plotted versus N, for several values of M.

The signal-to-noise ratio parameter employed is related to the total received signal energy to Gaussian noise spectral density ratio. This allows for consideration of arbitrary fractionalization of the received signal energy and for investigation of mismatched as well as frequency offset and time desynchronization, if desired. Programs for all procedures are listed.

TABLE OF CONTENTS

LIST OF ILLUSTRATIONS

LIST OF ILLUSTRATIONS (CONT'D)

LIST OF ILLUSTRATIONS (CONT'D)

LIST OF SYMBOLS

M	number of filter outputs added, figure 1
N	number of channels subject to or-ing, figure 2, (2)
$h(\tau)$	impulse response of filter, figure 1
underline	complex envelope
t_{nm}	sampling time in n-th channel on m-th filter output, figure 1
v_n	summer output of n-th channel, figure 1, (9)
w	maximum output from or-ing device, (2), (3)
$\hat{n}$	channel indication from or-ing device, (2)
$s(t)$	real signal function of time t, (4)
$n(t)$	real noise process, (5)
a,b	real, imaginary parts of signal output, (4)
x,y	real, imaginary parts of noise, (4)
c	complex envelope of filter output, (4)
N_d	double-sided noise spectral density (watts/Hz), (12)
N_o	single-sided noise spectral density (= $2N_d$), (12)
σ^2	noise power, (14)
d	total output signal-to-noise ratio measure, (15)
E_m	received signal energy in m-th component, (17)
P	cumulative distribution function, (18)
Q_M	Marcum's Q_M - function, (19)
F_n	auxiliary function, (22)
e_n	partial exponential, (23)

LIST OF SYMBOLS (CONT'D)

P_F	false alarm probability, (25)
P_{SD}	probability of signal detection, (26)
P_{AD}	probability of any detection, (27)
P_{CD}	probability of correct detection, (28)
ROC	Receiver Operating Characteristic

OPERATING CHARACTERISTICS FOR INDICATOR OR-ING OF INCOHERENTLY COMBINED MATCHED-FILTER OUTPUTS

INTRODUCTION

When multiple pulses are transmitted, in an effort to detect the presence of a target, the multiple echoes should be optimally processed and combined before a decision is reached. For received signals that are deterministic, except for independent random phases between pulses, the ideal processing consists of matched filtering, envelope detection, and combination according to a $\ln I_0$ rule [1; chapter VII, (1.7)]. Since the receiver input signal-to-noise ratio must be known in order to apply this rule, the slightly suboptimum alternative of combining (adding) squared envelopes is often adopted [1; ch. VII, (1.12)]; this is the situation to be considered here.

In addition, if the target has some movement in the radial direction, causing a Doppler shift of the echoes, a search must be conducted over frequency at the receiver, in order not to miss the received signal energy. For example, suppose a series of M tone bursts at a common center frequency are transmitted and echoed off a moving point target. Since the received center frequency will be unknown, groups of matched filters will be necessary, in order to cover the expected range of frequency shifts. Each one of the possible received center frequencies that must be processed is called a channel.

In figure 1, a block diagram of the processing in the n-th channel is depicted. The M narrowband filters in the n-th channel are indicated by impulse responses $\left\{h_{nm}(\tau)\right\}_{m=1}^{M}$. They are followed by detectors which extract the squared envelopes of the filter outputs. These detector outputs are then sampled at times $\left\{t_{nm}\right\}_{m=1}^{M}$, which should correspond to the times of peak signal at each filter output. The sampled outputs are then added, to yield channel output v_n.

The block diagram in figure 1 is not restricted to a transmitted sequence of M tone bursts at a common center frequency. In fact, due to the general filter impulse responses and sampling times allowed, it encompasses any sequence of orthogonal deterministic signals transmitted at arbitrary time delays and frequency offsets, provided they are known to the receiver. The processor in figure 1 also allows for unknown time delay to the target range and unknown frequency shift due to target movement, by virtue of the sampling times not being optimum, and the filter impulse responses not being matched to each received signal component. An example is afforded by the case where the filters are time-delayed and/or frequency-shifted versions of one another,

$$\underline{h}_{nm}(\tau) = \underline{h}(\tau - \tau_{nm}) \exp(i2\pi f_{nm}\tau), \tag{1}$$

corresponding to a time sequence of frequency-stepped pulses; here $\underline{h}$ is the complex envelope corresponding to impulse response h [1; pages 65-72].

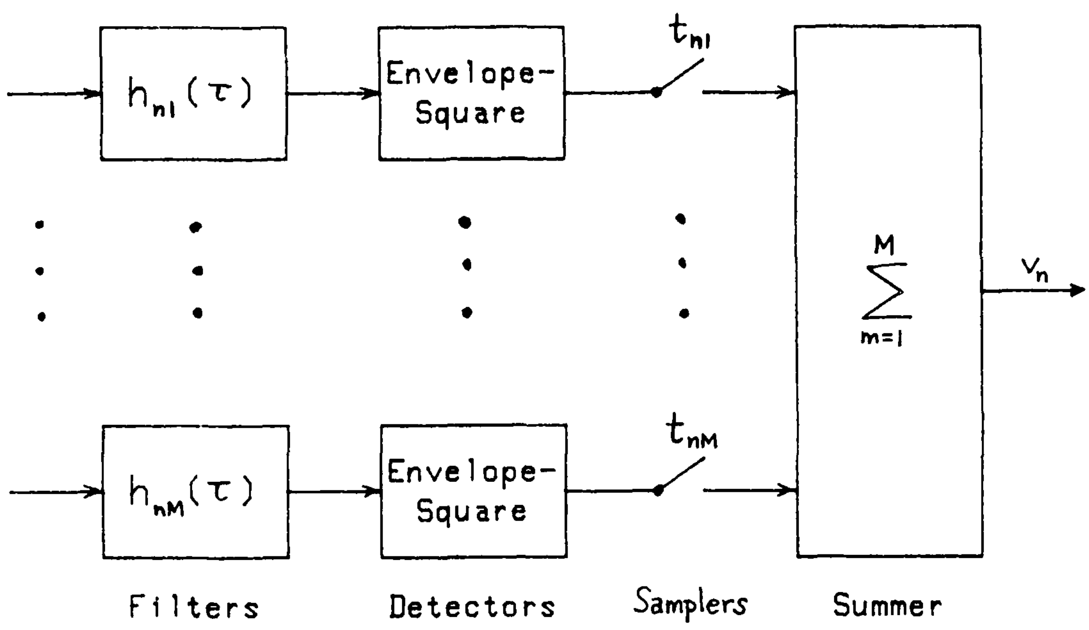

Figure 1. Pre-Processing for n-th Channel

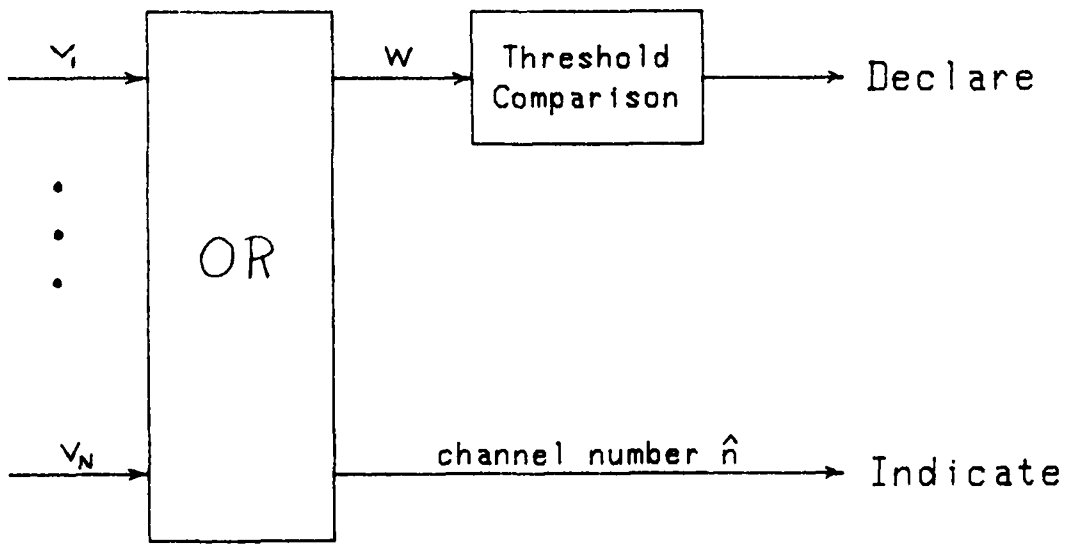

Figure 2. Indicator Or-ing of N Channels

Another instance which is covered by the processing indicated in figure 1 is where the transmitted signal encounters multipath and/or separated target highlight structure. For example, a single transmitted tone burst might be received as four pulses, due to two multipaths and two target highlights. Thus, the number M of filters employed in figure 1 is be interpreted as the total number of received signal components. Some results for the receiver operating characteristics of this processor are given in [1] and [2].

When the processing in the n-th channel indicated in figure 1 is completed, the total of N channels that must be considered is subjected to the indicator or-ing depicted in figure 2. Namely, the maximum of the N channel outputs is extracted, along with its identity,

$$w = \max\,(v_1,\ v_2,\ \ldots,\ v_N) = v_{\hat{n}}\ , \tag{2}$$

and compared with a fixed threshold:

$$\left\{\begin{array}{l} w < \text{threshold: declare no signal present} \\ w > \text{threshold: declare signal present in channel } \hat{n} \end{array}\right\}\ . \tag{3}$$

Thus, there are two possible outputs from figure 2, the first being a declaration of no signal present, and the second being a declaration of a signal present along with an indication of which channel contains the signal. (This latter information is useful for identifying the Doppler shift, for example, of a moving target.)

A false alarm occurs when output w in (2) exceeds the threshold, but there is no signal present at the input. On the other hand, a correct detection occurs only when the signal channel output exceeds the threshold and all the noise channel outputs. That is, we insist on accurately identifying the signal channel, in order to achieve a correct detection. The performance characteristics of the processor combination in figures 1 and 2 are of interest, namely the false alarm probability and the probability of correct detection, in terms of M, the number of filter outputs summed, N, the number of channels or-ed, and some signal-to-noise ratio measure at the receiver.

It should be observed that the M received signal components have been presumed to have undergone no fading. The only randomness in the received signals are the independent random phase shifts between components. Some results on fading signals, including partial fading between pulses, are given in [3]; however, or-ing was not considered there.

It is also assumed that the individual signal components are orthogonal with respect to each other, perhaps due to time separation and/or frequency shift. That is, at sampling instant t_{nm}, there is only one signal component contributing, with all the other signal components yielding no output at that filter at that time.

The processor considered in this study has undergone some analysis in the past [4]; however, several significant extensions have been made here. First, a different definition of detection probability has been adopted here, namely one which counts as correct detections only those events for

which the signal channel output exceeds both the threshold and all the other undesired noise channel outputs. Second, results are extended from a sinusoidal signal to arbitrary orthogonal deterministic signals and filters, with arbitrary sampling instants; this allows for analysis of the effects of filter-signal mismatch, Doppler offset, time desynchronization, multiple highlights, etc. Third, a fundamentally different signal-to-noise ratio parameter, d, is used here to characterize performance, namely, a measure of the total received signal energy to noise spectral density ratio, rather than the signal-to-noise ratio per pulse (usually assumed identical for all pulses); this allows for arbitrary fractionalization of the total received signal energy into component pulses. Fourth, the detection probability vs. false alarm probability curves are plotted on normal probability paper with total signal-to-noise ratio, d, as a parameter; this straightens out the curves, makes them nearly equi-spaced in d, and affords easy accurate interpolation in signal-to-noise ratio values. Finally, the current results are extended to much larger values of the number, N, of or-ing channels and much smaller false alarm probabilities P_F; in particular, values of N up to 1000, and values of P_F as small as 1E-10, are considered.

STATISTICS OF FILTER ENVELOPE-SQUARED OUTPUT

In this section, we derive the statistical properties of the output of figure 1. Suppose a real narrowband deterministic signal s(t) and a real random noise process n(t) have complex envelopes $\underline{s}(t)$ and $\underline{n}(t)$, respectively. Let the sum of these two processes excite a narrowband filter $h(\tau)$ with complex envelope impulse response $\underline{h}(\tau)$. The complex envelope of the filter output at time t is proportional to

$$c(t) = [\underline{s}(t) + \underline{n}(t)] \bullet \underline{h}(t) = a(t) + ib(t) + x(t) + iy(t), \quad (4)$$

where

$$a(t) + ib(t) = \int d\tau\ \underline{s}(\tau)\ \underline{h}(t-\tau) \quad (5)$$

is the deterministic signal output, and

$$x(t) + iy(t) = \int d\tau\ \underline{n}(\tau)\ \underline{h}(t-\tau) \quad (6)$$

is the random noise output process. Then the filter squared-envelope output at time t is

$$|c(t)|^2 = |a(t) + ib(t) + x(t) + iy(t)|^2 =$$

$$= [a(t) + x(t)]^2 + [b(t) + y(t)]^2. \quad (7)$$

More generally, for M filters, if signal $s_m(t)$ excites filter $h_m(\tau)$, the m-th filter squared-envelope output at sample time t_m is

$$|c_m(t_m)|^2 = [a_m(t_m) + x_m(t_m)]^2 + [b_m(t_m) + y_m(t_m)]^2 \quad \text{for } 1 \le m \le M. \tag{8}$$

Sample times $\{t_m\}_1^M$ can be selected arbitrarily; each individual t_m should be chosen to maximize the size of the m-th signal output, $a_m^2(t_m) + b_m^2(t_m)$.

If we sum these squared-envelope filter output samples, we have channel output

$$v = \sum_{m=1}^{M} |c_m(t_m)|^2 =$$

$$= \sum_{m=1}^{M} \left\{[a_m(t_m) + x_m(t_m)]^2 + [b_m(t_m) + y_m(t_m)]^2\right\} . \tag{9}$$

The signal and noise outputs, given in (5) and (6), apply for an arbitrary complex envelope signal $\underline{s}_m(t)$ and filter $\underline{h}_m(\tau)$ in the m-th branch of the receiver. The instantaneous output signal squared-envelope is

$$a_m^2(t) + b_m^2(t) = |a_m(t) + ib_m(t)|^2 = \left|\int d\tau\, \underline{s}_m(\tau)\, \underline{h}_m(t-\tau)\right|^2 , \tag{10}$$

while the instantaneous output noise squared-envelope is

$$x_m^2(t) + y_m^2(t) = |x_m(t) + iy_m(t)|^2 = \left|\int d\tau\, \underline{n}(\tau)\, \underline{h}_m(t-\tau)\right|^2 . \tag{11}$$

Here, we presume that a common broadband noise n(t) excites all the filters $\{h_m(\tau)\}$ in the receiver bank. Observe that if the m-th signal is subject to a random phase shift, according to the factor $\exp(i\theta_m)$, this cancels out of the envelope-squared signal term. Thus, all the results here apply not only to a deterministic signal, but also to one with an arbitrary phase shift. However, no fading of the received signal is allowed in any of the current results.

If the real input noise n(t) is white with double-sided spectral level N_d watts/Hz, then the correlation of complex envelope $\underline{n}(t)$ is [1; ch. II, (3.11) and (6.22)]

$$\overline{\underline{n}(t)\ \underline{n}^*(t-\tau)} = 4N_d\ \delta(\tau) = 2N_0\ \delta(\tau); \tag{12}$$

N_0 is the single-sided noise spectral density level in watts/Hz. By use of (6), this results in average noise powers for the m-th components, as

$$\overline{x_m^2(t)} = \overline{y_m^2(t)} = 2N_d \int d\tau\ \left|\underline{h}_m(\tau)\right|^2 . \tag{13}$$

We presume that all the filters have the same level (energy); thus, we define

$$\sigma^2 = \overline{x_m^2(t)} = \overline{y_m^2(t)} = 2N_d \int d\tau \left|\underline{h}_m(\tau)\right|^2 \quad \text{for } 1 \le m \le M. \tag{14}$$

This is an important restriction; greater generality is given in [2; appendices B and C].

We are now in position to employ the general results listed in appendix A, when the noise is Gaussian. Namely, define, as in (A-1),

$$d^2 = \frac{1}{\sigma^2} \sum_{m=1}^{M} \left[a_m^2(t_m) + b_m^2(t_m) \right] =$$

$$= \frac{1}{\sigma^2} \sum_{m=1}^{M} \left| \int d\tau \; \underline{s}_m(\tau) \; \underline{h}_m(t_m - \tau) \right|^2 =$$

$$= \frac{\sum_{m=1}^{M} \left| \int d\tau \; \underline{s}_m(\tau) \; \underline{h}_m(t_m - \tau) \right|^2}{2N_d \int d\tau \left| \underline{h}_m(\tau) \right|^2} . \qquad (15)$$

Observe that the absolute level of each filter, $\underline{h}_m$, cancels out in this ratio. However, d^2 does depend on the scale of each signal $\underline{s}_m$ and inversely on noise level N_d.

The maximum value of each term in these ratios is realized by choosing the m-th filter such that its impulse response

$$\underline{h}_m(\tau) = k \; \underline{s}_m^{\star}(T_m - \tau), \qquad (16)$$

where k is a complex constant selected to guarantee the equal energy requirement in (14), and T_m is a delay inserted for realizability, and by choosing sample time t_m equal to T_m. This is the matched filter to the m-th signal, sampled at the time of peak output. Thus, we have, in the best situation,

$$\max d^2 = \frac{1}{2N_d} \sum_{m=1}^{M} \int dt \left| \underline{s}_m(t) \right|^2 = \frac{1}{N_d} \sum_{m=1}^{M} E_m = \frac{E_T}{N_d} = \frac{2E_T}{N_o} , \tag{17}$$

where E_m is the received signal energy in the m-th real signal component $s_m(t)$, and E_T is the total received signal energy over all M paths (branches). Additional interpretations of d^2 are available in (A-21) et seq.

This maximum value of d^2 in (17) is realized only if the receiving filters are the matched filters (16), and if the filter outputs are sampled at the correct time instants. More generally, the generic value of d^2 in (15) allows for arbitrary signals, filters, and sampling instants, thereby affording the possibility of considering losses due to mismatch and desynchronization. The signals can be time-delayed and/or frequency-shifted versions of each other, if desired. A more thorough analysis and comparison is presented in [2; appendices B and C]. The received signals have undergone no fading in any of these considerations; thus the current analysis applies to a deterministic signal, except for random phase.

Reference to (A-2) and (A-6) now allows us to state the exceedance distribution function of channel output v in (9) as

$$\mathrm{Prob}(v > u) = 1 - P_v(u) = Q_M\,(d, \sqrt{u}/\sigma) \text{ for } u > 0, \tag{18}$$

where the Q_M-function is

$$Q_M(\alpha,\ \beta) = \int_\beta^\infty dx\ x \left(\frac{x}{\alpha}\right)^{M-1} I_{M-1}(\alpha x)\ \exp\left(\frac{x^2 + \alpha^2}{-2}\right). \tag{19}$$

Parameters d and σ in (18) are given by (15) and (14), respectively. These results pertain to the signal-bearing channel; the noise-only channel outputs correspond to setting d = 0.

FALSE ALARM AND DETECTION PROBABILITIES

The exceedance distribution function of the processor output v_n for the n-th channel (see figure 1) is given by (18) for signal present in that channel. For those channels with no signal present, the exceedance distribution is

$$1 - P_v^{(o)}(u) = Q_M(0,T) = E_{M-1}(T^2/2) \quad \text{for } u > 0, \tag{20}$$

where we have let

$$T = \sqrt{u}/\sigma \tag{21}$$

for notational convenience, and defined

$$E_n(x) = \exp(-x)\, e_n(x), \tag{22}$$

where

$$e_n(x) = \sum_{k=0}^{n} x^k/k! \tag{23}$$

is the partial exponential [5; 6.5.11].

FALSE ALARM PROBABILITY

Since the noises in the N channels subject to or-ing in figure 2 are presumed independent, the probability that <u>all</u> N outputs do not exceed a threshold value u is

$$[P_V^{(o)}(u)]^N = \left[1-E_{M-1}\left(\frac{u}{2\sigma^2}\right)\right]^N , \tag{24}$$

where cumulative distribution function $P_V^{(o)}$ was obtained from (20). The false alarm probability is then

$$P_F = 1 - [1 - E_{M-1}(T^2/2)]^N , \tag{25}$$

where we used (21).

DETECTION PROBABILITY

When signal is present in one channel, we have several alternative definitions of a detection probability. For example, we could define the probability of signal detection, P_{SD}, as the probability that the <u>signal</u> channel output exceeds threshold u, disregarding the noise channels completely; then directly from (18) and (21),

$$P_{SD} = Q_M(d,T), \tag{26}$$

which is, of course, independent of N.

However, it is possible that the noise channels could also cause a threshold crossing, even when the signal channel does not. We can then define a probability of any detection, P_{AD}, as the probability that <u>any</u> channel output exceeds the threshold u. This quantity is given by

$$P_{AD} = 1 - [P_v^{(o)}(u)]^{N-1} P_v(u) =$$

$$= 1 - [1 - E_{M-1}(T^2/2)]^{N-1} [1 - Q_M(d,T)], \qquad (27)$$

by use of (20) and (18). This is the case considered in [4; see (9) and (4)].

The problem with this latter definition is that, since we are interested in knowing which channel contains the signal, the probability P_{AD} contains some (rare) events which indicate the incorrect channel to contain the signal. The best alternative appears to be to define the probability of correct detection, P_{CD}, as the probability that the signal channel output exceeds the threshold u <u>and</u> exceeds all the noise outputs. In this case, the signal will be detected and its channel number correctly indicated. This probability is given by

$$P_{CD} = \int_u^{\infty} dt \; p_v(t) \; [P_v^{(o)}(t)]^{N-1}, \qquad (28)$$

where probability density function p_v and cumulative distribution function $P_v^{(o)}$ are given by (A-4) and (A-9), respectively. Substituting these expressions, letting $x = \sqrt{t}/\sigma$, and using (21), there follows the integral result

$$P_{CD} = \int_T^{\infty} dx\ x\ \left(\frac{x}{d}\right)^{M-1} I_{M-1}(dx)\ \exp\left(\frac{x^2+d^2}{-2}\right)\ [1-E_{M-1}(x^2/2)]^{N-1}\ . \qquad (29)$$

From physical reasoning or mathematical manipulations, it follows that

$$P_{CD} < P_{SD} < P_{AD} \quad \text{for } N > 1. \qquad (30)$$

For N = 1, no or-ing, all three detection probabilities are equal to $Q_M(d,T)$.

Also, from (29), since the bracketed term is greater than or equal to its value at x = T, we have the lower bound

$$P_{CD} > [1 - E_{M-1}(T^2/2)]^{N-1}\ Q_M(d,T) \quad \text{for } N > 1. \qquad (31)$$

Thus we have the tight bounds on the probability of correct detection:

$$[1 - E_{M-1}(T^2/2)]^{N-1}\ Q_M(d,T) < P_{CD} < Q_M(d,T)\ . \qquad (32)$$

To show how tight these bounds are, recall the false alarm probability in (25), in order to express the bounds as

$$(1 - P_F)^{\frac{N-1}{N}} \; Q_M(d,T) < P_{CD} < Q_M(d,T) \; . \tag{33}$$

For small false alarm probabilities,

$$(1 - P_F)^{\frac{N-1}{N}} \approx 1 - P_F \, \frac{N-1}{N} > 1 - P_F \; , \tag{34}$$

leading to

$$(1 - P_F) \; Q_M(d,T) < P_{CD} < Q_M(d,T); \tag{35}$$

thus the bounds in (32) are very tight for small false alarm probabilities. This is very convenient computationally, since it means that we will not have to evaluate the integral in (29) numerically, but need only compute the simpler quantities Q_M and E_{M-1}.

One special case of P_{CD} can be evaluated in closed form: for d = 0+, (28) yields

$$P_{CD}^{(o)} = \int_u^\infty dt \; p_v^{(o)}(t) \; [P_v^{(o)}(t)]^{N-1} =$$

$$= \frac{1}{N} \left\{ 1 - [P_v^{(o)}(u)]^N \right\} = \frac{1}{N} \, P_F \; , \tag{36}$$

the latter relation following from (25). This relation agrees with physical reasoning.

TIGHTNESS OF BOUND

To verify the accuracy afforded by using the upper bound $Q_M(d,T)$, instead of the exact result (29) for P_{CD}, a short comparative study of the two quantities was conducted; the numerical results are tabulated in appendix B. False alarm probabilities near the values .1, .01, .001, and detection probabilities near the values .5, .9, .99, .999 were considered, while M took on values 1,10, and N took on values 2,10,100,1000. These ranges of values encompass most of the cases of practical interest; there is no need to consider smaller P_F values, since the discrepancy is even smaller then. It will be observed that for $P_F < .1$ (the only cases plotted here), the differences between the exact P_{CD} and $Q_M(d,T)$ are inconsequential; in particular, see figure B-1.

GRAPHICAL RESULTS

In this section, we plot the analytical results for the false alarm probability (25) and the tight upper bound on the probability of correct detection (33); see (35). The number of filter outputs summed, M, ranges over the values

$$M = 1,2,3,4,5,6,7,8,9,10 = 1(1)10, \tag{37}$$

while the number of channel or-ed, N, ranges over the values

$$N = 1,\ 10,\ 100,\ 1000. \tag{38}$$

The parameter, d, on the plots is the generic signal-to-noise ratio defined by (15), for general signals and filters. The 40 combinations corresponding to (37) and (38) are plotted on normal probability paper in figures* 3 through 42. Values of d small enough to encompass the (poor quality) operating point $(P_F, P_{CD}) = (.01, .5)$ have been employed; while at the high quality end, values of d extending up to $(P_F, P_{CD}) = (1E\text{-}10, .999)$ have been used. The increment in d is .5 for all the results in figures 3 through 42.

---

*All the figures are collected together, after the Summary section.

It will be observed that the curves are approximately equispaced in parameter d, thereby allowing for ready accurate interpolation in d, given specified P_F and P_{CD}. The curves, for cases in which N = 1, are virtually straight lines, while those for N = 1000 have developed significant curvature; nevertheless, the equispaced nature of the results readily accommodates interpolation in all cases.

From these results, it is possible to extract a different type of performance characteristic, namely the required values of d to achieve a specified quality of performance in terms of false alarm probability and detection probability. In figures 43 through 48, these results are plotted for the six combinations of

$$M = 1,2,4 \quad \text{with } P_{CD} = .5,.9, \tag{39}$$

while N varies over 1(1)1000, and P_F takes on the values 1E-2, 1E-4, 1E-6, 1E-8, 1E-10. (Strictly, only the cases for N = 1, 10, 100, 1000 follow from figures 3 through 42; the remaining values of N were obtained directly from (25) and (33).)

The most striking feature of figures 43 through 48 is their slow increase with N, the number of channels subjected to or-ing. Certainly the increase in required d values was anticipated, since or-ing cannot improve performance capability; however, the amount of increase is not very significant. Thus, from figure 43, for P_F = 1E-10, d need only increase from 6.71 to 7.67 as N increases from 1 (no or-ing) to N = 1000. Greater increases are necessary for the larger P_F values.

SUMMARY

It will be easily observed from the graphical results in figures 3 through 42 that, for a fixed amount of or-ing (fixed N), the performance degrades as M increases. That is, for specified values of P_F and d, the values of P_{CD} decrease as M is increased. Alternatively, to maintain a specified performance pair P_F, P_{CD}, the values of d must be increased as M increases. This is due to the fact that parameter d in (15) or (17) is a total (or output) signal-to-noise ratio measure and that larger M corresponds to increased fractionalization of the received signal energy into more paths or branches. Since the filter-output combination rule is incoherent, namely adding squared envelopes, this fra tionalization cannot be made up by summation, and a loss occurs.

On the other hand, if we were to add more paths to a particular system, then both M <u>and</u> d would increase. Whether this results in an improvement or degradation depends on the relative amount of additional energy. Particular cases can be studied quantitatively by referring to figures 3 through 42. In addition, programs for the procedures in this report are listed in BASIC in appendix C, if additional cases of interest to the reader need to be investigated.

The maximum value of d^2 is given by (17) as $2E_T/N_o$; this can be realized only if the matched filters (16) are utilized and if the sampling times are properly selected. If these conditions are not met, the value of d^2 given by (15) must be employed. In any event, the figures are

parameterized by quantity d, regardless of what filters and sampling times are used. Thus a desired value of d for a mismatched situation will require larger signal levels for $\{\underline{s}_m\}$ in (15) than the values indicated by the ideal, (17). In this manner, the degradation caused by mismatch and/or desynchronization can be quantitatively assessed.

The received signal was assumed to have undergone no fading in the current analysis. Extensions to fading signals, but without or-ing, are available in [3]. This latter reference presumed a fixed threshold for decision variable comparisons (as did this analysis in (3) and (18)); extensions to a variable threshold, based on a finite sample size noise-level estimation procedure, are currently underway. Results on this normalizer in a fading environment will be reported on shortly by the author.

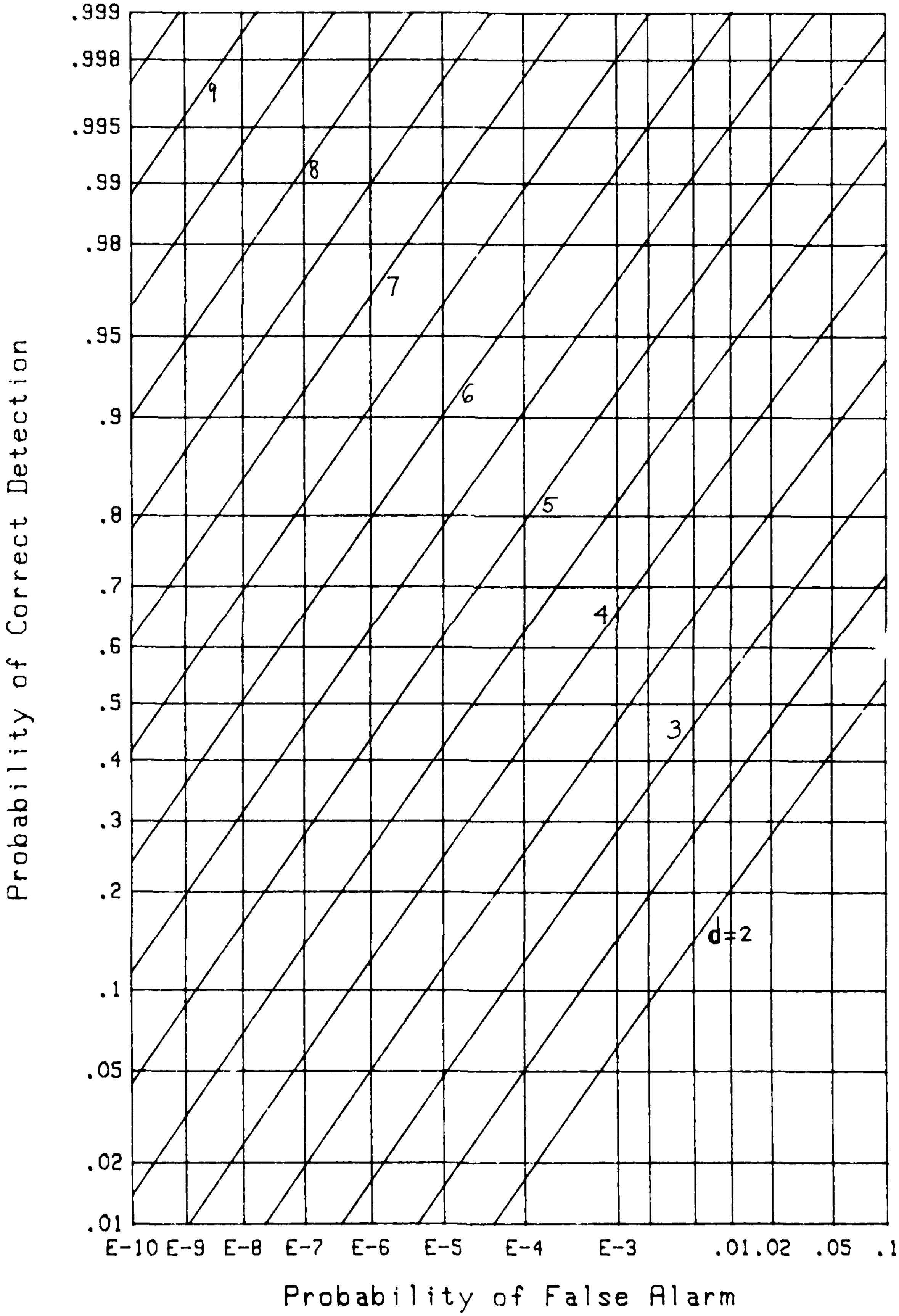

Figure 3. ROC for M=1, N=1

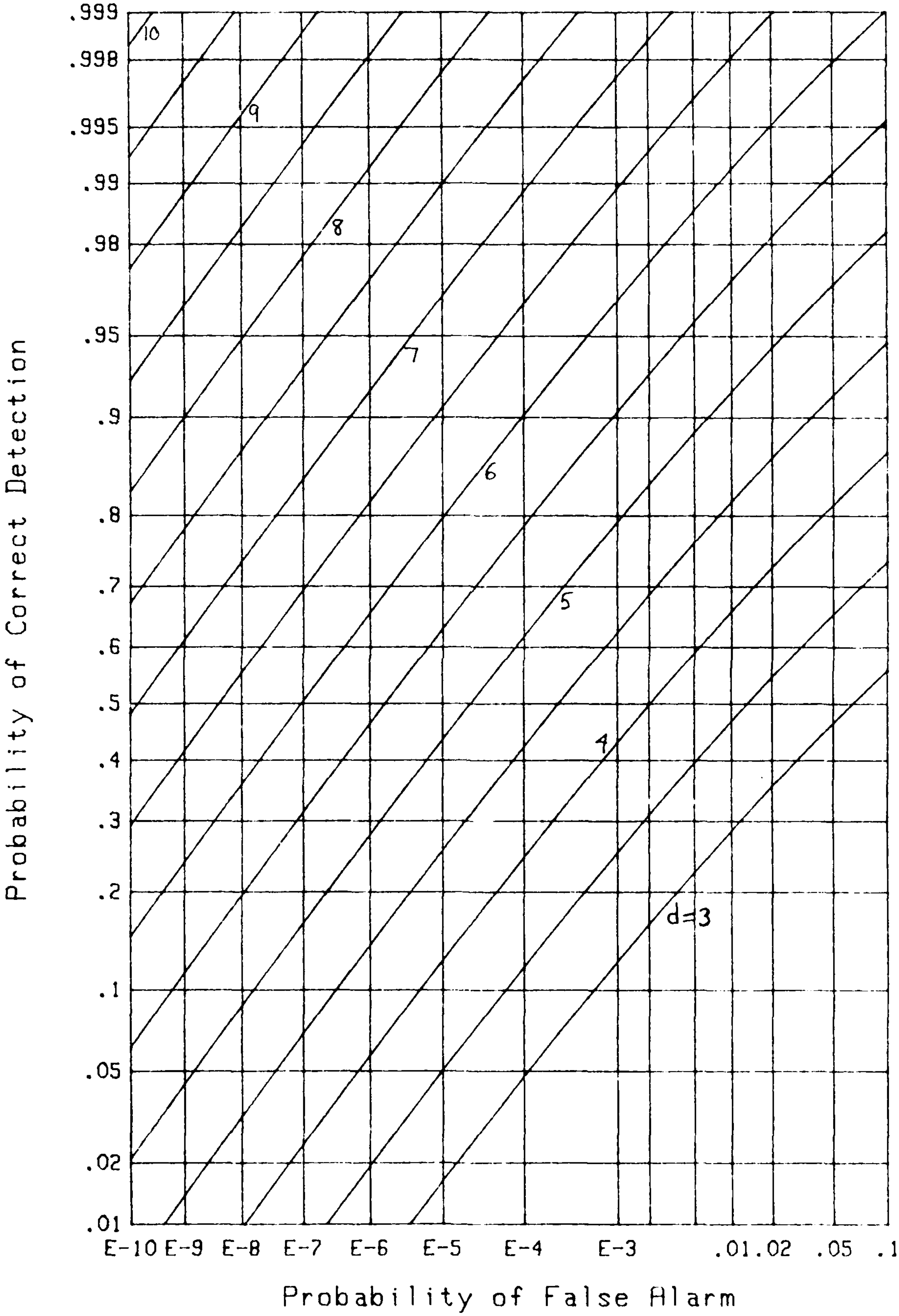

Figure 4. ROC for M=1, N=10

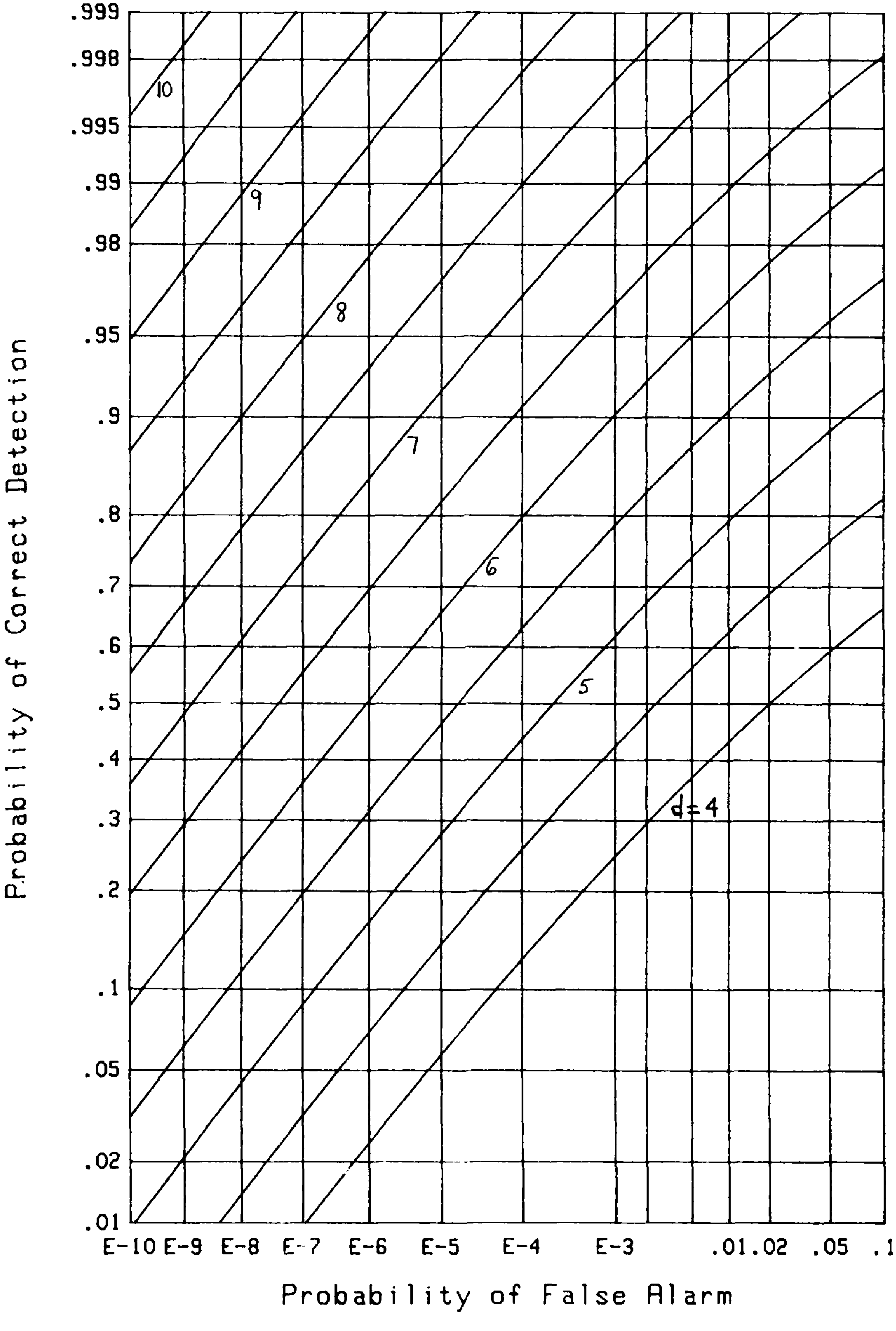

Figure 5. ROC for M=1, N=100

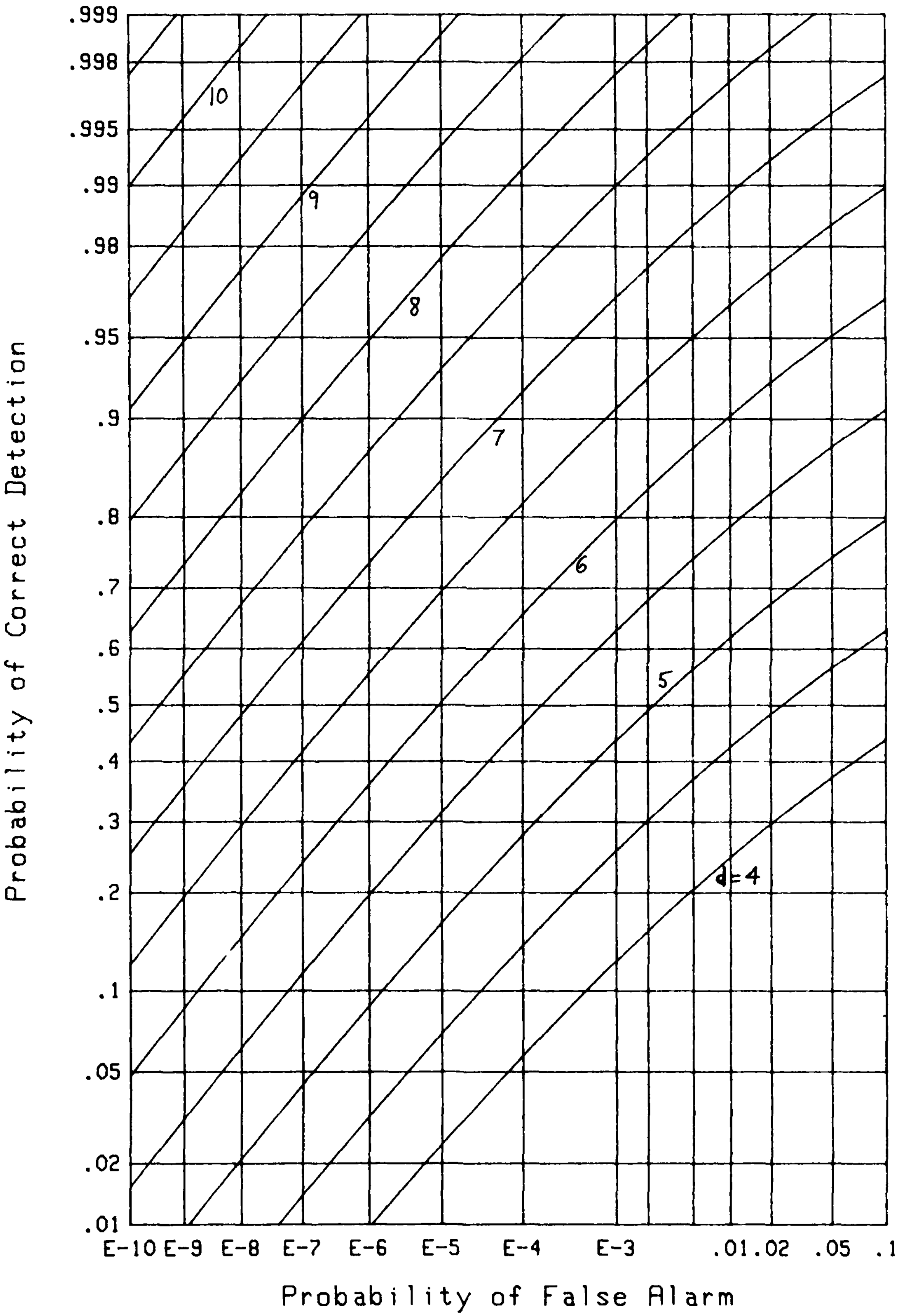

Figure 6. ROC for M=1, N=1000

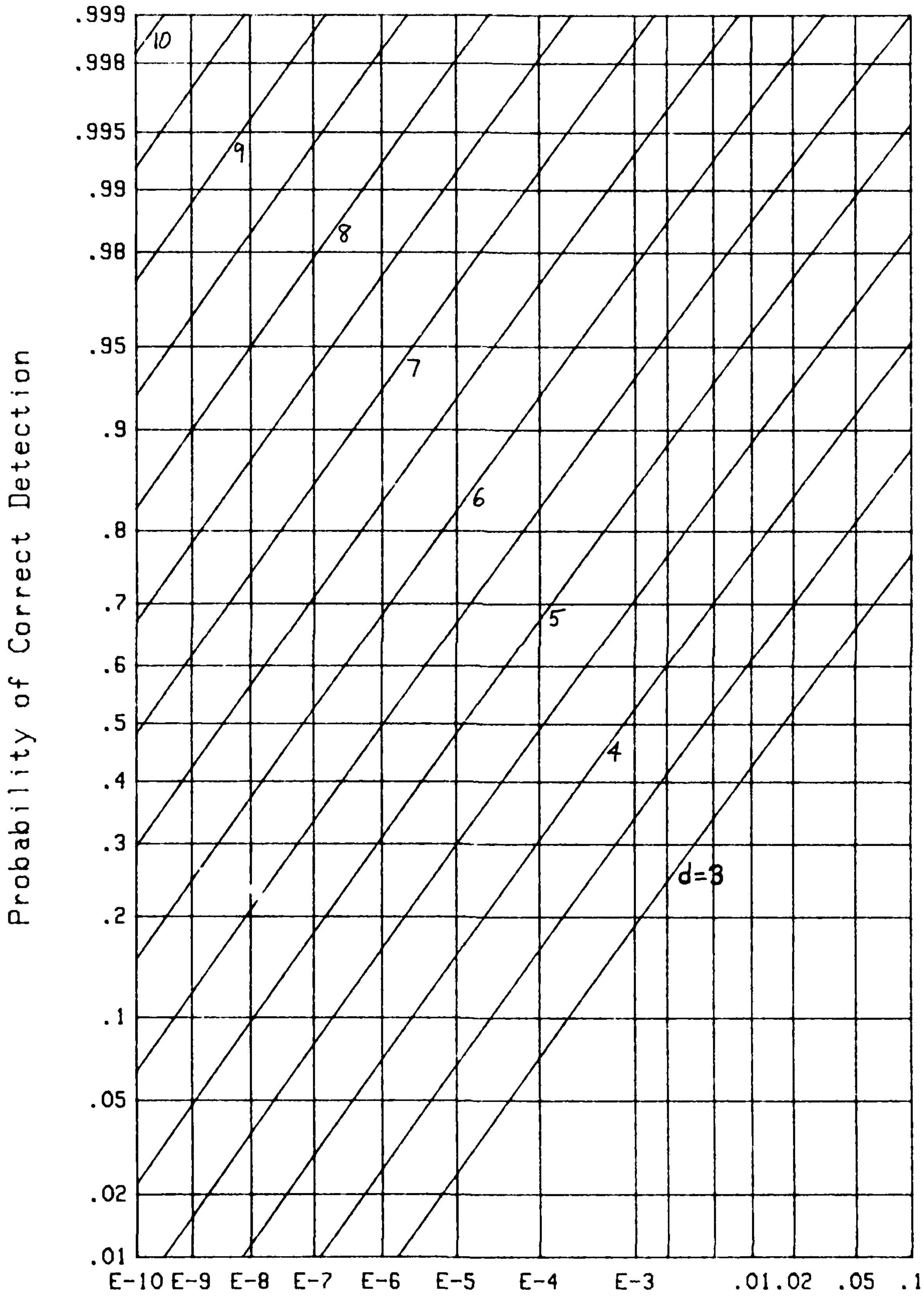

Figure 7. ROC for M=2, N=1

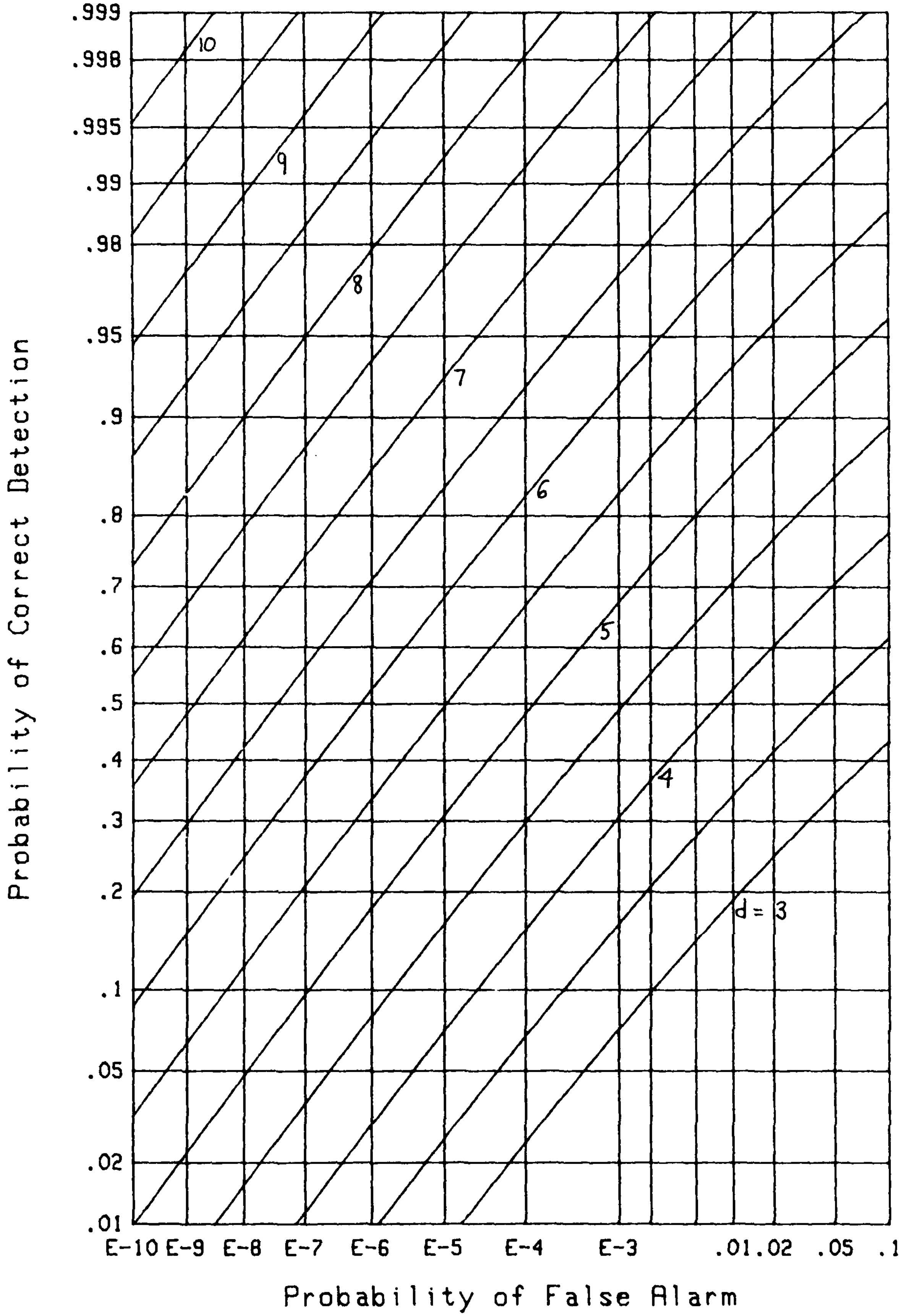

Figure 8. ROC for M=2, N=10

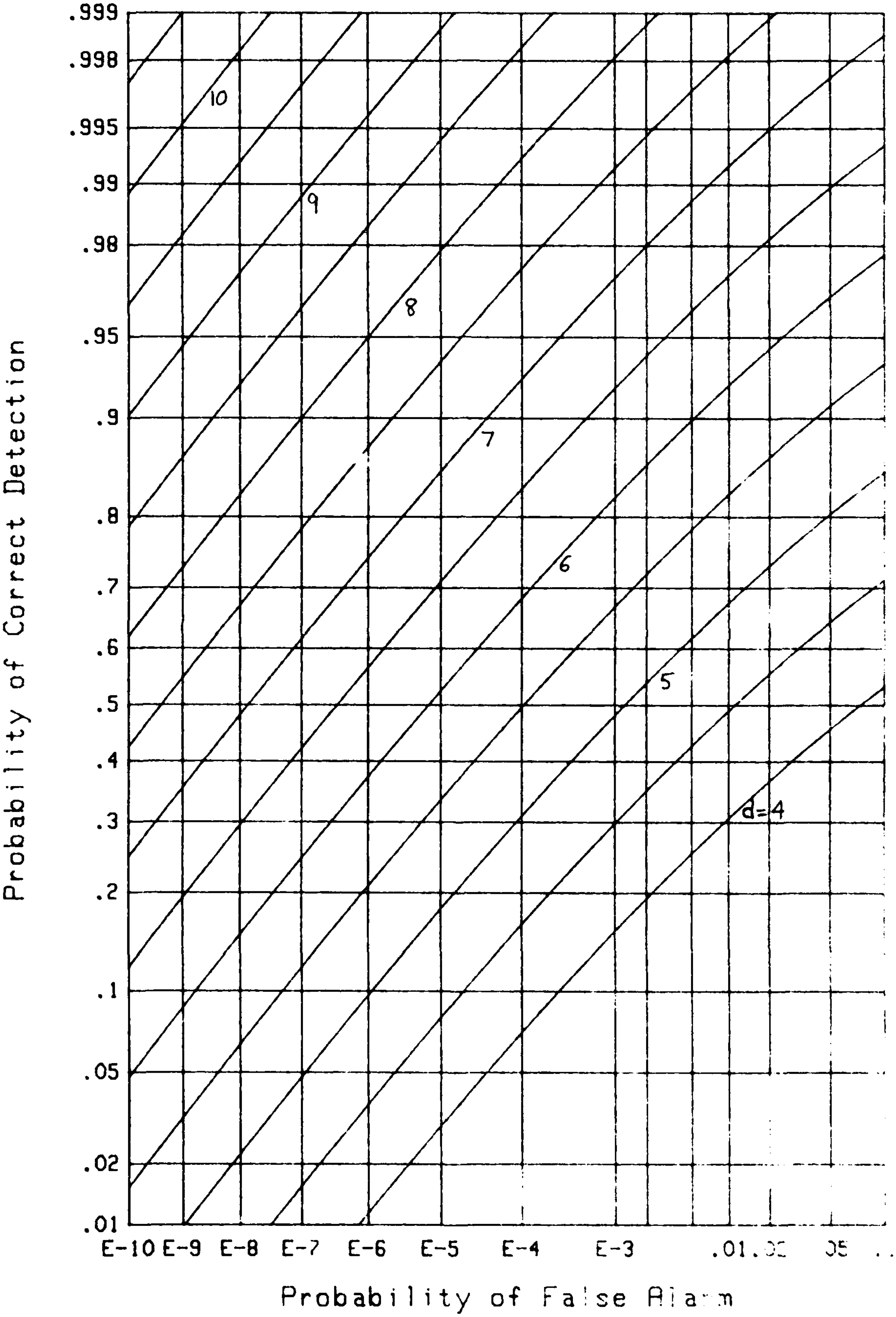

Figure 9. ROC for M=2, N=100

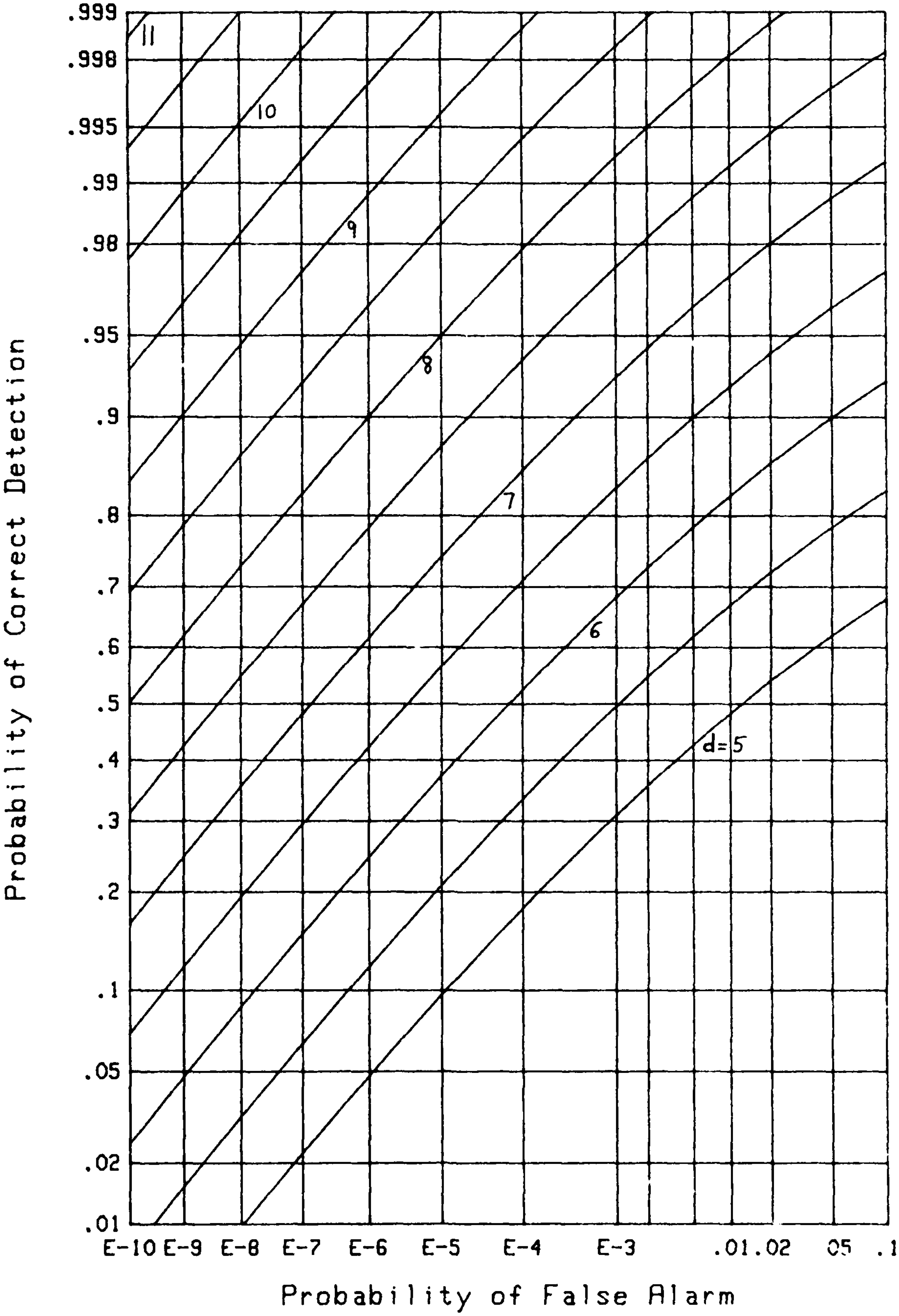

Figure 10. ROC for M=2, N=1000

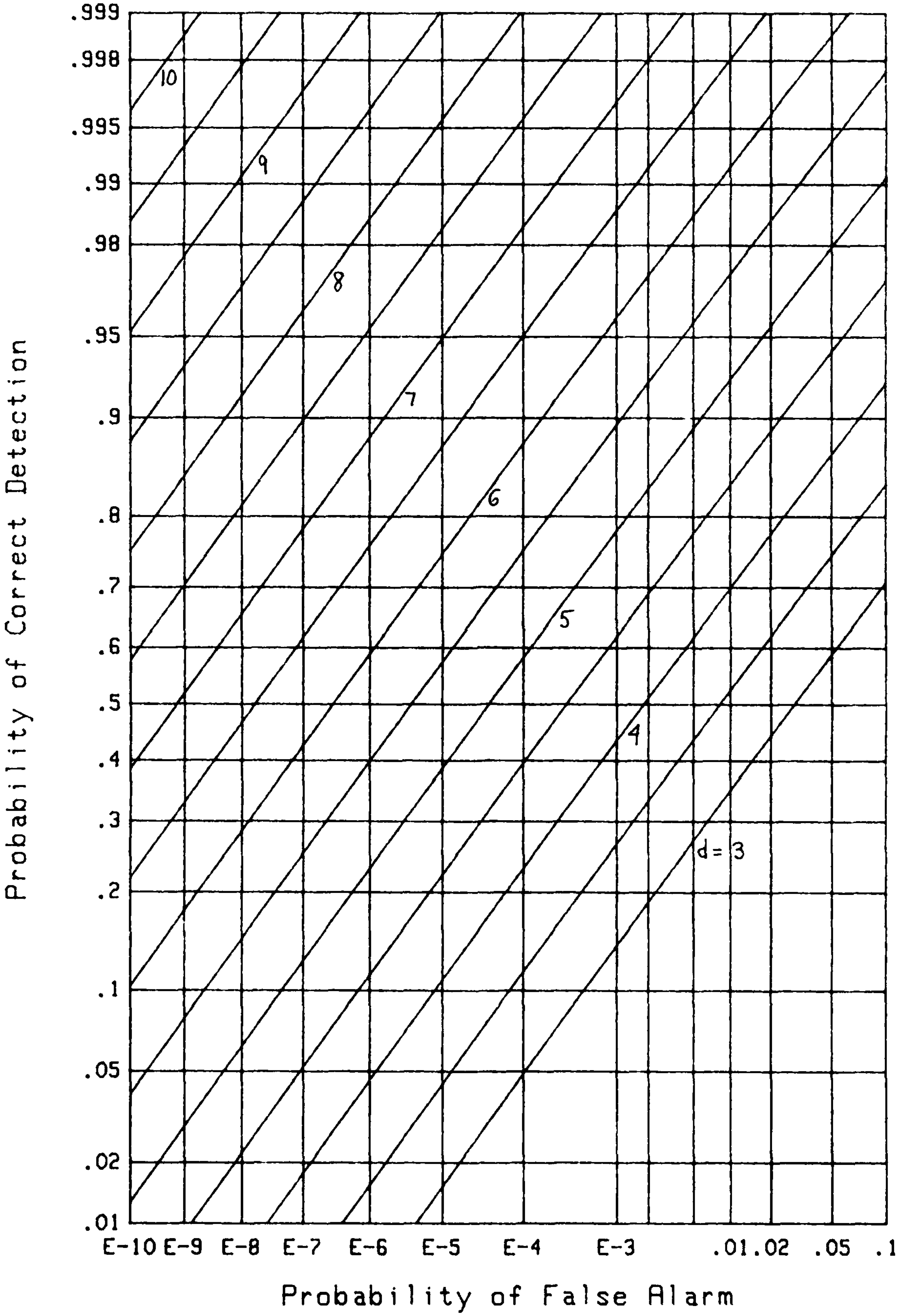

Figure 11. ROC for M=3, N=1

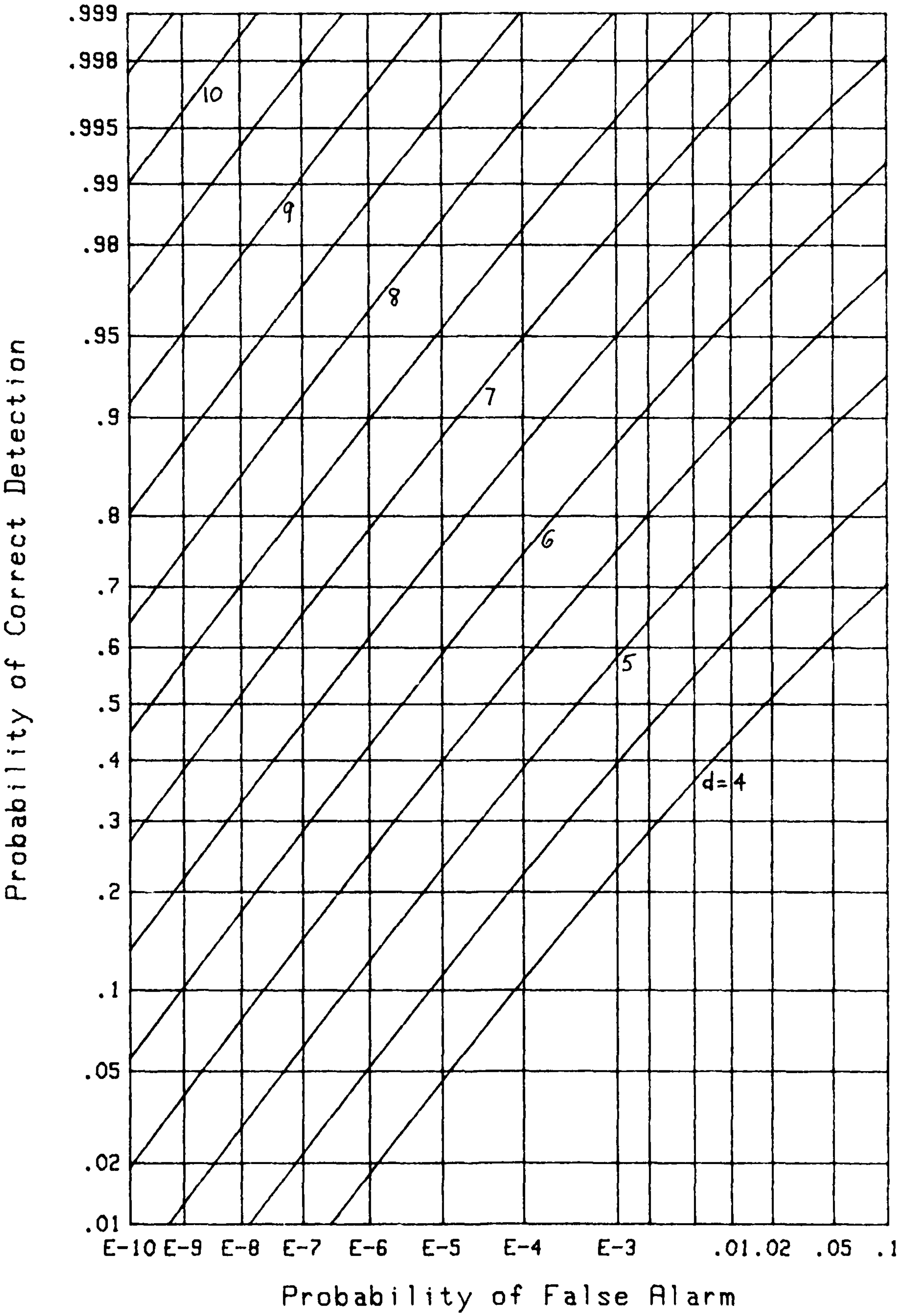

Figure 12. ROC for M=3, N=10

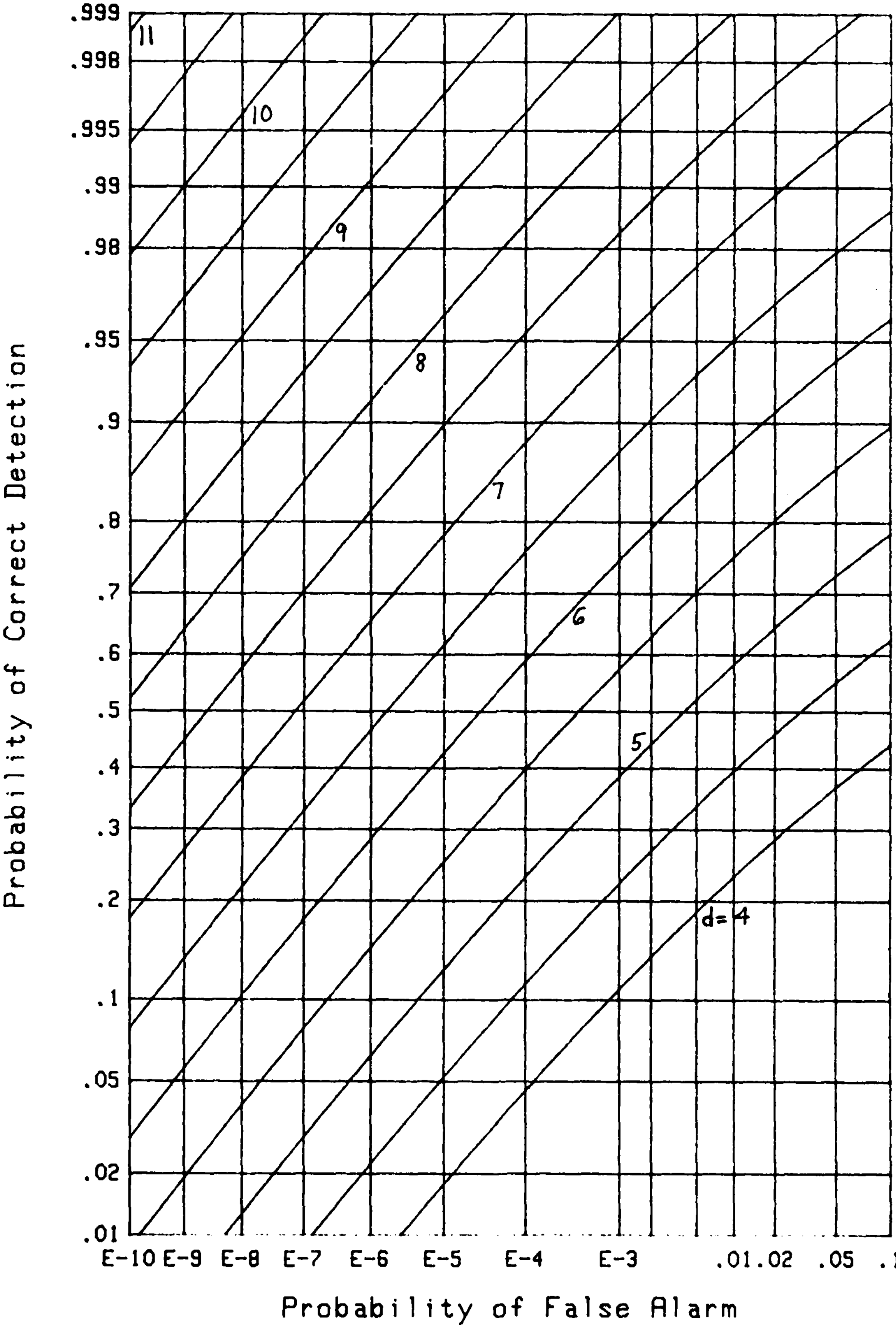

Figure 13. ROC for M=3, N=100

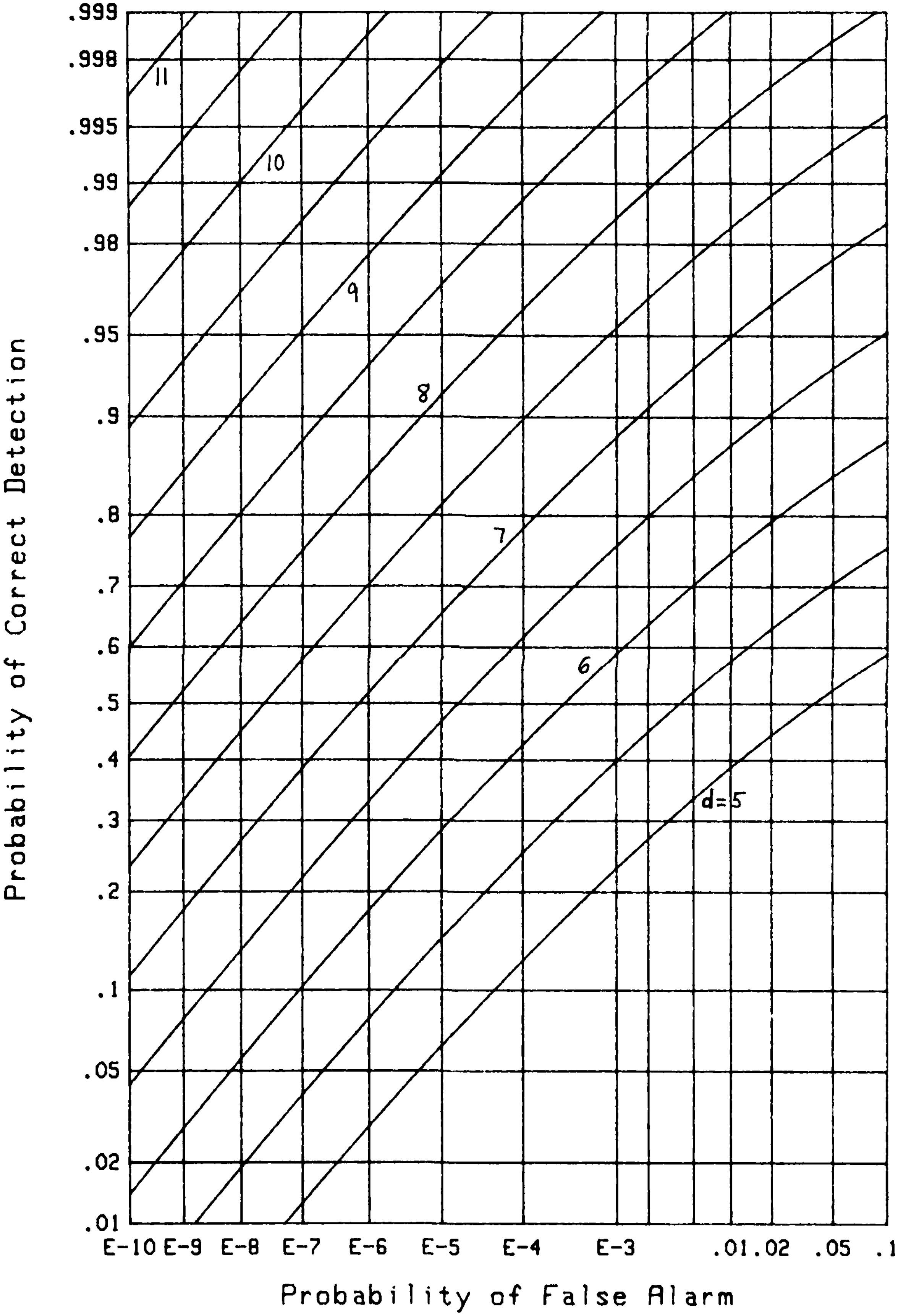

Figure 14. ROC for M=3, N=1000

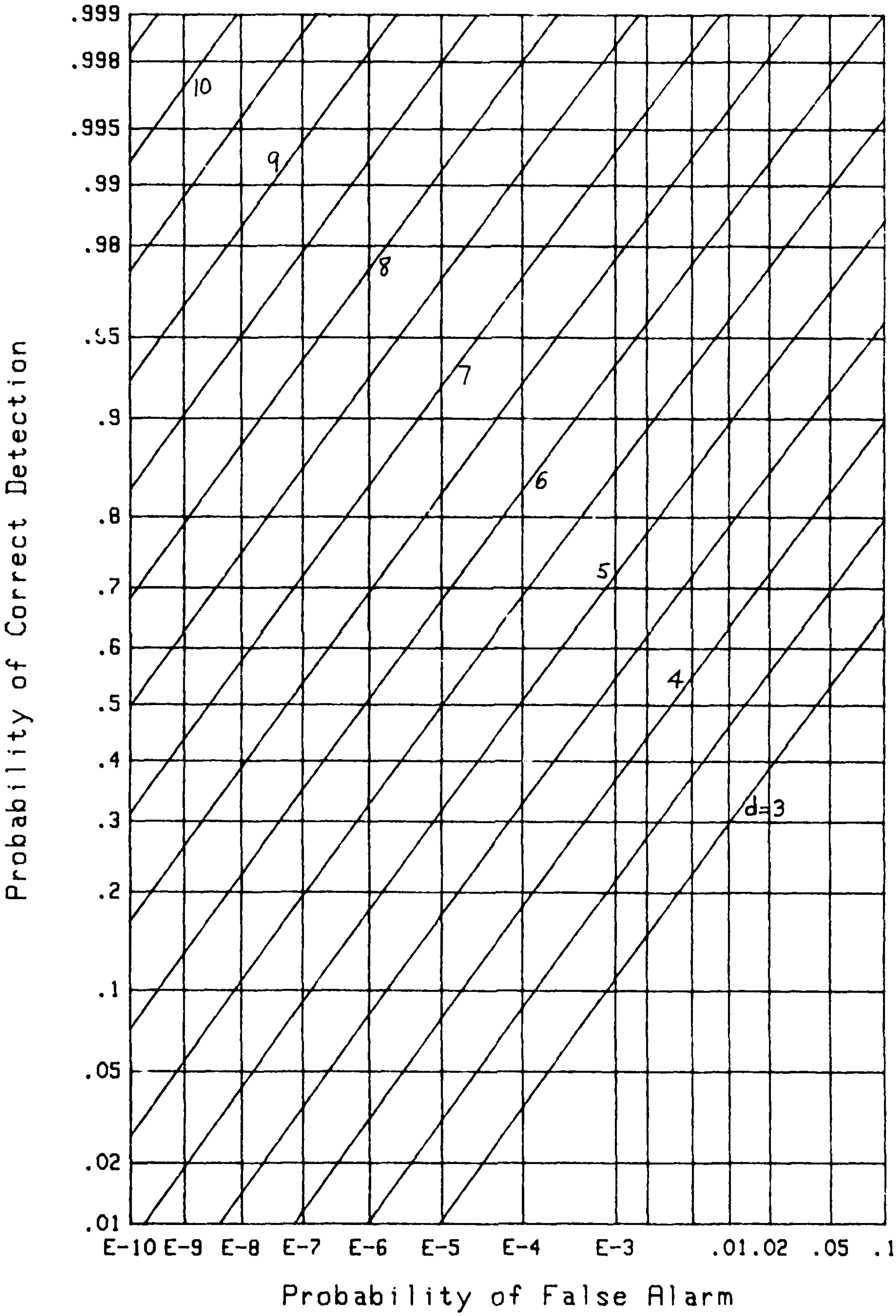

Figure 15. ROC for M=4, N=1

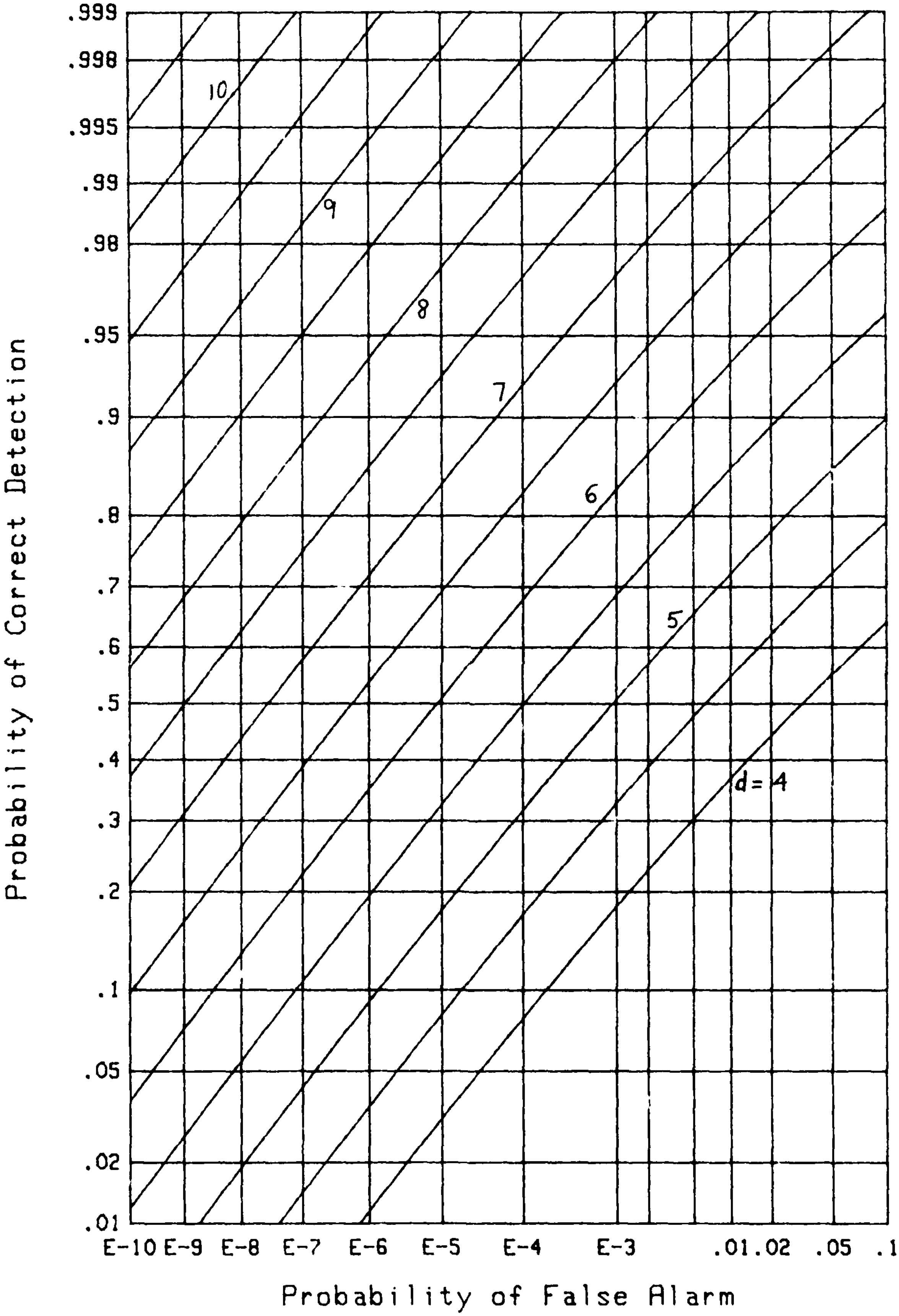

Figure 16. ROC for M=4, N=10

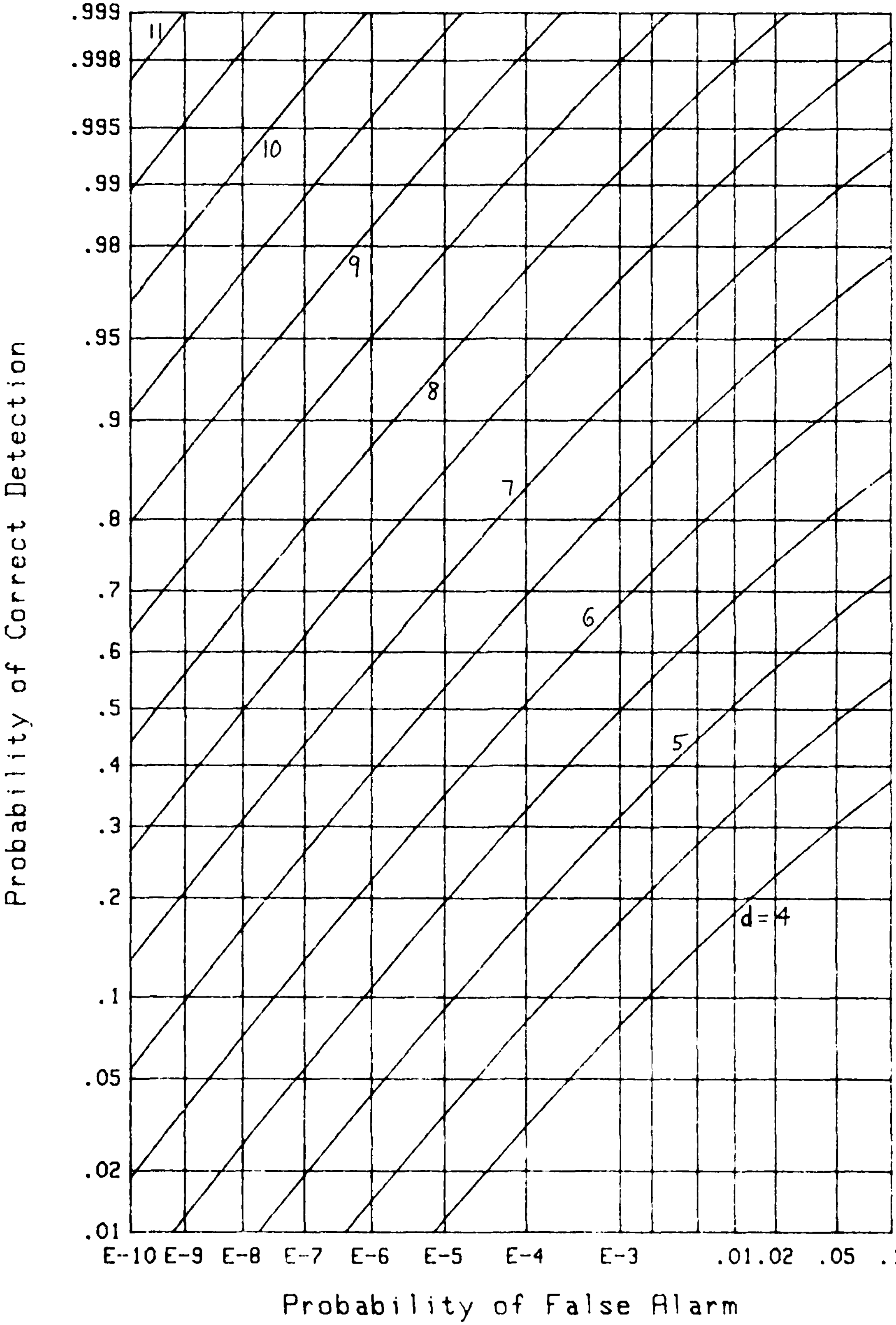

Figure 17. ROC for M=4, N=100

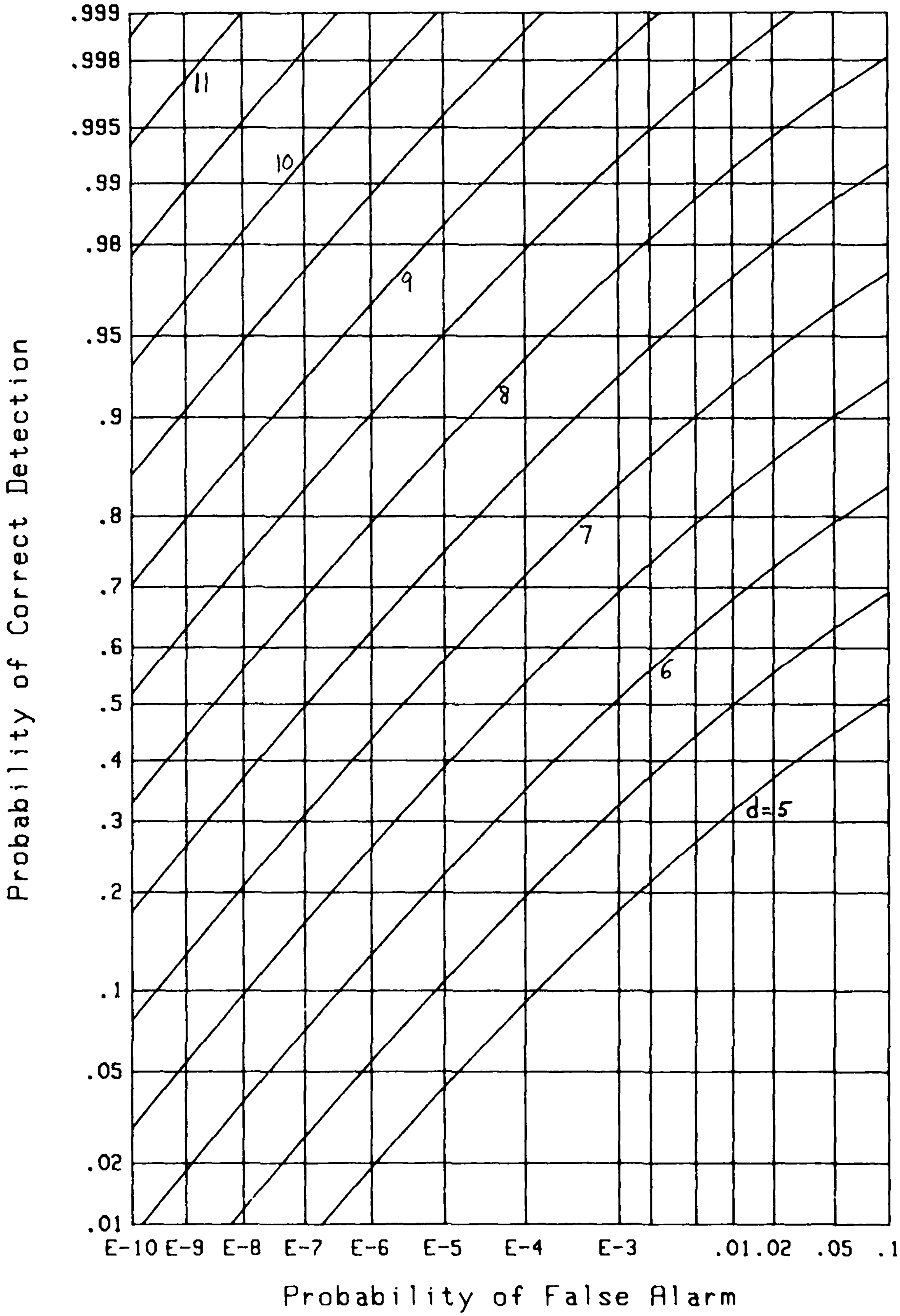

Figure 18. ROC for M=4, N=1000

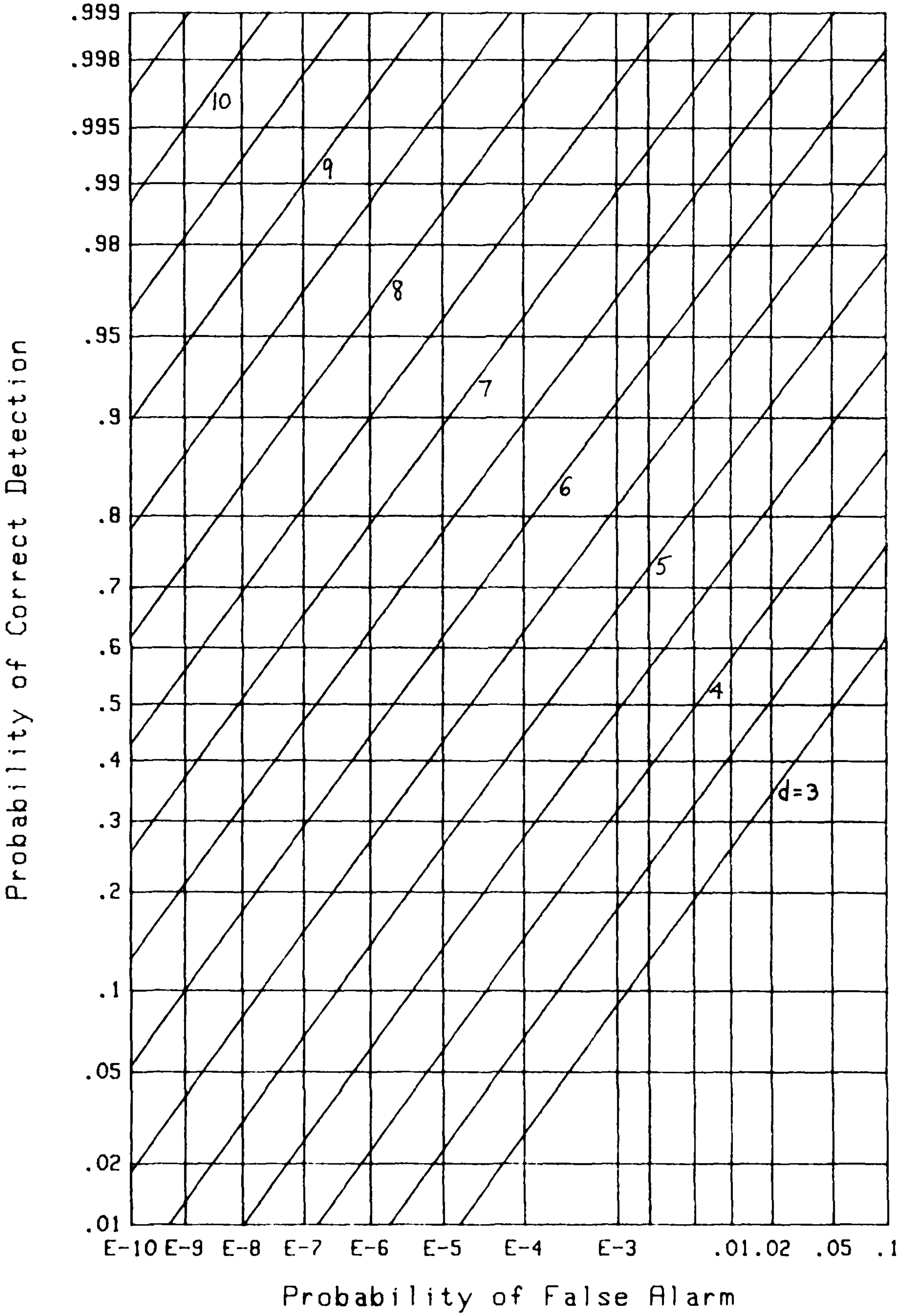

Figure 19. ROC for M=5, N=1

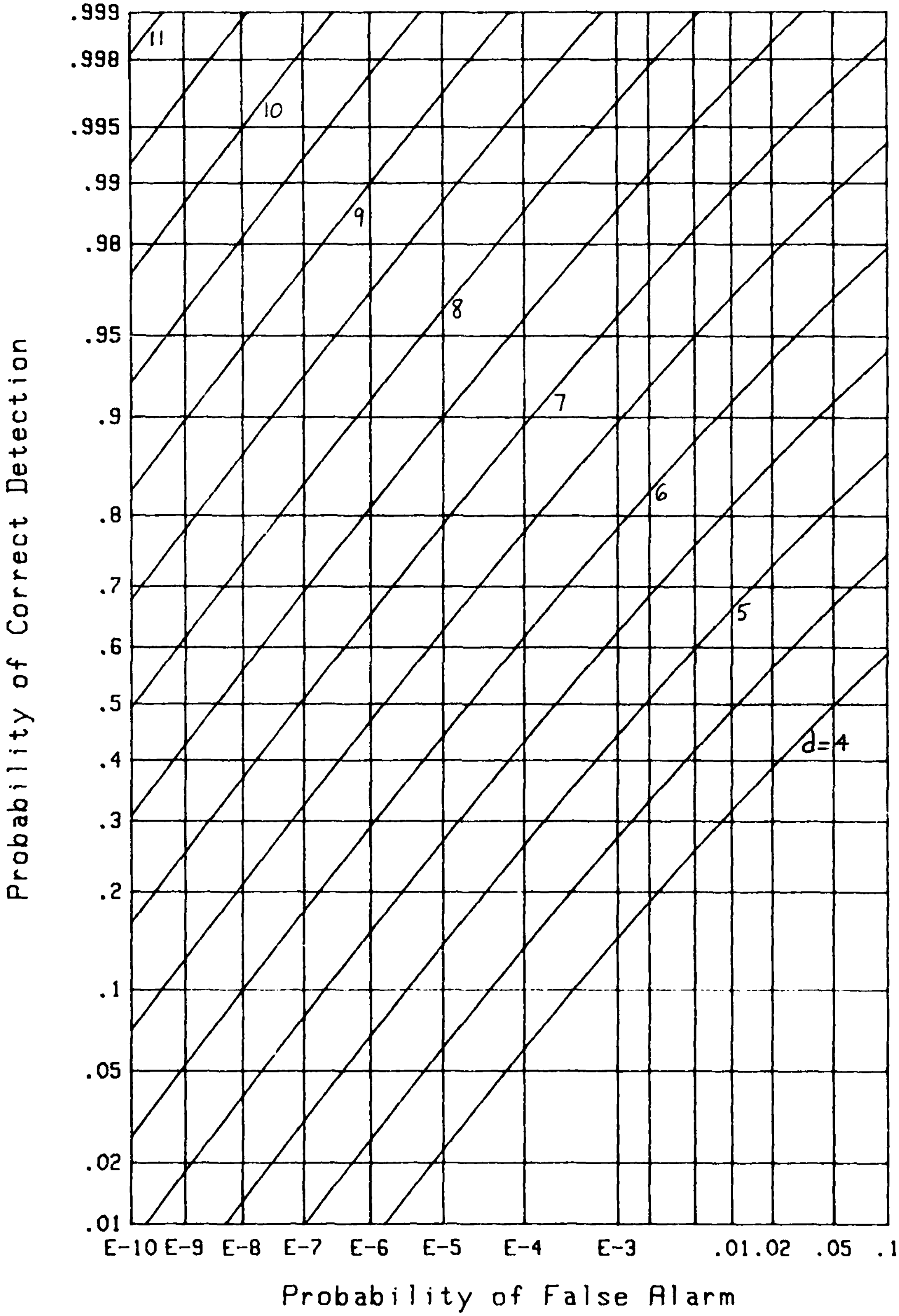

Figure 20. ROC for M=5, N=10

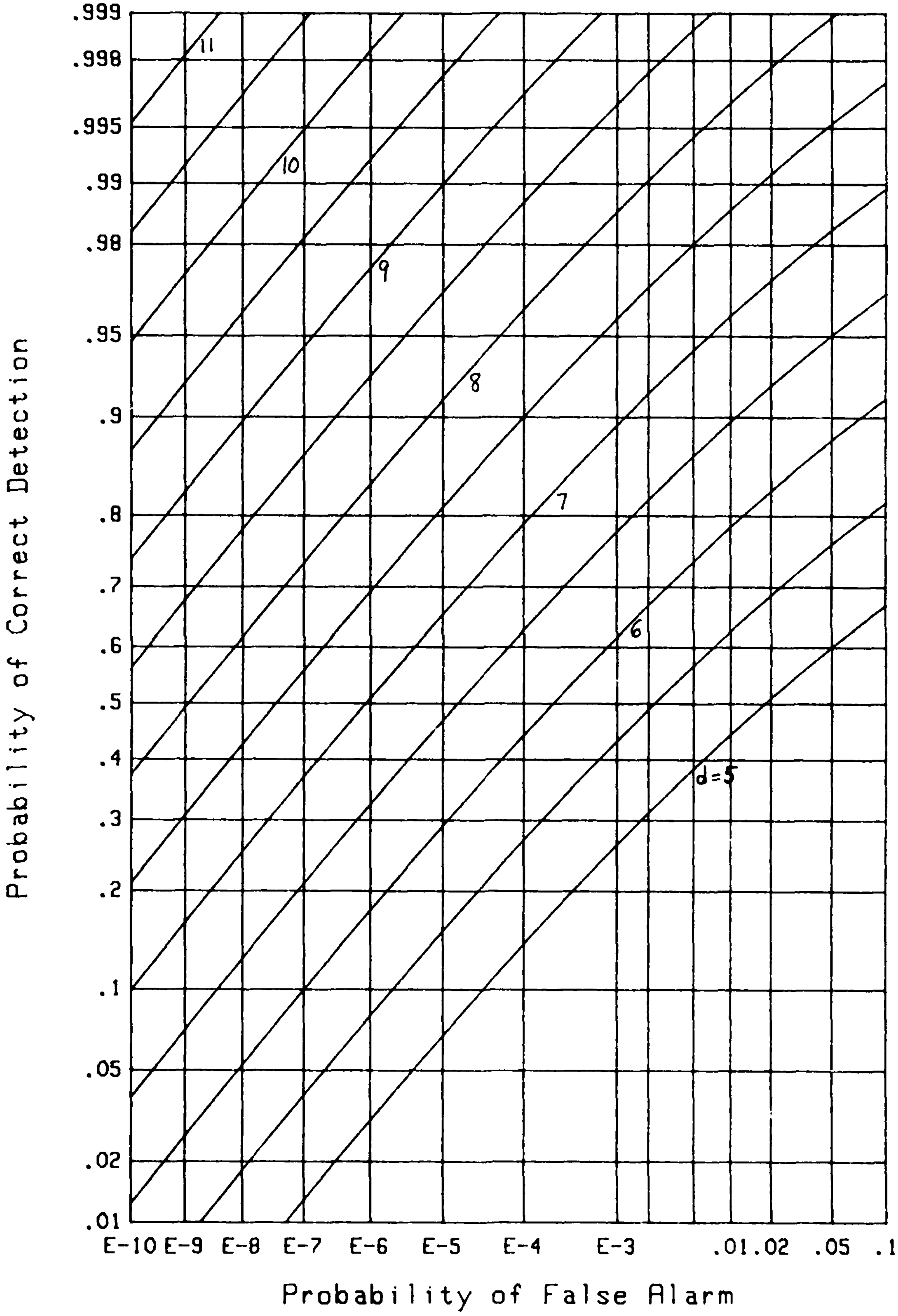

Figure 21. ROC for M=5, N=100

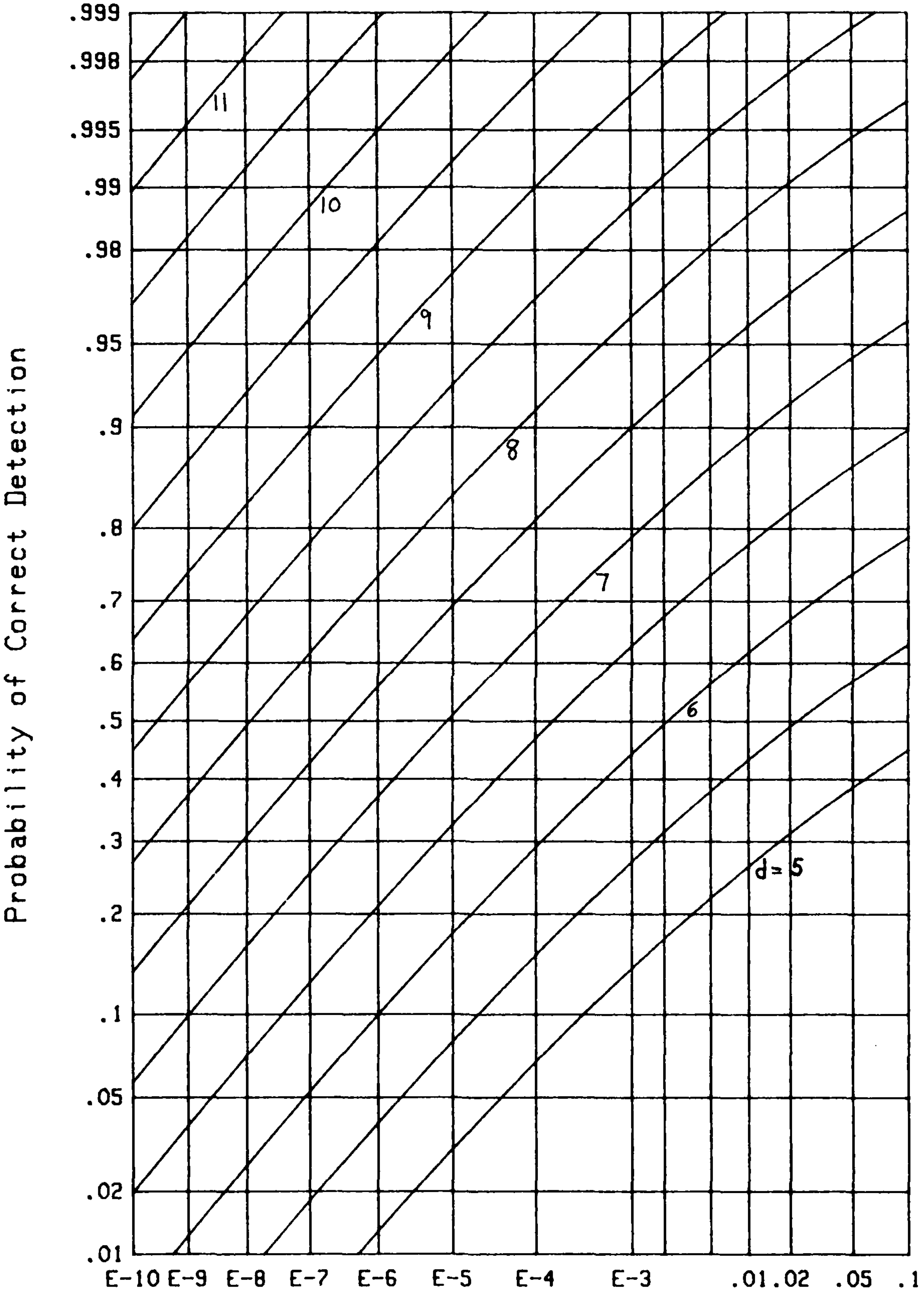

Figure 22. ROC for M=5, N=1000

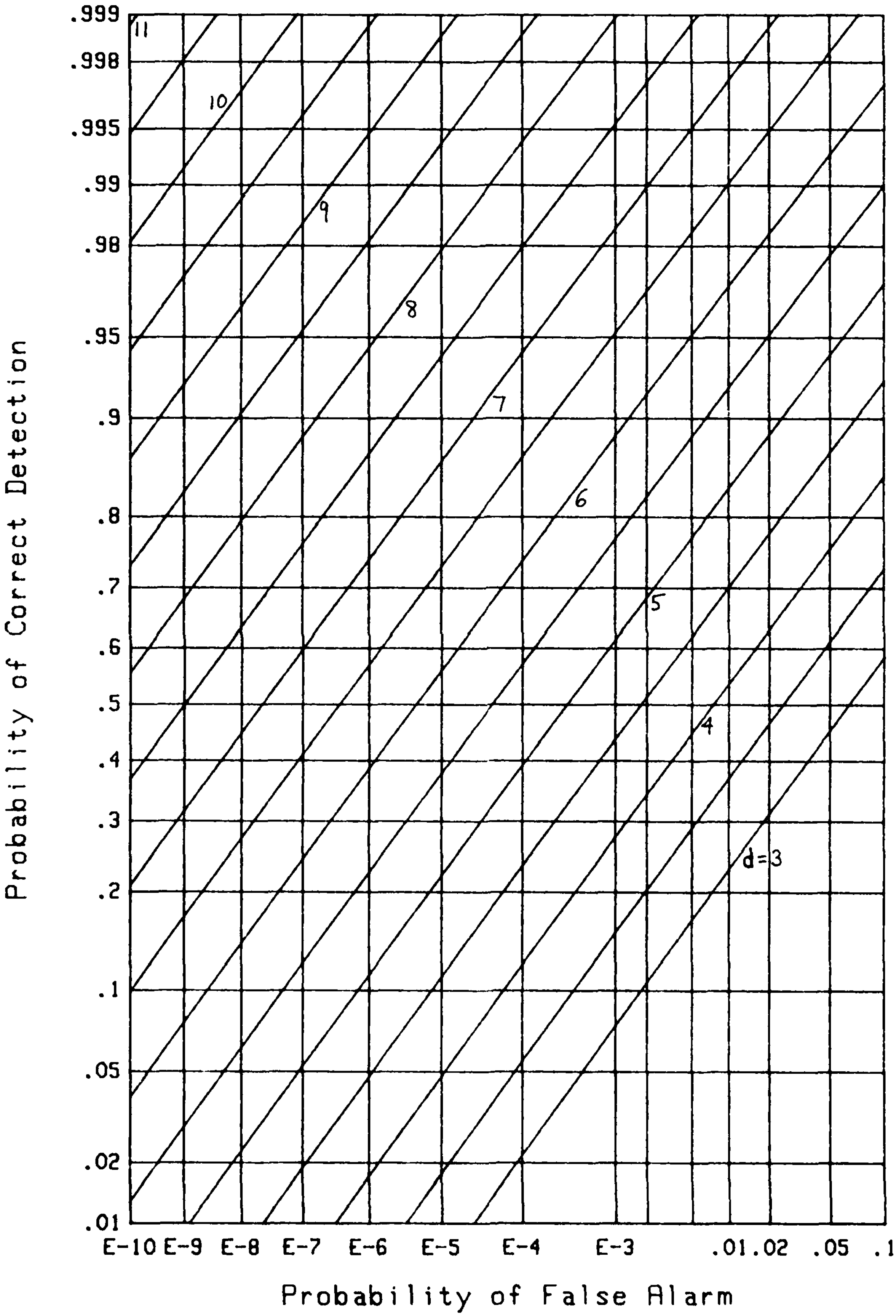

Figure 23. ROC for M=6, N=1

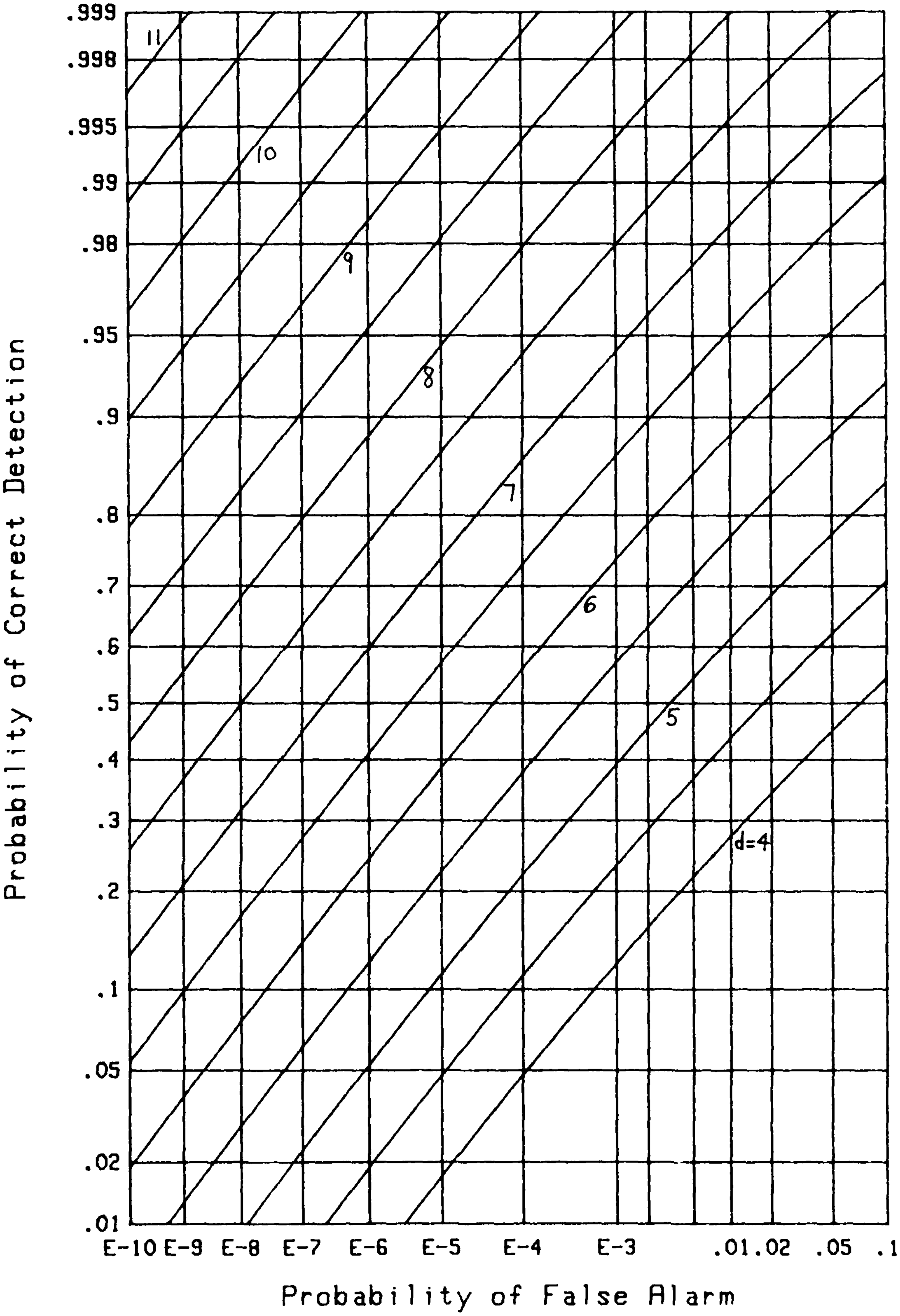

Figure 24. ROC for M=6, N=10

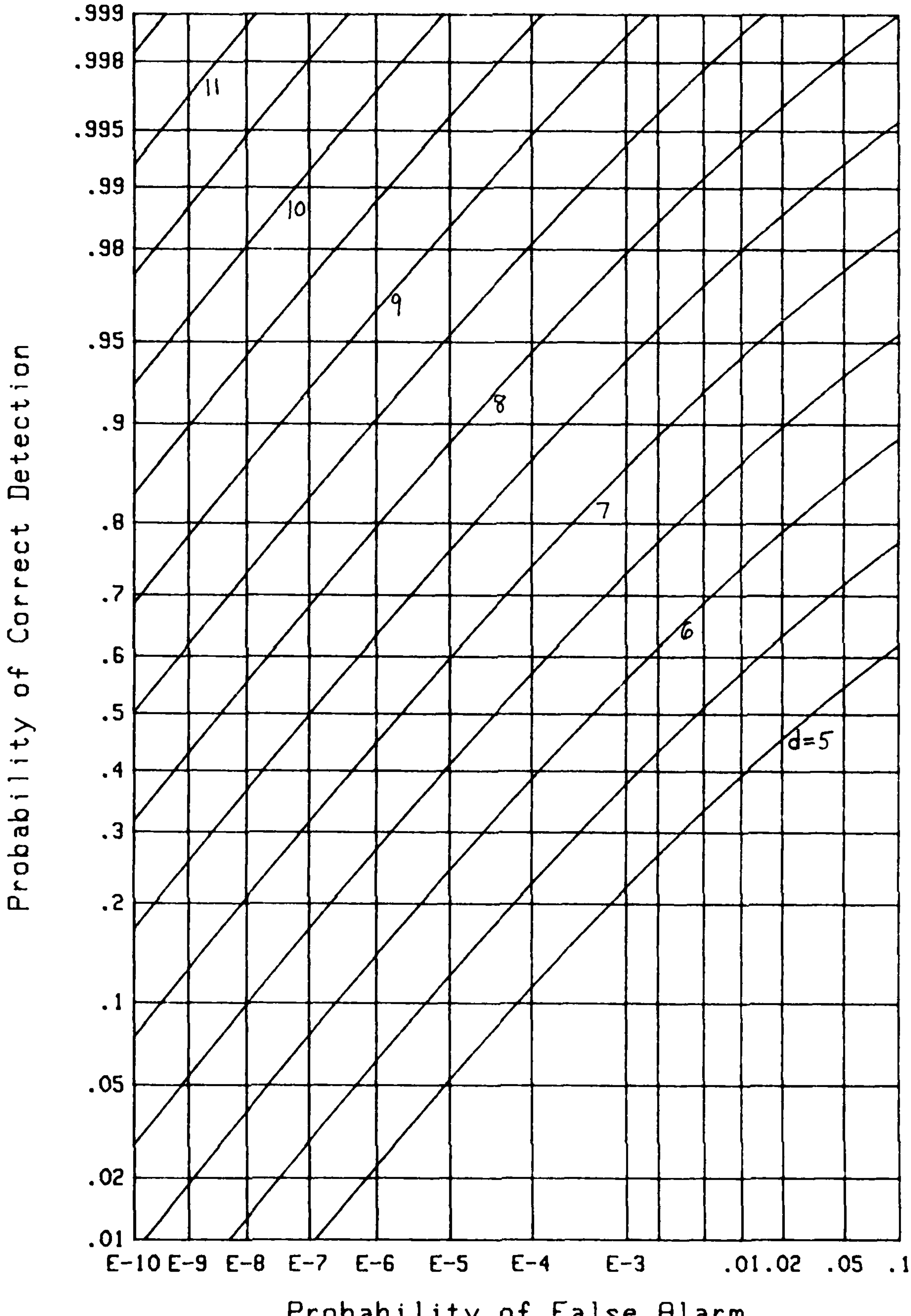

Figure 25. ROC for M=6, N=100

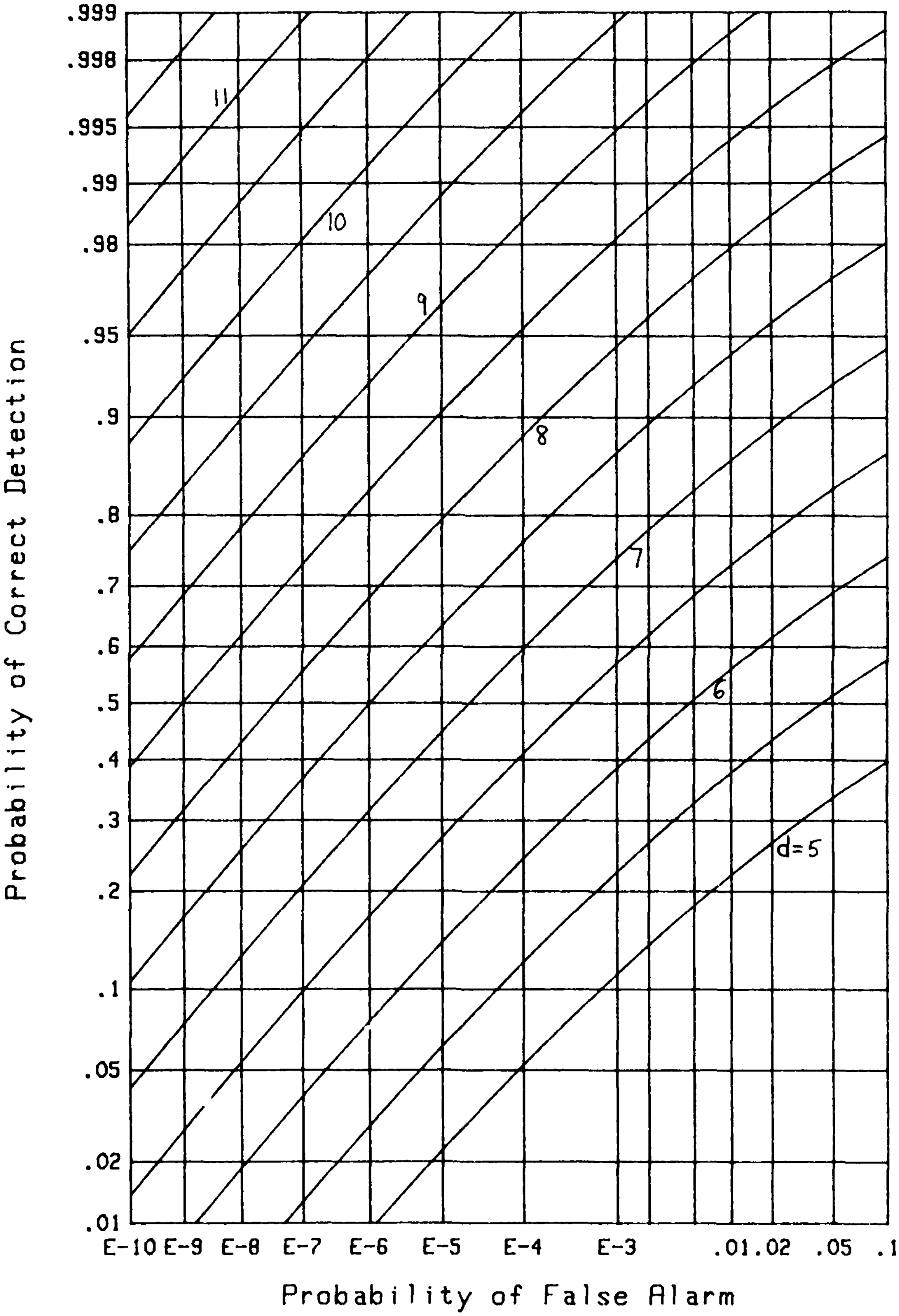

Figure 26. ROC for M=6, N=1000

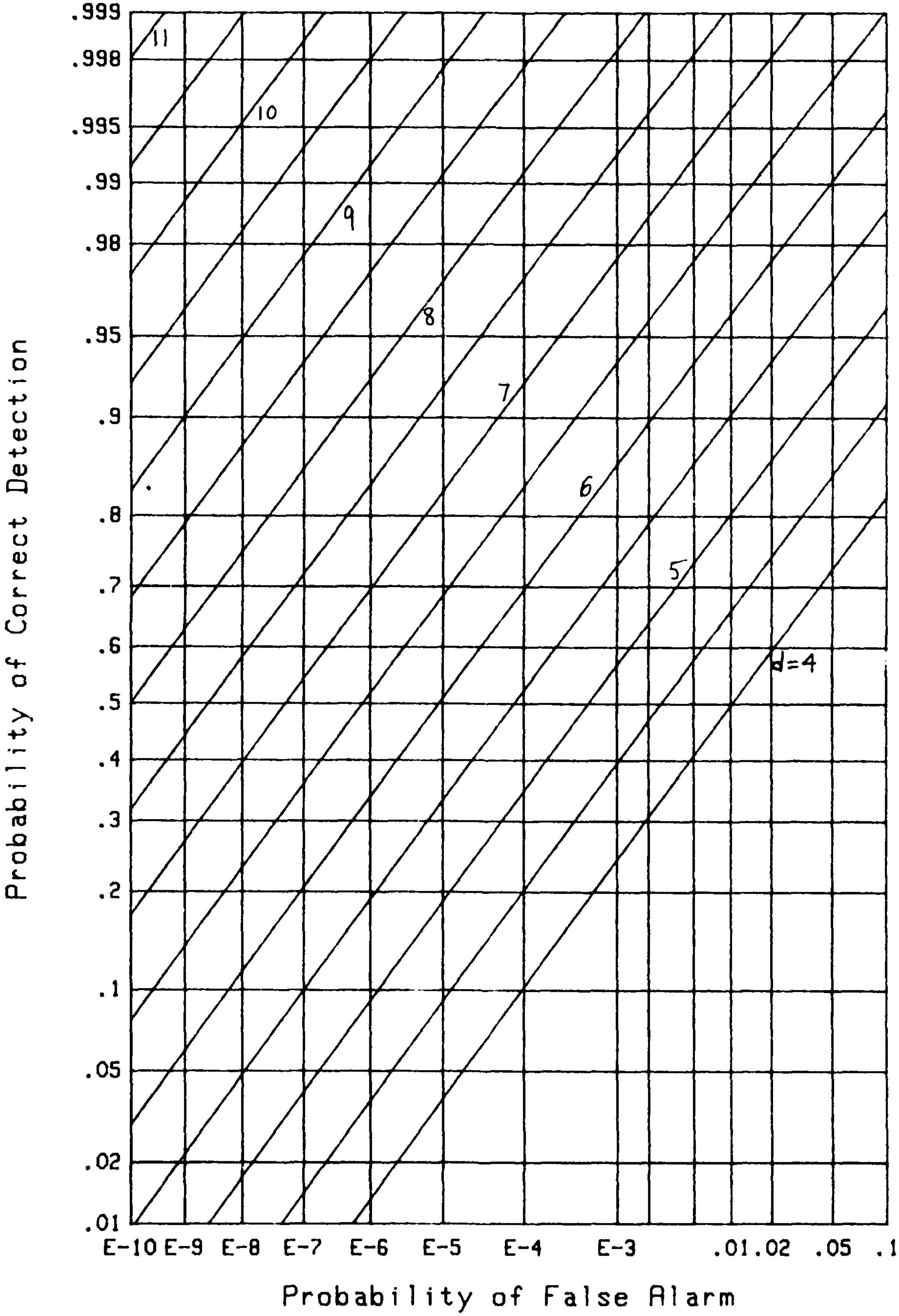

Figure 27. ROC for M=7, N=1

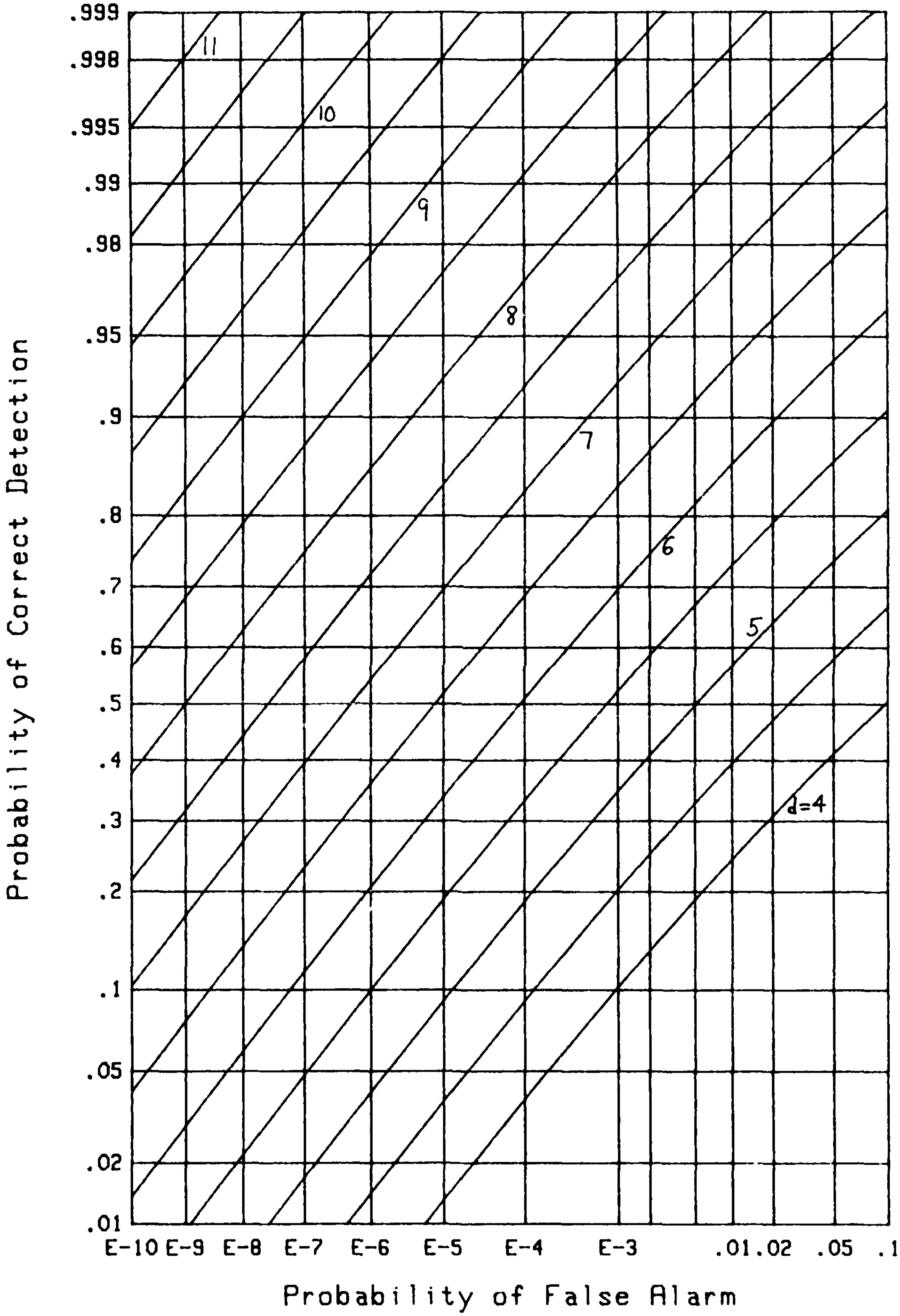

Figure 28. ROC for M=7, N=10

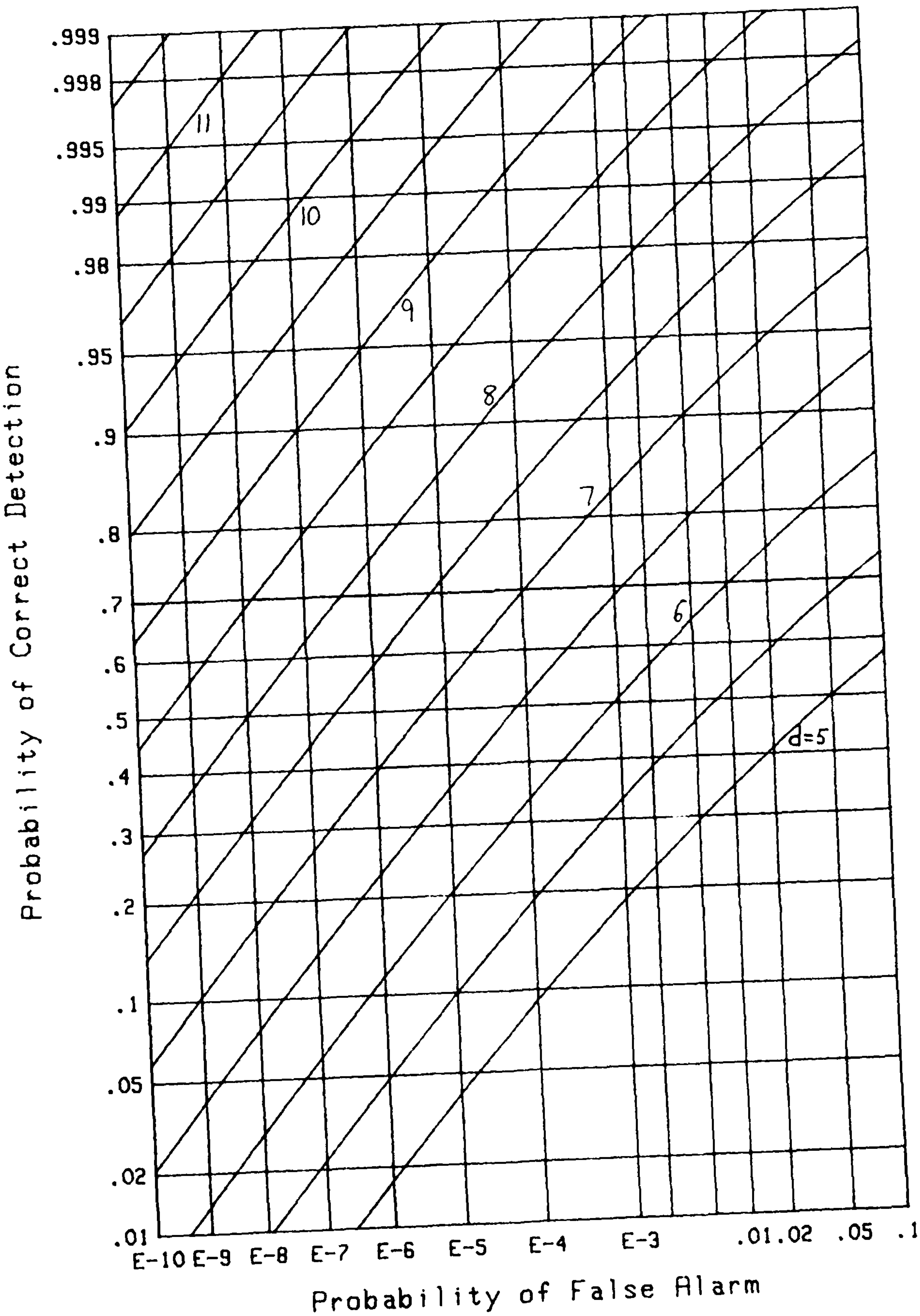

Figure 29. ROC for M=7, N=100

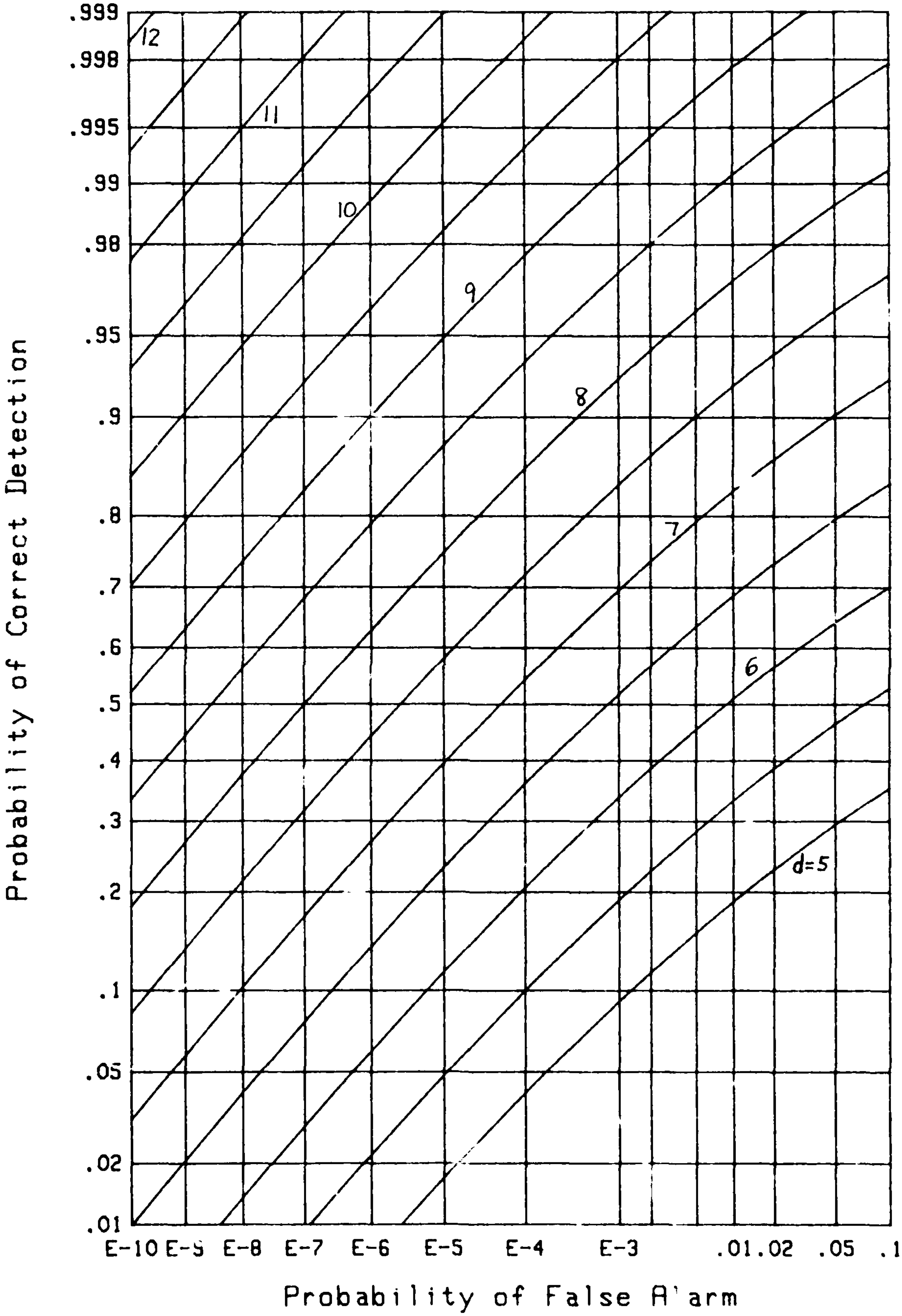

Figure 30. ROC for M=7, N=1000

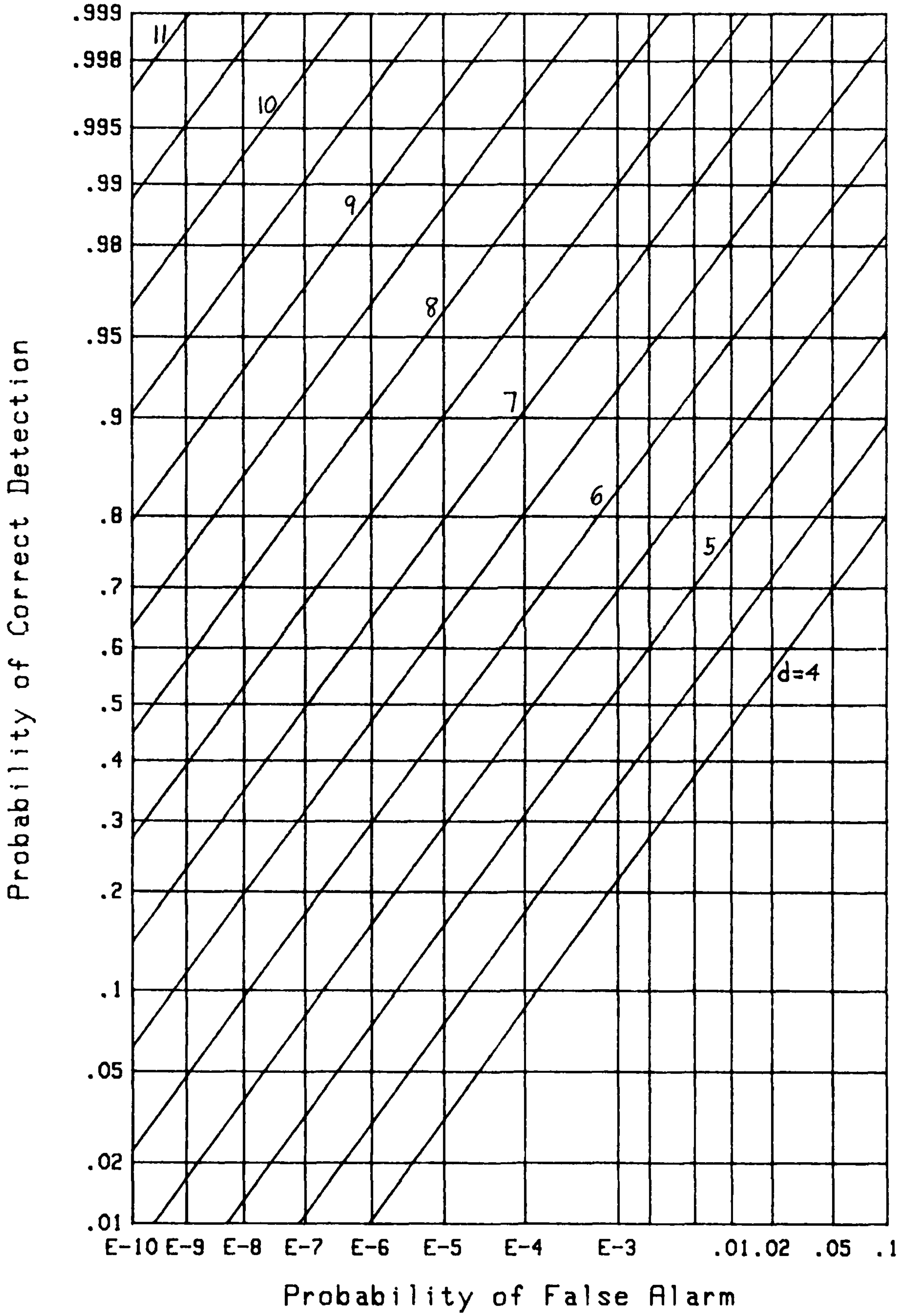

Figure 31. ROC for M=8, N=1

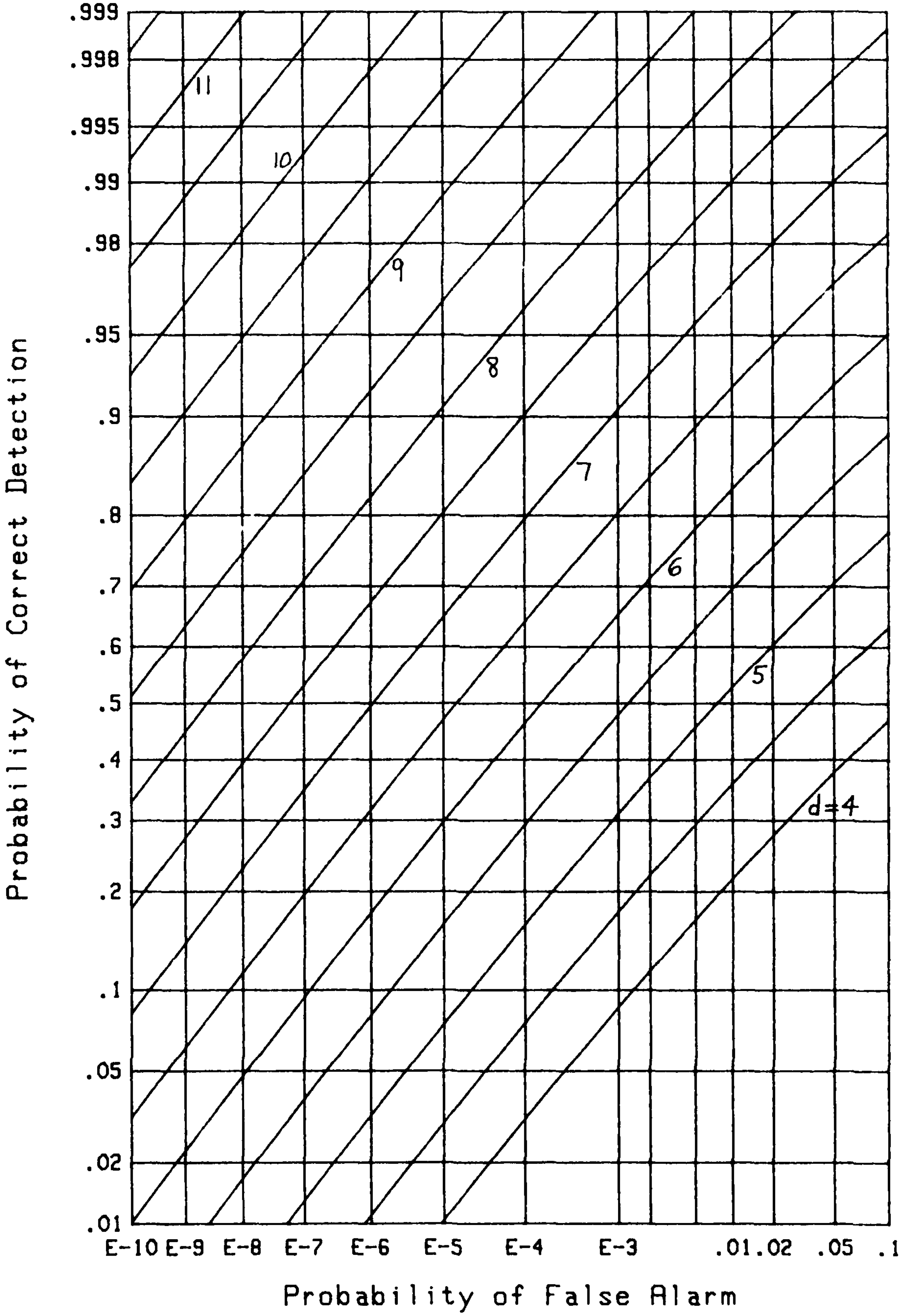

Figure 32. ROC for M=8, N=10

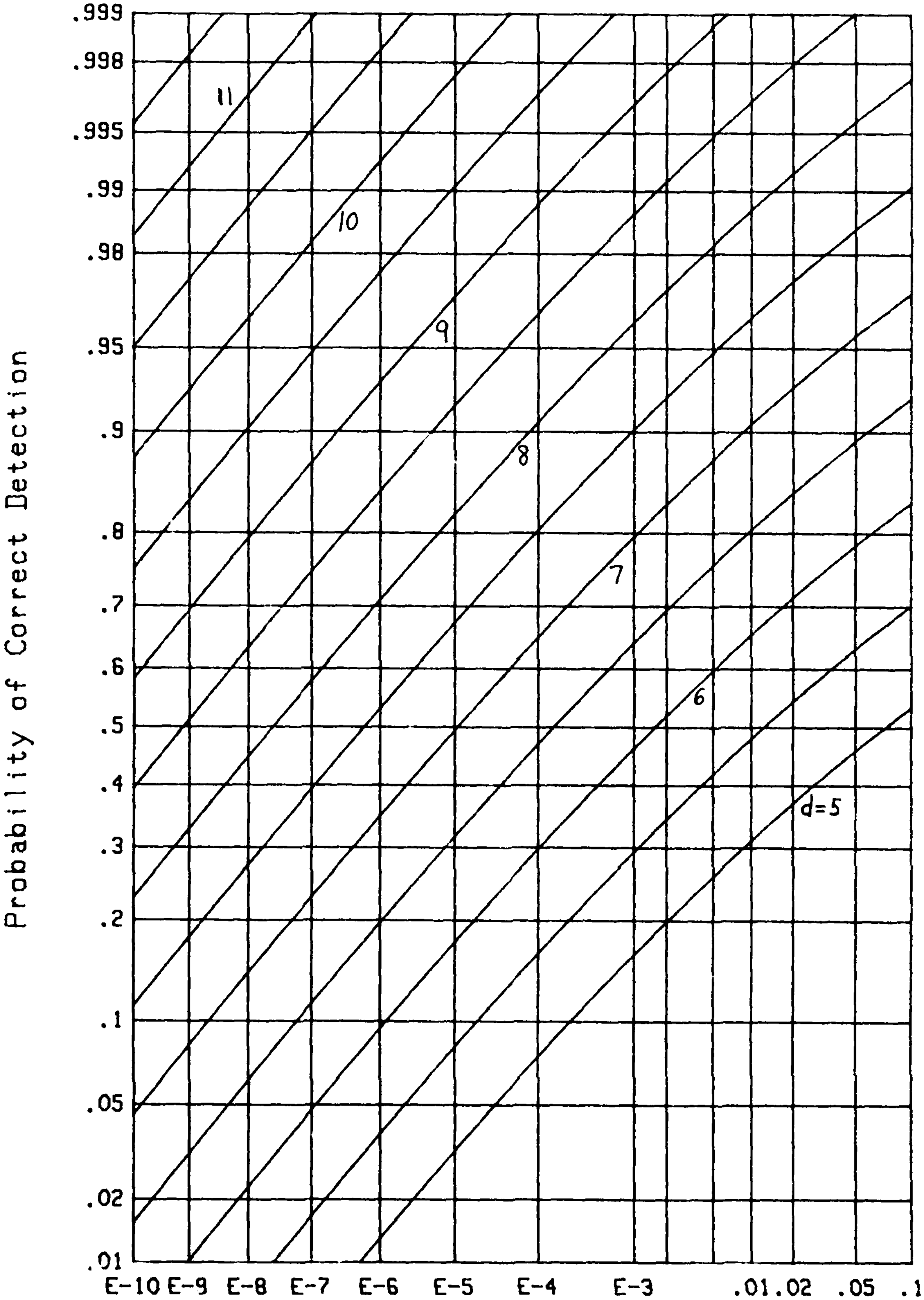

Figure 33. ROC for M=8, N=100

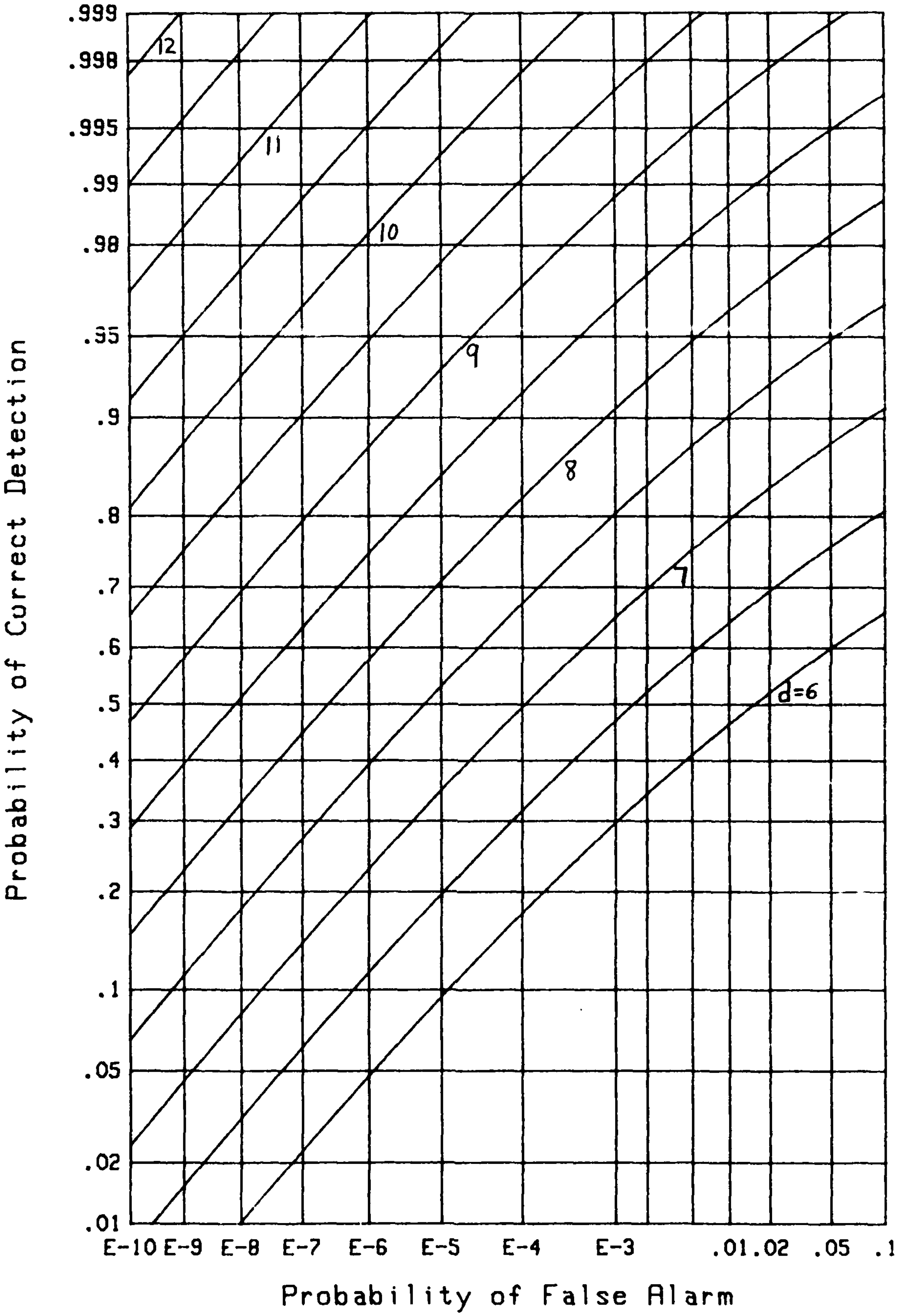

Figure 34. ROC for M=8, N=1000

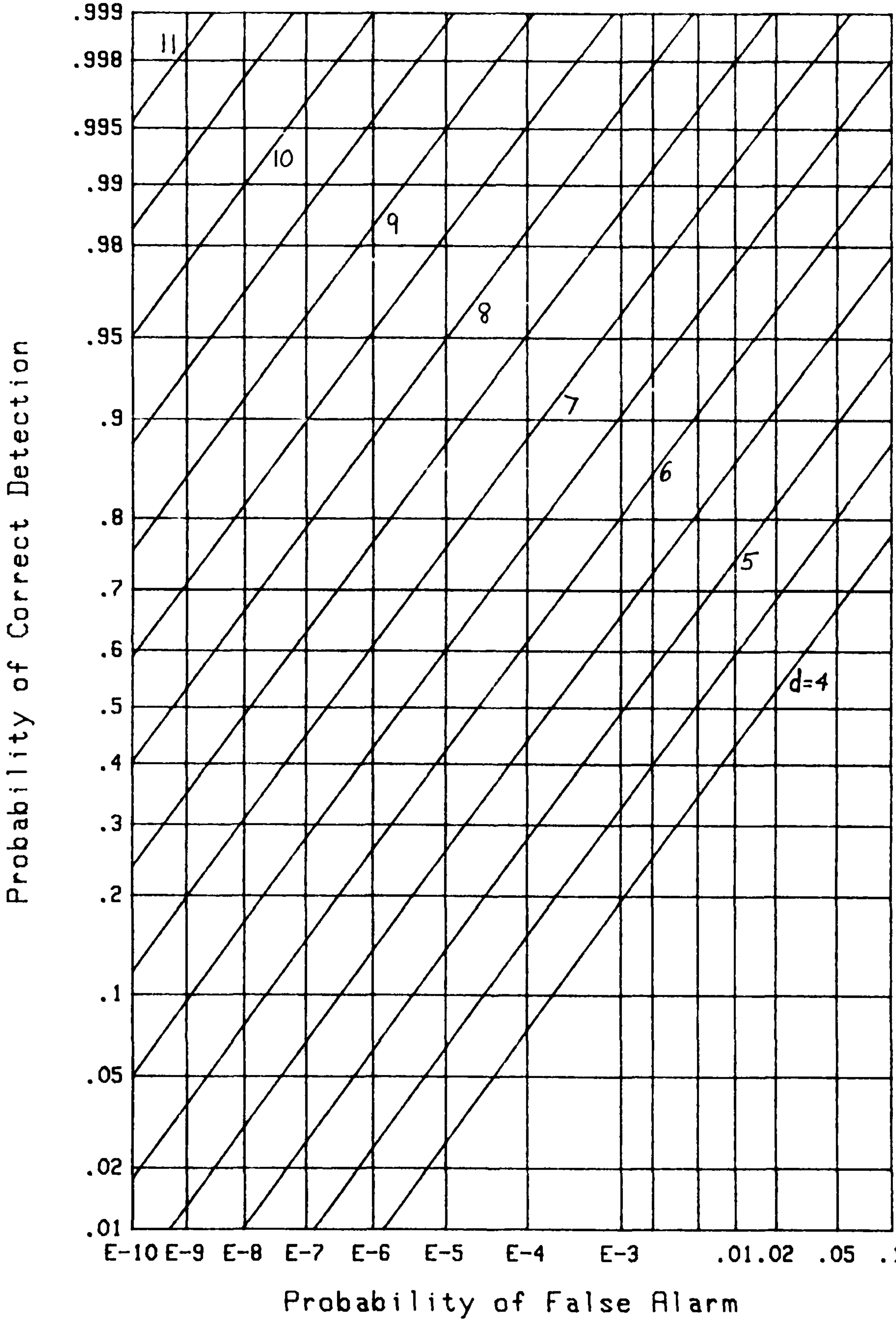

Figure 35. ROC for M=9, N=1

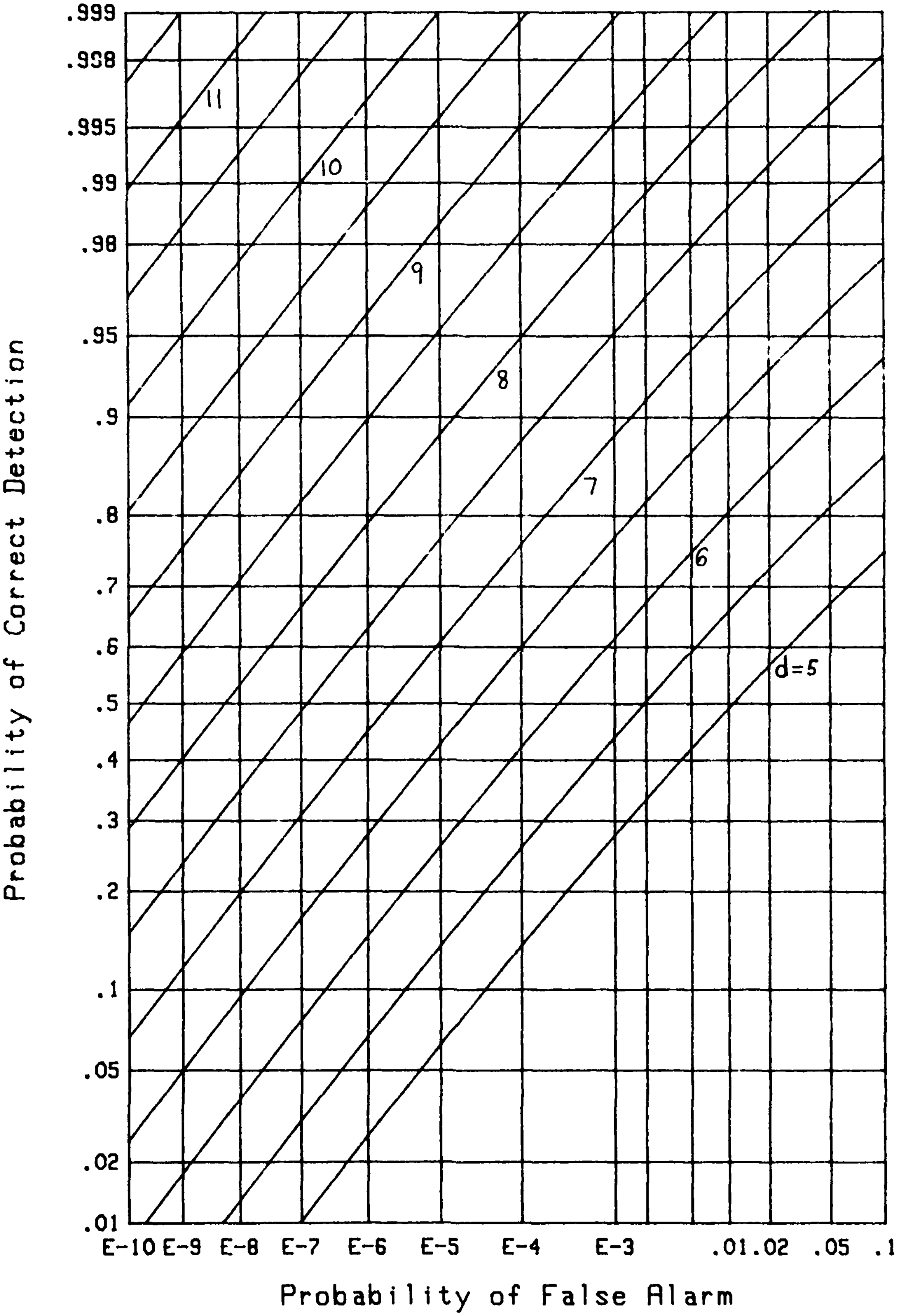

Figure 36. ROC for M=9, N=10

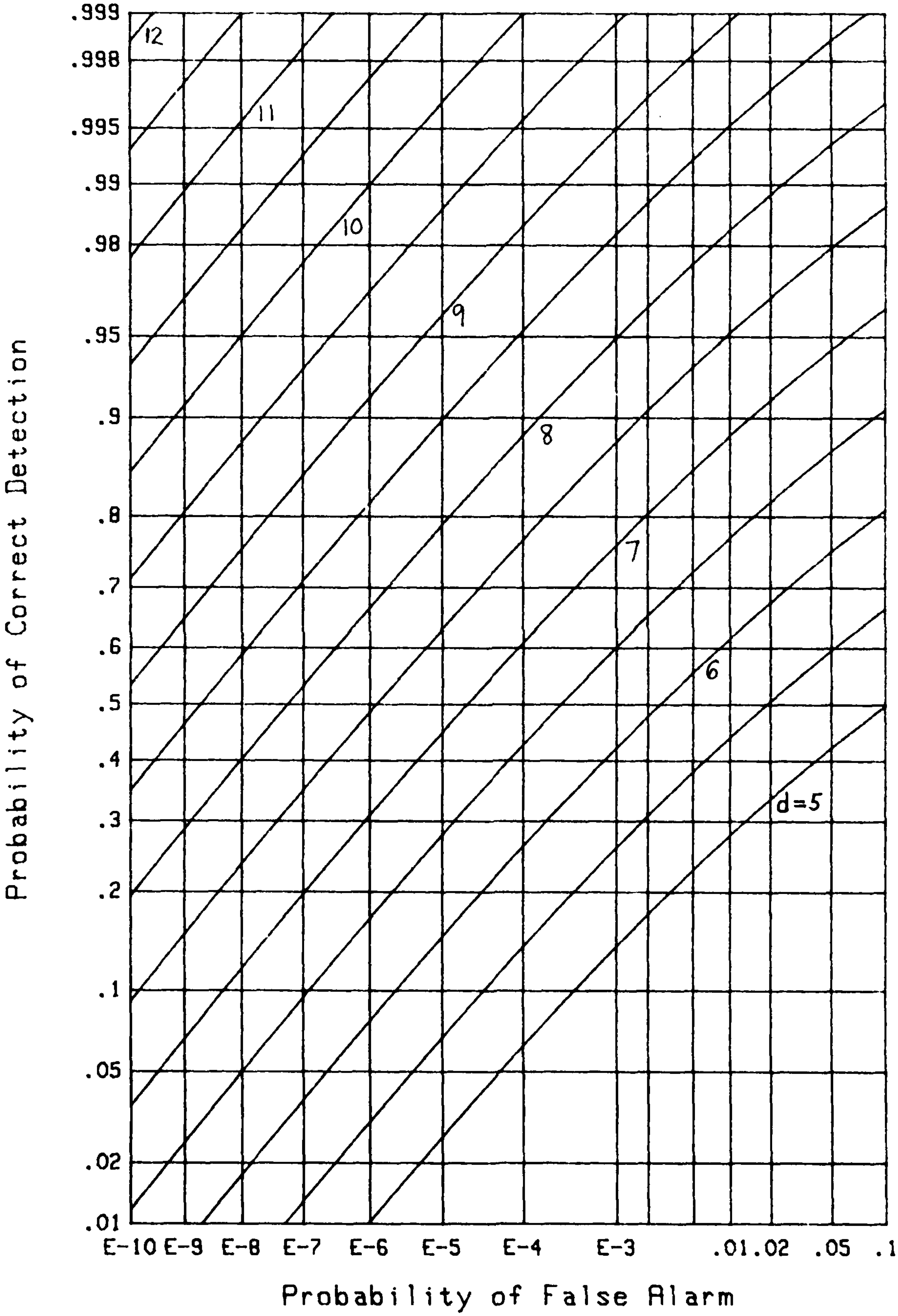

Figure 37. ROC for M=9, N=100

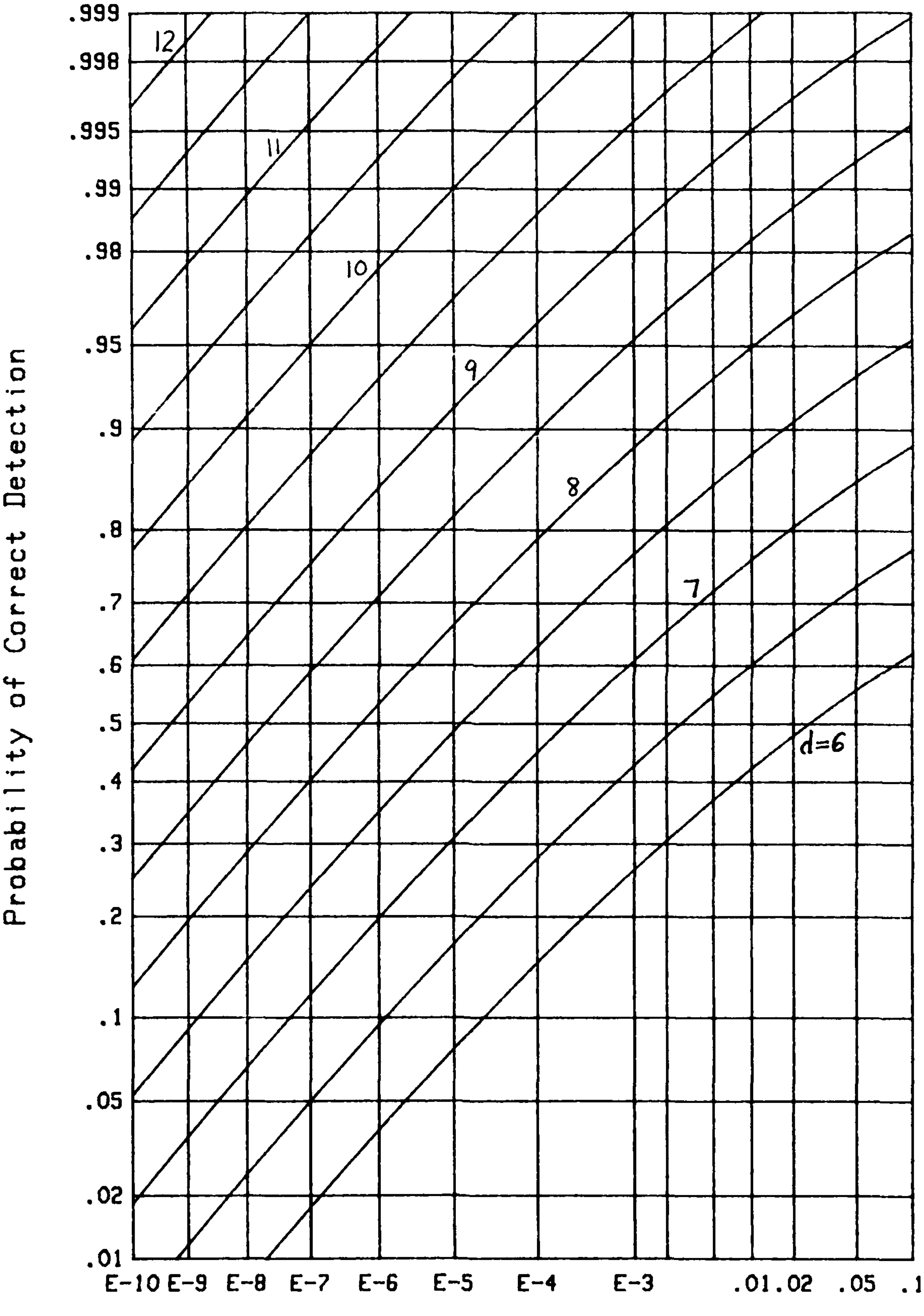

Figure 38. ROC for M=9, N=1000

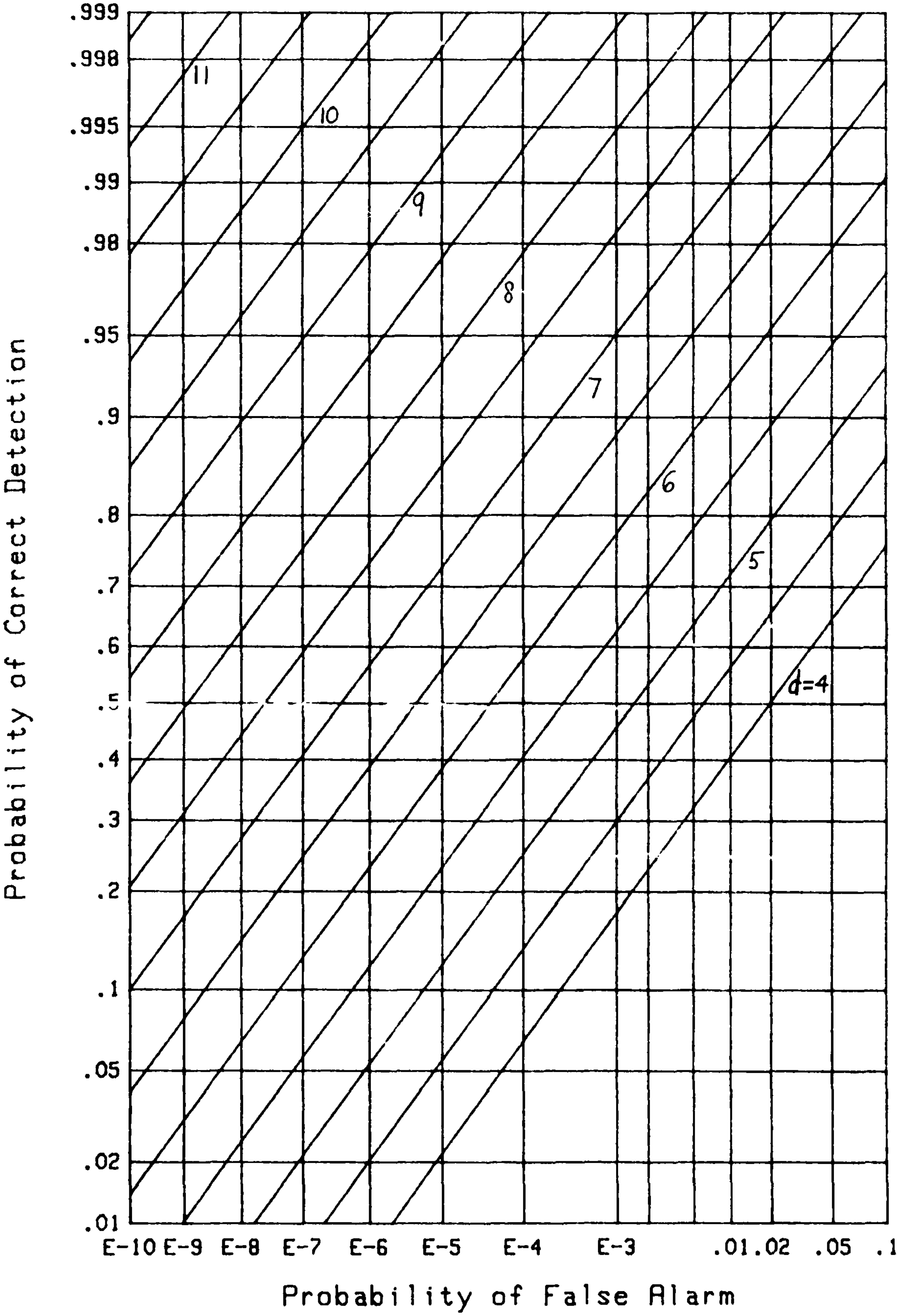

Figure 39. ROC for M=10, N=1

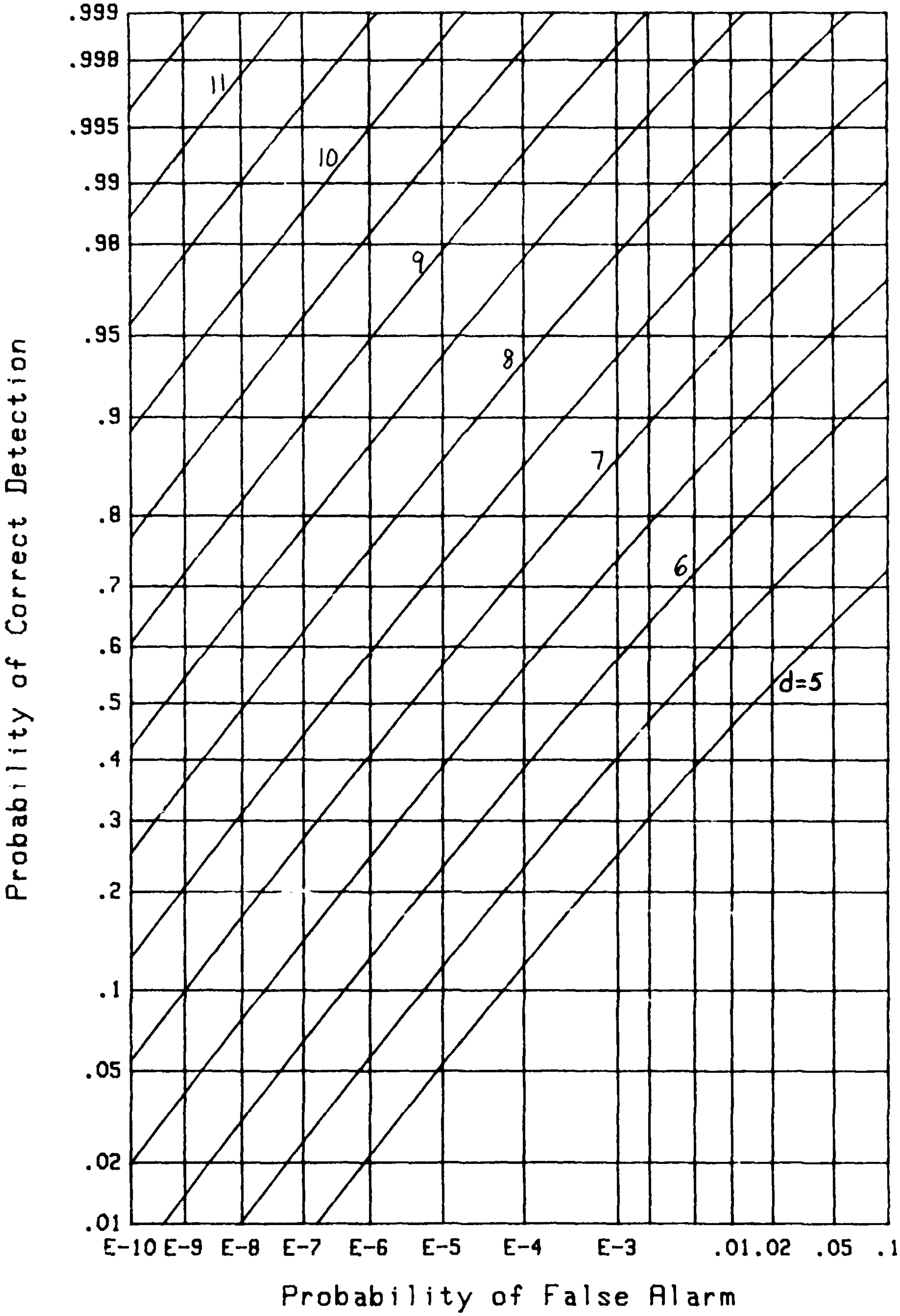

Figure 40. ROC for M=10, N=10

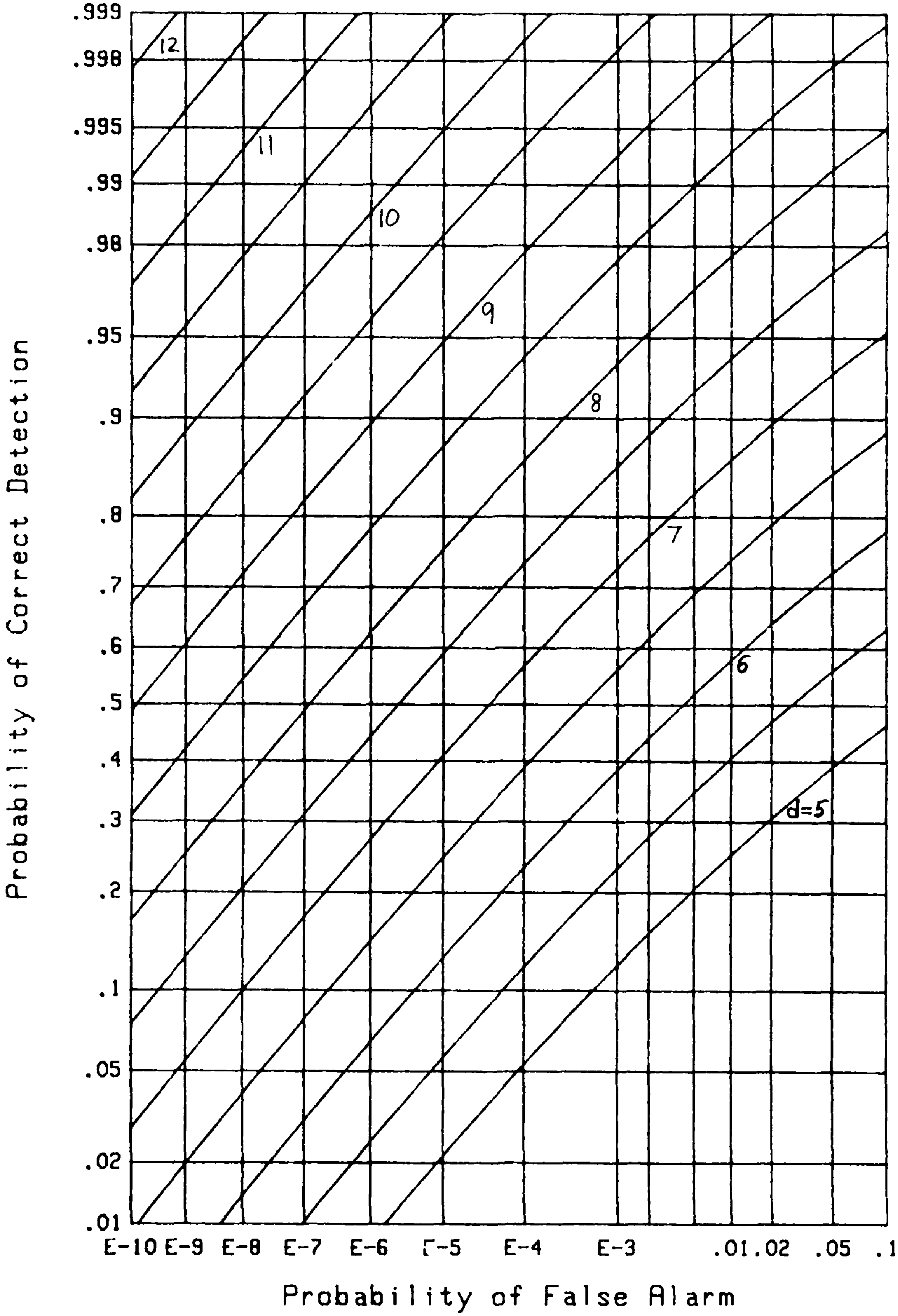

Figure 41. ROC for M=10, N=100

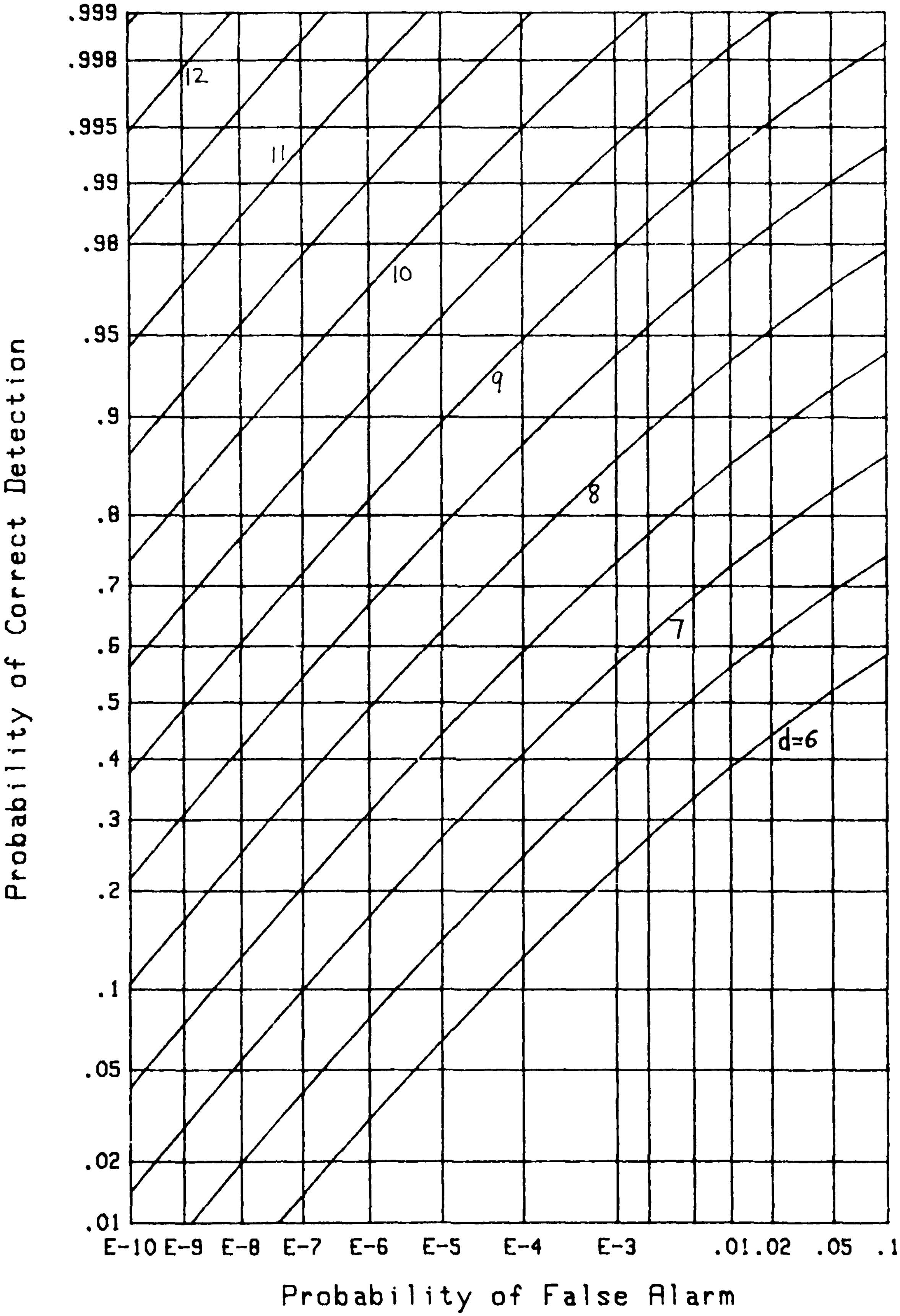

Figure 42. ROC for M=10, N=1000

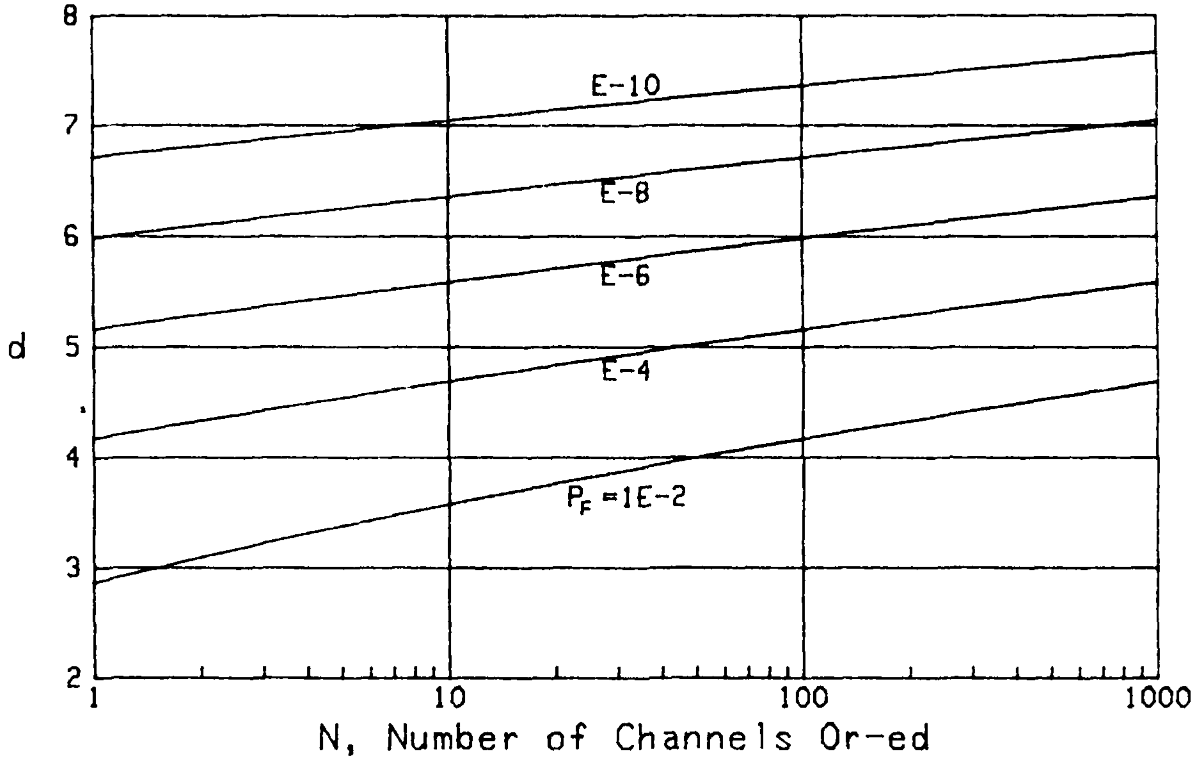

Figure 43. Required d Values for M=1, P_{CD}=.5

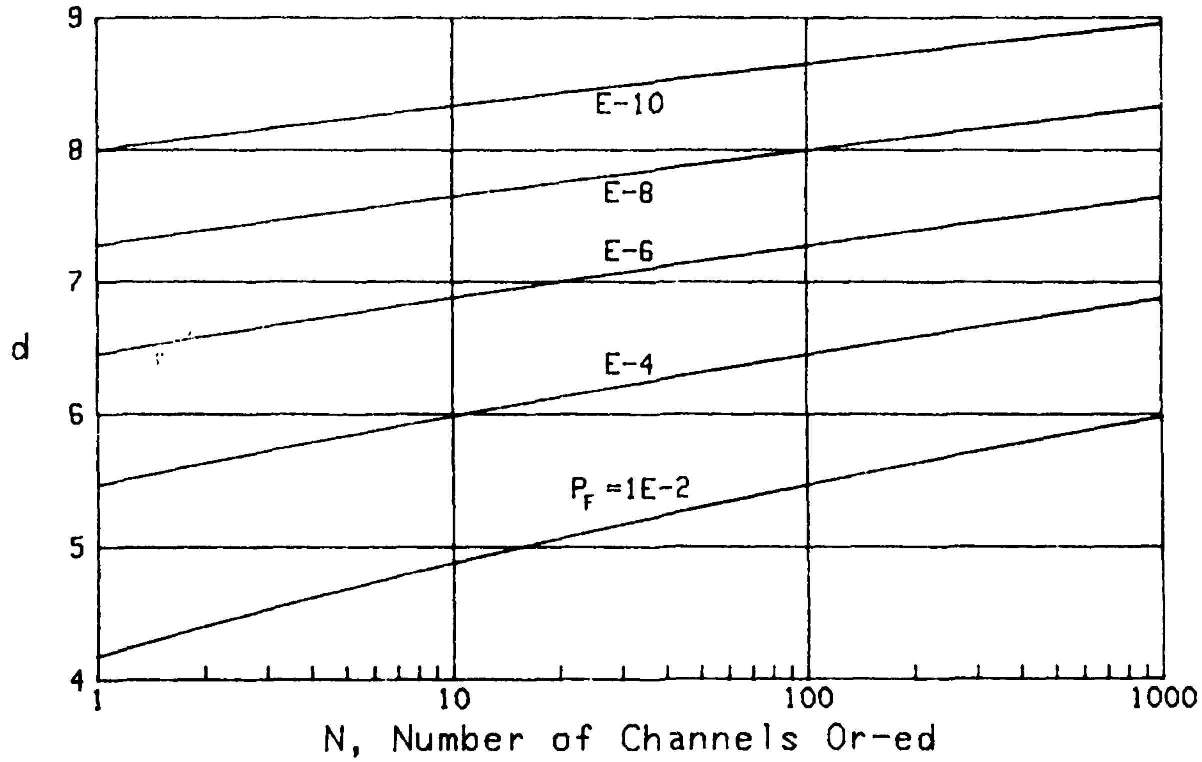

Figure 44. Required d Values for M=1, P_{CD}=.9

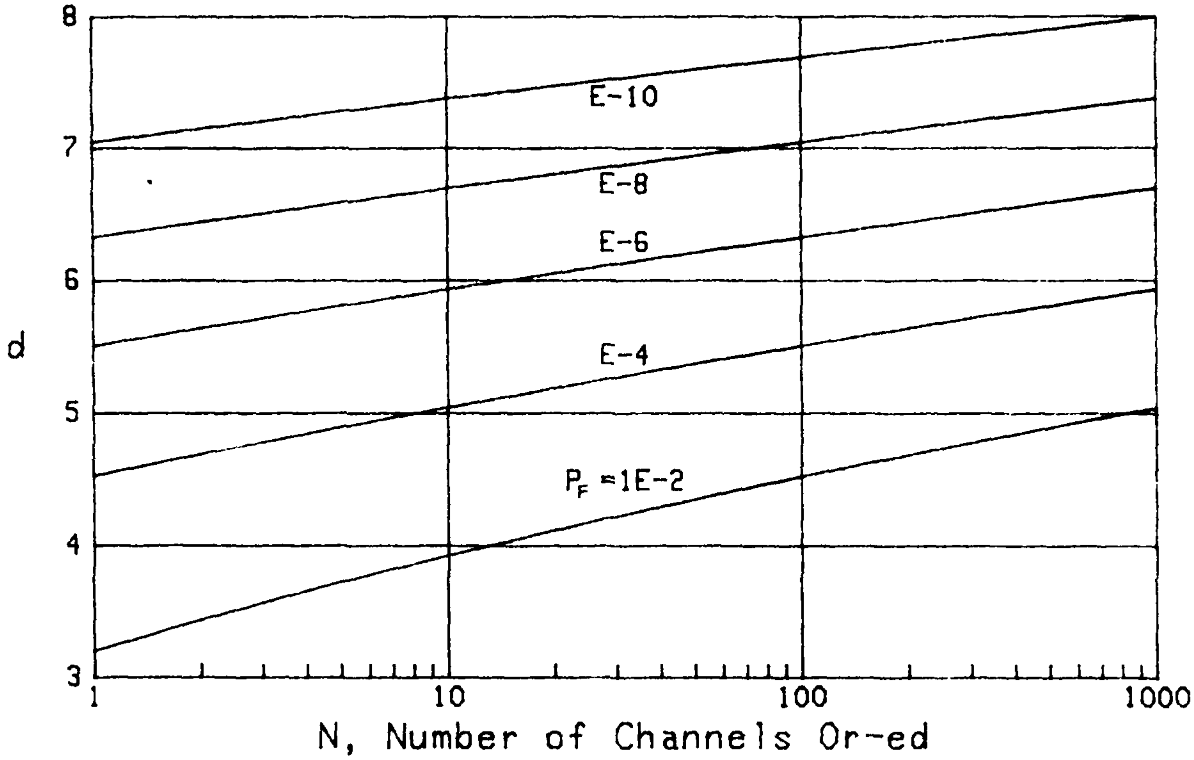

Figure 45. Required d Values for M=2, P_{CD}=.5

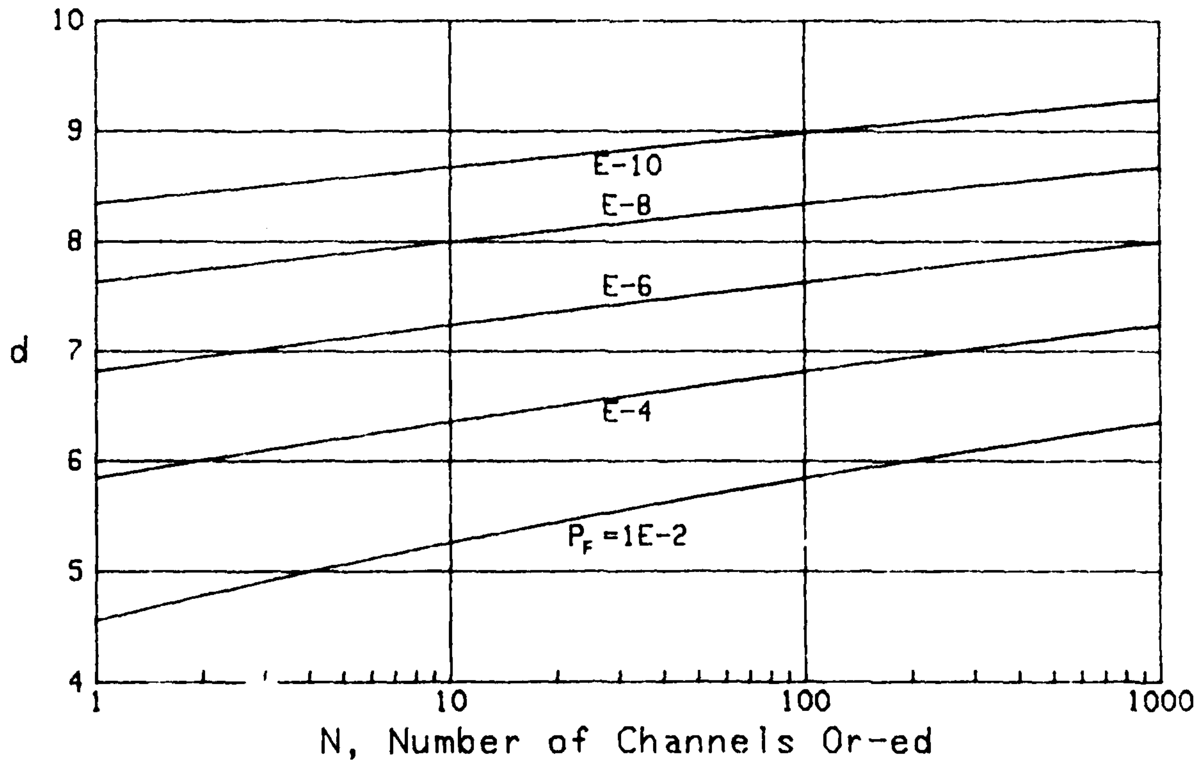

Figure 46. Required d Values for M=2, P_{CD}=.9

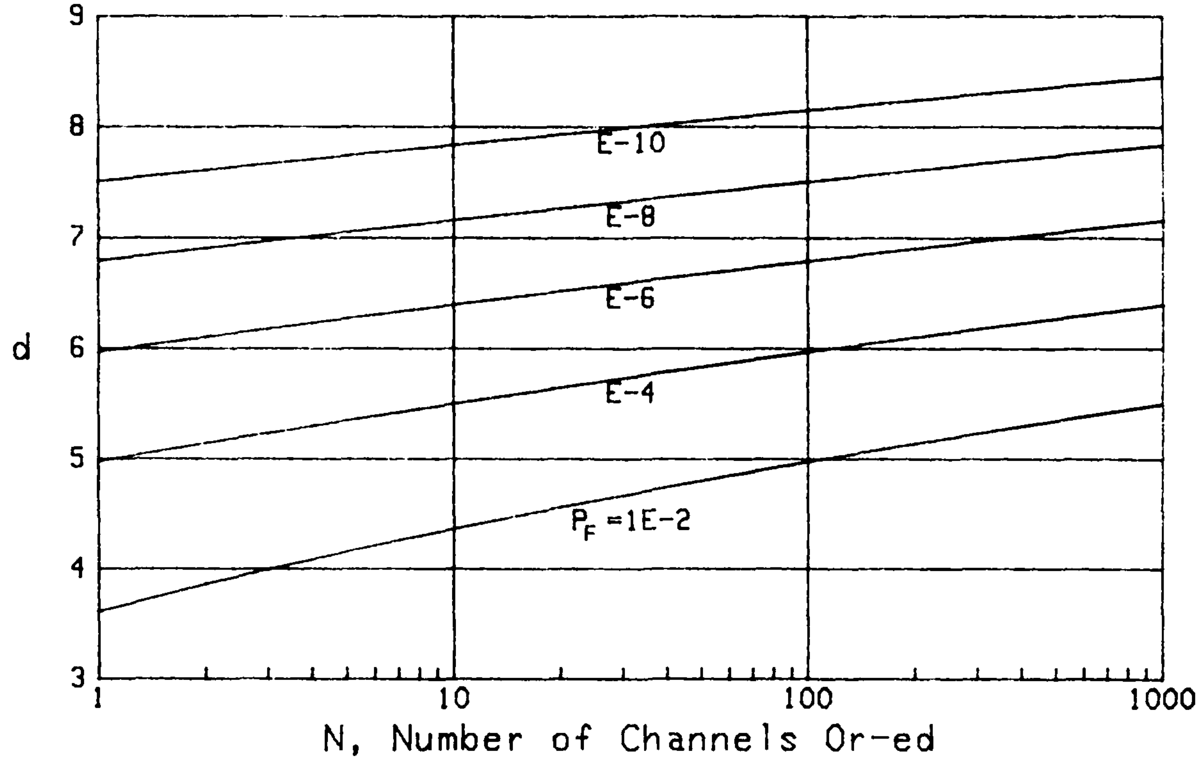

Figure 47. Required d Values for M=4, P_{CD}=.5

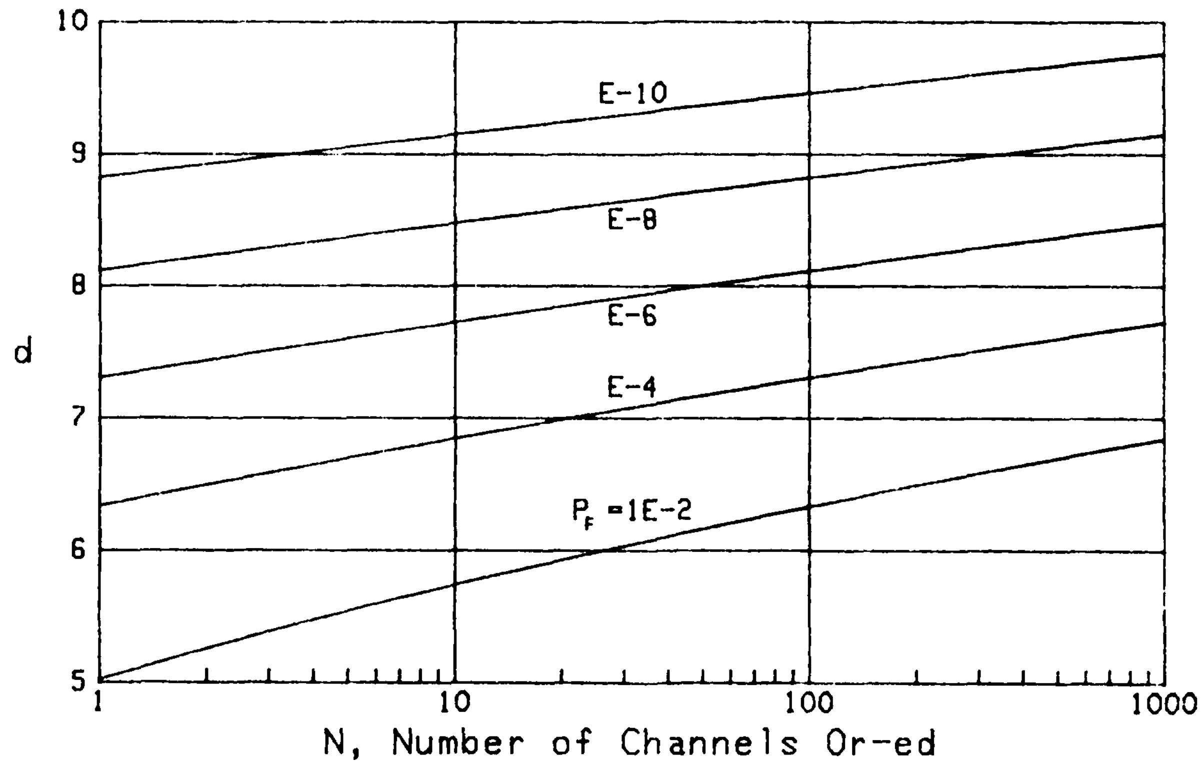

Figure 48. Required d Values for M=4, P_{CD}=.9

APPENDIX A. Q_M-FUNCTION RELATIONSHIPS

Let $\{x_m\}_1^M$ and $\{y_m\}_1^M$ be independent identically distributed Gaussian random variables, each with zero mean and common variance σ^2, and let $\{a_m\}_1^M$ and $\{b_m\}_1^M$ be arbitrary fixed constants. Define "total" parameter

$$d^2 = \frac{1}{\sigma^2} \sum_{m=1}^{M} (a_m^2 + b_m^2) \ . \tag{A-1}$$

Chi-Squared Variate

We are interested in the statistical description of the noncentral chi-squared random variable of 2M degrees of freedom,

$$v = \sum_{m=1}^{M} [(x_m + a_m)^2 + (y_m + b_m)^2] \ . \tag{A-2}$$

We will only list results here, and will not give detailed derivations.

The characteristic function of v is [6; page 11]

$$f_v(\xi) = \overline{\exp(i\xi v)} = (1 - i\xi 2\sigma^2)^{-M} \ \exp\left[\frac{i\xi d^2 \sigma^2}{1-i\xi 2\sigma^2}\right], \tag{A-3}$$

which is seen to depend on the arbitrary constants $\{a_m\}$ and $\{b_m\}$ only through the sum d^2 in (A-1). The probability density function of random variable v is [7; 6.631 4]

$$p_v(u) = \frac{1}{2\sigma^2}\left(\frac{\sqrt{u}}{d\sigma}\right)^{M-1} I_{M-1}\left(\frac{d\sqrt{u}}{\sigma}\right)\exp\left(-\frac{u}{2\sigma^2}-\frac{d^2}{2}\right) \quad \text{for } u > 0. \qquad \text{(A-4)}$$

The cumulative distribution function of random variable v is

$$\text{Prob}\ (v < u) = P_v(u) = \int_0^u dt\ p_v(t)\ , \qquad \text{(A-5)}$$

and the exceedance distribution function is

$$1 - P_v(u) = Q_M(d, \sqrt{u}/\sigma) \quad \text{for } u > 0, \qquad \text{(A-6)}$$

where the Q_M-function is

$$Q_M(\alpha, \beta) = \int_\beta^\infty dx\ x\left(\frac{x}{\alpha}\right)^{M-1} I_{M-1}(\alpha x)\ \exp\left(-\frac{x^2+\alpha^2}{2}\right). \qquad \text{(A-7)}$$

As special cases of (A-4) and (A-6), for d = 0, we have probability density function

$$p_v^{(o)}(u) = \frac{u^{M-1}}{(M-1)!\ (2\sigma^2)^M}\ \exp\left(\frac{-u}{2\sigma^2}\right) \quad \text{for } u > 0 \qquad \text{(A-8)}$$

and exceedance distribution function

$$1-P_v^{(o)}(u) = \exp\left(\frac{-u}{2\sigma^2}\right) e_{M-1}\left(\frac{u}{2\sigma^2}\right) = E_{M-1}\left(\frac{u}{2\sigma^2}\right) \quad \text{for } u > 0, \qquad \text{(A-9)}$$

where [5; 6.5.11]

$$e_n(x) = \sum_{k=0}^{n} x^k/k! \qquad \text{(A-10)}$$

is the partial exponential and where we define

$$E_n(x) = \exp(-x)\, e_n(x) \ . \qquad \text{(A-11)}$$

Returning to the general case of $d > 0$ for random variable v again, the cumulants of v are

$$\lambda_v(n) = \left(2\sigma^2\right)^n n!\left(\frac{M}{n} + \frac{d^2}{2}\right) \quad \text{for } n \geq 1 \ , \qquad \text{(A-12)}$$

the ν-th moments are

$$\overline{v^\nu} = (2\sigma^2)^\nu \frac{\Gamma(M+\nu)}{\Gamma(M)} \, {}_1F_1(-\nu;M;-d^2/2) \quad \text{for } \nu > -M, \qquad \text{(A-13)}$$

and the n-th moments are

$$\overline{v^n} = (2\sigma^2)^n \, n! \, L_n^{(M-1)}(-d^2/2). \qquad \text{(A-14)}$$

<u>Chi Variate</u>

The noncentral chi variate of $2M$ degrees of freedom is

$$z = v^{1/2} = \left\{\sum_{m=1}^{M} [(x_m + a_m)^2 + (y_m + b_m)^2]\right\}^{1/2} . \qquad \text{(A-15)}$$

Its probability density function is

$$p_z(u) = \frac{u}{\sigma^2}\left(\frac{u}{d\sigma}\right)^{M-1} I_{M-1}\left(\frac{du}{\sigma}\right) \exp\left(-\frac{u^2}{2\sigma^2} - \frac{d^2}{2}\right) \quad \text{for } u > 0, \qquad \text{(A-16)}$$

and its exceedance distribution function is

$$1 - P_Z(u) = Q_M(d,\ u/\sigma) \quad \text{for } u > 0. \tag{A-17}$$

As special cases of (A-16) and (A-17), for d = 0, we have probability density function

$$p_Z^{(o)}(u) = \frac{2\,u^{2M-1}}{(M-1)!\,(2\sigma^2)^M}\,\exp\left(\frac{-u^2}{2\sigma^2}\right) \quad \text{for } u > 0 \tag{A-18}$$

and exceedance distribution function

$$1 - P_Z^{(o)}(u) = E_{M-1}\left(\frac{u^2}{2\sigma^2}\right) \text{ for } u > 0, \tag{A-19}$$

in terms of the functions defined in (A-10) and (A-11).

In general, for d > 0, the ν-th moment of random variable z is

$$\overline{z^\nu} = \sigma^\nu\, 2^{\nu/2}\, \frac{\Gamma(M + \nu/2)}{\Gamma(M)}\, {}_1F_1(-\nu/2;M;-d^2/2) \quad \text{for } \nu > -2M. \tag{A-20}$$

The characteristic function and cumulants of z are not available in any compact form.

Special Case

If the constants in random variable v in (A-2), and in random variable z in (A-15), satisfy

$$a_m = A \cos \Theta_m, \quad b_m = A \sin \Theta_m, \tag{A-21}$$

where $\{\Theta_m\}$ are arbitrary, then (A-1) reduces to

$$d^2 = M\, A^2/\sigma^2, \tag{A-22}$$

independent of the particular values of $\{\Theta_m\}$. So if $\{\Theta_m\}$ were random variables instead of constants, the statistics of v and z in (A-2) and (A-15), respectively, would be unaffected. This conclusion follows immediately from (A-3).

In this latter case of random $\{\Theta_m\}$, if they are also uniformly distributed over 2π, it is sometimes useful to define an individual (common) signal-to-noise ratio

$$R = \frac{\overline{a_m^2}}{\overline{x_m^2}} = \frac{\overline{b_m^2}}{\overline{y_m^2}} = \frac{A^2/2}{\sigma^2} \quad \text{for all m.} \tag{A-23}$$

Then the parameter d^2 in (A-22) can be expressed as

$$d^2 = 2\, M\, R. \tag{A-24}$$

More generally, if

$$a_m = A_m \cos \Theta_m, \quad b_m = A_m \sin \Theta_m, \tag{A-25}$$

where $\{A_m\}$ are arbitrary constants, then (A-1) reduces to

$$d^2 = \frac{1}{\sigma^2} \sum_{m=1}^{M} A_m^2 . \tag{A-26}$$

Again, presuming $\{\theta_m\}$ to be uniformly distributed random variables over 2π, if we define the individual component signal-to-noise ratios as

$$R_m = \frac{\overline{a_m^2}}{\overline{x_m^2}} = \frac{\overline{b_m^2}}{\overline{y_m^2}} = \frac{A_m^2/2}{\sigma^2} , \tag{A-27}$$

then (A-26) can be expressed as

$$d^2 = 2 \sum_{m=1}^{M} R_m . \tag{A-28}$$

These relations, (A-24) and (A-28), afford an alternative interpretation of the "total" parameter d^2 in terms of component signal-to-noise ratios.

APPENDIX B. TABULATION OF P_{CD} AND $Q_M(d,T)$

For the eight possible combinations of M=1,10 with N=2,10,100,1000, values of the exact value of P_{CD} and the approximation afforded by $Q_M(d,T)$ are tabulated here. An explanation of table B-1, which pertains to M=1, N=2, follows:

For threshold T = 2.40, the false alarm probability P_F = .10912. Holding these values fixed, then as d is varied from 2.2 to 5.4, the detection probabilities vary over the values .5, .9, .99, .999 (approximately). This case is covered by the top four lines in table B-1.

When the threshold T is changed to 3.25, the new false alarm probability is P_F = .01015, and the second group of four lines in table B-1 pertains. This procedure is continued for all the M,N combinations, while P_F ranges over the values .1, .01, .001 (approximately). The comparisons for smaller P_F values are not conducted because the discrepancies are very small, as may be seen by inspection of the tables.

The greatest discrepancies between probabilities P_{CD} and $Q_M(d,T)$ occur in tables B-3 and B-4, where N=10. These particular cases are plotted in figure B-1, for false alarm probabilities in the .1 and .01 regime. For example, the two curves labelled by A, which pertains to M=1, N=10, $P_F \sim .1$, show a very slight difference between the two probabilities over the range (.5,.999). The label B actually pertains to two overlapping curves for M=1, N=10, $P_F \simeq .01$; that is, the plotted values for P_{CD} and

$Q_M(d,T)$ are indistinguishable at this level of false alarm probability. The situation for C and D is exactly similar, except that in these latter cases, we have M=10, N=10.

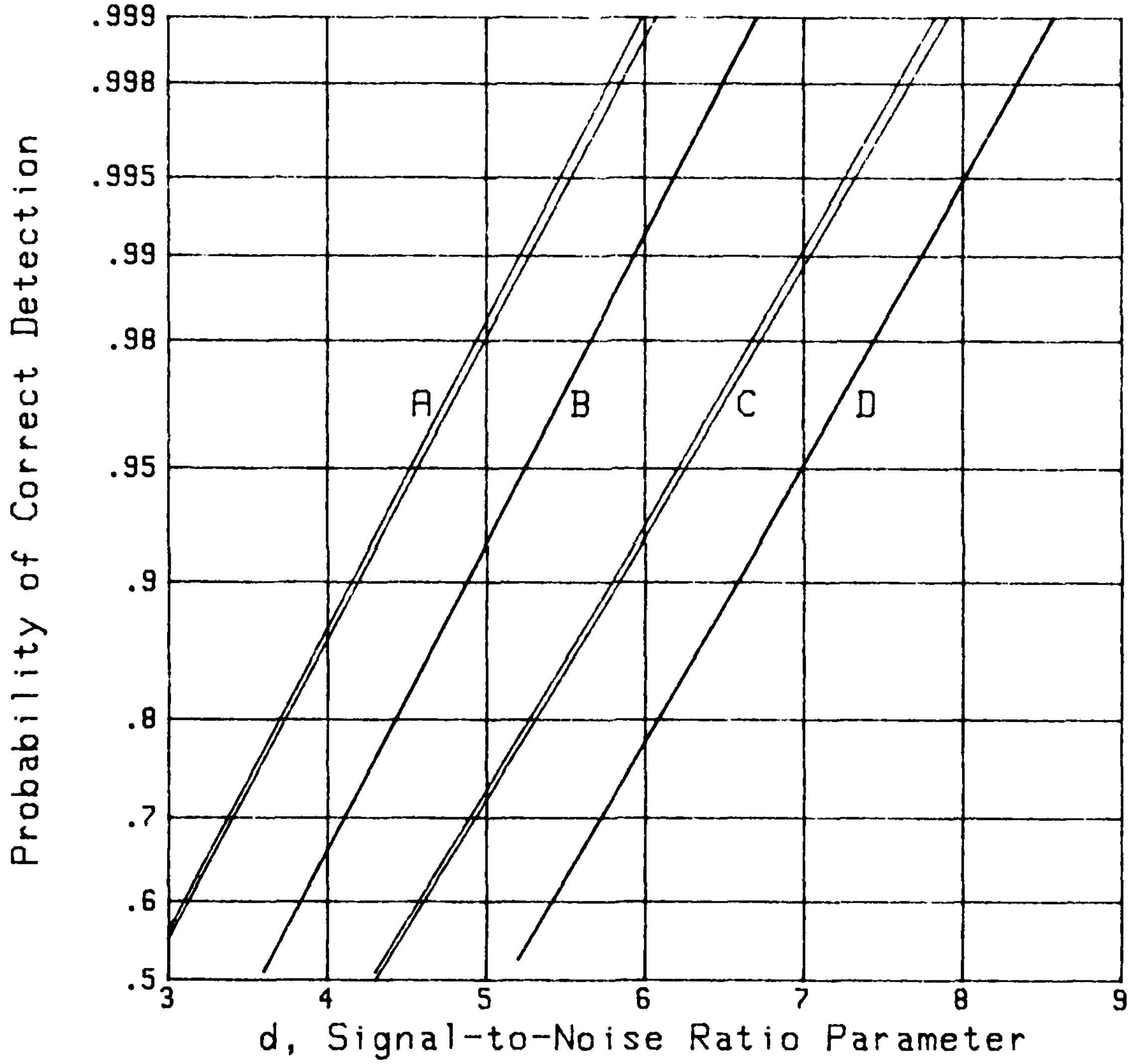

A: Table B-3, P_F =.10272
B: Table B-3, P_F =.01021
C: Table B-4, P_F =.10175
D: Table B-4, P_F =.01002

Figure B-1. Comparison of Probabilities

	d	P_{CD}	$Q_M(d,1)$
T = 2.40	2.2	.50220	.51005
P_F = .10912	3.6	.91017	.91506
	4.6	.98935	.99062
	5.4	.99890	.99915
T = 3.25	3.1	.50353	.50409
P_F = .01015	4.4	.89997	.90032
	5.5	.99099	.99106
	6.3	.99920	.99921
T = 3.89	3.8	.51653	.51658
P_F = .00104	5.0	.88951	.88954
	6.2	.99205	.99206
	6.9	.99905	.99905

Table B-1. Probability Comparison for M=1, N=2

	d	P_{CD}	$Q_M(d,1)$
T = 5.59	3.5	.49914	.50646
P_F = .10129	5.1	.89637	.90120
	6.4	.99083	.99185
	7.3	.99913	.99931
T = 6.32	4.6	.51111	.51166
P_F = .01013	6.1	.90493	.90526
	7.3	.99132	.99138
	8.1	.99905	.99906
T = 6.89	5.3	.49032	.49036
P_F = .00101	6.8	.90322	.90325
	8.0	.99162	.99162
	8.8	.99913	.99913

Table B-2. Probability Comparison for M=10, N=2

	d	P_{CD}	$Q_M(d,1)$
T = 3.01	2.9	.51382	.52498
P_F = .10272	4.2	.90180	.90857
	5.3	.99074	.99213
	6.1	.99909	.99933
T = 3.71	3.6	.51050	.51140
P_F = .01021	4.9	.90404	.90457
	6.0	.99161	.99171
	6.8	.99927	.99929
T = 4.29	4.2	.51145	.51153
P_F = .00101	5.5	.90544	.90548
	6.6	.99188	.99189
	7.3	.99903	.99903

Table B-3. Probability Comparison for M=1, N=10

	d	P_{CD}	$Q_M(d,1)$
T = 6.11	4.3	.49943	.51032
P_F = .10175	5.9	.90911	.91532
	7.1	.99133	.99257
	7.9	.99898	.99921
T = 6.73	5.2	.52682	.52769
P_F = .01002	6.6	.90232	.90282
	7.8	.99133	.99143
	8.6	.99908	.99910
T = 7.23	5.8	.51336	.51344
P_F = .00104	7.2	.90126	.90131
	8.4	.99160	.99160
	9.2	.99914	.99914

Table B-4. Probability Comparison for M=10, N=10

	d	P_{CD}	$Q_M(d,T)$
T = 3.70	3.6	.50535	.51547
P_F = .10105	4.9	.90037	.90628
	6.0	.99080	.99193
	6.8	.99914	.99931
T = 4.29	4.2	.51067	.51153
P_F = .01003	5.5	.90499	.90548
	6.6	.99180	.99189
	7.3	.99901	.99903
T = 4.79	4.7	.50637	.50645
P_F = .00104	6.0	.90378	.90382
	7.1	.99170	.99170
	7.8	.99900	.99900

Table B-5. Probability Comparison for M=1, N=100

	d	P_{CD}	$Q_M(d,T)$
T = 6.72	5.2	.52240	.53217
P_F = .09974	6.6	.89913	.90471
	7.8	.99064	.99169
	8.6	.99895	.99913
T = 7.23	5.8	.51258	.51344
P_F = .01033	7.2	.90082	.90131
	8.4	.99152	.99160
	9.2	.99913	.99914
T = 7.68	6.4	.52928	.52936
P_F = .00102	7.8	.91140	.91144
	8.9	.99112	.99113
	9.7	.99910	.99910

Table B-6. Probability Comparison for M=10, N=100

	d	P_{CD}	$Q_M(d,1)$
T = 4.27	4.2	.51031	.51962
P_F = .10403	5.5	.90369	.90884
	6.6	.99141	.99233
	7.3	.99892	.99909
T = 4.79	4.7	.50564	.50645
P_F = .01036	6.0	.90337	.90382
	7.1	.99162	.99170
	7.8	.99899	.99900
T = 5.25	5.2	.51839	.51846
P_F = .00103	6.5	.90916	.90920
	7.5	.99008	.99009
	8.3	.99911	.99911

Table B-7. Probability Comparison for M=1, N=1000

	d	P_{CD}	$Q_M(d,1)$
T = 7.22	5.8	.50897	.51785
P_F = .10332	7.2	.89822	.90320
	8.4	.99098	.99185
	9.2	.99903	.99917
T = 7.68	6.3	.49278	.49354
P_F = .01017	7.8	.91105	.91144
	8.9	.99105	.99113
	9.7	.99909	.99910
T = 8.08	6.8	.50022	.50029
P_F = .00105	8.2	.90129	.90133
	9.3	.98975	.98976
	10.1	.99894	.99894

Table B-8. Probability Comparison for M=10, N=1000

APPENDIX C. PROGRAM LISTING

```
10    M=10                          !  NUMBER OF FILTER OUTPUTS SUMMED
20    N=1000                        !  NUMBER OF CHANNELS OR-ED
30    DIM U(100),Do(1:10,0:3)          !  THRESHOLD VALUES
40    COM Pf(100),Pd1(100),Pd2(100),Pd3(100),Pd4(100),Pd5(100)
50    COM Pd6(100),Pd7(100),Pd8(100),Pd9(100),Pd10(100)
60    COM Pd11(100),Pd12(100),Pd13(100),Pd14(100),Pd15(100)
70    COM Pd16(100),Pd17(100)
80    DOUBLE M,N,I,J                !  INTEGERS
90    DATA 2,3,4,4,3,3,4,5,3,4,4,5,3,4,4,5,3,4,5,5
100   DATA 3,4,5,5,4,4,5,5,4,4,5,6,4,5,5,6,4,5,5,6
110   READ Do(*)                    !  STARTING VALUES FOR d
120   U=0.
130   U=U+.01
140   Pf=FNPf(U,M,N)
150     IF Pf>.1 THEN 130           !  UPPER LIMIT ON Pf
160   U1=MAX(U-.01,.01)
170   U=U+.01
180   Pf=FNPf(U,M,N)
190     IF Pf>1E-10 THEN 170        !  LOWER LIMIT ON Pf
200   U2=U
210   Delu=(U2-U1)/100.
220   FOR I=0 TO 100
230   U=U1+Delu*I
240   U(I)=U
250   Pf(I)=FNPf(U,M,N)
260   NEXT I
270   I=LGT(N)
280   Do=Do(M,I)
290     PRINTER IS PRT
300     PRINT M,N,Do
310     PRINTER IS CRT
320   FOR J=1 TO 17
330     Ds=Do+(J-1)*.5              !  TOTAL DEFLECTION PARAMETER d
340   FOR I=0 TO 100
350   U=U(I)                        !  THRESHOLD
360   Pd=FNPd(Ds,U,M)
370   Pd=MIN(Pd,.99999)
380   IF J=1 THEN Pd1(I)=Pd
390   IF J=2 THEN Pd2(I)=Pd
400   IF J=3 THEN Pd3(I)=Pd
410   IF J=4 THEN Pd4(I)=Pd
420   IF J=5 THEN Pd5(I)=Pd
430   IF J=6 THEN Pd6(I)=Pd
440   IF J=7 THEN Pd7(I)=Pd
450   IF J=8 THEN Pd8(I)=Pd
460   IF J=9 THEN Pd9(I)=Pd
470   IF J=10 THEN Pd10(I)=Pd
480   IF J=11 THEN Pd11(I)=Pd
490   IF J=12 THEN Pd12(I)=Pd
500   IF J=13 THEN Pd13(I)=Pd
510   IF J=14 THEN Pd14(I)=Pd
520   IF J=15 THEN Pd15(I)=Pd
530   IF J=16 THEN Pd16(I)=Pd
540   IF J=17 THEN Pd17(I)=Pd
550   NEXT I
560   NEXT J
```

```
570     FOR I=0 TO 100
580     Pf(I)=FNInvphi(Pf(I))
590     Pd1(I)=FNInvphi(Pd1(I))
600     Pd2(I)=FNInvphi(Pd2(I))
610     Pd3(I)=FNInvphi(Pd3(I))
620     Pd4(I)=FNInvphi(Pd4(I))
630     Pd5(I)=FNInvphi(Pd5(I))
640     Pd6(I)=FNInvphi(Pd6(I))
650     Pd7(I)=FNInvphi(Pd7(I))
660     Pd8(I)=FNInvphi(Pd8(I))
670     Pd9(I)=FNInvphi(Pd9(I))
680     Pd10(I)=FNInvphi(Pd10(I))
690     Pd11(I)=FNInvphi(Pd11(I))
700     Pd12(I)=FNInvphi(Pd12(I))
710     Pd13(I)=FNInvphi(Pd13(I))
720     Pd14(I)=FNInvphi(Pd14(I))
730     Pd15(I)=FNInvphi(Pd15(I))
740     Pd16(I)=FNInvphi(Pd16(I))
750     Pd17(I)=FNInvphi(Pd17(I))
760     NEXT I
770     CALL A
780     END
790     !
800     DEF FNInvphi(X)              !  AMS 55, 26.2.23
810     IF X=.5 THEN RETURN 0.
820     P=MIN(X,1.-X)
830     T=-LOG(P)
840     T=SQR(T+T)
850     P=1.+T*(1.432788+T*(.189269+T*.001308))
860     P=T-(2.515517+T*(.802853+T*.010328))/P
870     IF X<.5 THEN P=-P
880     RETURN P
890     FNEND
900     !
910     DEF FNPf(U,DOUBLE M,N)       !  FALSE ALARM PROBABILITY
920     T=FNE(.5*U*U,M-1)
930     Pf=1.-(1.-T)^N
940     RETURN Pf
950     FNEND
960     !
970     DEF FNPd(Ds,U,DOUBLE M)      !  DETECTION PROBABILITY
980     Pd=FNQm(M,Ds,U)              !  UPPER BOUND ON Pcd
990     RETURN Pd
1000    FNEND
1010    !
1020    DEF FNE(X,DOUBLE N)          !  exp(-x) e n(x)
1030    DOUBLE K                     !  INTEGER
1040    T=S=EXP(-X)
1050    FOR K=1 TO N
1060    T=T*X/K
1070    S=S+T
1080    NEXT K
1090    RETURN S
1100    FNEND
1110    !
```

```
1120    DEF FNQm(DOUBLE M,REAL A,B)      !  QM(A,B)
1130    Error=1.E-17
1140    DOUBLE M1,J                      !  INTEGERS
1150    Q3=.5*A*A
1160    Q4=.5*B*B
1170    Q5=EXP(-.5*(Q3+Q4))
1180    Q6=Q7=Q5
1190    M1=M-1
1200    FOR J=1 TO M1
1210    Q7=Q7*Q4/J
1220    Q6=Q6+Q7
1230    NEXT J
1240    Qm=Q5*Q6
1250    FOR J=1 TO 300
1260    Q5=Q5*Q3/J
1270    Q7=Q7*Q4/(J+M1)
1280    Q6=Q6+Q7
1290    Q9=Q5*Q6
1300    Qm=Qm+Q9
1310    IF Q9<=Error*Qm THEN 1340
1320    NEXT J
1330    PRINT "300 TERMS IN FNQm(M,A,B) AT ";M;A;B
1340    RETURN MIN(Qm,1.)
1350    FNEND
1360    !
1370    SUB A      !  PLOT PD VS PF ON NORMAL PROBABILITY PAPER
1380    COM Pf(*),Pd1(*),Pd2(*),Pd3(*),Pd4(*),Pd5(*)
1390    COM Pd6(*),Pd7(*),Pd8(*),Pd9(*),Pd10(*)
1400    COM Pd11(*),Pd12(*),Pd13(*),Pd14(*),Pd15(*)
1410    COM Pd16(*),Pd17(*)
1420    DIM A$[30],B$[32]
1430    DIM Xlabel$(1:30),Ylabel$(1:30)
1440    DIM Xcoord(1:30),Ycoord(1:30)
1450    DIM Xgrid(1:30),Ygrid(1:30)
1460    DOUBLE N,Lx,Ly,Nx,Ny,I      !  INTEGERS
1470    !
1480    A$="Probability of False Alarm"
1490    B$="Probability of Correct Detection"
1500    !
1510    Lx=12
1520    REDIM Xlabel$(1:Lx),Xcoord(1:Lx)
1530    DATA E-10,E-9,E-8,E-7,E-6,E-5,E-4,E-3,.01,.02,.05,.1
1540    READ Xlabel$(*)
1550    DATA 1E-10,1E-9,1E-8,1E-7,1E-6,1E-5,1E-4,1E-3,.01,.02,.05,.1
1560    READ Xcoord(*)
1570    !
1580    Ly=18
1590    REDIM Ylabel$(1:Ly),Ycoord(1:Ly)
1600    DATA .01,.02,.05,.1,.2,.3,.4,.5,.6,.7,.8,.9
1610    DATA .95,.98,.99,.995,.998,.999
1620    READ Ylabel$(*)
1630    DATA .01,.02,.05,.1,.2,.3,.4,.5,.6,.7,.8,.9
1640    DATA .95,.98,.99,.995,.998,.999
1650    READ Ycoord(*)
1660    !
1670    Nx=14
1680    REDIM Xgrid(1:Nx)
1690    DATA 1E-10,1E-9,1E-8,1E-7,1E-6,1E-5,1E-4,1E-3,.002,.005,.01,.02,.05,.1
1700    READ Xgrid(*)
1710    !
```

```
1720    Ny=18
1730    REDIM Ygrid(1:Ny)
1740    DATA .01,.02,.05,.1,.2,.3,.4,.5,.6,.7,.8,.9
1750    DATA .95,.98,.99,.995,.998,.999
1760    READ Ygrid(*)
1770    !
1780    FOR I=1 TO Lx
1790    Xcoord(I)=FNInvphi(Xcoord(I))
1800    NEXT I
1810    FOR I=1 TO Ly
1820    Ycoord(I)=FNInvphi(Ycoord(I))
1830    NEXT I
1840    FOR I=1 TO Nx
1850    Xgrid(I)=FNInvphi(Xgrid(I))
1860    NEXT I
1870    FOR I=1 TO Ny
1880    Ygrid(I)=FNInvphi(Ygrid(I))
1890    NEXT I
1900    X1=Xgrid(1)
1910    X2=Xgrid(Nx)
1920    Y1=Ygrid(1)
1930    Y2=Ygrid(Ny)
1940    Scale=(Y2-Y1)/(X2-X1)
1950    GINIT 200./260.                        !  VERTICAL PAPER
1960    PLOTTER IS 505,"HPGL"
1970    PRINTER IS 505
1980  ! PRINT "VS2"
1990    LIMIT PLOTTER 505,0.,200.,0.,260.      !  1 GDU = 2 mm
2000  ! VIEWPORT 20.,20.+103./Scale,19.,122.
2010    VIEWPORT 20.,85.,19.,122.
2020  ! VIEWPORT 22.,85.,59.,122.             !  TOP OF PAPER
2030  ! VIEWPORT 22.,85.,19.,62.              !  BOTTOM OF PAPER
2040    WINDOW X1,X2,Y1,Y2
2050    FOR I=1 TO Nx
2060    MOVE Xgrid(I),Y1
2070    DRAW Xgrid(I),Y2
2080    NEXT I
2090    FOR I=1 TO Ny
2100    MOVE X1,Ygrid(I)
2110    DRAW X2,Ygrid(I)
2120    NEXT I
2130    PENUP
2140    CSIZE 2.3,.5
2150    LORG 5
2160    Y=Y1-(Y2-Y1)*.02
2170    FOR I=1 TO Lx
2180    MOVE Xcoord(I),Y
2190    LABEL Xlabel$(I)
2200    NEXT I
2210    CSIZE 3.,.5
2220    MOVE .5*(X1+X2),Y1-.06*(Y2-Y1)
2230    LABEL A$
2240    MOVE .5*(X1+X2),Y1-.1*(Y2-Y1)
2250        LABEL "Figure 42. ROC for M=10, N=1000"
```

```
2260    CSIZE 2.3,.5
2270    LORG 8
2280    X=X1-(X2-X1)*.01
2290    FOR I=1 TO Ly
2300    MOVE X,Ycoord(I)
2310    LABEL Ylabel$(I)
2320    NEXT I
2330    LDIR PI/2.
2340    CSIZE 3.,.5
2350    LORG 5
2360    MOVE X1-.15*(X2-X1),.5*(Y1+Y2)
2370    LABEL B$
2380    PENUP
2390    PLOT Pf(*),Pd1(*)
2400    PENUP
2410    PLOT Pf(*),Pd2(*)
2420    PENUP
2430    PLOT Pf(*),Pd3(*)
2440    PENUP
2450    PLOT Pf(*),Pd4(*)
2460    PENUP
2470    PLOT Pf(*),Pd5(*)
2480    PENUP
2490    PLOT Pf(*),Pd6(*)
2500    PENUP
2510    PLOT Pf(*),Pd7(*)
2520    PENUP
2530    PLOT Pf(*),Pd8(*)
2540    PENUP
2550    PLOT Pf(*),Pd9(*)
2560    PENUP
2570    PLOT Pf(*),Pd10(*)
2580    PENUP
2590    PLOT Pf(*),Pd11(*)
2600    PENUP
2610    PLOT Pf(*),Pd12(*)
2620    PENUP
2630    PLOT Pf(*),Pd13(*)
2640    PENUP
2650    PLOT Pf(*),Pd14(*)
2660    PENUP
2670    PLOT Pf(*),Pd15(*)
2680    PENUP
2690    PLOT Pf(*),Pd16(*)
2700    PENUP
2710    PLOT Pf(*),Pd17(*)
2720    PENUP
2730    BEEP 500,2
2740    PRINTER IS CRT
2750    PLOTTER 505 IS TERMINATED
2760    SUBEND
```


Reverse Blank

REFERENCES

1. C. W. Helstrom, Statistical Theory of Signal Detection, Second Edition, Pergamon Press Inc., New York, NY, 1968.

2. A. H. Nuttall and R. Garber, "Receiver Operating Characteristics for Phase-Incoherent Detection of Multiple Observations," NUSC Technical Memorandum TC-179-71, Naval Underwater Systems Center, New London, CT, 28 September 1971.

3. A. H. Nuttall and E. S. Eby, Signal-To-Noise Ratio Requirements for Detection of Multiple Pulses Subject to Partially-Correlated Fading with Chi-Squared Statistics of Various Degrees of Freedom, NUSC Technical Report 7707, Naval Underwater Systems Center, New London, CT, 2 June 1986.

4. R. F. Dwyer, Or-ing Data Reduction Model with Applications in Passive Sonar, NUSC Technical Report 5231, Naval Underwater Systems Center, New London, CT, 3 October 1975.

5. Handbook of Mathematical Functions, U. S. Department of Commerce, National Bureau of Standards, Applied Mathematics Series No. 55, U. S. Government Printing Office, Washington, D.C., June 1964.

6. A. H. Nuttall, Exact Performance of General Second-Order Processors for Gaussian Inputs, NUSC Technical Report 7035, Naval Underwater Systems Center, New London, CT, 15 October 1983.

7. I. S. Gradshteyn and I. M. Ryzhik, Table of Integrals, Series and Products, Academic Press, Inc., New York, NY, 1980.

Technical Report 8027
11 September 1987

Accurate Efficient Evaluation of Bessel Transform; Programs and Error Analysis

A. H. Nuttall

ABSTRACT

The method of Filon numerical integration for Fourier transforms is extended to Bessel transforms of the form

$$G(\omega) = \int_0^\infty dx \; J_0(\omega x) \; g(x),$$

for general g(x). Specifically, for the two cases where g(x) is approximated by (a) straight lines, or (b) parabolas, over abutting panels, the corresponding integrals in the Bessel transform $G(\omega)$ are evaluated exactly (within computer round-off error). Although these integrals cannot be expressed in closed form (as for Filon's case), a recursive procedure and an asymptotic expansion yield rapid accurate evaluation of the required quantities.

Programs are furnished for both cases (a) and (b) in BASIC. Furthermore, two versions of each are furnished: a faster one requiring considerable storage, and a slower one requiring very little storage. The presence and location of aliasing is predicted and its magnitude is investigated numerically. The error dependence on the panel width used in both cases (a) and (b) is established by means of numerical examples, one with a very fast decay with ω, the other with a very slow decay with ω. Comparisons with standard Trapezoidal and Simpson's rules reveal that the new procedures are error <u>maintenance</u> procedures, tending to keep the absolute error for larger ω comparable to that near $\omega = 0$, whereas the standard rules are subject to aliasing errors that become very significant for larger ω.

Extensions to more general Bessel transforms are possible and procedures for obtaining them are outlined.

TABLE OF CONTENTS

TABLE OF CONTENTS (Cont'd)

LIST OF ILLUSTRATIONS

LIST OF SYMBOLS

x	variable of integration, (2)
$g(x)$	function to be transformed, (2)
$J_0(u)$	zero-th order Bessel function, (2)
ω	transform variable, (2)
$G(\omega)$	Bessel transform of $g(x)$, (2)
x_ℓ	lower limit of integral, (11)
x_r	upper limit of integral, (11)
h	panel width, sampling increment, (12)
x_n	general sample point in x, figure 1
g_n	sample value $g(x_n)$, figure 1
$A(u)$	indefinite integral of J_0, (13)
$J_1(u)$	first order Bessel function, (14)
$B_0(u)$	auxiliary function, (16)
$B_1(u)$	auxiliary function, (17)
I_n	integral contribution, (18)
y	normalized variable, (19)
ℓ, r	left and right integer limits, (20)
Θ	product ωh, (22)
Λ	sampling increment in ω, (25)
k	integer location of sample in ω, (25)
K_1, K_2	limits on k, (25)
S_ℓ, S_r	auxiliary quantities, (31)
Q_ℓ, Q_r	auxiliary quantities, (31)
D_n, F_n, R_n	auxiliary sequences, (32)

LIST OF SYMBOLS (Cont'd)

a(b)c	sequence a, a+b, a+2b, ..., c-b, c, (33)
$\sum_{2}$	Summation over every other term, (30)
$I_0(u)$	zero-th order modified Bessel function, (40)

ACCURATE EFFICIENT EVALUATION OF BESSEL TRANSFORM; PROGRAMS AND ERROR ANALYSIS

INTRODUCTION

The method of Filon integration for Fourier transforms [1], [2; pages 408-409], [3; pages 67-75], [4; page 400], [5; page 890], [6; pages 62-66], [7]

$$\int_{-\infty}^{+\infty} dx \exp(i\omega x)\ g(x) \tag{1}$$

is well established and very useful for accurate numerical work. Instead of the standard Simpson's rule, which would approximate the complete integrand $\exp(i\omega x)\ g(x)$ by parabolas over abutting pairs of panels, Filon's method approximates only the function $g(x)$ by parabolas, and carries out the corresponding integrals in (1) analytically. These closed form integrals are then evaluated with computer aid. Since the exponential in (1) is being handled exactly for all ω, the hope is that the error of approximating (1) by means of Filon's method will be substantially the same for larger ω as for small ω (where all the error arises from approximating $g(x)$). That is, Filon's method is expected to be an error maintenance procedure, whereby the absolute error does not increase significantly with ω. Certainly that is not the case for the Trapezoidal and Simpson rules, where significant aliasing severely limits the accuracy of the results for larger ω.

An alternative simpler procedure to Filon's method for Fourier transforms is to approximate g(x) by straight lines over abutting panels, and again to evaluate the resultant integrals in (1) analytically in closed form. This (less-accurate) procedure is documented in [8; pages 418-419], for example.

Here, we will extend these two procedures to a Bessel transform of the form

$$G(\omega) = \int_0^\infty dx\ J_0(\omega x)\ g(x)\ , \tag{2}$$

where g(x) is an arbitary given function, and J_0 is the zeroth-order Bessel function. One of the major differences we encounter, relative to Filon's method, is that the resultant integrals cannot all be evaluated in closed form. In order to circumvent this problem, we use a combination of a downward recursion and an asymptotic expansion, which are limited in accuracy only by the inherent round-off error of the computer utilized, thereby obtaining an efficient useful procedure for numerical evaluation of the pertinent integrals and functions.

To give a physical application where the Bessel transform arises, consider that we are interested in two-dimensional Fourier transform

$$\iint_{-\infty}^{+\infty} dx\ dy\ \exp(iux + ivy)\ f_2(x,y)\ , \tag{3}$$

where function f_2 has isotropic behavior. That is, suppose the dependence of f_2 is solely on the distance from the origin of coordinates:

$$f_2(x,y) = f_1(\sqrt{x^2 + y^2})\ . \tag{4}$$

Then (3) becomes

$$\iint_{-\infty}^{+\infty} dx\, dy\, \exp(iux + ivy)\, f_1\left(\sqrt{x^2 + y^2}\right) =$$

$$= 2\pi \int_0^{\infty} dr\, J_0(\omega r)\, r\, f_1(r)\ , \tag{5}$$

where we changed to cylindrical coordinates and have defined

$$\omega = (u^2 + v^2)^{1/2}\ . \tag{6}$$

Thus, (5) is of the form of (2), upon identification of $g(x)$ as $x\ f_1(x)$.

Suppose in (3) that the f_2 dependence on x,y is more general than (4), namely of the form

$$f_2(x,y) = f_1\left(\left[\left(\frac{x - x_0}{a}\right)^2 + \left(\frac{y - y_0}{b}\right)^2 - 2\rho\left(\frac{x - x_0}{a}\right)\left(\frac{y - y_0}{b}\right)\right]^{1/2}\right)\ , \tag{7}$$

which allows for a general center point of symmetry x_0, y_0, as well as a tilted elliptical shape. Then substitution in (3) yields, after a cylindrical coordinate change, the result

$$\frac{2\pi ab}{(1 - \rho^2)^{1/2}} \exp(iux_0 + ivy_0) \int_0^{\infty} dr\, J_0(\omega r)\, r\, f_1(r)\ , \tag{8}$$

where now

$$\omega = \left[\frac{a^2u^2 + b^2v^2 + 2\rho abuv}{1 - \rho^2}\right]^{1/2}\ . \tag{9}$$

Again, the fundamental Bessel transform of the form of (2) results, where $g(x)$ is $x\, f_1(x)$.

On the other hand, if $G(\omega)$ is specified in (2) for $\omega > 0$, the corresponding solution to this integral equation is

$$g(x) = x \int_0^\infty d\omega\, J_0(x\omega)\, \omega\, G(\omega) \;, \tag{10}$$

which is again a Bessel transform of the form of (2).

Thus, we have presented several instances where the transform given by (2) is of interest and must be accomplished accurately for large as well as small arguments of the transform variable ω.

LINEAR APPROXIMATION

The integral of interest here is

$$G(\omega) = \int_{x_\ell}^{x_r} dx \; J_0(\omega x) \; g(x) \; , \tag{11}$$

where left-end point x_ℓ could be zero, and right-end point x_r could be taken so large that $g(x)$ is essentially zero for $x > x_r$. (If x_ℓ is negative, the values of g could be folded over to the positive x-axis, using $g(x) + g(-x)$ as the new integrand, since $J_0(\omega x)$ is even in x.) We break interval x_ℓ, x_r into a number of abutting panels, each of the same width h, and fit g(x) by straight lines over each of those panels. The fits for the left-end point and an abutting (internal) point x_n are depicted in figure 1, where it is temporarily presumed that the adjacent sample values of

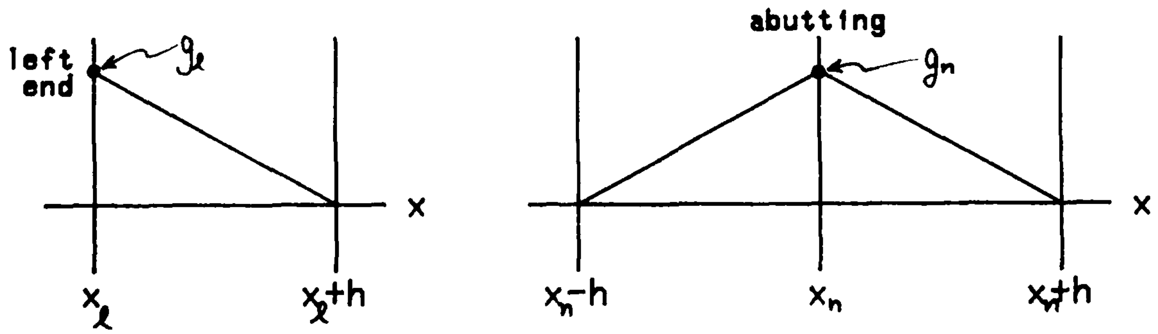

Figure 1. Linear Approximations to g(x)

function $g(x)$ are zero; this allows us to isolate the contribution of each sample of $g(x)$ to the total desired in (11). The straight lines pass through the function value $g_n = g(x_n)$ at sample value x_n, and are zero at the adjacent sample points. h is the sampling increment in x applied to $g(x)$. The situation at the right end is the mirror image of that at the left end, depicted in figure 1.

If ω is zero in (11), the approximation afforded to the integral by means of figure 1 is obviously

$$G(0) \cong h\left[\frac{1}{2}\, g_\ell + g_{\ell+1} + \ldots + g_{r-1} + \frac{1}{2}\, g_r\right] =$$

$$= h\left[\frac{1}{2}\, g(x_\ell) + g(x_{\ell+1}) + \ldots + g(x_{r-1}) + \frac{1}{2}\, g(x_r)\right] \quad \text{for } \omega = 0 \,, \tag{12}$$

which is just the Trapezoidal rule. For $\omega > 0$, considerably more effort is required; there is no need to consider $\omega < 0$, since $J_0(\omega x)$ is even in ω. Before we get into that derivation, we must introduce some auxiliary functions.

SPECIAL FUNCTION DEFINITIONS

Define the integral

$$A(u) = \int_0^u dt\ J_0(t) \ . \tag{13}$$

This function cannot be evaluated in closed form; a table of A(u) is available in [5; pages 492-493]. On the other hand, the integral

$$\int_0^u dt\ t\ J_0(t) = u\ J_1(u) \tag{14}$$

is immediately available by use of [5; 9.1.30]. And two integrations by parts, coupled with (13), yields the result

$$\int_0^u dt\ t^2\ J_0(t) = u^2\ J_1(u) + u\ J_0(u) - A(u)\ . \tag{15}$$

We will also find use for the auxiliary functions

$$B_0(u) \equiv A(u) - u\ J_0(u) = \int_0^u dt\ t\ (u - t)\ J_0(t)\ , \tag{16}$$

and

$$B_1(u) \equiv A(u) - J_1(u) = \int_0^u dt \left(1 - \frac{t}{u}\right) J_0(t)\ . \tag{17}$$

All of these functions, A, B_0, B_1, are zero at the origin and are odd. Numerical evaluation of these functions is considered in appendix A.

ABUTTING POINT

For an abutting (internal) point x_n in the interval (x_ℓ, x_r), as depicted on the right-hand side of figure 1, the contribution to integral (11), due to this single sample point $g_n = g(x_n)$, is

$$I_n = \int_{x_n - h}^{x_n} dx\ J_0(\omega x)\ g_n\ (1 + y) + \int_{x_n}^{x_n + h} dx\ J_0(\omega x)\ g_n\ (1 - y)\ , \tag{18}$$

where we have defined

$$y = \frac{x - x_n}{h}\ . \tag{19}$$

We now assume that the n-th sample point x_n is taken such that

$$x_n = n\ h \quad \text{for } \ell \le n \le r\ . \tag{20}$$

This makes

$$x_\ell = \ell h, \quad x_r = rh, \quad \text{i.e. } \frac{x_r}{x_\ell} = \frac{r}{\ell} = \text{rational}\ . \tag{21}$$

This constitutes a restriction on ratio x_r/x_ℓ in (11); it has been adopted here in order to minimize the number of calculations of the Bessel function J_0 later, when we consider the multiple values of ω desired for (11). (The procedure presented here can be extended to the general case where x_ℓ is *arbitrary and* $x_n = x_\ell + nh$, if desired.) If x_ℓ is zero, then the choice in (20) is no restriction at all.

APPROXIMATION TO INTEGRAL

An important parameter in this numerical integration procedure is the quantity

$$\Theta = \omega h \tag{22}$$

which is the product of "radian frequency" ω and the sampling increment h. As we shall see, values of Θ near π and 2π will constitute points of considerable aliasing; see [4; page 400] for a discussion of the Fourier transform case.

When the procedure in (18)-(19) is extended to include the left-end and right-end points of integral (11), and the various integrals evaluated with the help of (13)-(17), the total approximation is given by appendix B in several alternative forms, one of which is (B-7):

$$\begin{aligned}\omega\, G(\omega) \cong {} & \left[\ell g_{\ell+1} - (\ell + 1)g_{\ell}\right] B_1(\ell\Theta) - g_{\ell}\, J_1(\ell\Theta) + \\ & + \left[r\, g_{r-1} - (r - 1)g_r\right] B_1(r\Theta) + g_r\, J_1(r\Theta) + \\ & + \sum_{n=\ell+1}^{r-1} n\left[g_{n+1} - 2g_n + g_{n-1}\right] B_1(n\Theta) \ ,\end{aligned} \tag{23}$$

where

$$g_n = g(x_n) = g(nh) \ . \tag{24}$$

Reasons for this grouping of terms, including speed of execution and storage requirements, are discussed below.

SAMPLING INCREMENT FOR ω

When output variable ω in integral (11) is restricted to multiples of a sampling increment Δ, according to

$$\omega = k\Delta \quad \text{for } 1 \le K_1 \le k \le K_2 \ , \tag{25}$$

then $n\Theta = nk\Delta h$, meaning that the arguments of the $B_1(u)$ function in (23) are limited to integer multiples of $h\Delta$, the product of the sampling increment in input variable x and the sampling increment in output (transform) variable ω. The explicit relationship for $G(\omega) = G(k\Delta)$ is given by specializing (23) to the values (24), thereby obtaining

$$\begin{aligned} k\Delta\ G(k\Delta) \cong &\left[\ell\, g_{\ell+1} - (\ell+1)g_\ell\right] B_1(\ell k\Delta h) - g_\ell\, J_1(\ell k\Delta h) + \\ &+ \left[r\, g_{r-1} - (r-1)g_r\right] B_1(rk\Delta h) + g_r\, J_1(rk\Delta h) + \\ &+ \sum_{n=\ell+1}^{r-1} n\left[g_{n+1} - 2g_n + g_{n-1}\right] B_1(nk\Delta h) \quad \text{for } k \ge 1\ . \end{aligned} \tag{26}$$

COMPUTATION TIME CONSIDERATIONS

Thus, we need evaluate $B_1(u)$ only at $u = m\Delta h$, where m is an integer. Furthermore, not all values of integer m will be encountered as n and k sweep out their respective values given by (20) and (25). And since $B_1(u)$, defined in (17) and (13), is the most time-consuming aspect of the computation of (26), it behooves us <u>not</u> to compute $B_1(m\Delta h)$ at values of m that will not be encountered, and <u>not</u> to recompute $B_1(m\Delta h)$ at values of m

that are encountered more than once. This latter situation arises when m is highly composite; for example, $m = 12 = 4*3 = 6*2 = 12*1$ could be encountered several times as n and k vary in (26).

In order to incorporate this time-saving feature into the Bessel integral evaluations required by (26), the values of $B_1(nk\Delta h)$ are computed only once and stored in a one-dimensional array at linear location $m = nk$. Unfortunately, this speed-up feature is achieved at the expense of considerable storage, for if n and k range up to N and K, respectively, the one-dimensional storage array must have NK cells, of which most are empty when N and K are large.

When N and K are so large that storage is not feasible, such as when x_r in (11) is large, and large ω is desired in (25), then the alternative procedure of direct brute-force evaluation of (26) for $B_1(nk\Delta h)$, repeated as often as necessary, but without storage, is employed. Recomputation of $B_1(m\Delta h)$ for some m values occurs, but evaluation at unused m values never does.

Thus we have two alternatives and two corresponding programs for (26): one faster routine which may require considerable storage, and a slower procedure utilizing very little storage. The former is recommended when feasible, while the latter furnishes a back-up position. Programs for both procedures are listed in appendix B.

BEHAVIOR FOR SMALL Θ

When Θ is small, differences of functions with similar values are required in (23), as may be observed by the linear ω dependence on the left-side. The appropriate series development for this linear approximation approach to (11) is given in (B-11)-(B-12), through order Θ^2. Additional terms to order Θ^4, Θ^6 can be derived by extending the approach given there; however, an easier technique will be developed in the next section.

PARABOLIC APPROXIMATION

The integral of interest is again

$$G(\omega) = \int_{x_\ell}^{x_r} dx \; J_0(\omega x) \; g(x) \; . \tag{27}$$

However, now we approximate g(x) by parabolas over abutting pairs of panels, each of width h. The fits for a mid-point, an abutting point, the left-end point, and the right-end point are illustrated in figure 2. Again, the

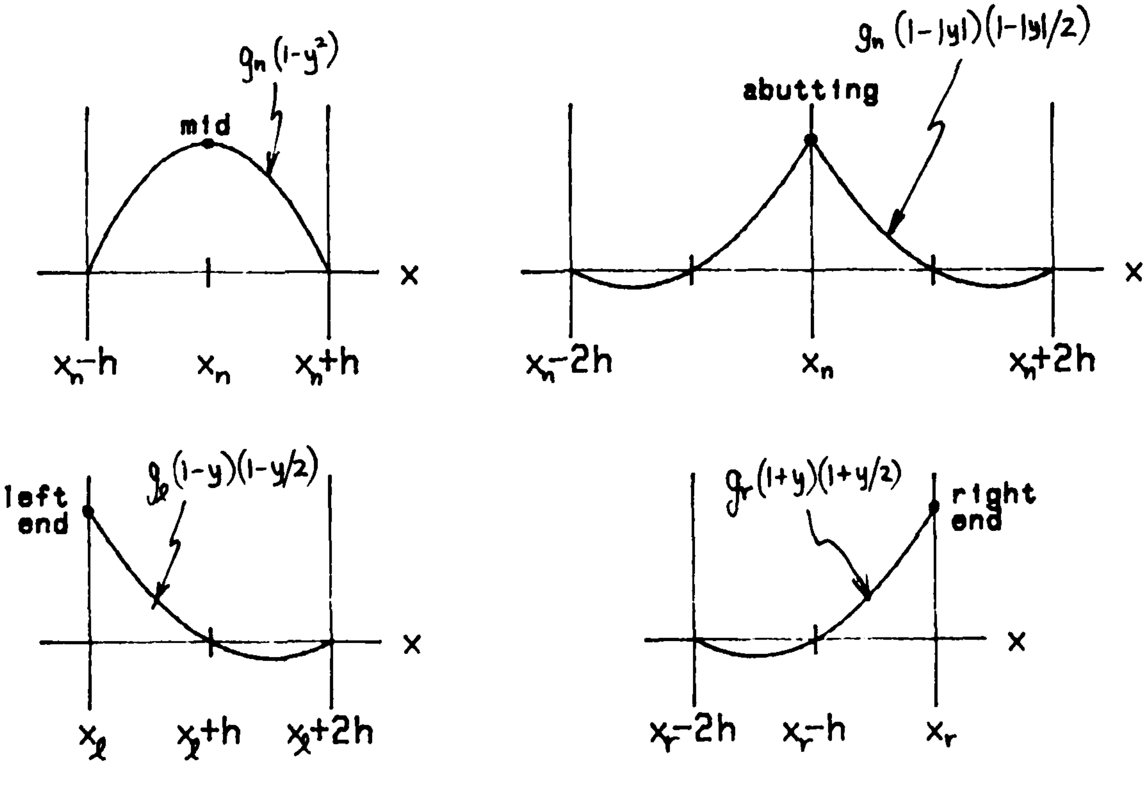

Figure 2. Parabolic Approximations to g(x)

contribution of each sample value $g_n = g(x_n)$ is isolated, by temporarily presuming that the neighboring sample values of g(x) are zero. The variable y in figure 2 is again the normalized quantity

$$y = \frac{x - x_n}{h} , \tag{28}$$

where h is the sampling increment in x applied to g(x).

If ω is zero in (27), the approximation afforded to the integral by means of figure 2 is

$$\begin{aligned} G(0) &\cong \frac{h}{3}\left[g_\ell + 4g_{\ell+1} + 2g_{\ell+2} + \ldots + 2g_{r-2} + 4g_{r-1} + g_r\right] = \\ &= \frac{h}{3}\left[g(x_\ell) + 4g(x_{\ell+1}) + 2g(x_{\ell+2}) + \ldots + 2g(x_{r-2}) + 4g(x_{r-1}) + g(x_r)\right] , \end{aligned} \tag{29}$$

which is Simpson's rule.

APPROXIMATION TO INTEGRAL

Since J_0 in (27) is even in ω, we only need to consider $\omega > 0$ in the following. The derivation of the approximation to integral (27), by means of the parabolic fits in figure 2, is carried out in appendix C, culminating in (C-10)-(C-12):

$$2\omega\, G(\omega) = \frac{1}{\theta^2} S_\ell\, B_0(\ell\theta) - Q_\ell\, B_1(\ell\theta) - 2g_\ell\, J_1(\ell\theta) -$$

$$- \frac{1}{\theta^2} S_r\, B_0(r\theta) + Q_r\, B_1(r\theta) + 2g_r\, J_1(r\theta) +$$

$$+ \frac{1}{\theta^2} \sideset{}{'}\sum_{n=\ell+2}^{r-2} D_n\, B_0\,(n\theta) - \sideset{}{'}\sum_{n=\ell+2}^{r-2} R_n\, B_1\,(n\theta)\ . \qquad (30)$$

The auxiliary sequences utilized in (30) are defined below:

$$S_\ell = g_{\ell+2} - 2g_{\ell+1} + g_\ell$$

$$S_r = g_r - 2g_{r-1} + g_{r-2}$$

$$Q_\ell = \ell(\ell+1)g_{\ell+2} - 2\ell(\ell+2)g_{\ell+1} + (\ell+2)(\ell+1)g_\ell$$

$$Q_r = (r-2)(r-1)g_r - 2r(r-2)g_{r-1} + r(r-1)g_{r-2} \qquad (31)$$

and

$$\left.\begin{aligned} D_n &= g_{n+2} - 2g_{n+1} + 2g_{n-1} - g_{n-2} \\ F_n &= g_{n+2} - 4g_{n+1} + 6g_n - 4g_{n-1} + g_{n-2} \\ R_n &= n^2 D_n + nF_n \end{aligned}\right\} \quad \text{for } n = (\ell+2)(2)(r-2)\ . \qquad (32)$$

The functions $B_0(u)$ and $B_1(u)$ are those defined in (13)-(17), and the slash on the summation symbol in (30) denotes skipping every other term, after starting at $n = \ell + 2$. A shorthand notation that will be used here is

$$n = \ell+2,\ \ell+4\ ,\ldots,\ r-4,\ r-2 = (\ell+2)(2)(r-2)\ . \qquad (33)$$

Several important observations should be made about the result in (30)-(32). The four quantities in (31) are evaluated only once at the end points $n = \ell$ and r. The sequences in (32) must be evaluated at all the points listed in (33), that is, at every <u>other</u> interior point. All of these computations should be done once and stored, when given the function $g(x)$, the limits x_ℓ, x_r, and sampling increment h, prior to ever considering which ω values will be of interest in (30). Input function $g(x)$ must be evaluated at all $x = x_n = nh$ for $n = \ell(1)r$.

The time-consuming calculations of $B_0(u)$ and $B_1(u)$ in (30) are only necessary at the values $u = n\Theta$ for $n = \ell(2)r$, and need not be evaluated at any of the in-between points $n = (\ell + 1)(2)(r - 1)$. The Bessel function $J_1(u)$ need only be evaluated at end points $u = \ell\Theta$ and $r\Theta$; however, this quantity shows up as a free by-product of evaluating $B_0(u)$ and $B_1(u)$, by the method indicated in appendix A.

SAMPLING INCREMENT FOR ω

When output variable ω in desired integral (27) is restricted to multiples of a sampling increment Δ, according to

$$\omega = k\Delta \quad \text{for} \quad 1 \le K_1 \le k \le K_2 \; , \tag{34}$$

then

$$\Theta = \omega h = k\Delta h \; , \tag{35}$$

and (30) takes on the form

$$2k\Delta \; G(k\Delta) \cong$$

$$= \frac{1}{(k\Delta h)^2} \; S_\ell \; B_0(\ell k\Delta h) - Q_\ell \; B_1(\ell k\Delta h) - 2g_\ell \; J_1(\ell k\Delta h) -$$

$$- \frac{1}{(k\Delta h)^2} \; S_r \; B_0(rk\Delta h) + Q_r \; B_1(rk\Delta h) + 2g_r \; J_1(rk\Delta h) +$$

$$+ \frac{1}{(k\Delta h)^2} \sum_{n=\ell+2}^{r-2} D_n \; B_0(nk\Delta h) - \sum_{n=\ell+2}^{r-2} R_n \; B_1(nk\Delta h) \; . \qquad (36)$$

At this point, the discussion in the sequel to (26) is directly relevant and should be reviewed. The only change in the presentation is to replace $B_1(u)$, there, by both $B_0(u)$ and $B_1(u)$ here. We again end up with two alternatives and two corresponding programs for evaluation of (36): one faster routine which may require considerable storage, and a slower procedure utilizing very little storage. Programs for both procedures are listed in appendix C.

BEHAVIOR FOR SMALL Θ

When Θ is small, differences of functions with similar values are required in (30), as may be observed by the linear ω dependence on the left side and the $1/\Theta^2$ dependence on the right side. This behavior is also typical for Filon's method, and indicates the need for a series expansion in powers of Θ for the right-hand side of (30) when Θ is small; see [5; (25.4.53)], for example. The appropriate series development for this parabolic approximation approach to (27) is given in (C-15)-(C-17), through order Θ^2. Additional terms to order Θ^4, Θ^6 can be derived by an obvious extension of the approach given there.

EXAMPLES

Two examples will be considered in this section; the first is a Rayleigh function,

$$g(x) = x \exp(-x^2/2) \quad \text{for } x > 0 \;, \tag{37}$$

for which Bessel transform (11) is [9; 6.631 4]

$$G(\omega) = \exp(-\omega^2/2) \;. \tag{38}$$

The second is a Gaussian function,

$$g(x) = \exp(-x^2) \quad \text{for } x > 0 \;, \tag{39}$$

leading to [9; 6.618 1]

$$G(\omega) = 1/2\sqrt{\pi}\, \exp(-\omega^2/8)\; I_0(\omega^2/8) \;. \tag{40}$$

These two examples are very different, in that transform (38) decays very quickly for large ω, whereas (40) decays very slowly for large ω. In fact, for the latter case [5; 9.7.1],

$$G(\omega) \sim 1/\omega \quad \text{as } \omega \to +\infty \;. \tag{41}$$

This difference will enable us to investigate both absolute and relative errors of the approximate numerical integration procedures developed earlier, over a wide range of values of ω.

ALIASING

The Bessel function J_0 is rather similar to a sinusoid; in fact, for large z [9; 9.2.1],

$$J_0(z) \sim \left(\frac{2}{\pi z}\right)^{1/2} \cos\left(z - \frac{\pi}{4}\right) \quad \text{as } z \to +\infty. \tag{42}$$

Then when argument x in transform (11) is sampled at increment h, we encounter the behavior

$$J_0(\omega x_n) = J_0(\omega hn) = J_0(\Theta n) \sim \left(\frac{2}{\pi \Theta n}\right)^{1/2} \cos\left(\Theta n - \frac{\pi}{4}\right) \tag{43}$$

for large Θn. Now when $\Theta = 2\pi$, the cosine yields the same values as for $\Theta = 0$; this leads us to expect larger errors for the numerical integration procedure when Θ is near 2π.

For a Fourier transform, this aliasing effect was studied quantitatively in [10; appendix A] for both the Trapezoidal rule and Simpson's rule. The former rule was shown to have a large aliasing lobe at $\Theta = \omega h = 2\pi$, while the latter rule had an additional large lobe at $\Theta = \pi$, due to the alternating character of the Simpson weights; see [10; (A-6) and (A-8)]. This leads us to anticipate that the linear approximation procedure developed here for Bessel transform (11) will be subject to aliasing near

$\Theta = 2\pi$, while the parabolic approximation will be degraded earlier, namely near $\Theta = \pi$. This will be borne out by the numerical examples to follow.

GRAPHICAL RESULTS

The Bessel transform numerical integration rule for the linear approximation to g(x) is given by (23) or (26), while the rule for the parabolic approximation to g(x) is given by (30) or (36). The exact transforms (38) and (40), and the absolute errors associated with these two rules, are depicted in figures 3 and 4 for the Rayleigh and Gaussian functions g(x) of (37) and (39), respectively, with sampling increment $h = .1$. The ordinates in all figures are the logarithm to the base 10 of the corresponding results, while the abscissas are linear in ω or Θ. The upper limit, x_r, of integration in (2) or (11) is taken large enough to guarantee a negligible contribution (less than 1E-20) to the truncation error.

In figure 3, the error for the parabolic fits is initially lower (for small ω) than for the linear fits; however, the linear error decays rapidly with ω, and stays below the parabolic error for larger ω. Both absolute errors flatten out and are not increasing with ω, at least for this range of ω values. The maximum value of Θ is .8, as indicated in the figure.

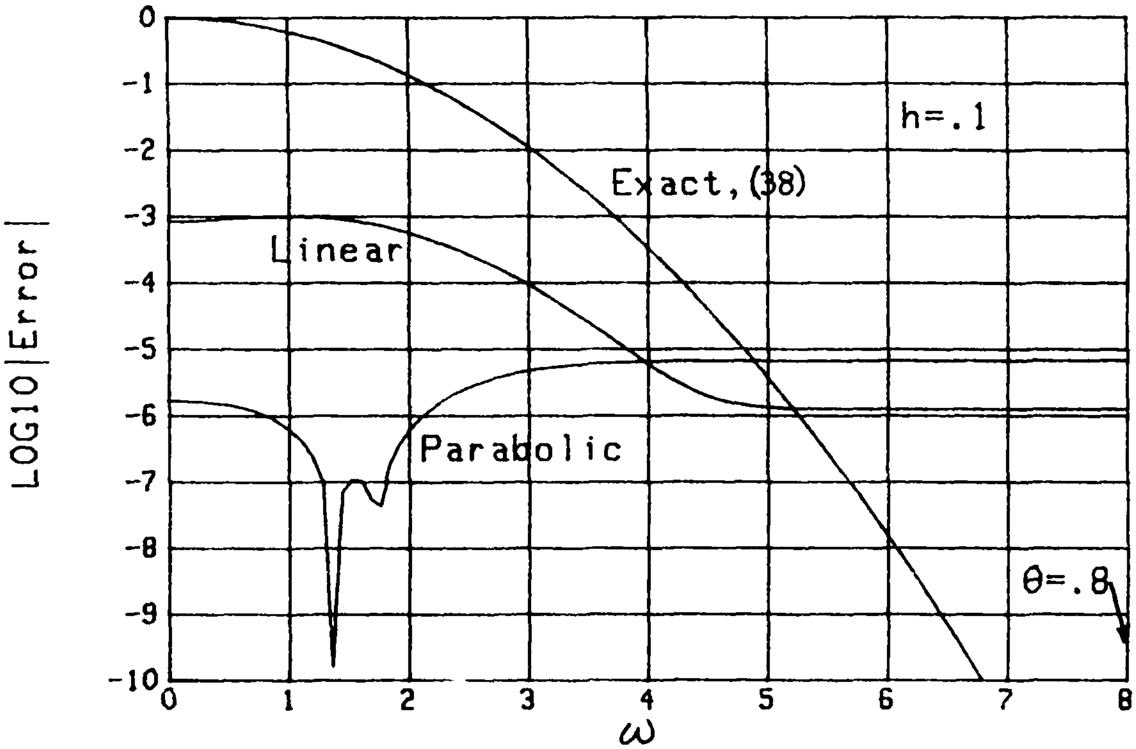

Figure 3. Errors for Rayleigh Function g(x)

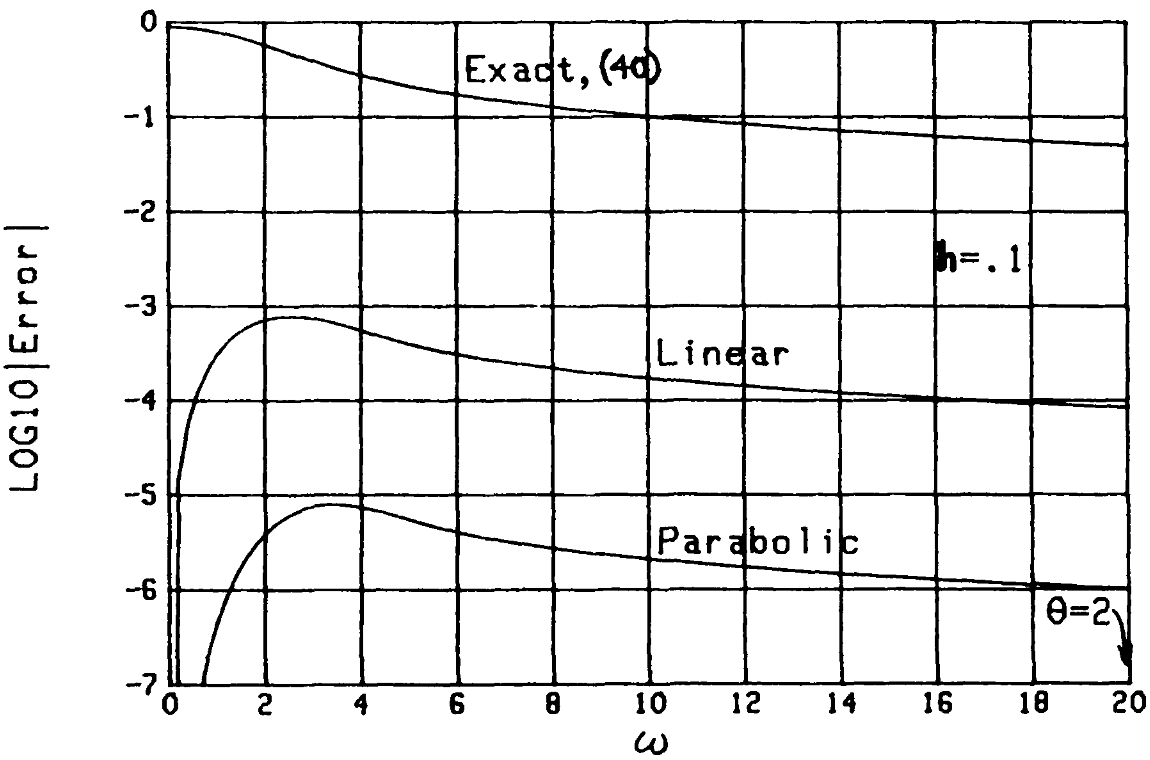

Figure 4. Errors for Gaussian Function g(x)

For the Gaussian function g(x), the parabolic error in figure 4 is everywhere less than the linear error. Both errors near and at $\omega = 0$ are extremely small; this fortuitous result for the linear fits is fully explained in [6; pages 92-93], especially in the paragraph under (3.4.5). It has to do with the fact that the integrand in (11) for this Gaussian case, namely $J_0(\omega x)\ \exp(-x^2)$, has zero odd derivatives at the limits of integration. This is not the case for the Rayleigh function; hence the much larger errors at $\omega = 0$ in figure 3 result.

COMPARISON OF PROCEDURES

To demonstrate the benefits to be accrued from the fitting procedures derived in this study, a comparison of the absolute errors for four different procedures is presented in figure 5 for the Rayleigh function (37). The sampling increment in x is h = .03. The variable ω now covers the range (0,120); the point where $\theta = \pi$ is indicated by a tic mark on the abscissa.

The Trapezoidal result is obtained by applying it to the <u>complete</u> integrand $J_0(\omega x)\ g(x)$ of (11). The error is essentially constant for all ω, including the region near $\theta = \pi$; thus, as expected, aliasing is not significant at $\theta = \pi$ for the Trapezoidal rule.

Application of the standard Simpson's rule to the complete integrand of (11) yields a very small error near $\omega = 0$, but a rapidly increasing error with ω, and a very large aliasing lobe centered around $\theta = \pi$. This confirms the expectations presented earlier in this section.

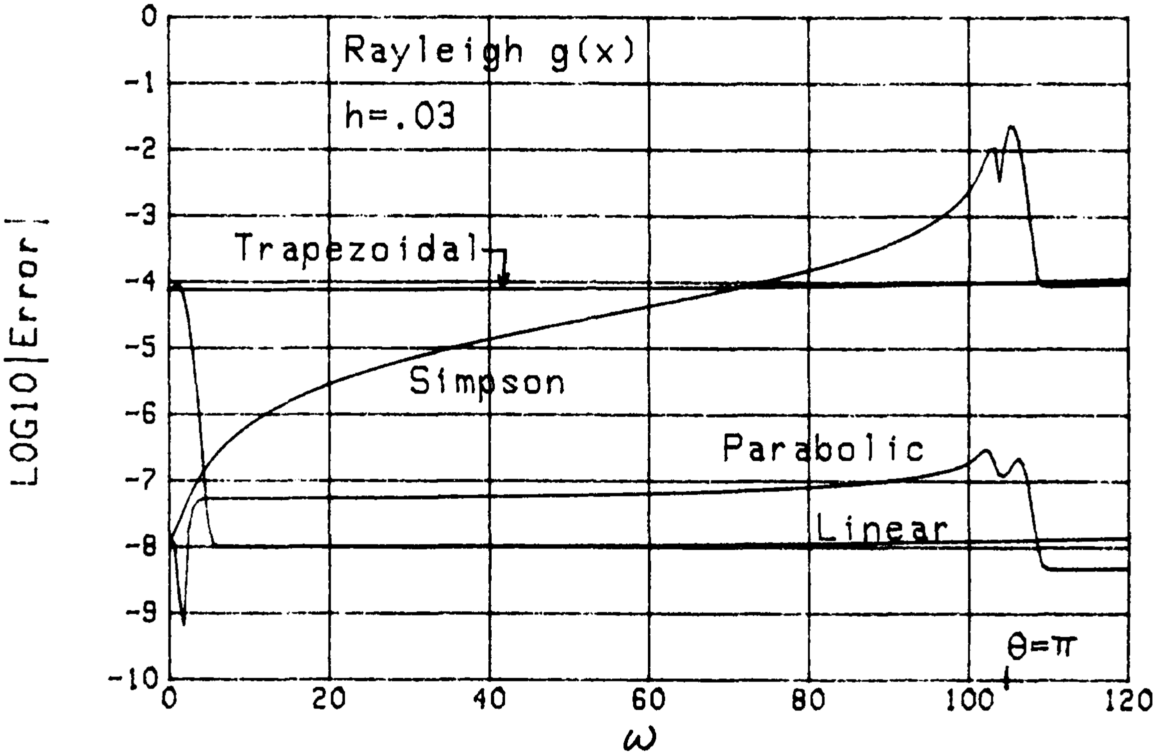

Figure 5. Errors for Four Procedures; $\omega < 120$

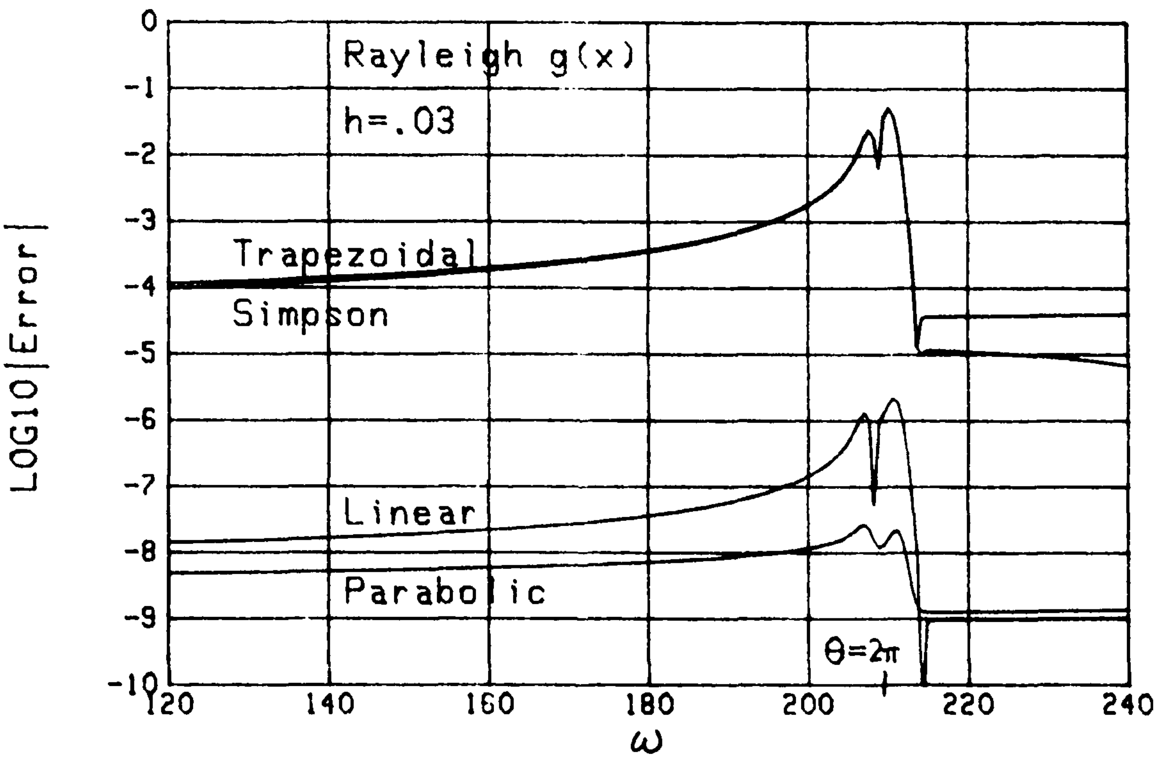

Figure 6. Errors for Four Procedures; $\omega > 120$

For the case of linear fits to g(x), rather than $J_0(\omega x)$ g(x), the error drops dramatically, by four orders of magnitude as ω increases, similar to figure 3. Furthermore, there is no aliasing at $\theta = \pi$.

The situation for the parabolic fits is that the absolute error starts out small and remains so, for all $\omega < 120$, there being a slight aliasing effect near $\theta = \pi$. However, it is 5 orders of magnitude smaller than the Simpson error in this region of ω.

The results in figure 6 extend the abscissa to cover the range of (120,240) in ω; that is, these curves are an extension of those in figure 5. Now all rules suffer aliasing in the neighborhood of $\theta = 2\pi$. The absolute error for the linear procedure increases by 2 orders of magnitude near $\theta = 2\pi$, while the parabolic error is just slightly larger; however, the latter is 6 orders of magnitude better than the standard Trapezoidal and Simpson rules for numerical integration. All of these results confirm the predicted presence and location of aliasing discussed earlier.

ERROR DEPENDENCE ON SAMPLING INCREMENT

In figure 7, we investigate the dependence of the error on increment h employed to sample x in (11). Here we apply the linear fit procedure to the Rayleigh function (37). The absolute error for small ω (< 2) decreases by a factor of 4 as h is halved; that is, the large error bump near $\omega = 0$ behaves as h^2 for small increments h. On the other hand, for larger ω (> 5),

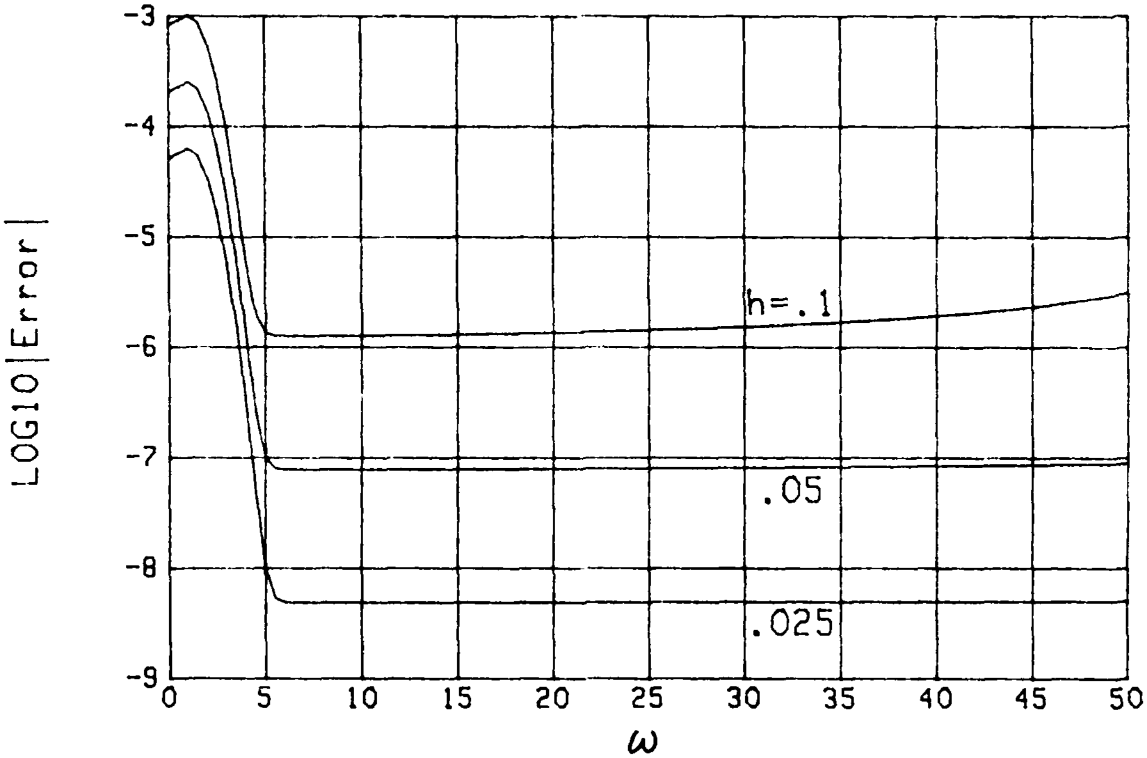

Figure 7. Linear Procedure, Rayleigh g(x)

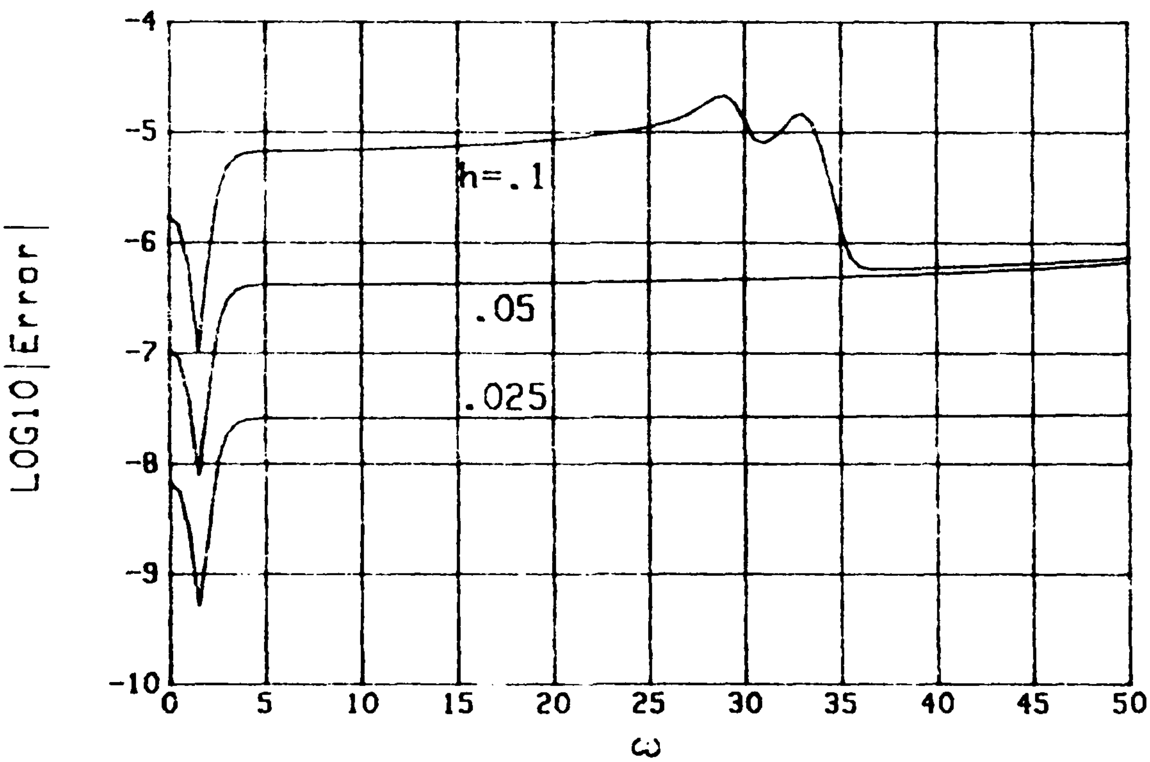

Figure 8. Parabolic Procedure, Rayleigh g(x)

the error decreases by a factor of 16 when h is halved; that is, the "saturation" level of error behaves as h^4 for small h. The slight flare in the error curve near $\omega = 50$, for $h = .1$, is an indication of the beginning of aliasing; that is, $\Theta = 5$ here, which is near the $\Theta = 2\pi$ location.

Still considering the Rayleigh function (37), but now switching to the parabolic procedure, the results in figure 8 demonstrate that the error drops by a factor of 16 as h is halved; thus, the error dependence is h^4 for all ω. The wiggles in the $h = .1$ curve near $\omega = 30$ are due to aliasing, since $\Theta = \pi$ for $\omega = 10\pi = 31.4$.

When the function g(x) is changed to the Gaussian example of (39), and the linear fitting procedure is employed, the errors are depicted in figure 9. Here, the error dependence is according to h^2 for all ω, until aliasing sets in. Aliasing is present in the $h = .1$ curve near $\omega = 64$, since $\Theta = 2\pi$ at $\omega = 62.8$ for that curve. Comparison of these errors with the exact answer in figure 4 reveals that the relative error is constant in the range $4 < \omega < 56$.

When the parabolic procedure is used instead on the Gaussian example, the error dependence is again according to h^4, until aliasing becomes dominant. The aliasing lobes in the $h = .1$ curve in figure 10 are centered at $\Theta = \pi$ and 2π, as before. The large increase in the error for the $h = .025$ curve, when ω exceeds 50, is a feature not seen previously. It may be due to the sum of distant aliasing of sidelobes which decay very slowly

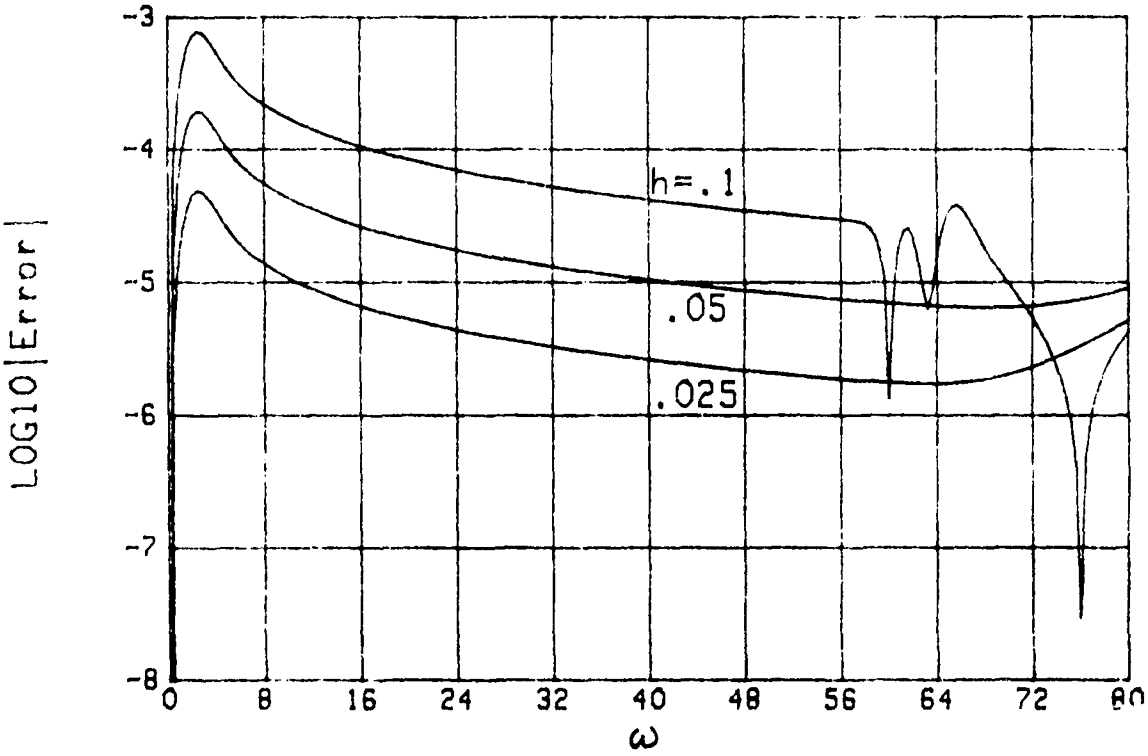

Figure 9. Linear Procedure, Gaussian g(x)

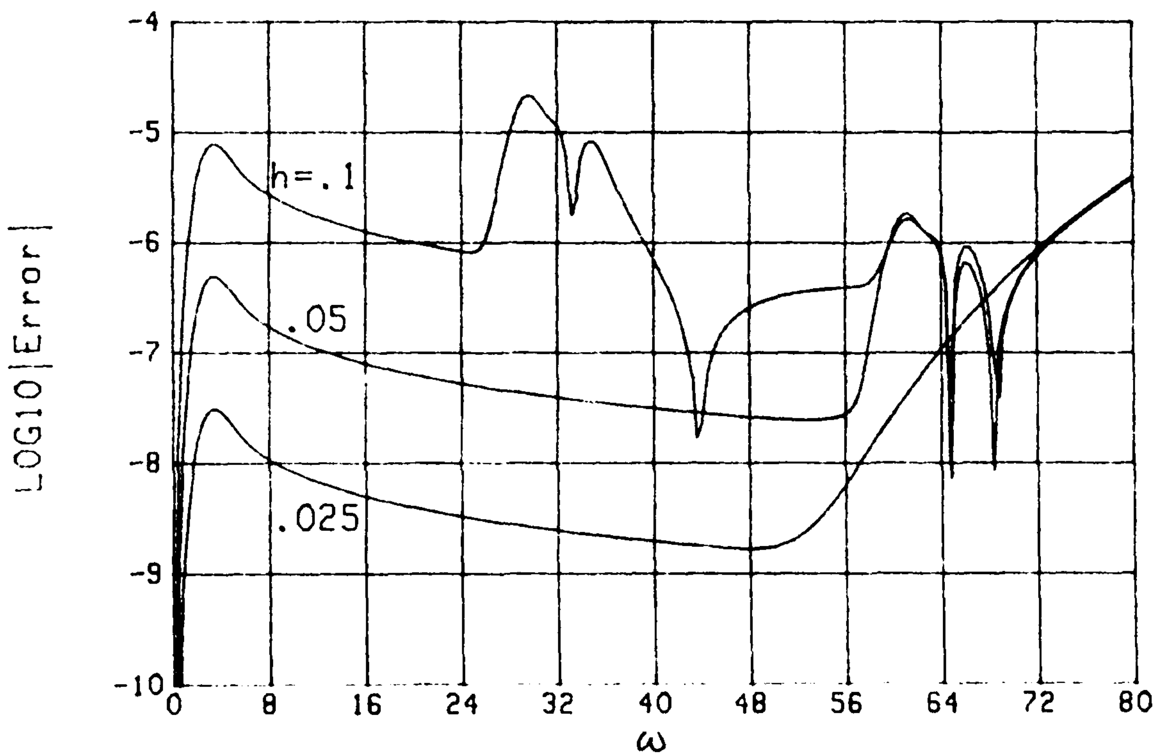

Figure 10. Parabolic Procedure, Gaussian g(x)

with ω; in fact, from (41), the exact answer only decays as $1/\omega$. The rapid decay of the Rayleigh transform, (38), apparently precluded this type of error from appearing in any of the numerical cases considered here for the Rayleigh $g(x)$.

SUMMARY

There is a marked difference between the form of these results and the Filon equations; namely, the term multiplying sample value $g_n = g(x_n)$ (in (B-3), for example) varies with n in such a fashion that no simplification or factoring is possible. In order to better explain this complication, let us investigate the evaluation of (18) when $J_o(\omega x)$ is replaced by $\exp(i\omega x)$; that is, consider evaluation of a Fourier transform, rather than a Bessel transform, for the moment. When the linear fits to g(x) in (18) are then integrated, there follows

$$I_n = g_n\, h \exp(in\Theta) \left[\frac{\sin(\Theta/2)}{\Theta/2}\right]^2 . \tag{44}$$

But the bracketed term here is a common factor (independent of n) that can be removed from the summation on n. This fortuitous simplification does not hold for the corresponding result (B-3) here, because whereas exp(iu) is periodic, $J_o(u)$ and A(u) are not.

In an effort to recover some of this loss in execution time, we therefore grouped the terms in (B-6) in an alternative form, pivoted around $B_1(n\Theta)$ rather than g_n; see (B-7). Perhaps another rearrangement of terms would be more advantageous for some purposes.

It is possible to extend the results here to other Bessel transforms. For example, suppose we are interested in the evaluation of first-order transform

$$\int dx \; J_1(\omega x) \; g(x) \; , \tag{45}$$

and we approximate g(x) either by straight lines or parabolas. The integrals in (13)-(15) are then replaced by

$$\int_0^u dt \; J_1(t) = 1 - J_0(u) \; ,$$

$$\int_0^u dt \; t \; J_1(t) = B_0(u) \; ,$$

$$\int_0^u dt \; t^2 \; J_1(t) = u^2 \; J_2(u) = 2u \; J_1(u) - u^2 \; J_0(u) \; , \tag{46}$$

where we used [5; (11.1.6) and (9.1.30)] and (16). Since all of these terms have already been encountered here, extension to transform (45) would not be difficult.

For the evaluation of the alternative transform

$$\int dx \; \frac{J_1(\omega x)}{x} \; g(x) \; , \tag{47}$$

we need the additional result [5; (11.1.1)]

$$\int_0^u dt\, \frac{J_1(t)}{t} = \frac{4}{u} \sum_{k=1}^{\infty} k\, J_{2k}(u) =$$

$$= \frac{4}{u}\Big[J_2(u) + 2\, J_4(u) + 3\, J_6(u) + \ldots\Big] . \qquad (48)$$

But this type of term is easily evaluated by means of the downward recurrence technique given in appendix A. In fact, immediately following the single line Se = Se + E, we have merely to add the line Sx = Sx + Se; when the downward recurrence is completed, the bracketed term in (48) results in storage location Sx (after the scaling correction).

APPENDIX A

NUMERICAL EVALUATION PROCEDURE FOR BESSEL INTEGRALS

The three fundamental Bessel integrals that must be evaluated are given by (13)-(17) as

$$A(u) = \int_0^u dt\ J_0(t)\ , \tag{A-1}$$

$$B_0(u) = A(u) - u\ J_0(u) = \int_0^u dt\ t\ (u - t)\ J_0(t)\ , \tag{A-2}$$

$$B_1(u) = A(u) - J_1(u) = \int_0^u dt\left(1 - \frac{t}{u}\right) J_0(t)\ . \tag{A-3}$$

By expanding J_0 in a power series [5; (9.1.10)], and integrating term by term, there follows from (A-1),

$$A(u) = \frac{u}{2}\sum_{k=0}^{\infty} \frac{(-u^2/4)^k}{k!\ k!\ (k+\frac{1}{2})} = u - \frac{u^3}{12} + \frac{u^5}{320} - \dots\ . \tag{A-4}$$

When this result is coupled with the series expansions of J_0 and J_1 in (A-2) and (A-3) respectively, there follows

$$B_0(u) = \frac{u^3}{4} \sum_{k=0}^{\infty} \frac{(-u^2/4)^k}{k!\,(k+1)!\,(k+\frac{3}{2})} = \frac{u^3}{6} - \frac{u^5}{80} + \frac{u^7}{2688} - \cdots \tag{A-5}$$

and

$$B_1(u) = \frac{u}{4} \sum_{k=0}^{\infty} \frac{(-u^2/4)^k}{k!\,(k+1)!\,(k+\frac{1}{2})} = \frac{u}{2} - \frac{u^3}{48} + \frac{u^5}{1920} - \cdots . \tag{A-6}$$

Although these power series could be used for small and moderate values of u, they are not useful for large u, due to the loss of significant digits caused by the alternating character of series (A-4)-(A-6). In fact, we will find that a downward recurrence will yield all the values of A, B_0, B_1, J_0, and J_1 very efficiently for small u, while an asymptotic expansion is equally attractive for large u.

DOWNWARD RECURRENCE

We start with [5; (11.1.2)] and (A-1):

$$A(u) = 2[J_1(u) + J_3(u) + J_5(u) + \ldots] . \tag{A-7}$$

Thus if we can evaluate all the odd-order Bessel functions, we can get A(u) from their sum. Also, $B_0(u)$ and $B_1(u)$ follow immediately from (A-2) and (A-3), if we can additionally get $J_0(u)$.

But the Bessel functions satisfy the downward recurrence [5; (9.1.27), line 1]

$$J_m(u) = \frac{2}{u}(m+1)\, J_{m+1}(u) - J_{m+2}(u) \qquad \text{(A-8)}$$

for $m \geq 0$. This recurrence can be started by guessing at $J_M(u) = 0$, $J_{M-1}(u) = 1E\text{-}250$ for example, and evaluating downward via (A-8) to $m = 0$. Since the error increases much slower than the size of the terms in (A-8) [5; table 9.4], the relative error of the terms is very small for the smaller values of m, if M is chosen large enough to start with. In order to accurately establish the absolute level of the sequence of $\{J_m\}$ values, we then use the check sum formula [5; (9.1.46)]

$$J_0(u) + 2[J_2(u) + J_4(u) + \ldots] = 1\ . \qquad \text{(A-9)}$$

In order to realize 15 decimal accuracy in A, B_0, B_1, J_0, J_1, it has been found sufficient to choose even integer M as

$$M = M(u) = 2\ \mathrm{INT}\left(20 + .56u - \frac{175}{12+u}\right) + 12 \quad \text{for } 0 \leq u < 45\ . \qquad \text{(A-10)}$$

While conducting the downward recurrence on m in (A-8), an even sum of $J_M + J_{M-2} + \ldots$, and an odd sum of $J_{M-1} + J_{M-3} + \ldots$, are maintained. After completion to $m = 0$, the even sum is subject to constraint (A-9), in order to establish the scale factor that must be applied to all the desired outputs; this is to correct for the initial arbitrary (incorrect) guess of $J_{M-1}(u) = 1E\text{-}250$. With this scale factor in hand, the odd sum in (A-7) can then be modified by means of one multiplication for the correct absolute level for A(u). Since the last two quantities yielded by recurrence (A-8)

are $J_1(u)$ and $J_0(u)$ (after scaling), we then have all the necessary ingredients to determine $B_0(u)$ and $B_1(u)$.

No array declarations or array storage is necessary in this procedure, since there is never any need to "go back up" the recurrence and correctly scale the $\{J_m(u)\}$ terms. This has been guaranteed (through numerical investigation) by the choice of M in (A-10). A further economy in the program for this two-term recurrence (A-8) has been achieved by splitting it into even and odd versions, thereby avoiding the usual temporary storage of the left-hand side of (A-8) until the right-hand side is updated. This compact program is listed below as subroutine SUB Besj. For given u, it outputs values for $J_0(u)$, $J_1(u)$, $A(u)$, $B_0(u)$, $B_1(u)$, provided that $0 \le u < 45$.

ASYMPTOTIC EXPANSION

For large u, the starting integer M in (A-10) gets too large to make downward recurrence a viable procedure. Instead, we resort to the asymptotic expansion [5; (11.1.11)]

$$A(u) = \int_0^u dt\, J_0(t) \sim 1 -$$

$$- \left(\frac{2}{\pi u}\right)^{1/2}\left[\cos\left(u - \frac{\pi}{4}\right)\sum_{k=0}^{\infty} \frac{(-1)^k\, a_{2k+1}}{u^{2k+1}} - \sin\left(u - \frac{\pi}{4}\right)\sum_{k=0}^{\infty} \frac{(-1)^k\, a_{2k}}{u^{2k}}\right] \qquad \text{(A-11)}$$

as $u \to +\infty$; here, we also used the definite integral result that $A(\infty) = 1$ [5; (11.4.17)]. The values of the coefficients are [5; (11.1.2)]

$$a_k = \left(\frac{1}{2}\right)_k \sum_{s=0}^{k} \left(\frac{1}{2}\right)_s \frac{1}{2^s s!} \tag{A-12}$$

and are conveniently obtained by recursion

$$T_s \equiv \left(\frac{1}{2}\right)_s \frac{1}{2^s s!} = \frac{s - \frac{1}{2}}{2s} T_{s-1} \quad \text{for } s \geq 1 \ . \tag{A-13}$$

The number of terms required in the summations in (A-11) depends on the value of u and the desired accuracy. For $u > 45$ and 15 decimal accuracy, it has been sufficient to terminate (A-11) at $k = \mathrm{INT}(u/2)$.

Since (A-11) yields only $A(u)$, it is necessary to calculate $J_o(u)$ and $J_1(u)$ additionally; this has been accomplished by use of [11; section 6.8]. All of these quantities are evaluated by means of subroutine SUB Bessel listed below. For input $u \geq 0$, this subroutine yields values of $J_o(u)$, $J_1(u)$, $A(u)$, $B_o(u)$, $B_1(u)$.

```
 10     SUB Bessel(X,J0,J1,A,B0,B1)   !  A = INTEGRAL(0,X) dt Jo(t)
 20     DOUBLE K,I                    !  INTEGERS
 30     IF X>45. THEN 60
 40     CALL Besj(X,J0,J1,A,B0,B1)    !  DOWNWARD RECURRENCE 9.1.27,1
 50     SUBEXIT
 60     I=INT(X)/2                    !  ASYMPTOTIC SERIES 11.1.11 & 12
 70     Rx=1./X
 80     F=.5*Rx
 90     T=.25
100     A=1.25
110     Re=.625*Rx
120     Im=P=1.
130     FOR K=1 TO I
140     P=-P
150     Sn=K+K
160     F5=Sn-.5
170     F=F*F5*Rx
180     T=T*F5/(Sn+Sn)
190     A=A+T
200     Be=F*A
210     Im=Im+P*Be
220     Sn=Sn+1.
230     F5=Sn-.5
240     F=F*F5*Rx
250     T=T*F5/(Sn+Sn)
260     A=A+T
270     Bo=F*A
280     Re=Re+P*Bo
290     IF Be*Be+Bo*Bo<1.E-26 THEN 310
300     NEXT K
310     F=X-.785398163397448
320     T=.797884560802865
330     A=1.-T*SQR(Rx)*(Re*COS(F)-Im*SIN(F))
340     J0=FNJo(X)                    !  J0 = Jo(X)
350     J1=FNJ1(X)                    !  J1 = J1(X)
360     B0=A-X*J0                     !  B0 = A(X) - X Jo(X)
370     B1=A-J1                       !  B1 = A(X) - J1(X)
380     SUBEND
390     !
400     SUB Besj(U,J0,J1,A,B0,B1)     !  J0 = Jo(U),  J1 = J1(U)
410     IF U>0. THEN 450              !   A = A(U) = INTEGRAL(0,U) dt Jo(t)
420     J0=1.                         !  B0 = A(U) - U Jo(U)
430     J1=A=B0=B1=0.                 !  B1 = A(U) - J1(U)
440     SUBEXIT
450     DOUBLE Mc,Ms                  !  INTEGERS
460     Mc=2*INT(20.+.56*U-175./(12.+U))+12
470     T=2./U
480     Se=E=0.
490     So=O=1.E-250
500     FOR Ms=Mc TO 2 STEP -2
510     E=T*(Ms+1)*O-E                !  9.1.27,1
520     Se=Se+E
530     O=T*Ms*E-O                    !  9.1.27,1
540     So=So+O
550     NEXT Ms
560     E=T*O-E
570     F=1./(Se+Se+E)                !  9.1.46
580     J0=E*F
590     J1=O*F
600     A=(So+So)*F                   !  11.1.2
610     B0=A-U*J0
620     B1=A-J1
630     SUBEND
640     !
```

```
650    DEF FNJo(X)           !  Jo(X) via Hart #5845, 6546, and 6946
660    Y=ABS(X)
670    IF Y>8. THEN 770
680    T=Y*Y
690    P=2271490439.5536033-T*(5513584.5647707522-T*5292.6171303845574)
700    P=2334489171877869.7-T*(47765559442673.588-T*(462172225031.71803-T*P))
710    P=185962317621897804.-T*(4414582939181598 2.-T*P)
720    Q=204251483.52134357+T*(494030.79491813972+T*(884.72036756175504+T))
730    Q=2344750013658996.8+T*(15015462449769.752+T*(64398674535.133256+T*Q))
740    Q=185962317621897733.+T*Q
750    Jo=P/Q
760    RETURN Jo
770    Z=8./Y
780    T=Z*Z
790    Pn=2204.5010439651804+T*(128.67758574871419+T*.90047934748028803)
800    Pn=8554.8225415066617+T*(8894.4375329606194+T*Pn)
810    Pd=2214.0488519147104+T*(130.88490049992388+T)
820    Pd=8554.8225415066628+T*(8903.8361417095954+T*Pd)
830    Qn=13.990976865960680+T*(1.0497327982345548+T*.0093525953294 0319)
840    Qn=37.510534954957112+T*(46.093826814625175+T*Qn)
850    Qd=921.56697552653090+T*(74.428389741411179+T)
860    Qd=2400.6742371172675+T*(2971.9837452084920+T*Qd)
870    T=Y-.78539816339744828
880    Jo=.28209479177387820*SQR(Z)*(COS(T)*Pn/Pd+SIN(T)*Z*Qn/Qd)
890    RETURN Jo
900    FNEND
910    !
920    DEF FNJ1(X)           !  J1(X) via Hart #6045, 6747, and 7147
930    Y=ABS(X)
940    IF Y>8. THEN 1040
950    T=Y*Y
960    P=.11073522244537306E-10-T*.63194310317443161E-14
970    P=.49105992765551294E-5-T*(.93821933651407445E-8-T*P)
980    P=.39831079839523 3-T*(.17057692643496171E-2-T*P)
990    P=5878.7877666568200-T*(61.218769973569439-T*P)
1000   P=69536422.632983850-T*(8356785.4873489143-T*(320902.74688539470-T*P))
1010   Q=139072845.26596769+T*(670534.68354822993+T*(1284.5934539663019+T))
1020   J1=X*P/Q
1030   RETURN J1
1040   Z=8./Y
1050   T=Z*Z
1060   Pn=3132.7529563550695+T*(174.31379748379025+T*1.2285053764359043)
1070   Pn=12909.184718961881+T*(13090.420511035065+T*Pn)
1080   Pd=3109.2814167700288+T*(169.04721775008610+T)
1090   Pd=12909.184718961879+T*(13066.783087844020+T*Pd)
1100   Qn=51.736532818365916+T*(3.7994453796980673+T*.036363466476034711)
1110   Qn=144.65282874995209+T*(174.42916890924259+T*Qn)
1120   Qd=1119.1098527047487+T*(85.223920643413404+T)
1130   Qd=3085.9270133323172+T*(3734.3401060163018+T*Qd)
1140   T=Y-2.3561944901923448
1150   J1=.28209479177387820*SQR(Z)*(COS(T)*Pn/Pd-SIN(T)*Z*Qn/Qd)
1160   IF X<0. THEN J1=-J1
1170   RETURN J1
1180   FNEND
```

APPENDIX B

DERIVATION OF INTEGRATION RULE FOR STRAIGHT LINE FITS TO g(x)

The situation of interest here is represented in figure 1, where straight lines are fit to g(x) between adjacent samples of g(x), taken at sample points $\{x_n\}$. In particular, the contribution to integral (11) of an (internal) abutting point x_n was set up in (18)-(19). By letting $t = \omega x$ in (18), and using (19), (20), and (22), namely

$$y = \frac{x - x_n}{h} \;, \quad x_n = nh \;, \quad \Theta = \omega h \;, \tag{B-1}$$

there follows, for the n-th contribution to the integral,

$$I_n = \frac{g_n}{\omega} \int_{(n-1)\Theta}^{n\Theta} dt \; J_0(t) \left(1 - n + \frac{t}{\Theta}\right) +$$

$$+ \frac{g_n}{\omega} \int_{n\Theta}^{(n+1)\Theta} dt \; J_0(t) \left(1 + n - \frac{t}{\Theta}\right) , \tag{B-2}$$

where $g_n = g(x_n) = g(nh)$. By reference to the auxiliary functions defined in (13)-(17), the sum of these two integrals can be expressed in the compact form

$$I_n = \frac{g_n}{\omega}\left\{(n + 1)\; B_1[(n + 1)\Theta] - 2n\; B_1[n\Theta] + (n - 1)\; B_1[(n - 1)\Theta]\right\}$$
$$\text{for } \ell < n < r \; . \tag{B-3}$$

The procedures in appendix A are now directly applicable to the evaluation of (B-3) for any n.

For the left-end point x_ℓ depicted on the left side of figure 1, the corresponding contribution to desired integral result (11) is, using (B-1) again,

$$I_\ell = \int_{x_\ell}^{x_\ell + h} dx \; J_0(\omega x) \; g_\ell \; (1 - y) =$$

$$= \frac{g_\ell}{\omega} \int_{\ell\Theta}^{(\ell+1)\Theta} dt \; J_0(t) \left(\ell + 1 - \frac{t}{\Theta}\right) =$$

$$= \frac{g_\ell}{\omega}\left\{(\ell + 1) \; B_1\left[(\ell + 1)\Theta\right] - (\ell + 1) \; B_1\left[\ell\Theta\right] - J_1\left[\ell\Theta\right]\right\} . \qquad \text{(B-4)}$$

The corresponding contribution to integral (11) for the right-end point x_r is given by

$$I_r = \int_{x_r - h}^{x_r} dx \; J_0(\omega x) \; g_r \; (1 + y) =$$

$$= \frac{g_r}{\omega} \int_{(r-1)\Theta}^{r\Theta} dt \; J_0(t) \left(\frac{t}{\Theta} - r + 1\right) =$$

$$= \frac{g_r}{\omega}\left\{(r - 1) \; B_1\left[(r - 1)\Theta\right] - (r - 1) \; B_1\left[r\Theta\right] + J_1\left[r\Theta\right]\right\} . \qquad \text{(B-5)}$$

(As a check, combination of (B-4) and (B-5), upon replacement of ℓ and r by n, yields (B-3), as it should. The "end correction terms" in J_1 cancel out for all internal points, n.)

The resultant approximation to desired integral (11) is given by the sum of (B-3)-(B-5):

$$G(\omega) = \int_{x_\ell}^{x_r} dx\; J_0(\omega x)\; g(x) \cong I_\ell + I_r + \sum_{n=\ell+1}^{r-1} I_n \; . \tag{B-6}$$

This particular grouping of terms is according to the function sample values $\{g_n\} = \{g(nh)\}$. An alternative grouping, according to the samples of function $B_1(u)$ instead, is given by

$$\begin{aligned} \omega\, G(\omega) \cong & \left[\ell\, g_{\ell+1} - (\ell + 1) g_\ell\right] B_1(\ell\Theta) - g_\ell\; J_1(\ell\Theta) + \\ & + \left[r\; g_{r-1} - (r - 1) g_r\right] B_1(r\Theta) + g_r\; J_1(r\Theta) + \\ & + \sum_{n=\ell+1}^{r-1} n\left[g_{n+1} - 2g_n + g_{n-1}\right] B_1(n\Theta) \; . \end{aligned} \tag{B-7}$$

Whereas $B_1(n\Theta)$ must be evaluated for all $\ell \leq n \leq r$, the J_1 function need only be evaluated at the end points $\ell\Theta$ and $r\Theta$.

When ω is restricted to be multiples of a sampling increment Δ, that is

$$\omega = k\Delta \quad \text{for } k = 1, 2, \ldots \tag{B-8}$$

then (B-7) yields, for $k \geq 1$, the approximation

$$\begin{aligned} k\Delta\ G(k\Delta) \cong & \left[\ell\, g_{\ell+1} - (\ell + 1) g_\ell\right] B_1(\ell k\Delta h) - g_\ell\ J_1(\ell k\Delta h) + \\ & + \left[r\, g_{r-1} - (r-1) g_r\right] B_1(rk\Delta h) + g_r\ J_1(rk\Delta h) + \\ & + \sum_{n=\ell+1}^{r-1} n\left[g_{n+1} - 2g_n + g_{n-1}\right] B_1(nk\Delta h)\ , \end{aligned} \tag{B-9}$$

where

$$g_n = g(nh)\ . \tag{B-10}$$

Since n and k are integers (see (20) and (B-8)), the evaluation of $B_1(u)$ in (B-9) is confined to integer multiples of Δh, i.e. $u = m\Delta h$. Further discussion on how to take advantage of this feature of (B-9) is given in the sequel to (26). The end result is that we have two alternative procedures for evaluation of (B-9) and two corresponding programs: one faster routine which may require considerable storage, and a slower procedure utilizing very little storage. Programs for both procedures are listed below.

BEHAVIOR FOR SMALL θ

When θ is small, the differences of like quantities in (B-3)-(B-5) can be circumvented by expanding B_1 and J_1 in power series in θ. Using the facts that

$$B_1(u) \sim \frac{u}{2} - \frac{u^3}{48} \quad \text{as } u \to 0 ,$$

$$J_1(u) \sim \frac{u}{2} - \frac{u^3}{16} \quad \text{as } u \to 0 , \tag{B-11}$$

the above results reduce to

$$I_n \sim g_n h\left[1 - \frac{1}{4}\theta^2\left(n^2 + \frac{1}{6}\right)\right],$$

$$I_\ell \sim \frac{1}{2} g_\ell h\left[1 - \frac{1}{4}\theta^2\left(\ell^2 + \frac{2}{3}\ell + \frac{1}{6}\right)\right],$$

$$I_r \sim \frac{1}{2} g_r h\left[1 - \frac{1}{4}\theta^2\left(r^2 - \frac{2}{3} r + \frac{1}{6}\right)\right], \tag{B-12}$$

as $\theta \to 0$. By use of the power series expansion developed for $B_1(u)$ in appendix A, these results could be extended to order θ^4, θ^6 if desired.

The total contribution to (11) is given by the sum in (B-6). As $\theta \to 0$, this reduces to the Trapezoidal rule, (12).

```
10   ! ZERO-TH ORDER BESSEL TRANSFORM USING LINEAR INTERPOLATION.
20   ! INTEGRAL(X1,Xr) dX Jo(WX) g(X) FOR W1<=W<=W2 IS STORED IN
30   ! Gw(Ks), where W = Ks*Delw.        Faster high-storage.
40     Delx=.025                      !  INCREMENT (h) IN X
50     L=0                            !  X1=L*Delx, L>=0
60     R=400                          !  Xr=R*Delx, R>L
70     Delw=.2                        !  INCREMENT (Δ) IN W
80     K1=0                           !  W1=K1*Delw, K1>=0
90     K2=40                          !  W2=K2*Delw, K2>=K1
100    DOUBLE L,R,K1,K2,K0,L1,R1,Ns,Ks,I        !  INTEGERS
110    DIM Gx(500),Dg(500),B1(50000),J1l(100),J1r(100),Gw(100)
120    K0=K1
130    K1=MAX(K1,1)
140    L1=L+1
150    R1=R-1
160    REDIM Gx(L:R),Dg(L1:R),B1(L*K1:R*K2)
170    REDIM J1l(K1:K2),J1r(K1:K2),Gw(K0:K2)
180    FOR Ks=K0 TO K2
190    Gw(Ks)=0.
200    NEXT Ks
210    FOR Ns=L TO R
220    Gx(Ns)=FNG(Ns*Delx)            !  SEE DEF FNG(X) = g(X)
230    NEXT Ns
240    Gl=Gx(L)
250    Gr=Gx(R)
260    IF K0>0 THEN 320
270    F=.5*(Gl+Gr)
280    FOR Ns=L1 TO R1
290    F=F+Gx(Ns)
300    NEXT Ns
310    Gw(0)=F*Delx
320    FOR Ns=L1 TO R
330    Dg(Ns)=Gx(Ns)-Gx(Ns-1)
340    NEXT Ns
350    D2=Delw*Delx
360    IF L=0 THEN 410
370    FOR Ks=K1 TO K2
380    I=L*Ks
390    CALL Bessel(I*D2,J0,J1l(Ks),A,B0,B1(I))
400    NEXT Ks
410    FOR Ks=K1 TO K2
420    I=R*Ks
430    CALL Bessel(I*D2,J0,J1r(Ks),A,B0,B1(I))
440    NEXT Ks
450    FOR Ns=L1 TO R1
460    FOR Ks=K1 TO K2
470    I=Ns*Ks
480    IF B1(I)<>0. THEN 500
490    CALL Bessel(I*D2,J0,J1,A,B0,B1(I))
500    NEXT Ks
510    NEXT Ns
```

```
520     T1=L*Dg(L1)-Gl
530     T2=R*Dg(R)-Gr
540     IF L=0 THEN 580
550     FOR Ks=K1 TO K2
560     Gw(Ks)=T1*B1(L*Ks)-Gl*J1l(Ks)
570     NEXT Ks
580     FOR Ks=K1 TO K2
590     F=T2*B1(R*Ks)-Gr*J1r(Ks)
600     Gw(Ks)=Gw(Ks)-F
610     NEXT Ks
620     FOR Ns=L1 TO R1
630     F=Ns*(Dg(Ns+1)-Dg(Ns))
640     FOR Ks=K1 TO K2
650     Gw(Ks)=Gw(Ks)+F*B1(Ns*Ks)
660     NEXT Ks
670     NEXT Ns
680     FOR Ks=K1 TO K2
690     Gw(Ks)=Gw(Ks)/(Ks*Delw)
700     NEXT Ks
710     PRINT Gw(*)
720     PAUSE
730     END
740     !
750     DEF FNG(X)                        !  g(X)
760       Gx=X*EXP(-.5*X*X)               !  RAYLEIGH EXAMPLE
770     RETURN Gx
780     FNEND
```

```
10  ! ZERO-TH ORDER BESSEL TRANSFORM USING LINEAR INTERPOLATION.
20  ! INTEGRAL(X1,Xr) dX Jo(WX) g(X) FOR W1<=W<=W2 IS STORED IN
30  ! Gw(Ks), where W = Ks*Delw.      Slower low-storage.
40    Delx=.025                    !  INCREMENT (h) IN X
50    L=0                          !  X1=L*Delx, L>=0
60    R=400                        !  Xr=R*Delx, R>L
70    Delw=.5                      !  INCREMENT (Δ) IN W
80    K1=0                         !  W1=K1*Delw, K1>=0
90    K2=100                       !  W2=K2*Delw, K2>=K1
100   DOUBLE L,R,K1,K2,K0,L1,R1,Ns,Ks        !  INTEGERS
110   DIM Gx(500),Dg(500),Gw(200)
120   K0=K1
130   K1=MAX(K1,1)
140   L1=L+1
150   R1=R-1
160   REDIM Gx(L:R),Dg(L1:R),Gw(K0:K2)
170   FOR Ks=K0 TO K2
180   Gw(Ks)=0.
190   NEXT Ks
200   FOR Ns=L TO R
210   Gx(Ns)=FNG(Ns*Delx)            !  SEE DEF FNG(X) = g(X)
220   NEXT Ns
230   Gl=Gx(L)
240   Gr=Gx(R)
250   IF K0>0 THEN 310
260   F=.5*(Gl+Gr)
270   FOR Ns=L1 TO R1
280   F=F+Gx(Ns)
290   NEXT Ns
300   Gw(0)=F*Delx
310   FOR Ns=L1 TO R
320   Dg(Ns)=Gx(Ns)-Gx(Ns-1)
330   NEXT Ns
340   D2=Delw*Delx
350   T1=L*Dg(L1)-Gl
360   T2=R*Dg(R)-Gr
370   IF L=0 THEN 430
380   T=L*D2
390   FOR Ks=K1 TO K2
400   CALL Bessel(T*Ks,J0,J1,A,B0,B1)
410   Gw(Ks)=T1*B1-Gl*J1
420   NEXT Ks
430   T=R*D2
440   FOR Ks=K1 TO K2
450   CALL Bessel(T*Ks,J0,J1,A,B0,B1)
460   F=T2*B1-Gr*J1
470   Gw(Ks)=Gw(Ks)-F
480   NEXT Ks
490   FOR Ns=L1 TO R1
500   F=Ns*(Dg(Ns+1)-Dg(Ns))
510   T=Ns*D2
520   FOR Ks=K1 TO K2
530   CALL Bessel(T*Ks,J0,J1,A,B0,B1)
540   Gw(Ks)=Gw(Ks)+F*B1
550   NEXT Ks
560   NEXT Ns
570   FOR Ks=K1 TO K2
580   Gw(Ks)=Gw(Ks)/(Ks*Delw)
590   NEXT Ks
600   PRINT Gw(*)
610   END
```

APPENDIX C

DERIVATION OF INTEGRATION RULE FOR PARABOLIC FITS TO g(x)

The situation of interest here is depicted in figure 2, where parabolas are fit to the samples of g(x), a pair of adjacent panels at a time. The derivation of the resultant approximation to integral (27) is broken down into the four cases illustrated in that figure.

It is again presumed, as in (20), that sample points of g(x) are taken at increment h, namely

$$x_n = nh \quad \text{for } \ell \le n \le r \;, \tag{C-1}$$

and that, in addition,

$$r - \ell \text{ is even} \;. \tag{C-2}$$

That is, the total number of panels employed in interval x_ℓ, x_r must be even. A breakdown of all the sample points $\{x_n\}$ into the four categories of figure 2 is depicted in figure C-1, where we have used the abbreviations

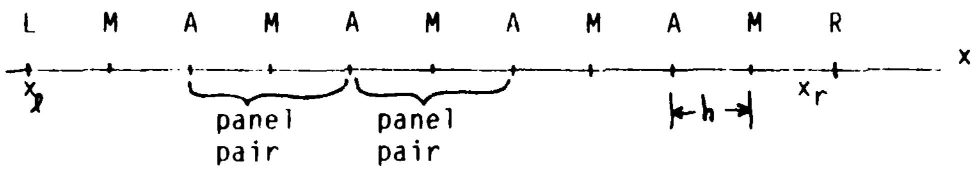

Figure C-1. Categorization of Sample Points

M = mid-point (of a panel pair),

A = abutting point (between two panel pairs),

L = left-end point,

R = right-end point. (C-3)

It is presumed in the following that $\omega > 0$; the case for $\omega = 0$ is given by (29), while $\omega < 0$ is immediately covered by observing that J_o is even.

Mid-Point

The contribution of a mid-point x_n to integral (27) is (see figure 2)

$$M_n = \int_{x_n-h}^{x_n+h} dx\ J_o(\omega x)\ g_n\ (1 - y^2) =$$

$$= \frac{g_n}{\omega} \int_{(n-1)\Theta}^{(n+1)\Theta} dt\ J_o(t) \left[1 - \left(\frac{t}{\Theta} - n\right)^2\right], \qquad \text{(C-4)}$$

where we utilized $t = \omega x$, (C-1), (28), and (22). Upon expansion of the square in (C-4), and use of (13)-(17), (C-4) reduces to the rather compact form

$$M_n = \frac{g_n}{\omega}\left\{(n^2 - 1)\,(B_1[(n-1)\Theta] - B_1[(n+1)\Theta]) - \right.$$

$$\left. - \frac{1}{\Theta^2}\,(B_0[(n-1)\Theta] - B_0[(n+1)\Theta])\right\} . \qquad \text{(C-5)}$$

This type of term is yielded for $n = \ell + 1,\ \ell + 3,\ \ldots,\ r - 3,\ r - 1$, as reference to figure C-1 will verify. Here, and in the following, for the sake of brevity, we do not document the rather detailed machinations that lead to the compact form (C-5) from the integral definition (C-4). The reader will have to reconstruct those nonprofitable manipulations, if interested.

At this juncture, instead of treating an abutting point with its associated 4 panels (see upper right of figure 2), we split it up into a panel pair with a left-end point and another panel pair with a right-end point. We thus have to consider a general left point and a general right point.

LEFT POINT

This case is obtained by looking at the bottom-left diagram in figure 2 and replacing ℓ by n everywhere. The contribution of this type of panel pair is

$$L_n = \int_{x_n}^{x_n+2h} dx\ J_0(\omega x)\ g_n\ (1 - y)\ (1 - y/2) =$$

$$= \frac{g_n}{\omega} \int_{n\Theta}^{(n+2)\Theta} dt\ J_0(t) \left[1 - \frac{3}{2}\left(\frac{t}{\Theta} - n\right) + \frac{1}{2}\left(\frac{t}{\Theta} - n\right)^2\right] =$$

$$= \frac{g_n}{2\omega}\Big\{(n+1)(n+2)\Big(B_1[(n+2)\Theta] - B_1[n\Theta]\Big) -$$

$$- \frac{1}{\Theta^2}\Big(B_0[(n+2)\Theta] - B_0[n\Theta]\Big) - 2\ J_1[n\Theta]\Big\} . \qquad \text{(C-6)}$$

This type of term is yielded for $n = \ell, \ell + 2, \ldots, r - 4, r - 2$, but not $n = r$; see figure C-1.

RIGHT POINT

This case pertains for the bottom-right diagram in figure 2 when r is replaced by n everywhere. The corresponding contribution to integral (27) is

$$R_n = \int_{x_n-2h}^{x_n} dx\ J_0(\omega x)\ g_n\ (1 + y)\ (1 + y/2) =$$

$$= \frac{g_n}{\omega} \int_{(n-2)\Theta}^{n\Theta} dt\ J_0(t) \left[1 + \frac{3}{2}\left(\frac{t}{\Theta} - n\right) + \frac{1}{2}\left(\frac{t}{\Theta} - n\right)^2\right] =$$

$$= \frac{g_n}{2\omega}\Big\{(n-1)(n-2)\Big(B_1[n\Theta] - B_1[(n-2)\Theta]\Big) -$$

$$- \frac{1}{\Theta^2}\Big(B_0[n\Theta] - B_0[(n-2)\Theta]\Big) + 2\ J_1[n\Theta]\Big\} . \qquad \text{(C-7)}$$

This type of term is yielded for $n = \ell + 2, \ell + 4, \ldots, r - 2, r$, but not $n = \ell$; see figure C-1.

ABUTTING POINT

We can now immediately obtain the integral contribution for an abutting point (top-right diagram of figure 2) by adding (C-6) and (C-7):

$$A_n = L_n + R_n =$$

$$= \frac{g_n}{2\omega}\Big\{(n+1)(n+2)\ B_1[(n+2)\Theta] - \frac{1}{\Theta^2}\ B_0[(n+2)\Theta] - 6n\ B_1[n\Theta] -$$

$$- (n-1)(n-2)\ B_1[(n-2)\Theta] + \frac{1}{\Theta^2}\ B_0[(n-2)\Theta]\Big\}\ , \qquad \text{(C-8)}$$

which holds only for $n = \ell + 2, \ell + 4, \ldots, r - 4, r - 2$; see figure C-1. As a notational shortcut, we say $n = (\ell + 2)(2)(r - 2)$ are the allowed values of n.

At this stage, we have succeeded in evaluating all the types of terms that have been depicted in figures 2 and C-1. The total approximation to integral (27) is therefore

$$G(\omega) \cong \sum_{n=\ell+1}^{r-1} M_n + \sum_{n=\ell+2}^{r-2} A_n + L_\ell + R_r\ , \qquad \text{(C-9)}$$

in terms of the contributions in (C-5)-(C-8), where the slash on the summation symbol denotes skipping every other term.

However, this grouping of terms in (C-9) is according to sample values $g_n = g(nh)$ of function $g(x)$. It is advantageous to re-arrange this sum, grouping terms instead according to sample values of functions $B_0(u)$ and $B_1(u)$, defined in (16) and (17). After considerable manipulations, the following alternative to (C-9) is obtained:

$$2\omega\ G(\omega) \cong \frac{1}{\Theta^2} S_\ell\ B_0(\ell\Theta) - Q_\ell\ B_1(\ell\Theta) - 2g_\ell\ J_1(\ell\Theta) -$$

$$- \frac{1}{\Theta^2} S_r\ B_0(r\Theta) + Q_r\ B_1(r\Theta) + 2g_r\ J_1(r\Theta) +$$

$$+ \frac{1}{\Theta^2} \sum_{n=\ell+2}^{r-2} D_n\ B_0(n\Theta) - \sum_{n=\ell+2}^{r-2} R_n\ B_1(n\Theta)\ . \qquad \text{(C-10)}$$

The auxiliary sequences utilized in (C-10) are defined below:

$$S_\ell = g_{\ell+2} - 2g_{\ell+1} + g_\ell$$

$$S_r = g_r - 2g_{r-1} + g_{r-2}$$

$$Q_\ell = \ell(\ell + 1)g_{\ell+2} - 2\ell(\ell + 2)g_{\ell+1} + (\ell + 2)(\ell + 1)g_\ell$$

$$Q_r = (r - 2)(r - 1)g_r - 2r(r - 2)g_{r-1} + r(r - 1)g_{r-2} \qquad \text{(C-11)}$$

and

$$\left.\begin{aligned} D_n &= g_{n+2} - 2g_{n+1} + 2g_{n-1} - g_{n-2} \\ F_n &= g_{n+2} - 4g_{n+1} + 6g_n - 4g_{n-1} + g_{n-2} \\ R_n &= n^2 D_n + nF_n \end{aligned}\right\} \text{for } n = (\ell + 2)(2)(r - 2)\ . \qquad \text{(C-12)}$$

It is important to observe from (C-10) that the Bessel integrals $B_0(u)$ and $B_1(u)$ need be evaluated only at $u = n\Theta$ for $n = \ell(2)r$, and need not be evaluated at the in-between points $n = (\ell + 1)(2)(r - 1)$. Of course, the input function $g(x)$ must be evaluated at all $x = x_n = nh$ for $n = \ell(1)r$. The quantities in (C-11) and (C-12) do not depend on $\Theta = \omega h$, and can be computed just once and stored, in preparation for use in (C-10).

If we are interested in evaluating integral $G(\omega)$ in (27) at values of ω equal to integer multiples k of some increment Δ, then we must substitute

$$\omega = k\Delta \quad \text{and} \quad \Theta = \omega h = k\Delta h \tag{C-13}$$

into (C-10). Then interest centers on computation of $B_0(u)$ and $B_1(u)$ at $u = m\Delta h$ for certain integers m. This consideration has been discussed in the sequel to (26).

BEHAVIOR FOR SMALL Θ

When Θ is small, differences of functions with similar values are required in (C-10). This same behavior obtains for Filon's method; see [5; (25.4.53)]. Accordingly, it is useful to have a series expansion for $G(\omega)$ about $\Theta = 0$, to be used for small Θ.

Since [5; (9.1.12)]

$$J_0(u) \sim 1 - \frac{1}{4}u^2 \quad \text{as } u \to 0 , \tag{C-14}$$

substitution in (C-4), along with the change of variable $y = t/\Theta - n$, yields the mid-point contribution

$$M_n = g_n\, h \int_{-1}^{1} dy\; J_0(\Theta(n+y))\,(1 - y^2) =$$

$$\sim g_n\, h \int_{-1}^{1} dy \left[1 - \frac{1}{4}\Theta^2(n+y)^2\right](1 - y^2) =$$

$$= \frac{4}{3} g_n\, h\left\{1 - \frac{1}{4}\Theta^2\left(n^2 + \frac{1}{5}\right)\right\} \quad \text{as } \Theta \to 0 \;. \tag{C-15}$$

A similar procedure for left point and right point contributions (C-6) and (C-7) gives

$$L_n = R_n \sim \frac{1}{3} g_n\, h\left\{1 - \frac{1}{4}\Theta^2\left(n^2 - \frac{2}{5}\right)\right\} \quad \text{as } \Theta \to 0 \;. \tag{C-16}$$

The total asymptotic contribution to $G(\omega)$ in (27) is therefore given by (a modified version of (C-9))

$$G(\omega) \sim \sum_{n=\ell}^{r-2} L_n + \sum_{n=\ell+2}^{r} R_n + \sum_{n=\ell+1}^{r-1} M_n \quad \text{as } \Theta \to 0 \;, \tag{C-17}$$

using (C-15) and (C-16). For $\Theta = 0$, this reduces to Simpson's rule, (29). Additional correction terms involving Θ^4, Θ^6 could be derived by using additional terms in expansion (C-14).

When ω is specialized to values $\omega = k\Lambda$ in (C-10), the result is as given in (36). Programs for both a faster high-storage procedure and a slower low-storage procedure are listed below.

```
10   ! ZERO-TH ORDER BESSEL TRANSFORM USING PARABOLIC INTERPOLATION.
20   ! INTEGRAL(Xl,Xr) dX Jo(WX) g(X) FOR W1<=W<=W2 IS STORED IN
30   ! Gw(Ks), where W = Ks*Delw.       Faster high-storage.
40     Delx=.03                       !  INCREMENT (h) IN X
50     L=0                            !  Xl=L*Delx, L >=0
60     R=300                          !  Xr=R*Delx, R-L MUST BE EVEN & >=4
70     Delw=1.                        !  INCREMENT (Δ) IN W
80     K1=0                           !  W1=K1*Delw, K1>=0
90     K2=40                          !  W2=K2*Delw, K2>=K1
100    DOUBLE L,R,K1,K2,K0,L1,L2,R1,R2,Ns,Ks,I  !  INTEGERS
110    DIM Gx(800),Gw(500),Sq(500),J1l(500),J1r(500)
120    DIM B0(20000),B1(20000)
130    K0=K1
140    K1=MAX(K1,1)
150    L1=L+1
160    L2=L+2
170    R1=R-1
180    R2=R-2
190    REDIM Gx(L:R),Gw(K0:K2),Sq(K1:K2),J1l(K1:K2),J1r(K1:K2)
200    REDIM B0(L*K1:R*K2),B1(L*K1:R*K2)
210    FOR Ks=K0 TO K2
220    Gw(Ks)=0.
230    NEXT Ks
240    FOR Ns=L TO R
250    Gx(Ns)=FNG(Ns*Delx)             !   SEE DEF FNG(X) = g(X)
260    NEXT Ns
270    Gl=Gx(L)
280    Gr=Gx(R)
290    IF K0>0 THEN 380
300    S1=S2=0.
310    FOR Ns=L1 TO R1 STEP 2
320    S1=S1+Gx(Ns)
330    NEXT Ns
340    FOR Ns=L2 TO R2 STEP 2
350    S2=S2+Gx(Ns)
360    NEXT Ns
370    Gw(0)=(Gl+Gr+4.*S1+2.*S2)*Delx/3.
380    Gl1=Gx(L1)
390    Gl2=Gx(L2)
400    Gr1=Gx(R1)
410    Gr2=Gx(R2)
420    Sl=Gl2-2.*Gl1+Gl
430    Sr=Gr-2.*Gr1+Gr2
440    Ol=L*L1*Gl2-2.*L*L2*Gl1+L2*L1*Gl
450    Or=R2*R1*Gr-2.*R*R2*Gr1+R*R1*Gr2
460    Gl2=Gl*2.
470    Gr2=Gr*2.
480    D2=Delw*Delx
490    FOR Ks=K1 TO K2
500    F=Ks*D2
510    Sq(Ks)=1./(F*F)
520    NEXT Ks
```

```
530     IF L=0 THEN 580
540     FOR Ks=K1 TO K2
550     I=L*Ks
560     CALL Bessel(I*D2,J0,J1l(Ks),A,B0(I),B1(I))
570     NEXT Ks
580     FOR Ks=K1 TO K2
590     I=R*Ks
600     CALL Bessel(I*D2,J0,J1r(Ks),A,B0(I),B1(I))
610     NEXT Ks
620     FOR Ns=L2 TO R2 STEP 2
630     FOR Ks=K1 TO K2
640     I=Ns*Ks
650     IF B0(I)<>0. THEN 670
660     CALL Bessel(I*D2,J0,J1,A,B0(I),B1(I))
670     NEXT Ks
680     NEXT Ns
690     IF L=0 THEN 740
700     FOR Ks=K1 TO K2
710     I=L*Ks
720     Gw(Ks)=Sq(Ks)*Sl*B0(I)-Ql*B1(I)-Gl2*J1l(Ks)
730     NEXT Ks
740     FOR Ks=K1 TO K2
750     I=R*Ks
760     F=Sq(Ks)*Sr*B0(I)-Qr*B1(I)-Gr2*J1r(Ks)
770     Gw(Ks)=Gw(Ks)-F
780     NEXT Ks
790     FOR Ns=L2 TO R2 STEP 2
800     G2=Gx(Ns+2)
810     G1=Gx(Ns+1)
820     H1=Gx(Ns-1)
830     H2=Gx(Ns-2)
840     Dn=G2-2.*G1+2.*H1-H2
850     Fn=G2-4.*G1+6.*Gx(Ns)-4.*H1+H2
860     Rn=Ns*(Ns*Dn+Fn)
870     FOR Ks=K1 TO K2
880     I=Ns*Ks
890     Gw(Ks)=Gw(Ks)+Sq(Ks)*Dn*B0(I)-Rn*B1(I)
900     NEXT Ks
910     NEXT Ns
920     F=Delw*2.
930     FOR Ks=K1 TO K2
940     Gw(Ks)=Gw(Ks)/(Ks*F)
950     NEXT Ks
960     PRINT Gw(*)
970     PAUSE
980     END
990     !
1000    DEF FNG(X)                          !  g(X)
1010      Gx=X*EXP(-.5*X*X)                 !  RAYLEIGH EXAMPLE
1020    RETURN Gx
1030    FNEND
```

```
10   ! ZERO-TH ORDER BESSEL TRANSFORM USING PARABOLIC INTERPOLATION.
20   ! INTEGRAL(Xl,Xr) dX Jo(WX) g(X) FOR W1<=W<=W2 IS STORED IN
30   ! Gw(Ks), where W = Ks*Delw.          Slower low-storage.
40     Delx=.03                        !   INCREMENT (h) IN X
50     L=0                             !   Xl=L*Delx, L>=0
60     R=300                           !   Xr=R*Delx, R-L MUST BE EVEN & >=4
70     Delw=1.                         !   INCREMENT (Δ) IN W
80     K1=0                            !   W1=K1*Delw, K1>=0
90     K2=120                          !   W2=K2*Delw, K2>=K1
100    DOUBLE L,R,K1,K2,K0,L1,L2,R1,R2,Ns,Ks   !   INTEGERS
110    DIM Gx(800),Gw(500),Sq(500)
120    K0=K1
130    K1=MAX(K1,1)
140    L1=L+1
150    L2=L+2
160    R1=R-1
170    R2=R-2
180    REDIM Gx(L:R),Gw(K0:K2),Sq(K1:K2)
190    FOR Ks=K0 TO K2
200    Gw(Ks)=0.
210    NEXT Ks
220    FOR Ns=L TO R
230    Gx(Ns)=FNG(Ns*Delx)             !   SEE DEF FNG(X) = g(X)
240    NEXT Ns
250    Gl=Gx(L)
260    Gr=Gx(R)
270    IF K0>0 THEN 360
280    S1=S2=0.
290    FOR Ns=L1 TO R1 STEP 2
300    S1=S1+Gx(Ns)
310    NEXT Ns
320    FOR Ns=L2 TO R2 STEP 2
330    S2=S2+Gx(Ns)
340    NEXT Ns
350    Gw(0)=(Gl+Gr+4.*S1+2.*S2)*Delx/3.
360    Gl1=Gx(L1)
370    Gl2=Gx(L2)
380    Gr1=Gx(R1)
390    Gr2=Gx(R2)
400    Sl=Gl2-2.*Gl1+Gl
410    Sr=Gr-2.*Gr1+Gr2
420    Ol=L*L1*Gl2-2.*L*L2*Gl1+L2*L1*Gl
430    Or=R2*R1*Gr-2.*R*R2*Gr1+R*R1*Gr2
440    Gl2=Gl*2.
450    Gr2=Gr*2.
460    D2=Delw*Delx
470    FOR Ks=K1 TO K2
480    F=Ks*D2
490    Sq(Ks)=1./(F*F)
500    NEXT Ks
```

```
510   IF L=0 THEN 570
520   T=L*D2
530   FOR Ks=K1 TO K2
540   CALL Bessel(T*Ks,J0,J1,A,B0,B1)
550   Gw(Ks)=Sq(Ks)*Sl*B0-Ql*B1-Gl2*J1
560   NEXT Ks
570   T=R*D2
580   FOR Ks=K1 TO K2
590   CALL Bessel(T*Ks,J0,J1,A,B0,B1)
600   F=Sq(Ks)*Sr*B0-Or*B1-Gr2*J1
610   Gw(Ks)=Gw(Ks)-F
620   NEXT Ks
630   FOR Ns=L2 TO R2 STEP 2
640   G2=Gx(Ns+2)
650   G1=Gx(Ns+1)
660   H1=Gx(Ns-1)
670   H2=Gx(Ns-2)
680   Dn=G2-2.*G1+2.*H1-H2
690   Fn=G2-4.*G1+6.*Gx(Ns)-4.*H1+H2
700   Rn=Ns*(Ns*Dn+Fn)
710   T=Ns*D2
720   FOR Ks=K1 TO K2
730   CALL Bessel(T*Ks,J0,J1,A,B0,B1)
740   Gw(Ks)=Gw(Ks)+Sq(Ks)*Dn*B0-Rn*B1
750   NEXT Ks
760   NEXT Ns
770   F=Delw*2.
780   FOR Ks=K1 TO K2
790   Gw(Ks)=Gw(Ks)/(Ks*F)
800   NEXT Ks
810   PRINT Gw(*)
820   PAUSE
830   END
840   !
850   DEF FNG(X)                        !   g(X)
860     Gx=X*EXP(-.5*X*X)               !   RAYLEIGH EXAMPLE
870   RETURN Gx
880   FNEND
```

REFERENCES

1. L. N. G. Filon, "On a Quadrature Formula for Trigonometric Integrals," Proc. Royal Soc. Edinburgh, vol. 49, pp. 38-47, 1928.

2. Z. Kopal, Numerical Analysis, J. Wiley and Sons, Inc., New York, NY, 1955.

3. C. J. Tranter, Integral Transforms in Mathematical Physics, J. Wiley and Sons, Inc., New York, NY, 1956.

4. J. W. Tukey, "The Estimation of Power Spectra and Related Quantities," On Numerical Approximation, Ed. R. E. Langer, Madison, WI, 1959.

5. Handbook of Mathematical Functions, U. S. Department of Commerce, National Bureau of Standards, Applied Mathematics Series No. 55, U. S. Government Printing Office, Washington, DC, June 1964.

6. P. J. Davis and P. Rabinowitz, Numerical Integration, Blaisdell Publishing Co., Waltham, MA, 1967.

7. S. M. Chase and L. D. Fosdick, "An Algorithm for Filon Quadrature," Communications of the ACM, vol. 12, no. 8, pp. 453-458, August 1969.

8. C. Lanczos, Applied Analysis, Third Printing, Prentice Hall, Inc., Englewood Cliffs, NJ, 1964.

9. I. S. Gradshteyn and I. M. Ryzhik, Table of Integrals, Series, and Products, Academic Press, Inc., New York, NY, 1980.

10. A. H. Nuttall, Accurate Efficient Evaluation of Cumulative or Exceedance Probability Distributions Directly From Characteristic Functions, NUSC Technical Report 7023, Naval Underwater Systems Center, New London, CT, 1 October 1983.

11. J. F. Hart et al, Computer Approximations, J. Wiley and Sons, Inc., New York, NY, 1968.

Technical Report 7995
1 April 1987

Efficient Evaluation of Polynomials and Exponentials of Polynomials for Equi-Spaced Arguments

A. H. Nuttall

ABSTRACT

A k-th order polynomial can be evaluated by means of k additions and no multiplications, when done in a recursive fashion at equi-spaced arguments. The evaluation of an exponential of a k-th order polynomial can be accomplished by k multiplications and no additions or exponentiations. Combinations of rational functions and exponentials can therefore be realized very efficiently by combining these properties.

TABLE OF CONTENTS

LIST OF SYMBOLS

$P_3(x)$	Third-order polynomial of x, (1)
α,β,γ,μ	Polynomial coefficients, (1)
x_0	Starting value of x, (2)
Δ	Increment in x, (2)
$Q_3(n)$	Third-order polynomial of n, (3)
a,b,c,d	Polynomial coefficients, (3),(4)
Q_2,Q_1	Difference polynomials, (5),(6)
$P_3(x)$	Exponential of third-order polynomial, (10)
$Q_3(n)$	Exponential of third-order polynomial, (11)

EFFICIENT EVALUATION OF POLYNOMIALS AND EXPONENTIALS OF POLYNOMIALS FOR EQUI-SPACED ARGUMENTS

INTRODUCTION

The evaluation of polynomials at equi-spaced arguments is a recurring task that arises in many applications. When a k-th order polynomial is written in nested form, its evaluation generally requires k additions and k multiplications at each argument of interest. For a set of equi-spaced arguments, we will demonstrate that the multiplications can be entirely circumvented (except during initialization) and that a recursive procedure employing only k additions per stage will suffice to generate the sequence of polynomial values.

For an exponential of a polynomial, an even greater savings is possible; namely, the exponential can be circumvented (except during initialization), and only k multiplications per stage are required in a recursive procedure. Memory storage is also kept at a minimum.

EVALUATION OF POLYNOMIAL

The procedure is best introduced by way of example. Suppose we want to evaluate third-order polynomial

$$P_3(x) = \alpha + \beta x + \gamma x^2 + \mu x^3 \tag{1}$$

at the set of equi-spaced arguments

$$x_n = x_o + n\Delta \quad \text{for } n = 0,\ 1,\ 2,\ \ldots\ . \tag{2}$$

That is, we are interested in the values

$$Q_3(n) \equiv P_3(x_n) = a + bn + cn^2 + dn^3 \quad \text{for } n = 0,\ 1,\ 2,\ \ldots\ , \tag{3}$$

where

$$a = \alpha + \beta x_o + \gamma x_o^2 + \mu x_o^3\ ,$$

$$b = \Delta(\beta + 2\gamma x_o + 3\mu x_o^2)\ ,$$

$$c = \Delta^2(\gamma + 3\mu x_o)\ ,$$

$$d = \Delta^3 \mu\ . \tag{4}$$

To this aim, define difference

$$Q_2(n) = Q_3(n) - Q_3(n-1) = b - c + d + (2c - 3d)n + 3dn^2\ . \tag{5}$$

Also define

$$Q_1(n) = Q_2(n) - Q_2(n-1) = 2c - 6d + 6dn\ , \tag{6}$$

and observe that

$$Q_1(n) - Q_1(n-1) = 6d \ . \qquad (7)$$

These last three recursions together read as

$$\left.\begin{aligned} Q_1(n) &= Q_1(n-1) + 6d \\ Q_2(n) &= Q_2(n-1) + Q_1(n) \\ Q_3(n) &= Q_3(n-1) + Q_2(n) \end{aligned}\right\} \text{ for } n = 1, 2, \ldots , \qquad (8)$$

and require only 3 additions for each n, with no multiplications whatsoever. The starting values for recursion (8) follow immediately from (6), (5), and (3), respectively:

$$\begin{aligned} Q_1(0) &= 2c - 6d \ , \\ Q_2(0) &= b - c + d, \\ Q_3(0) &= a \ . \end{aligned} \qquad (9)$$

Extension to a k-th order polynomial is obvious, and requires k additions per stage, with no multiplications.

EVALUATION OF EXPONENTIAL OF POLYNOMIAL

Suppose we want to evaluate the exponential of a third-order polynomial, namely

$$P_3(x) = \exp[\alpha + \beta x + \gamma x^2 + \mu x^3] \tag{10}$$

at the arguments listed in (2). That is, we want the values

$$Q_3(n) \equiv P_3(x_n) = \exp[a + bn + cn^2 + dn^3] \quad \text{for } n = 0, 1, 2 \ldots , \tag{11}$$

where a,b,c,d are given in (4).

To accomplish this goal, define ratio

$$Q_2(n) = Q_3(n)/Q_3(n-1) = \exp[b - c + d + (2c - 3d)n + 3dn^2] . \tag{12}$$

Also define

$$Q_1(n) = Q_2(n)/Q_2(n - 1) = \exp[2c - 6d + 6dn] , \tag{13}$$

and observe that

$$Q_1(n)/Q_1(n - 1) = \exp[6d] . \tag{14}$$

These last three recursions together read as

$$\left.\begin{aligned} Q_1(n) &= Q_1(n - 1) \exp[6d] \\ Q_2(n) &= Q_2(n - 1)\, Q_1(n) \\ Q_3(n) &= Q_3(n - 1)\, Q_2(n) \end{aligned}\right\} \quad \text{for } n = 1, 2, \ldots , \tag{15}$$

and require only 3 multiplications for each n, with no additions or exponentiations. The starting values for recursion (15) follow immediately from (13), (12), and (11), respectively:

$$
\begin{aligned}
Q_1(0) &= \exp[2c - 6d] , \\
Q_2(0) &= \exp[b - c + d] , \qquad (16)\\
Q_3(0) &= \exp[a] .
\end{aligned}
$$

Initialization requires the evaluation of four exponentials.

Extension to an exponential of a k-th order polynomial is obvious, and requires k multiplications per stage. Initialization requires the evaluation of k + 1 exponentials.

CONCLUSION

All the results above apply to complex coefficients a,b,c,d as well as complex arguments x_0,Δ. Only integer n needs to be real. However, since a complex multiplication involves 4 real multiplications and 2 real additions, the time of execution will naturally be larger.

The applicability of the above results to linear frequency-modulation with Gaussian amplitude-modulation follows readily, by restricting the order of the polynomial in (10) and (11) to $k = 2$; i.e., set $\mu = d = 0$. This particular case has been treated in [1]; in particular, the accuracy of the procedure has been investigated and found adequate for most applications. The evaluation of cosines or sines of real polynomials can be achieved by setting a,b,c,d in (11) to purely imaginary values.

When k equals 2 and a,b,c are complex, the quantities $Q_1(n)$ and $Q_2(n)$ are complex. Since a complex multiplication involves 4 real multiplications and 2 real additions, the number of operations per stage to generate $Q_1(n)$ and $Q_2(n)$ is 8 real multiplications and 4 real additions. As an example, if a,b,c are purely imaginary, $a = ia'$, $b = ib'$, $c = ic'$, then

$$Q_2(n) = \exp[i(a' + b'n + c'n^2)] =$$

$$= \cos[a' + b'n + c'n^2] + i \sin[a' + b'n + c'n^2] , \qquad (17)$$

meaning that the cosine and sine are capable of simultaneous generation at each stage. (Attempts to generate the cosine alone, with a lesser number of operations per stage, have not been successful.)

There is no need to set aside storage arrays for the recursive quantities in (8) or (15), if these numbers are used on the fly as they are generated. Then the computer coding for (8) is simply Q1 = Q1 + D6, Q2 = Q2 + Q1, Q3 = Q3 + Q2, while that for (15) is simply Q1 = Q1*E6, Q2 = Q2*Q1, Q3 = Q3*Q2, in the order listed. Generally, storage of only k temporary variables is required for a k-th order polynomial. On the other hand, if $Q_3(n)$ must be stored for later use, the only change in the coding above is to replace the Q3 lines by Q3(N) = Q3(N - 1) + Q2 and Q3(N) = Q3(N - 1)*Q2, respectively; there is no need to store Q1 or Q2 in arrays.

For general values of k, if the product of a rational function with an exponential of a polynomial must be calculated, it can be broken down into the evaluation of two polynomials and one exponential, as indicated above. Then one additional multiplication and division realizes the desired combination. Extensions to sums and products of such combinations are obvious. The orders, k, of the numerator and denominator polynomials, as well as the polynomial inside the exponential, need not be equal, but are completely arbitrary.

REFERENCES

[1] J. F. Kaiser, "On the Fast Generation of Equally-Spaced Values of the Gaussian Function A $\exp(-at^2)$," submitted to IEEE Trans. Acoust., Speech, Signal Processing, February 1987.

Technical Memorandum 871186
8 October 1987

Estimation of Signal and Noise Powers of Amplitude-Modulated Signal

A. H. Nuttall

ABSTRACT

A random signal of unknown power level is amplitude-modulated in a known deterministic fashion and observed in the presence of stationary noise of unknown level. Estimation of the signal power level is accomplished by a least-squares approach, resulting in an unbiased estimate. The variance of the estimate depends on the degree of modulation of the deterministic amplitude modulation, the background noise level, and the observation time.

INTRODUCTION

If a source of constant (unknown) strength moves on a known course and speed past an observing point, the received signal power level is modulated in a known deterministic manner. However, the absolute received signal power level may be unknown, and is further obscured by the presence of additive noise of unknown strength.

The mathematical problem of interest here is formulated as follows:

$$x(t) = m(t)\, s(t) + n(t) \tag{1}$$

is observed versus time t in an observation time interval of T seconds, where m(t) is a known deterministic amplitude-modulating function. Real signal s(t) and real noise n(t) are zero-mean stationary independent random processes with power levels

$$\overline{s^2(t)} = S, \quad \overline{n^2(t)} = N, \tag{2}$$

both of which are unknown. We wish to estimate the signal power S and determine the variance of the estimate, including its dependence on observation time T and modulation m(t).

The average received power varies with time according to

$$\overline{x^2(t)} = m^2(t)\, S + N, \tag{3}$$

as seen by reference to (1) and (2). A sample function x(t), as well as the modulation m(t), is depicted in figure 1. The common bandwidth of the assumed low-pass random processes, s(t) and n(t), is W Hz; for good estimation capability, it will be necessary to have TW >> 1. (Extension to the bandpass case should not be difficult, based on the results to be given.)

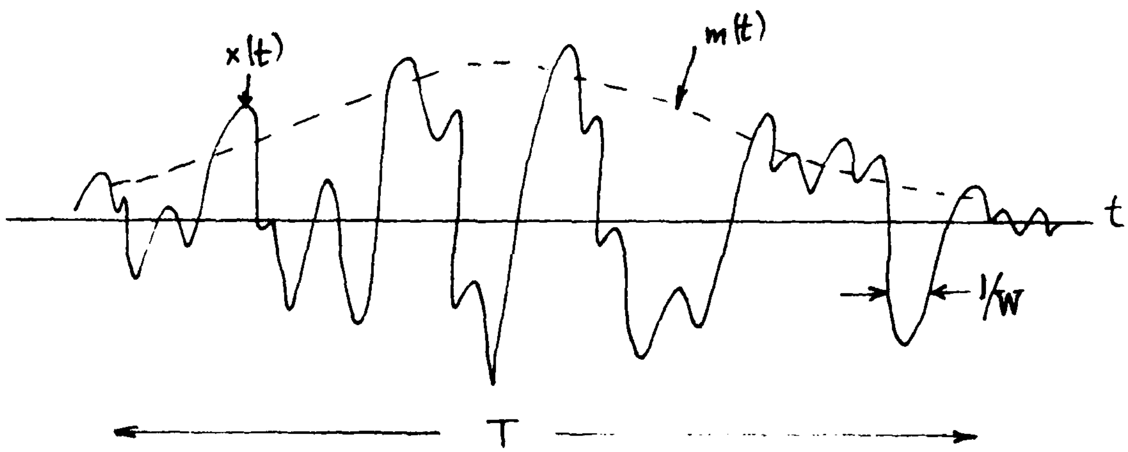

Figure 1. Sample Function and Modulation

PROBLEM SOLUTION

Definition of Error

We will attempt to fit the instantaneous sample power $x^2(t)$ of a particular observed member function (1) with a model of the form (3), namely

$$m^2(t)\ \tilde{S} + \tilde{N}, \tag{4}$$

where hypothesized values $\tilde{S}$ and $\tilde{N}$ will be chosen to minimize the error. Specifically, define instantaneous error

$$e(t) = x^2(t) - \left[m^2(t)\ \tilde{S} + \tilde{N}\right] \quad \text{for } t \in T. \tag{5}$$

Then the total integrated squared error over observation time T is

$$E \equiv \int_T dt\ e^2(t) = \int_T dt \left[x^2(t) - m^2(t)\ \tilde{S} - \tilde{N}\right]^2, \tag{6}$$

which is quadratic in hypothesized power values $\tilde{S}$ and $\tilde{N}$.

Minimization of Error

The partial derivatives of total error E with respect to $\tilde{S}$ and $\tilde{N}$ are

$$\frac{\partial E}{\partial \tilde{S}} = -2 \int_T dt \left[x^2(t) - m^2(t)\, \tilde{S} - \tilde{N}\right] m^2(t),$$

$$\frac{\partial E}{\partial \tilde{N}} = -2 \int_T dt \left[x^2(t) - m^2(t)\, \tilde{S} - \tilde{N}\right]. \qquad (7)$$

Setting both of these derivatives to zero, the optimal estimates, $\hat{S}$ and $\hat{N}$, of the unknown powers, S and N, are solutions of the two simultaneous linear equations

$$\hat{S}\, M_4 + \hat{N}\, M_2 = X_2,$$

$$\hat{S}\, M_2 + \hat{N}\, 1 = X_0, \qquad (8)$$

where

$$M_k \equiv \int_T dt\, m^k(t),$$

$$X_k \equiv \int_T dt\, m^k(t)\, x^2(t). \qquad (9)$$

Optimal Estimates

The solutions of linear equations (8) are

$$\hat{S} = \frac{T\, X_2 - M_2\, X_o}{T\, M_4 - M_2^2},$$

$$\hat{N} = \frac{M_4\, X_o - M_2\, X_2}{T\, M_4 - M_2^2}\ . \tag{10}$$

It should be observed that if amplitude modulation m(t) is constant over observation interval T, then determinant

$$D \equiv T\, M_4 - M_2^2 \tag{11}$$

is zero, and (8) can only be solved for the combination $\hat{S}m^2 + \hat{N}$, according to

$$\hat{S}\, m^2 + \hat{N} = \frac{1}{T} \int_T dt\ x^2(t) \quad \text{for } m(t) = m. \tag{12}$$

Therefore, in order to estimate S separately, it will be required that m(t) be nonconstant over T. However, we can anticipate that the stability of the estimate, $\hat{S}$, will be poor for modulations m(t) that are nearly constant over time T. The only way that D in (11) can be zero is if m(t) is constant over T, as may be easily seen from Schwartz's inequality.

Inspection of $\hat{S}$ in (10) reveals that it is inversely proportional to the level of m^2. Also, the product of $\hat{S}$ and the level of m^2 is

proportional to the level of x^2. This is consistent with the observation, based on (3), that it is only the product of $m^2(t)$ and S that matters, in so far as the received signal power is concerned. So, without loss of generality, one could set the maximum value of m(t) equal to 1, if desired; furthermore, if this convention is adopted, then S is directly the maximum value (over the observation interval) of the received average signal power versus time.

Mean of Signal Power Estimate

The mean of estimate $\hat{S}$ in (10) is given by

$$\overline{\hat{S}} = \frac{1}{D}\left(1\ \overline{X_2} - M_2\ \overline{X_0}\right), \tag{13}$$

where we used (11). Now (9) and (3) yield

$$\begin{aligned}\overline{X_k} &= \int_T dt\ m^k(t)\ \overline{x^2(t)} = \\ &= \int_T dt\ m^k(t)\left[m^2(t)\ S + N\right] = \\ &= M_{k+2}\ S + M_k\ N.\end{aligned} \tag{14}$$

Substitution of this result in (13), and the use of (11), yields

$$\overline{\hat{S}} = S. \tag{15}$$

That is, $\hat{S}$ is an unbiased estimate of the true power level S. (It may be shown in a similar fashion that $\hat{N}$ is an unbiased estimate of N; that is $\overline{\hat{N}} = N$.)

Variance of Estimate

An alternative form for $\hat{S}$ in (10) is more useful; by substituting (9) and (11), there follows

$$\hat{S} = \int dt\ g(t)\ x^2(t), \tag{16}$$

where

$$g(t) \equiv \begin{cases} \frac{1}{D}\left[T\ m^2(t) - M_2\right] & \text{for } t \in T \\ 0 & \text{otherwise} \end{cases} . \tag{17}$$

$g(t)$ is a deterministic function, dependent solely on $m^2(t)$ and T. Integrals without limits are over the range of nonzero integrands.

In order to determine the variance of $\hat{S}$, we first evaluate the mean square value:

$$\overline{\hat{S}^2} = \iint dt\ du\ g(t)\ g(u)\ \overline{x^2(t)\ x^2(u)}. \tag{18}$$

In order to proceed any further, we will assume that $x(t)$ is a (non-stationary) Gaussian random process; this is tantamount to assuming that $s(t)$ and $n(t)$ in (1) are Gaussian processes. (The results above for the mean of estimate $\hat{S}$ do not require this restriction, and apply for arbitrary statistics.) Therefore, we have the breakdown

$$\overline{x^2(t)\ x^2(u)} = \overline{x^2(t)}\ \overline{x^2(u)} + 2\ \overline{x(t)\ x(u)}^2 . \tag{19}$$

Substitution of the first term on the right hand side of (19) into (18) yields the square of the mean of $\hat{S}$. Consequently, the variance of $\hat{S}$ is

$$\mathrm{Var}(\hat{S}) = 2 \iint dt\, du\, g(t)\, g(u)\, \overline{x(t)\, x(u)}^{\,2} . \tag{20}$$

Consideration of the definition of x(t) in (1) now allows us to express

$$\overline{x(t)\, x(u)} = \overline{\left[m(t)\, s(t) + n(t)\right] \left[m(u)\, s(u) + n(u)\right]} =$$

$$= m(t)\, m(u)\, R_s(t-u) + R_n(t-u), \tag{21}$$

where R_s and R_n are the covariances of stationary processes s and n, respectively. Substitution of (21) into (20) yields

$$\mathrm{Var}(\hat{S}) = 2\iint dt\, du\, g(t)\, g(u) \left[m(t)\, m(u)\, R_s(t-u) + R_n(t-u)\right]^2 =$$

$$= 2 \iint dt\, d\tau\, g(t)\, g(t-\tau) \left[m(t)\, m(t-\tau)\, R_s(\tau) + R_n(\tau)\right]^2 =$$

$$= 2\int d\tau\, R_s^2(\tau)\, \phi_{gm^2}(\tau) + 4\int d\tau\, R_s(\tau)\, R_n(\tau)\, \phi_{gm}(\tau) +$$

$$+ 2\int d\tau\, R_n^2(\tau)\, \phi_g(\tau), \tag{22}$$

where we have defined autocorrelations

$$\phi_g(\tau) = \int dt\ g(t)\ g(t-\tau),$$
$$\phi_{gm}(\tau) = \int dt\ g(t)\ m(t)\ g(t-\tau)\ m(t-\tau),$$
$$\phi_{gm^2}(\tau) = \int dt\ g(t)\ m^2(t)\ g(t-\tau)\ m^2(t-\tau). \tag{23}$$

Approximation to Variance

The result in (22) for the variance of estimate $\hat{S}$ is exact, holding for any TW product. We will now specialize it to the case where

$$TW >> 1. \tag{24}$$

Representative plots of the various functions in (22) are displayed in figure 2. The covariances decay to zero within a delay 3/W, while the

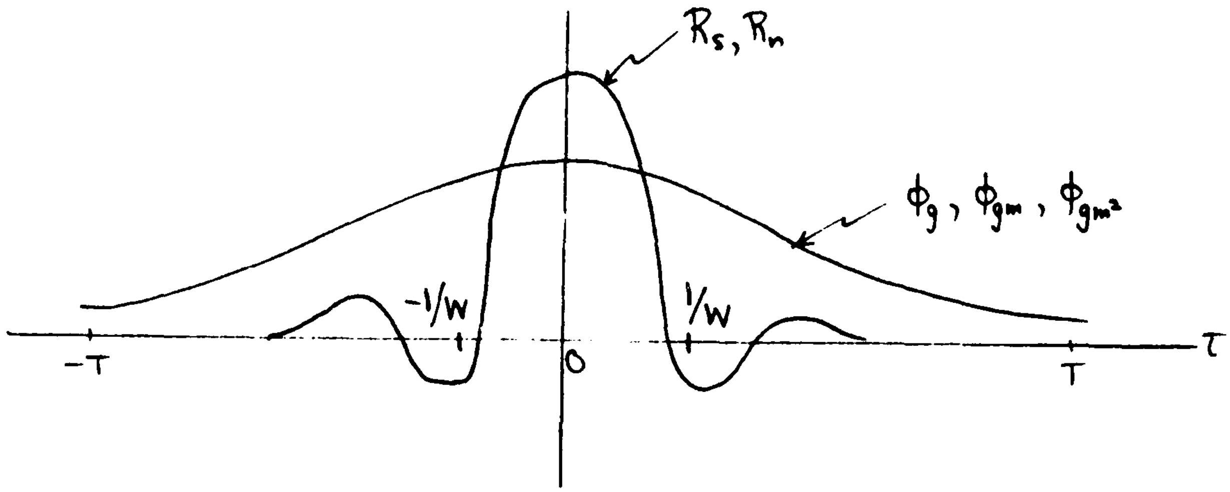

Figure 2. Representative Covariances and Autocorrelations

autocorrelations are more slowly varying, decaying to nearly zero at $\tau = T$. It is presumed that observation time T is approximately matched to the effective duration of modulation m(t). This allows (22) to be simplified to

$$\mathrm{Var}(\hat{S}) \cong 2\phi_{gm^2}(0)\int d\tau\, R_s^2(\tau) + + 4\,\phi_{gm}(0)\int d\tau\, R_s(\tau)\, R_n(\tau) + 2\,\phi_g(0)\int d\tau\, R_n^2(\tau). \qquad (25)$$

Alternative Forms for Autocorrelations

In order to simplify the scale factors that appear in (25), and to relate them back to the modulation m(t) by means of (17), we define some auxiliary quantities. Let the instantaneous power modulation be

$$a(t) = \left\{\begin{matrix} m^2(t) & \text{for } t \in T \\ 0 & \text{otherwise} \end{matrix}\right\}, \qquad (26)$$

and let

$$A = \frac{1}{T}\int dt\; a(t) = \frac{1}{T} M_2, \qquad (27)$$

which is the average power-modulation over observation time T. Define the "variable component" of $m^2(t)$ as

$$v(t) = a(t) - A = \left\{\begin{matrix} m^2(t) - A & \text{for } t \in T \\ 0 & \text{otherwise} \end{matrix}\right\}, \qquad (28)$$

and define integral

$$V_k = \int dt\; v^k(t) = \int dt\, \left[a(t) - A\right]^k. \qquad (29)$$

Then determinant D in (11) becomes

$$D = T\,M_4 - M_2^2 = T \int\limits_T dt\; m^4(t) - \left[\int\limits_T dt\; m^2(t)\right]^2 =$$

$$= T\int dt\; a^2(t) - \left[\int dt\; a(t)\right]^2 = T \int dt \left[a(t) - A\right]^2 = T\,V_2, \qquad (30)$$

while (17) becomes

$$g(t) = v(t)/V_2. \qquad (31)$$

That is, $g(t)$ is the ratio of the variable component to its own energy. Then since

$$m^2(t) = a(t) = A + v(t), \qquad (32)$$

we find

$$\phi_g(0) = \int dt\; g^2(t) = \frac{1}{V_2},$$

$$\phi_{gm}(0) = \int dt\; g^2(t)\; m^2(t) = \frac{A\,V_2 + V_3}{V_2^2},$$

$$\phi_{gm^2}(0) = \int dt\; g^2(t)\; m^4(t) = \frac{A^2\,V_2 + 2\,A\,V_3 + V_4}{V_2^2}, \qquad (33)$$

all in terms of the integrals (29) of the variable component (28) of $m^2(t)$.

Spectral Representations

By the use of Parseval's theorem, the three integrals over the covariances in (25) become

$$\int df\ G_s^2(f), \quad \int df\ G_s(f)\ G_n(f), \quad \int df\ G_n^2(f), \tag{34}$$

respectively, where G_s and G_n are the double-sided power density spectra of stationary processes s and n. Since the received processes will be pre-filtered to the band of the signal, it is reasonable to assume that s and n have identical spectral shapes. Then the bandwidth W, introduced in figure 1, can be made quantitative by defining it as the (positive frequency) effective bandwidth

$$W = \frac{\left[\int_0^\infty df\ G_s(f)\right]^2}{\int_0^\infty df\ G_s^2(f)} = \frac{\left[\int df\ G_s(f)\right]^2}{2\int df\ G_s^2(f)} = \frac{S^2}{2\int df\ G_s^2(f)} . \tag{35}$$

This enables us to express the three integrals in (34) as

$$\frac{S^2}{2W}, \quad \frac{SN}{2W}, \quad \frac{N^2}{2W}, \tag{36}$$

respectively.

Alternative Variance Expressions

When we combine (33)-(36) in (25), there results

$$\mathrm{Var}(\hat{S}) \cong \frac{A^2 V_2 + 2 A V_3 + V_4}{V_2^2} \frac{S^2}{W} +$$

$$+ 2 \frac{A V_2 + V_3}{V_2^2} \frac{SN}{W} + \frac{1}{V_2} \frac{N^2}{W} =$$

$$= \frac{1}{W V_2^2} \left[V_2 (AS + N)^2 + 2 V_3 S (AS + N) + V_4 S^2 \right]. \tag{37}$$

A more useful result is obtained if we let the dimensionless shape factor be defined as

$$U_k = \frac{\frac{1}{T} \int dt \; v^k(t)}{\left[\frac{1}{T} \int dt \; v^2(t) \right]^{k/2}} = \frac{V_k/T}{(V_2/T)^{k/2}}, \tag{38}$$

and define a variability factor

$$r^2 = \frac{\frac{1}{T} \int dt \left[a(t) - A \right]^2}{A^2} = \frac{V_2/T}{A^2}. \tag{39}$$

U_k depends solely on the variable component of $m^2(t)$, as defined in (28), while r^2 measures the relative strength of the variable component

and the average component, as defined in (27). Then (37) becomes

$$\mathrm{Var}(\hat{S}) \cong \frac{1}{TW} \frac{1}{r^2 A^2} \left[(AS+N)^2 + 2U_3\, r\, AS\, (AS+N) + U_4\, r^2\, (AS)^2 \right]. \tag{40}$$

Quality Ratio

A measure of the stability of estimate $\hat{S}$ is furnished by the quality ratio

$$Q = \frac{\mathrm{Av}(\hat{S})}{\mathrm{Std\ Dev}(\hat{S})} =$$

$$= \frac{\sqrt{TW}\, r\, R}{\left[(1+R)^2 + 2U_3\, r\, R\, (1+R) + U_4\, r^2\, R^2 \right]^{1/2}}, \tag{41}$$

where

$$R = \frac{AS}{N} = \frac{\frac{1}{T}\int dt\, \overline{\left[m(t)s(t) \right]^2}}{\overline{n^2(t)}} \tag{42}$$

is the observed signal-to-noise ratio. That is, AS is the mean signal power, averaged over the observation interval T. The fact that AS appear together in quality ratio (41) is consistent with the observations made in the sequel to (12). The result in (41) holds only for large TW; recall the assumption in (24) et sequel.

Large values for the quality ratio are desirable. However, increasing the bandwidth W will also increase the noise power N proportionately, if

the noise is white, thereby decreasing signal-to-noise ratio R. Increasing the observation time T is beneficial, to a point, depending on the nonzero extent of modulation m(t); however, since T is involved in U_2, U_3, r, A, the dependence of Q on T is very complicated and can only be ascertained by example. Larger variability factors, r, are desirable, but they also depend on T; if modulation m(t) is not under control, then only T can be varied in an attempt to realize large values of r.

If modulation m(t) is constant over T, then (39) and (41) yield r=0, Q=0, respectively. This is consistent with the observation in (12) that the signal power can not be separately estimated in this case.

Small Signal-to-Noise Ratio

If R << 1, then (41) reduces to

$$Q \cong \sqrt{T\,W}\, r\, R \quad \text{for } R \ll 1, \tag{43}$$

which is independent of shape factor U_k in (38). However, the variability factor r in (39) still plays an important role in the size of the quality factor Q.

EXAMPLE

Let the amplitude modulation m(t) in (1) be given by

$$m(t) = \exp\left(-\frac{t^2}{2\,T_1^2}\right) \qquad \text{for all } t. \tag{44}$$

T_1 is a measure of the effective extent of the modulation; that is,

$$m(\pm T_1) = \exp(-1/2) = .607,$$

$$a(\pm T_1) = m^2(\pm T_1) = \exp(-1) = .368. \tag{45}$$

Let observation time T in figure 1 extend over (-T/2, T/2), and define

$$\alpha_j = \frac{1}{T}\int_{-T/2}^{T/2} dt\, \exp(-j\, t^2/T_1^2) =$$

$$= \left(\frac{\pi}{j}\right)^{1/2} \frac{T_1}{T}\left[2\,\Phi\left(\left(\frac{j}{2}\right)^{1/2}\frac{T}{T_1}\right) - 1\right]; \qquad \alpha_0 = 1. \tag{46}$$

Here, the normal probability integral is

$$\Phi(x) = \int_{-\infty}^{x} du\, (2\pi)^{-1/2} \exp(-u^2/2). \tag{47}$$

The $\{\alpha_j\}$ are functions of the ratio of observation time T to effective duration T_1.

Then (26), (27), (44), and (46) yield

$$A = \alpha_1, \tag{48}$$

while (29) yields

$$\frac{V_k}{T} = \sum_{j=0}^{k} \binom{k}{j} (-A)^{k-j} \alpha_j. \tag{49}$$

In particular, using (48),

$$\begin{aligned} V_1 &= 0 \\ V_2/T &= \alpha_2 - \alpha_1^2, \\ V_3/T &= \alpha_3 - 3\alpha_2\alpha_1 + 2\alpha_1^3, \\ V_4/T &= \alpha_4 - 4\alpha_3\alpha_1 + 6\alpha_2\alpha_1^2 - 3\alpha_1^4. \end{aligned} \tag{50}$$

Then (38) and (39) yield

$$\begin{aligned} U_3 &= \frac{\alpha_3 - 3\alpha_2\alpha_1 + 2\alpha_1^3}{(\alpha_2 - \alpha_1^2)^{3/2}}, \\ U_4 &= \frac{\alpha_4 - 4\alpha_3\alpha_1 + 6\alpha_2\alpha_1^2 - 3\alpha_1^4}{(\alpha_2 - \alpha_1^2)^2}, \\ r^2 &= \frac{\alpha_2 - \alpha_1^2}{\alpha_1^2}. \end{aligned} \tag{51}$$

These quantities all depend on T/T_1 ; see (46).

We now have all the ingredients necessary to evaluate quality ratio Q in (41). Since

$$TW = T_1 W \frac{T}{T_1} , \tag{52}$$

we can express a normalized quality ratio as

$$\frac{Q}{(T_1 W)^{1/2}} = \frac{(T/T_1)^{1/2} \, r \, R}{\left[(1+R)^2 + 2U_3 \, r \, R \, (1+R) + U_4 \, r^2 \, R^2\right]^{1/2}} , \tag{53}$$

to accent the fundamental dependence on the ratio T/T_1. Also, from (42) and (48),

$$R = A \frac{S}{N} = \alpha_1 \frac{S}{N} , \tag{54}$$

giving input signal-to-noise ratio S/N as the only other fundamental parameter. The product $T_1 W$ of effective modulation duration and signal bandwidth is presumed large compared to 1, and can be chosen to fit the particular application. A program for the evaluation of (53) is attached below.

GRAPHICAL RESULTS

The normalized quality ratio in (53) is plotted vs T/T_1 in figure 3 for several signal-to-noise ratios, S/N. Here,

$$dB = 10 \log(S/N) \tag{55}$$

is used to label the curves. The curves increase rapidly with T/T_1 in the neighborhood of 2 to 4; however, they all saturate for large T/T_1, indicating the futility of attempting to observe over an interval where the signal strength has essentially decayed to zero.

The curves are also saturating at an upper bound, as may be seen by the crowding together near dB values of 20 in figure 3. Thus infinitely large signal-to-noise ratios result in a finite quality ratio (41), due to the inherent random character of the random signal process.

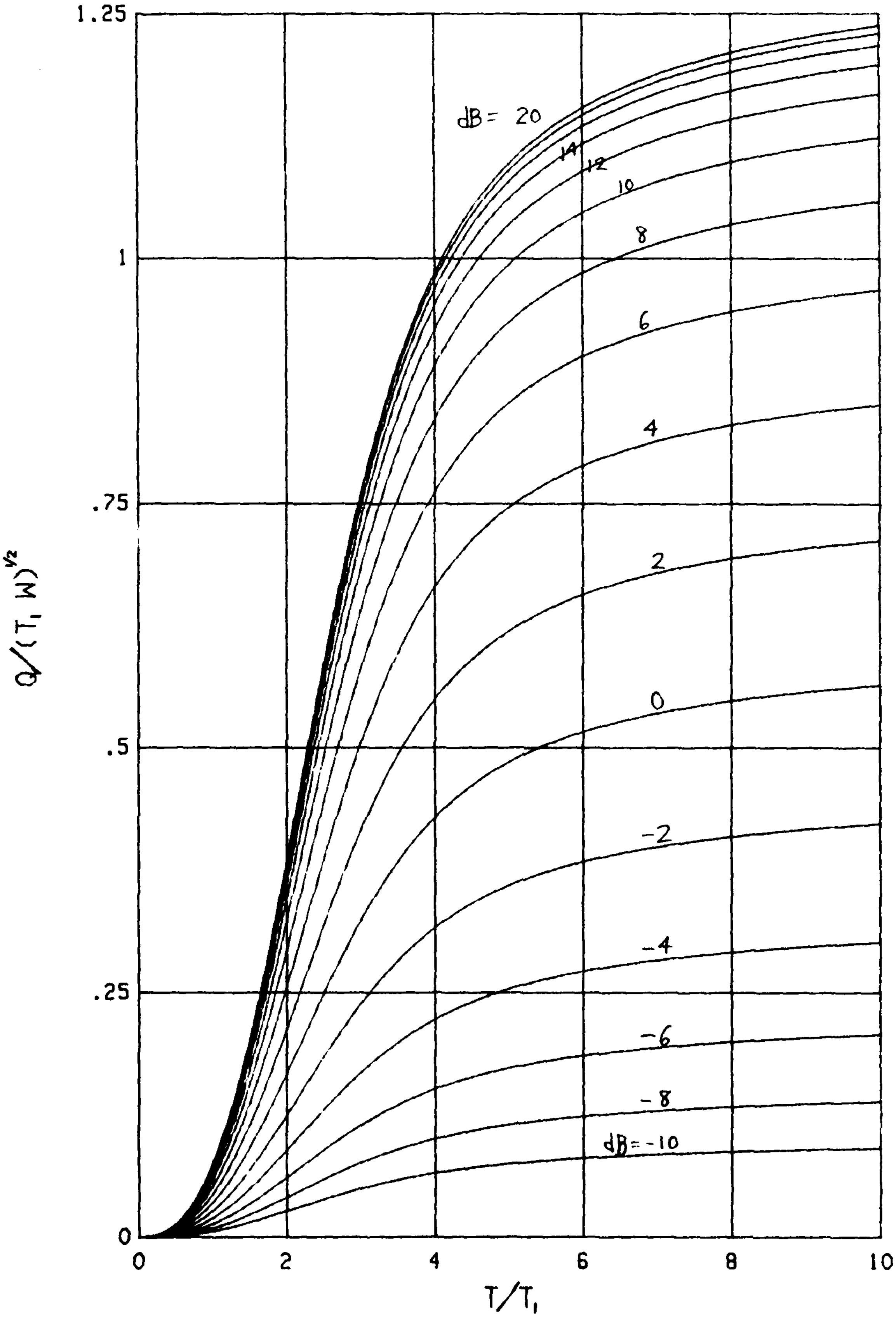

Figure 3. Normalized Quality Ratio

SUMMARY

A technique for estimating the unknown signal power of an amplitude-modulated signal in the presence of noise has been derived and evaluated in terms of its mean and variance. The estimate is unbiased, while the quality ratio depends strongly on the ratio of observation time to the effective-modulation duration.

PROGRAM

```
10     Sp=SQR(PI)
20     S5=SQR(.5)
30     S2=SQR(2.)
40     S3=SQR(3.)
50     FOR Db=-10. TO 20. STEP 2.
60     Sn=10.^(.1*Db)                      !  S/N
70     FOR Tt1=.1 TO 10 STEP .1            !  T/T1
80     Sq1=Sp/Tt1
90     Sq2=S5*Tt1
100    A1=Sq1*(2.*FNPhi(Sq2)-1.)           !  ALPHA1
110    A2=Sq1/S2*(2.*FNPhi(Sq2*S2)-1.)
120    A3=Sq1/S3*(2.*FNPhi(Sq2*S3)-1.)
130    A4=Sq1/2.*(2.*FNPhi(Sq2*2.)-1.)
140    P=A1*A1
150    F=A2-P
160    Sq=SQR(F)
170    Rs=Sq/A1                            !  r
180    U3=(A3-3.*A2*A1+2.*P*A1)/(F*Sq)
190    U4=(A4-4.*A3*A1+6.*A2*P-3.*P*P)/(F*F)
200    R=A1*Sn                             !  R
210    R1=1.+R
220    P=Rs*R
230    D=R1*R1+2.*U3*P*R1+U4*P*P
240    Nqr=P*SQR(Tt1/D)
250    PRINT Db,Tt1,Nqr
260    NEXT Tt1
270    PRINT
280    NEXT Db
290    END
300    !
310    DEF FNPhi(X)                        !  HART, page 140, #5708 & #5725
320    Y=ABS(X)*.70710678118654746
330    SELECT Y
340    CASE <8.
350    P=1631.7602687537147O+Y*(456.261458706092631+Y*(86.0827622119485951+Y*
(10.0648589749095425+Y*.564189586761813614)))
360    P=3723.50798155480672+Y*(7113.66324695404987+Y*(6758.21696411048589+Y*
(4032.26701083004974+Y*P)))
370    Q=7542.47951019347576+Y*(2968.00490148230872+Y*(817.622386304544077+Y*
(153.077710750362216+Y*(17.8394984391395565+Y))))
380    Q=3723.50798155480654+Y*(11315.1920818544055+Y*(15802.5359994020425+Y*
(13349.3465612844574+Y*Q)))
390    Phi=.5*EXP(-Y*Y)*P/Q
400    CASE <26.6
410    P=2.97886562639399289+Y*(7.40974060596474179+Y*(6.16020985310963054+Y*
(5.01904972678426746+Y*(1.27536664472996595+Y*.564189583547755074))))
420    Q=3.36907520698275277+Y*(9.60896532719278787+Y*(17.0814407474660043+Y*
(12.0489519278551290+Y*(9.39603401623505415+Y*(2.26052852076732697+Y)))))
430    Phi=.5*EXP(-Y*Y)*P/Q
440    CASE ELSE
450    Phi=0.
460    END SELECT
470    IF X>0. THEN Phi=1.-Phi
480    RETURN Phi
490    FNEND
```

Subject Matter Index